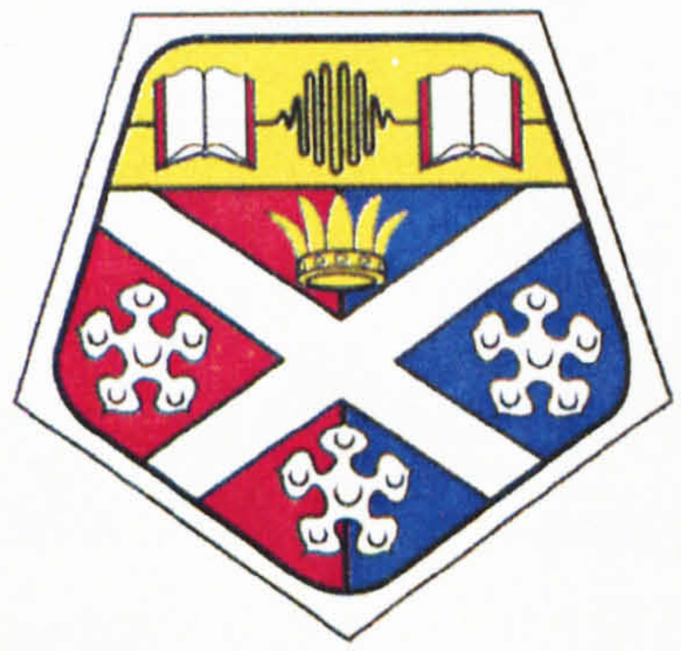

UNIVERSITY OF STRATHCLYDE

Department of Chemical and Process Engineering

"Heat and Mass Transfer Models for Binary Hydrocarbon Mixtures in Reflux Condensation"

Derek Cuthbertson

A thesis submitted for the degree of Doctor of Philosophy

Declaration

"The copyright of this thesis belongs to the author under the terms of the United Kingdom Copyright Acts as qualified by University of Strathclyde Regulation 3.49. Due acknowledgements must always be made of the use of any material contained in, or derived from, this thesis."

Derek Cuthbertson

Acknowledgements

The author wishes to express his sincere gratitude to the following individuals and organisations:

Mr. Jim M McNaught, the project industrial supervisor, and the academic supervisor Prof. Colin D Grant, for all their valuable support, guidance, and encouragement during this work.

All the technical staff at the TÜV National Engineering Laboratory (NEL) who assisted during this research, in particular Mr. Tom Clark, Brendan Robson, Tommy Gallagher and Linda Rowan.

AEA Technology and the Heat Transfer and Fluid Flow Service (HTFS), for providing me with the opportunity to participate in this research.

The Postgraduate Training Partnership (PTP) Scheme for three years of useful learning in an industrial environment, especially Mr. Jim T R Watson and Mr. Dennis Boam the past and present PTP-Coordinators at NEL.

The UK Department of Trade and Industry, the Engineering and Physical Sciences Research Council (EPSRC), and the TÜV National Engineering Laboratory for providing funding.

Abstract

This thesis presents an investigation into the the important issues in the design of reflux condensers. The main focus is on heat and mass transfer, particularly in applying standard models to the design, although flooding is also considered as it is crucial to the design. New data have been collected on an improved HTFS Reflux Condensation Facility at NEL to provide information to back up the theoretical arguments presented.

n-Penane (pentane) and 2,2,4-trimethylpentane (iso-octane) were condensed separately and in binary mixtures with three different bulk compositions. Single component data on the condensation of both pentane and iso-octane were used to measure heat transfer resistances in the condensate film while mixture data were used to measure separations and resistances in the vapour. Experimental separations were extremely low, always less than one ideal stage, a fact caused by the tube geometry and operating conditions which promoted very high mass transfer rate factors. Condensate and vapour resistances were both lower than would be expected in an equivalent condenser operated in co-current mode. It was argued that this was due to the countercurrent flow of vapour which served to increase turbulence at the phase interface. In the flooding analysis, the single vertical tube was deliberately flooded while condensing iso-octane allowing the flooding point to be defined in terms of condensate drainage and facility behaviour.

The experimental data were modelled to analyse the application of the film theory and equilibrium models to reflux condenser design. The film theory model proved to be by far the most accurate of the two with tube length (area) predictions to within ±23% and the majority of separations to within ±30% of the actual. The equilibrium model predicted tube lengths up to three and a half times longer than the actual tube length while the low experimental separations meant that composition changes were very overpredicted by both intergral and differetial condensation curves.

The reason for the failure of the equilibrium model was the high rate factors that are experienced in reflux condensers and this facility especially. High rate factors lead to large reductions in the vapour sensible heat transfer coefficient when correcting for the effect of mass transfer. This upsets the balance achieved by overpredicting both heat transfer in the vapour and overprediction of temperature-enthalpy (T-h) gradient. This balance normally leads to the equilibrium model being reasonable accurate.

This was addressed by proposing a rate factor based correction to the equilibrium method. The correction reduced the vapour composition predicted by equilibrium thus reducing the T-h gradient and the predicted tube length. This correction is applicable to all cases of rate controlled binary condensation in the absence of a non-condensing gas although it will only be significant when rate factors are large such as in reflux condensers. A simple correction factor was used to prove that the correction improves the model, with predicted compositions and tube lengths in some cases more accurate than those of the film theory model.

Contents

Declaration ii

Acknowledgements i

Abstract ii

Contents iv

Nomenclature ix

1 Introduction 1

1.1 Reflux Condensation 1

1.2 Background to Project 4

1.3 Aims and Objectives 5

1.4 Thesis Layout 5

2 Literature Review 7

2.1 Introduction 7

2.2 Theory of Condensation 7

2.3 Heat Transfer in the Condensate Film 9

2.3.1 Condensate film hydrodynamics *9*

2.3.2 Film heat transfer resistance *11*

2.3.3 Prediction of film heat transfer coefficients *12*

2.4 Heat Transfer in the Vapour 16

2.5 Flooding 19

2.5.1 Flooding Mechanism *20*

2.5.2 Definition of the flooding point *24*

2.5.3 Flooding point correlations *27*

2.6 Equilibrium Based Design Method 31

2.6.1 Condensation curves *35*

2.6.2 Theoretical Assessment of Condensation curves in reflux condenser design *39*

2.6.3 Experimental evaluation of the equilibrium method *41*

2.7 Film Theory Design Method....43
2.7.1 Heat transfer....43
2.7.2 Mass transfer....44
2.7.3 Downstream development....46
2.7.4 Liquid Mixing....47
2.8 Summary....48

3 Experimental Equipment and Methods....50
3.1 The Test Facility....50
3.1.1 Test Fluid Circuit....51
3.1.2 Coolant Circuit....55
3.1.3 Measurement Systems....55
3.2 Data Analysis....60
3.2.1 Analysis spreadsheet....60
3.2.2 Physical properties....61
3.2.3 Vapour / Liquid equilibrium calculations....64
3.3 Experimental Method....66
3.3.1 Controlled variables....66
3.3.2 General procedure....67
3.3.3 Data collection procedure....68

4 Data Analysis Calculations....71
4.1 Mass and energy balances....71
4.2 Mass balance calculations....73
4.2.1 Density to composition conversion....75
4.3 Heat balance calculations....76
4.3.1 Heat losses....77
4.3.2 Estimation of heat losses....77
4.4 Heat Transfer Coefficients....81
4.4.1 Overall mean heat transfer coefficient....82
4.4.2 Coolant heat transfer coefficient....82
4.4.3 Condensate film heat transfer coefficient....86
4.4.4 Vapour heat transfer coefficient....86
4.5 Uncertainty Analysis Method....89
4.5.1 Combined measurement uncertainties....89
4.5.2 Propagated Uncertainties....95

5 Experimental Data and Results 99
5.1 Experimental Programme 99
5.1.1 Single component data 101
5.1.2 Mixture data 102
5.2 Heat balances 103
5.2.1 Location of heat losses 106
5.2.2 Estimation of heat losses 107
5.3 Temperature profiles and saturation conditions 110
5.3.1 Single component 110
5.3.2 Mixtures 113
5.3.3 Saturation temperature problem 114
5.4 Heat Transfer Coefficients 123
5.4.1 Correlation for the coolant heat transfer coefficient 123
5.4.2 Condensing film heat transfer coefficients 125
5.4.3 Vapour heat transfer coefficients 132
5.5 Separations achieved in the condenser 138
5.6 Uncertainty analysis results 141
5.6.1 Standard uncertainties for the main measurements 141
5.6.2 Uncertainty of calculated results 142
5.7 Summary 148

6 Flooding Analysis 150
6.1 Experimental data set 150
6.2 Visual Observations 151
6.3 Flooding mechanism 153
6.4 Definition of the flooding point 155
6.4.1 Facility behaviour 155
6.4.2 Temperature profiles 156
6.4.3 System pressure 157
6.4.4 Pressure Drop 159
6.5 Flooding velocity correlations 161
6.5.1 Effect of tube diameter 163
6.5.2 Effect of tube end cut 167
6.6 Summary 169

7 Film Theory Based Modelling 171
7.1 Introduction 171
7.2 Method summary 171
7.3 Implementation of the method 172
7.3.1 Calculation of local condensing fluxes 173
7.3.2 Downstream development and simulation solution 176
7.3.3 Prediction of heat transfer coefficients 178
7.4 Analysis of individual runs 179
7.4.1 Structure of the output file 179
7.4.2 Temperature profiles 182
7.5 Results Summary 183
7.5.1 Tube length predictions 183
7.5.2 Prediction of vapour temperature 187
7.5.3 Composition of the outlet vapour 188
7.5.4 Discussion on separation 191
7.6 Film theory modelling by other workers 194
7.7 Summary 199

8 The Silver, Bell and Ghaly (Equilibrium) Method 201
8.1 Method summary 201
8.2 Condensation curves 202
8.2.1 Integral 202
8.2.2 Differential (unmixed) 203
8.2.3 Differential (mixed) 203
8.3 Experimental analysis 203
8.3.1 Implementation of the method 203
8.3.2 T-h relationship and separation 205
8.3.3 Tube length predictions 207
8.4 Link between heat and mass transfer rate factors 214
8.5 Proposed correction to the equilibrium method 216
8.5.1 Justification for a correction 216
8.5.2 Basis for correction 217
8.5.3 Form of the correction 218
8.5.4 Limits check 219

8.6 Application of correction to equilibrium method....220
8.6.1 Correction factor F....220
8.6.2 Compositions and T-h relationship....222
8.6.3 Tube length predictions....224
8.7 Summary....226

9 Summary, conclusions and recommendations....227
9.1 Summary....227
9.2 Conclusions....229
9.2.1 Experimental work....229
9.2.2 Flooding....230
9.2.3 Film theory based modelling....230
9.2.4 Equilibrium method modelling....231
9.3 Recommendations for future work....232
9.3.1 Flooding....232
9.3.2 Film theory modelling....233
9.3.3 Equilibrium model....233
9.3.4 Heat transfer enhancement....234

References....235

List of figures....242

List of tables....245

Appendix A: Instrument Calibrations....246
Appendix B: Sample Uncertainty Analysis....254
Appendix D: VLE Calculation Functions....279
Appendix E: Single Component Data And Calculation Results....285
Appendix F: Binary Mixture Data And Calculation Results....314
Appendix G: Film Theory Simulation Code....331

Nomenclature

Letters

A	[m²]	Heat transfer area
c	[kg/m³]	Concentration
c	[-]	Sensitivity coefficient (uncertainty analysis)
$\tilde{c}$	[kmol/m³]	Molar concentration
Cp	[J/kgK]	Specific heat capacity
$\tilde{C}p$	[J/kmolK]	Molar specific heat capacity
D	[m]	Tube diameter
D_{AB}	[m²/s]	Binary diffusion coefficient
D_e	[m]	Equivalent hydraulic diameter
E	[-]	Number of ideal stages
f	[-]	Friction factor
F	[-]	Equilibrium method correction factor
G	[m]	Coolant channel dimensions
g	[m²/s]	Acceleration due to gravity
$g(Pr)$	[-]	Temperature gradient parameter
h	[m]	Height
h	[J/kg]	Specific enthalpy
Δh_v	[J/kg}	Latent heat of vaporisation
L	[m]	Tube length
$\dot{M}$	[kg/s]	Mass flow rate
$\tilde{M}$	[kg/kmol]	Molar mass
$\dot{m}$	[kg/m²s]	Mass flux
$\dot{N}$	[kmol/s]	Molar flow rate
$\dot{n}$	[kmol/m²s]	Molar flux
P	[Pa]	Pressure
$\dot{Q}$	[W]	Heat load
$\dot{q}$	[W/m²]	Heat flux
R	[-]	Ratio of measurable heat out to heat in

r	[-]	Ratio of total to component flux
s	[m]	Film thickness
$s(x_i)$	[-]	Standard deviation
T	[°C]	Temperature
$\Delta\overline{T}$	[°C]	Logarithmic mean temperature difference
U	[W/m²K]	Overall heat transfer coefficient
u	[m/s]	Velocity
$U(x_i)$	[-]	Expanded uncertainty
$u(x_i)$	[-]	Standard uncertainty
$\dot{V}$	[m³/s]	Volume flow rate
x	[-]	Liquid mass fraction
x	[m]	Wall thickness
$\tilde{x}$	[-]	Liquid mole fraction
$\dot{x}$	[-]	Vapour quality
x_i	[-]	Measurement value in uncertainty analysis
y	[-]	Vapour mass fraction
$\tilde{y}$	[-]	Vapour mole fraction
Z	[-]	Ratio of sensible to total heat transfer
z	[m]	Width

Greek symbols

α	[W/m²K]	Heat transfer coefficient
α^*	[-]	Dimensionless heat transfer coefficient
β	[mol/m²s]	Mass transfer coefficient
β	[K^{-1}]	Coefficient of expansion
β^*	[mol/m²s]	Modified mass transfer coefficient
δ	[m]	Film thickness
ϕ	[-]	Rate factor
η	[kg/ms]	Dynamic viscosity
λ	[W/mK}	Thermal conductivity
ν	[m/s]	Kinematic viscosity

θ	[-]	Mass transfer correction factor
θ	[-]	Fraction of inlet vapour left uncondensed
θ	[°]	Angle of tube end cut
ρ	[kg/m³]	Density
σ	[N/m]	Surface tension
τ	[N/m²]	Shear stress

Subscripts

A	Air extraction
B	Boiler
b	Bulk
b	Bottom of the tube
Ba	Bartleman
c	Coolant
$CabC$	Cabinet ceiling
$CabW$	Cabinet wall
$corr$	Corrected
cs	Condensing side
D	Dump Condenser
DB	Dittus-Boelter
$Duct$	Air extraction duct
E	Error
eff	Effective
F	Cabinet floor
FV	Film Velocity correction
f	Condensate film
$flood$	Flooding
G	Gnielinski
g	Gas phase
H	Heat transfer
h	Height
$HTFS$	HTFS method

I	Iso-octane
I	Instrument uncertainty
i	Inside
i	Vapour / liquid interface
in	Inlet
inc	Incremental
j	Component identity
L	Heat losses
l	Liquid
M	Mass transfer
o	Outside
out	Outlet
P	Pentane
P	Petukhov
R	Reflux condenser
S	Sensible
S	Steady state uncertainty
s	Condensate surface
Sat	Saturation
T	Total
t	Top of the tube
tr	Tube root diameter
v	Vapour
VCC	Vapour containment cabinet
W	Wave correction
w	Wall
w	Width
λ	Phase change

Overstrikes

$\bar{}$	Mean
$\tilde{}$	Molar

Dimensionless groups

Bo	Bond number
Fr	Froude number
Gr	Grashof number
K	Kutateladze number
Nu	Nusselt number
Pr	Prandtl number
Ra	Raleigh number
Re	Reynolds number
Sc	Schmidt number

1 Introduction

1.1 Reflux Condensation

Condensers are heat exchangers that are used to change the state of one or more components from vapour to liquid by exchanging heat with a coolant. Reflux condensation is the term used to describe the condensation of an upwardly flowing vapour into a condensate that flows counter-currently under the influence of gravity. The most popular design geometry for this type of condenser is a vertical shell and tube exchanger with the vapour and condensate in the tubes and the coolant in the shell. Historically, other geometries such as plate-fin and inclined shell and tube have also been employed.

A reflux condenser can be considered as a mass transfer device as well as a heat exchanger. The principle is similar to that of a distillation column in that at any point in the tubes, the heavier components will condense preferentially. This leads to a separation as the condensate will be richer in the heavier components than any uncondensed vapour. Theoretically, it is expected that a reflux condenser will produce more separation than a co-current condenser of similar geometry.

Applications of reflux condensers include distillation overheads partial condensers, where the reflux condenser is known as a dephlegmator, knock-back and vent condensers associated with reaction vessels, and air cooled steam condensers. The process of reflux condensation has also been employed in the nuclear industry where emergency cooling systems condense steam in an inverted U-tube.

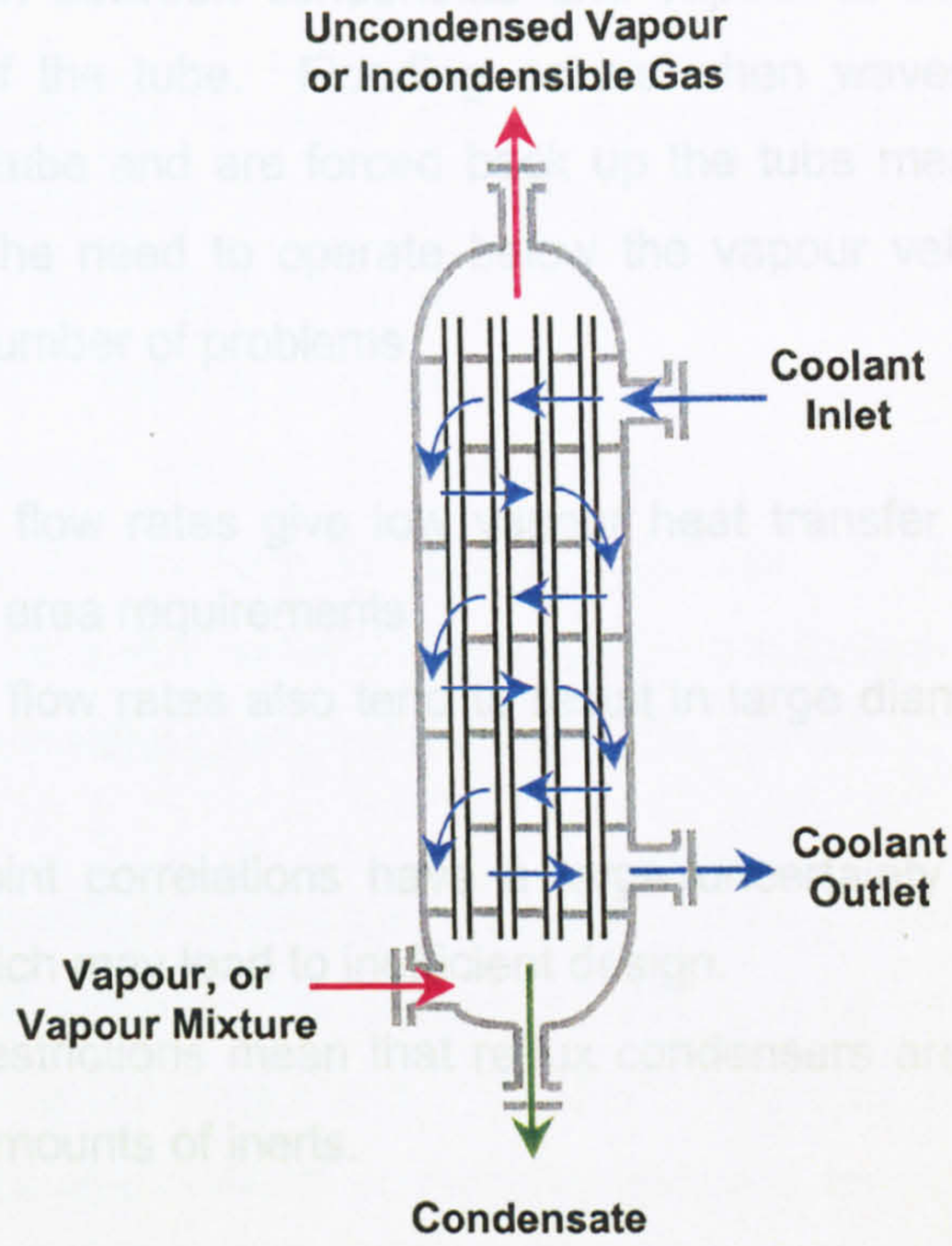

Figure 1.1: Schematic diagram of a vertical shell and tube reflux condenser

Reflux condensers offer a number of advantages over competing technologies.

(i) Dephlegmators are capital cost effective. A single unit can be flange mounted onto the top of a column providing a capital saving over an equivalent total condenser, reflux drum and pump. Running costs are also lower as there is no pump.

(ii) In a reflux condenser, inerts are flushed to the top of the tube by the vapour flow hence the unit is self venting.

(iii) The countercurrent flow means that cooling condensate is reheated by hot vapour. Not only is the condensate cooling minimised, but lighter components may re-evaporate resulting in an additional rectification effect.

There is however one grave disadvantage to the use of the reflux condensation process. Interaction between condensate and vapour at the tube entrance may result in flooding of the tube. Flooding occurs when waves on the condensate surface bridge the tube and are forced back up the tube meaning that the tube is unable to drain. The need to operate below the vapour velocity which results in flooding causes a number of problems

(i) Low vapour flow rates give low vapour heat transfer coefficients and as a result larger area requirements.

(ii) Low vapour flow rates also tend to result in large diameter shells, which are expensive.

(iii) Flooding point correlations have a large uncertainty so safety factors are required which may lead to inefficient design.

(iv) Flow rate restrictions mean that reflux condensers are not suitable for fluids with large amounts of inerts.

Other potential disadvantages include the reflux ratio being difficult to control, and flow maldistributions that could arise from the very low pressure drop experienced in reflux condensers.

Customer demand has resulted in the inclusion of reflux condensers into the HTFS shell and tube design and rating package TASC. The HTFS philosophy is to base design methods on theory validated by experimental data. This has led to the commissioning of this project to study in more detail the heat and mass transfer mechanisms involved in reflux condensation with the aim of developing and validating a model suitable for inclusion into TASC.

The thermal design of a reflux condenser is based on heat and mass transfer in the vapour and condensate films, with consideration given to estimation of the flooding point. In this project the most important issue was developing understanding of the underlying heat and mass transfer processes and applying this to the thermal design. To this end, pure fluids and binary mixtures were both studied. Accurate thermal designs are of limited use though, if poor understanding of flooding results in the need for large safety factors. Because of this, the process of flooding and prediction of the flooding point have also been studied.

1.2 Background to Project

This project was carried out as part of the Postgraduate Training Partnership (PTP) scheme. This scheme was introduced jointly by the Department of Trade and Industry (DTI) and the Engineering and Physical Sciences Research Council (EPSRC) in 1992 to provide a framework for partnerships between research and technology organisations (RTOs) and higher education institutes (HEI). These partnerships provide the backing for a post graduate student, known as a PTP Associate, to study for a PhD while being based in the industrial environment of the RTO, with EPSRC providing financial backing to the associate.

The PTP scheme benefits the associate in that he or she is able to conduct research in an industrial environment while receiving training in a variety of skills such as management and financial awareness. The RTO and HEI also benefit as they are able to improve ties and extend common objectives leading to research that is relevant to industry.

The partnership responsible for this project was between the National Engineering Laboratory (NEL), based in East Kilbride, and the University of Strathclyde, in Glasgow. Industrial sponsorship was received from Hyprotech UK Ltd (formerly AEA Technology) under the HTFS brand.

The National Engineering Laboratory was founded in 1947 as a government run research facility. Now privately owned as a business of TÜV Product Service, it provides state of the art research from a team of highly skilled professionals. With a global client base including government and industrial organisations NEL provides consultancy, design, modelling, certification and testing in a multi-disciplinary field backed up by extensive experimental facilities.

1.3 Aims and Objectives

In order to satisfy the overall aim of the project and successfully model the process of reflux condensation, a number of key objectives were specified.

- Upgrading of the existing experimental facility to allow collection of quality reliable data.

- Expansion of the data bank for the condensation of single hydrocarbons and binary hydrocarbon mixtures under refluxing conditions.

- Improve understanding of the detailed mass and heat transfer mechanisms particularly in the vapour phase.

- Improve the understanding of flooding in a reflux condenser to allow improved prediction of the flooding point.

1.4 Thesis Layout

In Chapter 2, the theory of the processes of condensation and of reflux condensation are summarised. This is followed by a detailed literature review where some of the important issues around the design of reflux condensers are considered. This review focuses on the phenomenon of flooding, and application of standard thermal design methods to reflux condensers.

The experimental facility is described in Chapter 3 with consideration given to the improvements made by the author. The measurement systems, data collection and data analysis tools are summarised, and with a detailed description of the experimental method highlight the improvements not only in hardware but also in operating procedures.

In Chapter 4 the techniques and equations used to analyse the experimental data are presented. This is followed by a description of the method used to produce a detailed uncertainty analysis of the experimental data. The experimental data and results are then presented in Chapter 5 along with a summary of the uncertainty analysis findings.

The issue of flooding is tackled in Chapter 6. Visual observations and experimental data are used to focus discussion on the flooding mechanism and prediction of the flooding point.

The two major condenser thermal design methods based on film theory and equilibrium models were applied to the experimental data and are discussed in Chapters 7 and 8. Simulations written in Visual Basic are used to model the experimental data, and the results of the simulation used to compare and contrast the two methods.

Finally, a summary is given in Chapter 9 followed by conclusions and recommendations for future work.

2 Literature Review

2.1 Introduction

In this chapter, a summary of the theory of the process of condensation is presented. This is then followed by a detailed literature review on the main topics associated with the thermal design of reflux condensers. Correlations for heat transfer in the vapour and condensate films are presented and discussed, as are the two main standard thermal design methods for reflux and co-current condensers. The issue of flooding is also considered as the flooding point is a vital issue to any reflux condenser design.

2.2 Theory of Condensation

When a condensate first begins to form on a cooled surface, it appears as small droplets. As condensation proceeds these droplets grow in size and number and begin to join together. In the vast majority of cases, the surface will become completely covered with condensate in the form of a thin liquid film. This is known as filmwise condensation. In some situations however the droplets do not join together and remain as separate patches of condensate; this is known as dropwise condensation. It is difficult to sustain dropwise condensation without treating the cooled surface specifically for that objective. In reflux condensers, filmwise condensation is the mechanism expected therefore dropwise condensation is not considered any further in this work.

The most popular theory of the process of binary mixture condensation was presented by Colburn & Drew (1937). They considered all heat and mass transfer in the gas-phase to take place in a one-dimensional laminar film adjacent to the vapour and liquid interface. This is shown in Figure 2.1.

A binary vapour with temperature T_v and bulk composition $\tilde{y}_b$ cools through the gas film towards the vapour liquid interface. The vapour at the interface, $\tilde{y}_i$, is assumed to be in equilibrium with the condensate of surface composition $\tilde{x}_i$, at the local dew point temperature T_i.

The heat flux from the vapour to the coolant, $\dot{q}_T$, is the sum of the sensible cooling fluxes of the vapour and condensate, $\dot{q}_v$ and $\dot{q}_f$ respectively, and the latent heat released by condensation, $\dot{q}_\lambda$ although in reflux condensation the condensate cooling term is expected to be small.

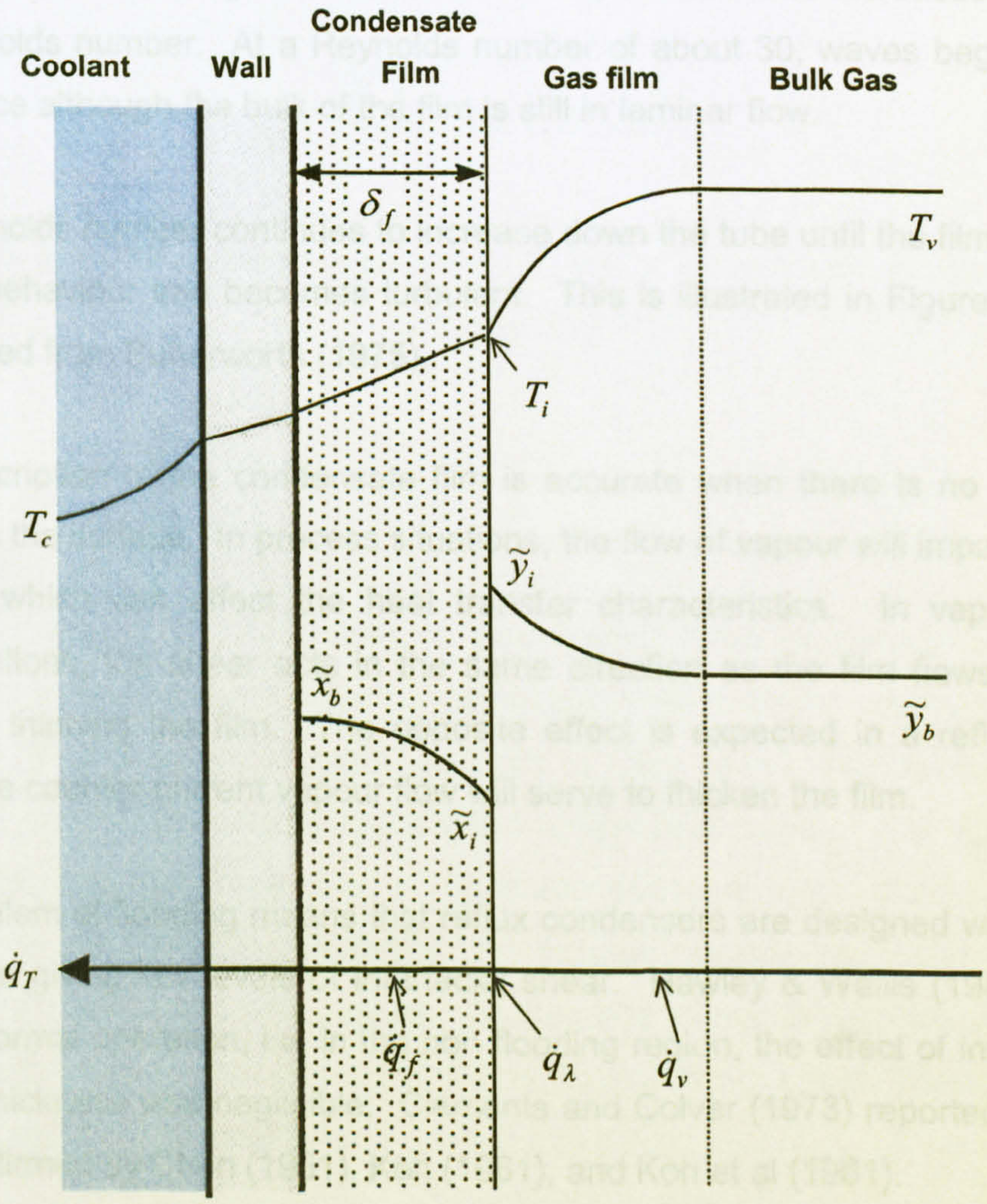

Figure 2.1: Film theory of binary mixture condensation, Colburn & Drew (1937)

2.3 Heat Transfer in the Condensate Film

The literature for heat transfer in condensing films on vertical surfaces is extensive. Unfortunately, most of these studies were based on co-current condenser arrangements, and there are relatively fewer data available for reflux condensers. Film condensation in general will be summarised briefly, with reflux condensation considered in more detail.

2.3.1 Condensate film hydrodynamics

Under condensing conditions, a film forming at the top of a tube will fall under the influence of gravity. Initially, the small mass flow rate results in a smooth laminar film, but as the film progresses down the tube, the flow rate increases and so does the Reynolds number. At a Reynolds number of about 30, waves begin to form on the surface although the bulk of the film is still in laminar flow.

The Reynolds number continues to increase down the tube until the film departs from laminar behaviour and becomes turbulent. This is illustrated in Figure 2.2, which is reproduced from Butterworth (1975).

This description of the condensate film is accurate when there is no vapour shear acting on the surface. In process situations, the flow of vapour will impart a drag onto the film which can affect the heat transfer characteristics. In vapour downflow configurations, the shear acts in the same direction as the film flows and has the effect of thinning the film. The opposite effect is expected in a reflux condenser where the counter-current vapour flow will serve to thicken the film.

The problem of flooding means that reflux condensers are designed with low vapour flow rates giving low levels of interfacial shear. Hawley & Wallis (1982) found that during normal operation, i.e. in the non flooding region, the effect of interfacial shear on film thickness was negligible. Clements and Colver (1973) reported that this was also confirmed by Chen (1961), Koh (1961), and Koh et al (1961).

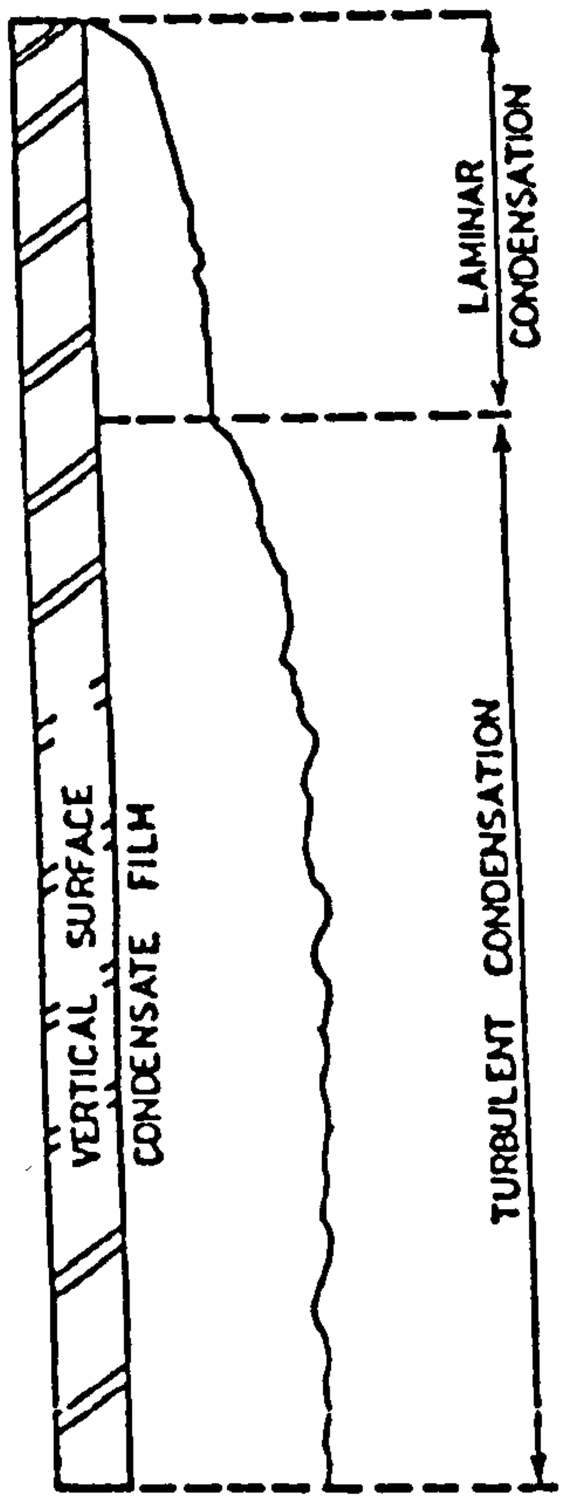

Figure 2.2: Filmwise condensation on a vertical surface with no vapour shear (Butterworth, 1975) .

Recently, Gross et al. (2002) used an experimental reflux condenser tube to quantify the effect of vapour shear on the condensate film heat transfer coefficient over a wide range of Reynolds and Prandtl numbers. They found that at some Reynolds numbers, shear stress had a small effect on the heat transfer characteristics of the film. With very thin films (Re_l < 10), shear stress reduced the Nusselt number, whereas in the laminar-wavy region, the Nusselt number increased in a parabolic fashion with increasing shear stress. As the enhancements reported were small and it is safe to assume that shear stress has no significant effect, interfacial shear will not be considered further here.

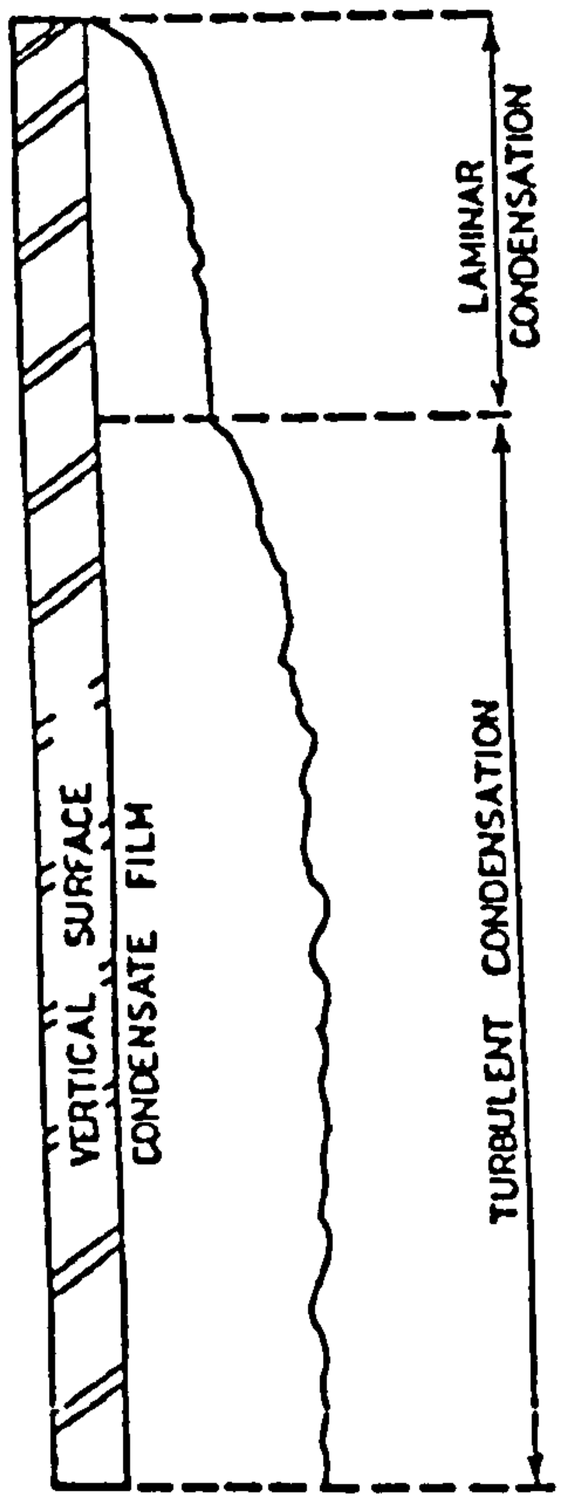

Figure 2.2: Filmwise condensation on a vertical surface with no vapour shear (Butterworth, 1975) .

Recently, Gross et al. (2002) used an experimental reflux condenser tube to quantify the effect of vapour shear on the condensate film heat transfer coefficient over a wide range of Reynolds and Prandtl numbers. They found that at some Reynolds numbers, shear stress had a small effect on the heat transfer characteristics of the film. With very thin films ($Re_l < 10$), shear stress reduced the Nusselt number, whereas in the laminar-wavy region, the Nusselt number increased in a parabolic fashion with increasing shear stress. As the enhancements reported were small and it is safe to assume that shear stress has no significant effect, interfacial shear will not be considered further here.

2.3.2 *Film heat transfer resistance*

In the laminar flow regime there is no cross mixing, and heat is transferred purely by conduction through the film. It follows that as the film thickens and Reynolds number increases, the resistance to heat transfer (which is the film thickness divided by thermal conductivity) also increases. This is also true in the laminar wavy region but the effect of waves is to reduce the resistance compared with purely laminar flow. It is believed that this is because the effective thickness of the film is smaller between the wave crests (Gross, 1992).

This is shown in Figure 2.3. In the laminar and laminar-wavy regions the film heat transfer coefficient decreases with increasing Reynolds number, with a smaller gradient in the laminar-wavy region.

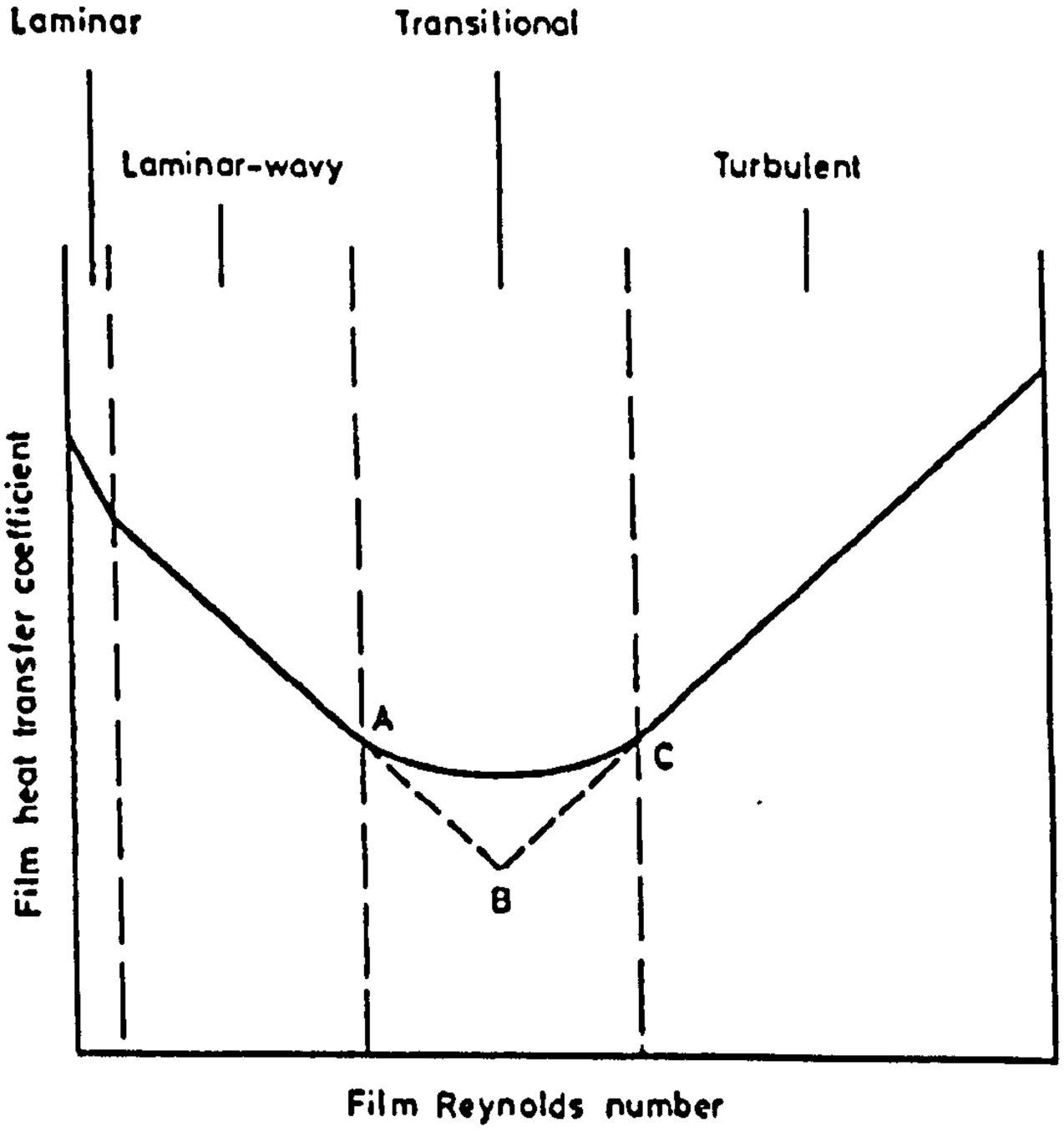

Figure 2.3: Typical variation of condensate heat transfer coefficient with film Reynolds number (on log-log scales) (Butterworth, 1975)

Figure 2.3 also shows the transition to fully turbulent flow. In the turbulent regime, the resistance of the film to heat transfer decreases even though the film thickness increases. This is due to the presence of turbulent eddies that cause mixing to dominate over conduction.

2.3.3 Prediction of film heat transfer coefficients

In the laminar region, it is widely accepted that the analysis of Nusselt (1916) is accurate. As reported by Clements and Colver (1973), most other studies of laminar film condensation have tended to agree with Nusselt's findings. Examples of these works are Minkowycz & Sparrow (1966), and Poots & Miles (1967) who investigated the effect of variable fluid properties whereas Bromley (1952) and Koh (1961) considered sub cooling and temperature distributions in the film respectively.

By defining a dimensionless film heat transfer coefficient α_f^* as

$$\alpha_f^* = \frac{\alpha_f}{\lambda_l}\left[\frac{\eta_l^{\,2}}{\rho_l(\rho_l-\rho_g)g}\right]^{1/3} \tag{2.1}$$

Nusselt's analysis, which is applicable at film Reynolds numbers up to 30, can be written in terms of the Reynolds number,

$$\alpha_f^* = 1.1\, Re_f^{-1/3} \tag{2.2}$$

where α_f^* is the local heat transfer coefficient for a vertical plain surface. In the laminar-wavy region, the correlation of Kutadeladze (1963) is used. This is a correction to Nusselt's analysis allowing for the formation of waves on the condensate surface, and is applicable up until the film becomes turbulent.

$$\alpha_f^* = 0.756\, Re_f^{-0.22} \tag{2.3}$$

Different workers such as Carpenter & Colburn (1951), Chunangad (1992), and Palen et al. (1993) have suggested different Reynolds numbers for the onset of turbulent flow. McNaught and Walker (1987) sought to rectify this by defining 3 transitional points.

A The Reynolds number at which the film heat transfer coefficient departs from typical laminar-wavy behaviour (Re_A).

B The intersection of the Kutateladze (1963) correlation for laminar-wavy flow and the Chun & Seban (1971) correlation for fully turbulent flow (Re_B).

C The Reynolds number (Re_C) at which fully turbulent behaviour begins; characterised by the point at which the Chun and Seban (1971) correlation gives the same dimensionless heat transfer coefficient as at transition point A.

They argued that the locations of these transition points were not fixed Reynolds number values but were variable dependent on the fluid properties. Although this finding was backed by Butterworth (1975) and adopted as the HTFS recommendation, it was contradicted by Blangetti and Schlunder (1978). They reported that while condensing steam in the downflow arrangement no transition region was found. The McNaught and Walker (1987) analysis allows for this in the calculation of the transition points. In some cases, the calculated values of Re_A, Re_B and Re_C indicate that there is no transition region.

A number of correlations exist for heat transfer in turbulent films. McNaught and Walker (1987) argued that the correlation of Chun and Seban (1971), equation (2.4), that they used in their estimation of the transition regions was the most suitable to vertical condensers.

$$\alpha_f^* = 0.0038\, Re_f^{0.4}\, Pr_l^{0.65} \qquad (2.4)$$

This was preferred over the work of Dukler (1960) and Labuntsov (1957), equation (2.5)

$$\alpha_f^* = 0.023\, Re_f^{0.25}\, Pr_l^{0.5} \qquad (2.5)$$

These correlations were all developed for co-current, or downflow, condenser arrangements, but should be applicable to reflux condensers if the assumption of negligible vapour shear is accurate.

Unfortunately there have been few studies of film heat transfer in reflux condensers. Among the literature available, the work of Clements & Colver (1973) stands out. They studied the effects of pressure and composition gradients on the reflux condensation of light hydrocarbons and found no significant effect. This is important as it means that pure component data, where the only resistance is that of the film, can be used to estimate the film coefficient in mixture condensation where vapour resistances become significant.

Chunangad (1992) performed a detailed review of reflux condenser design and formulated a strategy for determining the local film heat transfer coefficient based on whether or not vapour shear effects were significant. Gravitational and frictional stresses were evaluated and vapour shear considered negligible if the frictional value was less than half of the gravitational value.

For gravity controlled condensation, or insignificant shear, the methods of Nusselt (1916), equation (2.2), and Kutadeladze (1963), equation (2.3), were used for film Reynolds numbers of up to 30 and between 30 and 1,600 respectively. For Reynolds numbers greater then 1600, Chunangad suggested either the Colburn (1934) correlation, displayed in graphical form in Figure 2.4, or the Labuntsov (1957) correlation. Except for the use of the Colburn (1934) chart, this is the same method as proposed by ESDU (1989).

For significant vapour shear, Chunangad proposed the use of the correlation devised by Soliman et al (1968). This is a general correlation for annular flow condensation and is displayed in equation (2.6). The gravity controlled and shear controlled values were then compared. If there was a large difference, the arithmetic mean was used, otherwise, the higher of the two values was selected.

$$\alpha_f = 0.036\,\mathrm{Pr}_l^{0.65}\,\frac{\lambda_l\,\rho_l^{0.5}\,\tau_w^{0.5}}{\eta_l} \qquad (2.6)$$

Two recent studies of reflux condensation in a vertical tube reported contradictory results with reference to the film coefficient. Bartleman (2001) found that although the film coefficient was predicted better by the HTFS method than the Nusselt correlation, there was still a consistent under-prediction (Figure 2.5).

Bartleman argued that the higher coefficients measured than predicted by Nusselt's theory confirmed the presence of waves on the surface. The under-prediction by the HTFS method came from the fact that it was developed for vapour and liquid in co-current flow. He suggested that the counter-current nature of the vapour in reflux condensation may cause increased waviness in the film perhaps even leading to turbulence at lower than expected Reynolds numbers.

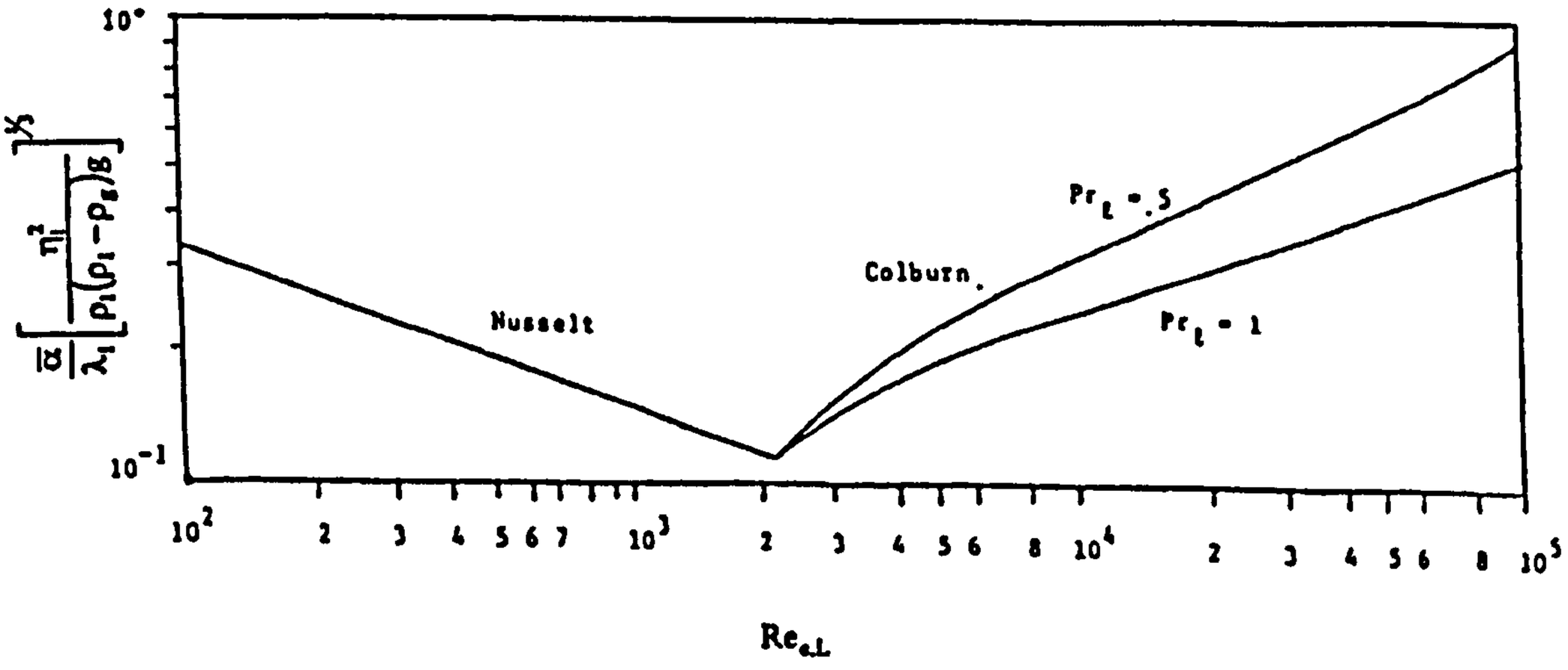

Figure 2.4: Colburn (1934) correlation for condensation on a vertical surface with no vapour shear

To enable a more accurate prediction of the coefficients in a particular reflux condensation research facility, Bartleman suggested a correction to the HTFS method, equation (2.6), which would increase the coefficient.

$$Nu_{f,Ba} = 1.0415\, Nu_{f,HTFS} + 1.362*10^{-4}\, Re_f \qquad (2.7)$$

Al-Shammari (2001) compared his data for the condensation of steam with the ESDU method, as displayed in Figure 2.6. At the film Reynolds numbers reported, the HTFS and ESDU methods are the same allowing for comparison with the work of Bartleman (2001). Al-Shammari (2001) found that although there was relatively high scatter in his results, the ESDU/HTFS method actually over predicted most of his data. It was suggested that this could be attributed to vapour shear due to turbulent vapour flow, which would thicken the film and reduce the coefficients.

It is clear from these findings that although reflux condenser film heat transfer coefficients are reasonably well predicted by the classical co-current correlations there is still an uncertainty as to the effect of the counter-current vapour flow. If accurate design methods are to be proposed, then this issue should be resolved.

2.4 Heat Transfer in the Vapour

In a reflux condenser, it is expected that the vapour fed to the tubes will be in fully developed turbulent flow. In this regime, single phase heat transfer will be by forced convection, with condensation having an effect on the heat transfer characteristics. The general approach is to calculate the rate of heat transfer expected for the vapour flowing alone and apply a two phase correction as discussed in 2.6 later.

Single phase heat transfer is a well studied topic with many correlations available to estimate the heat transfer coefficient. Among these are the classic Colburn (1933) and Dittus & Boelter (1930) equations. The Dittus-Boelter solution was validated experimentally over the range $0.7 \leq Pr \leq 120$, $2500 \leq Re \leq 12400$.

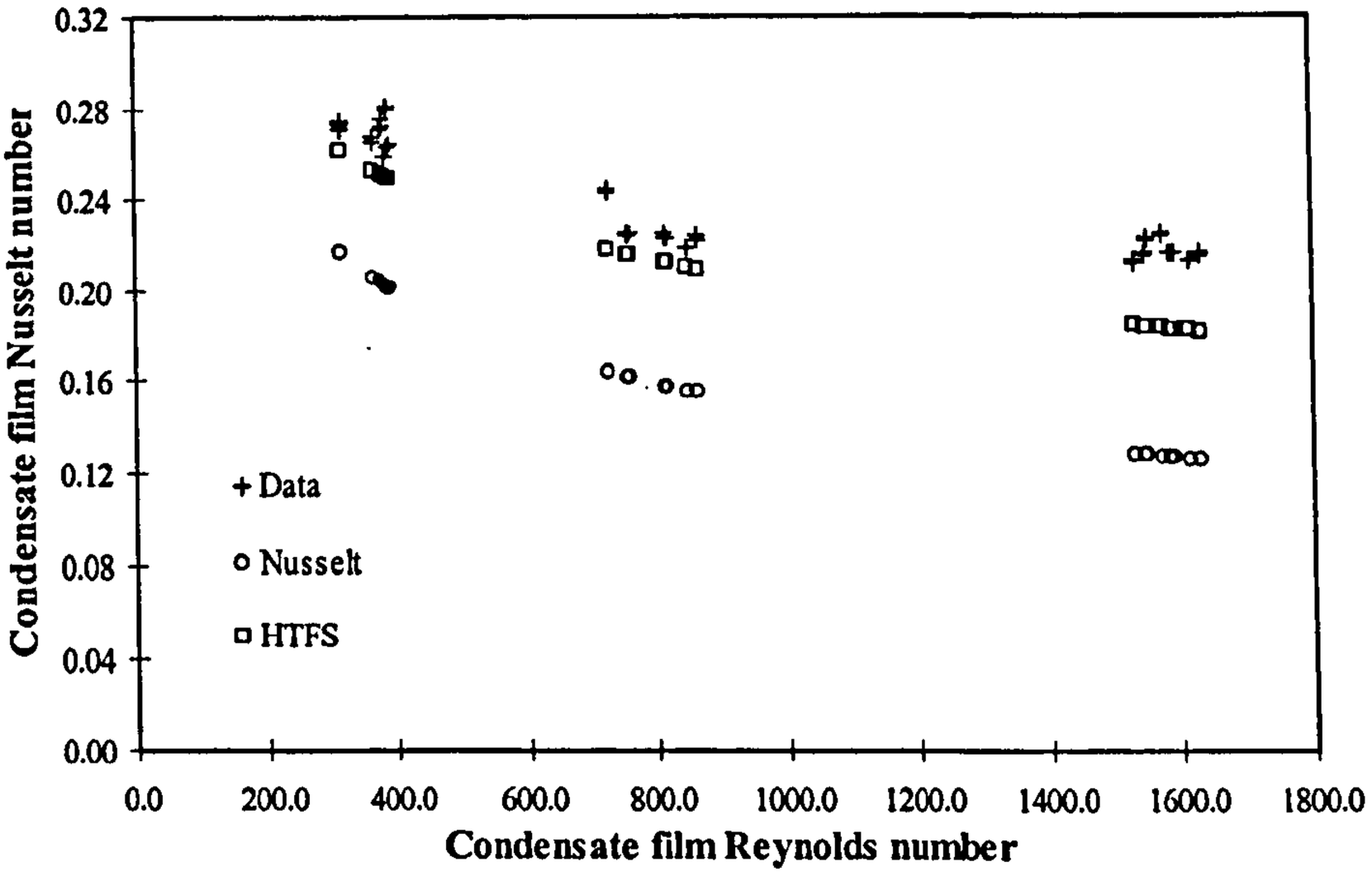

Figure 2.5: Comparison of Bartleman (2001) data with Nusselt (1916) and HTFS method

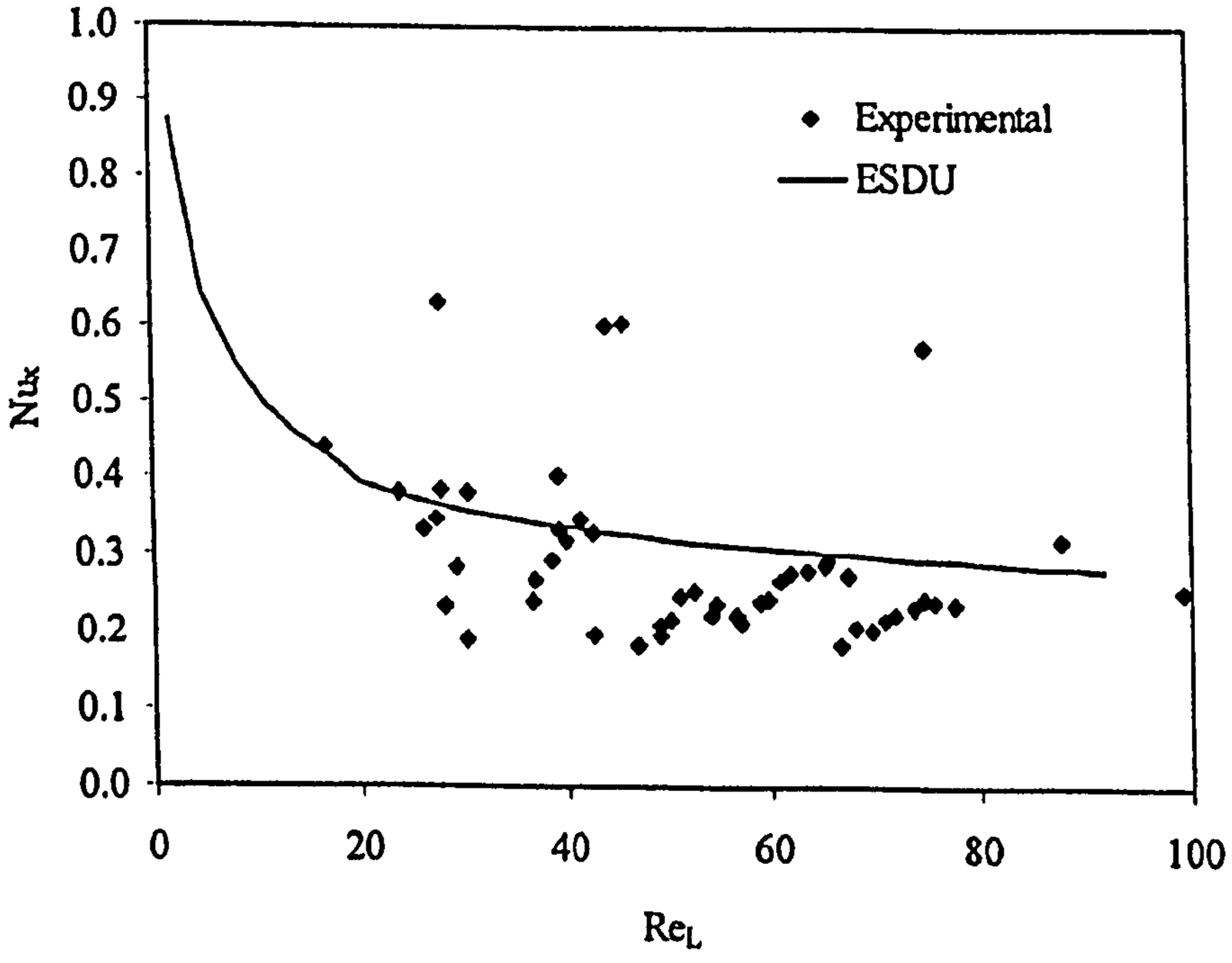

Figure 2.6: Comparison of Al-Shammari (2001) data with ESDU (1989) method

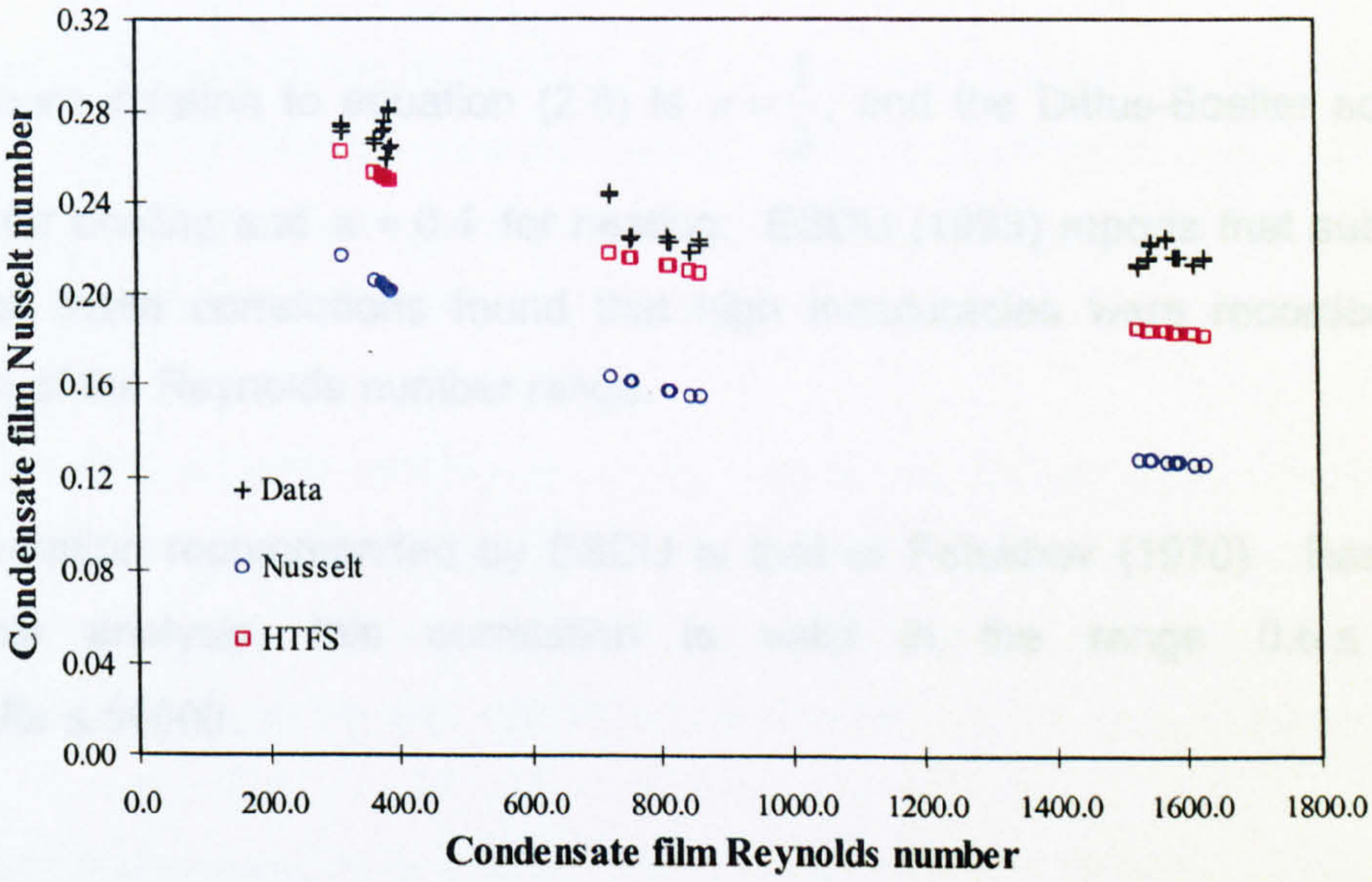

Figure 2.5: Comparison of Bartleman (2001) data with Nusselt (1916) and HTFS method

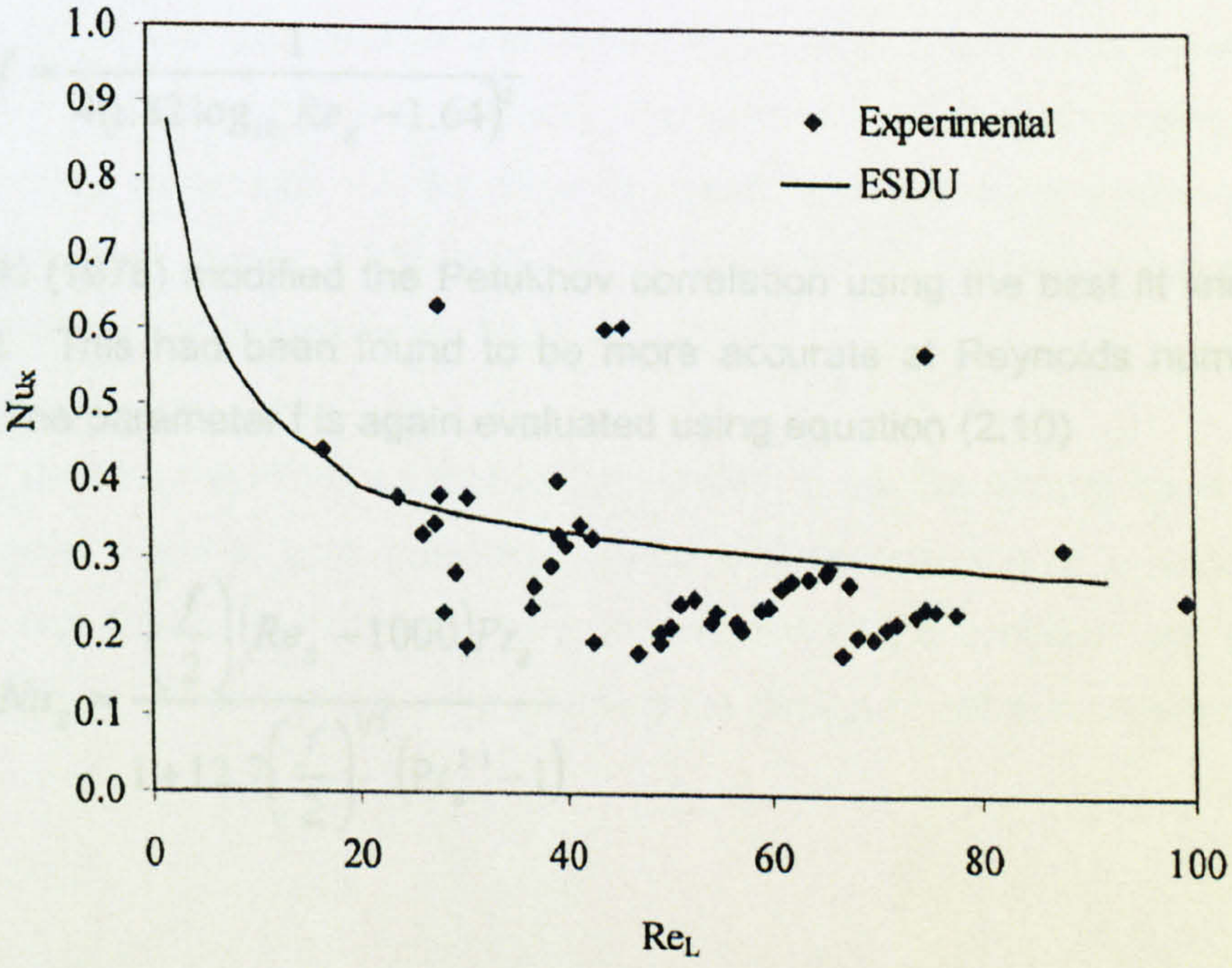

Figure 2.6: Comparison of Al-Shammari (2001) data with ESDU (1989) method

$$Nu_g = 0.023\, Re_g^{0.8}\, Pr_g^n \tag{2.8}$$

The Colburn solution to equation (2.8) is $n = \frac{1}{3}$, and the Dittus-Boelter solution is $n = 0.3$ for cooling and $n = 0.4$ for heating. ESDU (1993) reports that subsequent testing of these correlations found that high inaccuracies were recorded at the extremes of the Reynolds number range.

The correlation recommended by ESDU is that of Petukhov (1970). Based on a theoretical analysis, this correlation is valid in the range $0.6 \le Pr \le 60$, $4000 \le Re \le 50000$.

$$Nu_g = \frac{\left(\frac{f}{2}\right) Re_g\, Pr_g}{1.07 + \left(12.7\left(\frac{f}{2}\right)^{1/2}\left(\mathrm{Pr}_g^{2/3} - 1\right)\right)} \tag{2.9}$$

where

$$f = \frac{1}{4\left(1.82 \log_{10} Re_g - 1.64\right)^2} \tag{2.10}$$

Gnielinski (1976) modified the Petukhov correlation using the best fit line to a large data set. This had been found to be more accurate at Reynolds numbers above 10000. The parameter f is again evaluated using equation (2.10)

$$Nu_g = \frac{\left(\frac{f}{2}\right)\left(Re_g - 1000\right) Pr_g}{1 + 12.7\left(\frac{f}{2}\right)^{1/2}\left(\mathrm{Pr}_g^{2/3} - 1\right)} \tag{2.11}$$

2.5 Flooding

The major drawback in the application of a reflux condenser is the phenomenon of flooding. Flooding occurs when the vapour velocity reaches a critical limit which causes condensate drainage from the tubes to be impaired or even stopped altogether, and as such represents the operational limit of a reflux condenser.

It is desirable to operate condensers at high vapour velocities to promote good heat transfer in the vapour. Flooding thus leads to a trade off as the condenser must be operated at a low enough velocity so that the condensate can drain freely but this lowers the vapour heat transfer coefficients and leads to large area requirements.

The result of this trade off is that for optimum performance of a reflux condenser, it should be operated close to but never reaching the flooding point. The definition of the flooding point itself is thus crucial to the design of the condenser as is the selection of a suitable correlation to predict the vapour velocity at the flooding point.

Flooding is a problem affecting many two phase countercurrent flow operations including falling film evaporators and wetted wall columns, and as a result there have been many studies of the phenomenon. Between the numerous studies, there have been varying definitions of the flooding point, various tube entrance and exit geometries, and various fluids used. All of these factors combined have resulted in large differences in the predicted flooding velocities.

It should be noted at this point that as the flooding is not the central focus of this work the intention is not to give a detailed review and comparison of a large number of flooding correlations but rather to give an overview of the problem with the intention of discussing the important factors affecting the design of reflux condensers.

2.5.1 Flooding Mechanism

It is apparent from the available literature on flooding in two phase counter-current flow that there is still no clear understanding of the detailed mechanism leading to flooding. A number of theories have been put forward describing this process, but as yet no agreement has been reached.

Classically, there were two widely accepted theories; bridging of waves and droplet entrainment. More recently a Bernoulli or lift effect, as droplets exit the tube, has been cited.

In reflux condensation, vapour and condensate flows are both at their maximum at the tube inlet meaning that this area will always flood first. This is an important point as it is the major difference between flooding with condensation and flooding in a adiabatic system where flooding may start further up the tube, for example at the liquid injection point.

2.5.1.1 Wave Formation

This mechanism was described by Deakin et al (1978). These workers condensed steam in a custom built glass single tube reflux condenser with measurements and visual observations both recorded. The flooding point was approached by increasing the vapour flow rate in a step wise manner. Deakin found that as vapour velocity increased, so did disturbances in the condensate film in the form of waves (see Figure 2.7, ii). At some point, these waves bridged the tube and a churn flow was observed local to the bottom of the tube (iii).

Upon further increasing the vapour flow, hence velocity, the region of churn flow increased in size until the entire tube was filled and slugs were ejected from the top of the tube (v). At this point the condensate flow had become greatly reduced, and further increasing of the velocity caused the condensate to stop draining altogether with co-current annular upward flow observed (vi).

This view is backed by Imura et al. (1977) and McQuillan et al. (1985) who said that flooding occurred as a result of the formation and motion of a large disturbance wave on the surface of the liquid film. McQuillan and his co. workers used photographs of a perspex tube to show that waves that formed on the surface of the liquid grew in size but decelerated as they travelled downwards. Eventually the waves became stationary at the base of the tube before moving upwards to cause flooding. They also noted that some droplets were entrained after breaking off from the wave but this was seen as a minor occurrence.

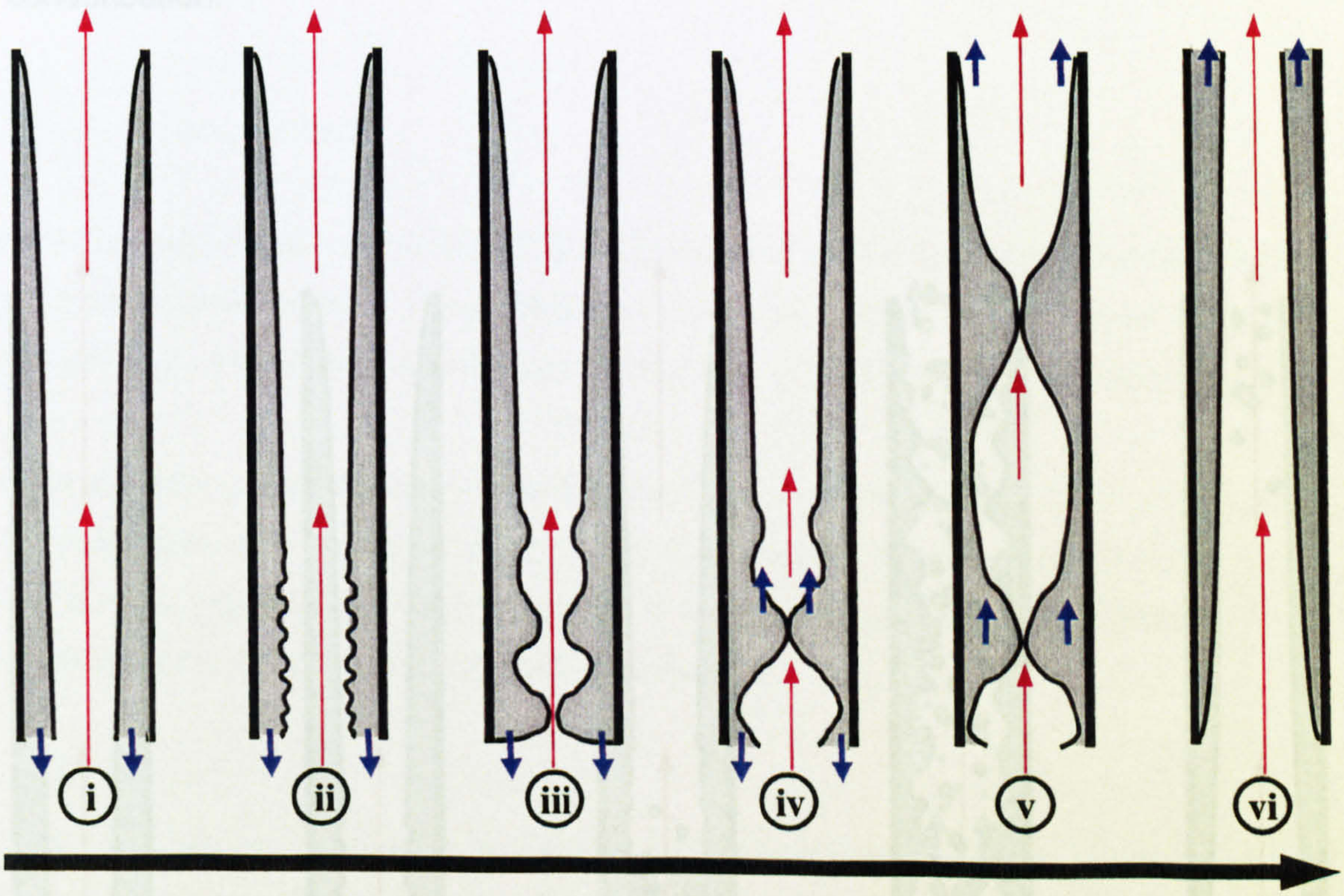

Figure 2.7: Wave formation as mechanism of flooding

2.5.1.2 *Droplet entrainment*

In this mechanism, flooding occurs when larger droplets are torn off the surface of the film and carried upwards (see Figure 2.8 iii and iv). Experimental work by Dukler and Smith (1979) and Zabaras and Dukler (1988) under adiabatic conditions indicated that increasing gas velocity caused the formation of large waves at the liquid inlet. At a critical gas velocity, droplets were torn off this wave and flooded the tube. No upward wave movements were reported.

This description highlights the differences associated with adiabatic and reflux condensation flooding experiments. In the work above, flooding initiated at the liquid injection point some way up the tube, a phenomenon that would not occur in reflux condensation.

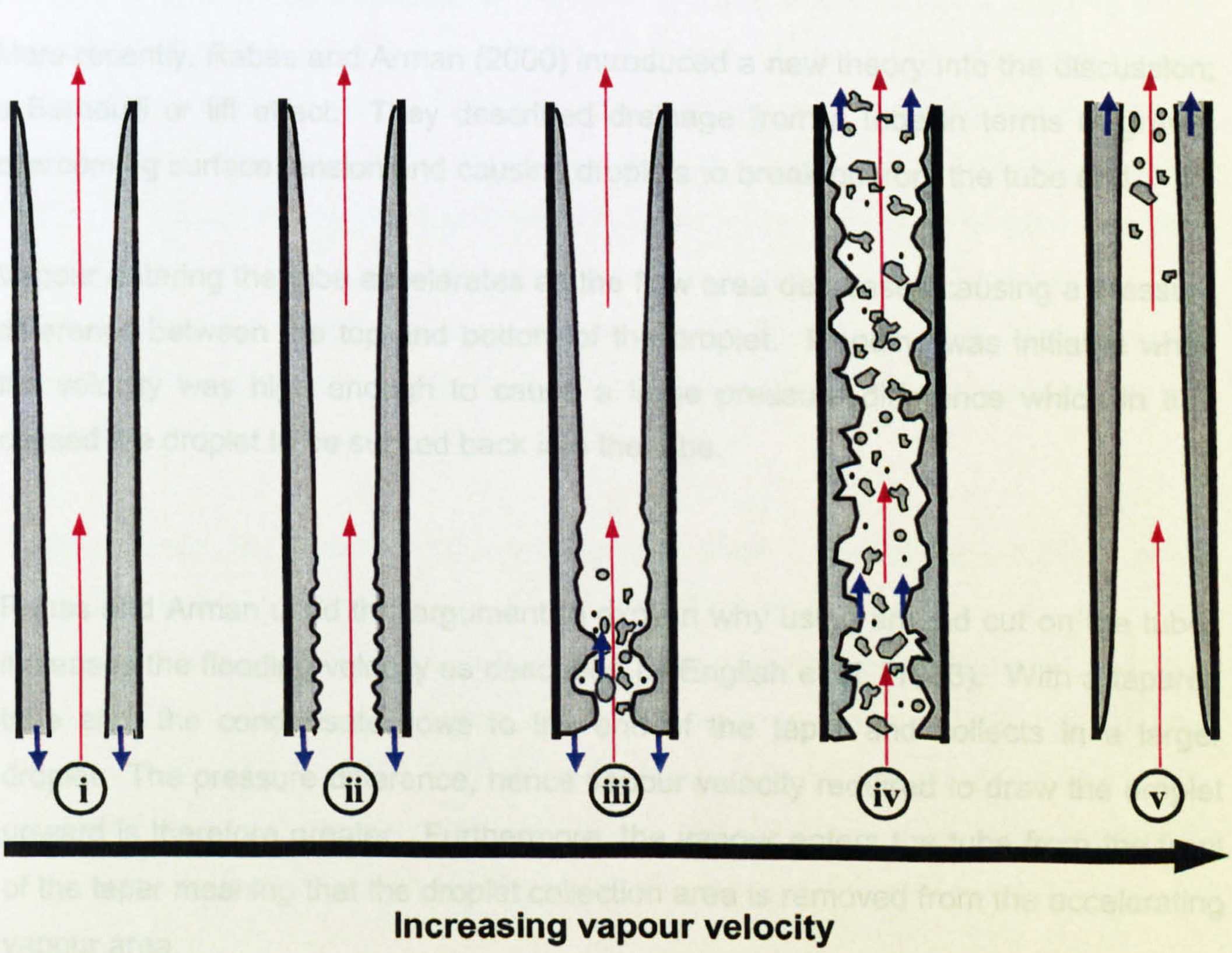

Figure 2.8: Droplet entrainemt as the flooding mechanism

Both of the mechanisms discussed above were described by Jayanti et al. (1996), who proposed that either of the two mechanisms were possible depending on the diameter of the tube.

For bridging and upward transport of waves to prevail, they stated that the gas/vapour force on the waves would have to be large. This would occur in small diameter tubes where ring type waves formed round the circumference causing a relatively large reduction in gas flow area in turn causing a large increase in drag.

This would not occur in larger tubes where it would be more difficult for a ring type wave to form and the area reduction would be relatively less than in a smaller tube. However, in larger tubes, large amplitude waves would have droplets torn off resulting in flooding when these droplets became entrained.

2.5.1.3 Bernoulli effect

More recently, Rabas and Arman (2000) introduced a new theory into the discussion; a Bernoulli or lift effect. They described drainage from a tube in terms of gravity overcoming surface tension and causing droplets to break off from the tube end.

Vapour entering the tube accelerates as the flow area decreases causing a pressure difference between the top and bottom of the droplet. Flooding was initiated when the velocity was high enough to cause a large pressure difference which in turn caused the droplet to be sucked back into the tube.

Rabas and Arman used this argument to explain why using an end cut on the tubes increases the flooding velocity as described by English et al. (1963). With a tapered tube end, the condensate flows to the end of the taper and collects in a larger droplet. The pressure difference, hence vapour velocity required to draw the droplet upward is therefore greater. Furthermore, the vapour enters the tube from the front of the taper meaning that the droplet collection area is removed from the accelerating vapour area.

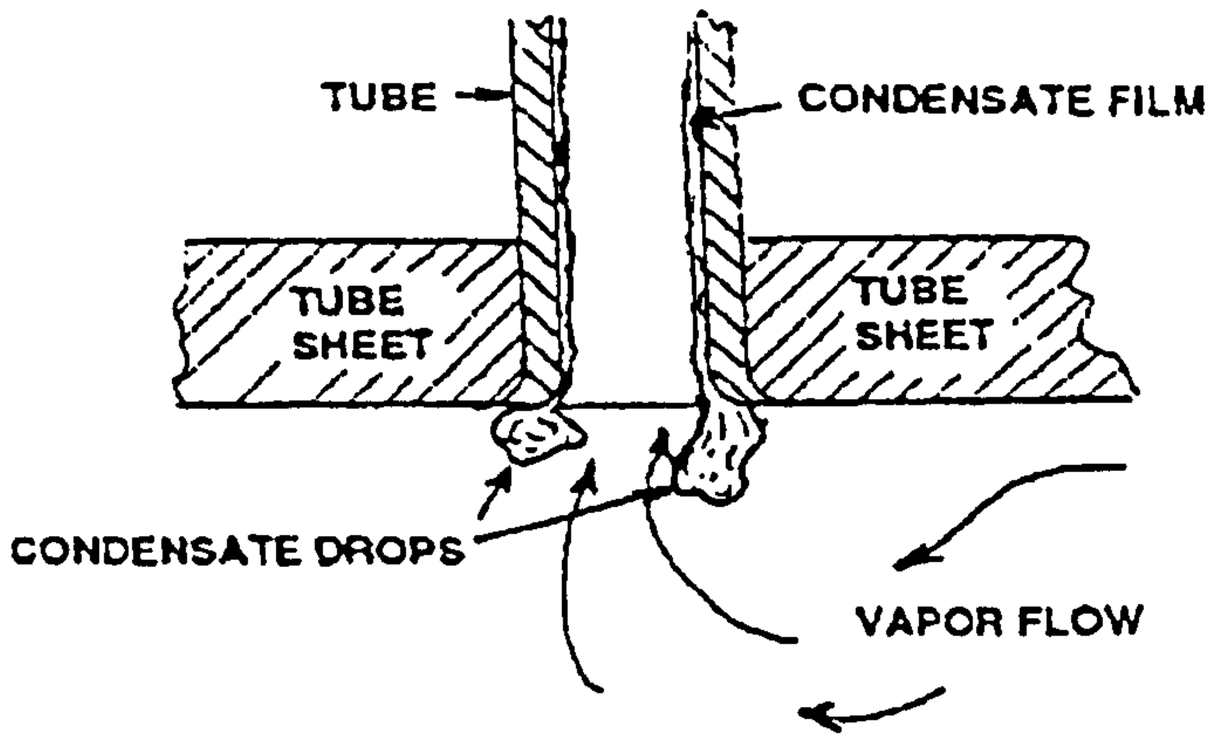

Figure 2.9: Bernoulli effect as the flooding mechanism (from Rabas & Arman (2000))

2.5.2 Definition of the flooding point

In the design of reflux condensers, the most important issue around flooding is the prediction of the flooding point and the operation of the condenser at a vapour velocity lower than this point. Generally, the flooding point is defined as the vapour velocity that causes the tube to flood. However, due to the lack of agreement in the flooding mechanism, the point at which the tube can be said to be flooded has been very arbitrary and has been expressed by different workers in different ways. The problem with this is that different correlations for the flooding velocity are based on a number of flooding point definitions and the accuracies of the correlations are dependent on the definition used.

In most cases, the flooding point definition has been based on observations of the liquid film behaviour backed up by pressure drop measurements. Based on the theory of wave formation, McQuillan & Whalley (1985) and Vijayan et al (2001) defined flooding as occurring when waves first begin to move vertically up the tube. Deakin et al (1978) found that wave bridging caused the condensate to drain intermittently in a churn flow, but noted that at this point the reflux operation was still observed and there was no liquid carryover.

They defined the flooding point as the velocity that first caused liquid to be ejected out of the top of the condenser. Other definitions based on this theory include disruption of the liquid film (Hewitt & Wallis 1963) and loss of stability (Imura, et al 1977). Where the droplet entrainment theory was preferred, Rabas & Arman (2000) stated that "some liquid begins to be entrained" at the flooding point whereas Diehl & Koppany (1969) based their definition on a sharp increase in entrainment rate.

Definitions which refer to the liquid injection point, such as Jeong & No (1996) and Zapke & Kroger (1996) are applicable only to adiabatic systems and again serve to highlight the differences between these systems and reflux condensation.

Where there is general agreement in this area is in the shape of the curve of pressure drop through the tube against vapour mass flux at the inlet. Proposed by Deakin (1977), this curve describes the transition from smooth downward liquid drainage through to concurrent upward annular flow

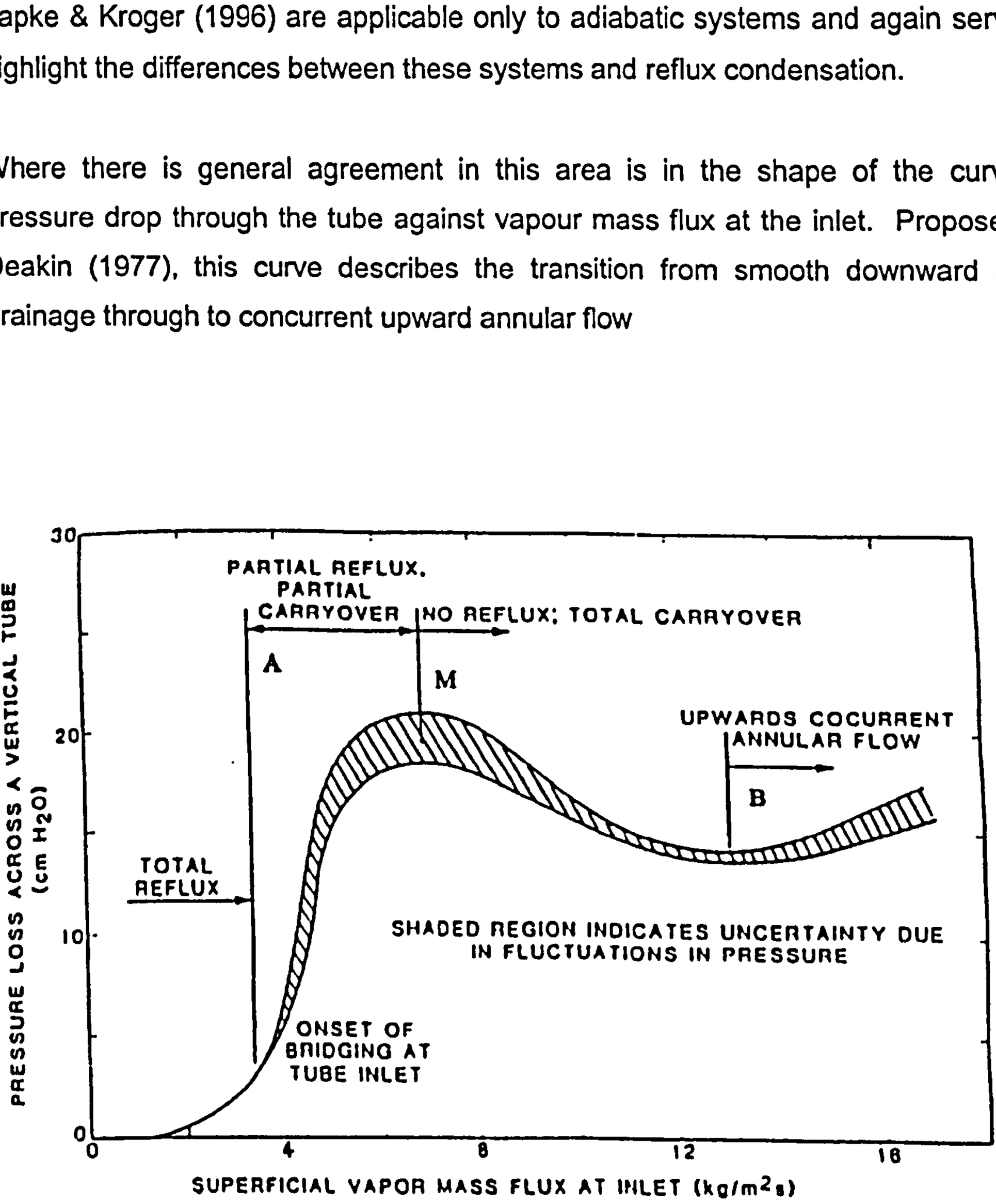

Figure 2.10: Pressure drop and vapour mass flux during flooding (Deakin, 1977)

Important points to note are the dramatic rise in pressure drop around the point where bridging of waves was said to occur, the fact that there is a maximum at the transition point between partial and total carryover, and a minimum at the transition to fully annular upward flow.

As stated, there is agreement between many workers in the shape of the curve, but disagreement is noted in the fixing of the flooding point on this curve. The definitions described earlier refer to various points between the onset of wave bridging and total carryover which on the curve fall anywhere between the point where pressure drop begins to rise sharply up to the maximum turning point. For example, English, et al (1963) based their flooding point on the second break point of a similar curve (Figure 2.11), representing the maximum in Figure 2.10.

Based on the preceding discussion, when using a particular flooding correlation, it is important to bear in mind the definition of the flooding point used by the author. In future work, it would be best if a consistent flooding point was defined and universally accepted as this would allow more accurate comparisons between new correlations.

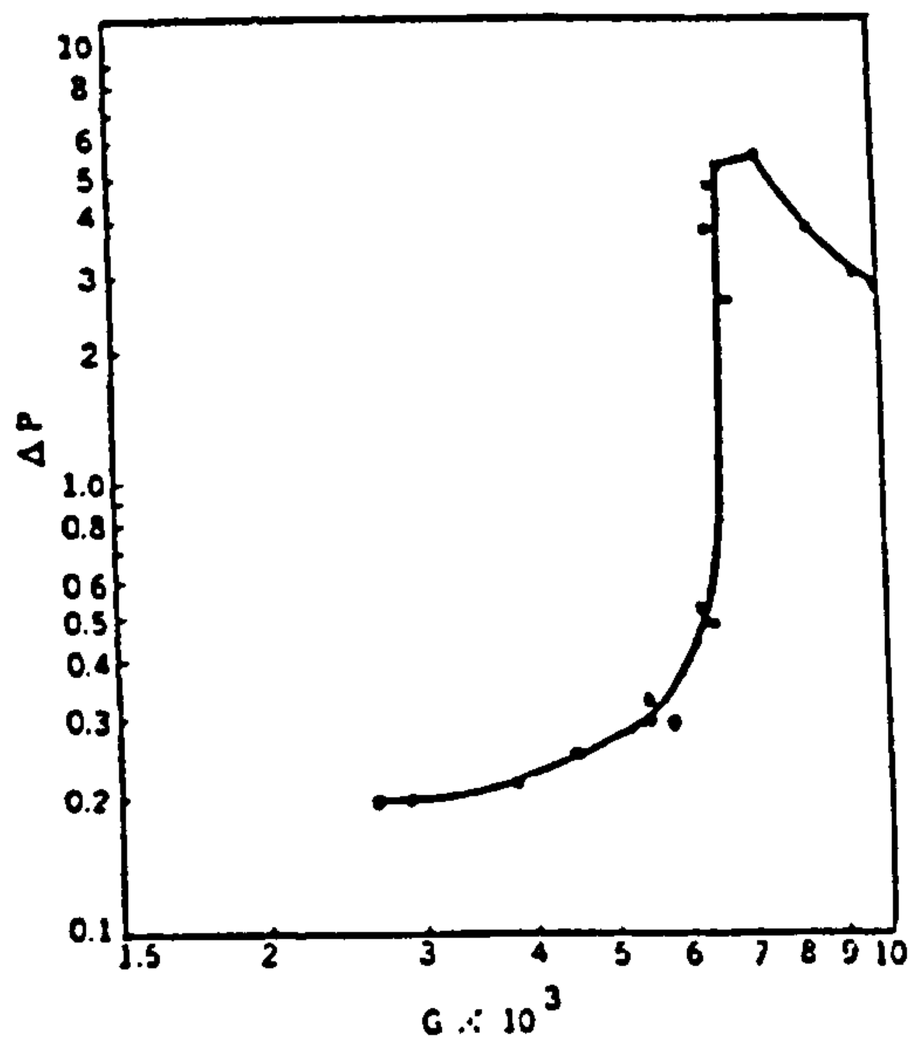

Figure 2.11: Pressure drop v's gas mass flow rate as reported by English et al (1963)

2.5.3 *Flooding point correlations*

There are many correlations available for the prediction of flooding velocity in both reflux condensation and adiabatic systems, based on many different geometries and fluids. Authors who have conducted a review of a number of different correlations include Deakin (1977), Imura et al (1977), and McQuillan & Whalley (1985). All of these reviews found considerable differences between correlations.

Imura and his co-workers indicated that the choice of correlation was dependent on the tube geometry, selected from Figure 2.12, a suggestion backed by Deakin (1977). Bearing in mind that the most suitable correlation in terms of geometry may have been developed for adiabatic and not reflux flow, Deakin also said that the velocity yielded by the this correlation should be compared with one specifically developed for reflux condensation and the lowest value taken.

The most comprehensive study was that of McQuillan & Whalley (1985). They combined the data from a large number of other workers into a single databank and tested 22 correlations against it (17 empirical and 5 theoretical). They also modified the correlation of Alekseev at al (1972) into a more workable format and found that it was the most successful in predicting the flooding point over the wide range of data.

In his thesis on the sizing of reflux condensers, Chunangad (1992) devised a strategy for the design of a reflux condenser such that flooding would be avoided. His idea was to use a number of correlations to predict the flooding point and select the most conservative value as outlined below

Chunangad (1992) method for flooding point prediction in a reflux condenser.

1. Compare design geometry with Figure 2.12. Select most appropriate correlation and calculate flooding velocity.

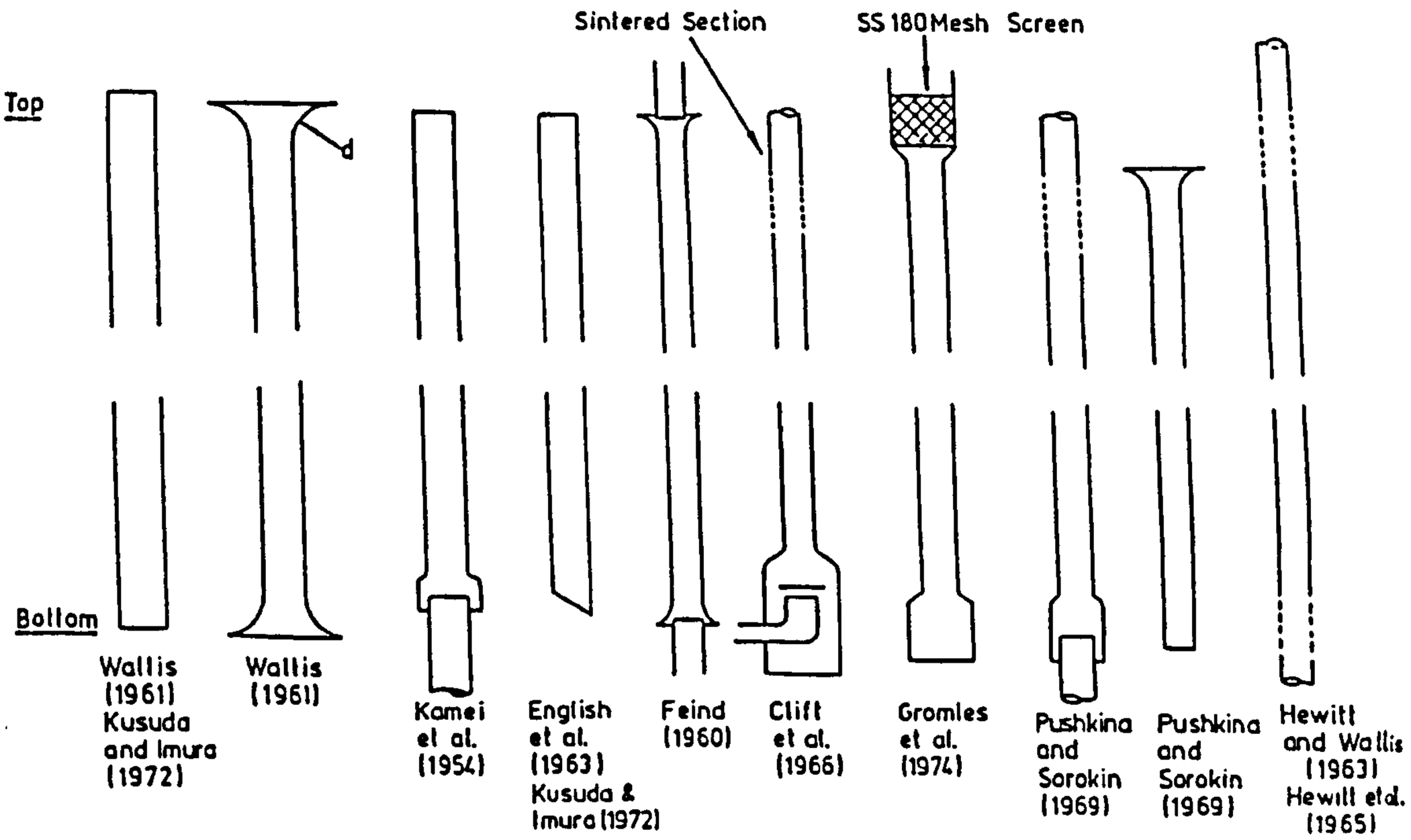

Figure 2.12: Flooding studies/correlations and geometries (Imura et al. (1977))

2. Calculate flooding velocity using Alekseev (1972) correlation as modified by McQuillan & Whalley (1985)

$$u_{g,flood} = \frac{K_g\left(g\sigma\left(\rho_l - \rho_G\right)\right)^{0.25}}{\rho_g^{0.5}} \tag{2.12}$$

where K_g is the Kutateladze number

$$K_g = 0.286\, Bo^{0.26}\, Fr^{-0.22}\, F \tag{2.13}$$

and the Bond number, Bo, Froude number, Fr, and liquid viscosity correction, F, are

$$Bo = \frac{D^2 g\left(\rho_l - \rho_g\right)}{\sigma} \tag{2.14}$$

$$Fr = \frac{u_l D}{4}\left[\frac{g(\rho_l - \rho_g)^3}{\sigma^3}\right]^{\frac{1}{4}} \tag{2.15}$$

$$F = \left(1 + \frac{\eta_l}{10^{-3}}\right)^{-0.18} \tag{2.16}$$

3. Calculate flooding velocity using English, et al (1963) correlation

$$u_{g,flood} = 1550 \frac{D^{0.3}\rho_l^{0.46}\sigma^{0.09}}{\rho_g^{0.5}\eta_l^{0.14}(\cos\theta)^{0.32}\left[\frac{\dot{M}_l}{\dot{M}_G}\right]^{0.07}} \tag{2.17}$$

where θ is the angle of taper on the tube end, measured from the horizontal. Note that in this equation, imperial units must be used.

4. Calculate flooding velocity using Diehl & Koppany (1969). Again, note that imperial units must be used.

$$u_{gf} = F_1 F_2 \left(\frac{\sigma}{\rho_g}\right)^{0.5} \tag{2.18}$$

where

$$F_1 = \left[\frac{D_i}{(\sigma/80)}\right]^{0.4}, \text{ for } \frac{D_i}{(\sigma/80)} < 1 \tag{2.19}$$

$$F_1 = 1, \text{ for } \frac{D_i}{(\sigma/80)} \geq 1 \tag{2.20}$$

$$F_2 = \left[\frac{\dot{M}_l}{\dot{M}_v}\right]^{-0.25} \tag{2.21}$$

5. Select lowest value as design flooding velocity

Although the author is of the opinion that this is a sensible approach to the flooding problem, it does highlight the large uncertainties in the prediction of the flooding point. The modified Alekseev correlation (Step 2) was found to be the most accurate over a wide range of experimental flooding data (McQuillan & Whalley, 1985) and as such is the correlation recommended by HTFS. The equation proposed by English et al (1963) (Step 3) includes a factor based on the degree of end cut, and the Diehl & Koppany (1969) solution (Step 4) is a function of the tube diameter.

Add to that the fact that a totally different correlation may be the most suitable for the required geometry (Step 1) and there may well be 4 completely different velocities predicted. Merely selecting the lowest prediction as the flooding point and designing to operate below that value may result in designs that are overly safe.

Each of the flooding velocity correlations described above were developed for a single tube. In a practical environment however there will always be a tube bank in a reflux condenser, with associated issues of flow maldistribution. ESDU (1989) discusses this phenomenon and, bearing in mind that flow rates may be different in different tubes, recommends that a factor of 0.7 be applied to the predicted velocity to ensure conservative design. Potentially this will make conservative designs even more safe resulting in exchangers with larger than necessary diameters. It is therefore vital that the whole flooding issue in reflux condensers is addressed and some consensus reached.

2.6 Equilibrium Based Design Method

The most commonly used design procedure for the condensation of vapour mixtures is the equilibrium method. This is an approximate general method that takes its name from the assumption of equilibrium between the vapour and the condensate allowing the use of equilibrium condensation curves. The equilibrium method was first proposed by Silver (1947), then reinvented by Bell and Ghaly (1972). A similar method was devised by Ward (1960).

The simplicity of the equilibrium method comes from the fact that complex mass transfer calculations are omitted. A proportional relationship between mass transfer resistance and heat transfer resistance was assumed to exist, and the mass transfer resistance compensated for by over estimating the heat transfer resistance.

The total resistance to heat transfer in a condenser is the sum of the resistances of the vapour, condensate film, coolant, tube wall and fouling. The film, wall, coolant and fouling resistances can be grouped together to give an effective condensing side heat transfer coefficient, denoted by α_c.

The design equation for required area in a condenser is

$$A = \int_0^{Q_T} \frac{1}{U(T_v - T_c)} dQ \qquad (2.22)$$

where the local overall heat transfer coefficient, U, is related to total local heat flux by

$$\dot{q}_T = U(T_v - T_c) \qquad (2.23)$$

A further assumption of the equilibrium method is that all of the heat (sensible and latent) is transferred from the vapour/liquid interface (denoted by i) through the entire thickness of the condensate film giving

$$\dot{q}_T = \alpha_{fc}(T_i - T_c) \tag{2.24}$$

Further, the vapour sensible heat flux is related to the gas-side heat transfer coefficient by

$$\dot{q}_g = \alpha_v(T_v - T_i) \tag{2.25}$$

Combining equations (2.23), (2.24) and (2.25) to remove the unknown interfacial temperature gives

$$\frac{1}{U} = \frac{1}{\alpha_{fc}} + \frac{\dot{q}_v}{\dot{q}_T \alpha_v} \tag{2.26}$$

The ratio of sensible heat flux to total heat flux (or sensible to total heat duty) is denoted by Z to give

$$\frac{1}{U} = \frac{1}{\alpha_{fc}} + \frac{Z}{\alpha_v} \tag{2.27}$$

This is the Ward (1960) formulation of the equilibrium method. Silver (1947), and Bell and Ghaly (1972) considered condensate cooling and included this in the analysis of sensible heat transfer. This would be expected in a co-current condenser where the condensate and vapour are both cooled as they travel through the condenser together.

One of the advantages of a reflux condenser is that the counter-current geometry causes hot vapour travelling upwards to interact with cooling condensate travelling downwards. The result is that the condensate is reheated (leading to further evaporation and the rectification effect), and the condensate leaves at close to the inlet temperature of the vapour. This suggests that the Ward formulation is more suitable to the design of reflux condensers, an observation that is also made in ESDU (1989).

Substituting equation (2.27) into the design equation (2.22) gives

$$A = \int_0^{Q_T} \frac{1 + \frac{Z\alpha_{fc}}{\alpha_v}}{\alpha_c (T_v - T_c)} dQ \qquad (2.28)$$

In the case where $Z = 0$, there is no sensible heat exchanged from the vapour, and equation (2.28) reduces to the form for a pure component condensing isothermally.

By splitting the condenser up into a number of increments, the design equation can be evaluated numerically. The increments are chosen such that the condensing curve can be approximated linearly hence Z can be evaluated from equation (2.29) over each increment.

$$Z = \dot{M}_v Cp_v \frac{\Delta T_{inc}}{\Delta Q_{inc}} \qquad (2.29)$$

The area of the increments are calculated independently and summed to give the total area required to meet the specified duty. The method is subject to selection of an appropriate condensation curve as is discussed below.

McNaught and Emerson (1977) developed the method further to include a correction factor for the effect of mass transfer on the sensible heat transfer in the vapour. By performing an Ackerman analysis, they incorporated "equivalent laminar film theory" into the heat and mass transfer calculations.

$$\dot{q}_g = \alpha_v \left(\frac{\phi_H}{e^{\phi_H} - 1} \right) (T_v - T_i) = \alpha_v \theta_H \tag{2.30}$$

where

$$\phi_H = \sum_{j=1}^{n} \left(\dot{M}_j C p_j \right) / \alpha_v \tag{2.31}$$

This should not be confused with the correction of Ackerman (1937) and Colburn & Drew (1937) for the effect of mass transfer on the heat flux at the condensate surface. In that situation the correction factor derived was $\frac{\phi_H}{1 - e^{-\phi_H}}$.

In Figure 2.1, the temperature profile through the gas film was represented as a curve. In the case of sensible cooling with no mass transfer this profile would be linear as shown below in Figure 2.13. Mass transfer effects serve to modify the temperature profile and increase the resistance to heat transfer with higher mass transfer rates having a larger effect. The correlations presented earlier estimate heat transfer coefficient for a dry gas so including the correction (2.30) makes the coefficient a better representation of the true process of the condensation of a binary mixture.

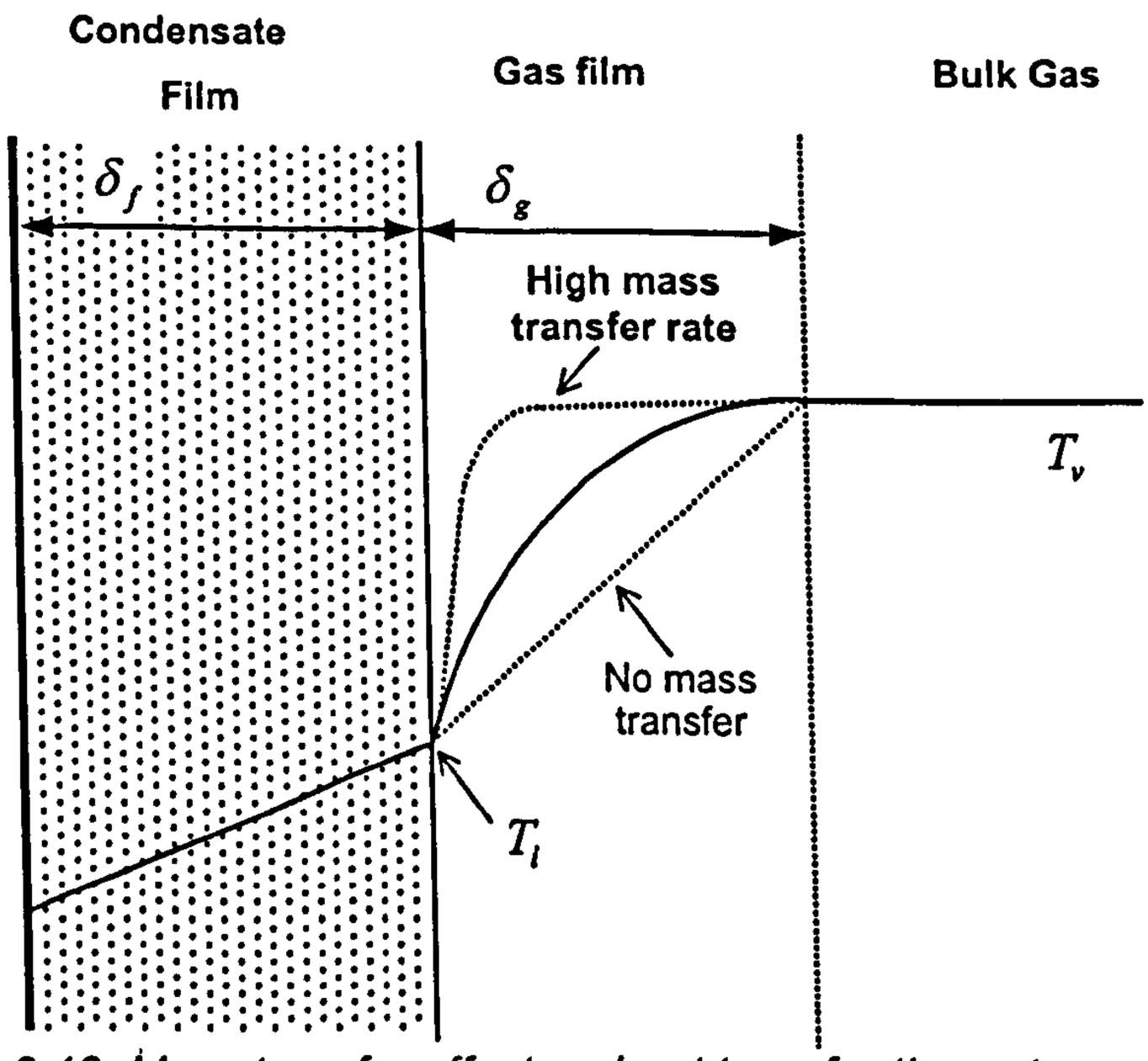

Figure 2.13: Mass transfer effect on heat transfer through gas film

2.6.1 *Condensation curves*

The main simplifying step in the equilibrium method is the use of a pre-determined cooling or condensation curve in the estimation of the parameter Z. It follows that the accuracy of the method depends on how well the condensation curve represents the true process. In general there are two types of condensation curve, the integral and differential curves as shown in Figure 2.12, but recently a second form of the differential curve has been proposed.

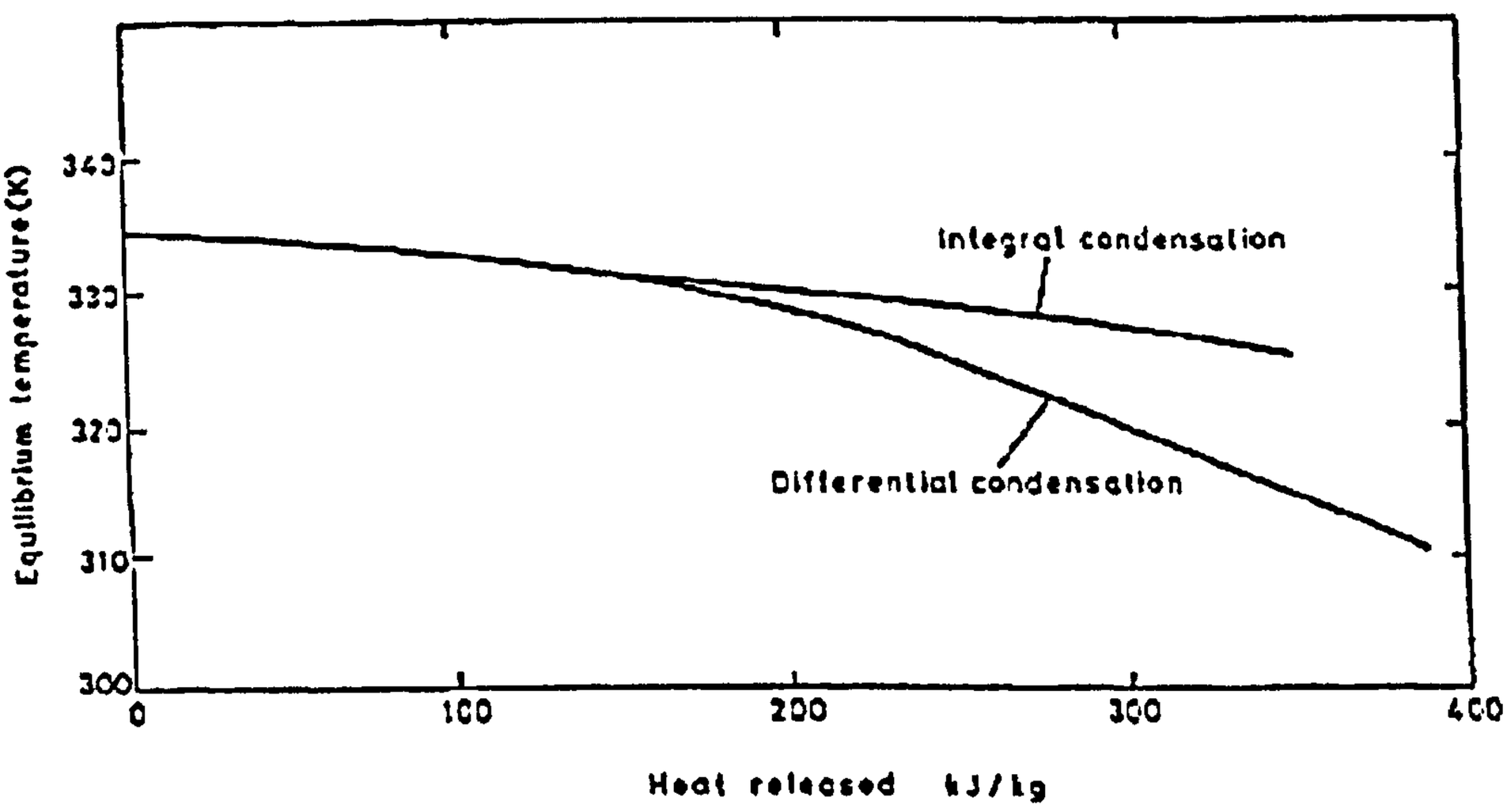

Figure 2.14: Example of a condensation (heat release) curve

(from McNaught, 1984)

2.6.1.1 *Integral condensation curve*

The integral curve is used to represent a process where the vapour and liquid remain in intimate contact such that the bulk liquid is in equilibrium with the bulk vapour. An example of this is in a co-current vertical condenser.

Consider a temperature/composition (T-xy) diagram for a binary mixture at a known pressure, Figure 2.15. The saturation curves divide the diagram into three distinct regions. Above the dew curve the mixture exists as a superheated vapour and below the bubble curve it exists as a subcooled liquid with the two-phase region in the middle.

The integral condensation of a saturated vapour into a saturated liquid is represented by a vertical line from the dew curve to the bubble curve. At any temperature between the dew and bubble points, a horizontal tie line can be drawn to give the compositions of the vapour and condensate. The mole fraction of the mixture existing as vapour, θ, is defined as the fraction of the tie line between the bubble curve and the vertical line (the ratio of DC to DE).

Using the T-xy diagram, the vapour and liquid enthalpies can be calculated at a number of temperatures and used to describe the heat released as the vapour cools through a condenser thus allowing the condensation curve to be drawn.

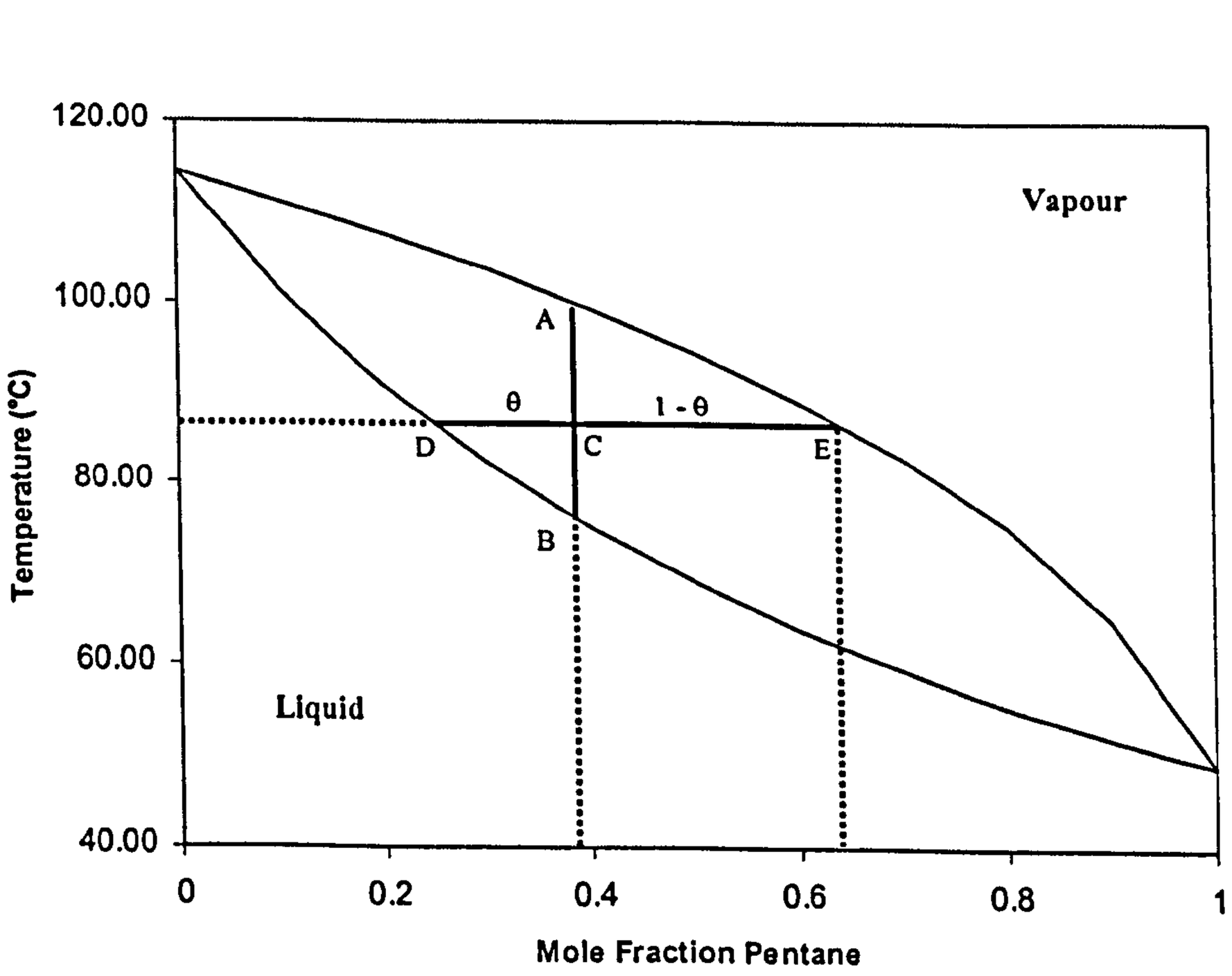

Figure 2.15: T-xy diagram for integral condensation of pentane and iso-octane

2.6.1.2 Differential condensation curve

The original differential curve represents a process where the vapour and liquid are separated from each other such as in a horizontal shell and tube condenser where the vapour condenses in the shell and condensate falls into a liquid pool. In this situation, the bulk vapour is in equilibrium only with the newly forming condensate and not the bulk liquid.

Due to the removal of previously formed condensate, the lighter component is removed from the vapour at a faster rate than in integral condensation. This causes the equilibrium temperature to drop at a faster rate resulting in the larger gradient in the differential heat release curve.

Jibb et al. (1999) liken this differential process to the situation expected in a reflux condenser where there is no mixing in the liquid film. As new condensate forms, it lies on top of the previously formed condensate thus there is no contact between the vapour and the old condensate. This is also the view taken by ESDU (1989) where the recommendation is given that the differential curve should be used in the design of reflux condensers.

The construction of the T-xy diagram shown in Figure 2.16 for the differential unmixed curve is a step wise process where a number of stages are selected and a fraction of the vapour condensed in each stage. The condensate formed in each stage is effectively removed and plays no further part in the equilibrium calculations. A mass balance is required to calculate the vapour fraction, θ, in each stage from

$$\theta = \frac{\dot{M}_v}{\dot{M}_v + \dot{M}_l} \tag{2.32}$$

where $\dot{M}_v$ represents the vapour flow rate leaving the stage and $\dot{M}_l$ is the liquid condensate formed in the stage.

In the first stage, a vertical line is drawn down from the dew curve. An iterative solution is then used to find the temperature that gives the correct value of θ when a horizontal tie line is drawn. Following this tie line to the dew curve gives the composition of vapour leaving this stage and entering the next stage. This process is followed for the number of stages specified.

Developing the T-xy diagram this way allows the vapour and condensate compositions leaving each stage to be estimated and the condensation curve to be drawn.

2.6.1.3 Differential (mixed) condensation

The situation in a reflux condenser where there is perfect mixing in the liquid film would result in equilibrium between the local vapour and all of the local condensate. To describe the equilibrium in a countercurrent flow situation similar to this process, Jibb et al. (1999) introduced a third curve, differential (mixed).

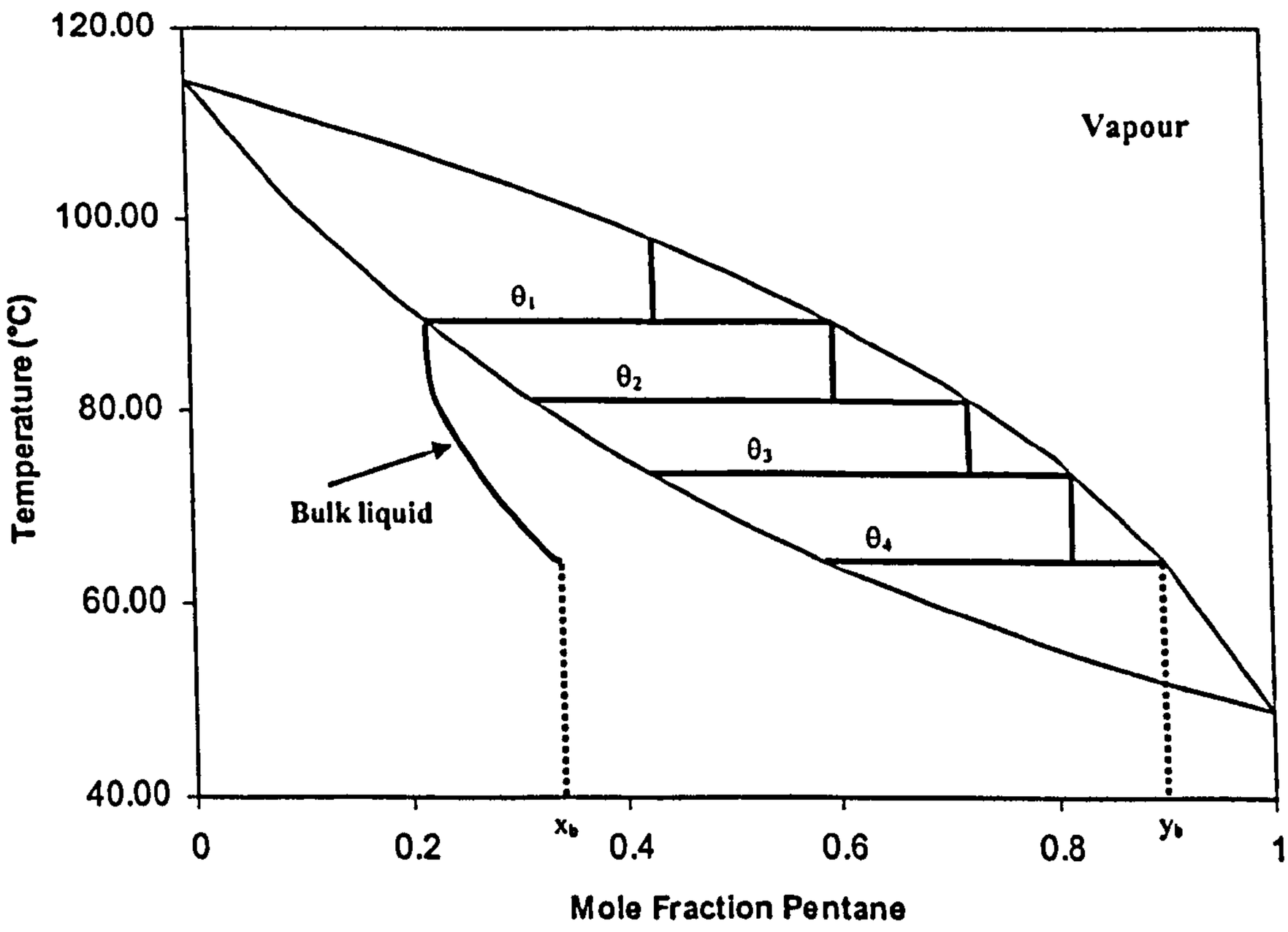

Figure 2.16: T-xy diagram for partial differential condensation (4 stages) of a pentane and iso-octane mixture

It is different from the integral curve as a number of separate equilibria are considered instead of one overall equilibrium, and it is different from the original differential (unmixed) curve as the unmixed curve does not consider previously formed condensate. As in the unmixed case, a number of stages are selected and a mass balance solved over each stage.

The construction of this curve is similar to the unmixed curve except that previously formed condensate is considered in the mass balance. This means that overall and component balances are required and as the composition of the condensate leaving the first stage is unknown the solution is iterative.

For the equilibrium method to be suitable as a design tool for reflux condensers, a condensing curve must be selected that accurately represents the true process behaviour. The following discussion is aimed at determining which if any of the curves are theoretically suitable, and whether or not the findings are confirmed experimentally.

2.6.2 Theoretical Assessment of Condensation curves in reflux condenser design

The integral curve assumes equilibrium along the whole length of the condenser. The counter-current geometry of reflux condensation means that such an equilibrium is physically unrealistic therefore it can said with confidence that the integral curve is unsuitable.

The main assumption in the differential (unmixed) curve is that there is no mixing in the condensate film. In most cases, the limitations imposed by flooding cause reflux condensation to take place at low liquid Reynolds numbers, in the laminar or laminar-wavy region. Although there will be little turbulent mixing in these regimes, there will still be a concentration gradient over the thickness of the film, thus promoting mixing by mass diffusion.

A recent study of mixing in liquid films was conducted by Al-Shammari (2001). This was a theoretical analysis of mixing on a vertical plate. They reported that even at low Reynolds numbers ($Re_l \leq 64$) the film was fully mixed within 10cm of the top of the plate. The problem was simplified by considering the film to be a pure solvent brought into contact with a solute gas. The solute spread across the film, and total mixing was defined as occurring when the mean concentration in the film was 99% of the saturation value.

In reflux condensation of a binary mixture the problem is much more complex. The film will initially be richer in the more volatile component as this will concentrate in the rising vapour. As the film falls, more condensate forms. This newly forming condensate will be more concentrated in the least volatile component thus establishing the concentration gradient across the film. Further, it is expected that as the film falls and comes into contact with hotter vapour, some of the most volatile component will re-evaporate. As have been described, there are therefore a number of mass transfer processes occurring simultaneously creating a complex problem.

Although Al-Shammari (2001) simplified the problem, the analysis presented still showed that cross film mixing due to mass transfer was a relatively quick process and concluded that the film can be classed as well mixed.

Applying this result to reflux condensation, a well mixed film is expected, even in the laminar region of flow. This would suggest that the unmixed version of the differential curve is inappropriate for the design of reflux condensers.

One of the main reasons for designing reflux condensers is to take advantage of the rectification effect observed when the most volatile component is preferentially re-evaporated. The assumption of the differential unmixed curve that no liquid mixing takes place means that the condensate from the top of the tube (which is richer in the lighter component) is ignored, thus the rectification effect is ignored. Again, it would seem that this choice of curve is not reasonable.

The mixed differential curve would seem to be the curve best suited to reflux condenser design but there are still some assumptions made in the construction of the curve that are not totally realistic. Firstly, the assumption of perfect mixing is non-conservative. At the top of the tube the film is relatively unmixed, and further down the tube mixing will not be infinitely fast.

2.6.3 Experimental evaluation of the equilibrium method

Two recent studies, Bartleman (2001) and Al-Shammari et al. (2002) have used experimental data to attempt to evaluate the accuracy of the equilibrium method. Al-Shammari et al. (2002) compared experimental data collected by themselves to three equilibrium models based on each of the curves described above. Working with a number of binary mixtures of methanol and water condensing in a single tube, data was collected over varied process conditions resulting in methanol feed compositions of 0.26 to 0.43 and vapour exit compositions of 0.67 to 0.81.

All of the data showed significantly better separations than would be expected in a single equilibrium stage with heat removal i.e. integral condensation. The differential mixed curve, which allows for the rectification effect, over-predicted all of the separations. These differential mixed predictions are the maximum possible separations that could theoretically have been achieved.

The unmixed differential curve however produced the best predictions, a result that the author indicated was surprising and disappointing as the expected rectification effect was not achieved. In the preceding discussion, the unmixed curve was deemed to be inappropriate, but these experimental results contradict that conclusion.

Similarly, Bartleman (2001) used a single tube to represent conditions in a reflux condenser. In this body of work, Bartleman condensed steam, pentane, iso-octane, and mixtures of pentane and iso-octane in a newly commissioned research facility.

Whereas Al-Shammari and his co-workers concentrated on the separation aspect of the equilibrium method, Bartleman concentrated on the prediction of the vapour heat transfer coefficients. As the coolant and condensate film coefficients are well predicted in condensers, it is accurate prediction of the controlling vapour resistances that will lead to good estimates of the surface area requirements. It is worth noting however that Bartleman reported experimental separations equal to less than one equilibrium stage. This is a disappointing result as not only was the rectification effect not observed, but the separations were less than would be expected in a co-current condenser.

Bartleman chose to compare his experimental values with predictions based on the integral curve. To achieve this, a standard design tool for co-current condensers was provided with the relevant inputs based on the experimental values. It was then run in checking mode to produce the exit vapour temperature and an estimate of the surface area required for the specified heat load. These results made it possible to evaluate equation (2.29) as if the integral curve had been calculated.

As composition measurements were only available at the inlet and outlet of the tube, the condenser was treated as one complete stage, an approach justified by the linear nature of the condensation curves obtained.

Bartleman found that the equilibrium method used in conjunction with the integral condensation curve under-predicted the effective vapour side heat transfer coefficient leading to an over estimation of the area requirement. The inclusion of the mass transfer correction term (McNaught & Emerson 1977) actually caused the data to be further underpredicted.

Bartleman's data gave a temperature enthalpy gradient smaller than that expected from integral condensation. As the differential curves have a larger gradient than the integral, it would seem that the use of a differential curve would not improve matters. Bartleman concluded that there were a number of objections to the use of condensation curves, and that the equilibrium method was inappropriate for the thermal design of reflux condensers.

This view was backed by Al-Shammari et al. (2002) who concluded that reflux condensers should not be designed using the equilibrium method, and that the film theory method was the correct approach to use. This conclusion will be discussed further in Chapter 8.

2.7 Film Theory Design Method

A more realistic approach to the design of a condenser is the application of film theory as proposed by Colburn & Hougen (1934) for the condensation of a single vapour from a gas. This was later expanded to a binary vapour with no gas by Colburn & Drew (1937) in their work on downflow condensers. In this approach local condensing fluxes are calculated by solving heat and mass transfer rate equations simultaneously at a number of points in the condenser. Temperature and concentration profiles are then determined by integration of the classic equations of downstream development.

Film theory models are more realistic than equilibrium based models, but their complexity has, in part, led to equilibrium models being favoured in industry. An example of the increased complexity is the requirement for extra physical properties such as diffusion rates.

2.7.1 Heat transfer

Referring back to Figure 2.1, an overall heat flux is defined from the vapour liquid interface to the coolant to include condensate, wall, coolant and fouling resistances.

$$\dot{q}_T = U\left(T_i - T_c\right) \tag{2.33}$$

This flux is made up of latent heat and sensible vapour cooling contributions. As described in section 2.4, heat transfer in the vapour is caused by convection due to mass transfer and conduction due to a temperature gradient between the bulk vapour and the cooler interface, and both of these mechanisms must be considered.

Using a correlation to obtain a heat transfer coefficient for single phase heat transfer, α_G, the vapour sensible cooling flux is written as equation (2.34). The correction term is as defined in equations (2.30) and (2.31) and represents the difference between single phase heat transfer and heat transfer with condensation.

$$\dot{q}_G = \alpha_v \frac{\phi_H}{e^{\phi_H} - 1}(T_v - T_i) = \alpha'_v(T_v - T_i) \tag{2.34}$$

The flux due to the release of latent heat depends on the condensing vapour flux

$$\dot{q}_L = \dot{n}_T \Delta\tilde{h}_v \tag{2.35}$$

Applying the principle of continuity of energy across the interface

$$\dot{q}_T = \dot{q}_G + \dot{q}_L \tag{2.36}$$

and substituting in equations (2.33), (2.34) and (2.35) gives

$$U(T_i - T_c) = \alpha'_v(T_v - T_i) + \dot{n}_T \Delta h_v \tag{2.37}$$

The use of mass transfer equations is then required to estimate the total and component condensing fluxes that solve this equation.

2.7.2 Mass transfer

The mass transfer flux across the interface is made up of a diffusive flux from the concentration difference and a convective flux from the removal of latent heat. If the diffusive flux is assumed to obey Fick's Law and the gas film thickness is denoted by s, the individual component fluxes can be written as

$$\dot{n}_j = -\tilde{c} D_{12} \frac{d\tilde{y}}{ds} + \tilde{y}_j \dot{n}_T \tag{2.38}$$

If the ratio of component to total flux is denoted by r_j, this can be rearranged to

$$\dot{n}_T\, ds = \frac{-\tilde{c} D_{12}}{\left(r_j - \tilde{y}_j\right)} dy \tag{2.39}$$

Integrating over the thickness of the film with boundary conditions $\tilde{y}_j = \tilde{y}_{jB}$ at $s = 0$, and $\tilde{y}_j = \tilde{y}_{jS}$ at $s = S$ results in the classical Colburn-Drew (1937) equation.

$$\dot{n}_T = \beta_{1,2} \ln\left[\frac{r_j - \tilde{y}_{jS}}{r_j - \tilde{y}_{jB}}\right] \tag{2.40}$$

where β_{12} is the mass transfer coefficient.

$$\beta_{1,2} = \frac{\tilde{c} D_{12}}{S} \tag{2.41}$$

By defining a rate factor, Φ_M, as the ratio of total condensing flux to mass transfer coefficient, the component condensing fluxes can be evaluated

$$\dot{n}_i = \beta_{1,2} \frac{\phi_M}{e^{\phi_M} - 1}\left(\tilde{y}_{jB} - \tilde{y}_{jS}\right) + \tilde{y}_{jB}\dot{n}_T = \beta^*_{1,2}\left(\tilde{y}_{jB} - \tilde{y}_{jS}\right) + \tilde{y}_{jB}\dot{n}_T \tag{2.42}$$

where

$$\phi_M = \frac{\dot{n}_T}{\beta_{1,2}} \tag{2.43}$$

2.7.3 *Downstream development*

Simultaneous solution of the heat and mass transfer equations defined earlier will yield the component condensing fluxes at a single point in the condenser. It is then necessary to integrate the equations of downstream development to determine temperature and concentration profiles over a small increment in the condenser, and either the corresponding surface area requirement or flow rate.

The calculations require knowledge of the vapour and coolant temperatures and flow rates at the condenser inlet. A full derivation of the following equations is given in Al-Shammari (2001).

Over the increment in question, the temperature change of the bulk vapour and coolant are given by the following equations

$$\frac{dT_G}{dA} = -\frac{\alpha_v^*(T_v - T_i)}{\dot{N}_G Cp_G} \tag{2.44}$$

$$\frac{dT_c}{dA} = -\frac{\alpha_c(T_i - T_c)}{\dot{M}_c Cp_c} \tag{2.45}$$

Vapour mole flux is related to the incremental area and change in vapour flow rate by equation (2.46). This equation can be applied in two ways. In a process design, flow rates through the condenser will be specified and this equation used to determine the area requirements. Conversely, in a rating calculation for an existing exchanger, this equation is used to calculate the change in flow rate over a specified area increment.

$$\frac{d\dot{N}_G}{dA} = -\dot{n}_T = -\sum_{j=1}^{N} \dot{n}_j \tag{2.46}$$

Finally, the composition change of the bulk gas is calculated from equation (2.47)

$$\frac{d\tilde{y}_{jB}}{dA} = -\frac{\dot{n}_j - \tilde{y}_{jB}\dot{n}_T}{\dot{N}_G} \tag{2.47}$$

2.7.4 *Liquid Mixing*

During the solution of the mass and heat transfer equations, it is necessary to evaluate the interfacial temperature between the gas film and the condensate film. This is achieved by assuming local equilibrium between the two phases and taking the condensate surface temperature to be the corresponding dew point temperature.

The role of liquid mixing is crucial as the condensate composition at the interface must be known. Liquid mixing will be driven by a combination of diffusive mass transfer due to concentration gradients and turbulent eddies due to the flow regime. There are two extremes to consider.

2.7.4.1 *Perfect mixing*

The condensate film is assumed to be in fully turbulent flow with an infinite mass transfer coefficient. The result is that cross mixing is assumed to be infinitely fast hence a uniform concentration profile exists. The interfacial composition is then equal to the bulk composition, calculated from condensation rates further up the tube.

$$\tilde{x}_{jS} = \tilde{x}_{jB} = \frac{\dot{N}_{j,f}}{\dot{N}_f} \tag{2.48}$$

2.7.4.2 *No Mixing*

The opposite case is where laminar flow and a negligible mass transfer coefficient are assumed resulting in no cross mixing. Newly forming condensate is said to "bury" existing condensate and the surface composition is determined from the local molar condensing rates.

$$\tilde{x}_{jS} = r_j = \frac{\dot{n}_j}{\dot{n}_T} \tag{2.49}$$

Al-Shammari (2001) concentrated his study on the importance of liquid mixing in reflux condensation. As discussed earlier, he used a detailed falling film model and found that mixing was a fast enough process that the film could be assumed to be well mixed less than 10cm from the top of the tube. This was confirmed by film theory based modelling of experimental data which showed that the data were predicted more closely by perfect mixing models with no mixing only in the first increment at the top of the tube. The modelling work conducted by Al-Shammari will be discussed in more detail in Chapter 7.

2.8 Summary

A literature review has been conducted on some of the main topics of concern in the thermal design of reflux condensers. Firstly, heat transfer in the condensate film and vapour were considered, with the focus on the application of co-current correlations to the countercurrent situation in a reflux condenser. It was shown that recent experimental studies have given conflicting results, but that using co-current correlations gave reasonably accurate predictions of the condensate heat transfer.

Much of the review concentrated on the flooding phenomenon as this is vitally important to the design of a reflux condenser. The review found that there were a number of different interpretations of the flooding point. These arose from the general disagreement in the mechanism dominating the approach to flooding and led in part to the varied results given by different flooding correlations.

It was reported that most studies of flooding were based on adiabatic situations where flow rates remained constant meaning that some of the flooding definitions were not applicable to the case of reflux condensation where flows are at a maximum at the bottom of the tube.

The application of two major co-current condenser design methods to reflux condensers was also reviewed. A summary of the derivations of the equilibrium (Silver) method, and film theory (Colburn-Drew) method were given, and the application of the equilibrium method discussed in detail. The equilibrium method relies on condensation curves accurately representing the physical system, and it was found that there were objections to the use of each of the three theoretical curves.

The equations presented for the film theory method were for the countercurrent flow of vapour and condensate in a reflux condenser, and a discussion on the application of the method will be covered fully in Chapter 7.

It is clear from the discussion presented that there are still many uncertainties associated with the process of reflux condensation. The understanding of the underlying heat and mass transfer mechanisms in the process need to be improved through experimental and theoretical analysis, and this used to further design methods. On the issue of flooding, there is a requirement for work focussed purely on reflux condensers so that flooding point predictions can be improved and reflux condensers designed and operated as close to the flooding point as possible.

3 Experimental Equipment and Methods

This chapter describes the equipment used to collect all experimental data reported in this thesis. The facility measurement and analysis system and the methods used to collect and analyse the results are discussed, detailing the strengths and weaknesses of the system.

The HTFS Reflux Condensation Facility is situated at the TUV National Engineering Laboratory (NEL) in East Kilbride. It was designed by Dr. C. Chu in 1994 and commissioned by Alan Bartleman, a PTP associate, in 1997. Bartleman (2001) gives a detailed description of the facility as used by him when evaluating design methods for reflux condensation.

In the period October 1999 to December 2000, the author conducted a programme of upgrades aimed at improving the overall performance of the facility. The measurement systems were almost completely overhauled, and some alterations were made to the facility. All calibration and operating procedures were improved incorporating some of the changes suggested by Bartleman (2001).

3.1 The Test Facility

The main features of the HTFS Reflux Condensation Facility, as described by Bartleman (2001), are a boiler, reflux condenser, dump condenser and sampling loop. These pieces of equipment comprise the test fluid circuit and are housed, except for the sampling loop, in a vapour containment cabinet (VCC). A coolant circuit provides mains water to the two condensers and rejects heat to the main NEL chilled water supply via a small shell and tube heat exchanger.

For safety purposes, the facility is located in a small outhouse which is isolated from the control area in the main building. A further safety precaution is the vapour containment cabinet. Effectively a sealed box, this prevents the possible build up of hydrocarbon vapours in the outhouse.

The VCC is vented by a fan which draws air out continually. The air outlet duct is situated at the bottom of the cabinet with the inlet duct at the top of the opposite wall. If any hydrocarbons are released, the heavy vapours will sink and be vented to atmosphere.

3.1.1 Test Fluid Circuit

3.1.1.1 Boiler

The total volume of the boiler was about 35 litres, 20 of which taken up by liquid test fluid. Heat was supplied from 6 cartridge heaters each with a capacity of 1 kW. These heaters were kept fully submerged in the liquid.

Vapour leaving the boiler entered the test condenser where a proportion was condensed and returned back to the boiler via a stub pipe protruding into the vapour space. Condensate flowing from the stub pipe was gathered in a collecting tray and redirected to the bottom of the boiler where it was introduced back into the bulk liquid. Two windows, perpendicular to each other, allowed visual observations to be made of the condensate as it drained. This feature was useful during studies of the flooding phenomenon when a CCTV camera was set up and the behaviour of the condensate studied from the control area. These main features are shown in Figure 3.1 below.

Vapour conditions in the boiler were measured by a pressure transducer and precision resistance thermometer (PRT). The location of these instruments is also shown in Figure 3.1.

3.1.1.2 Test condenser

The test (or reflux) condenser was made up of three identical test sections each of length 503 mm and internal diameter of 45mm. A diagram of a single test section can be seen in Figure 3.2. A small rectangular groove was cut into the outside of the tube to create a flow channel for the coolant. This allowed high velocity coolant to be used over a relatively large area resulting in a high coolant heat transfer coefficient while maintaining a significant measurable temperature rise.

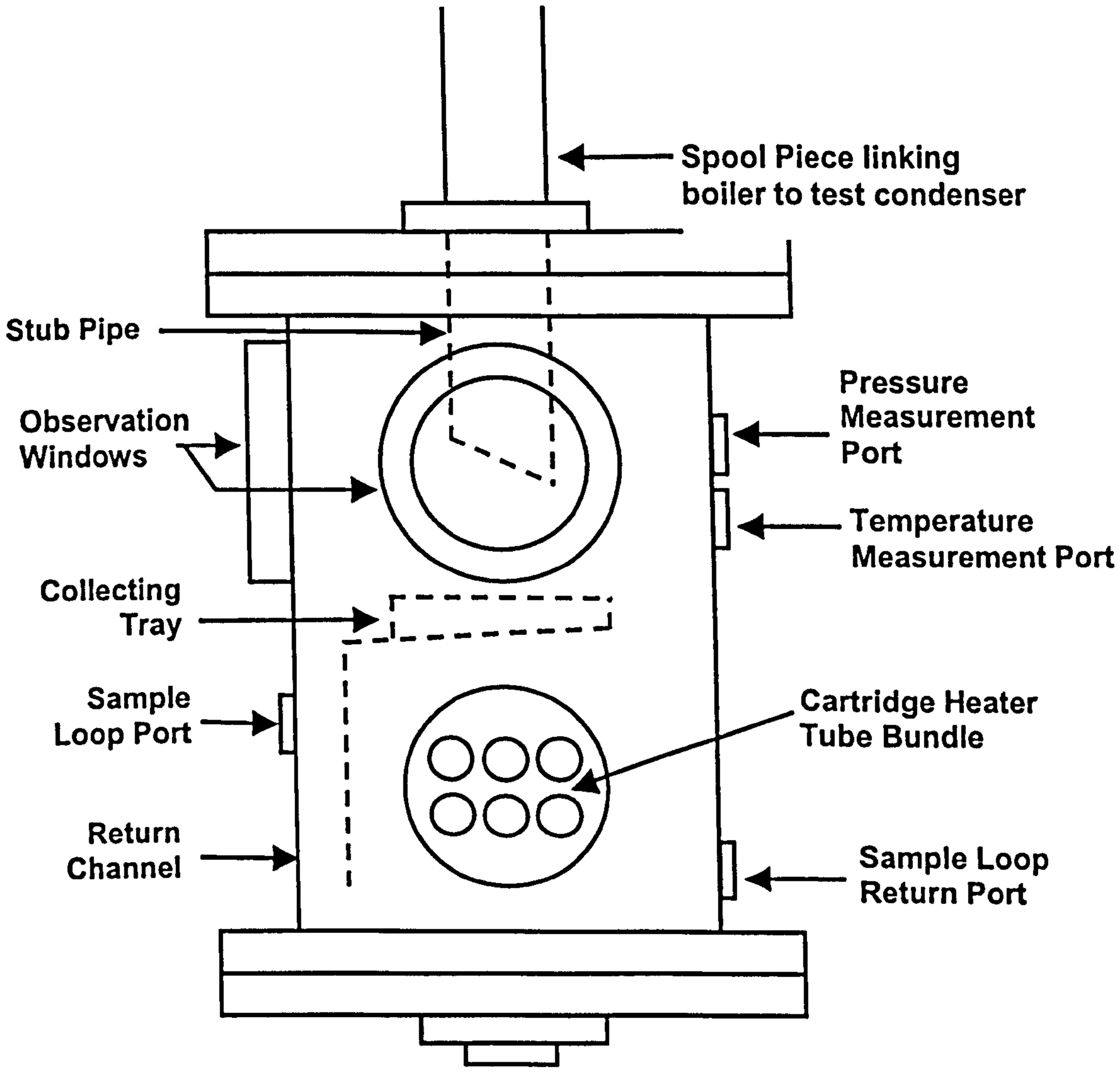

Figure 3.1: Boiler Main Features

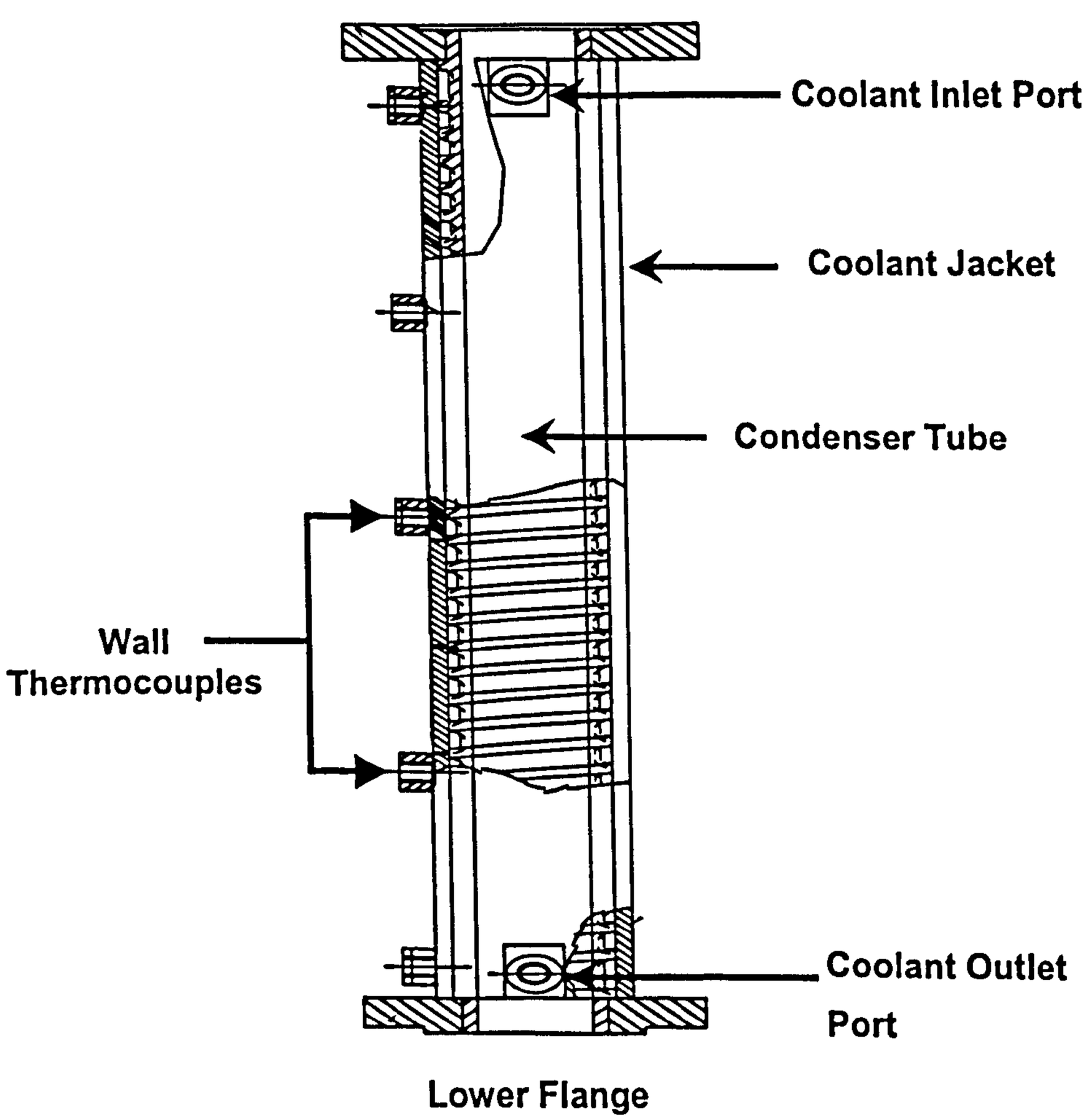

Figure 3.2: Reflux condenser test section

Coolant temperatures were measured at the inlet and outlet of the test condenser using PRTs and between the individual test sections with class 1 thermocouples. The vapour temperature at the outlet of each test section was measured using a class 1 thermocouple, and three class 2 thermocouples provided data on the wall temperature along the test section.

3.1.1.3 Dump condenser

The dump Condenser was 2m long with an internal diameter of 45mm. Any vapours passing through the reflux condenser were condensed in the dump condenser.

The coolant flowed in an annular jacket with PRTs measuring the temperatures at the inlet and outlet. The temperature of the condensate, usually sub-cooled, was measured by a class 2 thermocouple at the base of the condenser.

Condensate produced in the dump condenser was returned to the base of the boiler through the lower leg.

3.1.1.4 Sampling loop

The sampling loop was used to make on-line measurements of composition of the condensate from the reflux and dump condensers. Samples were withdrawn either from the condensate return channel in the boiler or the bottom of the dump condenser and passed through small bore pipes to the control area. A water bath cooled the samples to a known temperature before a vibrating u-tube densitometer measured the density of the sample. The sample was then returned to the boiler in similar small bore pipes. In-house calibration of the densitometer (see Appendix A) allowed the measured density to be converted to a sample composition.

The sampling loop was designed to operate on very small flow rates meaning that it could be operated with little or no disruption to the rest of the facility. The major disadvantage of the system however was that only one sample could be tested at a time. This meant that there was a time difference between the measurement of the composition in the two condensers.

3.1.2 Coolant Circuit

Coolant was supplied to the reflux and dump condensers from a closed loop containing mains water. Heat gained by this coolant while passing through the condensers was rejected to the central NEL chilled water supply through a small shell and tube heat exchanger. A line diagram of the coolant loop is displayed in Figure 3.3.

Coolant temperatures at the inlet to the reflux condenser were controlled using a three-way valve which was set by a PID controller based on thermocouple measurements at the condenser inlet port. The system worked by recycling a fraction of the warm coolant into the feed to the condenser thus bypassing the shell and tube exchanger. This allowed the conditions inside the reflux condenser to be altered by increasing or decreasing the coolant temperature at the inlet over the range 10 to 50°C. In practice however coolant inlet temperatures were kept in the range 30 to 42.5°C.

A similar system existed for the dump condenser although it was not used and coolant was always fed to this condenser at 15°C.

A series of valves existed adjacent to the reflux condenser which allowed the coolant to enter into any of the three test sections. This system was in place to allow the length of the condenser to be altered. In practice it proved difficult to operate with fewer than three test sections because the nominally uncooled test sections were not isolated from the cooled section, and condensate tended to form in the uncooled section due to conduction from the cooled sections.

3.1.3 Measurement Systems

Most of the facility upgrades planned and implemented by the author were concentrated on the collection of reliable and accurate data. Every aspect of the data collection and analysis system was improved and the details of this are discussed below.

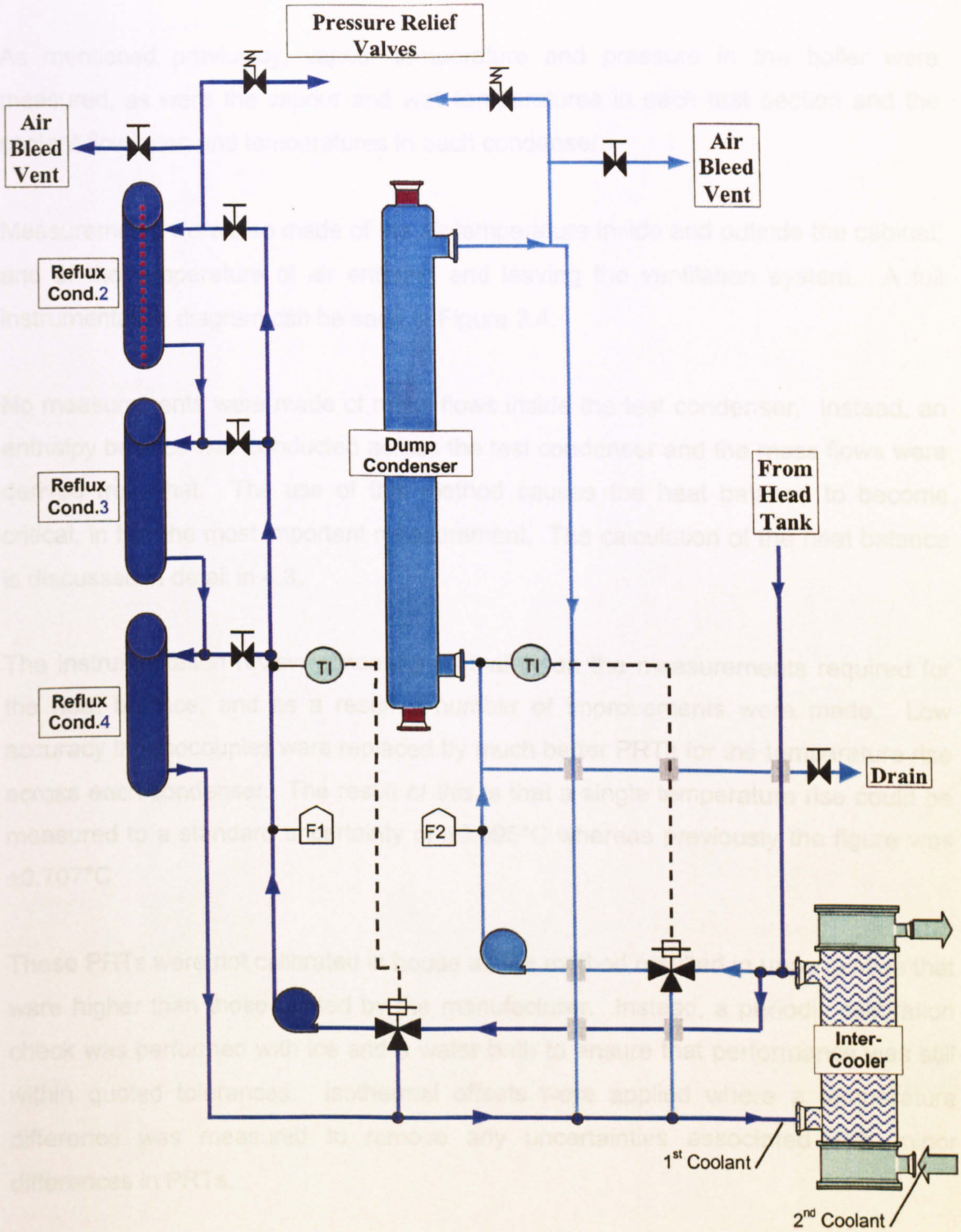

Figure 3.3: Line diagram of coolant circuit

3.1.3.1 Instrumentation

As mentioned previously, vapour temperature and pressure in the boiler were measured, as were the vapour and wall temperatures in each test section and the coolant flow rates and temperatures in each condenser.

Measurements were also made of the air temperature inside and outside the cabinet, and of the temperature of air entering and leaving the ventilation system. A full instrumentation diagram can be seen in Figure 3.4.

No measurements were made of mass flows inside the test condenser. Instead, an enthalpy balance was conducted across the test condenser and the mass flows were derived from that. The use of this method causes the heat balance to become critical, in fact the most important measurement. The calculation of the heat balance is discussed in detail in 4.3.

The instrumentation review concentrated mainly on the measurements required for the heat balance, and as a result a number of improvements were made. Low accuracy thermocouples were replaced by much better PRTs for the temperature rise across each condenser. The result of this is that a single temperature rise could be measured to a standard uncertainty of ±0.095°C whereas previously the figure was ±0.707°C

These PRTs were not calibrated in house as the method resulted in uncertainties that were higher than those quoted by the manufacturer. Instead, a periodic calibration check was performed with ice and a water bath to ensure that performance was still within quoted tolerances. Isothermal offsets were applied where a temperature difference was measured to remove any uncertainties associated with minor differences in PRTs.

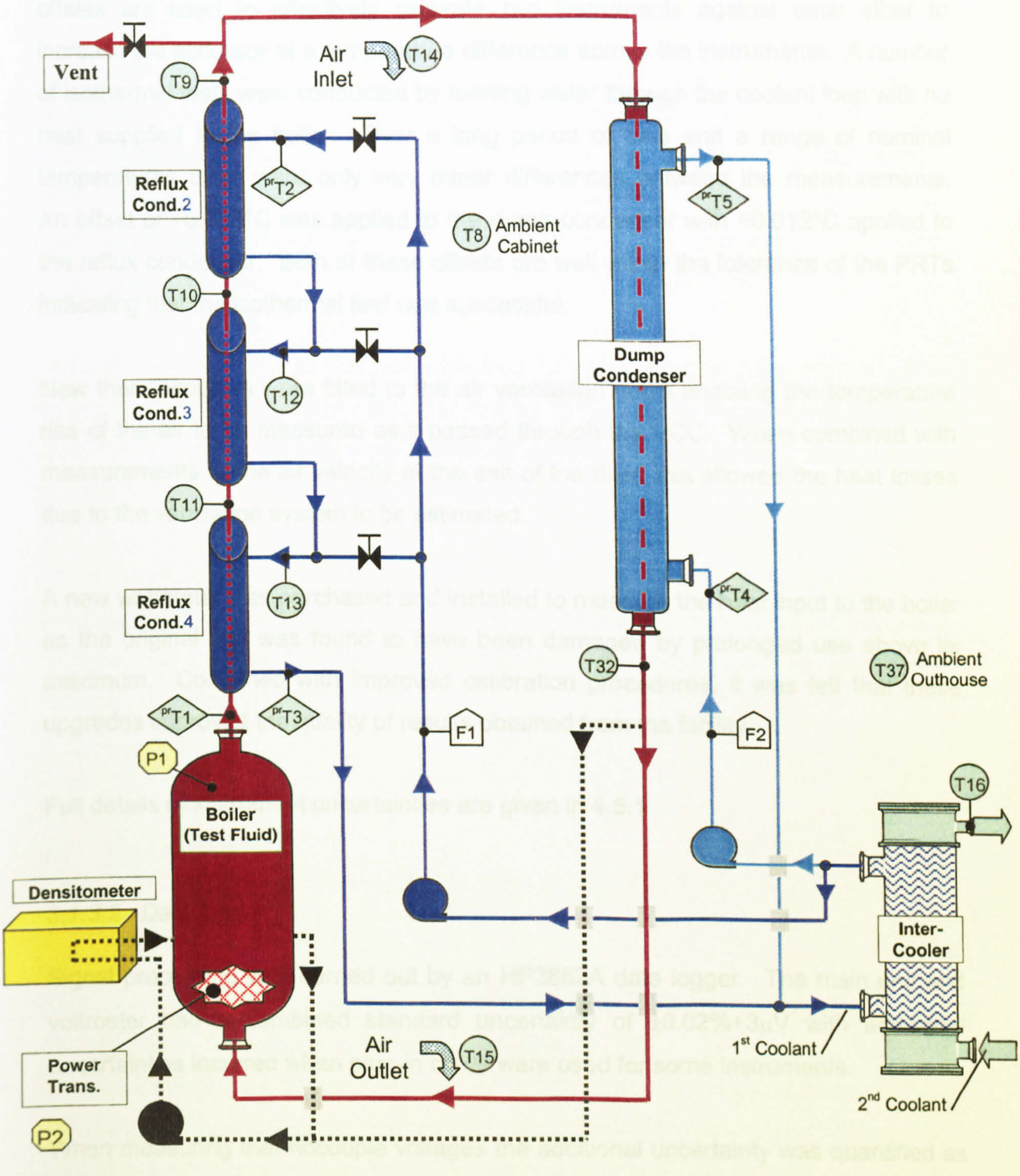

Figure 3.4: Facility instrumentation diagram

Two instruments are unlikely to give exactly the same measurement. Isothermal offsets are used to effectively calibrate two instruments against each other to increase the accuracy of a temperature difference across the instruments. A number of isothermal tests were conducted by running water through the coolant loop with no heat supplied to the boiler. Over a long period of time and a range of nominal temperatures there were only very minor differences between the measurements. An offset of –0.088°C was applied to the dump condenser with +0.012°C applied to the reflux condenser. Both of these offsets are well within the tolerance of the PRTs indicating that the isothermal test was successful.

New thermocouples were fitted to the air ventilation ducts enabling the temperature rise of the air to be measured as it passed through the VCC. When combined with measurements of the air velocity at the exit of the duct, this allowed the heat losses due to the ventilation system to be estimated.

A new wattmeter was purchased and installed to measure the heat input to the boiler as the original unit was found to have been damaged by prolonged use above its maximum. Combined with improved calibration procedures, it was felt that these upgrades improved the quality of results obtained from the facility.

Full details of instrument uncertainties are given in 4.5.1

3.1.3.2 Data logger

Signal processing was carried out by an HP3852A data logger. The main unit and voltmeter had a combined standard uncertainty of ±0.02%+3μV with additional uncertainties incurred when plug-in cards were used for some instruments.

When measuring thermocouple voltages the additional uncertainty was quantified as ±0.1°C due to cold junction compensation and when measuring flow rates was quantified as 0.04%. Resistance measurements were not subject to further uncertainties as all the PRTs used were the 4-wire type (TC Ltd, 1999).

3.1.3.3 Data acquisition software

Data were recorded using a unique Visual Basic based data acquisition program developed in house specifically for this work. Although in the main designed and coded by technical staff at NEL the author had some input into the design stage and took part in the commissioning. The program was based on a standard format used in other NEL research facilities, and was designed and coded to programming quality assurance standards.

The software incorporated features such as a rig monitor and stability monitor. The rig monitor was used to view a layout of the facility with all the measurements shown thus giving a complete picture of the facility and the stability monitor was used to indicate the behaviour of the main instruments over time.

The software also allowed all of the test conditions to be recorded, and when the flooding phenomenon was studied, comments relating to visual observations were recorded. The output from the program was a file designed to be input directly into the analysis spreadsheet.

3.2 Data Analysis

3.2.1 Analysis spreadsheet

Results were analysed on a spreadsheet developed by the author based on similar spreadsheets for other experimental facilities at NEL. The spreadsheet was designed not just as an analysis tool, but to fulfil a number of requirements. Raw data and results were to be displayed in a meaningful format and the spreadsheet was to be fully self contained so that all relevant information such facility geometries and physical properties were available.

3.2.2 Physical properties

In order to make the analysis spreadsheet as self contained as possible, physical property functions were built into the code. A standard NEL visual basic module was included which predicted physical properties as a function either of temperature, or pressure and temperature. Common fluids like air and water were included, but the hydrocarbons studied in this research were not. The author carried out work aimed at including pentane and isooctane properties into the module over the full working range of the reflux condensation facility.

The method used to achieve this goal is discussed below, and some consideration is given to the uncertainties of estimated property values.

3.2.2.1 Overview of the method

Physical property data were extracted from a commercially available package (PPDS v2.32) for both pentane and isooctane over the temperature range 0 to 100 °C and pressure range 0 to 2 bar (abs). These data were plotted and regression analysis used to fit polynomial curves. The physical property was then described by a polynomial equation as a function of temperature.

For vapour properties, curves were fitted at a number of different pressures, and the value at a known pressure was estimated by linear interpolation between the curves immediately above and below the required pressure.

A visual basic function was written to calculate any required hydrocarbon property from four inputs; the measured temperature and pressure, pentane mole fraction (which could be 1 or 0 if a pure component property was required), and a flag number to indicate the required property.

This function then called a number of other functions to calculate either a vapour or liquid property for each pure component, and a mixture property based on the mass or mole fraction of pentane using a weighted average. A summary of the extraction of the polynomial equations is given below, and a full list of the equations is given in appendix C.

3.2.2.2 Liquid properties

Saturation line values were used in the estimation of liquid properties. In the case of enthalpy, the datum was set at 0°C such that the property would be zero at the bottom of the working range.

Although it was known that the condensate film could become sub-cooled, the degree of sub-cooling was assumed to be small and have a negligible effect on all the required physical property values except specific enthalpy.

Each property was plotted against temperature with both pentane and isooctane on the same axis. A polynomial trendline was then fitted for each component and the equation of the line extracted. This is displayed in Figure 3.5 below, using density as the example. The residual values of the curve fits were found to be almost exactly unity, thus the assumption was made that the curve fit procedure did not cause any significant uncertainties.

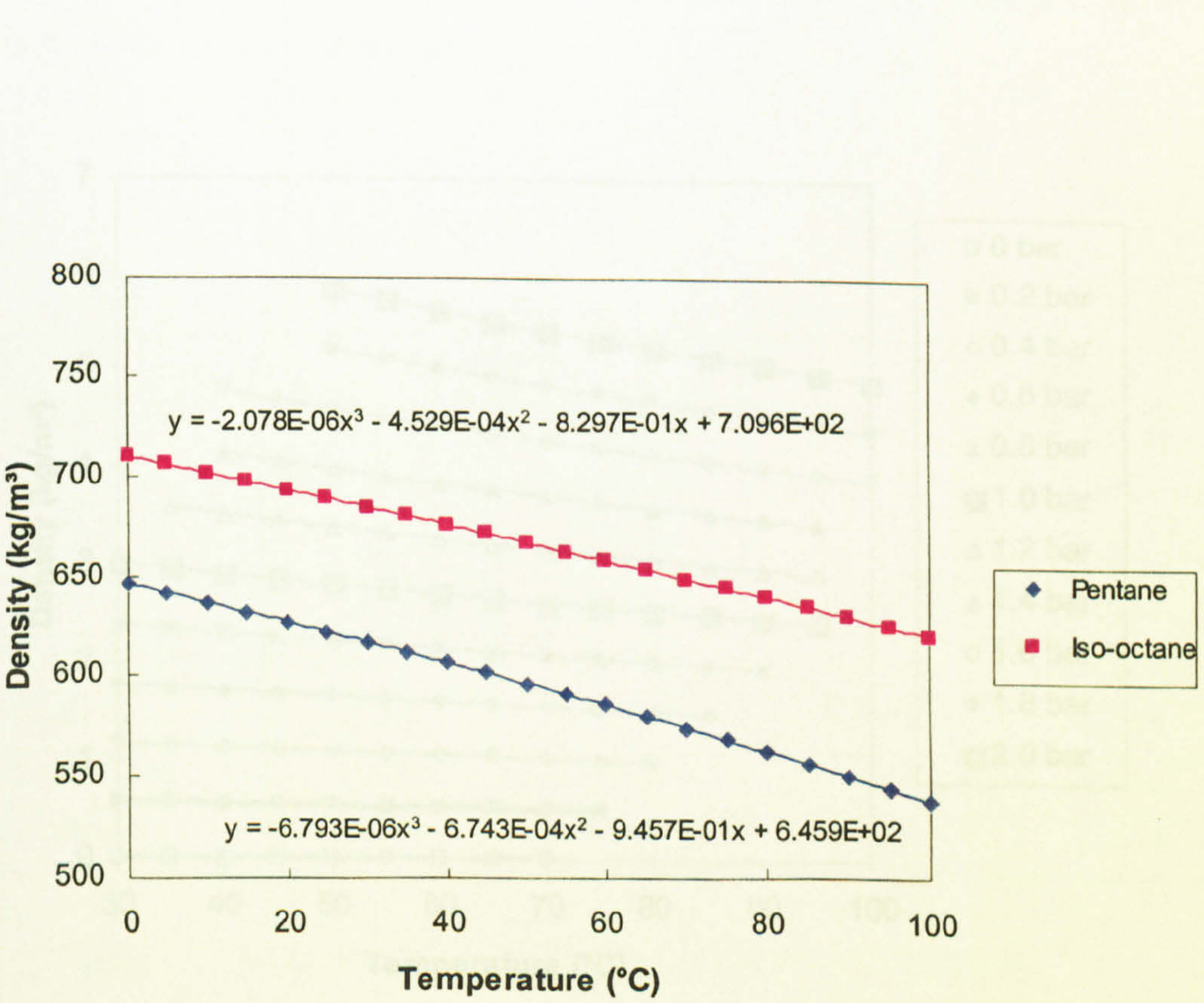

Figure 3.5: Saturated liquid density as a function of temperature

3.2.2.3 Vapour properties

The situation was more complex for vapours as their properties are a function of pressure to a much higher degree than liquids. A similar method was used as described above, but for vapours the graphs contained values of the physical property against temperature at a number of different pressures as shown in Figure 3.6.

Visual Basic code was developed to calculate the property at the required pressure. Within the working range, the code used a checking procedure to find the property curve at the first pressure value above the required value, followed by property curve immediately below the required pressure and then interpolate between the two.

Vapour specific enthalpy was referred to a datum of liquid specific enthalpy at 0°C. This meant that the vapour and liquid enthalpies had the same basis, thus simplifying any enthalpy changes where a change of phase occurred.

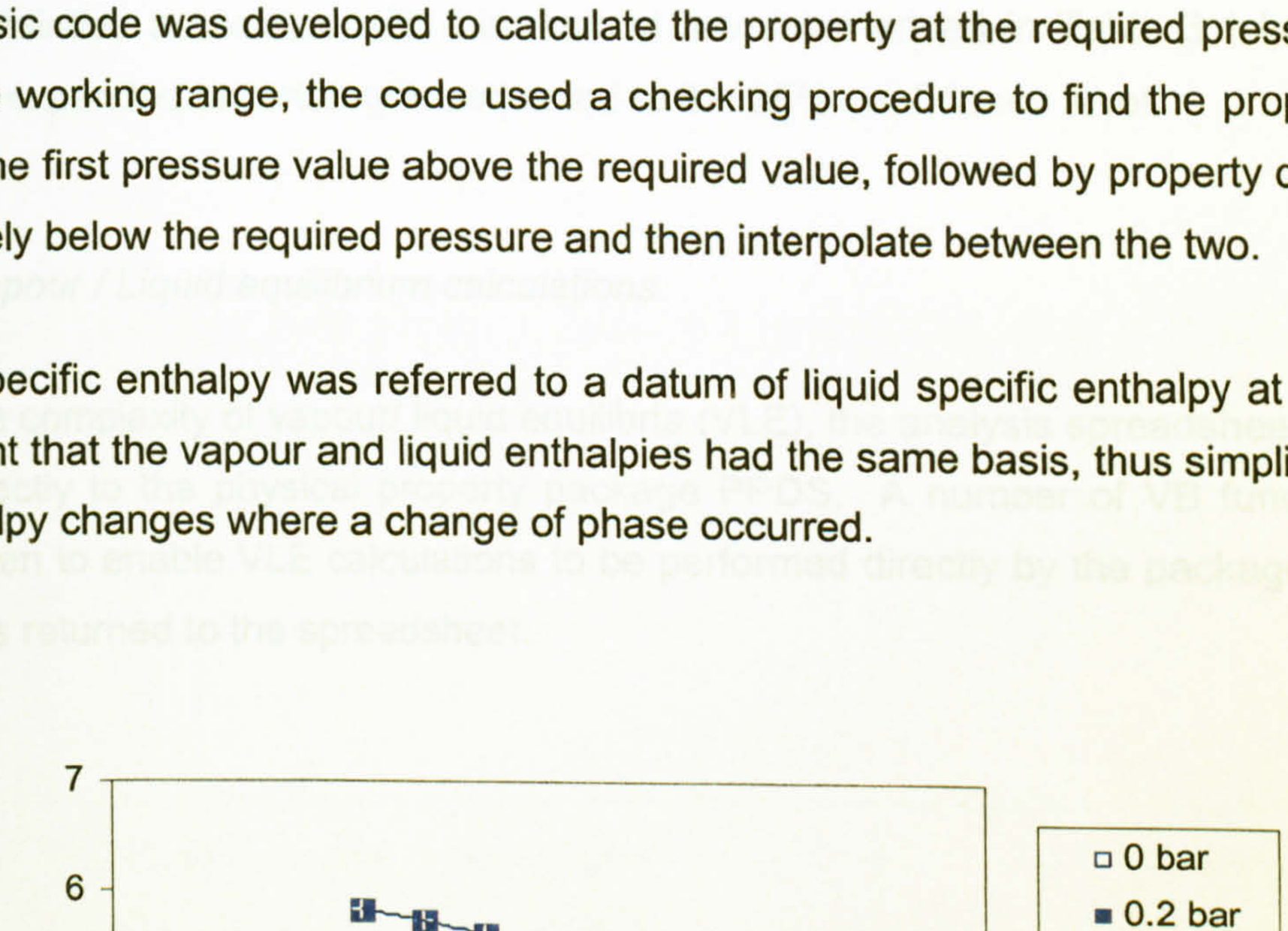

Figure 3.6: Pentane vapour density as a function of temperature and pressure

3.2.2.4 Physical property uncertainty analysis

The use of interpolation in the manner described above incurred additional uncertainties for any pressure value that did not lie on one of the curves. A full statistical analysis was carried out to compare the calculated values to the raw data values over the entire working range. By comparing predicted values with the data extracted from PPDS it could be shown that in most cases, the added uncertainty was very small when compared with the uncertainty of the original data.

The uncertainties associated with this method are summarised in Table 3.1 below, where the expanded uncertainty is estimated to the 95% confidence level.

3.2.3 Vapour / Liquid equilibrium calculations

Due to the complexity of vapour/ liquid equilibria (VLE), the analysis spreadsheet was linked directly to the physical property package PPDS. A number of VB functions were written to enable VLE calculations to be performed directly by the package and the results returned to the spreadsheet.

Property	**Pentane**		**Iso-octane**	
	Mean Difference (%)	Expanded uncertainty (%)	Mean Difference (%)	Expanded uncertainty (%)
Density (kg/m³)	0.062	0.23	0.216	0.538
Specific Heat Capacity	0.010	0.014	0.109	0.356
Dynamic Viscosity	0.004	0.004	0.005	0.008
Thermal Conductivity	0.009	0.016	0.008	0.013
Specific Enthalpy	0.005	0.008	0.015	0.040

Table 3.1: Summary of vapour properties uncertainty analysis

The advantages of this were that accurate results were obtained, and with most of the required information coded into the function (e.g. equations used), only inputs of either temperature or pressure, along with pentane mole fraction were required. The main disadvantage, however, was that the spreadsheet was no longer stand alone, thus limiting its use to a PC containing the physical property package. Passing data between the programs also resulted in longer processing times.

Each function was called from a cell in the spreadsheet. The variable inputs (temperature, pressure, mole fraction) and other constant values such as component number and VLE model were then passed to the property package where the VLE calculation was performed. The package then passed the required value back to the function which in turn returned it to the cell.

The functions used are summarised in Table 3.2, and the full code is included in Appendix D.

Calculated Value	Function name	Description	Inputs
Dew Point Temperature	fn_Tdew	Dew point temperature of saturated vapour mixture	P, $\tilde{y}_P$
Bubble Point Temperature	fn_Tbub	Bubble point temperature of saturated liquid mixture	P, $\tilde{x}_P$
Dew Point Pressure	fn_Pdew	Dew point pressure of saturated vapour mixture	T, $\tilde{y}_P$
Bubble point composition	fn_EqLiqComp	Liquid pentane mole fraction in equilibrium with input vapour composition	P, $\tilde{y}_P$
Dew Point composition	fn_EqVapComp	Vapour pentane mole fraction in equilibrium with input liquid composition	P, $\tilde{x}_P$

Table 3.2: VLE function summary

3.3 Experimental Method

This project was a follow up to the work of Bartleman (2001), and as such, the experimental work was based on Bartleman's findings. The same hydrocarbons were used; n-pentane and iso-octane (2,2,4-trimethylpentane), both AnalR grade supplied by McQuilken and Co. of Glasgow, with the on improved accuracy over a wider range.

Three sets of tests were carried out; single component for each of the fluids, flooding tests using iso-octane, and mixture tests. After recommissioning of the upgraded facility, pure component tests were performed. The aims of these tests were to validate the work on improving the overall heat balance and to expand the range of the mean film heat transfer coefficient against Reynolds number curve.

Following on from this, a flooding test was carried out to study the behaviour of the facility under flooding and non-flooding (normal) conditions to enable prediction of the flooding point. The bulk of the test work concentrated on binary mixtures of the hydrocarbons. The objective of these tests, which proved more complicated because of the requirement for composition measurements, was to provide useful data to enable further modelling of the reflux condensation process.

3.3.1 Controlled variables

The facility was designed to allow control of the heat supplied to the boiler, the coolant flow rates and inlet temperatures to both condensers, and the length of the reflux condenser. Bartleman (2001) found that altering the condenser length by shutting off the coolant supply to one or more of the test sections was unreliable with condensate forming in the uncooled test sections, so in this project only the full length was utilised.

Coolant flow rates were controlled by a valve from a switch located next to an indicator. The coolant flow rates were left constant through all the tests since the analogue nature of this system made it difficult to reproduce settings. Conversely, the control mechanism for the coolant inlet temperatures used a PID controller with digital settings that resulted in accurate control allowing inlet temperatures to be repeated.

In all of the tests carried out therefore, only the heat supplied to the boiler and the coolant inlet temperature to the reflux condenser were altered. The mass of vapour generated and hence the velocity was set by the power input to the boiler. Increasing the power to the heaters caused a higher heater surface temperature, and the liquid boiled more vigorously resulting in a higher vapour mass flow at a higher temperature. The ratio of condensate to vapour flow (reflux ratio) was controlled by the temperature driving force which in turn was set by the coolant inlet temperature. Reducing the inlet temperature of the coolant caused a higher driving force which increased the reflux ratio and reduced the overall system pressure and temperatures.

3.3.2 General procedure

The general operating procedure was based on the procedure developed during the preceeding project on this facility. Some changes were made, mostly due the use of the new data acquisition program and data collection method.

At the start of each test day, the vacuum pump was run for a short time to remove any inerts that may have leaked into the system. When the pressure was well below saturation pressure at the ambient boiler temperature the pump was stopped and vapour flashed off to return the system to saturation. This was potentially more of a problem in the pure iso-octane tests because of the very low saturation pressures.

Once the system stabilised, the coolant pumps and boiler heaters were switched on. The facility was then left for between 2 and 4 hours to heat up and approach steady-state. During this period, the rig monitor (see Figure 3.7) was left on and checked every half hour to ensure normal operation. When the overall heat balance reached 0.85 – 0.90 the rig monitor was switched off and replaced by the stability monitor (see Figure 3.8). The stability monitor was used to chart the progress towards steady state. Steady state was defined as being achieved when the overall heat balance was level over a period of five minutes; this usually occurred at heat balances of 0.95 –1.00.

After about half an hour of steady state operation, results were recorded. The settings were then changed and the facility left to reach steady state again before the process was repeated.

In most cases the heat input level was held constant and the coolant inlet temperature altered and 2 to 3 sets of data were recorded in a day.

3.3.3 Data collection procedure

Before every test run a number of settings were entered into the data acquisition program. These included the date, the test name, and the test fluid. Because of the requirement for composition measurements during mixtures tests, there were differences in the collection methods for each of the tests.

3.3.3.1 Pure component

After allowing the facility to run at steady state, three sets of measurements were made. These were denoted by n.1, n.2, and n.3, where n was the run number. In true steady state all three would have been the same, however slight fluctuations caused slight differences to appear. The effect of these fluctuations was reduced as each set of measurements was the mean of 10 scans.

3.3.3.2 Flooding

The only difference between the flooding tests and the initial single component tests was that a record was made of the condensate flow pattern as it drained from the tube. The data acquisition program was modified slightly to allow for this. Visual observations were made just before data collection started using a monitor placed next to the facility PC, and checked a number of times during scanning to ensure that the pattern did not change. This became standard procedure for all subsequent tests as a check that the facility was in fact operating in the non-flooding region.

3.3.3.3 Mixtures

As stated above, the facility was left to operate at steady state for about half an hour before any data were recorded. In the mixture tests this was important as a build up of condensate was required from each of the condensers to create a condensate pool so that a sample could be removed. The reflux ratio was always kept below 0.95 so that enough condensate formed in the dump condenser for the same reason.

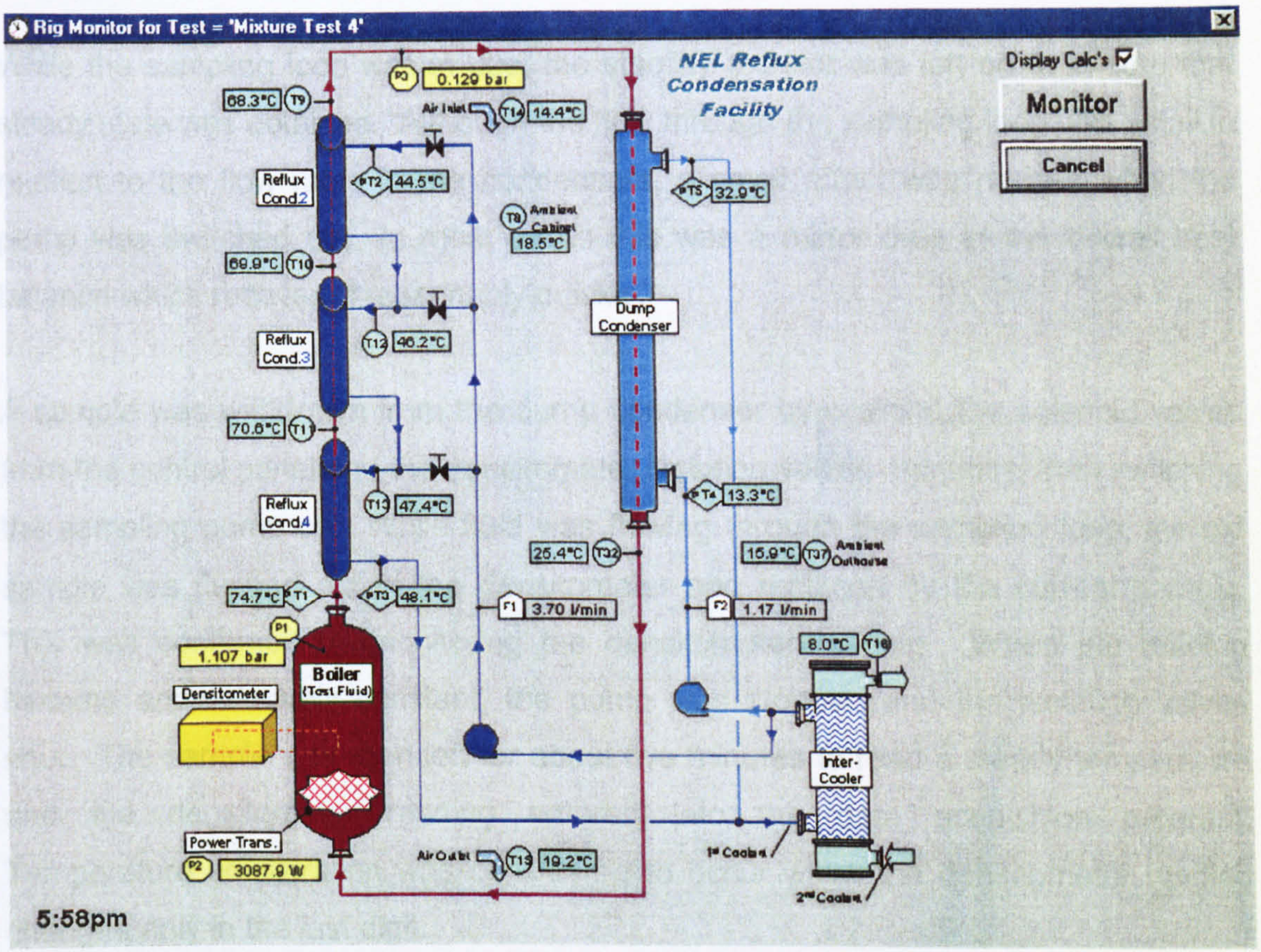

Figure 3.7: Screenshot of the rig monitor

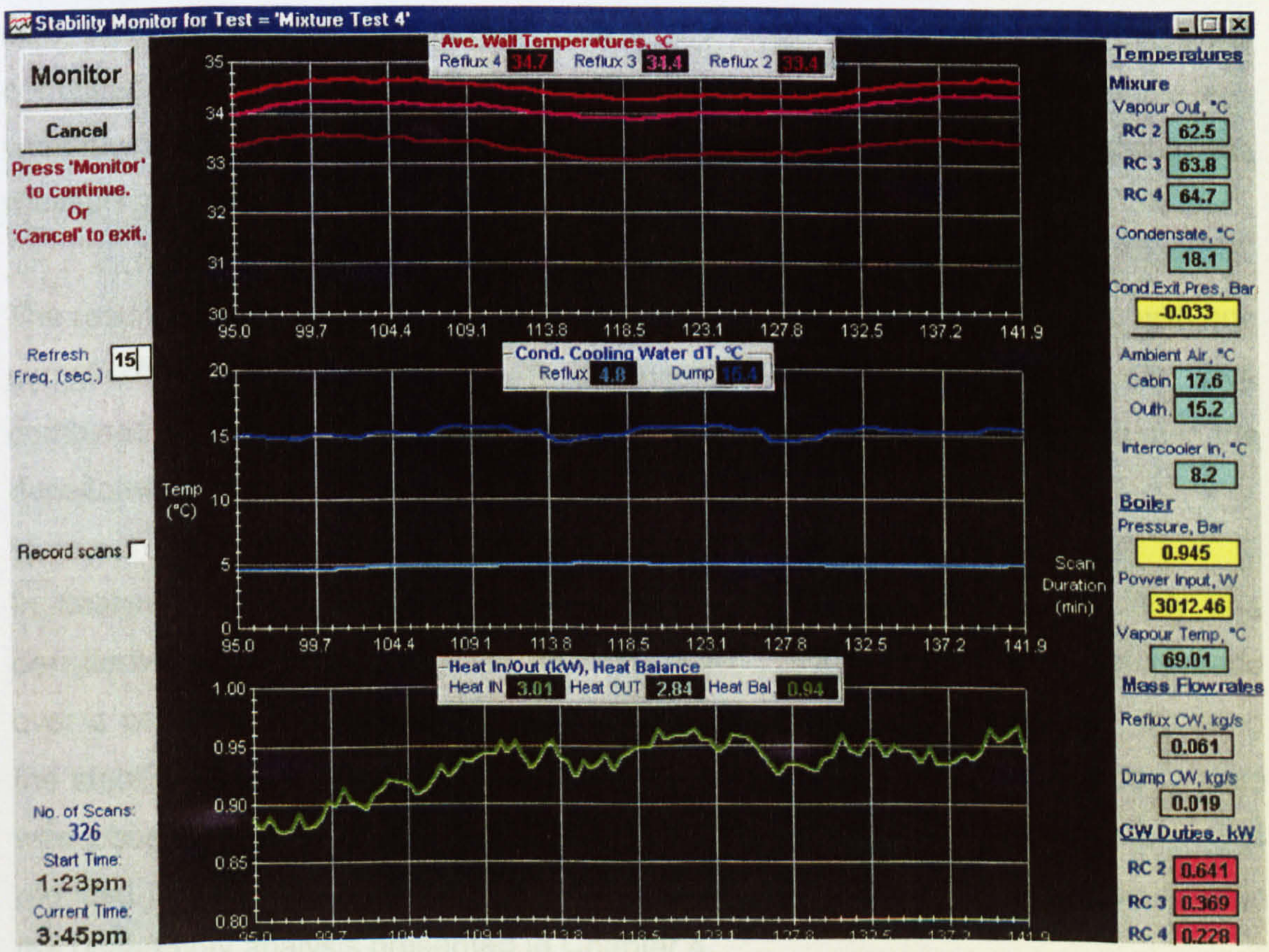

Figure 3.8: Screenshot of the stability monitor

While the sampling loop was in use, the stability monitor was left on to ensure that steady state was obtained. Although the flow through the sampling loop was small in relation to the flow rates in the condensers, a small effect was noticed when the pump was switched on. In most cases this was a minor drop in the overall heat balance which recovered reasonably quickly.

A sample was withdrawn from the dump condenser by opening the solenoid valves from the control panel and the densitometer isolating valves manually, then switching the sampling pump on. While fluid was flowing through the sampling loop, the old sample was flushed out of the densitometer and replaced by the current sample. This was confirmed by monitoring the densitometer reading. When the reading became approximately constant, the pump was stopped and the isolating valves shut. The sample was then left for about five minutes to read a steady temperature and the densitometer reading entered into the data acquisition program. Temperature equilibration was considered to occur when the densitometer reading changed only in the last digit.

For every sample, three sets of data were recorded and denoted by nD1, nD2 and nD3, where n was the run number. As in the single component work, every set contained the mean of 10 scans. Once the three sets were recorded, a sample was withdrawn from the reflux condenser and the process repeated giving the measurement sets nR1, nR2, and nR3.

The result was that for each data point, there were 6 sets of measurements, with one sample from each condenser. In the analysis spreadsheet, the 6 sets were combined to give one mean set denoted by n, which was completed by including the densitometer measurements.

In designing a data collection system the author considered that with only one densitometer this method was the most accurate. With measurements being made over a period of time, it was important that steady state was maintained. By using the stability monitor it was possible too check this, and in most cases, steady state was observed save for minor fluctuations. The effect of these fluctuations was reduced by taking many measurements and averaging them. This is discussed in the uncertainty analysis presented in Chapter 4.

4 Data Analysis Calculations

4.1 Mass and energy balances

The flow of mass and energy across a reflux condenser are illustrated in Figure 4.1. The diagram represents condensation of a vapour mixture, with vapour and liquid mole fractions used to represent composition changes.

Vapour at mass flow rate $\dot{M}_{v,in}$ and temperature $T_{v,in}$ enters the bottom of the tube and condenses into a falling film as it rises through the condenser. The condensate leaves from the bottom of the tube at $T_{f,out}$ and mass flow rate $\dot{M}_{f,out}$ while uncondensed vapour exits the top of the tube at $\dot{M}_{v,out}$ and $T_{v,out}$. Coolant is passed through the condenser where its temperature increases as it gains the heat released by condensation.

The assumption was made of no heat losses from the condenser. This is discussed in detail in 4.3.1. The further assumption that no condensation took place above the top of the condenser tube was also made. This meant that there would be no condensate flow into the condenser, as would be expected if there were significant heat losses above the coolant inlet point.

There are two special cases to be considered here. Firstly the case of total reflux, where all of the vapour is condensed in the test condenser. In this case there is no vapour flow out of the condenser and the mass balance is simple. There will also be no overall change in composition between the vapour and condensate.

$$\dot{M}_{v,in} = \dot{M}_{f,out} \tag{4.1}$$

$$\tilde{y}_{j,in} = \tilde{x}_{j,out} \tag{4.2}$$

Secondly, in the case of single component condensation, the composition terms can be ignored, again simplifying the mass balance. Single component condensation occurs almost isothermally, a fact that is evident in the experimental results. There are no sensible heat effects in the vapour and the only sensible heat transfer expected is conduction from the cold wall through the condensate film resulting in sub-cooling of the film.

$$T_{v,in} = T_{v,out} \tag{4.3}$$

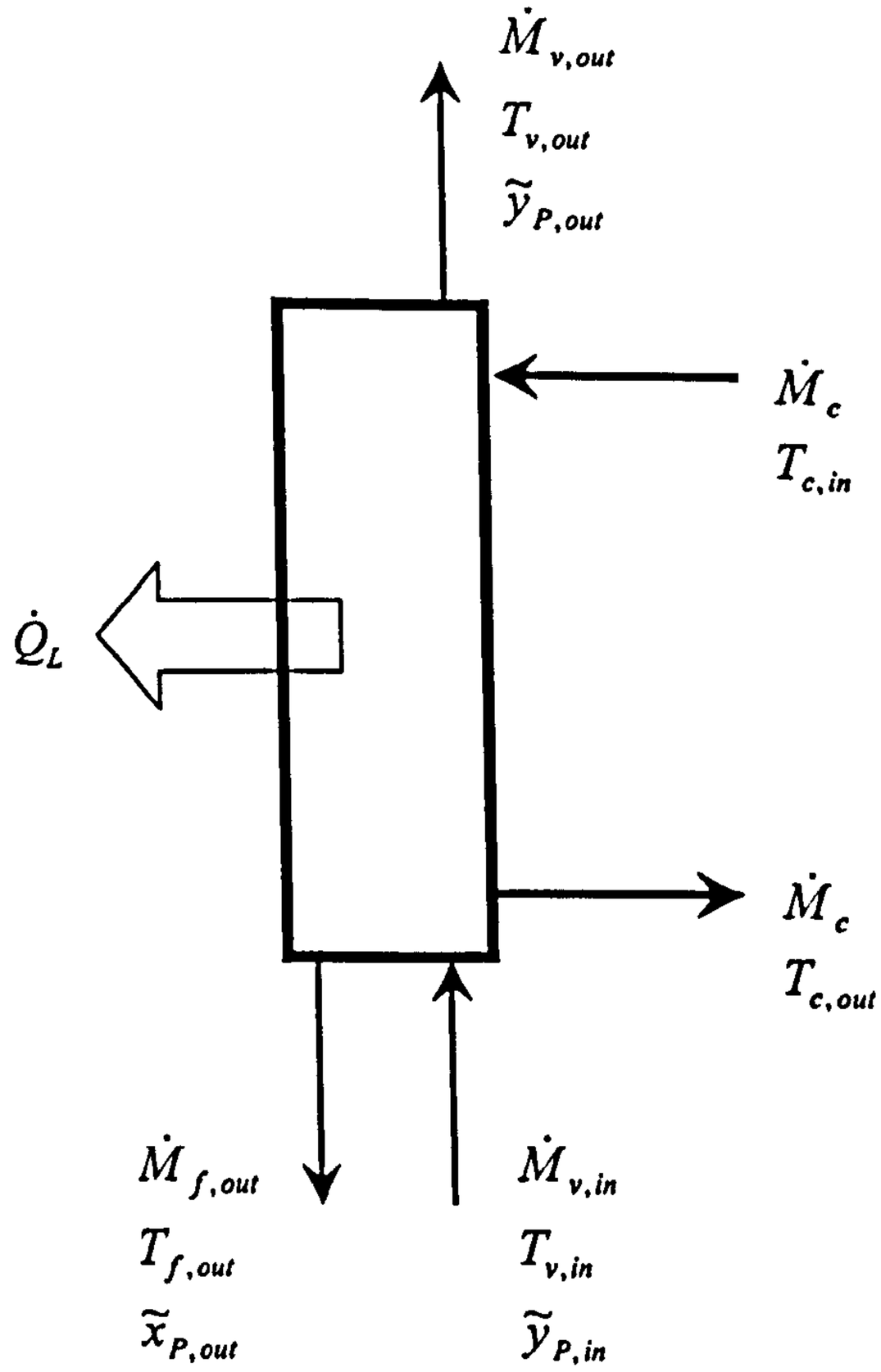

Figure 4.1: Mass and energy balances over the reflux condenser

4.2 Mass balance calculations

The total and component mass balances over the reflux condenser tube give

$$\dot{M}_{v,in} = \dot{M}_{v,out} + \dot{M}_{f,out} \tag{4.4}$$

$$\dot{M}_{v,in}\,\tilde{y}_{P,in} = \dot{M}_{f,out}\,\tilde{x}_{P,out} - \dot{M}_{v,out}\,\tilde{y}_{P,out} \tag{4.5}$$

As no flow rate measurements were made on the process side, the mass balance was fully specified by performing an enthalpy balance over the test condenser tube. Assuming negligible heat losses from the condenser jacket, this gives

$$\dot{M}_{v,in}\,h_{v,in} + \dot{M}_{c}\,h_{c,in} = \dot{M}_{v,out}\,h_{v,out} + \dot{M}_{f,out}\,h_{f,out} + \dot{M}_{c}\,h_{c,out} \tag{4.6}$$

Rearranging

$$\begin{aligned} \dot{M}_{v,in}\,h_{v,in} - \dot{M}_{v,out}\,h_{v,out} - \dot{M}_{f,out}\,h_{f,out} &= \dot{M}_{c}\,h_{c,out} - \dot{M}_{c}\,h_{c,in} \\ &= \dot{M}_{c}\left(h_{c,out} - h_{c,in}\right) \\ &= \dot{Q}_{c} \end{aligned} \tag{4.7}$$

Originally, two compositions were measured using the densitometer, namely the condensate from the reflux and dump condensers. As all of the vapour leaving the reflux condenser was condensed in the dump condenser, it can be said that the composition of the vapour was measured at the outlet. Analysis of the results showed that there was a problem with the measurements of composition in the reflux condenser and as a result all of these measurements were rejected as being unreliable. This is discussed fully in 5.3.3. As one composition measurement was not enough to calculate the mass balance, the composition of feed vapour from the boiler was estimated from VLE calculations by assuming full saturation.

The flow rate of vapour leaving the reflux condenser was calculated from measurements on the dump condenser. As total condensation occurred in the dump condenser equation (4.7) can be simplified

$$\dot{M}_{fD,out}\left(h_{vD,in}-h_{fD,out}\right)=\dot{Q}_{c,D} \tag{4.8}$$

The flow rate of vapour leaving the reflux condenser was then found by rearranging this equation to give

$$\dot{M}_{vR,out}=\dot{M}_{fD,out}=\frac{\dot{Q}_{c,D}}{\left(h_{vD,in}-h_{fD,out}\right)} \tag{4.9}$$

In order to evaluate condensate enthalpies temperatures were required. In the dump condenser, the condensate temperature was measured but no such data was available in the reflux condenser. Since the value was known to lie between the vapour and wall temperature, an estimation was made based on the work of Rosenhow (1956).

$$T_{f,out}=0.68T_{v,in}+0.32\overline{T}_{w} \tag{4.10}$$

In Rosenhow's work on the condensation of a vapour mixture, the vapour temperature in (4.10) was actually the interfacial temperature, but this was not available in the present work. Bartleman (2001) analysed the effect of using the bulk vapour temperature instead of the interfacial temperature and found that using an estimated interfacial temperature had less than a 1% effect on the condensate film heat transfer coefficient and less than a 10% difference on the vapour side heat transfer coefficients. As there was no measurement of interfacial temperature, Bartleman felt that using the vapour inlet temperature was justified.

Although the mass balance was fully specified by equations (4.4), (4.5) and (4.7), the fact that the reflux condenser condensate composition was unknown meant that there were 4 unknowns; $\dot{M}_{v,in}$, $\dot{M}_{f,out}$, $\tilde{y}_{f,out}$, $h_{f,out}$. An iterative solution was therefore required. This was achieved by guessing the condensate composition and solving.

4.2.1 Density to composition conversion

As the densitometer measured only sample density, it was necessary to convert this to composition manually. Throughout the measurement process, the densitometer measuring cell was kept at a constant temperature of 20°C. This effectively removed any uncertainties associated with the effect of temperature on density. Data on the relationship between density and mass fraction of pentane and iso-octane mixtures were extracted from PPDS v2.2. Mass fraction was selected as the relationship is very linear, unlike the mole fraction/density relationship which is a curve. The conversion from density to composition was then based on the equation of the line.

$$x_P = 2.290*10^{-5}\rho^2 - 4.534*10^{-2}\rho + 2.042*10^{1} \qquad (4.11)$$

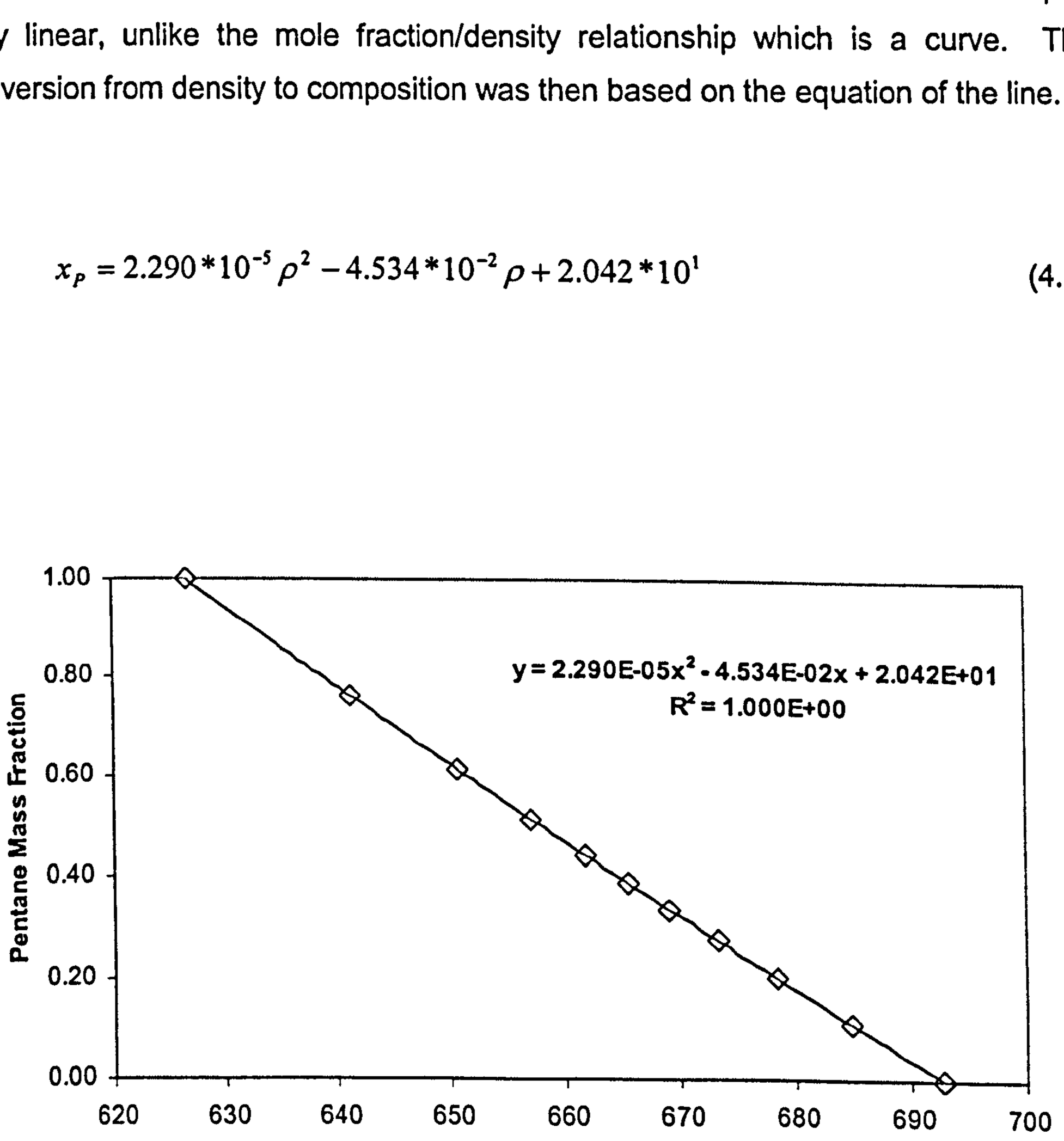

Figure 4.2: Mass fraction against density for pentane and iso-octane liquid mixture at 20°C

4.3 Heat balance calculations

The heat balance over the reflux facility is a measurement of how accurately the heat flows have been accounted for. As no mass flow measurements were made in the test fluid circuit, the heat flows became vital to the mass balance. As a result of this, the author spent time developing the heat balance estimation to improve the accuracy.

The balance of heat over the facility is described by (4.12) below. This states that the heat input to the boiler is accounted for in the coolant heat loads across the test and dump condensers plus the heat transferred between the facility hot surfaces and the air inside the vapour containment cabinet.

$$\dot{Q}_B = \dot{Q}_R + \dot{Q}_D + \dot{Q}_L \tag{4.12}$$

If an attempt is made to measure or estimate the heat losses, then a fourth term can be added to the right hand side of (4.12) to give (4.7) below

$$\dot{Q}_B = \dot{Q}_R + \dot{Q}_D + \dot{Q}_L + \dot{Q}_E \tag{4.13}$$

The $\dot{Q}_L$ term now represents heat losses that are accounted for, and $\dot{Q}_E$ is an error term caused by a combination of the measurement uncertainties and errors in the estimation of heat losses.

The accuracy of the heat balance was calculated by defining a term R_Q as the ratio of measured heat out to heat input.

$$R_Q = \frac{\dot{Q}_{c,R} + \dot{Q}_{c,D} + \dot{Q}_L}{\dot{Q}_B} \tag{4.14}$$

In the ideal situation where there are no significant measurement uncertainties and the heat losses are measured accurately, the error term $\dot{Q}_E$ would approach zero and R_Q would be 1 (or 100%).

4.3.1 Heat losses

During normal operation, test fluid temperatures in the boiler and reflux condenser reached almost 90°C. With the air inside the VCC at ambient temperature before operation, it was expected that heat would be transferred from the hot unlagged surfaces of the test fluid circuit to the cooler air causing the air to heat up. This was confirmed experimentally as results showed that the ambient temperature inside the VCC was always greater then the ambient temperature of the surroundings once steady state had been reached. To combat this, most of the hot surfaces inside the VCC were well insulated.

The air extraction system was in place to remove any possible leakage of hydrocarbon vapour from the bottom of the VCC. With no extraction system the VCC would effectively be a stagnant volume of air with free convection and possibly radiation from the hot surfaces as the modes of heat transfer. The presence of the flow of air however caused forced convection away from some of the hot surfaces. It resulted in the extraction of warm air, which was replaced by cooler air from the surroundings.

4.3.2 Estimation of heat losses

Experimental results taken with the vapour containment cabinet (VCC) closed showed that as the rig heated up and approached steady state, the air temperature inside the cabinet increased. When steady state had been reached, no further increase in air temperature in the VCC was recorded.

At this point the assumption can be made that the heat transferred from all of the hot surfaces to the air in the VCC was exactly balanced by the heat lost from the VCC to the surroundings. If this was not the case, the temperature in the cabinet would either continue to increase (if the rig was losing heat at a faster rate then the VCC), or begin to decrease (if the VCC was losing heat at a faster rate then the rig).

By making this assumption, the total heat lost by all of the hot surfaces can be calculated by estimating the heat rejected by the VCC to the surroundings. As stated earlier, heat is lost by the hot surfaces by free and forced convection and by radiation. Calculating the heat transfer coefficient for each relevant mode for each separate surface would be extremely time consuming and at best very approximate. Estimating the heat lost by the VCC to the surroundings was a much simpler process that can be calculated far more accurately.

There were only three routes by which heat could be transferred from the VCC to the surroundings:

1. Through the walls of the VCC.
2. Through the floor of the VCC.
3. Warm air removed by the extraction system and replaced by cooler air from the surroundings.

The heat loads due to each of these routes should be calculated separately and then summed to give the total heat lost from the VCC.

$$\dot{Q}_L = \dot{Q}_W + \dot{Q}_F + \dot{Q}_A \tag{4.15}$$

4.3.2.1 VCC Walls

A number of assumptions were made in order to estimate the extent of heat lost through the VCC walls

- Perfect mixing of air inside the VCC resulting in a uniform temperature throughout the cabinet.
- The walls were deemed to be flat plates such that the effect of fittings from the ceiling and screws on all the walls were assumed negligible.
- The walls were made of stainless steel with a thermal conductivity of 16 W/mK.

- Air inside the cabinet was quiescent. This was not strictly correct as the extraction system caused a flow of air over part of the cabinet however most of this flow was over the bottom of the cabinet and did not affect a large part off the VCC walls.
- The surroundings were quiescent such that heat could only be transferred from the walls via free convection and radiation.

Making the further assumption that the outside temperature of the cabinet walls was the same as the air temperature inside the cabinet meant that any value calculated would be a slight over estimate.

Heat transfer coefficients were calculated for free convection from the horizontal upward facing ceiling and the four walls of the cabinet using the equations described in Incropera and De Witt (1981).

For the vertical wall, the average Nusselt number over the full height x was described by equation (4.13)

$$\overline{Nu}_x = \frac{\alpha_v x_W}{\lambda_W} = \frac{4}{3}\left(\frac{Gr_L}{4}\right)^{\frac{1}{4}} g(\mathrm{Pr}) \tag{4.16}$$

where the Grashof Number Gr_L was defined as

$$Gr_L = \frac{g\beta(T_{vcc} - T_S)L^3}{\upsilon^2} \tag{4.17}$$

and the temperature gradient parameter $g(\mathrm{Pr})$ is a function of the Prandtl number

$$g(\mathrm{Pr}) = \frac{0.75\mathrm{Pr}^{1/3}}{\left(0.609 + 1.221\mathrm{Pr}^{1/3} + 1.238\mathrm{Pr}\right)^{1/4}} \tag{4.18}$$

The cabinet ceiling was taken as a horizontal plate, the mean Nusselt number was defined as either (3.16) or (3.17) below

$$\overline{Nu} = \frac{\alpha_h z_W}{\lambda_W} = 0.54\, Ra^{1/4}, \qquad (10^4 \le \mathrm{Ra} \le 10^7) \qquad (4.19)$$

$$\overline{Nu} = \frac{\alpha_h z_W}{\lambda_W} = 0.15\, Ra^{1/3}, \qquad (10^7 \le \mathrm{Ra} \le 3.1510^{11}) \qquad (4.20)$$

The vertical and horizontal Nusselt numbers were then used to determine the respective resistances to heat transfer allowing the total heat lost through the four vertical walls and the horizontal ceiling was then calculated.

$$\dot{Q}_W = A_{CabW}\left(T_{VCC} - T_S\right)\alpha_{CabW} + A_{CabC}\left(T_{VCC} - T_S\right)\alpha_{CabC} \qquad (4.21)$$

4.3.2.2 VCC Floor

The VCC floor was a steel plate raised about 20mm above the floor of the outhouse. It was covered by a thick layer of absorbent material to soak up any liquid leaks. There was very little draft under the floor and it was assumed that the heat lost through the floor was negligible.

4.3.2.3 Air Extraction System

The air extraction system was driven by a single speed fan and operated whenever the rig was filled with hydrocarbons. Measurements were made of the air velocity at the outlet of the extracted air as well as the geometry of the ducting. From these measurements, a value was calculated of the air mass flow rate through the VCC.

$$\dot{M}_A = A_{duct}\, u_A\, \rho_A \qquad (4.22)$$

The density of the air was taken at the assumed pressure of 1.01325 bar and the measured outlet temperature.

Two new thermocouples were installed; one at the inlet and one at the outlet each placed 5 cm inside the extraction ducting on the VCC side. These thermocouples gave reasonably accurate measurements of the air temperature entering and leaving the cabinet, allowing the heat load associated with the system to be estimated.

$$\dot{Q}_A = \dot{m}_A (h_{A,out} - h_{A,in}) \tag{4.23}$$

4.4 Heat Transfer Coefficients

The reflux condenser was described by the general heat exchanger equation (4.24), where the heat load was defined as the heat gained by the coolant (4.7).

$$\dot{Q}_R = \overline{U}\, A_i\, \Delta\overline{T} \tag{4. 24}$$

The area was found from the internal diameter of each test section and the combined length of the condenser (4.25), while the logarithmic mean temperature difference was defined in terms of the temperature differences between the vapour and the coolant at the inlet and outlet of the test section (4.26).

$$A_i = \frac{\pi d_i^2}{4} L \tag{4.25}$$

$$\Delta\overline{T} = \frac{(T_{v,in} - T_{C,out}) - (T_{v,out} - T_{C,in})}{\ln\left[\dfrac{(T_{v,in} - T_{C,out})}{(T_{v,out} - T_{C,in})}\right]} \tag{4.26}$$

4.4.1 Overall mean heat transfer coefficient

The mean overall heat transfer coefficient, $\overline{U}$, was described by the resistances of the coolant and tube wall, and the total condensing side resistance.

$$\frac{1}{\overline{U}} = \left(\frac{d_i}{d_o}\right)\frac{1}{\overline{\alpha}_C} + \left(\frac{d_i}{d_{tr}}\right)\frac{x_w}{\lambda_w} + \frac{1}{\overline{\alpha}_{cs}} \tag{4.27}$$

In equation (4.27), the total condensing side resistance is the combination of the resistance of the condensate film and the effective resistance of the condensing vapour.

$$\frac{1}{\overline{\alpha}_{cs}} = \frac{1}{\overline{\alpha}_f} + \frac{1}{\overline{\alpha}_{v,eff}} \tag{4.28}$$

This applied when mixtures were condensed, however when a pure component was condensed, isothermal condensation occurred. There was no heat transfer in the vapour, only mass transfer across the interface, hence there was no resistance to heat transfer. The total condensing side resistance was thus taken to be equal to the resistance of the condensate film.

$$\frac{1}{\overline{\alpha}_{cs}} = \frac{1}{\overline{\alpha}_f} \tag{4.29}$$

4.4.2 Coolant heat transfer coefficient

The unique geometry of the HTFS Reflux Condensation Facility meant that a correlation for the mean coolant heat transfer coefficient had to be found experimentally. Bartleman (2001) employed the Wilson Plot technique to develop a correlation stated in terms of the heat transfer coefficient.

For this work, Bartleman's data were taken and re-worked to incorporate the physical property calculations discussed in 3.2.2. A new correlation was then developed with the method altered slightly to produce a correlation stated in terms of the dimensionless mean Nusselt number (4.30)

$$\overline{Nu}_c = \frac{\alpha_c D_e}{\lambda_c} \tag{4.30}$$

In the above equation, D_e, represents the equivalent hydraulic diameter. This is necessary as the flow channel is rectangular. The equivalent hydraulic diameter was defined in terms of the cross sectional area and the wetted perimeter with the assumption that the channel was completely filled with coolant. G_h and G_w are the dimensions of the rectangular channel.

$$D_e = \frac{4 * \text{Channel Area}}{\text{Wetted Perimeter}} = \frac{4\, G_h\, G_w}{2\,(G_h + G_w)} \tag{4.31}$$

4.4.2.1 Wilson Plot method

The overall mean heat transfer coefficient in the reflux condenser was expressed in terms of the individual heat transfer coefficients:

$$\frac{1}{\overline{U}_m} = \frac{1}{\overline{\alpha}_f} + \frac{D_i}{D_{tr}}\frac{x_w}{\lambda_w} + \frac{D_i}{D_o}\frac{1}{\overline{\alpha}_c} \tag{4.32}$$

D_i, D_o and D_{tr} were taken to represent the inside, outside and tube root diameters respectively. The tube root diameter is taken as the diameter of the tube at the innermost point of the coolant flow channel.

This equation can be simplified by making the assumptions that the film heat transfer and wall resistances were constant. Previously, Bartleman justified these assumptions by stating that over the full set of data, the wall heat transfer coefficient changed by less than 1% with the mean film heat transfer changing by a maximum of 5.7%

$$\frac{1}{\overline{U}_m} = Y + \frac{D_i}{D_o}\frac{1}{\overline{\alpha}_c} \tag{4.33}$$

where

$$Y = \frac{1}{\overline{\alpha}_f} + \frac{D_i}{D_{tr}}\frac{x_w}{\lambda_w} \tag{4.34}$$

In order to determine a correlation for mean coolant heat transfer coefficient, a suitable expression must be decided upon and substituted into the previous equation. The Dittus-Boelter (1930) correlation for mean heat transfer coefficient in turbulent flow states that the Nusselt number is a function of Reynolds number and Prandtl number;

$$Nu_c = f(Re_c, Pr_c) \tag{4.35}$$

For fully turbulent flow in a straight pipe, the correlation given was

$$Nu_c = 0.023\, Re_c^{0.8}\, Pr_c^{0.4} \tag{4.36}$$

This was corrected for flow in a helical pipe by McAdams (1954);

$$Nu_{c,C} = Nu_{c,S}\left(1 + 3.5\frac{D_{t,i}}{D_c}\right) \tag{4.37}$$

In this equation, $Nu_{c,C}$ is the mean Nusselt number in a coiled tube, $Nu_{c,S}$ is the mean Nusselt number in a straight tube with similar geometry, $D_{t,i}$ is the inside diameter of the tube and D_c is the diameter of the coil (taken at the centre of the tube).

As stated earlier, the complex geometry of the reflux condenser renders this correlation invalid although the principles are the same. By replacing the factors 0.023 and $(1+3.5(D_{t,i}/D_c))$ with a constant K unique to this condenser, the mean Nusselt number for flow inside the rectangular channel was expressed as

$$\overline{Nu}_c = K\, Re_c^{0.8} Pr_c^{0.4} \tag{4.38}$$

The mean coolant heat transfer coefficient can then be written in terms of the Reynolds and Prandtl numbers.

$$\overline{\alpha}_c = \left(\frac{\lambda_c}{D_e}\right) K\, Re_c^{0.8} Pr_c^{0.4} \tag{4.39}$$

And by then substituting this into the original expression for mean overall heat transfer coefficient;

$$\frac{1}{\overline{U}} = Y + \frac{D_i}{D_o}\frac{D_e}{\lambda_c}\frac{1}{K}\frac{1}{Re_c^{0.8}\, Pr_c^{0.4}} \tag{4.40}$$

By then plotting $1/\overline{U}$ against $\left(D_i D_e/D_o\,\lambda_c\right)\left(1/Re_c^{0.8}\, Pr_c^{0.4}\right)$ for a range of operating conditions, a straight line was obtained with gradient equal to $1/K$ and vertical axis intercept equal to Y. From this the dimensionless factor K was calculated to give the final expression of mean coolant heat transfer coefficient.

4.4.3 Condensate film heat transfer coefficient

With the availability of vapour, coolant and wall temperatures, it was possible to evaluate local condensing condensate film heat transfer coefficients in the single component runs at a number of points in the condenser from equation (4.41). Using (4.38) above, the coolant coefficient was found, allowing the local heat flux to be calculated and used to determine the condensate coefficient.

$$\dot{q}_T = \alpha_c(T_w - T_c) = \alpha_f(T_v - T_w) \tag{4.41}$$

The mean condensate film heat transfer coefficient was found by rearranging (4.27) to give (4.42). As discussed earlier, in the condensation of a pure fluid, the resistance of the condensate film is taken to be the only resistance on the condensing side

$$\frac{1}{\alpha_f} = \frac{1}{\overline{U}} - \left(\frac{d_i}{d_o}\right)\frac{1}{\alpha_C} - \left(\frac{d_i}{d_w}\right)\frac{x_w}{\lambda_w} \tag{4.42}$$

4.4.4 Vapour heat transfer coefficient

The analysis used to determine the mean condensate film heat transfer coefficient in the single component data, equation (4.42), was also applied to the mixture data. This allowed the total resistance on the process (condensing) side to be calculated. The condensate side resistance was assumed to be made up purely of contributions from the condensate film and vapour. Using a correlation developed from experimental data, the condensate heat transfer coefficient was calculated allowing the mean effective vapour resistance to be calculated.

$$\frac{1}{\overline{\alpha}_{v,eff}} = \frac{1}{\overline{\alpha}_{cs}} - \frac{1}{\overline{\alpha}_f} \tag{4.43}$$

It is necessary at this stage to fully define the mean effective vapour heat transfer coefficient to allow a complete analysis of vapour side resistances. This analysis is based on the work of Silver (1947) and McNaught (1979) and follows many of the arguments of the equilibrium method for condenser design.

As discussed in the literature review in section 2.6, the total heat flux in a condenser is expressed as

$$\dot{q}_T = U(T_v - T_c) \tag{2.23}$$

This overall resistance is made up of coolant, condensate film and vapour contributions.

$$\dot{q}_T = \alpha_c(T_w - T_c) = \alpha_f(T_i - T_w) = \alpha_{v,eff}(T_v - T_i) \tag{4.44}$$

The effective vapour side resistance has sensible and latent heat contributions. Where α_v is the heat transfer coefficient for sensible heat transfer from the vapour this gives

$$\dot{q}_T = \dot{q}_{vS} + \dot{q}_{vL} = \alpha_v(T_v - T_i) + \dot{m}_f \Delta h_v \tag{4.45}$$

$$\dot{q}_{vS} = \alpha_v(T_v - T_i) \tag{4.46}$$

It should be noted that in reflux condensation, the counter-current vapour and condensate flow reduces the chances of condensate sub-cooling, and as a result, in this analysis sensible cooling of the condensate film is assumed to be negligible.

Given that the temperature difference $(T_v - T_i)$ is applied to both α_v and $\alpha_{v,eff}$, then equations (4.44) and (4.46) can be combined to give

$$\alpha_{v,eff} = \frac{\alpha_v}{\left(\frac{\dot{q}_v}{\dot{q}_T}\right)} \tag{4.47}$$

The next part of the analysis was carried out by Bartleman (2001) and allows the mean vapour heat transfer coefficient to be evaluated from the mean effective vapour heat transfer coefficient. It was necessary to apply this analysis to the data collected in this project to expand the data set reported by Bartleman.

The heat fluxes in equation (4.44) can be replaced by the rates of heat transfer calculated from experimental data.

$$\left(\frac{\dot{q}_v}{\dot{q}_T}\right)=\left(\frac{d\dot{Q}_v}{d\dot{Q}_T}\right)=\frac{\dot{M}_v\,Cp_v\,dT}{\dot{M}_{v,in}\,dh}=\dot{x}_v\,Cp_v\,\frac{dT}{dh} \qquad (4.48)$$

where the term $\dot{x}_v$ represents vapour quality. Assuming a linear temperature-enthalpy profile through the tube and a mean vapour quality, the differential term could be estimated

$$\frac{dT}{dh}=\frac{T_{v,in}-T_{v,out}}{\dfrac{\dot{Q}_{c,R}}{\dot{M}_{v,in}}} \qquad (4.49)$$

By substituting (4.48) and (4.49) into equation (4.47) and, the mean sensible vapour heat transfer coefficient could then be evaluated

$$\overline{\alpha}_v=\overline{\alpha}_{,eff}\left(\frac{\dot{x}_{v,mean}\,Cp_v\left(T_{v,in}-T_{v,out}\right)}{\dot{Q}_{c,R}/\dot{M}_{v,in}}\right) \qquad (4.50)$$

4.5 Uncertainty Analysis Method

Any measurement of a value (measurand) is an estimate of the true value and is subject to a number of errors depending on the measuring system. The ISO "Guide to Uncertainty Measurement" (ISO GUM) (1993) states that no measurement is complete unless there is an uncertainty associated with it. It is thus crucial to perform an analysis of the errors and uncertainties in a series of measurements and if possible reduce them.

In the past there has been some confusion about the terms error and uncertainty, and often they have been taken to mean the same thing. This is not the case, and in this work, the following definitions have been used.

Error: The difference between the value of a measurand and the absolute true value.

Uncertainty: The range within which the true value is likely to lie. This is not a fixed value; it is a function of the level of confidence interval, usually 95%.

Using these definitions, the differences between error and uncertainty are apparent. The uncertainty describes a range of values within which the error is likely to lie. Performing an uncertainty analysis allows this range to be estimated, though the actual errors can never be calculated.

The uncertainty analysis presented here was split into two parts. The first section concerned the uncertainty associated with measurements made on the experimental facility, while the second part concentrates on the uncertainty of calculation results (propagated uncertainties) such as the coolant heat loads.

4.5.1 Combined measurement uncertainties

There are two components that make up the combined standard uncertainty of a measurement x_i; instrument uncertainty, $u_I(x_i)$, and steady state uncertainty, $u_s(x_i)$.

Instrument uncertainty is defined as the uncertainty introduced by the instrument due to the fact that the instrument can only make an estimate of the true value, and steady state uncertainty is defined as the uncertainty caused by minor fluctuations in the process over small time increments. It should be noted that steady state uncertainty only applies when repeat measurements are made of the same value assuming that the value should not change over time. These are estimated individually and combined in quadrature (root-sum-square method) to give the combined measurement standard uncertainty

$$u(x_i) = \sqrt{u_I(x_i)^2 + u_S(x_i)^2} \tag{4.51}$$

Although the terminology of random and systematic uncertainties is no longer used, the instrument uncertainty can be likened to systematic uncertainties, and the steady state to random uncertainties.

4.5.1.1 Measurement uncertainties

These uncertainties are usually quantified by the instrument manufacturer using in house testing, and quoted as part of the instrument specification. They are often split up into components such as accuracy, hysteresis, non-linearity and temperature coefficient. These components can be combined to give total instrument uncertainty using the root-sum-square method described above.

It is the norm for a manufacturer to quote the expanded uncertainty to the 95% confidence interval level. When this value is converted back to standard uncertainty, it is stated (ISO/WD 5618.4) that a statistical coverage factor of 2 should be used. In some cases, manufacturers will quote tolerance limits, and in this case ISO/WD 5618.4 suggests assuming a rectangular (uniform) probability distribution rather than the normal distribution. This distribution results in equal probability that a measurement will fall anywhere in the quoted range and has a coverage factor of $\sqrt{3}$.

When an instrument is calibrated, the main purpose of the calibration is to reduce the specified uncertainty. A calibration therefore is only useful if its uncertainty is smaller than the quoted instrument uncertainty. If known, the calibration uncertainty overrides the value quoted by the manufacturer, however if it is not known and cannot be estimated the specified value must be used. The uncertainty used for each instrument is summarised in Table 4.1.

4.5.1.2 Steady state uncertainties

When a number of repeat measurements are made, the steady state uncertainty, $u_s(x_i)$, of a measurement is defined as the standard deviation of the mean. When n measurements are made in a set $x_{i.k}$ and the mean value $\bar{x}_i$ is used, the standard deviation of the sample is used to calculate the standard deviation of the mean.

$$s(x_i) = \sqrt{\frac{1}{n-1}\sum_{k=1}^{n}\left(x_{i,k} - \bar{x}_i\right)^2} \tag{4.52}$$

$$u_s(x_i) = s(\bar{x}_i) = \frac{s(x_i)}{\sqrt{n}} \tag{4.53}$$

Instrument	Expanded unc. (tolerance)	Dimension	Standard unc.	Source of value
Boiler Pressure Transducer	0.30	% of reading	0.15	Manufacturers Spec and calibration
Watt Meter	0.20	% of reading	0.10	Manufacturer Spec
Flow Meters	0.40	% of reading	0.20	Litre Meter Calibration
Coolant PRTs	0.135	°C	0.068	Manufacturer Spec
Boiler PRT	0.19	°C	0.095	Manufacturer Spec
Thermocouples Class 1	0.50	°C	0.25	Manufacturer Spec
Thermocouples Class 2	1.00	°C	0.50	Manufacturer Spec
Densitometer	n/a	% of reading	0.0303	Analysis of in house calibration

Table 4.1: Instrument uncertainties

For single component work on the reflux facility this method sufficed, as each measurement was simply the mean of 10 scans. For mixture analysis, however, the situation was more complex. The data collection method described in 3.3.3 resulted in a measurement being the mean of 60 scans. The 60 scans were made in 6 groups each of 10 scans, but the value of each scan was not recorded and only the mean and standard deviation of each group were available.

In order to determine the standard deviation of all 60 scans, the statistical technique known as "Analysis of Variance" (ANOVA) was used. This technique quantifies the variance within each group separately from the variance between the groups and combines them both using the "Total Sum of Squares Method".

For a measurement x_i whose value is the mean of *p* values $x_{i,m}$ which in turn are the means of *n* scans $x_{i,k}$, it can be said that the total sum of squares is equal to the "Between conditions" sum of squares and the "residual" sum of squares combined.

$$Total\ SSq = Between\ Condition\ SSq + Residual\ SSq$$

$$Total\ SSq = \left[(q-1)\,s\left(x_{i,m}\right)^2 n\right] + \left[\sum_{m=1}^{p}\left[(n-1)s\left(x_{i,k}\right)^2\right]\right] \qquad (4.54)$$

Since the number of scans and sets of data combined are always the same for the reflux facility, this general form of the equation can be simplified.

$$Total\ SSq = 50\,s\left(x_{i,m}\right)^2 + \left[9\sum_{m=1}^{p}\left[s\left(x_{i,k}\right)^2\right]\right] \qquad (4.55)$$

The total sum of squares is also equal to the overall degrees of freedom times the variance of all the values where the variance is equal to the standard deviation of the values squared and in this case is the unknown.

$$Total\ SSq = Overall\ degrees\ of\ freedom * St\ dev\ of\ all\ values\ squared$$
$$Total\ SSq = \left[(n * p) - 1\right] * s(x_i)^2 \qquad (4.56)$$

Rearrangement of (4.56) allows the standard deviation of all 60 scans to be calculated.

$$s(x_i) = \sqrt{\frac{Total\ SSq}{59}} \tag{4.57}$$

The standard steady state uncertainty is then equal to the standard deviation of the mean as defined in (4.53).

In practice, this method was incorporated into a Visual Basic function so that the steady state uncertainty was automatically calculated when the 6 separate measurements were combined. This resulted in every measurement having an associated steady state uncertainty, and allowed the combined standard measurement uncertainty to be calculated.

4.5.1.3 Example of combined standard measurement uncertainty

This example is based on the data collected during the second mixture test Run 1. A full list of the measurement uncertainties for a similar run is displayed in Appendix B. It was felt that this run gives a good representation of all the data collected. The example given here is for the measurement of power into the boiler.

The result of the analysis presented in Table 4.2 is that the standard uncertainty of the measurement of heat input to the boiler is ±4.65 W (±0.118%). It is interesting to note that the instrument uncertainty is much more significant than the steady state uncertainty. This implies that the rig is very stable over the course of the full 60 scans.

Data							
Instrument:	Power Meter	Instrument standard uncertainty			0.115 (% of reading)		
Data group	D1	D2	D3	R1	R2	R3	Mean x_i
Measurement (mean of 10 scans)	3923.89	3922.36	3927.61	3938.82	3936.63	3937.34	3931.11
Standard Deviations	2.99	4.30	3.91	4.04	5.03	3.77	

Calculations		
Estimation of standard deviation		
Conditional Sum SQ		2696.72
Residual Sum SQ		886.98
Total Sum SQ		3583.70
Standard Deviation	$s(x_i)$	7.794
St. Dev. (mean)	$s(\bar{x}_i)$	1.006
Component Uncertainties		
Steady state Uncertainty	$u_s(x_i)$	1.006
Instrument Uncertainty	$u_I(x_i)$	4.537
Combined standard measurement uncertainty		
Absolute	$u(x_i)$ (W)	4.65
Dimensionless	u(x$_i$) (%)	0.118

Table 4.2: Uncertainty analysis example: Power measurement for run M2.2

4.5.2 Propagated Uncertainties

This part of the uncertainty analysis describes the technique used to calculate the propagated uncertainties associated with the results. Propagated uncertainties are the uncertainties of calculation results. The combined measurement uncertainties discussed in 4.5.1 are analysed to estimate the effect of each measurement on the final calculation. An example of this is the heat balance. By analysing the effect of uncertainties of all the inputs (temperatures, flows, and power) a value can be assigned to the overall uncertainty of the heat balance calculation.

An analysis of this type can be used not only to indicate a value for the propagated uncertainty, but also to show which of the inputs have a significant effect on the final answer, thus indicating which instruments to target to reduce the overall uncertainty. The method summarised below was described in ISO WD 5168.3 and is known as a Type B analysis.

4.5.2.1 Sensitivity coefficients

It is necessary to consider that the various inputs to a calculation may all affect the outcome of the calculation to varying degrees. For example a high uncertainty in one measurement may have little or no effect on the result whereas smaller uncertainties may have a greater effect. It is therefore required to perform a sensitivity analysis on the calculation to determine sensitivity coefficients for each of the inputs.

The sensitivity coefficient is defined as the rate of change of the output quantity y with respect to the input quantity x_i. Although this may be obtained by partial differentiation, it is much more convenient in a practical situation to use finite differences.

$$c_i = \frac{\delta y}{\delta x_i} \approx \frac{\Delta y}{\Delta x_i} \tag{4.58}$$

The sensitivity coefficient for each input is found by applying a small increment to the input and recalculating the output. A suitable value for the increment is normally the standard uncertainty as this is usually small compared to the value of the input quantity ($\Delta x_i = u(x_i)$).

$$y = f(x_1, x_2, x_3 ... x_N) \tag{4.59}$$

$$(y + \Delta y) = f(x_1 + \Delta x_1, x_2, x_3 ... x_N) \tag{4.60}$$

The sensitivity coefficient is then

$$c_1 = \frac{\Delta y}{\Delta x_1} \tag{4.61}$$

This process is repeated for all the inputs into the calculation.

4.5.2.2 Combination of uncertainties

Once the standard uncertainties and sensitivity coefficients for all the measurements have been calculated, they are combined to give the overall standard uncertainty of the calculation using equation (4.62) below.

$$u_c(y) = \sqrt{\sum_{i=1}^{N} c_i^2 u^2(x_i)} \tag{4.62}$$

In the situation where the calculation is itself used in a further calculation (e.g. coolant heat loads in the heat balance) this value of standard uncertainty is the value that is used. However, if the uncertainty of the calculation is to be quoted as part of the result it must be expanded to a pre determined confidence interval.

The expanded uncertainty is calculated by applying a coverage factor, k, to the standard uncertainty. In this thesis, the coverage factor used was $k = 2$ which gives a level of confidence of approximately 95%.

$$U = U_{95} = k\,u_c(y) \tag{4.63}$$

4.5.2.3 Example of propagated uncertainties

As with the previous example, this example is based on the data collected during the second mixture test Run 1. This time however, the coolant heat load across the reflux condenser is used. The coolant heat load is calculated using the right hand side of equation (4.7). The increments used in the calculation of sensitivity coefficients were the combined standard measurement uncertainties calculated using the method described above.

It should be noted that in this example, as in all of the uncertainty calculations performed for this work, absolute uncertainties were used, and were only converted to dimensionless form at the end of the calculation.

The result of the analysis presented in Table 4.3 is that the combined standard uncertainty of the estimation of coolant heat load across the reflux condenser is ±27.08 W (±1.82%). This is the value that would be used in any further calculations involving the condenser heat load (heat/mass balance).

If quoting the condenser heat load as a final result, the expanded uncertainty would be used. The expanded uncertainty of the coolant heat load in the reflux condenser is ±54.16W (±3.64%) to a level of confidence interval of 95%.

It is interesting to note that the absolute standard uncertainty was low compared to most of the other runs. However, because the selected run had a relatively low heat load, the dimensionless value is quite high. This can be quite a common occurrence and illustrates the need for both absolute and dimensionless values to give the full picture.

A full uncertainty analysis for pentane run P2.2 is included in appendix B. It was felt that this run was representative of the experimental data, and shows how the methods described above were utilised in order to perform a full analysis across all of the facility calculations.

Data for run M2.2			
Measurement	Flow rate	Tc_{in}	Tc_{out}
Value (x_i)	$5.816*10^{-5}$	39.359	45.540
Standard uncertainty $(u(x_i) = \Delta x_i)$	$1.39*10^{-7}$	0.079	0.078

Calculations		
Nominal Value	y (W)	1489.28
Sensitivity coefficients		
Flow rate	c_1	$2.56*10^{7}$
Tc_{in}	c_2	$-2.41*10^{2}$
Tc_{out}	c_3	$2.41*10^{2}$
Combined Standard Uncertainty		
Absolute	$u_c(y)$ (W)	27.08
Dimensionless	$u_c(y)$ (%)	1.82
Expanded uncertainty		
Absolute	$U(y)$ (W)	54.16
Dimensionless	$U(y)$ (%)	3.64

Table 4.3: Uncertainty analysis example: Propagated uncertainty of dump condenser heat load

5 Experimental Data and Results

In this chapter, the data collected during the project are presented together with the results of the basic analysis. The quality of the data is considered by examining temperature profiles and heat balances, and discussion is given to the heat transfer coefficients and separations achieved.

Three separate sets of data were collected, all of which contribute to the findings of the project. Single component tests on AnalR grade n-pentane (pentane) and 2,2,4-trimethylpentane (iso-octane) were conducted as were single component flooding tests with iso-octane and binary mixture tests using pentane and iso-octane. The three sets of data are considered separately in this chapter and in Chapter 6.

5.1 Experimental Programme

This project is a follow up to the work of Alan Bartleman, to whom credit is due for the hard work of commissioning the experimental facility. When designing the experimental programme for this project, the data presented by Bartleman (2001) were reviewed and operating ranges selected to confirm and expand his findings. One example of this is in the single component work where in the results presented here condensate film heat transfer coefficients were measured over a much wider range of Reynolds numbers.

It is for the same reason that pentane and iso-octane were selected as the test fluids. These fluids were chosen for the Bartleman (2001) work for a number of key reasons:

- Customers of the sponsoring organisation HTFS indicated their preference for hydrocarbons as the test fluid.

- The two components had to be miscible, have well known physical properties and vapour/liquid equilibrium.

- To enable accurate composition measurements from mixture densities, the two components had to have sufficiently different densities

- The boiling points of the fluids had to be different enough for separation to occur but within the upper operating limit of the facility of 120°C.

- It was paramount that the fluids were not overly dangerous as the design of the facility meant the operator had to handle the fluids manually during filling and emptying.

The experimental programme was thus designed to study the behaviour of the two single hydrocarbons and a binary mixture in normal (non-flooding) operation with some test work to analyse behaviour at and above the flooding limit.

Prior to the main body of test work, a single component test on iso-octane was carried out to act as a re-commissioning test after the improvements to the facility and operating procedures described in Chapter 3 were implemented. The data from this test are not reported. A second commissioning test was also carried out before the first mixture data were collected to confirm the operation of the sampling loop. Again the data are not reported here.

In all, 30 single component runs are reported (13 iso-octane and 17 pentane runs), each consisting of 3 repeats. 55 binary mixture runs (spread over three bulk liquid compositions) are also reported as are 17 flooding runs. To allow a more complete flooding analysis, some of the single component data were added to the data set giving a range from well below to well above the flooding point. The flooding data are considered further in Chapter 6. All the reported data can be viewed in full in Appendix E, and a short summary of the controlled variables is given in Table 5.1.

5.1.1 Single component data

The main objective of the single component tests was to collect data to allow evaluation of the condensate film heat transfer coefficient at any local point in the tube over a wider range of conditions than those presented by Bartleman.

The operating limits were found by trial and error. In the lower limit, there had to be a large enough vapour flow to ensure condensation in the dump condenser. With total condensation in the reflux condenser the heat transfer area is unknown and there was no way to indicate at what height in the tube the condensate film began to form. The lower limit was found by a combination of low heat input and a small temperature difference between the vapour and cooling water to discourage a fast condensation rate

The upper limit was the vapour velocity that caused flooding to occur at the tube entrance. It was found that in the pentane tests, the flooding point could never be reached and the upper limit was set by the maximum available heat input and a large temperature difference between the vapour and coolant.

	Pure	Mixtures	Flooding
Bulk Fluids	Iso-octane Pentane	3 compositions of iso-octane/pentane mixture	Iso-octane
Runs	30	55	17
Heat Input	1.5 – 6.0 kW	2.5 – 5.8 kW	2.0 – 4.8 kW
Pressure	0.10 – 1.99 bar	0.76 – 1.93 bar	0.16 – 0.33 bar
Boiler Temperature	35.3 – 57.5 °C	71.0 – 99.5 °C	45.1 – 64.0 °C
Coolant inlet temperature	19.6 – 39.5 °C	29.2 – 44.2 °C	34.0 – 35.9 °C
Coolant outlet temperature	29.3 – 49.5 °C	37.3 – 53.8 °C	41.9 – 53.3 °C
Coolant flow rate	$6*10^{-5}$ m³/s	$6*10^{-5}$ m³/s	$6*10^{-5}$ m³/s

Table 5.1: Summary of experimental programme

5.1.2 Mixture data

Mixture tests were used to collect data to allow development of the modelling techniques discussed in Chapter 7. The ranges were designed to incorporate and expand on the results reported by Bartleman (2001).

The lower operating limit was similar to that of the pure component tests in that partial condensation was a requirement in the reflux condenser. It was more crucial in the mixture tests as the composition of the vapour leaving the reflux condenser was measured via the condensate in the dump condenser. To allow accurate measurements of there had to be a significant temperature rise in the dump condenser coolant.

Due to the presence of pentane, the flooding position was never reached in the mixture tests and hence the upper limit was set by the maximum heat input of the facility and the pressure and temperature limits of the physical property equations, 2 bar and 100 °C respectively.

The bulk liquid compositions selected were pentane mole fractions 0.245, 0.150 and 0.340 denoted by mixture 1, mixture 2 and mixture 3 respectively. The first and last of these were repeats of mixtures tested by Bartleman with the intention of expanding the range of data for each bulk composition.

A number of runs in both the single component and mixture tests were rejected. The runs in question and the reasons for rejecting the data are detailed below.

	Runs rejected	Reason
Single component	I6.1 I6.2 I6.3 I11.1 I11.2 I11.3	Tube accidentally flooded
	I10.1 I10.2 I10.3	Steady state not yet reached
Mixtures	M1.8 M1.9	$T_{v\,in,\,sat}$ >100 °C (outside physical property range)
	M3.5 M3.10	Large difference between $T_{v\,out}$ and $T_{v\,out,\,sat}$
	M1.18 M3.6	Composition measurement error

Table 5. 2: Data rejection criteria

5.2 Heat balances

Based on the heat flows displayed in Figure 5.1, the overall heat balance for the experimental facility was defined as the ratio of measured heat removed from the facility, $\dot{Q}_o$, to the heat input to the boiler, $\dot{Q}_B$, calculated using equation (4.11). It was assumed that all of the heat supplied from the cartridge heaters was transferred to the vapour entering the tube (negligible heat losses in the boiler) and the heat input was taken as the value measured by the wattmeter. It was also assumed that there were no heat losses from either of the condensers. The heat out was taken as the heat gained by the coolant in the reflux and dump condensers as measured by the respective PRTs and flow meters.

In all of the data, the heat gained by the coolant was less than the heat input to the boiler. As the level of heat supplied to the boiler was increased the heat balance improved, and better heat balances were recorded in the single component data than in the mixture data. This is displayed in Figure 5.2. These findings are similar to those of Bartleman (2001), who recorded heat balances of 0.85 – 0.93 for pure component work and 0.83 – 0.87 for binary mixtures on the same facility. Bartleman indicated that either heat losses or inaccurate measurements were to blame for the poor values, and although he did not measure heat loss he suggested there was scope for a more detailed analysis.

In this work, the instrumentation was overhauled and measurements on the coolant side and the wattmeter were known to be accurate. These results therefore suggest that the assumption of no heat losses was incorrect.

If heat losses were to blame for the poor heat balance, then it stands to reason that higher losses would be expected when the facility runs at a higher temperature when the heat input is also higher. This seems to contradict Figure 5.2 which indicates that the heat balance improved at higher heat input levels. In Figure 5.2 the heat balance was reported as the ratio of heat out to heat in. This is slightly misleading as it does not give any information on the levels of heat loss at each respective data point. The same data are presented in Figure 5.3 and Figure 5.4 where the differences between $\dot{Q}_o$ and $\dot{Q}_B$ are plotted against the heat input and boiler temperature respectively.

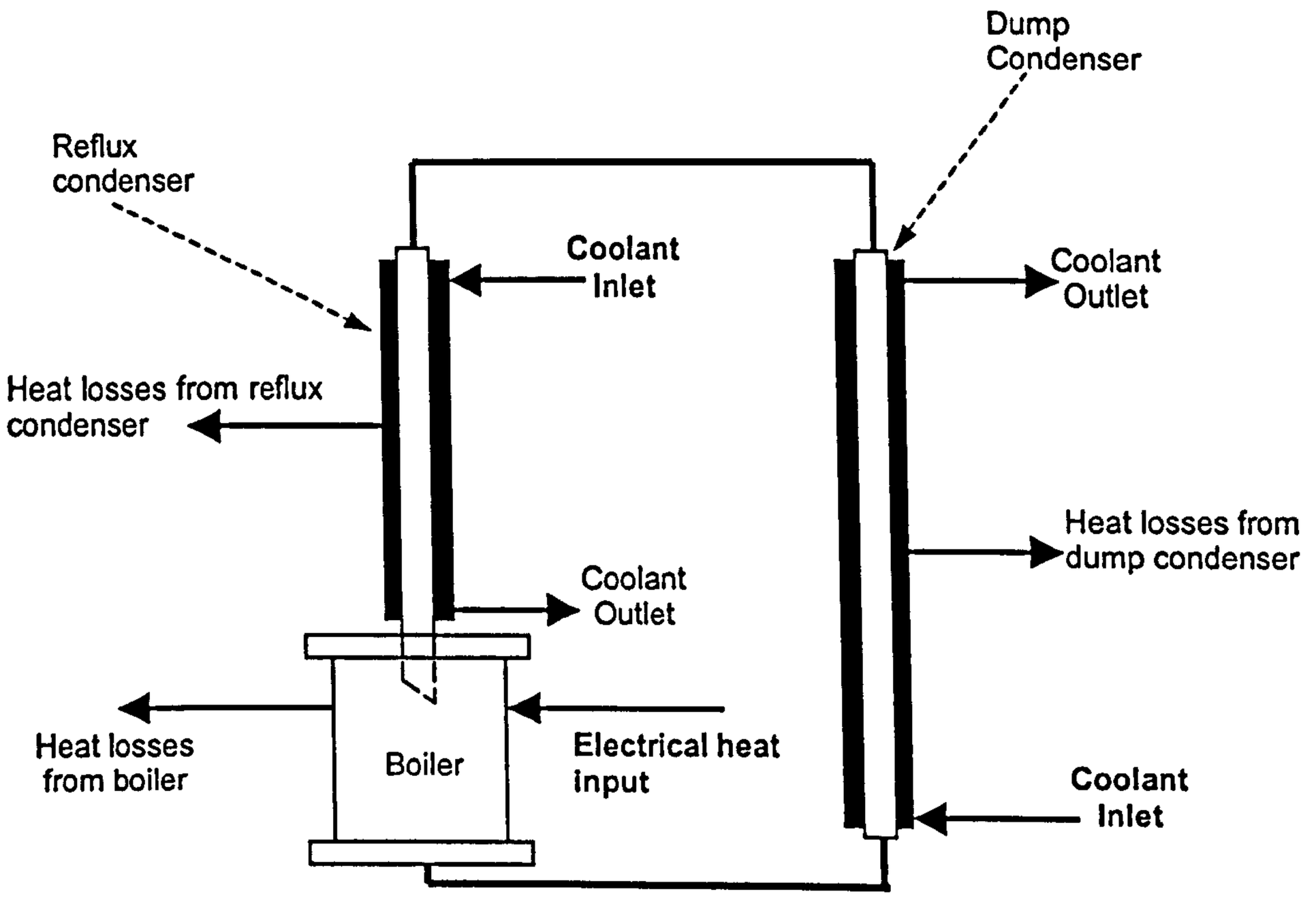

Figure 5.1: Heat flows in the experimental facility

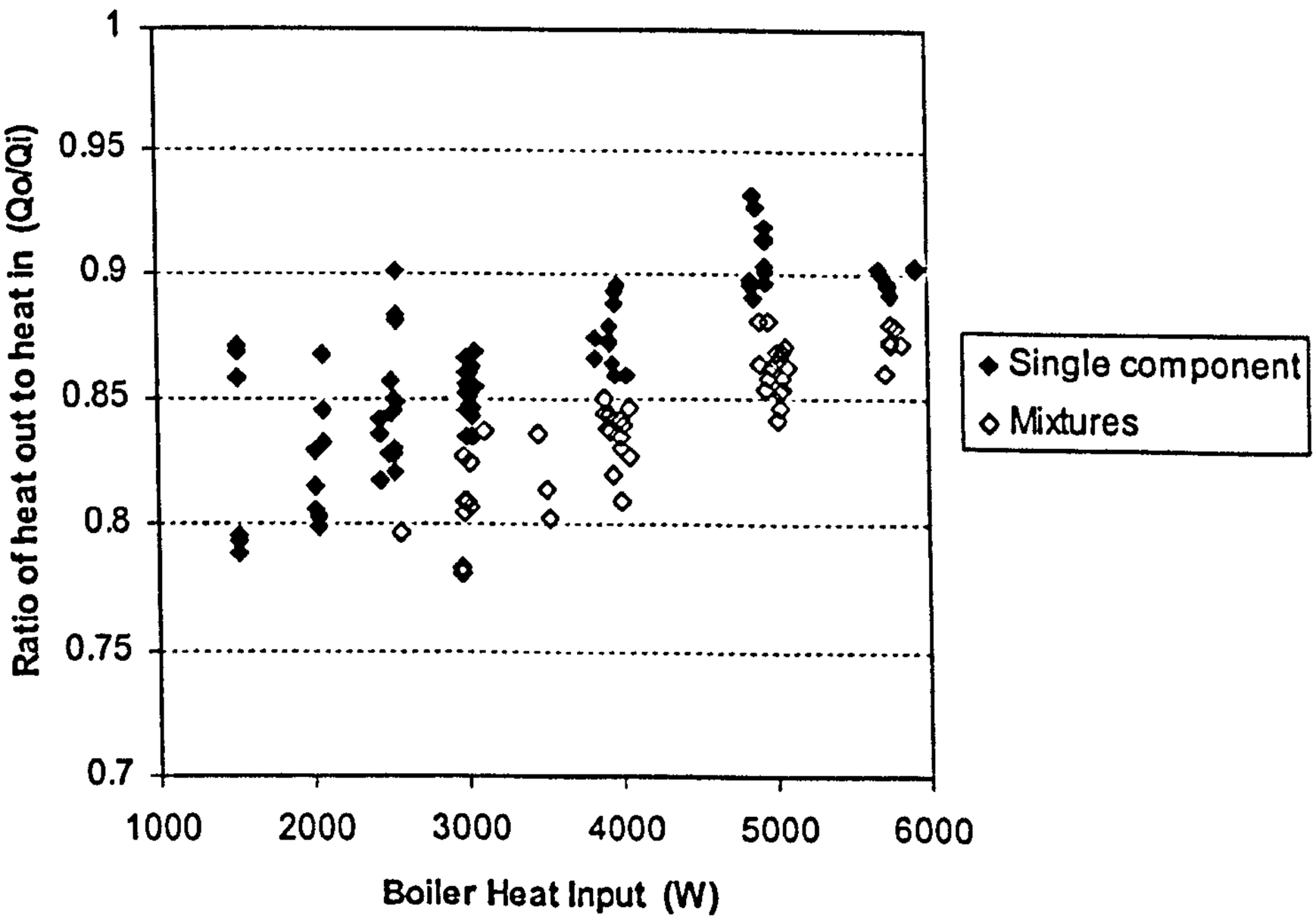

Figure 5.2: Overall heat balance results

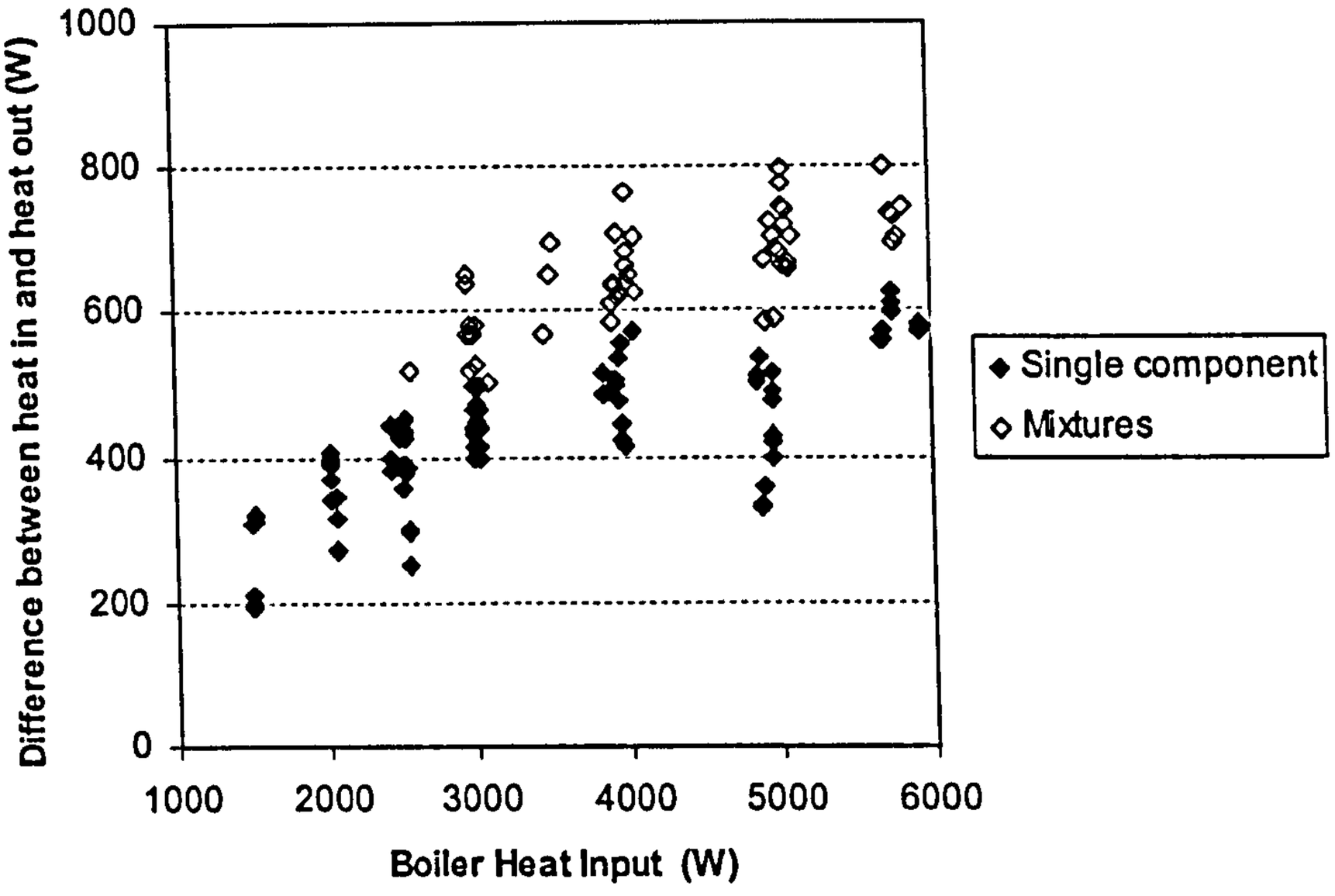

Figure 5.3: Difference between heat input and calculated heat out against heat input

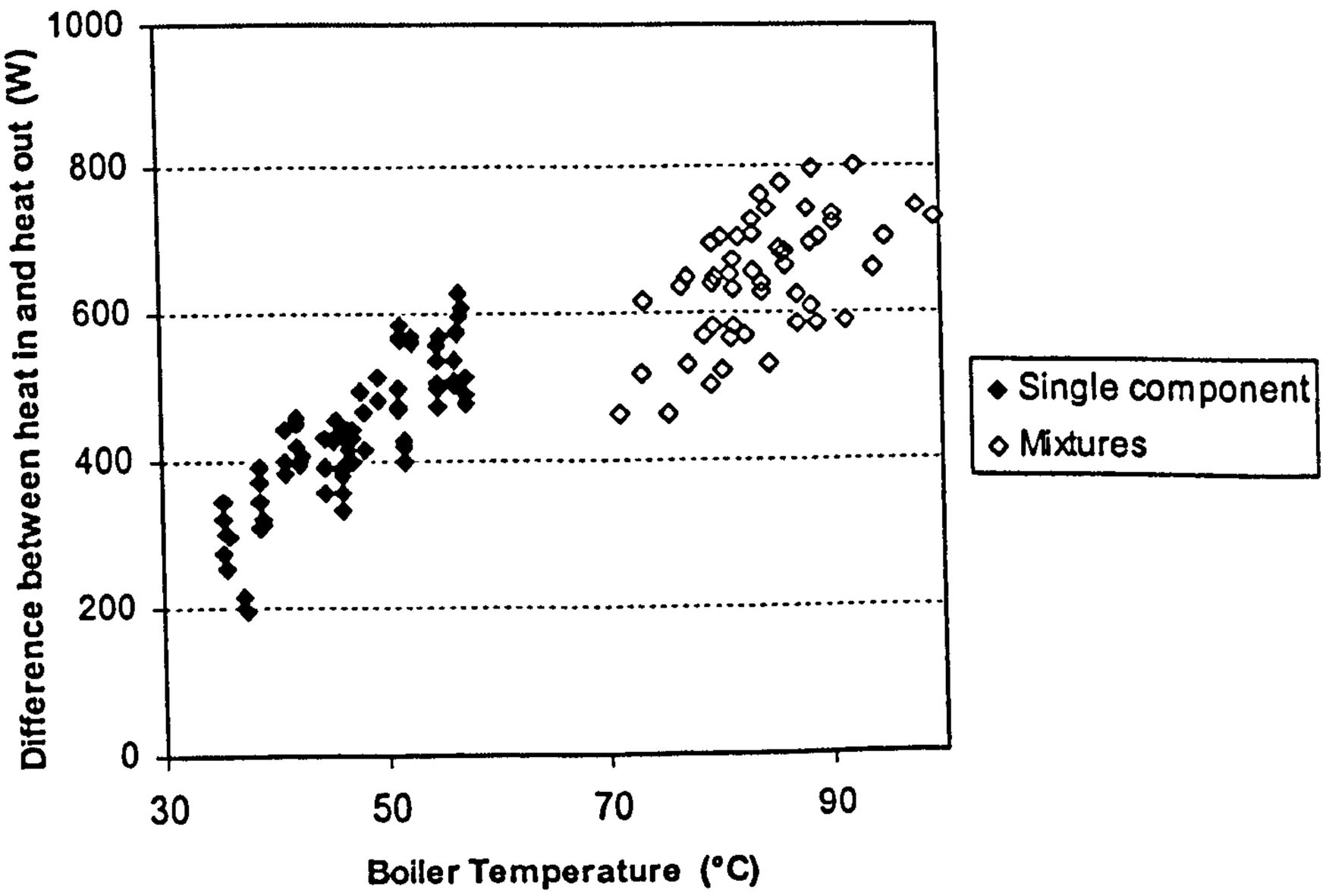

Figure 5.4: Difference between heat input and heat out against boiler temperature

It is apparent from these figures that more heat is unaccounted for when the facility runs at a higher temperature. This seems to confirm that there were unexpected heat losses in the facility. With the heat balance measurements crucial to the mass balance it was vital to discover the location of the heat losses.

So far, the sampling loop has not been considered in the heat balance. The sampling loop was run only for short intervals when collecting data in the mixture tests. When the results were actually collected the pump was shut off and the densitometer isolated to allow the reading to stabilise. With no flow round the loop and the small surface area of the narrow bore pipes in the loop, it was assumed that the heat lost in the sampling loop was negligible.

5.2.1 Location of heat losses

After a detailed investigation it was concluded that practically all the heat losses were from the boiler. Both of the condensers were well lagged as were the coolant pipes and no significant loss of heat was expected from them. This leaf the boiler as the most likely place for any heat to be lost. In later tests, a thermocouple was fitted to the surface of the lagging at the bottom test section. To obtain a worst case scenario, the entire condenser surface was assumed to be at this temperature. Calculations showed that the expected rate of heat loss from the condenser was of the order of 1.5% of the heat input, a value that was assumed negligible.

The boiler was also the hottest part of the facility, and although most of the surface of the boiler is lagged, the two view ports and surrounding flanges were not. When the facility was running, these flanges, the pressure measurement tapping and the temperature measurement probe were found to be hot to touch. Further, the flow of air round the vapour containment cabinet (to purge any potential hydrocarbon leak) was found to be concentrated over the boiler towards the adjacent outlet duct.

A simple CFD model of the cabinet and the main equipment inside the cabinet was constructed to visualise the flow of air round the facility. Figure 5.5 shows the air flow accelerating over parts of the boiler surface to the outlet duct, and confirms the air to be practically stagnant over most of the lagged surface of the reflux condenser. Although there is a significant flow over most of the dump condenser the temperatures were usually too low in the dump condenser for there to be any significant heat lost.

It was further assumed that all of the heat transferred to the air was removed from the cabinet by the air. This means that there was no heat transfer between the air and the cabinet walls. Calculations using the free convection method described in the previous chapter indicated that the amount of heat lost through the cabinet walls was a maximum of 3 W proving the assumption to be justified.

The conclusions of the investigation were that the boiler had unlagged hot surfaces, (which the condensers did not), and that the flow of air caused heat to be transferred from the boiler surfaces by forced convection unlike the reflux condenser where heat would be transferred by free convection. It was therefore concluded that, effectively, all of the unexpected heat losses were from the boiler. Some heat losses from the boiler were confirmed by visual observations made using the view ports. Condensation was visible on the inside walls of the boiler and on the temperature measurement probe.

Taking this one step further, if all the heat lost from the boiler was transferred to the circulating air, then measurements of the temperature rise of the air should give a good estimation of the heat losses.

5.2.2 Estimation of heat losses

Thermocouples were fitted just inside the openings of the entrance and exit air ducts and readings taken of the air velocity inside the ducts. These readings agreed with the flow rates quoted by the fan manufacturer, a value that was kept constant through the test work.

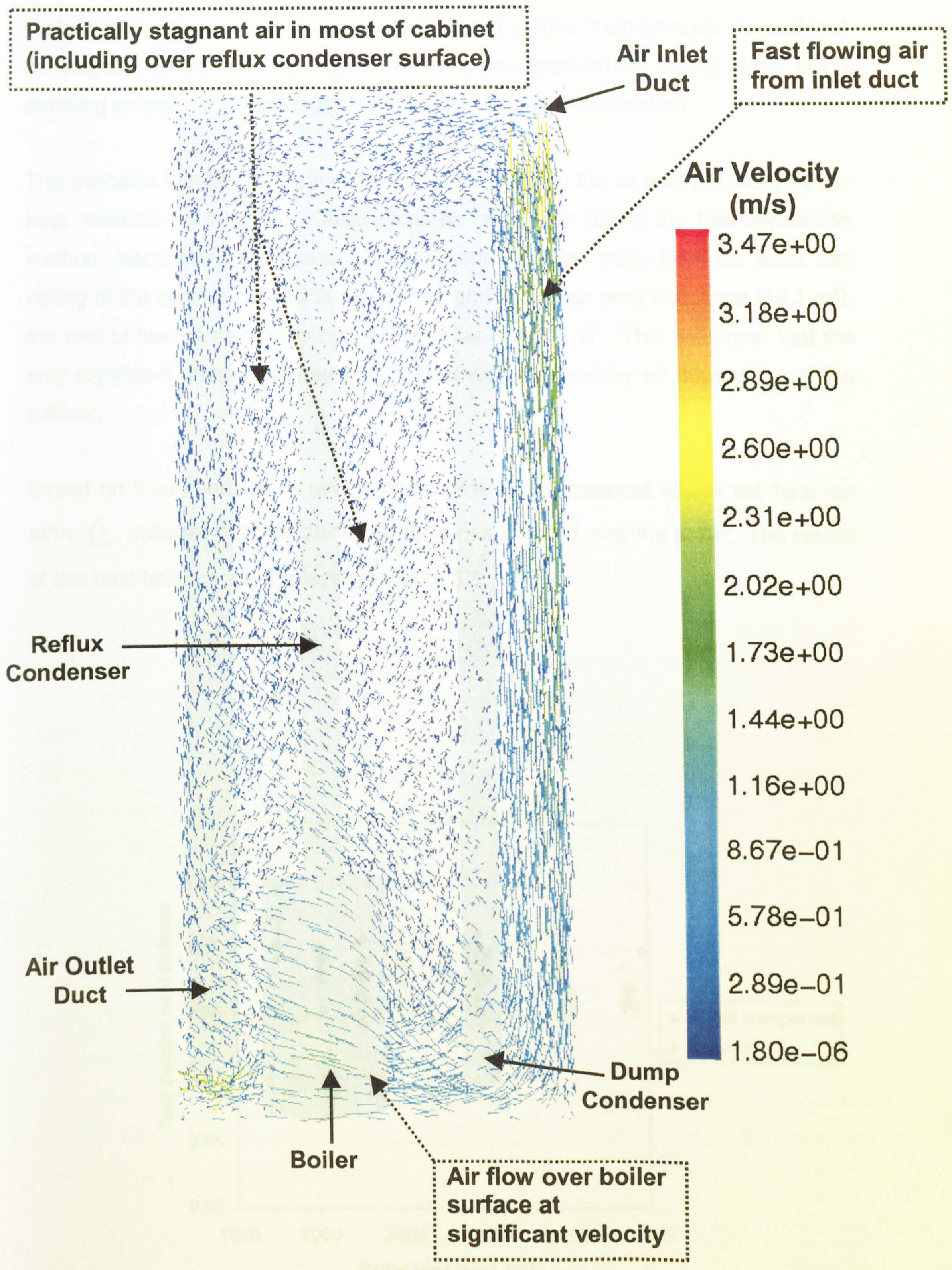

Figure 5.5: CFD representation of air flow over major equipment in experimental facility

A thermocouple was also fitted to a relatively stagnant area high up in vapour containment cabinet (i.e. well away from the boiler). This thermocouple showed that the stagnant air slowly heated up as the facility was approaching steady state. Upon reaching steady state, the temperature was found to remain constant.

This indicates that the heat transferred from the boiler to the air was balanced by the heat removed from the air. Calculations on convection (using the free convection method described in the previous chapter) and radiation away from the walls and ceiling of the cabinet showed that even though the surface area was large (19.1 m²), the rate of heat removal was only of the order of 1 – 5 W. This confirmed that the only significant unexpected removal of heat was removed by air flowing out of the cabinet.

Based on these findings, a new heat balance was considered where the heat out term, $\dot{Q}_o$, included the heat gained by the air as it flowed over the boiler. The results of this heat balance are displayed in Figure 5.6.

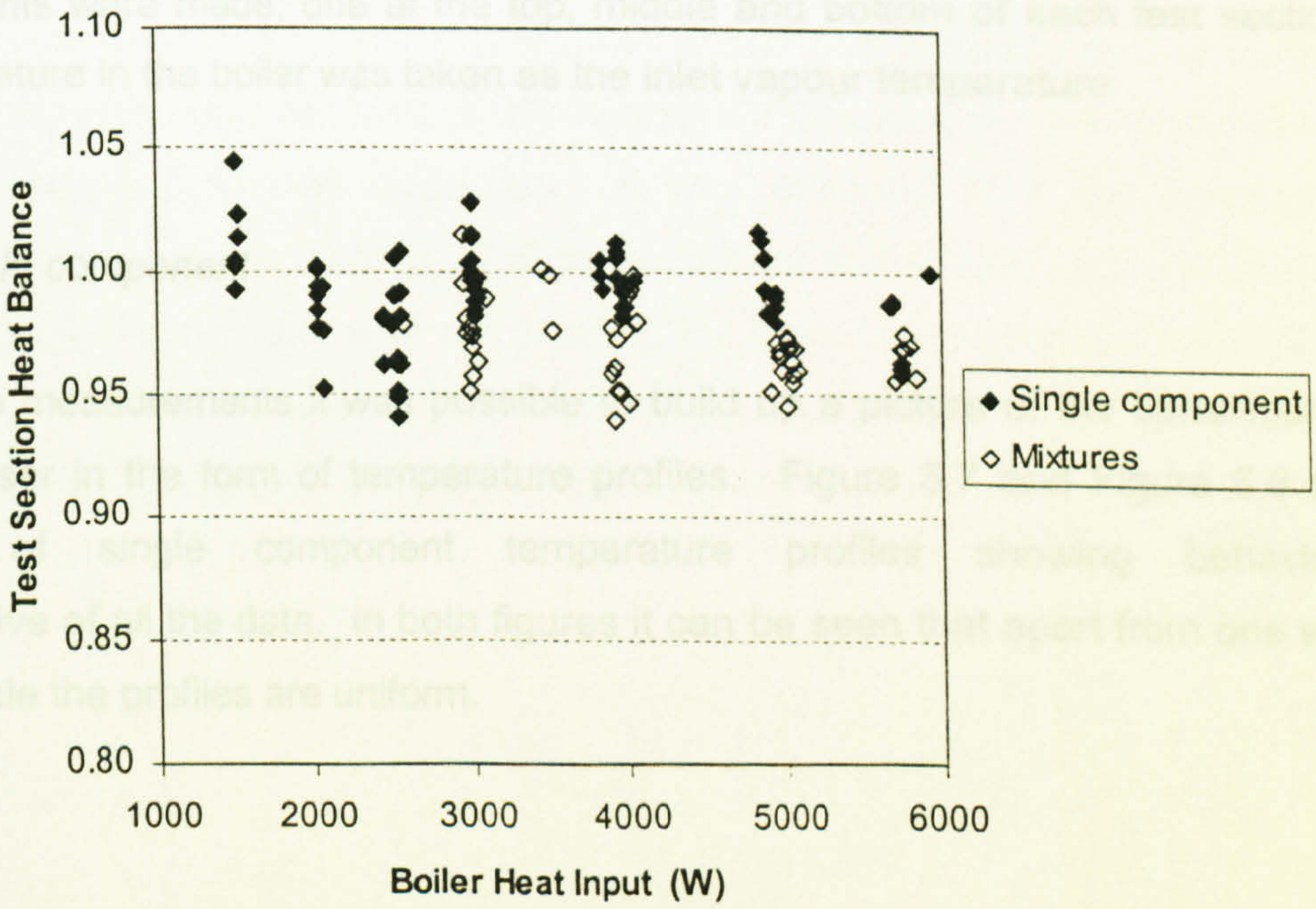

Figure 5.6: Overall heat balance with heat losses included in heat out term

In the single component data the ratio of heat out to heat in was in the range 0.94 – 1.04 with a mean of 0.99 whereas in the mixture data the ratio lay in the range 0.95 – 1.01 with a mean of 0.97. These results indicate that the heat gained by the air from the boiler was a relatively accurate estimation of the heat losses from the process.

The importance of the heat balance is the effect on the calculation of mass balance where the coolant temperature rises are crucial. The positive side is that the findings above indicate that the cooling water temperature rise measurements were accurate, but the negative is that the wattmeter measurement could not be used directly to accurately estimate the amount of vapour generated. This value would have been useful as an independent check on the mass balance.

5.3 Temperature profiles and saturation conditions

As discussed in chapter 3, the temperatures of the vapour and coolant were measured at the top of the reflux condenser and at two intermediate points. The reflux condenser was made up of three duplicate test sections with the intermediate points located between adjacent test sections. The temperature of coolant leaving the bottom of the tube was also measured. In total, 9 wall temperature measurements were made; one at the top, middle and bottom of each test section. The temperature in the boiler was taken as the inlet vapour temperature

5.3.1 Single component

Using these measurements it was possible to build up a picture of the behaviour of the condenser in the form of temperature profiles. Figure 5.7 and Figure 5.8 are examples of single component temperature profiles showing behaviour representative of all the data. In both figures it can be seen that apart from one wall thermocouple the profiles are uniform.

The vapour saturation temperature was calculated from the pressure in the boiler using PPDS. In both Figure 5.7 and Figure 5.8 it can be seen that the temperature in the boiler (i.e. vapour inlet temperature) is close to the expected saturation temperature . In general there was better agreement in the pentane data than in the iso-octane data with agreements to within ±0.3°C and ±1.0°C respectively.

This is an important result as it establishes that the temperature and pressure measurements agree with each other, a point that is discussed in 5.3.3. As there was no measurement of the (small) pressure drop, the saturation temperature at the top of the tube was taken to be the same as the value at the bottom of the tube.

Based on the assumption of no heat losses from the condenser, the relative sizes of the coolant and process side heat transfer coefficients can be estimated. In all of the single component data, there was a much larger temperature difference between the vapour and wall than the wall and coolant. This means that the largest resistance is on the process side. In single component condensation there are no gas phase heat transfer resistances, so it can be said that the condensate film is the controlling resistance.

It should be noted that the profile of the vapour temperature is slightly curved. The difference in temperature between the boiler and the vapour outlet was in the range 0.9 – 1.8°C for pentane and 1.4 – 1.7°C for iso-octane. Condensation of a saturated pure vapour through heat removal is an isothermal process, so no temperature vapour temperature drop was expected. It was assumed that the measured temperature drop was a combination of slight superheat in the boiler and a pressure drop. As the reflux condenser was not flooding the pressure drop through the tube would be expected to be very small, so any pressure drop would have been associated with the contraction from the boiler to the reflux tube.

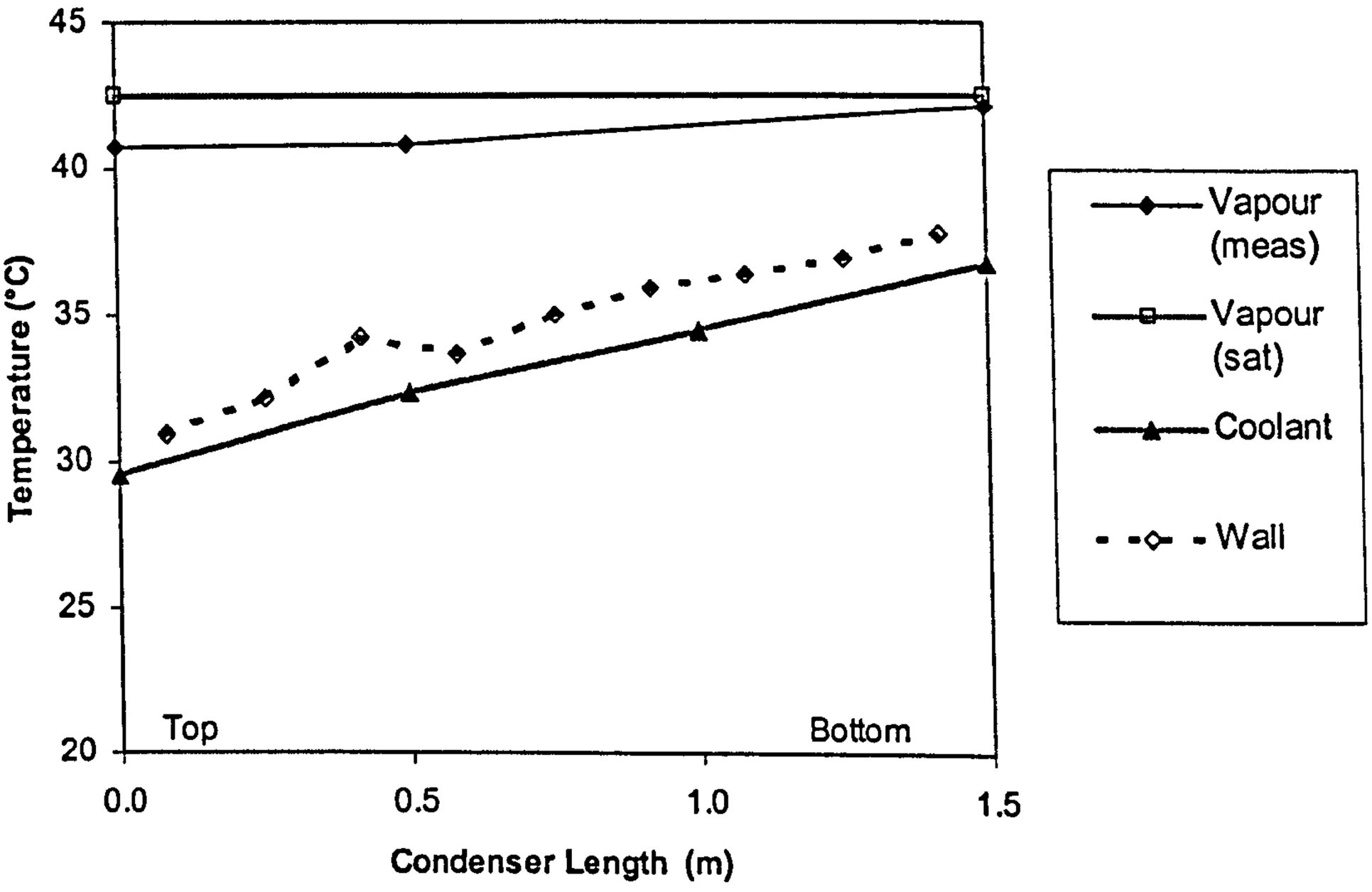

Figure 5.7: Temperature profile for pentane run 2.2

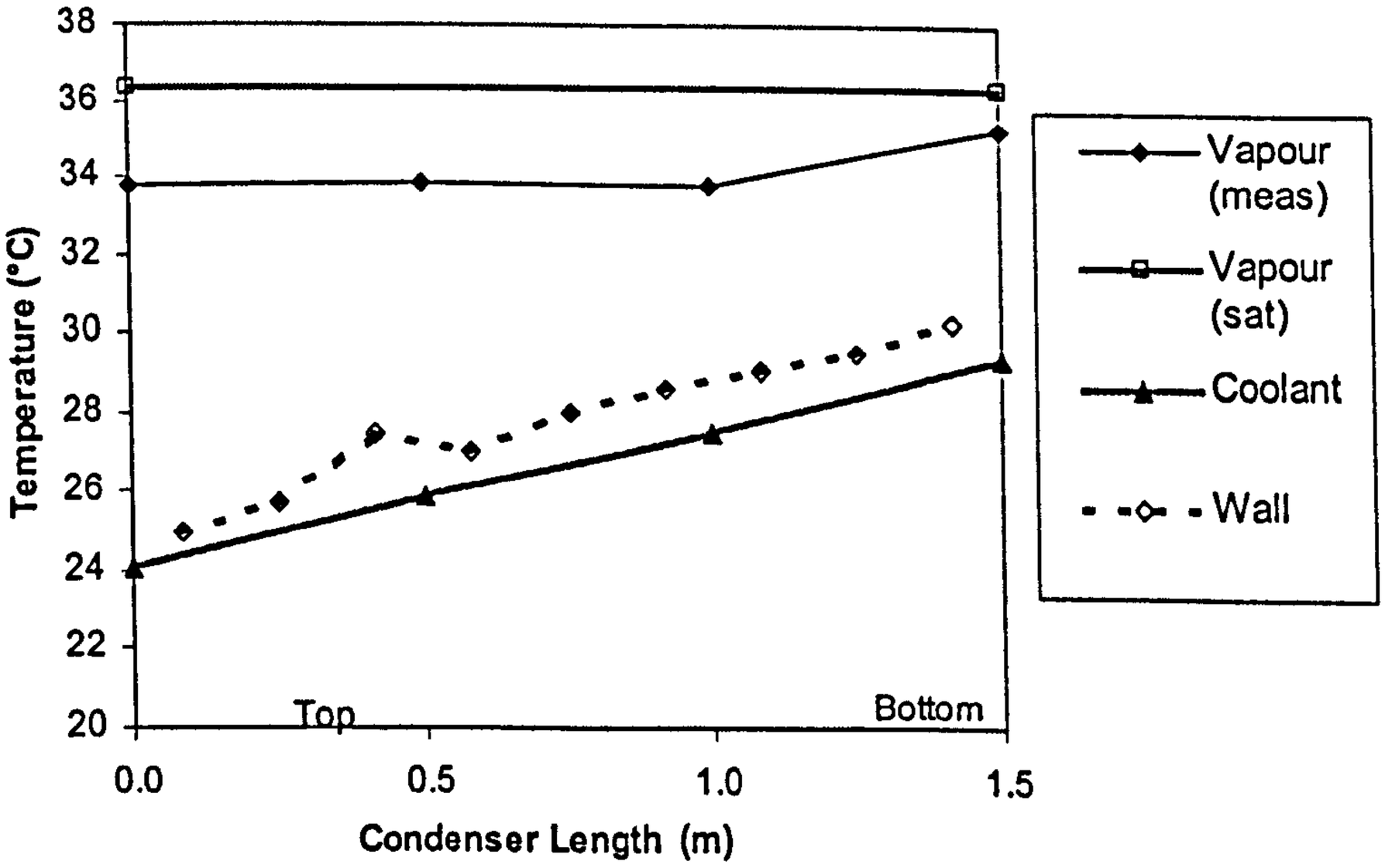

Figure 5.8: Temperature profile for iso-octane run 5.2

Some calculations were performed to estimate the pressure drop. Assuming an entrance loss of a single velocity head, these calculations showed that the entrance pressure drop would have been less than 10 Pa. As the temperature drop associated with this is almost negligible, it was assumed that the vapour was slightly superheated in the boiler.

It was noticed that, in some cases, the vapour temperature measured at the top of the tube was higher than the temperature at the two intermediate points in the tube. The cause of this was put down to experimental error with the intrusive thermocouples. The probes measuring vapour temperature at the two intermediate points were subject to the condensate film flowing over them. It was assumed that conduction along the probe length caused the measured temperature to be slightly lower than the actual temperature. The effect was larger in the highest of the intermediate measuring positions as the temperature difference between the coolant and vapour was higher causing the condensate film to be more subcooled at that point.

This effect did not occur in the measurement at the top of the reflux condenser tube as the thermocouple was positioned slightly above the starting location of the condensate film, nor at the vapour inlet where the measurement was made in the boiler.

5.3.2 Mixtures

Applying a similar analysis to mixture temperature profiles (see Figure 5.9 and Figure 5.10) yields some important observations. Again, the temperature difference between the vapour and wall is much larger than the difference between wall and coolant indicating a much higher resistance on the process side than the coolant side.

It should be noted that in the mixture data the ratio of these two temperature differences changed with a much higher relative resistance on the process side than in the single component data. As it is not expected that the coolant heat transfer coefficient would change significantly, this is consistent with the fact that there are gas-phase resistances expected in the condensation of mixtures and confirms that the reflux condenser was behaving as expected.

Although the saturation temperature was calculated in the same way as the single component data (using the measured pressure in the boiler), there is a drop in its value through the condenser. This is due to the change in composition of the vapour as the heavier component iso-octane is condensed preferentially.

Surprisingly, there is a large difference between then measured temperature at the vapour inlet and the dew point temperature based on the calculated vapour composition. Over all the mixture data this difference is in the range 2.2 to 7.1°C with a mean value of 4.2°C. In all cases the measured temperature is lower than the saturation temperature, a surprising result as with the cartridge heaters in the boiler a degree of superheat may be expected. At the top of the tube there is much better agreement between measured temperature and predicted dew point based on the measured composition in the dump condenser. Here the maximum difference was 1.1°C indicating that the vapour approached saturation through the condenser. The causes and implications of these findings are discussed below. but it should be noted that the vapour inlet composition used in the estimation of saturation temperature was calculated using the original mass balance based on the two condensate compositions measured in the densitometer.

5.3.3 Saturation temperature problem

The large differences between measured and saturated temperature at the reflux condenser inlet shed doubt on the measurements inside the boiler and the measurements that contribute to the mass balance. If the measured and saturated temperatures had been equal, that would have served as an independent check on the accuracy of the mass balance, which is important since neither the vapour inlet flow rate nor composition were measured directly.

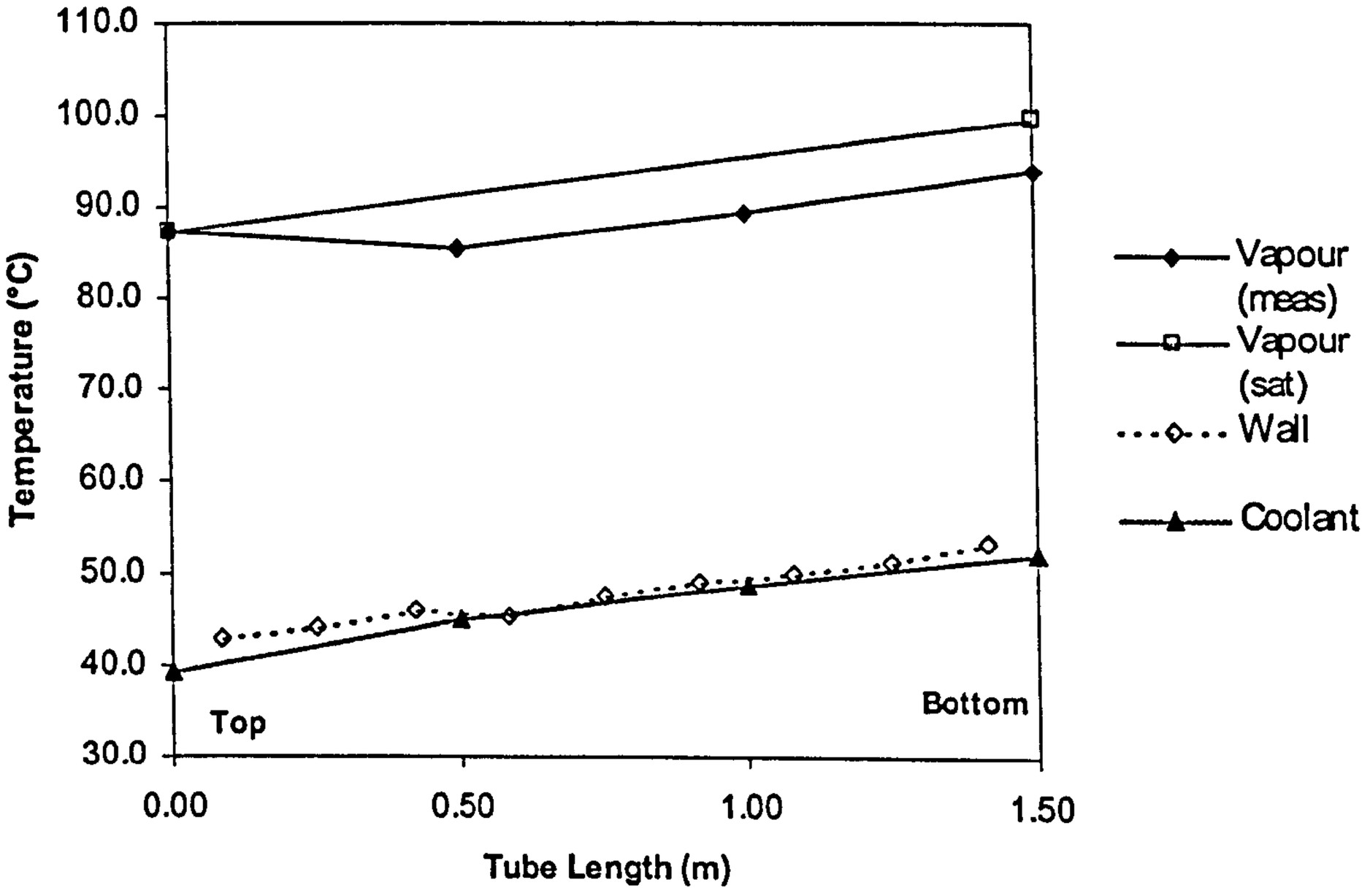

Figure 5.9: Temperature profile for mixture run M1.6

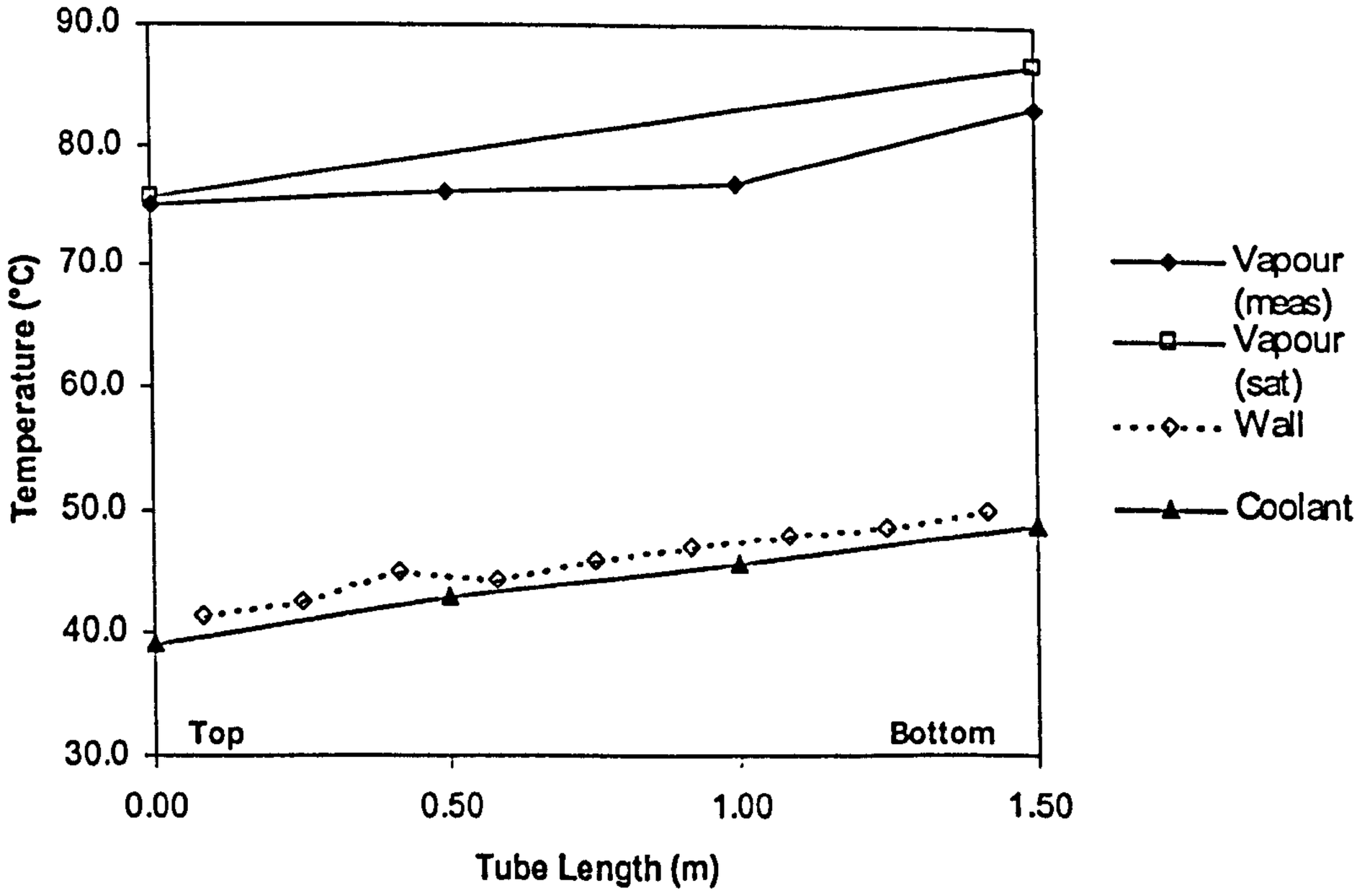

Figure 5.10: Temperature profile for mixture run M3.1

It should be noted at this point that similar results were reported by Bartleman (2001) who blamed a poor measurement of pressure in the boiler. Bartleman had used a gauge transducer with an operating range above atmospheric pressure and extrapolated the calibration to sub-atmospheric pressures. As a result, the pressure measurements were unreliable and were ignored. Calculated saturation pressures based on measured temperatures were therefore used in all of Bartleman's calculations.

In the instrument review conducted for this work, the transducer used in the previous project was replaced by a more accurate instrument with an operating range from absolute zero upwards hence this measurement has been ruled out as the cause of the error.

Also as part of the instrument review, the thermocouple measuring temperature in the boiler was replaced by a more accurate platinum resistance thermometer (PRT). This also was expected to measure accurately. Remembering that the measured temperatures in the single component work were well matched by the calculated saturation temperatures (where there is no mass balance involved), there is more evidence that both of these instruments operated properly.

5.3.3.1 Mass balance accuracy

The mass balance was based on the composition of the condensates from the reflux and dump condensers and the coolant temperature rise in each of the condensers. As discussed in 5.2.2, the overall mass balance was confirmed by good heat balance results. In the mixture data the saturation and measured temperatures at the vapour outlet were found to be very close in all of the data. This is the only place where the calculated saturation conditions were based on a single direct composition measurement confirming that the densitometer and sampling loop were operating properly.

To check measurements of the condensate from the reflux tube a series of runs were conducted with total condensation occurring in the reflux condenser.

With total condensation, the composition of condensate returned from the reflux tube would be exactly the same as the vapour entering the tube meaning that the vapour composition could be measured directly and not inferred by a mass balance. Further, it was expected that this value would be accurate as it was known that the sampling loop and densitometer operated as expected. In the data from these tests a large difference was again observed between the expected saturation temperature and measured temperature.

This confirmed that the cause of the error in the mixture data was not the mass balance. Had there been a mass balance error, then the large differences would have been eliminated by running at total condensation. The only conclusion to be drawn was that one of the instruments, although operating properly, was not measuring the expected condition.

5.3.3.2 Pressure measurement

Air leakage tests early in the project proved that the rig was never totally air tight. To combat this problem, the vacuum pump was run for a few seconds before data was collected. One of the advantages of reflux condensers is that they are self venting, with inerts flushed to the top of the reflux tube. The vacuum line was positioned in the top leg between the reflux and dump condensers, so running the vacuum pump would cause any inerts collected here to be removed. Any inerts not purged would be flushed round to the dump condenser by the rush of vapour created when the drop in pressure caused some liquid to flash off.

As a precaution, the six runs used to test the reflux tube at total condensation were split into two halves. Three runs were carried out just after evacuation, and the other three after the rig had been left to stand idle for a weekend. In terms of the saturation temperature problem, exactly the same results were recorded, and air leakage or inaccurate pressure measurement were therefore ruled out as the cause of the error.

5.3.3.3 Temperature measurement

In the preceding heat balance discussion, the fact that heat was lost from the boiler to the surroundings was used to account for previously unaccounted heat losses. One of the causes of this was deemed to be conduction along the length of the temperature probe. The 6 mm diameter probe was fixed into the boiler wall by a compression gland and terminated into a large heavy duty steel end cap which protected the electrical connections.

When the facility was running, the end cap, which was unlagged, was found to be hot to touch. Using the viewing window to the front of the boiler it was possible to see condensation on the measuring probe. Typically, a droplet would form toward the end nearest the boiler wall, and travel along the probe before falling off. During the highest temperature runs, there was more than one of these droplets per second.

Bearing in mind that there was a significant air flow over the part of the boiler in question, it was proposed that heat was conducted along the probe and rejected to the air. This caused parts of the probe near the wall to be slightly cooler than the vapour. This in itself would not cause the probe to measure incorrectly as the measurement is based on the temperature at the end of the probe. It did however result in the probe becoming covered in a thin film of condensate. The possibility arose that the probe was measuring the condensate temperature and not that of the vapour.

There are two reasons why this would have a much less significant effect on the temperature measurement in the pure fluid runs. During the pure fluid runs the liquid boiled at a much lower temperature and the facility as a whole ran at lower temperatures. The driving force for condensation on the probe, the temperature difference between the vapour and the air in the cabinet, was therefore much smaller. If any condensate did form on the probe, there would be no significant effect on the temperature measurement as the condensate would form at the same temperature as the vapour.

This is different to the mixture tests where the condensate forming on the probe would have a different composition and possibly different dew point temperature than the vapour. In general, the heavier component, iso-octane, would condense preferentially thus reducing its partial pressure in the vapour surrounding the probe. The effect of this would be to reduce the dew point temperature of the condensing vapour and the film surrounding the probe. However, considering a standard T-xy diagram for integral condensation (Figure 2.15) it can be shown that in this case the condensate would form at the same temperature as the vapour.

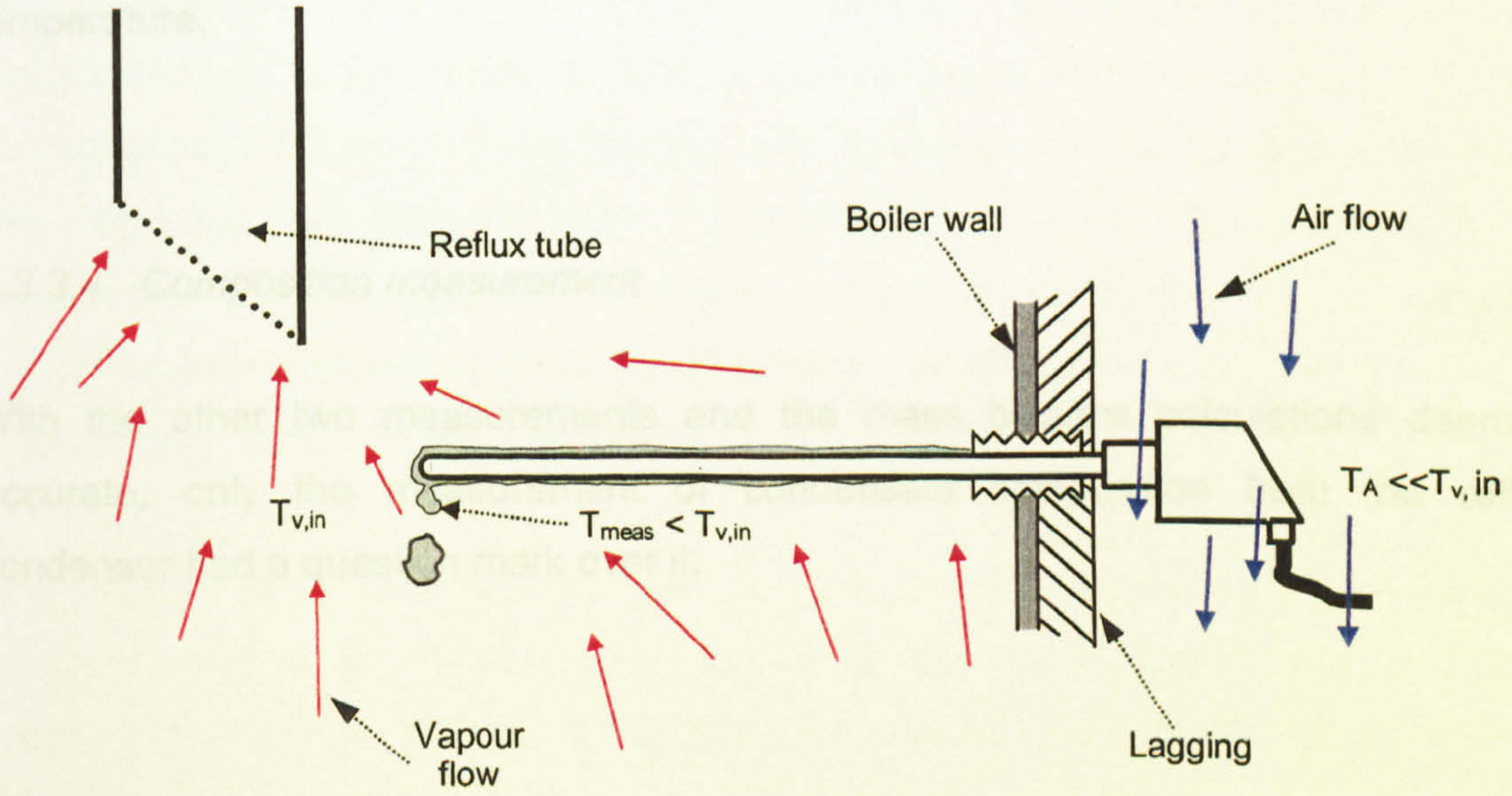

Figure 5.11: Schematic diagram of condensate film forming on temperature probe

If a saturated binary vapour at point A on Figure 2.14 is cooled and partially condensed, the resulting vapour and condensate compositions (tie line DE) are fixed by the value of θ. This is the ratio of vapour left uncondensed to total vapour flow. In the case of a few droplets condensing in the large vapour space in the boiler it can be assumed that the amount of vapour is infinitely larger than the amount of condensate. This means that θ approaches unity meaning that point E approaches point A. The condensate at the vapour-liquid interface forms at the same temperature as the bulk vapour, and any difference between the condensate and vapour temperatures can only be subcooling from contact with the probe.

As the condensate film was very thin and only the parts of the probe near the wall were expected to be cooler than the vapour, it was therefore assumed that the droplets falling into the boiler were at the same temperature as the vapour.

This would indicate that heat losses from the temperature probe did not cause the temperature measurement to be inaccurate. More evidence of this conclusion was gathered by running an extra test with the third mixture (not reported). In this test, a new smaller temperature probe was installed with a smaller end cap. The end cap was also lagged to isolate it from the air flow in the cabinet. In this test, fewer droplets were observed falling from the probe (as would be expected), but the same differences were found between measured temperature and calculated saturation temperature.

5.3.3.4 Composition measurement

With the other two measurements and the mass balance calculations deemed accurate, only the measurement of condensate composition from the reflux condenser had a question mark over it.

The original boiler design diagrams were consulted to obtain information on the condensate collection tray and channel. It was realised that condensate collecting on the tray and running off into the channel was able to interact with warmer vapour as the runoff from the tray was uncovered. Vapour and condensate interactions could also occur in the stub pipe between the reflux condenser and the boiler. Potentially, some of the cooler condensate could be re-evaporated causing a change in condensate composition and incurring a source of error.

In this situation, the lighter component, pentane, would evaporate preferentially and the measured composition would have a lower pentane mole fraction than the condensate leaving the tube. If there was actually more pentane leaving the tube than was measured, then it follows that there would have to also be more pentane in the feed vapour. Further, with a higher pentane mole fraction in the vapour, the expected saturation temperature would be closer to the measured temperature.

By this logic, it seems that previously unaccounted vapour/condensate interaction was the likely the cause of the large difference in temperatures. There are also other uncertainties surrounding the condensate sample withdrawn from the boiler.

For example, at the base of the boiler the condensate channel opened up into the bulk liquid area. With vapour rising above the bulk liquid and condensate falling into the collection channel a natural circulation existed. The condensate flow rate was small compared to the amount of bulk liquid, and the opportunity was there for back mixing through diffusion. Given that the bulk liquid was boiling vigorously, the mixing rate may have been relatively high. As the condensate had a higher pentane mole fraction than the bulk liquid any back mixing reaching the level of the sampling port would case the measurement to be affected in the same way described above for unaccounted vapour-liquid interactions.

It is impossible to know whether or not these situations actually occurred in the condensate channel. What is clear though is that the temperature and pressure measurements in the boiler and the mass balance calculations can be ruled out as the cause of the large errors.

The same cannot be said about the measurement of condensate composition. The densitometer was measuring accurately, but there is a large uncertainty as to whether or not it the samples had the same composition as the condensate leaving the bottom of the reflux tube. It was therefore assumed that the composition measurements in the reflux condenser were unreliable, and they were not used in any of the calculations.

This means that only one composition measurement was available for the mass balance. The pentane mole fraction in the vapour at the bottom of the tube was therefore estimated from the temperature and pressure measurements by assuming saturation. The reflux condensate composition was then found by mass balance as described in 4.2.

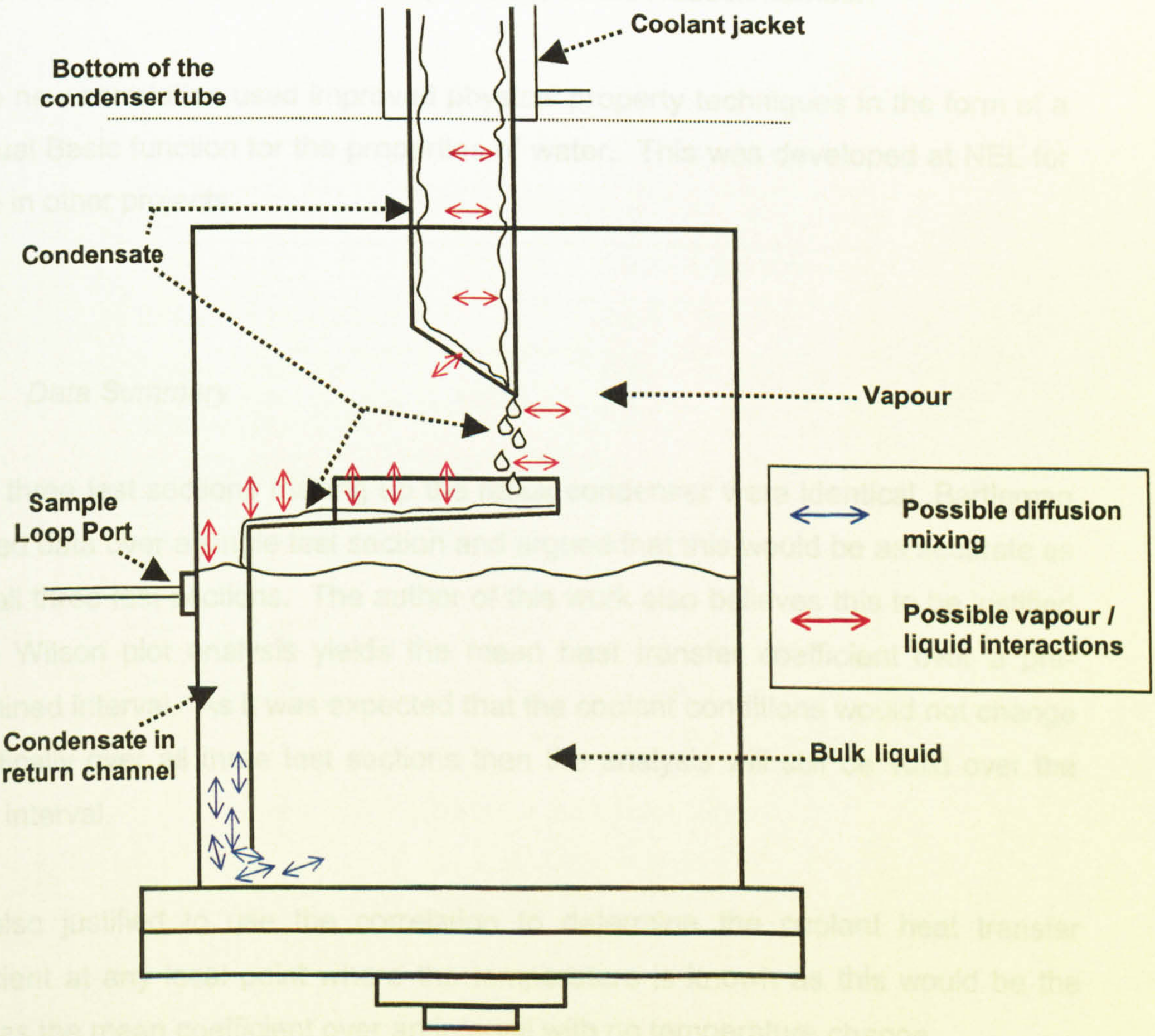

Figure 5.12: Possible causes of composition measurement error

5.4 Heat Transfer Coefficients

5.4.1 Correlation for the coolant heat transfer coefficient

The unique nature of the reflux condenser geometry meant that standard correlations were unsuitable for predicting the coolant heat transfer coefficient when modelling the reflux condenser. A correlation was developed and reported by Bartleman (2001) using the Wilson Plot technique the over a range of coolant conditions. For this work, the author performed a similar analysis, using Bartleman's data, in order to improve on the original correlation. There were two reasons for this:

- Bartleman stated the mean coolant heat transfer coefficient directly in terms of the Reynolds and Prandtl numbers. The analysis was altered slightly to produce a correlation in dimensionless form, in terms of the Nusselt number.

- The new correlation used improved physical property techniques in the form of a Visual Basic function for the properties of water. This was developed at NEL for use in other projects.

5.4.1.1 Data Summary

As the three test sections making up the reflux condenser were identical, Bartleman collected data over a single test section and argued that this would be as accurate as using all three test sections. The author of this work also believes this to be justified as the Wilson plot analysis yields the mean heat transfer coefficient over a pre-determined interval. As it was expected that the coolant conditions would not change dramatically over all three test sections then the analysis will still be valid over the longer interval.

It is also justified to use the correlation to determine the coolant heat transfer coefficient at any local point where the temperature is known as this would be the same as the mean coefficient over an interval with no temperature change.

The main issue of concern over using only the bottom test section was that there may be unaccounted for condensation in the higher test sections. Two possible causes were identified; conduction upwards from the cold wall of the bottom test section to the middle test section resulting in a temperature driving force in the middle test section, and coolant leakage past the isolation valves meaning that the upper test sections were partially cooled.

The coolant and wall temperatures in the upper two test sections were analysed and it was found that the differences between these temperatures and the vapour temperature were almost zero, and were well within the expected tolerances of the thermocouples. It was concluded that it was safe to use only one test section in the collection of data for the Wilson plot analysis. The full set of data used in the development of the correlation is reported in Appendix A6 of Bartleman (2001). A short summary of the relevant ranges is given below.

Facility conditions	
Heat Input	5.90 – 6.05 kW
Boiler Temperature	39.1 – 52.6 °C
Boiler Pressure	7,600 – 14,900 Pa
Coolant flow rate	$6.2*10^{-5}$ - $1.7*10^{-4}$ m^3/s
Coolant inlet temperature	21.2 – 40.1 °C
Coolant Outlet Temperature	34.6 – 48.9 °C
Calculated values	
Coolant Reynolds number	11,950 – 37,740
Coolant Prandtl number	4.19 – 5.29

Table 5.3: Wilson plot data summary

5.4.1.2 Estimation of correlation coefficient

The data was plotted and regression analysis used to obtain the best fit line as displayed in Figure 5.13. There is some scatter in the data but an R^2 value of 0.91 indicates a good fit. The resulting gradient was 61.11 giving the value of K as 0.0164. The final correlation is given in equation (5.1).

$$Nu_c = 0.0164\ Re_c^{0.8}\ Pr_c^{0.4} \qquad (5.1)$$

Using the coolant and wall temperatures, together with the heat load over the test section it was possible to calculate the coolant heat transfer coefficient directly from the data. These values were used to check on the accuracy of the Wilson plot method by comparing the calculated values with those predicted by the correlation over the full set of data. This comparison is displayed in Figure 5.14. It was found that the correlation predicted the calculated coefficients within 11%. In the condensation of hydrocarbons, the controlling resistance was expected to be on the process side. With that in mind, 11% is an acceptable accuracy when it comes to modelling the process.

5.4.2 Condensing film heat transfer coefficients

The main purpose of the single component test work in this project was to study the behaviour of the condensate film heat transfer coefficient under refluxing conditions. The coefficients calculated from the experimental data were compared with the classic Nusselt (1916) theory and the HTFS method, (McNaught, 1984) for predicting condensing film coefficients in vapour down-flow.

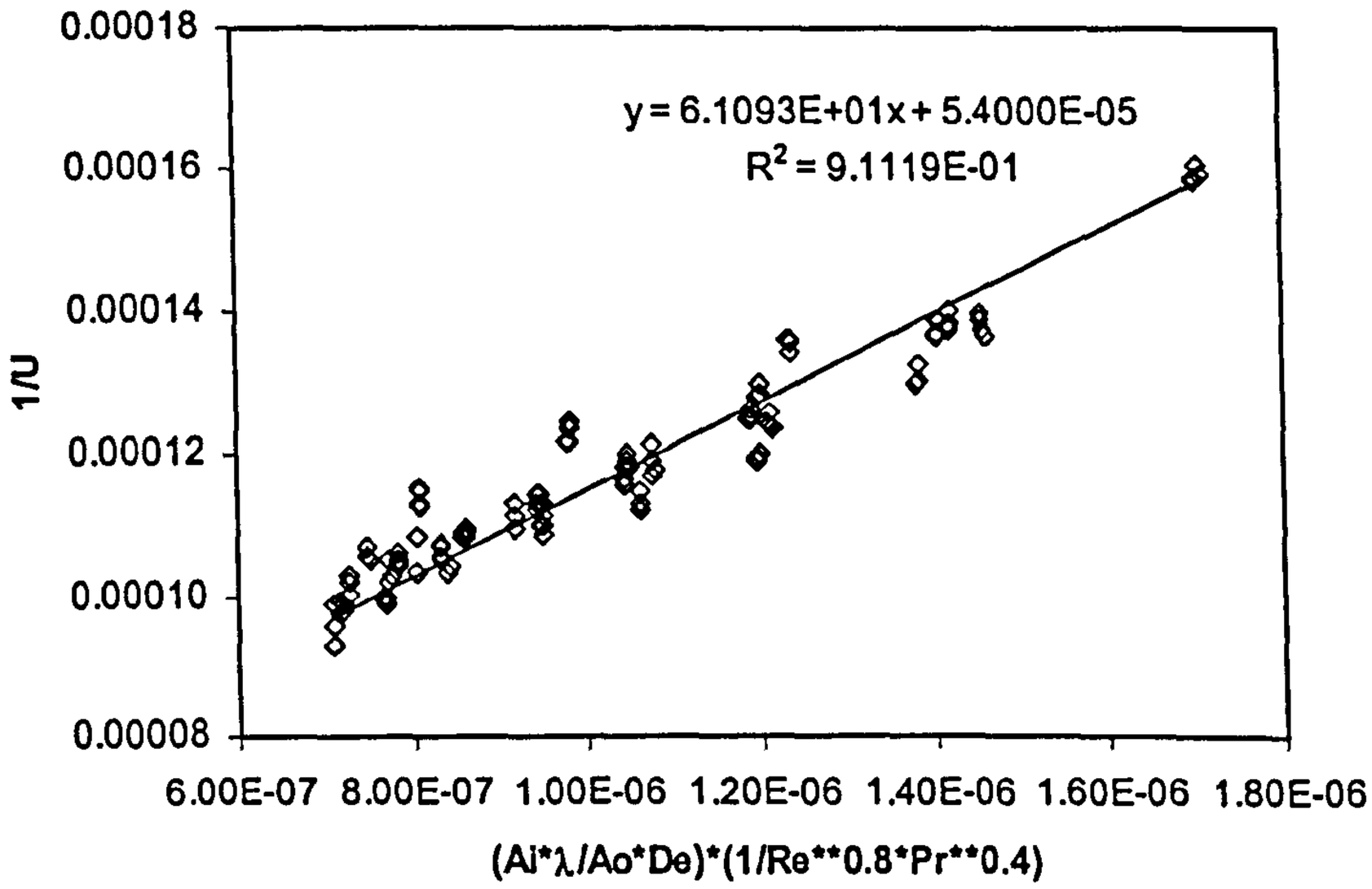

Figure 5.13: Wilson plot for steam condensing over a range of coolant conditions

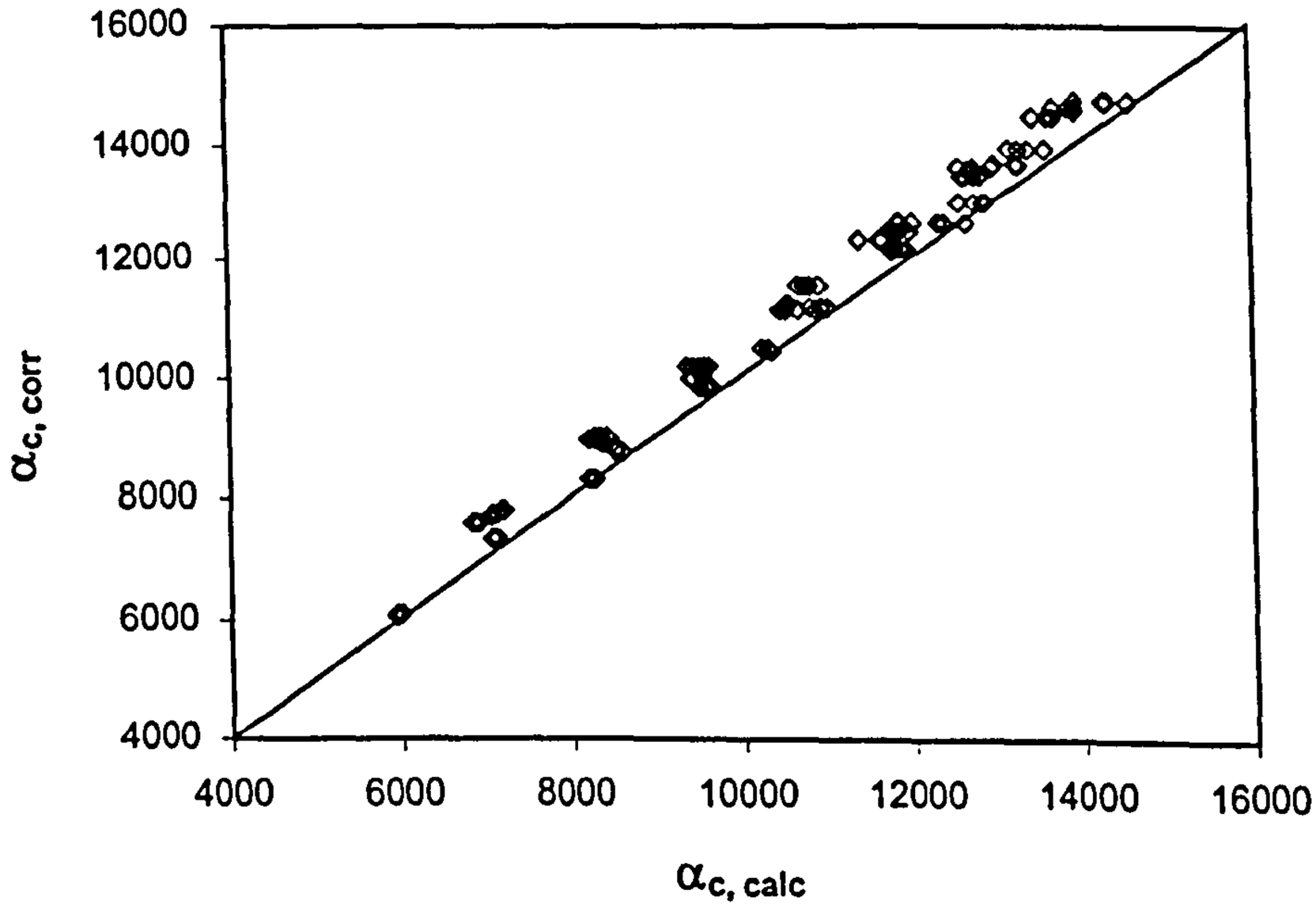

Figure 5.14: Comparison of coolant heat transfer coefficients calculated directly from data and predicted by Wilson plot correlation

5.4.2.1 Local coefficients

In order to calculate local heat transfer coefficients, vapour, wall and coolant temperatures were required. The only place coolant and vapour temperatures were measured was between the test sections, but by using the wall temperature measurement closest to the bottom of each test section, it was possible to evaluate the local coefficients at the bottom of each test section. Obviously using measurements that are not at the same point in the tube introduces an uncertainty into the calculations, but due to the small wall temperature changes this uncertainty will be small compared to the standard uncertainty of the thermocouples.

Using equation (5.1) to estimate the coolant coefficient, local condensate film heat transfer coefficients were evaluated by rearranging equation (4.41) to give

$$\alpha_f = \frac{\alpha_c (T_w - T_c)}{(T_v - T_w)} \tag{5.2}$$

The data for all the single component runs were plotted in dimensionless form, denoted by α_f^*, against the local film Reynolds number to give Figure 5.15. On this figure it is obvious that the trend is for the condensate heat transfer coefficient to decrease as the film Reynolds number increased, i.e. as the film travels down the tube. This is an expected result due to the thickening of the film as vapour condenses and adds to the mass of the film.

Two points of concern with this figure are the level of scatter and the fact that some of the runs showed a higher coefficient at the bottom of the lowest test section (TS4) than the middle section (TS3). Both of these problems can be attributed to experimental error. The wall thermocouples (class 2 with a standard uncertainty of ±0.5°C) had a high uncertainty relative to the small temperature differences.

In the pentane tests, the thermocouple measuring vapour temperature at the bottom of the middle test section was not working. The average of the boiler temperature and that at the bottom of the top test section was taken to be the temperature at this point. Using an average in this way assumes a linear vapour temperature profile, but analysis of the iso-octane data (see Figure 5.8 for an example) showed that the profile was not linear thus incurring a further uncertainty into the value used.

5.4.2.2 Mean coefficients

The high uncertainties associated with measuring the local condensate heat transfer coefficients were overcome by concentrating instead on the mean condensate film coefficients. As described in 4.4.3, the mean coefficient, $\overline{\alpha}_f$, was calculated from the mean overall heat transfer coefficient, $\overline{U}$, and mean coolant coefficient, $\overline{\alpha}_c$ by equation (4.39).

As the calculation of mean overall coefficient is based on a logarithmic temperature difference across the length of the tube, the only temperature measurements used are those of the coolant and vapour at each end of the tube. This removes the reliance on intermediate vapour and wall temperatures. This combined with the higher temperature differences meant that the mean condensate coefficient could be calculated much more accurately then the local coefficient. The estimation of the uncertainties of local and mean heat transfer coefficients is reported in 5.6.2.3.

In Figure 5.16 the data are presented against the film Reynolds number at the bottom of the tube. Also plotted are Nusselt's analysis for gravity controlled condensation on a vertical surface, and the HTFS method which takes into account ripples and waves on the surface of the film. At the Reynolds numbers in question, the HTFS method uses the correlation of Kutadeladze (1963)

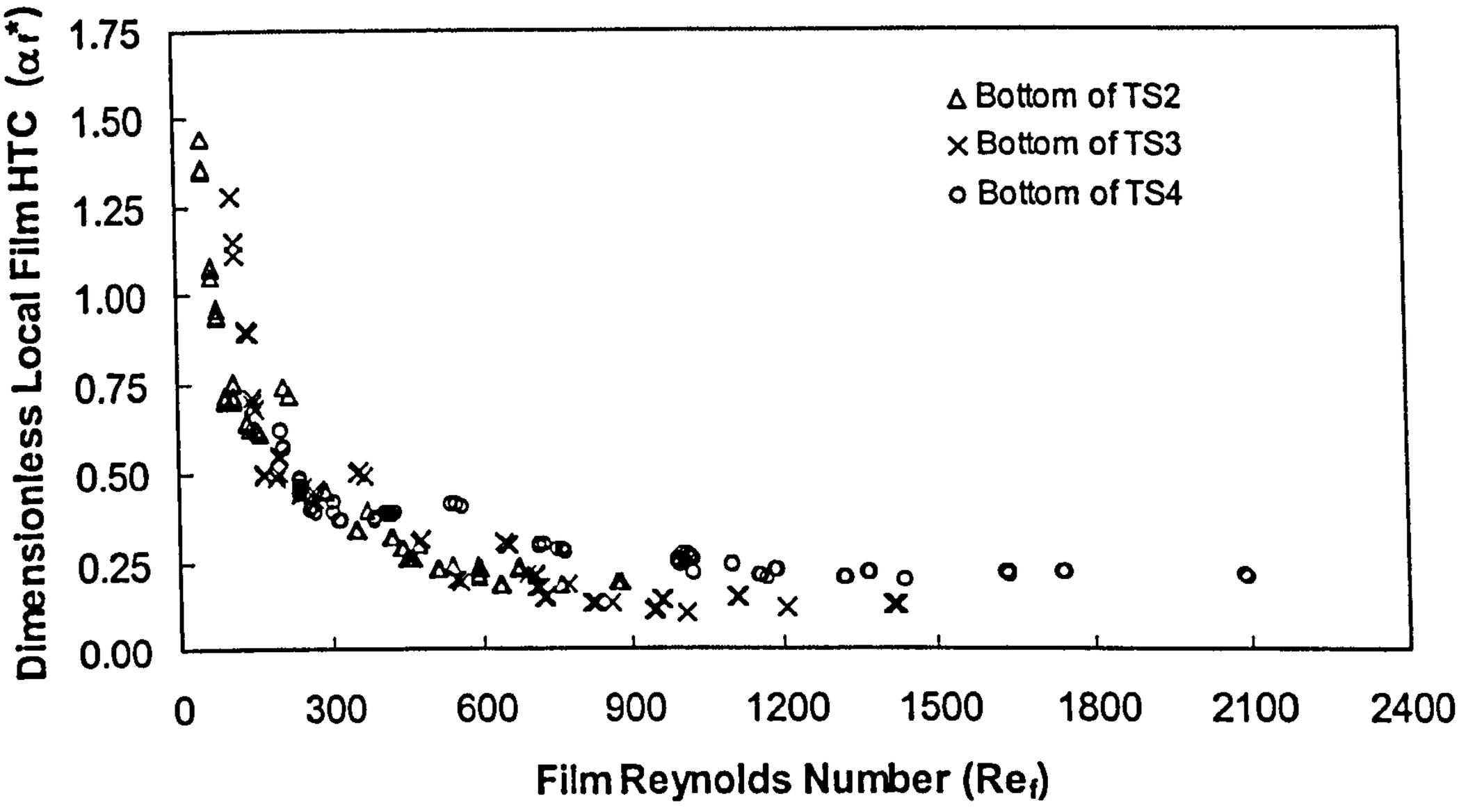

Figure 5.15: Dimensionless local condensate film heat transfer coefficients

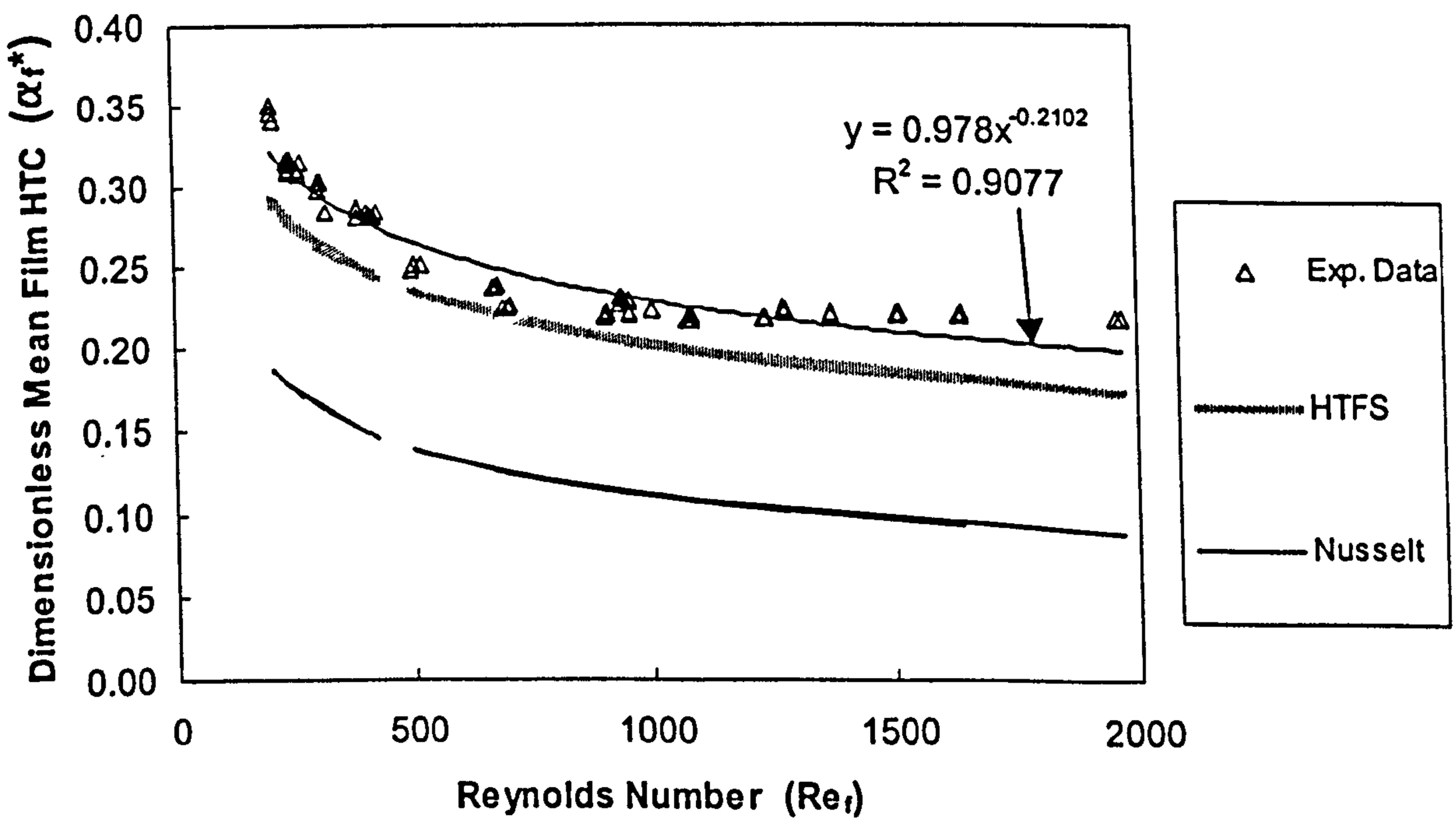

Figure 5.16: Mean condensate film heat transfer coefficients against film Reynolds number at the bottom of the tube

The results agree with the findings of Bartleman (2001) in that the coefficient is higher than would be expected in a co-current condenser. (using the Kutateladze correlation). Bartleman (2001) suggested that this was an effect of countercurrent flow that caused the waves on the film surface to increase in size thus increasing the heat transfer area. This is the opposite to the argument of Al-Shammari (2001) who found most of his film coefficients to be smaller than would be expected in a co-current condenser. He argued that the effect of vapour shear in countercurrent flow would be to thicken the film and increase the heat transfer resistance.

There is no overlap in the Reynolds number ranges in the iso-octane and pentane data and they can be considered separately. In both cases, there is a levelling off of the film heat transfer coefficient towards the higher end of the Reynolds number scales. The author believes that this is due to the approach of the flooding point causing turbulent behaviour to appear in the film at lower Reynolds numbers than would otherwise be expected.

When running the facility, it was found that the transition to flooding was very sudden when iso-octane was the test fluid. When the data was collected, care was taken to run the facility close to the flooding point to utilise the full range available. In fact one set of runs was rejected (iso-octane runs 6.1, 6.2 and 6.3) when the tube was accidentally flooded. In the iso-octane data in Figure 5.16 the film coefficient drops dramatically at lower Reynolds numbers but levels off suddenly in line with disturbances in the film that indicated the approach to flooding (see Chapter 6 for more details on observations of the film draining from the tube).

Referring back to Figure 2.2 in the literature review, in co-current condensation it is expected that there will be a gradual transition from laminar to laminar-wavy then finally turbulent flow in the condensate film. It is believed that in the data here the effect of disturbances in the film is to cause the transition between laminar and turbulent flow to occur at a very low Reynolds number.

The flooding point was never reached during the pentane tests, but disturbances in the film were still observed. In the film coefficient data presented here, the coefficient at first drops at a slower rate than the iso-octane data, in line with the expectation of the film becoming rippled and entering the laminar wavy regime. There is then the levelling off at higher Reynolds numbers, and in fact there is a slight increase in the mean coefficient. This again is in line with the transition to turbulence in the film where it would be expected that the film coefficient would increase at higher Reynolds numbers.

5.4.2.3 Correlation for the film heat transfer coefficient

In order to determine vapour side heat transfer coefficients in the mixture work and allow modelling of the experimental data, it was required to have a correlation to predict both the local and mean condensate heat transfer coefficient. Although the Kutateladze (1963) correlation gave reasonable good predictions of the mean coefficient, there was a constant underprediction. Regression analysis was therefore used to determine a correlation in a similar form based on the data reported here. This is displayed in Figure 5.16. The curve is a similar shape to that of the Nusselt (1916) and Kutateladze (1963) therefore smoothing out the effect of the approach of the flooding point.

$$\overline{\alpha}_f^* = 0.978\, Re_{f,out}^{-0.210} \tag{5.3}$$

As discussed earlier, the uncertainties around the measurement of local condensate coefficients were much higher than the mean coefficients. As a result if this it was decided to use the mean coefficient data to derive a correlation for local coefficients. The mean condensate film heat transfer coefficient over a range of Reynolds numbers 0 to $Re_{f,out}$ can be obtained by integration of the local coefficients over the full range.

$$\frac{1}{\overline{\alpha}_f^*} = \frac{1}{Re_{f,out}} \int_0^{Re_{f,out}} \frac{d\,Re_f}{\alpha_f^*} \tag{5.4}$$

To obtain local coefficients from the mean data, it is justifiable to reverse the process and differentiate

$$\frac{1}{\alpha_f^*} = \frac{d}{d\,Re_f}\left(\frac{Re_f}{\overline{\alpha}_f^*}\right) \tag{5.5}$$

which, from (5.3), gives the correlation for local condensate heat transfer coefficient as

$$\alpha_f^* = 0.808\,Re_f^{-0.210} \tag{5.6}$$

5.4.3 Vapour heat transfer coefficients

In Figure 5.17, the mean overall, total condensing side, condensate film, and effective vapour heat transfer coefficients are plotted against condensate heat flux for the first mixture. It can be seen that the mean overall and total condensing side heat transfer coefficients are almost identical. This confirms the findings from the temperature profiles in Figure 5.9 and Figure 5.10 that the condensing side resistance is more dominant than that of the coolant and wall.

Figure 5.17 also shows the relative contributions of the condensate film and effective vapour resistances to the total resistance on the condensing side. In practically all cases, the vapour resistance controls the rate of heat transfer although at higher heat fluxes the condensate and vapour resistances approach each other and in the last data point the condensate film is controlling. As heat flux increases it follows that the Reynolds number of the condensate film will increase and so the condensate heat transfer coefficient is seen to decrease slightly over the data.

The opposite effect is seen in the effective vapour heat transfer coefficient where the resistance to heat transfer decreases at higher heat flux. This arises because an increased heat flux in the facility is associated with an increased vapour flow rate which in turn generates a higher vapour heat transfer coefficient.

This illustrates one of the major practical drawbacks of reflux condensers. The need to keep vapour velocities low to avoid flooding means that vapour flow rates are low compared to co-current condensers. This means that vapour heat transfer coefficients are much lower in reflux condensers.

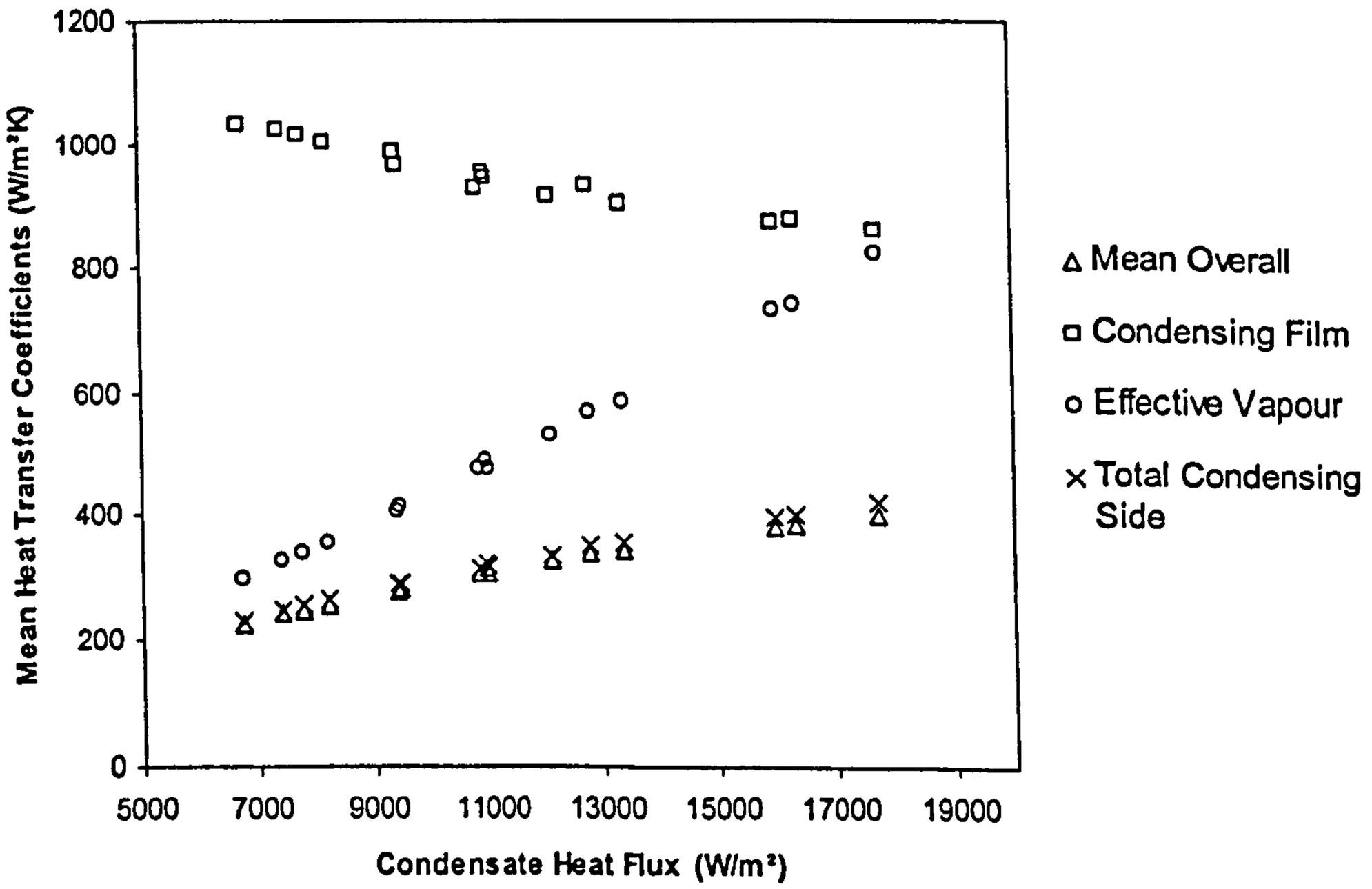

Figure 5.17: Condensate and effective vapour contributions to mean condensing side coefficient for mixture 1

5.4.3.1 Mean Coefficients

The results displayed in Figure 5.18 show that there is a high level of spread in the mean sensible vapour heat transfer coefficient, as calculated using equation (4.50). By plotting the three mixtures individually it can be seen that the same smooth trend appears but that at any given mean vapour Reynolds numbers the values are different for each mixture. The only differences in the three mixtures was the composition of the bulk liquid leading to different feed vapour compositions. It is unclear why this should have any effect as composition should have no effect on the sensible heat transfer characteristics of the vapour. It may be that there was some outside influence, such as different amounts of incondensible gas or impurities, that had an effect.

These results were compared with three commonly used correlations for heat transfer from a turbulent vapour to a dry stationary wall, namely the correlations of Dittus-Boelter (1930) (equation 2.8), Petukhov (1970) (equations 2.9 and 2.10) and Gnielinski (1976) (equations 2.10 and 2.11). The three correlations were also corrected for the effect of mass transfer by applying equations 2.30 and 2.31. Each of these correlations predicts a local coefficient at a given set of conditions. To allow comparison with the mean vapour coefficients measured experimentally, they were evaluated at the mean vapour Reynolds number.

Figure 5.18 shows that each of the correlations over predicts the experimental data. Including the mass transfer correction term caused the data to be underpredicted. As mass transfer effects are known to reduce the rate of heat transfer (as described in 2.6) it was expected that these correlations would overpredict the data, but the inclusion of the mass transfer correction term should have improved the accuracy. These results suggest that the use of these correlations and the mass transfer correction term are inadequate to accurately model the heat transfer process in a reflux condenser.

In order to improve the prediction of the vapour heat transfer coefficients two further corrections were considered for the effect of countercurrent flow and waves on the surface of the condensate film.

In reflux condensation, vapour velocities tend to be low to avoid flooding. As the condensate flows in the opposite direction the relative velocity between the condensate and vapour may be significantly higher then the vapour velocity. To include this into the analysis, the condensate film thickness was evaluated using the theory of laminar film flow and used to estimate the mean bulk condensate velocity at the bottom of the tube. This serves as an approximation to the liquid velocity at the vapour/liquid interface.

$$\delta_f = 0.68\left[\frac{\mu_f^2}{g\,\rho_f^2}\right]^{\frac{1}{3}} Re_f^{\frac{1}{3}} \tag{5.7}$$

$$u_f = \frac{\rho_f\, g\, \delta_f^2}{2\mu_f} \tag{5.8}$$

The vapour velocity was then taken to be relative to this value and a modified vapour inlet Reynolds number evaluated . The vapour heat transfer coefficient was then evaluated at the mean of the modified inlet Reynolds number and outlet Reynolds number giving an increased value over the uncorrected coefficient. As there is no condensate film at the top of the tube, the outlet vapour Reynolds number was not corrected.

In 5.4.2.2 it was suggested that the approach of the flooding point caused the condensate film to approach turbulence at lower Reynolds numbers than would be expected. This, and the fact that the condensate heat transfer coefficient was always higher than the value predicted by Nusselt's theory of laminar film condensation confirmed the presence of waves on the condensate film. It is possible that these waves improve diffusive heat transfer by disrupting the vapour and liquid interface. The increase in diffusive heat transfer associated with these waves was therefore accounted for by applying the correction of Di Cave et al (1987).

$$\alpha_{v,DiC} = \alpha_v\left[1 + 0.00397 Re_f^{0.476}\left(\frac{\eta_l}{\eta_g}\right)^{0.271}\right] \tag{5.9}$$

These corrections were applied to the heat transfer coefficients predicted by Petukhov's correlation and compared to the experimental data in Figure 5.19. In this figure the data is the same as that reported in Figure 5.18 as are the predictions of the Petukhov correlation (with and without the mass transfer correction factor). Of the two additional corrections, it can be seen that the film velocity correction is more significant than the wave correction.

The wave correction gave good predictions of the Mixture 2 data but tended to underpredict most of the data points whereas the film velocity correction, although overpredicting the majority of data points, falls almost exactly in the centre of the data spread. The Mixture 3 data was best predicted by applying both corrections together, but these predictions gave large overpredictions of the other 2 mixtures. These results suggest that when it comes to modelling the experimental condenser the vapour heat transfer coefficient should be based on a standard correlation corrected for the effects of film velocity and mass transfer.

Consideration was given to the idea that the uncertainties introduced when calculating $\overline{\alpha}_v$ from the mean effective vapour coefficient, $\overline{\alpha}_{v,eff}$, had caused the spread in the data. In order to obtain a mean value, a mean vapour quality was used, as were the calculated rate of heat transfer in the tube and the vapour flow rate at the inlet. There is also the uncertainty associated with comparing the experimental data, which were mean coefficients, against correlations that resulted in local values at a mean Reynolds number.

It was expected that measuring local coefficients would have reduced these uncertainties, but unfortunately these were not available. As described earlier, the mean effective and mean sensible vapour heat transfer coefficients were related by the ratio of sensible to total heat transfer. This is also true of the equivalent local coefficients. As flow rates were required to measure this ratio and there were no local mass balance measurements it was only possible to estimate this ratio over the full tube length.

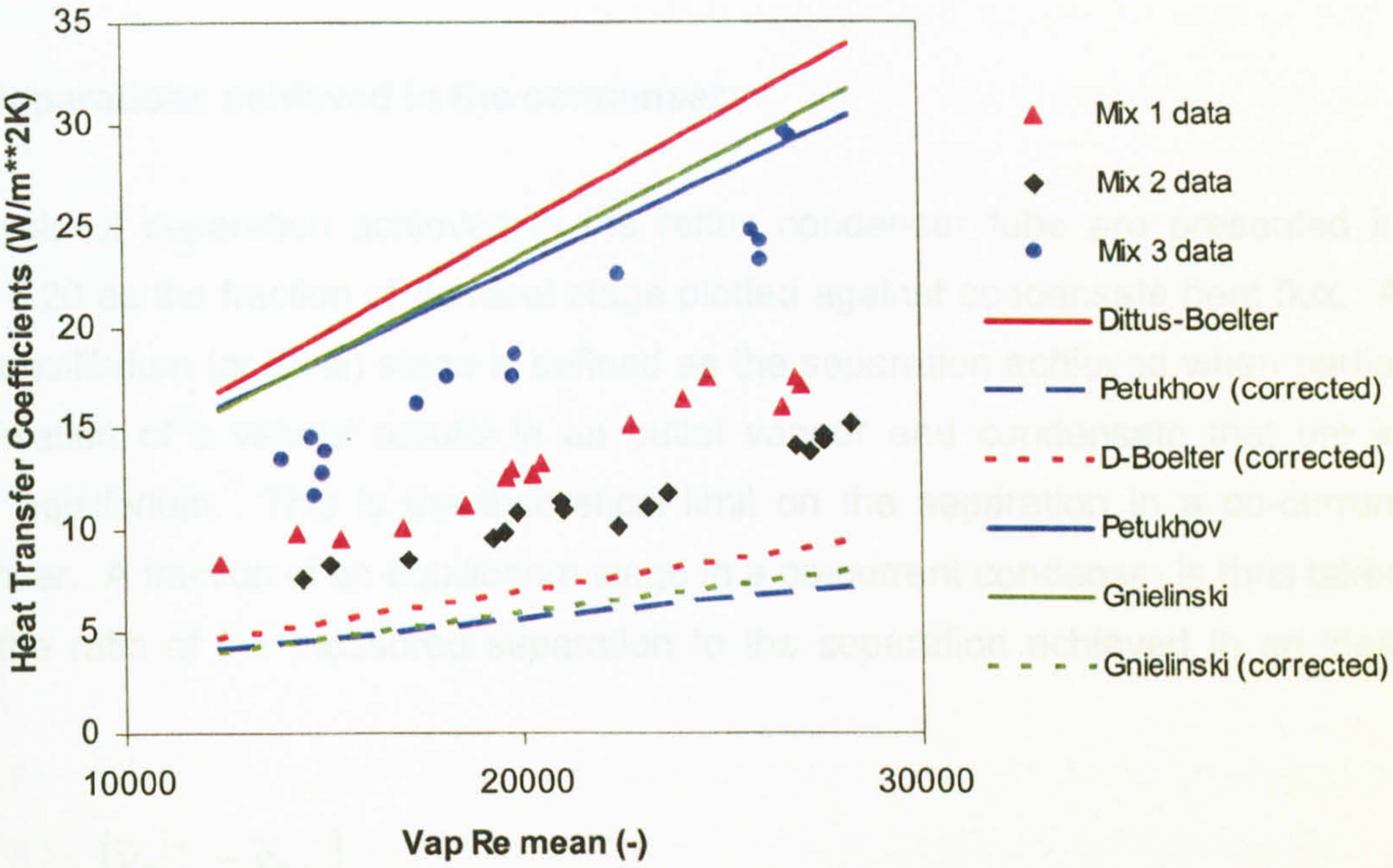

Figure 5.18: Comparison of mean sensible vapour heat transfer coefficients and common correlations for heat transfer to a dry stationary wall

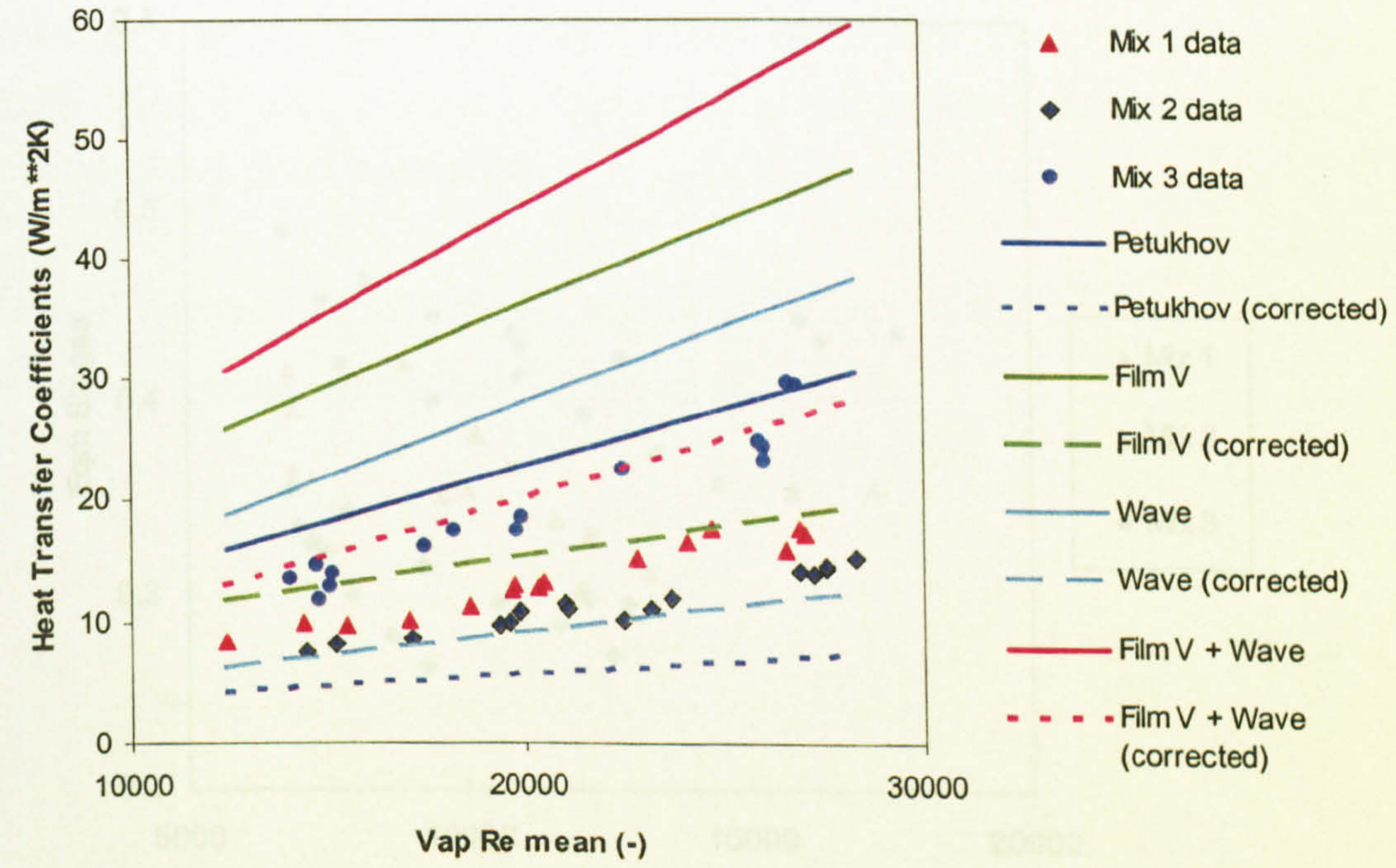

Figure 5.19: Comparison of mean sensible vapour heat transfer coefficients and additional corrections to Petukhov (1970) correlation

5.5 Separations achieved in the condenser

The levels of separation achieved in the reflux condenser tube are presented in Figure 5.20 as the fraction of an ideal stage plotted against condensate heat flux. A single equilibrium (or ideal) stage is defined as the separation achieved when partial condensation of a vapour results in an outlet vapour and condensate that are in overall equilibrium. This is the theoretical limit on the separation in a co-current condenser. A fraction of an equilibrium stage in a co-current condenser is thus taken to be the ratio of the measured separation to the separation achieved in an ideal stage.

$$E = \frac{\left(\tilde{y}_{P,out} - \tilde{y}_{P,in}\right)}{\left(\tilde{y}^{*}_{P,out} - \tilde{y}_{P,in}\right)} \tag{5.10}$$

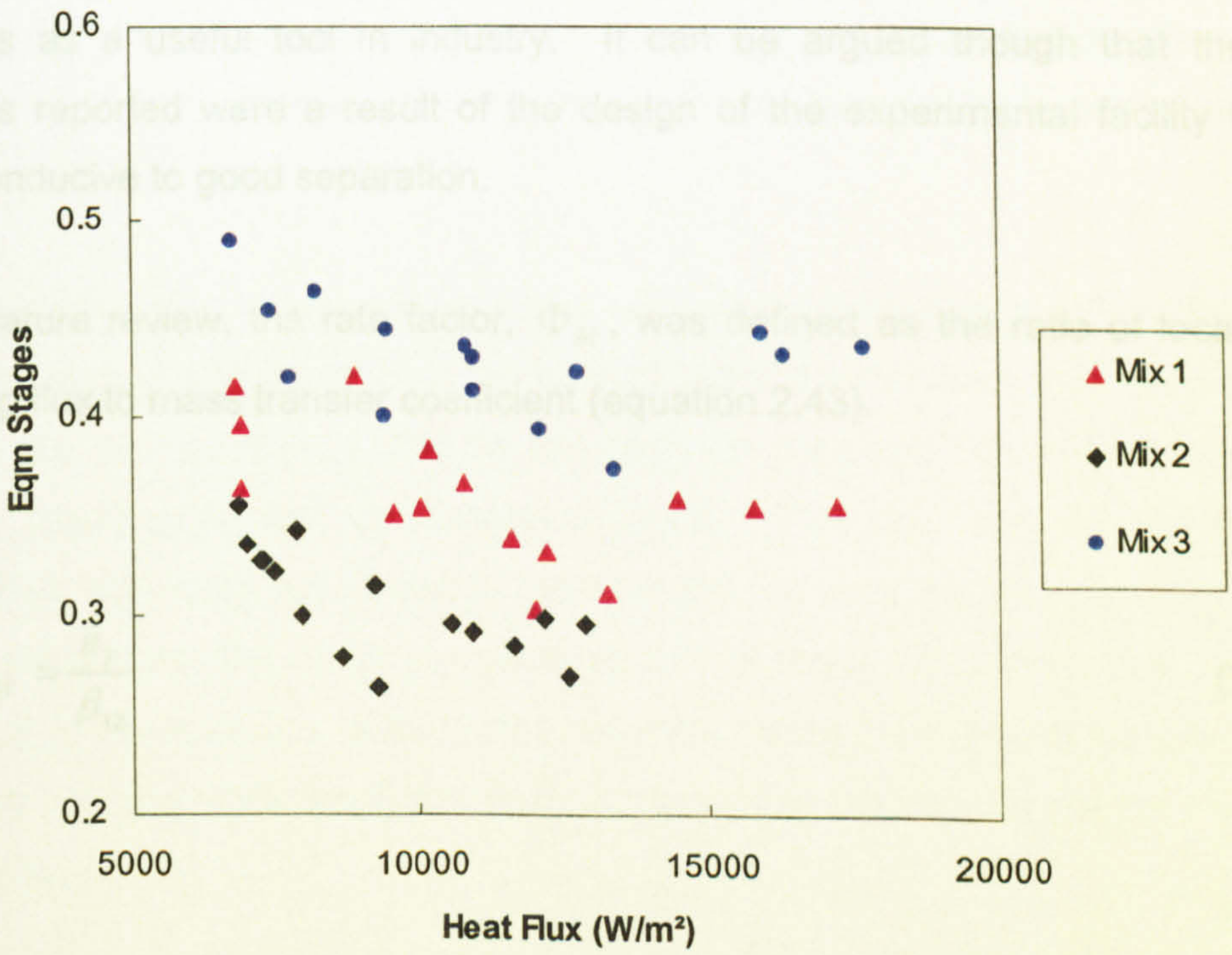

Figure 5.20: Measured separations through the reflux condenser

This definition has to be altered slightly for reflux condensers where the vapour and condensate flow in opposite directions. The term $\tilde{y}^*_{P,out}$, representing the vapour leaving the top of the tube if equilibrium was reached, is taken to be the vapour that would be in equilibrium with the condensate leaving at the bottom of the tube, $\tilde{x}_{P,out}$.

The trend that is apparent in Figure 5.20 is that the amount of separation decreases as condensate heat flux increases. The most important feature of the experimental separations though is that in all cases, the separation is a lot less than one equilibrium stage and in fact never greater than half an equilibrium stage.

One of the theoretical advantages of a reflux condenser is that the countercurrent flow geometry allows for extra separation compared to a co-current condenser. In all of the data recorded here though, the separations seem to be much lower than would be expected in an equivalent co-current condenser where the outlet streams left in equilibrium.

As the extra separative capacity of a reflux condenser is the main advantage of a reflux condenser then these results cast some doubt on the viability of reflux condensers as a useful tool in industry. It can be argued though that the low separations reported were a result of the design of the experimental facility which was not conducive to good separation.

In the literature review, the rate factor, Φ_M, was defined as the ratio of local total condensing flux to mass transfer coefficient (equation 2.43).

$$\Phi_M = \frac{n_T}{\beta_{12}} \qquad (2.43)$$

An analysis of the link between this rate factor and the level of separation was given by Webb & Al-Shammari (2002). By rearranging the Colburn-Drew equation (2.40) they showed that the rate of separation depends solely on the value of the rate factor.

$$\Phi_M = \ln\left[\frac{r-\tilde{y}_i}{r-\tilde{y}_B}\right] \tag{2.40}$$

At negligible rate factor, $\Phi_M \to 0$, the term in brackets on the right hand side of this equation must approach unity, therefore the composition of the vapour at the interface must approach that of the bulk vapour, $\tilde{y}_i \to \tilde{y}_B$. This gives the maximum separation possible.

In the opposite situation, for the rate factor to approach infinity, $\Phi_M \to \infty$, the term in brackets must be minimised. Physically the smallest value $\tilde{y}_i$ can have is that of the condensate, $\tilde{x}_i$. In this situation there is no separation.

This means that the rate factor must be minimised to allow for good separation. It is therefore required to operate at low condensation rate or high mass transfer coefficient.

The condensation rate in any condenser is controlled by the temperature difference between the vapour and coolant. In the mixture tests reported here, this temperature difference was of the order of 30K for low heat flux runs and 50K in high heat flux runs thus resulting in fast condensation rates. The only way to reduce the condensation rate would have been to increase the temperature of the coolant at the inlet. In some runs, the outlet temperature of the coolant was over 50K. It was decided not to increase this value further as heat losses from the condenser jacket would have become more significant thus compromising the accuracy of the heat and mass balances.

Much discussion has already been given to the low flow rates imposed on reflux condensers by the flooding limit and the effect this has on the vapour heat transfer coefficients. As the mass transfer coefficient is dependent on the vapour heat transfer coefficient, low mass transfer coefficients can be expected in reflux condensers compared to co-current condensers.

The geometry of the reflux tube used in this project was also an important feature. The 0.045m tube diameter (large compared to most industrial condensers) meant that the vapour velocity was relatively low for the amount of condensate. The knock on effect was that the mass transfer coefficient was relatively low for the condensing fluxes, giving relatively large rate factors. As discussed above, high rate factors result in low separation thus explaining the experimental results.

Based on the argument above, poor separation would also be expected if the tube was operated in the vapour down flow orientation. One way to confirm this is by constructing a model of the experimental data for a co-current condenser. This is achieved in chapter 7 where the film theory model of Colburn and Drew is applied to both a reflux condenser and an equivalent co-current condenser.

5.6 Uncertainty analysis results

5.6.1 Standard uncertainties for the main measurements

It is the intention in this section to present estimates for the standard uncertainties of each of the main measurements. The standard uncertainty of a measurement was based either on the manufacturers quoted uncertainty or the calibration uncertainty (whichever was larger) combined with the uncertainty caused by fluctuating repeat measurements (measured by the standard deviation of the repeats). Because of the different methods used to obtain the single component and mixture data, and the different ranges involved in some of the measurements, these are presented separately. The standard uncertainty of each measurement was calculated for all of the test runs. The data are reported in Table 5.4 in absolute form as the maximum and mean of all the accepted runs in each set.

Although these maximum uncertainties were not used in the calculation of propagated uncertainties, they show the uncertainty bounds found in the data. In cases where there is large maximum uncertainty, it indicates that there was some sort of fluctuation of the system while the data logger was recording the repeat scans.

5.6.2 Uncertainty of calculated results

The process of calculating propagated uncertainties, directly from the measurements can be complicated and laborious. For example, the calculation of mean overall heat transfer coefficient requires the heat load over the condenser, the heat transfer area (for which there is no uncertainty) and the logarithmic temperature difference as displayed in (5.11).

$$\overline{U} = \frac{\dot{Q}_R}{A_i \, \theta_m} \tag{5.11}$$

It is possible to substitute the equations for each of the required values in to this equation to give the mean coefficient purely in terms of the measured quantities

$$\overline{U} = \frac{\left(\frac{\dot{V}_{c,R}}{\rho_{c,R}}(T_{c,Rour} - T_{c,Rin})\right) + \left(\frac{\dot{V}_{c,D}}{\rho_{c,D}}(T_{c,Dour} - T_{c,Din})\right) + (u_A \, \rho_A \, A_{Ex})}{A_i \left[\frac{(T_{v,in} - T_{c,out}) - (T_{v,out} - T_{c,in})}{\ln\left[\frac{(T_{v,in} - T_{c,out})}{(T_{v,out} - T_{c,in})}\right]}\right]} \tag{5.12}$$

Using this relatively simple example, it is easy to see that complex equations can arise when working out the propagated uncertainty directly from measurements. If physical property uncertainties are considered, then the equations for the prediction of the properties in question should also be included and the complexity increases further. To simplify this process so that it could be incorporated in to the analysis spreadsheet, the calculations were handled in blocks.

	Measurement	Unit	Single component		Mixture data	
			Max	Mean	Max	Mean
Reflux Condenser (end points)	Boiler pressure	Pa	330.02	127.50	290.21	193.88
	Boiler Temperature	°C	0.212	0.099	0.129	0.102
	Vapour Temp TS2	°C	0.979	0.310	0.277	0.256
	Coolant Flow rate	m^3/s	$5.00*10^{-7}$	$3.18*10^{-7}$	$3.62*10^{-7}$	$1.83*10^{-7}$
	Coolant inlet temp	°C	0.117	0.073	0.80	0.072
	Coolant outlet temp	°C	0.137	0.073	0.075	0.070
Reflux condenser (intermediate temperatures)	Vapour out TS3 / in TS2	°C	0.927	0.299	0.642	0.292
	Vapour out TS4 / in TS3	°C	0.699	0.513	0.528	0.504
	Coolant out TS2 / in TS3	°C	0.391	0.260	0.263	0.252
	Coolant outTS3 / in TS4	°C	0.290	0.255	0.261	0.252
	Wall temperature	°C	0.507	0.504	0.501	0.501
Dump condenser	Coolant flow rate	m^3/s	$3.56*10^{-7}$	$1.67*10^{-7}$	$2.32*10^{-7}$	$0.89*10^{-7}$
	Coolant inlet temp	°C	0.517	0.104	0.222	0.096
	Coolant outlet temp	°C	0.192	0.082	0.109	0.074
	Condensate temperature	°C	0.655	2.438	0.513	0.502
Miscellaneous	Heat Input	W	53.81	5.91	8.57	5.25
	Extraction air inlet temp	°C	0.30	0.58	0.330	0.265
	Extraction air outlet temp	°C	0.25	0.26	0.264	0.252
	Reflux condensate composition	Mole/Mole	N/A	N/A	0.044	0.038
	Dump condensate composition	Mole/Mole	N/A	N/A	0.034	0.030

Table 5.4: Standard uncertainties of measurements

Referring again to the example above, the standard uncertainty of the logarithmic temperature difference and the heat load were calculated separately. These were then combined to give the uncertainty of the mean overall heat transfer coefficient. This method was repeated for all of the main calculations with the results presented below

5.6.2.1 Heat balances

The overall heat balance was taken to be the ratio of heat out to heat in where the heat output included a contribution from the heat gained by the air passing over the boiler as defined in (5.13).

$$R_{\dot{Q}} = \frac{\dot{Q}_{c,R} + \dot{Q}_{c,D} + \dot{Q}_L}{\dot{Q}_i} \tag{5.13}$$

The uncertainty budget for a typical run (Pentane run 2.2) is displayed below. In this example, the expanded uncertainty of the overall heat balance was taken as 0.044 (4.52%) to a confidence interval of approximately 95%.

The results of the uncertainty analysis on the heat balance data are presented in Table 5.6.

It can be seen from this table that the heat balance uncertainty is much higher in the iso-octane data than all the others (including the flooding data which was recorded using iso-octane as the test fluid). This is put down to the fact that to avoid flooding, the facility was operated at lower levels of heat input in the iso-octane tests. In Figure 5.21 it can be seen that the uncertainty is highly dependent on the heat input. Of the calculations that make up the overall heat balance, the heat gained by the air has the highest percentage uncertainty. In runs where there was a low heat input, this uncertainty becomes much more significant resulting in larger uncertainties at lower heat inputs.

Component	Nominal Value	Standard Uncertainty	Sensitivity Coefficient
$\dot{Q}_i$	3013.1 W	3.53 W (0.12 %)	-3.26*10^{-4}
$\dot{Q}_{c,R}$	1764.1 W	24.8 W (2.82 %)	3.319*10^{-4}
$\dot{Q}_{c,D}$	799.8 W	21.3 W (2.67 %)	3.319*10^{-4}
$\dot{Q}_{A,Ex}$	404.0 W	58.4 W (14.47 %)	3.319*10^{-4}
		Combined standard uncertainty	
$R_{\dot{Q}}$	0.985	0.022	2.26%
		Expanded uncertainty	
		0.044	4.52 %

Table 5.5: Uncertainty budget for calculation of heat balance in run P2.2

	Single component			Mixtures		
	Pentane	Iso-octane	Flooding	Mix 1	Mix 2	Mix 3
Maximum exp unc.	0.053	0.112	0.062	0.056	0.060	0.049
(%)	5.24	10.96	6.03	5.73	5.90	4.97
Mean exp unc	0.037	0.068	0.041	0.036	0.042	0.036
(%)	3.72	6.89	4.26	3.78	4.21	3.67

Table 5.6: Summary of results of overall heat balance uncertainty analysis

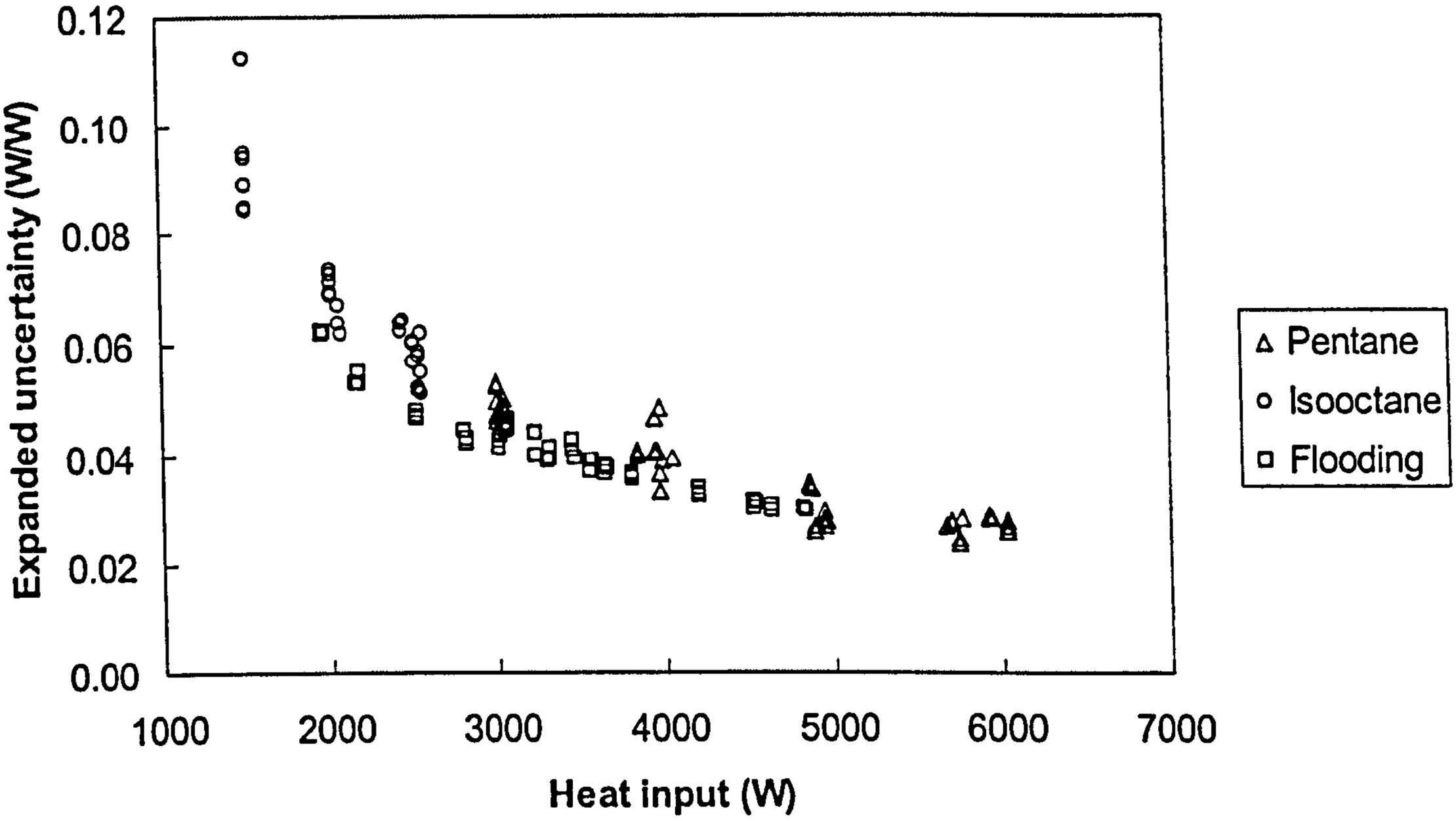

Figure 5.21: Heat balance expanded uncertainty against heat input for single component data

		Single component				Mixtures			
		Maximum		Mean		Maximum		Mean	
		(kg/s)	(%)	(kg/s)	(%)	(kg/s)	(%)	(kg/s)	(%)
Reflux Condensate	$\dot{m}_{fo,R}$	$8.71*10^{-4}$	10.71	$4.57*10^{-4}$	7.46	$8.00*10^{-4}$	7.73	$4.68*10^{-4}$	7.15
Dump condensate, reflux vapour out	$\dot{m}_{f,D}$ $\dot{m}_{vo,R}$	$1.66*10^{-4}$	32.84	$7.72*10^{-4}$	7.15	$1.53*10^{-4}$	7.82	$9.28*10^{-5}$	3.95
Reflux vapour in	$\dot{m}_{vi,R}$	$4.38*10^{-4}$	4.68	$2.44*10^{-4}$	3.10	$8.06*10^{-4}$	6.14	$4.78*10^{-4}$	5.18
Vapour inlet mole fraction	$\tilde{y}_{Pv,in}$	N/A	N/A	N/A	N/A	0.048	12.90	0.038	8.70

Table 5.7: Summary of mass balance uncertainty analysis results

5.6.2.2 Mass balances

The mass balance uncertainty analysis was used to determine how accurately the mass flows and component balances could be estimated in both the single component and mixture data. In the calculation of condensate mass flow in the reflux condenser, the film temperature was assumed (equation 4.5). For the purposes of uncertainty analysis, it was assumed that the uncertainty of this temperature was 5K. It was possible to calculate the uncertainty of the film temperature if the equation used was assumed to be completely correct. As this is unlikely to be the case, it was decided to assume a large value for the uncertainty. This did not apply to the dump condenser as the condensate temperature was measured in the pool at the bottom of the condenser.

The results of the analysis are presented in Table 5.7. Again, all values assume a coverage factor of 2 to a confidence interval of approximately 95%. It should be noted that as physical property uncertainties were not included, the uncertainty of the vapour velocity at the tube inlet is taken to be the same as that of the vapour inlet flow rate.

5.6.2.3 Heat transfer coefficients

In section 5.4.2.3 it was argued that the use of wall temperature measurements caused a high uncertainty in the calculation of local condensate film heat transfer coefficient. This was compounded by the low temperature differences across the wall which were in some cases lower than the uncertainty of the measuring thermocouples.

The uncertainty analysis method was applied to the calculation of overall mean, local condensate film and mean condensate film heat transfer coefficients. The results, displayed in Table 5.8 as expanded uncertainties (with a confidence interval of 95%) confirmed this argument.

The analysis estimated the uncertainty bounds of the mean condensate film coefficient to be ±7.3% in the pentane data and ±10.9 in the iso-octane data. This compares to the local coefficients where in the top test section the uncertainty was as high as ±270%, and although the accuracy improves further down the tube the uncertainty is still far too high to be acceptable.

These findings highlight the usefulness of the uncertainty analysis. Evidence has been provided to back the decision to use a correlation based on the mean condensate coefficient as opposed to the local coefficients when modelling the process.

5.7 Summary

The experimental data recorded in this project has been presented and the results discussed in this chapter. As this is a follow up project, consideration was given to the results of the previous project and the improvements highlighted.

Previously unexplained heat losses were attributed to the circulating air flow removing heat from the unlagged hot surfaces of the boiler. Using the temperature rise of the air these losses were quantified and included in the overall heat balance. The heat balances reported were good with the assumption of negligible heat loss from the condenser jacket justified implying that the mass balances were accurate.

		Pentane				Iso-octane			
		Max		Mean		Max		Mean	
		W/m²K	%	W/m²K	%	W/m²K	%	W/m²K	%
Local TS2	$\alpha_{f,TS2}$	9425.8	269.6	1748.1	103.3	9216.1	267.7	3446.5	157.7
Local TS3	$\alpha_{f,TS3}$	669.2	100.9	665.3	100.2	678.0	102.1	667.5	100.5
Local TS4	$\alpha_{f,TS4}$	926.4	91.58	922.4	91.19	940.2	92.96	926.2	91.57
Mean film	$\overline{\alpha}_f$	91.6	7.26	41.8	3.65	108.2	10.86	50.5	5.75
Overall mean	$\overline{U}$	69.66	6.33	32.4	3.20	85.5	9.63	40.9	5.17

Table 5.8: Summary of results of heat transfer coefficient uncertainty analysis

Temperature profiles showed the differences between mixture and single component tests and indicated that the condensate film controlled the rate of condensation in the condensation of a pure fluid. This was confirmed by estimating the component resistances both locally at three points and over the full length of the condenser tube.

Single component tests on both pentane and iso-octane were used to develop correlations for the mean and local condensate film heat transfer coefficient over a wide range of film Reynolds numbers. These were then incorporated into the analysis of mixture data allowing the vapour heat transfer coefficients to be estimated. It was thus confirmed that the rate of condensation of a binary mixture is controlled by the heat transfer resistance of the vapour phase.

It was also found that standard correlations for heat transfer to a dry stationary wall corrected for the effect of mass transfer were inadequate in modelling the sensible vapour heat transfer coefficient. Corrections for the effect of waves on the condensate film and the relative velocity between the vapour and condensate were applied. It was found that the film velocity correction led to improved predictions of the measured vapour heat transfer coefficients

Finally, the measured separations over the tube were discussed. These were found to be on the low side, always less than a single equilibrium stage, but this was attributed to the design of the facility.

6 Flooding Analysis

In this chapter, the phenomenon of flooding is studied. Since flooding is the major drawback to the use of reflux condensers, any thermal design of such a unit must consider the point at which flooding will occur and ensure operation below the flooding point. In addition, the requirement to operate below the flooding point leads to low gas phase heat and mass transfer coefficients. These low values can mean that a reflux condenser is impractical compared to a co-current condenser and it is therefore important to operate as close as possible to the flooding condition.

It was shown in the literature review in 2.5 that there are a number of uncertainties around the flooding phenomenon that need to be addressed in relation to the experimental facility. It is the aim of this chapter to consider these uncertainties and attempt to improve understanding of flooding in reflux condensers.

In order to achieve the specified aim, a number of objectives were selected:

- Add to the very limited data set available on flooding under reflux condensation conditions.
- Use visual observations and measurements to accurately determine the flooding point and mechanism of flooding.
- Propose a formal definition for the flooding point in a reflux condenser.
- Test a number of popular correlations for their suitability under refluxing conditions.

6.1 Experimental data set

The general experimental method was described in 3.3.2 with some alterations made for flooding tests with pure iso-octane noted in 3.3.3.2 Typically, a coolant inlet temperature was selected and kept constant with the boiler heat load increased in small steps. At each different heat load, a visual observation was made of the flow of condensate from the bottom of the reflux condenser tube, and three sets of results were taken. This progressed from the normal operating (non-flooding) region past the flooding point.

In later tests a digital video recorder was used to make permanent records of the visual observations. Selections from the video footage have been converted to Mpeg files and uploaded on the CD included as part of this thesis. These video files can be combined with the data presented in this thesis to give a more complete data set. This fulfils the first objective as it adds to the data available in open literature on flooding in a reflux condenser tube.

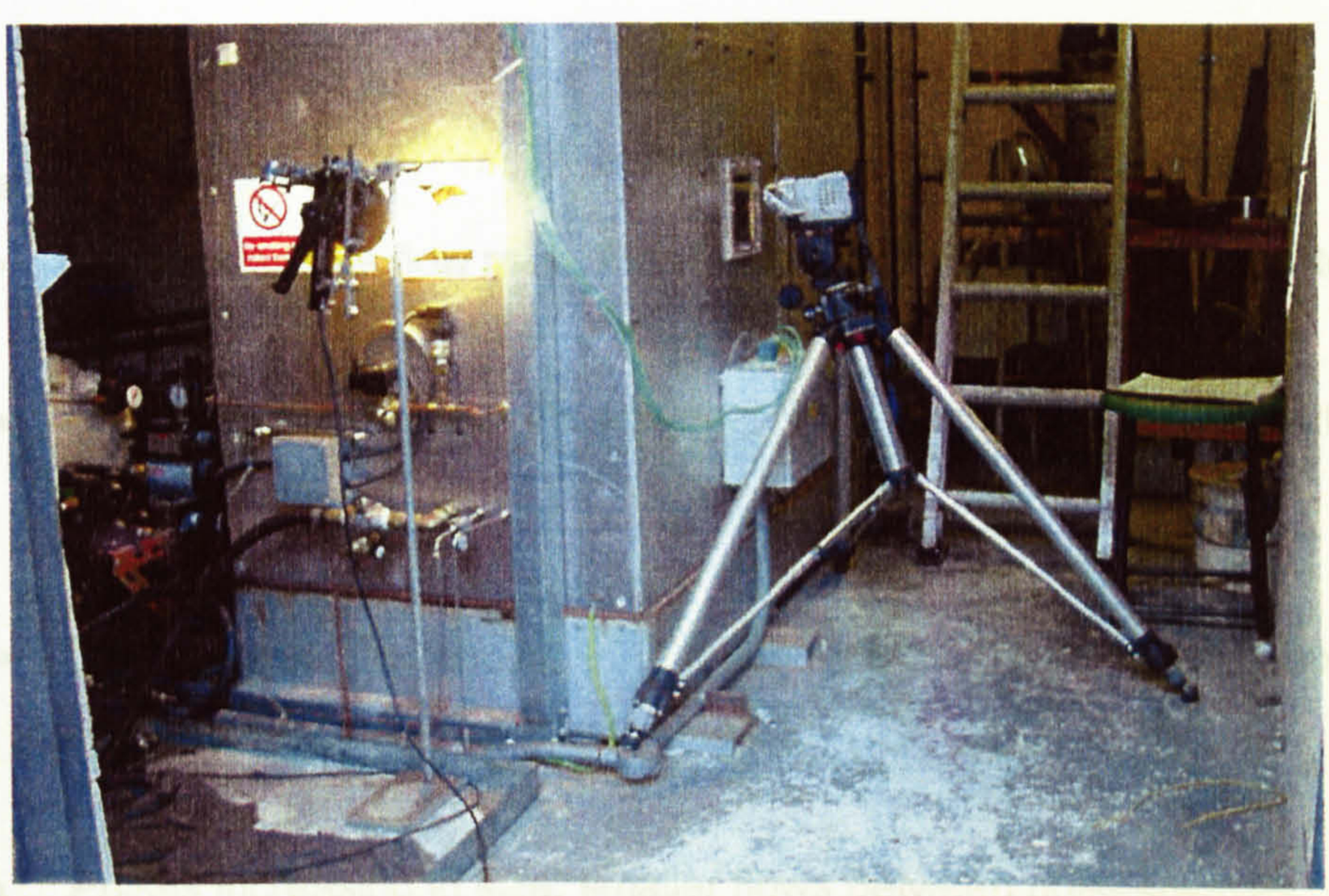

Figure 6.1: Digital video camera and light source for flooding observations

6.2 Visual Observations

It is known that in reflux condensation, vapour and condensate flows are at their maximum values at the bottom of the tube where the vapour enters and the condensate exits. Consequently, this is the area of the tube that floods first (Deakin, 1977). This is an important feature of flooding in a reflux condenser as it is the main difference in flooding between reflux and adiabatic conditions where flows are constant through the tube.

In the absence of a clear Perspex tube where the condensate flow in the tube can be viewed directly (such as the one used in the McQuillan et al. (1985) study), the flow pattern of condensate draining from the tube can be used to deduce behaviour further up the tube. For example, in normal operation with a laminar condensate film a smooth consistent smooth flow pattern will be expected.

Waves appearing on the surface will result in inconsistent amounts of condensate draining from the tube and the film looking more disturbed.

The following is a description of the visual observations made while stepping up from normal operation through the flooding point. Most of the flow patterns described were also recorded and can be viewed on the attached CD. All variables apart from boiler heat load were kept constant.

Low Heat Input

- Low condensate flow rate. Film very smooth and trickled out of tube.

- Condensate flow rate increasing. Film slightly disturbed with some minor splashing (video 1).

- Disturbances increasing. Constant small pulses at about 2Hz representing surface waves (video 2).

- Pulses increasing in size, smaller flows between pulses/waves.

- Drainage fully intermittent. Pulses now slug with no drainage at all in between except for small amounts of condensate collecting on rim which were carried back up tube (videos 3 and 4).

- Observations dependent on system pressure. Intermittent drainage with slugs of liquid decreasing in size at lower pressures (video 5). Cyclical periods of no drainage and intermittent drainage at higher pressures (video 6 parts 1, 2 and 3)

- Stable at lower pressures with almost no drainage. Every 10 seconds or so a single large slug of liquid would drain. Again small amounts of condensate on rim before disappearing up tube. At higher pressures cyclical behaviour again observed.

Increasing Heat Input

Maximum Heat Input

These observations are in fact very similar to those of Deakin (1977), except that Deakin made no reference to the condensate on the tube rim. It is important to discuss these observations to investigate what they say about behaviour further up the tube and the mechanism leading to flooding.

6.3 Flooding mechanism

In the literature review, three possible mechanisms were discussed and each of these must be considered in turn.

The Bernoulli effect proposed by Rabas & Arman (2000) resulted from a pressure difference across a droplet which caused the droplet to be sucked up the tube. When large condensate flows were present, this effect was not observed indicating that the momentum was too great for the pressure difference to overcome and the effect was lost.

In some of the observations described above when the facility was stabilised and partial upward flow had been established, small amounts of condensate were seen to collect on the rim and disappear back up the tube. Typically this occurred in the gaps between draining slugs. This seems to confirm the presence of the Bernoulli effect, but suggests that only small amounts of condensate were affected. It can therefore be said with confidence that although present, the Bernoulli effect is not the cause of flooding.

With no visual observation inside the tube itself it is difficult to make any definite judgements on droplet entrainment, but with the available evidence some theories can be proposed. At higher flow rates below the flooding point and above the flooding point, a certain amount of liquid splashing was observed. The cause of splashing can be attributed to turbulence in the condensate and the effect of vapour shearing droplets off the surface. None of the droplets seen breaking away from the main body appeared to be carried up the tube. The angle of the view port and the diagonal cut on the end of the reflux tube meant that there was a good view of vapour entering the tube. With no droplets moving upwards in the main vapour flow it seems very unlikely that droplet entrainment was the cause of the tube becoming flooded.

Workers who identified droplet entrainment as the flooding mechanism, such as Dukler & Smith (1979) and Moalem & Dukler (1984), reported no upwards movement of waves. In those cases, the intermittent drainage reported here would not have been observed. It therefore seems that droplet entrainment was not the flooding mechanism in this body of work.

This leaves wave bridging as the most likely cause of flooding, a conclusion that is further confirmed by a more detailed interpretation of the visual observations. As described earlier, increasing the vapour flow rate (hence increasing condensate flow rate and vapour velocity) caused the waves on the condensate surface to grow in size. In fact, a point was reached where there was no significant drainage at all between waves.

No drainage between waves suggests that the upward flow of vapour holds up the condensate flow for a short period of time. This is most likely to occur if waves bridge the tube and form a total blockage in the shape of a slug. Momentarily the vapour flow is enough to contain this slug, and possibly even cause a slight upward flow. As more condensate forms and falls onto the slug it becomes too heavy and eventually overcomes the vapour and falls out of the tube. The possibility of this scenario occurring is confirmed by the fact that Deakin (1977) witnessed the bottom of the tube becoming flooding while condensation took place as normal further up the tube.

It seems likely that this is the correct mechanism as further increases in the vapour flow will lead to a point where the condensate is unable to overcome the vapour and upward flow is reached. Firstly, the waves themselves should move a greater distance up the tube as the pressure increase in the boiler gives a greater driving force, and eventually upward concurrent annular flow should be established.

Again the expected behaviour is confirmed by visual observations made here. Increasing time gaps between wave/slug draining indicate that either the waves moved upwards or fluctuated inside the tube before overcoming the vapour. At the highest vapour flows no significant drainage was observed confirming almost total upwards flow.

It can therefore be said with confidence that the mechanism of flooding in this experimental facility was the bridging of waves. It is now crucial to define a point at which the tube can be said to be flooded. The vapour velocity at which this occurs is known as the flooding point.

6.4 Definition of the flooding point

It has been shown earlier that the bottom part of a reflux condenser tube can become flooded, but ultimately condensation will continue with intermittent instead of constant drainage. The flooding point must therefore be defined as the point where flooding causes a loss of condenser performance.

In most of the previous literature, the flooding point was defined in terms of the vapour velocity that would cause the tube to flood. The same definition will be used in this work, but the term flooding point will also be used to describe the overall conditions in the facility, for example the flooding point in terms of heat load would be the heat load that gives a vapour velocity high enough to flood the tube.

In order to achieve this it is necessary to tie in the visual observations with measurements on the experimental facility. The effect of the stepwise increases in heat load on the facility behaviour was thus examined.

6.4.1 Facility behaviour

In almost all of the single component data reported here, the reflux tube was operated as a partial condenser in the non-flooding region. This was to ensure condensation over the full length of the tube with some vapour carryover into the dump condenser. At some conditions, there was little or no temperature rise in the dump condenser indicating almost total condensation in the reflux tube. In this situation, the vapour temperature measurements were used to indicate the presence of vapour at the outlet of the reflux tube.

An increase in boiler heat load resulted in higher boiling temperatures leading to more vapour at a higher temperature and pressure. The resultant increase in temperature difference between the vapour and coolant meant that the condensation rate was also higher and more condensate was formed.

This trend continued as the flooding point approached. One point to note is that in some cases, the increase in vapour density due to higher pressure meant that the vapour velocity did not increase. This has no effect on the analysis as the flooding velocity is partly a function of condensate flow rate. In the same tube, it is easier to flood a higher condensate flow rate therefore a smaller vapour flow rate or lower velocity would be required.

As waves began to form on the condensate indicating the approach to flooding, the trend described above was followed. Eventually, a point was reached when in some cases the boiler pressure dropped, partial condensation was no longer sustained and all the vapour condensed in the bottom two sections of the reflux tube. This is indicated by analysing two temperature profile diagrams, at heat input levels below and above the flooding point. The change in behaviour occurred at the point where drainage first became truly intermittent with gaps of no drainage between the slugs.

6.4.2 Temperature profiles

Consider Figure 6.2. This represents run 7.1 from flooding test 3, where the reflux ratio was 0.985. It is similar to the other single component temperature profiles reported in section 5.3 in that there is almost no change in vapour temperature through the reflux condenser. Another important point is that the coolant temperature increases at a faster rate at the top of the tube indicating that the condensation duty is highest in the top test section. In fact 52% of the reflux condenser duty is in the top section with 29% and 19% in the middle and bottom sections respectively. This is an expected result as the temperature difference between the coolant and the vapour is highest at the top of the tube, and the condensate film heat transfer coefficient is also higher (as the film is thinner) as discussed earlier.

The temperature cross in the middle section of the tube has been attributed to the fact that class 2 thermocouples were used for the wall temperature measurements. As discussed earlier, these thermocouples are less accurate than the RTDs and class 1 thermocouples used for the coolant and vapour measurements and the difference between the coolant and wall temperatures is less than the tolerance of these thermocouples.

In Figure 6.3, taken from run 11.1 in the same test there are a number of differences. Firstly, it can be seen that there is a dramatic drop in the vapour temperature through the condenser with the vapour at the top of the tube around 10K cooler than in the boiler. Also, in this run, only 36% of the duty is in the top test section with 41% and 23% in the middle and bottom sections.

These temperature profiles confirm that when the flooding point is reached there is a change in the behaviour of the facility. This can be investigated further by considering the overall system pressure and the pressure drop at the flooding point.

6.4.3 System pressure

The effect of flooding on system pressure can be seen in Figure 6.4, where the boiler pressure is plotted against heat input. The flooding point in each test is marked on the graph by a small vertical line through the respective data series and was defined in terms of the visual observations and rig stability. In all of the four tests conducted, increasing the heat supplied to the boiler caused the pressure to rise below and above the flooding point. In one out of the four tests, Test 4, a drop in pressure is observed at the flooding point. This drop in pressure, measuring around 4,300 Pa highlights the instabilities caused by flooding as it was not observed in any of the other tests and the reason for it is unclear.

The pressure drop recorded in Test 3 occurred when the vacuum pump was run for a short time leading to the facility stabilising again as discussed in section 6.2. The close correspondence of the visual observations with the change in temperature profiles and the general instabilities in the facility, there is further evidence that the point at which condensate drainage becomes intermittent is the point at which flooding is initiated.

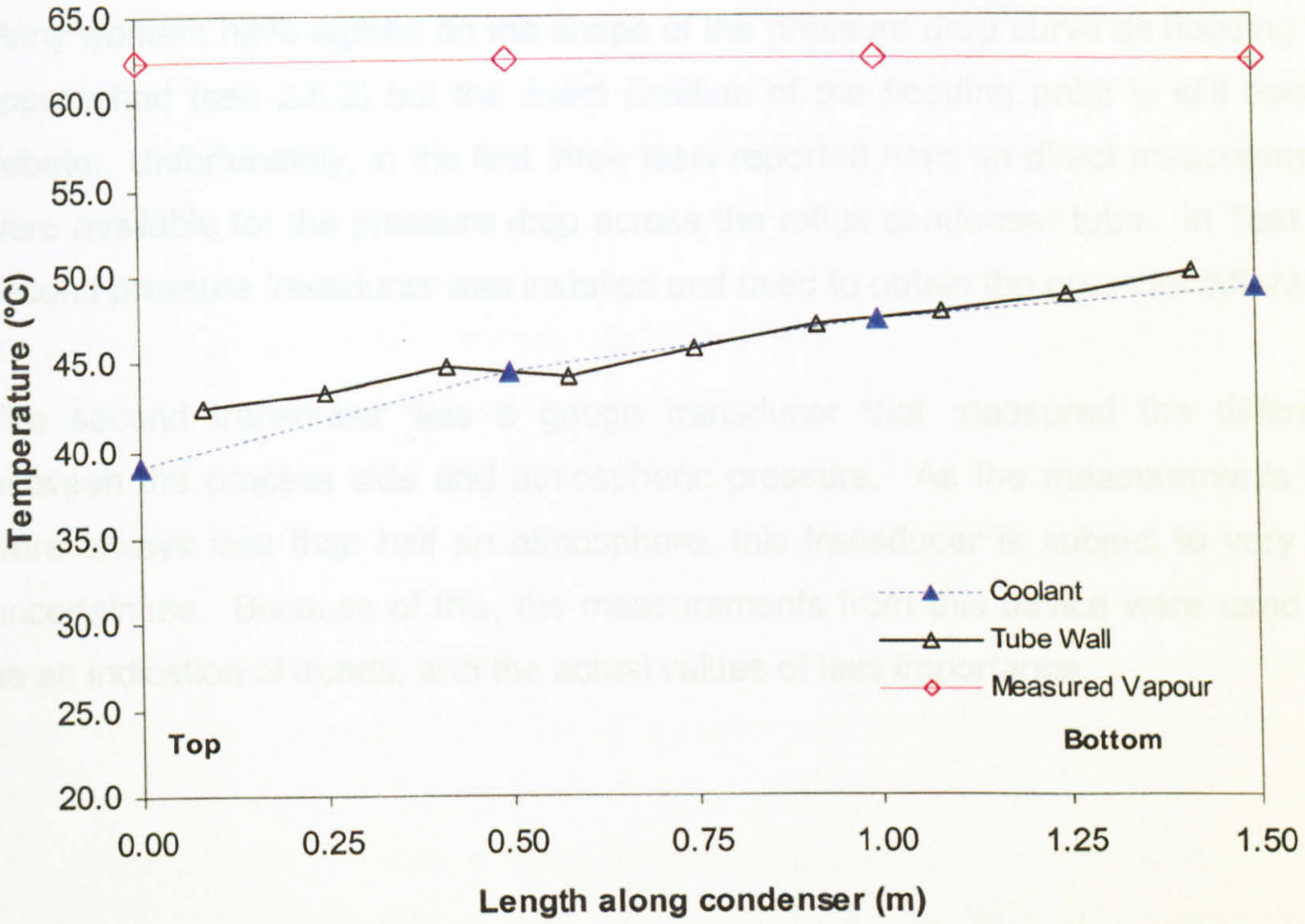

Figure 6.2: Temperature profiles for Flooding Test 3, Run 7.1 (non-flooding)

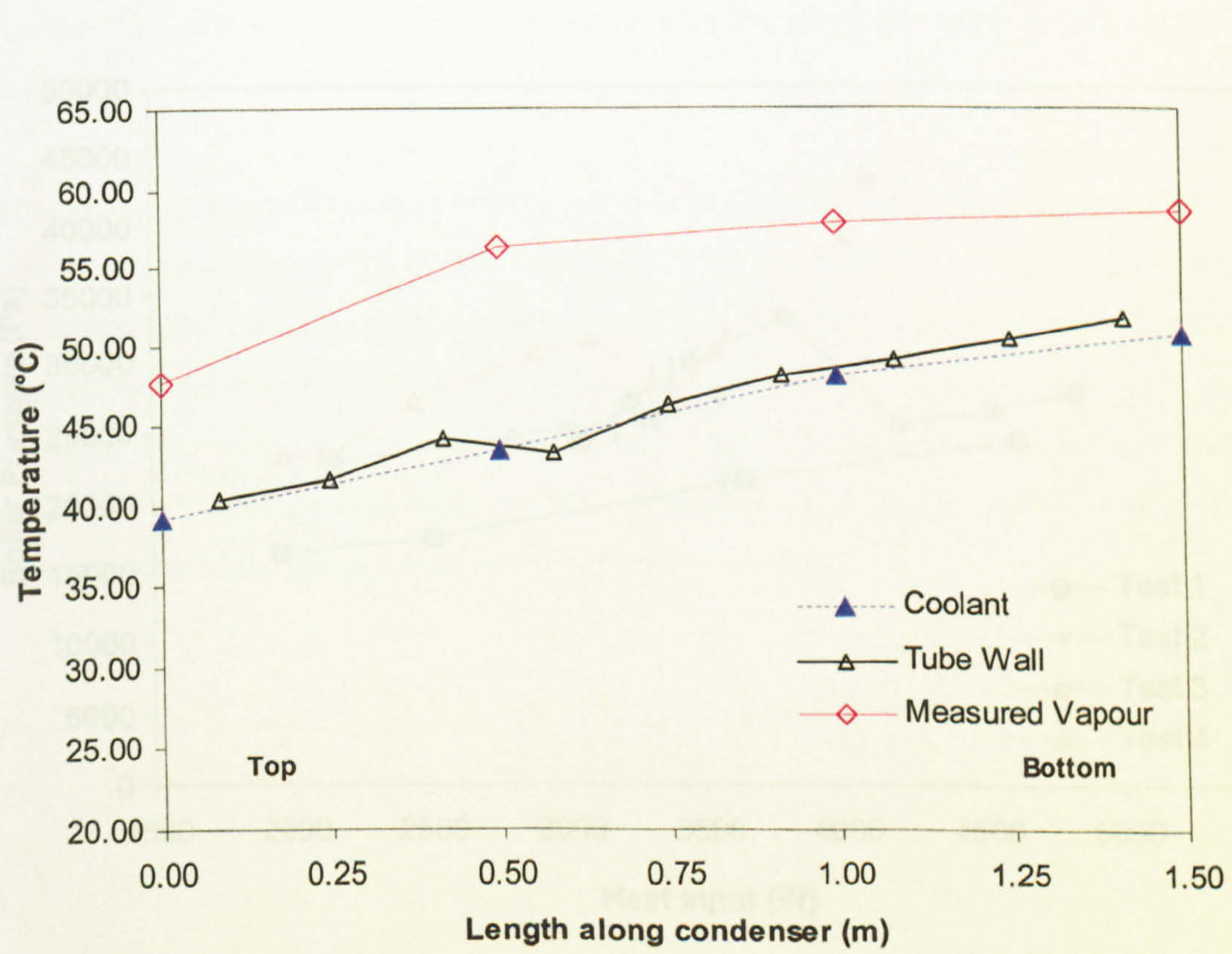

Figure 6.3: Temperature profile for Flooding Test 3, Run 11.1 (flooding)

6.4.4 *Pressure Drop*

Many workers have agreed on the shape of the pressure drop curve as flooding was approached (see 2.5.2) but the exact position of the flooding point is still open to debate. Unfortunately, in the first three tests reported here no direct measurements were available for the pressure drop across the reflux condenser tube. In Test 4, a second pressure transducer was installed and used to obtain the pressure difference. The second transducer was a gauge transducer that measured the difference between the process side and atmospheric pressure. As the measurements here were always less than half an atmosphere, this transducer is subject to very high uncertainties. Because of this, the measurements from this device were used only as an indication of trends, with the actual values of less importance.

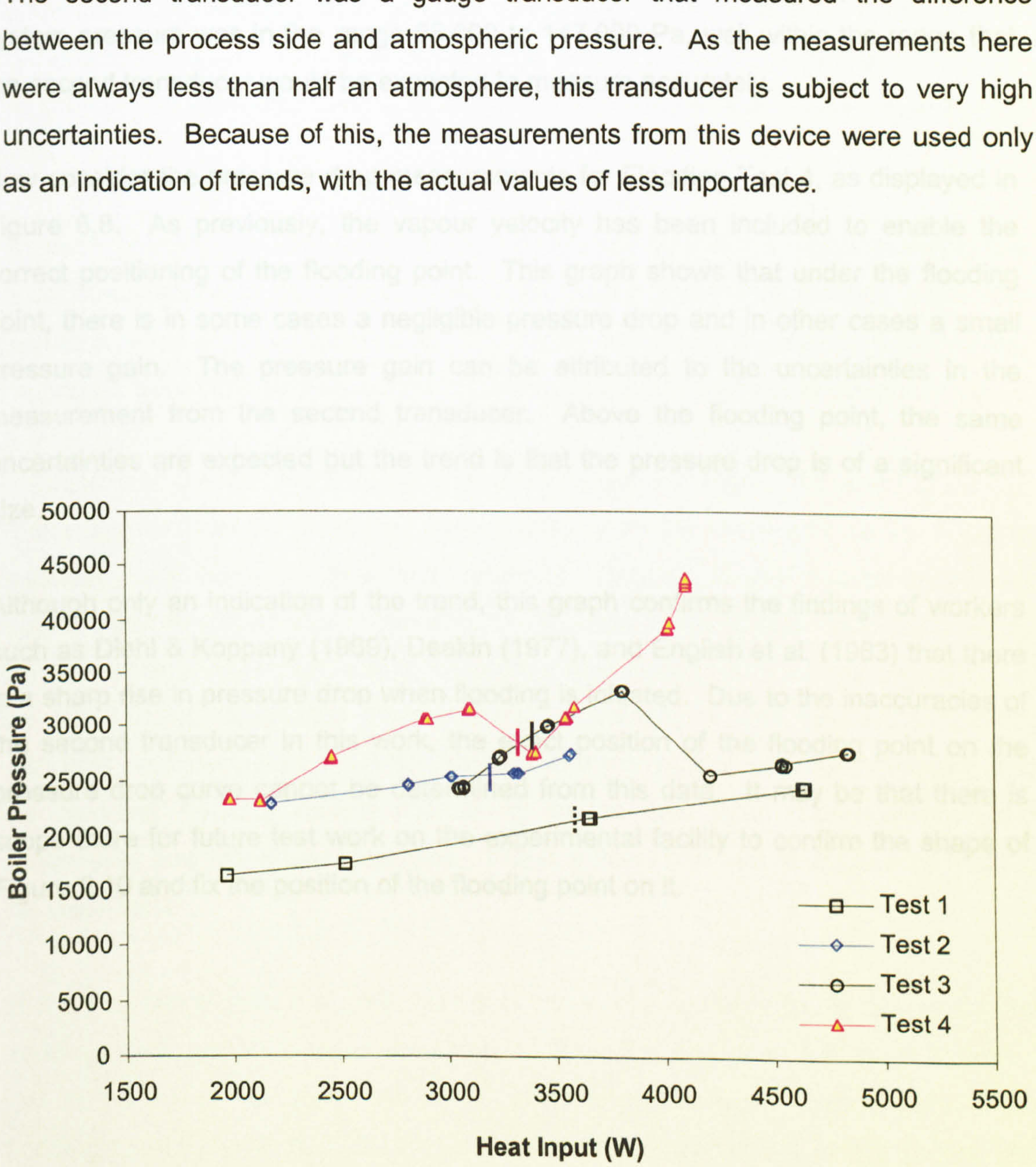

Figure 6.4: Boiler pressure and heat load for all four flooding tests

It was seen in Chapter 5 that the facility ran at a much higher system pressure when pentane was included in the test fluid. With this in mind, consider the pressure drop across the reflux tube in the Mixture Test 4. In this test, the facility was operated well below the flooding point and the system pressure was high enough that the uncertainties associated with the pressure measurement at the vapour outlet are vastly reduced.

The measured pressure drop across the tube was in the range –108 to +945 Pa, a result that is normal for reflux condensers (ESDU, 1993). This is important as the system pressure was in the range 95,000 to 147,000 Pa, well within the range that the second transducer would be expected to measure accurately.

Now consider the pressure drop measurements for Flooding Test 4, as displayed in Figure 6.8. As previously, the vapour velocity has been included to enable the correct positioning of the flooding point. This graph shows that under the flooding point, there is in some cases a negligible pressure drop and in other cases a small pressure gain. The pressure gain can be attributed to the uncertainties in the measurement from the second transducer. Above the flooding point, the same uncertainties are expected but the trend is that the pressure drop is of a significant size.

Although only an indication of the trend, this graph confirms the findings of workers such as Diehl & Koppany (1969), Deakin (1977), and English et al. (1963) that there is a sharp rise in pressure drop when flooding is initiated. Due to the inaccuracies of the second transducer in this work, the exact position of the flooding point on the pressure drop curve cannot be determined from this data. It may be that there is scope there for future test work on the experimental facility to confirm the shape of Figure 2.10 and fix the position of the flooding point on it.

6.5 Flooding velocity correlations

In this section, some of the most popular flooding correlations are tested against the experimental data. The correlations selected were those of English et al. (1963), Diehl & Koppany (1969), and Alekseev et al. (1972) as modified by McQuillan & Whalley (1985). These correlations were the ones selected by Chunangad (1992) in his strategy for calculating the flooding velocity over a wide range of reflux condenser conditions. Chunangad also suggested comparing the inlet geometry with Figure 2.12 and selecting the correlation (adiabatic or reflux) based on similar geometry. In this project, the geometry used is most similar that used in the English et al (1963) work.

For each flooding test, the data are plotted against heat input, again allowing the visual observations to be related to particular data points. The flooding point was defined in terms of visual observations and facility behaviour as described above and the graphs were otherwise sectioned off purely on the basis of visual observations.

The results of the first two flooding tests are displayed in Figure 6.5 and Figure 6.6. These figures show the measured vapour velocity on the same axis as the flooding velocities predicted by the different correlations. They are plotted against boiler heat input to allow the visual observations to be attributed to the correct velocities. Figure 6.5 represents the first test, where the coolant inlet temperature was set to 40°C. In the non-flooding region, the measured vapour velocity is well below the flooding velocities predicted by all three correlations with the vapour velocity increasing and the predicted flooding velocity decreasing as the heat input (hence vapour and condensate flow rates) was increased. This is a trend that was also followed in all of the latter tests.

In the first test (Figure 6.5), the third data point was selected to be just above the flooding point, and as a result the location of the flooding point has been indicated just to the left of this point. All three correlations give good predictions with the flooding point (6.5 m/s at 3.25 kW) lying between the predictions of the English (6.2 m/s) and Alekseev (6.7 m/s) correlations and the Diehl & Koppany correlation giving a safe prediction well below the other two (5.8 m/s).

In the second test, with the coolant inlet temperature set to 35°C, the English and Alekseev correlations again gave predictions close to each other at 5.5 m/s but in this case they both slightly over-predicted the flooding velocity of 5.25 m/s at 3.5 kW. The Diehl & Koppany prediction was again on the low side although this means that it is the only safe prediction at 4.6 m/s.

Figure 6.7 and Figure 6.8 display the results of the final two flooding tests, both of which had the coolant inlet temperature set to 40°C. The third test differed from the rest in that the system pressure was deliberately reduced above the flooding point by running the vacuum pump for a short period of time. This caused the rig to stabilise with partial condensation re-established in the reflux condenser tube. The measured vapour velocity in this region is well above the values predicted by all of the correlations, and the visual observations indicated that although the tube was still flooding there were smaller amounts of condensate draining from the tube. This confirmed that partial upward flow and carryover had been established, and at the last data point there was very little drainage from the tube at all.

With the flooding point selected as before giving 4.8 m/s at 3.4 kW, the English and Alekseev correlations again give very good predictions of 5.1 kW with the Alekseev correlation the closest to the actual value. The Diehl & Koppany correlation gave the most conservative estimate at 4.3 kW, and at the second data point suggests that the tube should be flooded when all other indicators said the flooding point had not been reached.

In Figure 6.8, the problems associated with the instabilities caused by flooding can be highlighted. Below the flooding point, the data and predicted velocities have fairly smooth trends and with the flooding point as indicated on the chart it seems that the Diehl & Koppany correlation should give the most accurate value. In this test however there was a marked drop in the system pressure when flooding was instigated (see Figure 6.4) which resulted in a decrease in vapour density causing in turn a sharp increase in vapour velocity. The effect of this drop in pressure is also apparent in the predicted flooding velocities which also rise sharply.

At values just above the flooding point, both the English and Alekseev correlations gave good but slightly unsafe values with the Diehl & Koppany correlation again the only one to have a value lower than the measured vapour velocity. At the two data points around 4kW, there was a significant decrease in the vapour flow rate. Looking at the results for these points in detail showed that the overall heat balances were lower than most of the other data. This can only be blamed on the instabilities associated with flooding resulting in fluctuating heat balances a fact that confirmed experimentally by the instrument stability monitor.

The real issue when designing a reflux condenser is to ensure operation below the flooding point. To this end, it is predictions below the flooding point that are crucial rather than the values after flooding. From this point of view, the Diehl & Koppany correlation was the most accurate at predicting the flooding point in test 4.

6.5.1 Effect of tube diameter

Although the tube diameter was included as a variable in all three of the correlations considered here the work of Diehl and Koppany (1969) is perhaps the most interesting in this respect. They used experimental data to confirm earlier findings that there was a critical value of tube diameter below which the flooding velocity depended on the tube diameter. In their correlation the flooding velocity was a function of $d_i^{0.4}$ at diameters less than the critical diameter. The critical diameter (measured in inches) was taken to be a function of the condensate surface tension (measured in dyne/cm).

$$d_{i,c} = \frac{\sigma_f}{80} \tag{6.1}$$

This proposed critical diameter is inconsistent with the theory of wave bridging as the mechanism of flooding. As tube diameters increase, a larger wave on the condensate film would be required to bridge the tube. This implies a larger condensate flow rate and heavier wave.

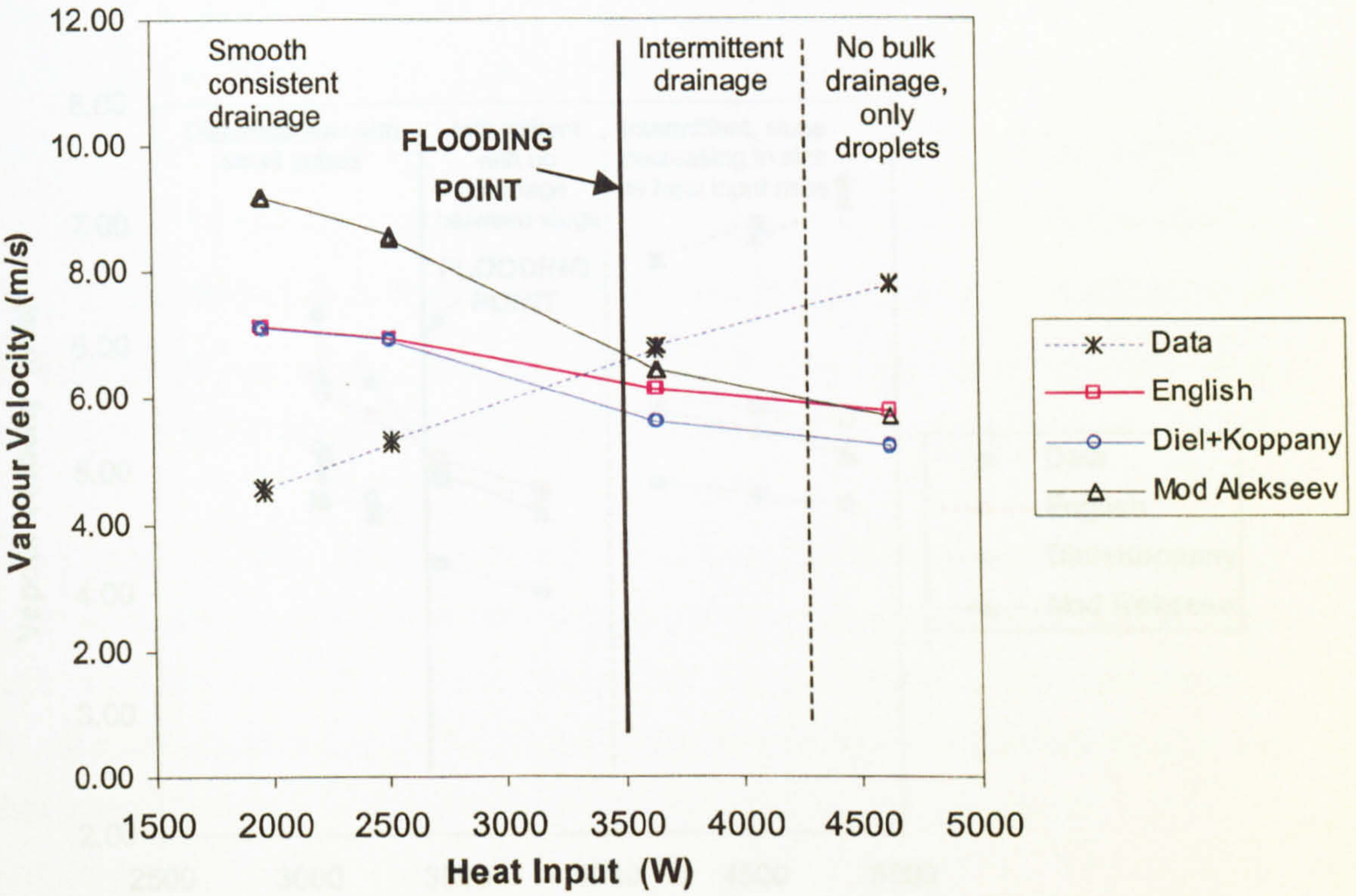

Figure 6.5: Comparison of correlations for Flooding Test 1 ($T_{c,in}$ =40°C)

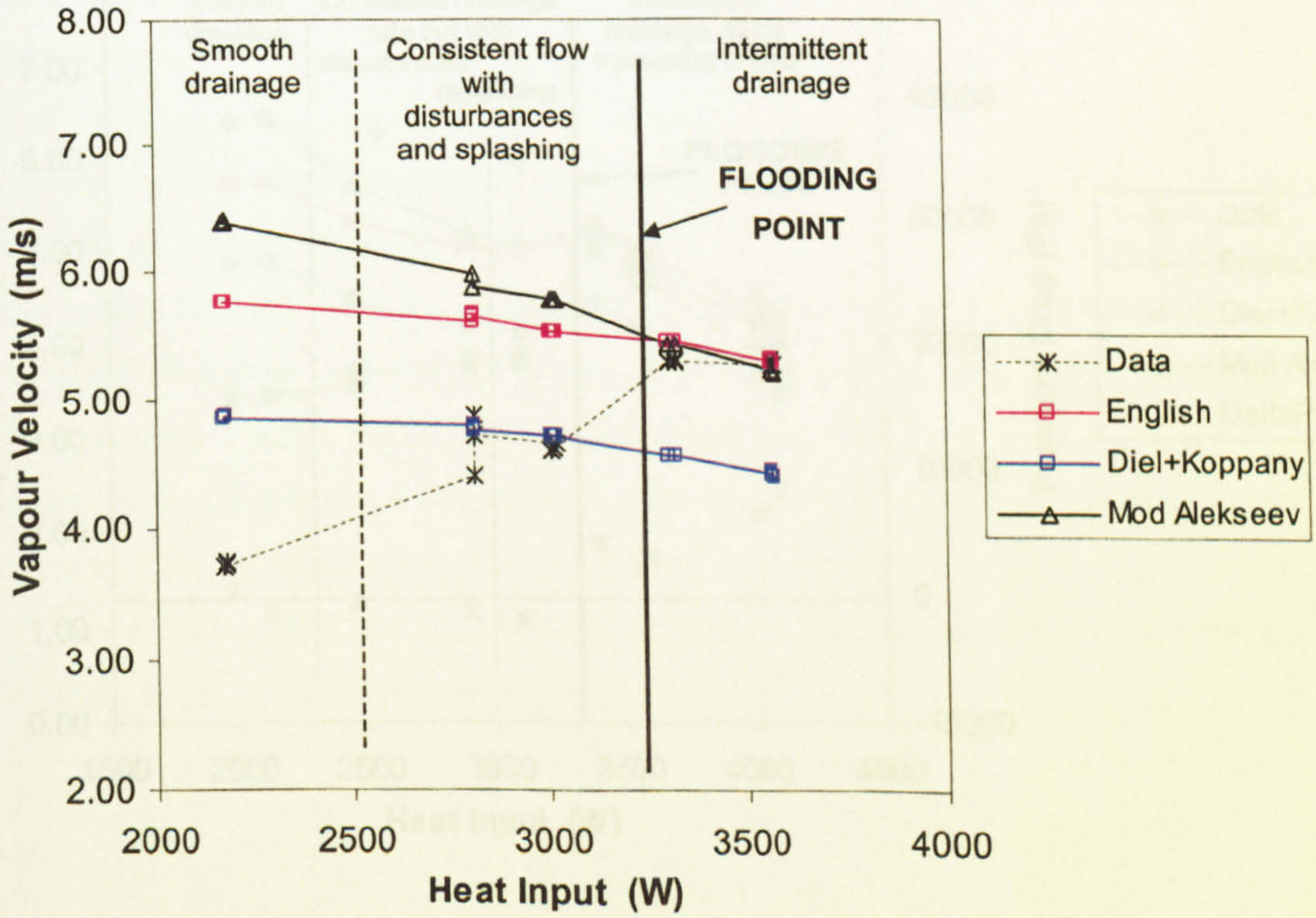

Figure 6.6: Comparison of correlations for Flooding Test 2 ($T_{c,in}$=35°C)

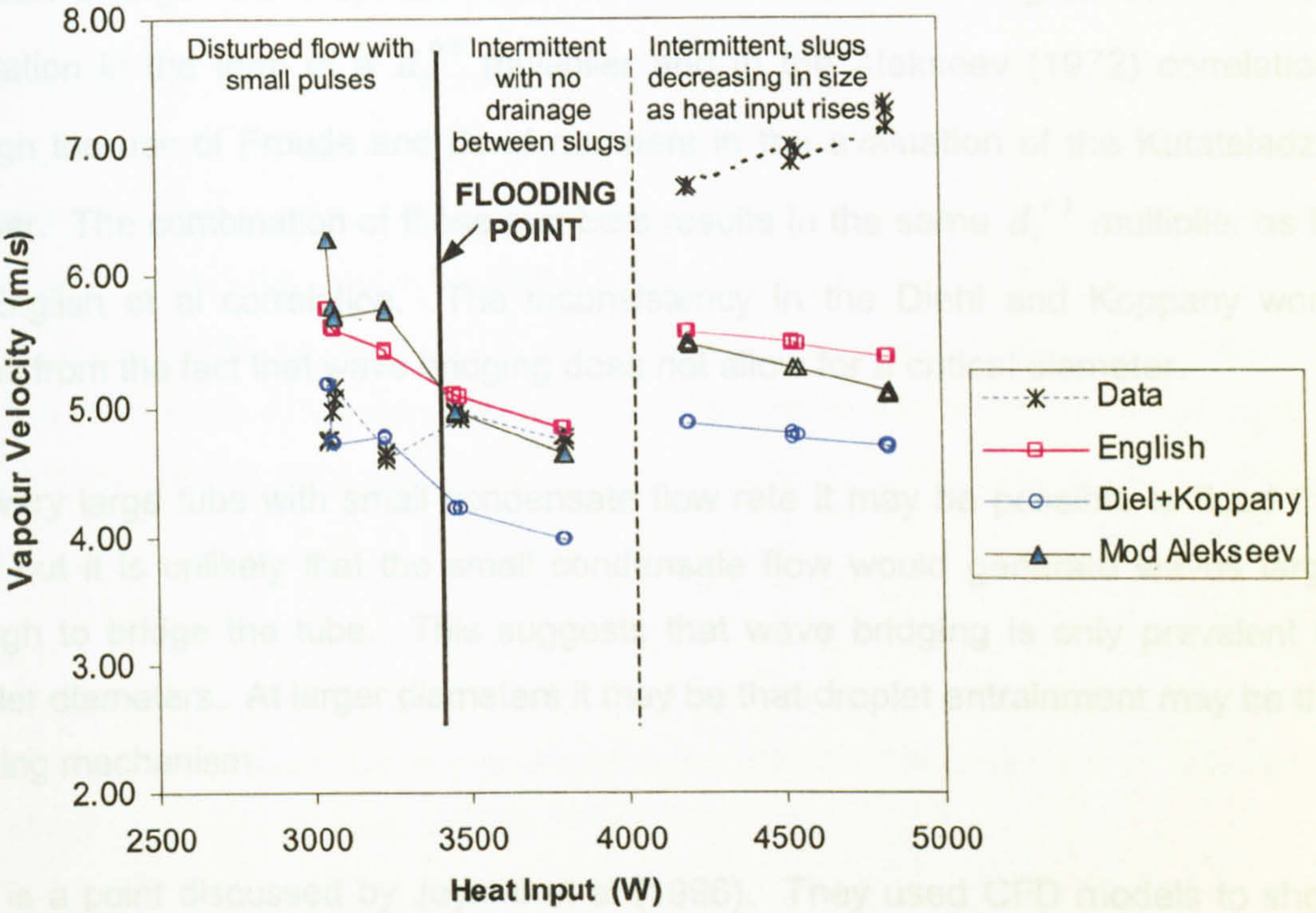

Figure 6.7: Comparison of correlations for Flooding Test 3 ($T_{c,in}$=40°C)

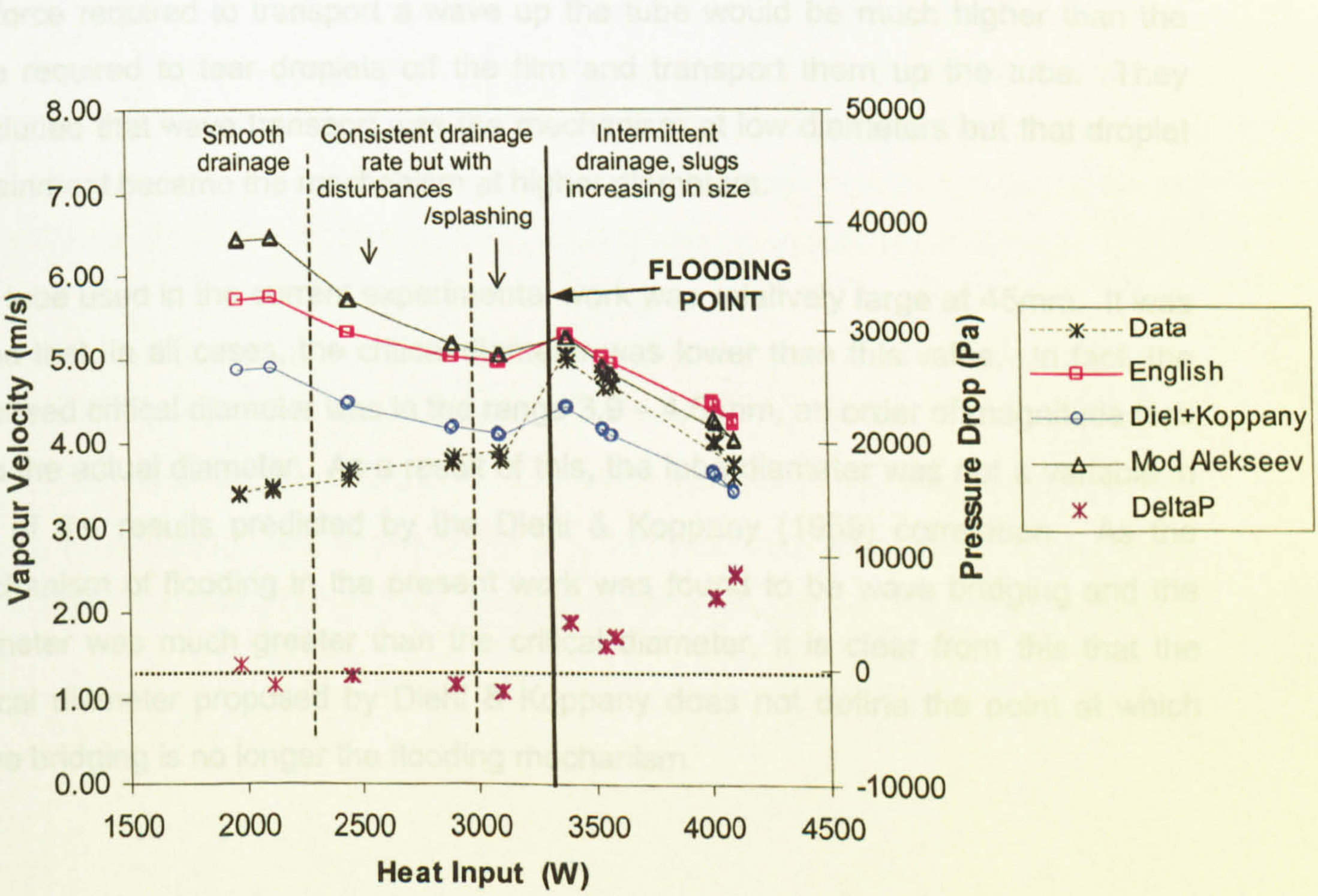

Figure 6.8: Comparison of correlations for Flooding Test 4 ($T_{c,in}$=40°C) with pressure drop also shown

It is therefore sensible to suggest a higher vapour velocity would be required to transport a larger wave up the tube. This is built into the English et al (1963) correlation in the form of a $d_i^{0.3}$ multiplier and in the Alekseev (1972) correlation through the use of Froude and Bond numbers in the evaluation of the Kutateladze number. The combination of these numbers results in the same $d_i^{0.3}$ multiplier as in the English et al correlation. The inconsistency in the Diehl and Koppany work comes from the fact that wave bridging does not allow for a critical diameter.

In a very large tube with small condensate flow rate it may be possible to flood the tube, but it is unlikely that the small condensate flow would generate waves large enough to bridge the tube. This suggests that wave bridging is only prevalent at smaller diameters. At larger diameters it may be that droplet entrainment may be the flooding mechanism.

This is a point discussed by Jayanti et al (1996). They used CFD models to show that the flooding velocity was very dependent on tube diameter. A larger diameters the force required to transport a wave up the tube would be much higher than the force required to tear droplets off the film and transport them up the tube. They concluded that wave transport was the mechanism at low diameters but that droplet entrainment became the mechanism at higher diameters.

The tube used in the current experimental work was relatively large at 45mm. It was found that, in all cases, the critical diameter was lower than this value. In fact, the proposed critical diameter was in the range 3.9 – 4.5 mm, an order of magnitude less than the actual diameter. As a result of this, the tube diameter was not a variable in any of the results predicted by the Diehl & Koppany (1969) correlation. As the mechanism of flooding in the present work was found to be wave bridging and the diameter was much greater than the critical diameter, it is clear from this that the critical diameter proposed by Diehl & Koppany does not define the point at which wave bridging is no longer the flooding mechanism.

6.5.2 Effect of tube end cut

Of the three correlations considered, only the equation of English et al (1963) includes the angle of taper at the bottom of the tube. These workers found that increasing the angle of taper caused an increase in the gas flow rate required to flood their experimental tube. As the angle of taper increased, so did the gas rate at the flooding point and at an angle of 75°, this increase was a significant 54%. Rabas & Arman (2000) argued that the reason for this was the that flooding was caused by a Bernoulli lift effect as discussed in 2.5.1.3. English et al included the angle of taper in their correlation in the form of a $(\cos\theta)^{-0.32}$ multiplier.

In the experimental work reported here the tube was cut to a 45° taper. Using the English et al correlation, this would increase the predicted vapour rate by a factor of 1.23 when compared to a flat cut tube.

If a flat tube had been used in this work, it is expected that the actual vapour velocity required to flood the tube would have been lower. In this case, the English correlation would have predicted a lower value, but the other two correlations would not. This possibly explains why the Diehl & Koppany correlation tended to give very safe estimates. It therefore also suggests that the Alekseev (1972) correlation would overpredict the data had a flat tube been used leading to unsafe predictions.

This can be illustrated by considering Figure 6.9 and Figure *6.10*. In these graphs, the predictions of Diehl & Koppany (1969) and Alekseev (1972) for Flooding Tests 1 and 3 have been adjusted to include the same $(\cos\theta)^{-0.32}$ multiplier suggested by English et al (1963). The result of this is to increase the values predicted by these two therefore allowing for the 45° end cut present on the end of the experimental tube.

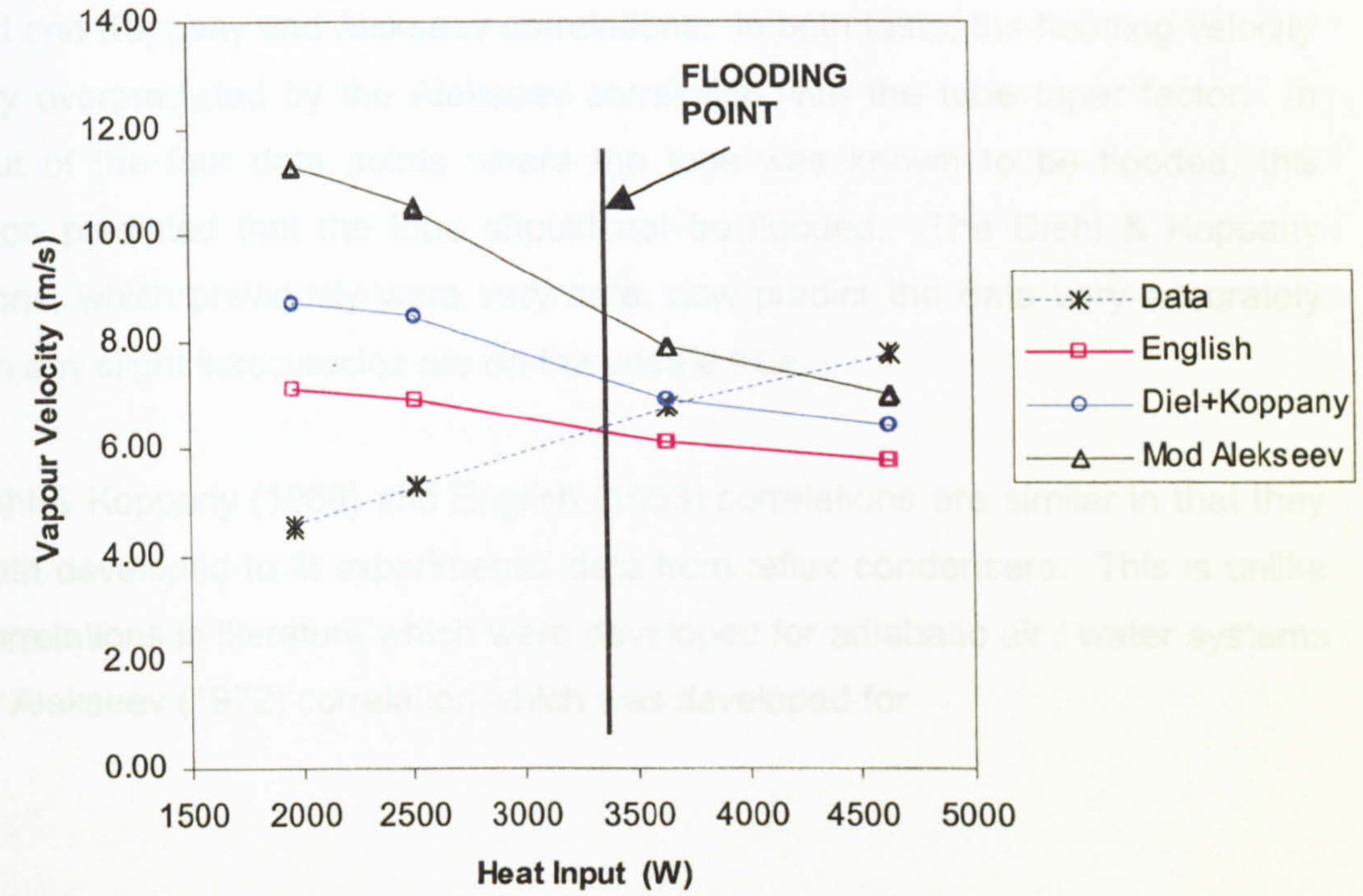

Figure 6.9: Comparison of Flooding Test 1 ($T_{c,\,in}$=40°C) data with correlations modified to include English et al (1963) tube taper factor

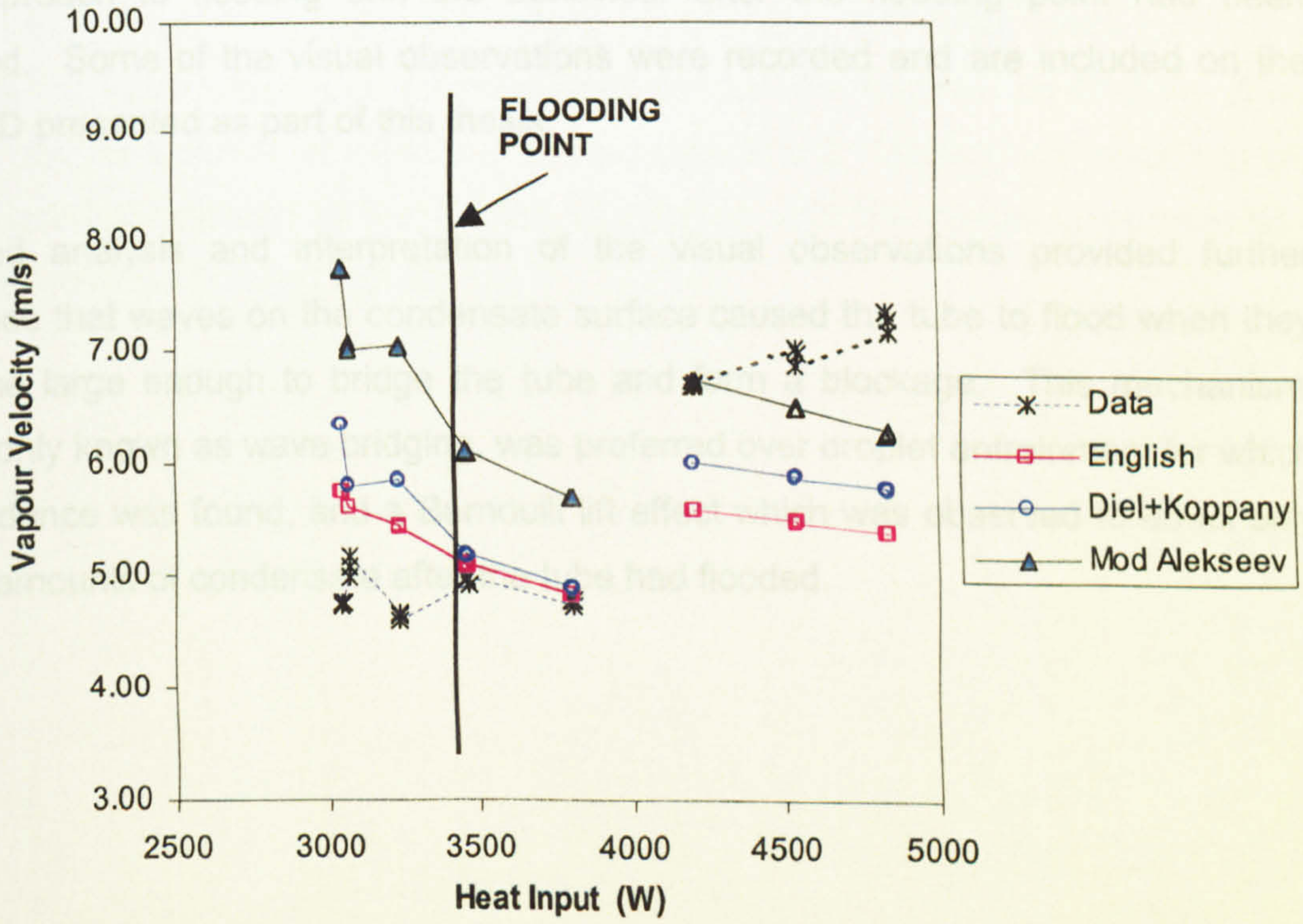

Figure 6.10: Comparison of Flooding Test 3 ($T_{c,\,in}$=40°C) data with correlations modified to include English et al (1963) tube taper factor

It can be seen from these figures that there is a significant effect on the predictions of the Diehl and Koppany and Alekseev correlations. In both tests, the flooding velocity was very overpredicted by the Alekseev correlation with the tube taper factor. In three out of the four data points where the tube was known to be flooded, this correlation predicted that the tube should not be flooded. The Diehl & Koppany predictions, which previously were very safe, now predict the data very accurately although any slight inaccuracies are on the unsafe side.

The Diehl & Koppany (1969) and English (1963) correlations are similar in that they were both developed to fit experimental data from reflux condensers. This is unlike most correlations in literature which were developed for adiabatic air / water systems and the Alekseev (1972) correlation which was developed for

6.6 Summary

This work has added to the available data on flooding inside a single reflux condenser tube. Measurements and visual observations were combined to describe the approach to flooding and the behaviour after the flooding point had been reached. Some of the visual observations were recorded and are included on the data CD presented as part of this thesis.

Detailed analysis and interpretation of the visual observations provided further evidence that waves on the condensate surface caused the tube to flood when they became large enough to bridge the tube and form a blockage. This mechanism, commonly known as wave bridging, was preferred over droplet entrainment for which no evidence was found, and a Bernoulli lift effect which was observed to affect only small amounts of condensate after the tube had flooded.

Through the combination of measurements and visual observations it was found that there was a change in behaviour at the point where condensate drainage became intermittent with a slug flow. There was a marked increase in heat transfer at this point causing the tube to change from a partial to total condenser, and a number of general instabilities were observed. A sharp rise in pressure drop was also recorded at this point. There was no facility to measure any condensate carryover, but as the bottom part of a reflux condenser tube will always flood first it is appropriate to define the flooding point in terms of behaviour at the bottom of the tube.

The flooding point was thus defined as "the vapour velocity (or set of conditions resulting in a vapour velocity) that caused condensate leaving the tube to change from film flow to a slug flow with resulting instabilities and increased pressure drop".

Based on this definition, it was found that three commonly used correlations; English et al (1963), Diehl & Koppany (1969) and Alekseev (1972) as modified by McQuillan & Whalley (1985), were are reasonably successful in determining the flooding point. In each case, the Diehl & Koppany correlation gave the safest prediction with the English and Alekseev correlations vying for the most accurate. The effect of tube diameter and end cut were also discussed. The Diehl and Koppany and Alekseev correlations which were proposed without a tube taper correction were modified to include the same tube taper correction proposed in the English correlation. It was found that the inclusion of this correction led the Diehl & Koppany correlation to give very similar predictions to the English correlation and the Alekseev correlation to overestimate the flooding velocity.

7 Film Theory Based Modelling

7.1 Introduction

The film theory model of the condensation of a binary mixture as proposed by Colburn & Drew (1937) was applied to the experimental data and the results reported in this chapter. Film theory is widely regarded as physically the most accurate model of condensation although its application to reflux condensers has been sparse. Notable work on reflux condensers has included Di Cave et al (1987) and Al-Shammari (2002) both of which are discussed in this chapter.

7.2 Method summary

This is a short summary of the important equations in film theory as applied to vertical condensers. A more complete derivation is given in 2.5 in the literature review.

An overall heat flux, $\dot{q}_T$ was defined from the vapour-liquid interface to the coolant. The resistance over this interval included contributions from the condensate film, wall and coolant. By applying continuity of energy across the interface this heat flux was equal to the sum of latent and sensible heat fluxes in the vapour.

$$U(T_i - T_c) = \alpha'_g(T_v - T_i) + \dot{n}_T \Delta h_v \tag{2.37}$$

Local mole condensing fluxes were evaluated by re-writing the classic Colburn-Drew mass transfer equation, (2.40), to give (2.42).

$$\dot{n}_T = \beta_{1,2} \ln\left[\frac{r_j - \tilde{y}_{jS}}{r_j - \tilde{y}_{jB}}\right] \tag{2.40}$$

$$\dot{n}_j = \beta^*_{1,2}(\tilde{y}_{jB} - \tilde{y}_{jS}) + \tilde{y}_{jB}\dot{n}_T \tag{2.42}$$

$$\dot{n}_T = \sum \dot{n}_j \tag{7.1}$$

These equations were solved simultaneously by finding the local condensing fluxes that solved the heat transfer equations. As the overall mass balance was specified at the start of the calculation this allowed the area requirement to be estimated.

$$\frac{d\dot{N}_g}{dA} = -\dot{n}_T = -\sum_{j=1}^{N} \dot{n}_j \tag{2.46}$$

Temperature and concentration profiles through the condenser were then found by integrating standard equations of downstream development.

$$\frac{dT_g}{dA} = -\frac{\alpha'_G (T_G - T_i)}{\dot{N}_G Cp_G} \tag{2.44}$$

$$\frac{dT_c}{dA} = -\frac{\alpha_c (T_i - T_c)}{\dot{M}_c Cp_c} \tag{2.45}$$

$$\frac{d\tilde{y}_{jB}}{dA} = -\frac{\dot{n}_j - \tilde{y}_{jB}\dot{n}_T}{\dot{N}_G} \tag{2.47}$$

7.3 Implementation of the method

In order to successfully evaluate the local heat and mass transfer and downstream development equations, a simulation program was written in Visual Basic. The simulation integrated directly with the analysis workbook and used the same physical property and VLE functions. Two versions of the simulation program were used, each for a different purpose. The code for the simulations is included in Appendix G.

- Function fn_ColDrew_Reflux

  This version used cell references to read data directly from the spreadsheet and returned the unknown boundary conditions to a row of cells. This was used to run the simulation on a number of experimental runs simultaneously.

- SUB ColDrew_Reflux

  This subroutine version of the program prompted the user to select a column from which the required data were read. An output file was created and the results at each increment displayed and stored in it. This version was used to obtain the detailed profiles through the condenser tube at a cost of being slow to implement.

When simulations of this type are applied to co-current condensers, the boundary conditions at the vapour inlet are all known. The solution is then a simple run through to determine the boundary conditions at the vapour outlet.

Countercurrent vapour and condensate flows in reflux condensers make the situation more complex. The condensate composition at the outlet (bottom of the tube) depends on the condensing fluxes further up the tube which are of course unknown at the start of the calculation. If the simulation is started at the vapour inlet at the bottom of the tube, the solution is therefore iterative. A guess value must be assumed for the condensate composition and an iterative approach used until the boundary conditions at the top of the tube converge to a sensible solution. In the simulation developed here, the condensate composition was changed until the component balances at the top of the tube were solved to give zero condensate flow at exactly the top of the tube.

The issue of liquid mixing was discussed in the literature review 2.5.4. In order to estimate the temperature at the vapour-liquid interface local equilibrium is assumed. The condensate composition, which depends on the extent of liquid mixing, is therefore crucial. As Al-Shammari (2002) concluded that the condensate film in a reflux condenser could be assumed to be well mixed all of the simulations reported here assumed perfect mixing in the condensate.

7.3.1 Calculation of local condensing fluxes

The following algorithm was used to solve the local heat and mass transfer equations at a number of locations in the tube.

Step 1. Mixture and component physical properties estimated at bulk vapour temperature

$$\rho_v,\ Cp_v,\ \widetilde{C}p_v,\ \lambda_v,\ \eta_v,\ D_{AB}$$

$$Cp_{v,P},\ Cp_{v,I},\ h_P,\ h_I,\ \Delta h_{v,P},\ \Delta h_{v,I}$$

Step 2. Pentane mole fraction at interface

$\widetilde{x}_{P,i} = \widetilde{x}_{P,B}$ (perfect mixing assumed)

Step 3. Vapour interfacial composition and dew point temperature from previously defined VB functions

$$\widetilde{y}_{Pen,i} = fn\_EqmVapComp(P_{sat}, \widetilde{x}_{P,i})$$

$$T_i = fn\_Tdew(P_{sat}, \widetilde{y}_{P,i})$$

Step 4. Vapour heat transfer coefficient estimated (see 7.3.3)

α_v

Step 5. Mass transfer coefficient calculated from Chilton-Colburn analogy (1934)

$$\beta_G = \frac{\alpha_v}{\widetilde{C}p_v}\left(\frac{Pr_v}{Sc}\right)^{2/3} \tag{7.2}$$

Step 6. Total condensing flux estimated

$\dot{n}_T$

Step 7. Calculate mass transfer rate factor

$$\phi_M = \frac{n_T}{\beta_G} \tag{2.43}$$

Step 8. Corrected mass transfer coefficient

$$\beta_G^* = \left[\frac{\phi_M}{e^{\phi_M} - 1}\right]\beta_G \tag{7.3}$$

Step 9. Condensing mole fluxes

$$\dot{n}_P = \beta_G^*\left(\tilde{y}_{P,B} - \tilde{y}_{P,i}\right) + \tilde{y}_{PB}\dot{n}_T \tag{2.42}$$

$$\dot{n}_I = \dot{n}_T - \dot{n}_P \tag{7.4}$$

Step 10. Heat transfer rate factor

$$\phi_H = \frac{\dot{n}_T\, Cp_v}{\alpha_v} \tag{7.5}$$

Step 11. Corrected heat transfer coefficient

$$\alpha_v^* = \left[\frac{\phi_H}{e^{\phi_H} - 1}\right]\alpha_v \tag{2.30}$$

Step 12. Estimate condensate film heat transfer coefficient

$$\alpha_f$$

Step 13. Heat flux from interface to coolant

$$\frac{1}{U} = \frac{1}{\alpha_f} + \frac{1}{\alpha_w} + \frac{1}{\alpha_c} \tag{7.6}$$

$$\dot{q}_1 = \frac{T_i - T_c}{U} \tag{7.7}$$

Step 14. Component enthalpies at interface

$$h_{P,i},\ h_{I,i}$$

Step 15. Heat flux from vapour to interface (latent and sensible)

$$\dot{q}_2 = \alpha_v^*(T_v - T_i) + \dot{n}_P(h_{P,B} - h_{P,i} + \Delta h_{v,P})\tilde{M}_P \tag{7.8}$$
$$+ \dot{n}_P(h_{I,B} - h_{I,i} + \Delta h_{v,I})\tilde{M}_I$$

Step 16. Compare $\dot{q}_1$ and $\dot{q}_2$. Iterate from Step 6 until $\dot{q}_1 = \dot{q}_2$

7.3.2 Downstream development and simulation solution

The condenser was split into 20 increments with an equal amount of condensation in each stage. The following algorithm was then used to calculate the area requirements and temperature profiles (by integrating the downstream development equations using finite differences) and perform the iterations leading to a sensible solution. It should be noted that in the following algorithm *in* and *out* refer to incremental conditions whereas *IN* and *OUT* refer to the boundary conditions at the top and bottom of the simulated tube.

Step 1. Amount of vapour condensed in each stage from overall mass / mole balance

$$d\dot{N}_v = \frac{\dot{N}_{v,IN} - \dot{N}_{v,OUT}}{20} \quad (7.9)$$

Step 2. Starting guess for condensate composition at outlet

$$\widetilde{x}_{P,OUTguess}$$

Step 3. Solve local heat and mass transfer equations for condensing fluxes over increment (see 1.3.1)

$$\dot{q}\,,\ \dot{n}_P\,,\ \dot{n}_I\,,\ \alpha_v^*\,,\ \beta_G^*\,,\ T_i$$

Step 4. Calculate increment area

$$A_{inc} = \frac{d\dot{N}_v}{\dot{n}_P + \dot{n}_I} \quad (7.10)$$

Step 5. Heat load for increment

$$\dot{Q}_{inc} = \frac{\dot{q}}{A_{inc}} \quad (7.11)$$

Step 6. Component balance over increment

$$\dot{N}_{vP,\,out} = \tilde{y}_{P,\,in}\dot{N}_{V,\,in} - \left(\dot{n}_P\, A_{inc}\right) \tag{7.12}$$

$$\dot{N}_{lP,\,in} = \tilde{x}_{P,\,out}\dot{N}_{l,\,out} - \left(\dot{n}_P\, A_{inc}\right) \tag{7.13}$$

Step 7. Compositions out of increment

$$\tilde{y}_{P,\,out} = \frac{\dot{N}_{vP,\,out}}{\dot{N}_{v,\,out}} \tag{7.14}$$

$$\tilde{x}_{P,\,in} = \frac{\dot{N}_{lP,\,in}}{\dot{N}_{l,\,in}} \tag{7.15}$$

Step 8. Change in vapour and coolant temperatures

$$T_{v,\,out} = T_{v,\,in} - A_{inc}\left[\frac{\alpha_V^*\left(T_{v,\,in} - T_i\right)}{\dot{N}_{V,\,in}\tilde{C}p_{v,in}}\right] \tag{7.16}$$

$$T_{c,\,in} = T_{c,\,out} - A_{inc}\left[\frac{\dot{q}}{\dot{M}_c Cp_c}\right] \tag{7.17}$$

Step 9. Steps 3 – 8 repeated for all 20 increments to get boundary conditions at the top of the tube.

$$\dot{N}_{lP,\,IN},\ \dot{N}_{vP,\,OUT},\ \tilde{y}_{P,\,OUT},\ T_{v,\,OUT},\ T_{c,\,IN}$$

Step 10. Iterate value of $\tilde{x}_{P,\,OUTguess}$ from Step 2 until $\dot{N}_{lP,\,IN} = 0$ (no condensate flow into top of tube).

Step 11. Total area requirement and heat load

$$A_{tot} = \sum A_{inc} \tag{7.18}$$

$$\dot{Q}_{tot} = \sum \dot{Q}_{inc} \tag{7.19}$$

7.3.3 Prediction of heat transfer coefficients

The accuracy of any simulation of this type will depend on how well the heat transfer processes are modelled. It was therefore decided to base the heat transfer coefficients on the results reported in Chapter 5 rather than standard correlations. Local condensate film coefficients were therefore predicted using equation (5.6), which corrected for the extra disturbances in the film caused by countercurrent vapour flow, while the vapour coefficients were predicted using Petukhov's correlation corrected for the relative film velocity as described in 5.4.3.

$$Nu_c = 0.0164\, Re_c^{0.8}\, Pr_c^{0.4} \tag{5.1}$$

$$\alpha_f = 0.808\, \mathrm{Re}_l^{-0.210} \tag{5.6}$$

$$Nu_v = \frac{\left(\frac{f}{2}\right) Re_v^{*}\, Pr_v}{1.07 + \left(12.7\left(\frac{f}{2}\right)^{1/2}\left(\mathrm{Pr}_v^{2/3} - 1\right)\right)} \tag{2.9}$$

where

$$f = \frac{1}{4\left(1.82 \log_{10} Re_v - 1.64\right)^2} \tag{2.10}$$

and

$$Re_v^{*} = f\left(u_v - u_f\right) \tag{7.20}$$

7.4 Analysis of individual runs

The subroutine based version of the film theory simulation created a set of output files each containing a detailed results table for a single experimental run. 2 samples of these output files are displayed on the following pages one of each where the tube length was well predicted (run 1.6, Figure 7.1) and where the tube length was under-predicted (run 2.10, Figure 7.2). These tables allow the important trends through the simulated condenser tube such as temperature and composition profiles to be analysed and discussed.

7.4.1 Structure of the output file

Each output files include 5 distinct coloured regions. The two yellow areas contained all of the data used as inputs to the simulation (top region) and a summary of the main results (bottom region). To the far right hand side, the orange region contained a summary of the iterations indicating the path followed to arrive at a sensible solution. The values 1E+20 and 2E+20 were flags used to indicate the physically impossible situations of a pentane mole fraction in the vapour above unity and a negative vapour flow rate respectively. The simulation was coded to react to these flags and change the guess value for condensate composition accordingly.

The blue and yellow areas displayed the data at each stage of the simulation, with the flows temperatures and compositions in the blue area and the results from the local heat and mass transfer calculations in the green area. At the bottom of the tube, the values in the blue area are the same values displayed in the yellow data region. These were then passed into the local heat and mass transfer calculations described in 7.3.1 and the results of the calculations used to increment the flows, temperatures and compositions. As the tube was split into 20 increments with input and output values, there were 21 sets of values in the blue region.

Colburn_Drew Analysis: Perfect Mixing Model Reflux Condenser

Date 20010823
Rnum 1-6_R

DATA				
Bulk Vapour		Coolant		Reflux Ratio
Temp	93.95942	Temp	52.2	0.754
Press	154128.5	HTC	6497	
Mole Flow	1.16E-04	Mass Flow	5.76E-02	
Mol Fr	0.517			

		Flows and temperatures through the condenser									Results from heat and mass transfer step									
	Inc	yP	xP	Nvap	Nliq	NliqPen	Qcum	Tbulk	Twater	Twall	q	Len	nPen	nIso	Ucond	dTGbydA	Tdew	BetaGx	Rate Factor	Vapour HTC
Top	21	0.617		2.84E-05		-1.19E-11	3074.9	88.474	39.389	43.010										
	20	0.617	0.617	3.28E-05	4.37E-06	2.69E-06	2937.2	88.479	39.960	43.500	23525	0.041	0.000460	0.000286	484.9	0.0862	63.35	1.233E-06	6.408	15.0
	19	0.617	0.616	3.72E-05	8.73E-06	5.38E-06	2799.5	88.493	40.532	43.747	22998	0.042	0.000449	0.000281	479.5	0.3478	63.39	4.485E-06	5.097	17.8
	18	0.616	0.615	4.15E-05	1.31E-05	8.05E-06	2661.6	88.525	41.105	44.087	20890	0.047	0.000405	0.000257	440.5	1.0071	63.45	1.008E-05	4.199	19.6
	17	0.616	0.613	4.59E-05	1.75E-05	1.07E-05	2523.2	88.579	41.679	44.479	19379	0.051	0.000371	0.000240	413.2	2.0381	63.54	1.765E-05	3.574	21.3
	16	0.614	0.610	5.03E-05	2.18E-05	1.33E-05	2384.2	88.658	42.256	44.905	18193	0.054	0.000343	0.000228	392.1	3.3850	63.66	2.689E-05	3.103	23.0
	15	0.612	0.607	5.46E-05	2.62E-05	1.59E-05	2244.2	88.766	42.837	45.358	17214	0.058	0.000318	0.000219	374.8	4.9682	63.81	3.750E-05	2.729	24.5
	14	0.610	0.603	5.90E-05	3.06E-05	1.84E-05	2103.1	88.904	43.422	45.832	16380	0.061	0.000294	0.000212	360.2	6.7079	63.99	4.925E-05	2.424	6.0
	13	0.607	0.599	6.34E-05	3.49E-05	2.09E-05	1960.5	89.074	44.014	46.325	15655	0.064	0.000272	0.000207	347.4	8.5346	64.20	6.191E-05	2.168	27.6
	12	0.604	0.594	6.77E-05	3.93E-05	2.33E-05	1816.1	89.277	44.613	46.837	15016	0.068	0.000251	0.000203	336.2	10.3915	64.45	7.532E-05	1.950	29.1
	11	0.600	0.588	7.21E-05	4.37E-05	2.57E-05	1669.6	89.514	45.221	47.367	14447	0.072	0.000231	0.000200	326.2	12.2344	64.73	8.934E-05	1.761	30.6
	10	0.595	0.582	7.65E-05	4.80E-05	2.79E-05	1520.6	89.788	45.840	47.915	13938	0.076	0.000211	0.000197	317.2	14.0291	65.05	1.038E-04	1.596	32.1
	9	0.590	0.574	8.08E-05	5.24E-05	3.01E-05	1368.8	90.098	46.470	48.482	13482	0.080	0.000192	0.000196	309.0	15.7498	65.41	1.187E-04	1.451	33.5
	8	0.583	0.566	8.52E-05	5.68E-05	3.22E-05	1213.7	90.447	47.114	49.069	13072	0.084	0.000173	0.000195	301.7	17.3767	65.81	1.339E-04	1.322	35.0
	7	0.576	0.557	8.96E-05	6.11E-05	3.41E-05	1055.0	90.836	47.772	49.678	12706	0.088	0.000154	0.000195	295.1	18.8947	66.27	1.492E-04	1.207	36.4
	6	0.569	0.548	9.39E-05	6.55E-05	3.59E-05	892.1	91.266	48.448	50.310	12381	0.093	0.000136	0.000196	289.1	20.2913	66.77	1.648E-04	1.104	37.9
	5	0.560	0.537	9.83E-05	6.99E-05	3.75E-05	724.7	91.738	49.143	50.966	12094	0.098	0.000119	0.000197	283.9	21.5563	67.34	1.803E-04	1.011	39.4
	4	0.551	0.525	1.03E-04	7.42E-05	3.90E-05	552.2	92.253	49.859	51.650	11846	0.103	0.000101	0.000199	279.4	22.6805	67.96	1.960E-04	0.928	40.9
	3	0.540	0.513	1.07E-04	7.86E-05	4.03E-05	374.2	92.811	50.597	52.362	11635	0.108	0.000084	0.000201	275.6	23.6557	68.66	2.115E-04	0.854	42.4
	2	0.529	0.499	1.11E-04	8.30E-05	4.14E-05	190.2	93.412	51.361	53.104	11462	0.114	0.000068	0.000204	272.6	24.4738	69.42	2.270E-04	0.788	43.9
Bottom	1	0.517	0.484	1.16E-04	8.73E-05	4.23E-05	0.0	93.959	52.150		11326	0.119	0.000052	0.000208	270.9	25.0066	70.27	2.422E-04	0.729	45.5
												Total 1.520								

Iterations		
No.	xPout	NliqPen
1	0.4166	1E+20
2	0.4266	1E+20
3	0.4366	1E+20
4	0.4466	1E+20
5	0.4566	1E+20
6	0.4666	-2.15E-06
7	0.4766	-9.31E-07
8	0.4842	5.28E-08
9	0.4838	-1.47E-09
10	0.4838	-1.19E-11

Results Summary	
yP bot	0.517
yP top	0.617
xP bot	0.484
Tube length	1.52
Heat load	3075
Tvap out	88.47
Tcw in	39.39

Figure 7.1: Detailed simulation results for run M1.6

Colburn_Drew Analysis: Perfect Mixing Model Reflux Condenser

Date 20011127
Rnum 2-10_R

DATA				
Bulk Vapour		Coolant		Reflux Ratio
Temp	77.447	Temp	41.2	0.761
Press	79128.19	HTC	6098	
Mole Flow	6.10E-05	Mass Flow	5.80E-02	
Mol Fr	0.401			

		Flows and temperatures through the condenser									Results from heat and mass transfer step										
	Inc	yP	xP	Nvap	Nliq	NliqPen	Qcum	Tbulk	Twater	Twall	q	Len	nPen	nIso	Ucond	dTGbydA	Tdew	BetaGx	Rate Factor	Vapour HTC	
Top	21	**0.503**		**1.46E-05**		3.93E-12	**1670.6**	**73.040**	**34.319**	**36.492**											
	20	0.503	0.502	1.69E-05	2.32E-06	1.16E-06	1592.5	73.050	34.641	36.729	13253	0.042	0.000197	0.000196	345.0	0.2034	46.81	1.335E-06	5.69	8.8	
	19	0.502	0.500	1.92E-05	4.64E-06	2.32E-06	1514.2	73.081	34.963	36.877	12738	0.043	0.000188	0.000190	334.2	0.8779	46.92	4.925E-06	4.35	10.6	
	18	0.501	0.497	2.15E-05	6.96E-06	3.46E-06	1435.7	73.139	35.286	37.081	11673	0.048	0.000169	0.000176	308.4	2.0105	47.07	9.319E-06	3.64	11.6	
	17	0.499	0.493	2.38E-05	9.28E-06	4.57E-06	1357.0	73.225	35.611	37.317	10944	0.051	0.000155	0.000167	291.0	3.4688	47.25	1.455E-05	3.14	12.5	
	16	0.497	0.489	2.62E-05	1.16E-05	5.67E-06	1277.8	73.340	35.937	37.575	10404	0.054	0.000144	0.000161	278.2	5.1102	47.47	2.038E-05	2.77	13.4	
	15	0.494	0.483	2.85E-05	1.39E-05	6.73E-06	1198.1	73.483	36.265	37.849	9987	0.056	0.000133	0.000158	268.3	6.8148	47.73	2.661E-05	2.48	14.3	
	14	0.490	0.478	3.08E-05	1.62E-05	7.76E-06	1117.8	73.652	36.596	38.137	9658	0.059	0.000124	0.000155	260.6	8.4950	48.02	3.311E-05	2.24	15.2	
	13	0.486	0.472	3.31E-05	1.86E-05	8.75E-06	1036.9	73.847	36.929	38.436	9397	0.061	0.000115	0.000154	254.5	10.0924	48.34	3.977E-05	2.05	16.1	
	12	0.481	0.465	3.54E-05	2.09E-05	9.70E-06	955.2	74.066	37.266	38.746	9188	0.063	0.000107	0.000154	249.7	11.5713	48.69	4.651E-05	1.89	16.9	
	11	0.475	0.458	3.78E-05	2.32E-05	1.06E-05	872.7	74.305	37.606	39.065	9024	0.065	0.000100	0.000154	245.9	12.9126	49.08	5.327E-05	1.75	17.8	
	10	0.469	0.450	4.01E-05	2.55E-05	1.15E-05	789.5	74.564	37.949	39.392	8896	0.066	0.000093	0.000155	242.9	14.1083	49.48	6.001E-05	1.63	18.6	
	9	0.463	0.442	4.24E-05	2.78E-05	1.23E-05	705.3	74.841	38.296	39.727	8799	0.068	0.000086	0.000157	240.8	15.1580	49.92	6.671E-05	1.53	19.4	
	8	0.456	0.434	4.47E-05	3.02E-05	1.31E-05	620.3	75.132	38.646	40.070	8729	0.069	0.000079	0.000159	239.2	16.0661	50.38	7.335E-05	1.45	20.3	
	7	0.449	0.425	4.70E-05	3.25E-05	1.38E-05	534.3	75.437	39.000	40.420	8682	0.070	0.000073	0.000161	238.3	16.8397	50.87	7.990E-05	1.37	21.1	
	6	0.442	0.416	4.94E-05	3.48E-05	1.45E-05	447.5	75.754	39.358	40.776	8656	0.071	0.000067	0.000164	237.8	17.4874	51.37	8.636E-05	1.30	21.9	
	5	0.434	0.407	5.17E-05	3.71E-05	1.51E-05	359.8	76.080	39.719	41.139	8648	0.072	0.000062	0.000167	237.8	18.0188	51.90	9.272E-05	1.24	22.8	
	4	0.426	0.398	5.40E-05	3.94E-05	1.57E-05	271.1	76.414	40.085	41.508	8656	0.072	0.000056	0.000170	238.3	18.4432	52.45	9.898E-05	1.19	23.6	
	3	0.418	0.388	5.63E-05	4.18E-05	1.62E-05	181.6	76.754	40.453	41.883	8679	0.073	0.000051	0.000174	239.1	18.7702	53.02	1.051E-04	1.14	24.4	
	2	0.410	0.379	5.86E-05	4.41E-05	1.67E-05	91.2	77.099	40.826	42.263	8715	0.073	0.000046	0.000178	240.3	19.0086	53.61	1.112E-04	1.10	25.2	
Bottom	1	**0.401**	**0.369**	**6.10E-05**	**4.64E-05**	1.71E-05	0.0	**77.447**	**41.202**		8762	**0.074**	0.000041	0.000182	241.7	19.1670	54.22	1.172E-04	1.07	26.0	
												Total 1.249									

Iterations		
No.	xPout	NliqPen
1	0.3010	1E+20
2	0.3110	1E+20
3	0.3210	1E+20
4	0.3310	1E+20
5	0.3410	1E+20
6	0.3510	1E+20
7	0.3610	-7.5E-07
8	0.3710	2.85E-07
9	0.3682	-7.32E-08
10	0.3688	-8.39E-09
11	0.3689	2.28E-10
12	0.3689	3.93E-12

Results Summary	
yP bot	0.401
yP top	0.503
xP bot	0.369
Tube length	1.25
Heat load	1671
Tvap out	73.04
Tcw in	34.32

Figure 7.2: Detailed simulation results for run M2.10

7.4.2 Temperature profiles

Comparing the data returned in the output files to the measured experimental data in the form of a temperature profile is a useful analysis tool. The temperature profile for run M1.6 (run 6 of mixture 1) is displayed in Figure 7.3. This is a similar diagram to Figure 5.9 but with the simulated vapour and coolant temperatures included. This run was selected for this purpose as the tube length was predicted to within 2.2cm, an important fact as the temperatures are plotted against tube length.

It is apparent from Figure 7.3 that the coolant and wall temperature profiles were predicted almost perfectly. This is partially a vindication of the coolant heat transfer coefficient but also a result of the form of simulation used. The majority of heat transferred from the vapour is in the form of latent heat. As the ratio of condensate to vapour and thus overall mass balance was specified at the start of the simulation, the predicted heat load will be close the experimental value even if the sensible heat transfer is poorly simulated.

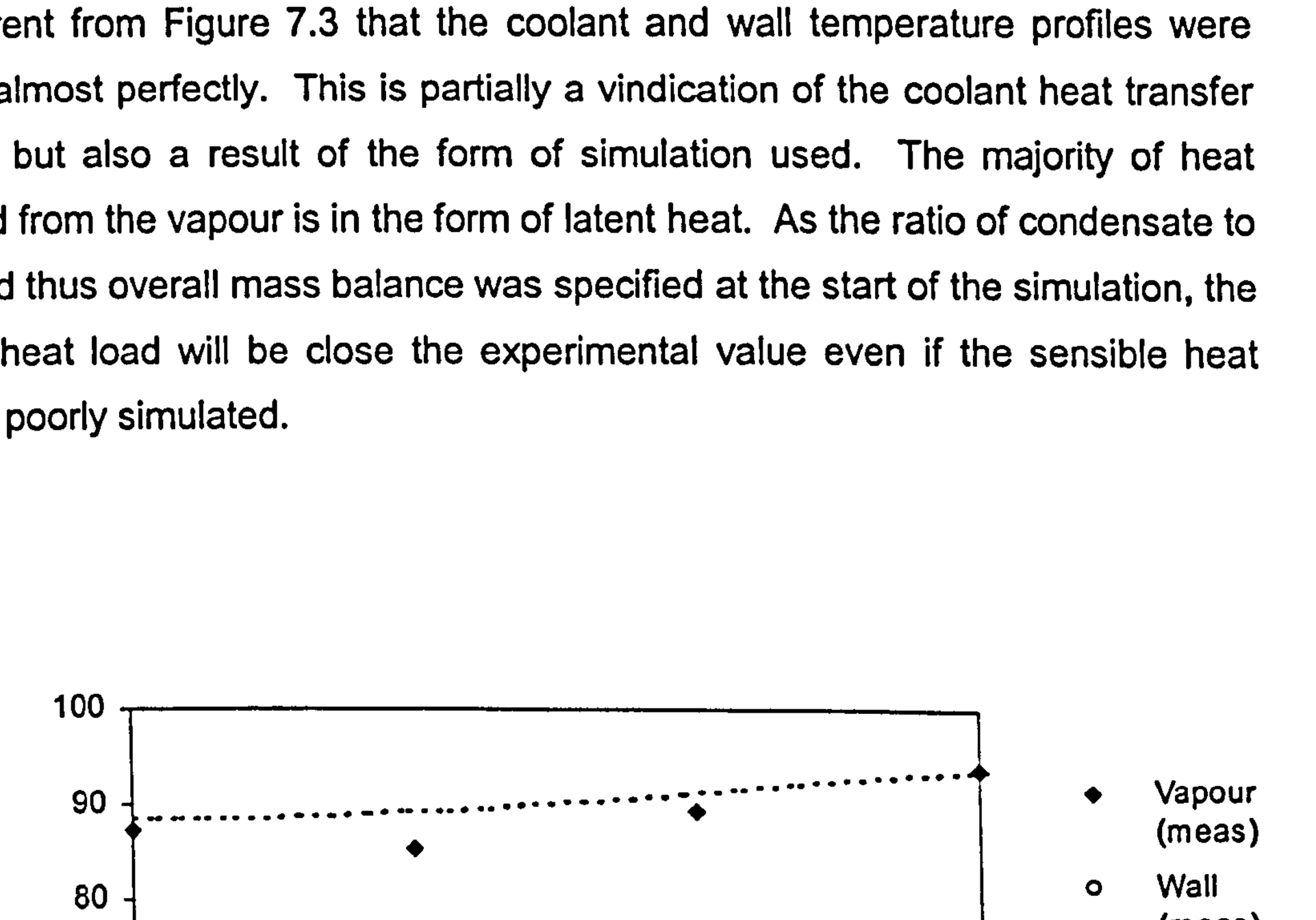

Figure 7.3: Temperature profile for run M1.6

If the heat load is similar to that in an experimental run then it follows that the coolant profile will be well modelled and in fact in all of the film theory simulations, the coolant temperature change was within 0.55°C of the experimental value. Of course, if the heat load is accurate and the coolant heat transfer coefficient badly modelled this would be indicated in the simulation by poor modelling of the wall temperature profile.

It is also noticeable that the vapour temperature profile is less well predicted. This was a common result that is discussed in more detail later. The important point to be noted from the shape of the profile is that the vapour temperature drop is steepest at the bottom of the tube with the gradient reducing through the tube. This agrees with experimental measurements that showed a larger temperature drop at the bottom of the tube.

7.5 Results Summary

The success or otherwise of the film theory simulation can be assessed by comparing experimental data with model predictions. Given a known inlet stream and amount of vapour to be condensed, the simulation predicted the outlet streams and area required to meet the duty. Of the two outlet streams, it is only necessary to consider the vapour stream, as the condensate temperature is of limited importance and the composition of the condensate is not independent of the vapour composition.

7.5.1 Tube length predictions

The predicted area requirements are presented in Figure 7.4 and summarised in Table 7.1 in terms of the length of tube with exactly the same cross section as the test condenser. Overall, the simulation produces relatively accurate results although the tendency is for an under-prediction of the required area. In all, there were 46 data points. In 71.3 % of these points, the tube length was predicted to within 10% of the actual length of 1.5m with 91.3% of the predictions within 20% of the tube length.

The clear trend in Figure 7.4 is that the predicted area (expressed as tube length) increases as the condensate heat flux increases. If the heat transfer coefficients used in the simulation had been the same as those measured experimentally, and the model was an accurate representation of the process then tube lengths close to the actual value would be expected. It is therefore important to establish whether this trend in Figure 7.4 was caused by the limitations of the model itself or the heat transfer coefficients used in the simulation program. As the resistance in the vapour was controlling, the effect of the sensible vapour coefficient was analysed.

Although the simulation evaluates heat transfer coefficients locally at a number of points in the tube, the limitations of the experimental facility meant that local vapour heat transfer coefficients were not measurable. In 5.4.3 it was found that mean sensible heat transfer coefficients measured experimentally, $\overline{\alpha}_{v,exp}$, were best predicted by modifying the correlation of Petukhov (1970) for the effects of mass transfer and film velocity, $\overline{\alpha}^{*}_{vP,FV}$ and evaluating at the mean vapour Reynolds number. This was displayed in Figure 5.19. These same corrections were applied when predicting the local coefficients in the simulation as it was expected that similar trends would be repeated locally.

The effect of the sensible vapour heat transfer coefficient on the tube length is illustrated well by Figure 7.5. In this figure, tube lengths predicted by the simulation are plotted against the difference between $\overline{\alpha}_{v,exp}$ and $\overline{\alpha}^{*}_{vP,FV}$ expressed as a percentage of the experimental value.

Length unit	Mix 1	Mix 2	Mix 3
m	1.20 – 1.54	1.15 – 1.43	1.33 – 1.61
% of actual	79.8 – 102.9	76.9 – 95.5	88.5 – 107.6

Table 7.1: Tube length predictions for each mixture

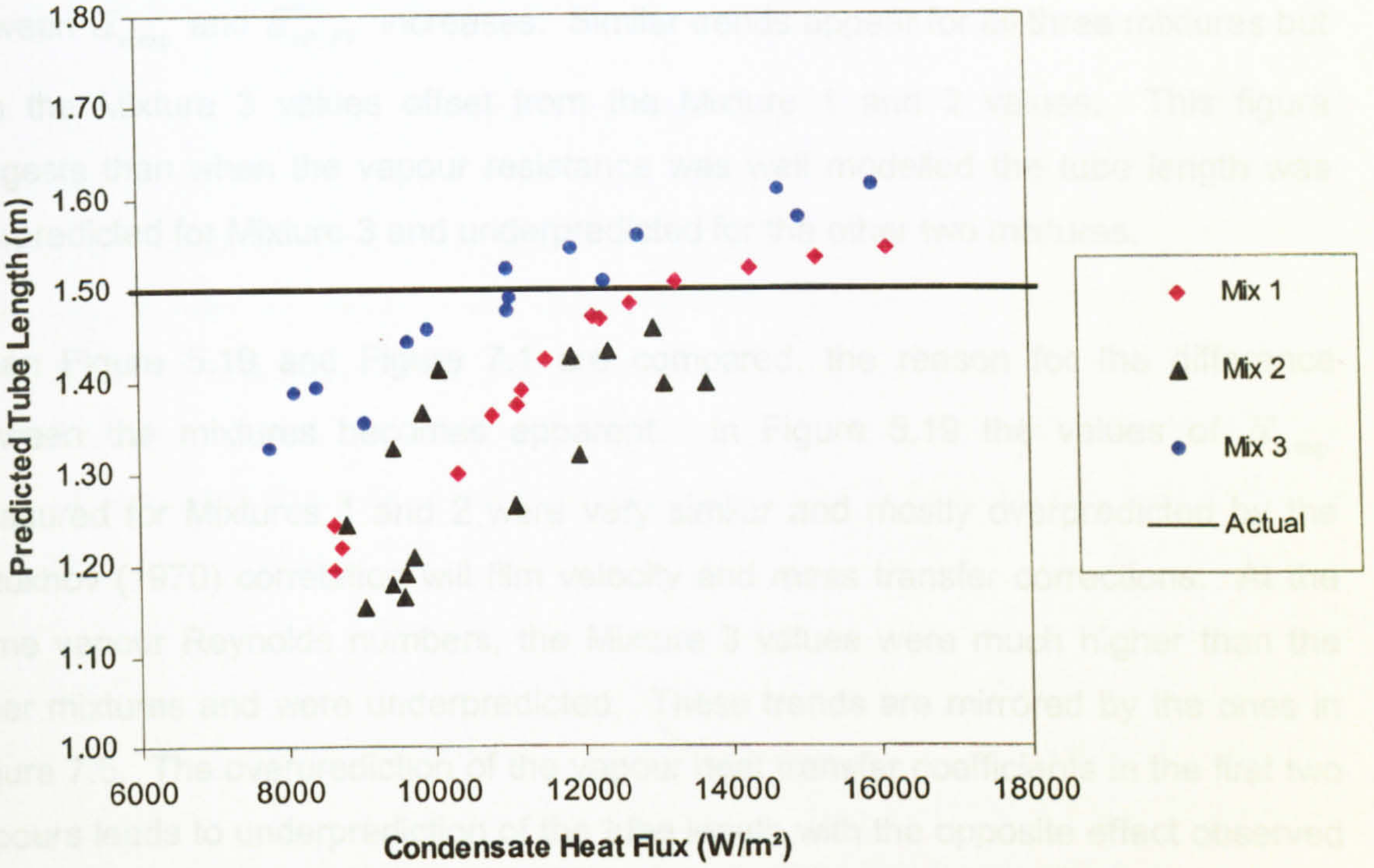

Figure 7.4: Tube lengths predicted by the film theory simulation

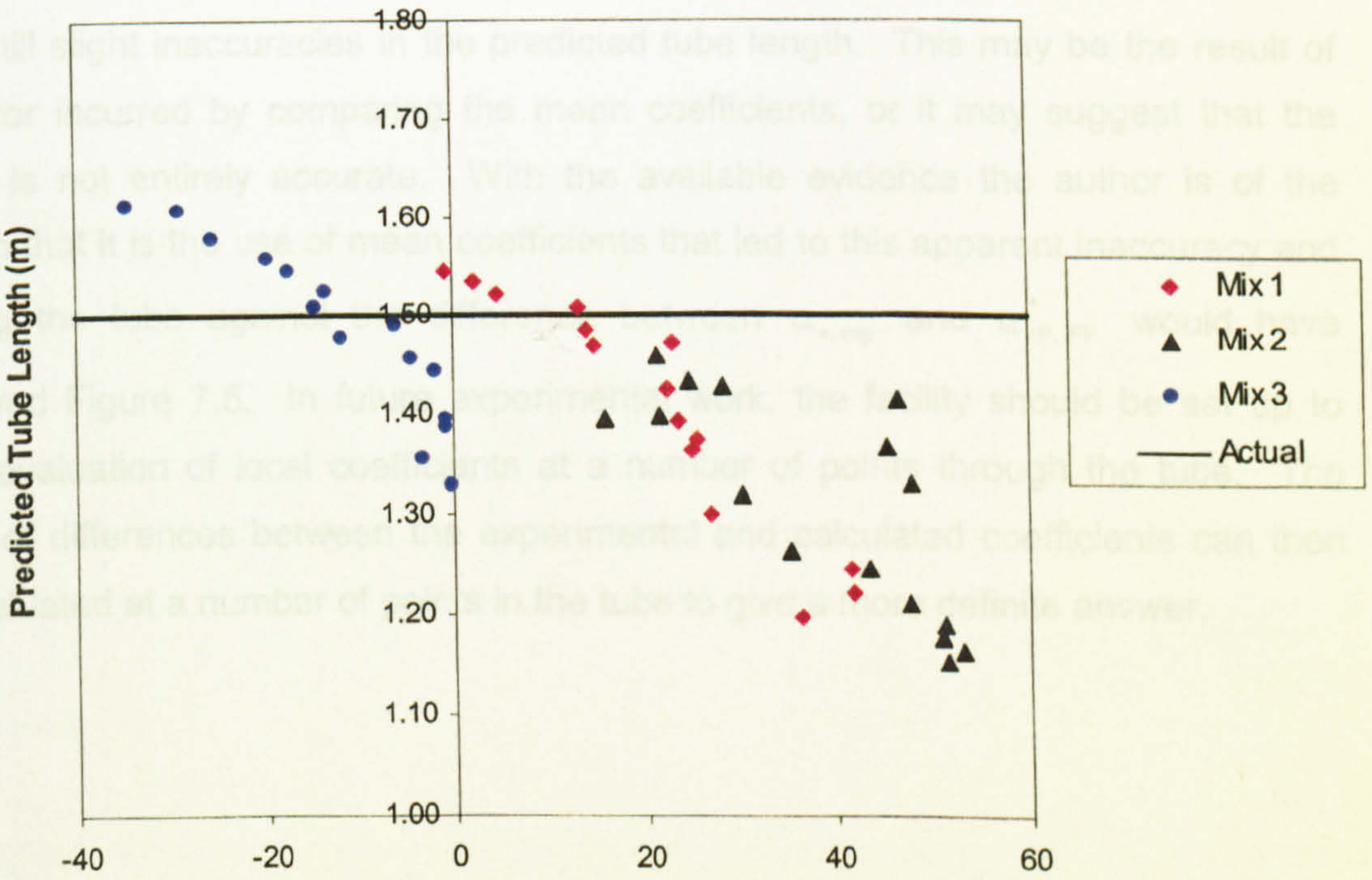

Figure 7.5: Predicted tube lengths against difference between calculated and mean experimental vapour heat transfer coefficient

It shows the sensitivity of the model to the selection of vapour heat transfer coefficient by indicating that the tube length inaccuracies increase as the difference between $\overline{\alpha}_{v,\exp}$ and $\overline{\alpha}^{\bullet}_{vP,FV}$ increases. Similar trends appear for all three mixtures but with the Mixture 3 values offset from the Mixture 1 and 2 values. This figure suggests than when the vapour resistance was well modelled the tube length was overpredicted for Mixture 3 and underpredicted for the other two mixtures.

When Figure 5.19 and Figure 7.1 are compared, the reason for the difference between the mixtures becomes apparent. In Figure 5.19 the values of $\overline{\alpha}_{v,\exp}$ measured for Mixtures 1 and 2 were very similar and mostly overpredicted by the Petukhov (1970) correlation will film velocity and mass transfer corrections. At the same vapour Reynolds numbers, the Mixture 3 values were much higher than the other mixtures and were underpredicted. These trends are mirrored by the ones in Figure 7.5. The overprediction of the vapour heat transfer coefficients in the first two vapours leads to underprediction of the tube length with the opposite effect observed in Mixture 3.

In the data points where the values of $\overline{\alpha}_{v,\exp}$ and $\overline{\alpha}^{\bullet}_{vP,FV}$ were almost equal, there were still slight inaccuracies in the predicted tube length. This may be the result of the error incurred by comparing the mean coefficients, or it may suggest that the model is not entirely accurate. With the available evidence the author is of the opinion that it is the use of mean coefficients that led to this apparent inaccuracy and plotting the tube against the difference between $\alpha_{v,\exp}$ and $\alpha^{*}_{vP,FV}$ would have improved Figure 7.5. In future experimental work, the facility should be set up to allow evaluation of local coefficients at a number of points through the tube. The effect of differences between the experimental and calculated coefficients can then be evaluated at a number of points in the tube to give a more definite answer.

7.5.2 *Prediction of vapour temperature*

The outlet temperatures predicted by the simulation are plotted against the experimental values in Figure 7.6. It is apparent that in all of the simulated runs the vapour temperature was over-predicted by +0.2°C to +4.0°C. Alternatively, it can be said that the level of vapour cooling was underestimated in the simulation. When considered in the context of temperature drop through the tube, these over-predictions are quite large. With the highest experimental temperature drop at just 8.3°C, the worst case was when the predicted temperature drop was just 54.0% of the experimental value.

The fact that the tube length was over-predicted in only a few cases indicated that the reason for this was not linked to the value of the vapour heat transfer coefficient. In the equation (7.16) for vapour temperature out of an increment the only variables were the vapour heat transfer coefficient and the interfacial temperature.

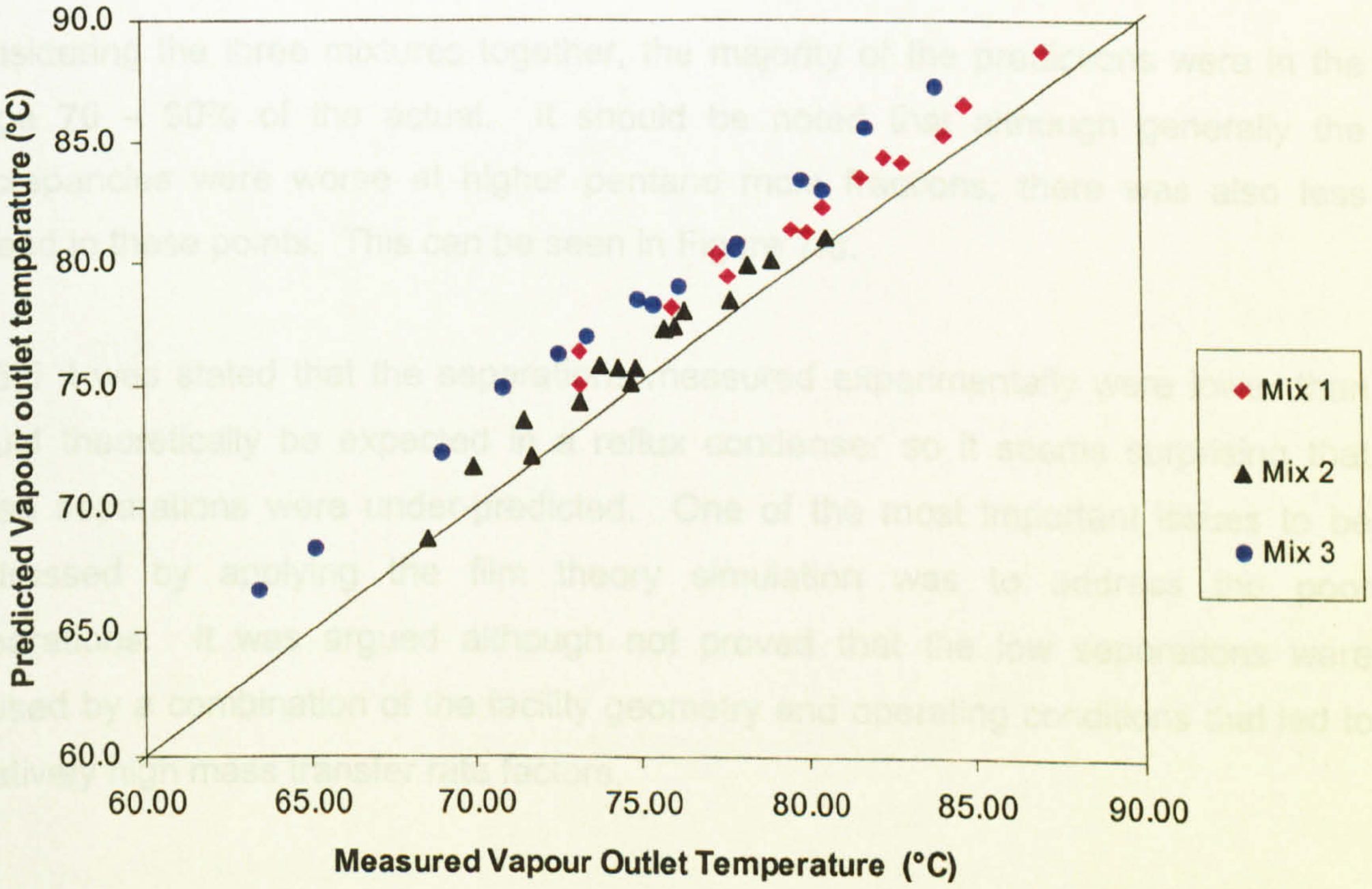

Figure 7.6: Predicted bulk vapour temperatures at the outlet

This suggests that the under-prediction in vapour cooling is linked to the levels of separation predicted by the simulation. The interfacial temperature was taken to be the dew point temperature of a vapour in local equilibrium with the bulk condensate at that point. An under-prediction in separation would therefore lead to an over-prediction in the dew point temperature and an under-prediction in the level of bulk vapour cooling. This link is explored further in 7.5.3.

7.5.3 Composition of the outlet vapour

The mole fractions of pentane in the simulated outlet vapours were compared to the experimental values in Figure 7.7. It can be seen from this chart that in all but a few cases the simulation predicted a lower pentane mole fraction and hence less separation than was measured experimentally. The maximum difference between the simulated composition and the experimental value was only +0.061. Although this seems a small value, the separations recorded were small and it is perhaps more relevant to consider the change in vapour composition through the tube than just the composition at the outlet. In the first mixture, worst prediction of the change in composition was 58.2% of the actual value, with 68.7% and 57.8% the worst for mixtures 2 and 3 respectively.

Considering the three mixtures together, the majority of the predictions were in the range 70 – 90% of the actual. It should be noted that although generally the discrepancies were worse at higher pentane mole fractions, there was also less spread in these points. This can be seen in Figure 7.8.

In 5.5 it was stated that the separations measured experimentally were lower than would theoretically be expected in a reflux condenser so it seems surprising that these separations were under-predicted. One of the most important issues to be addressed by applying the film theory simulation was to address the poor separations. It was argued although not proved that the low separations were caused by a combination of the facility geometry and operating conditions that led to relatively high mass transfer rate factors.

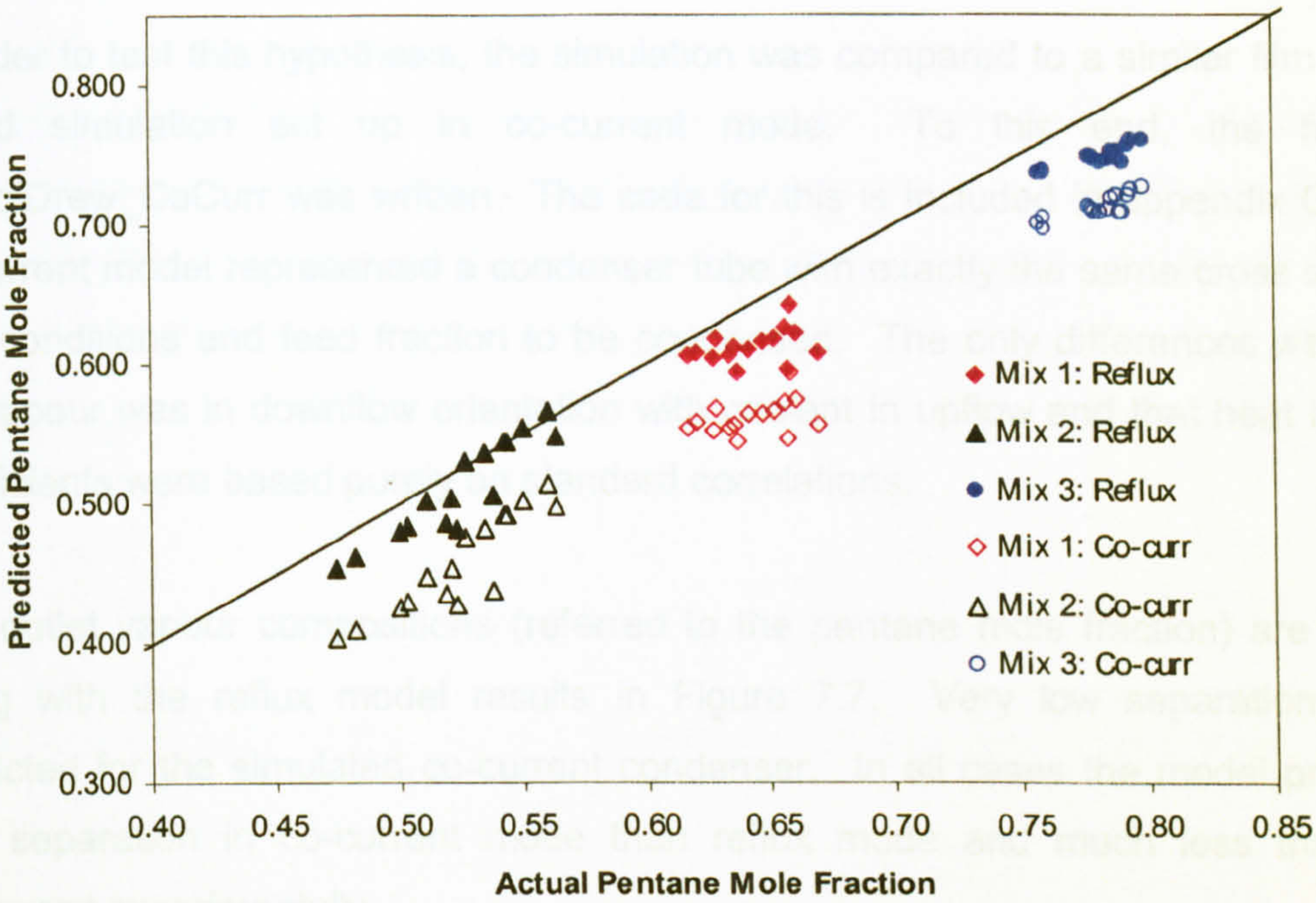

Figure 7.7: Predicted vapour compositions for reflux and co-current condenser models

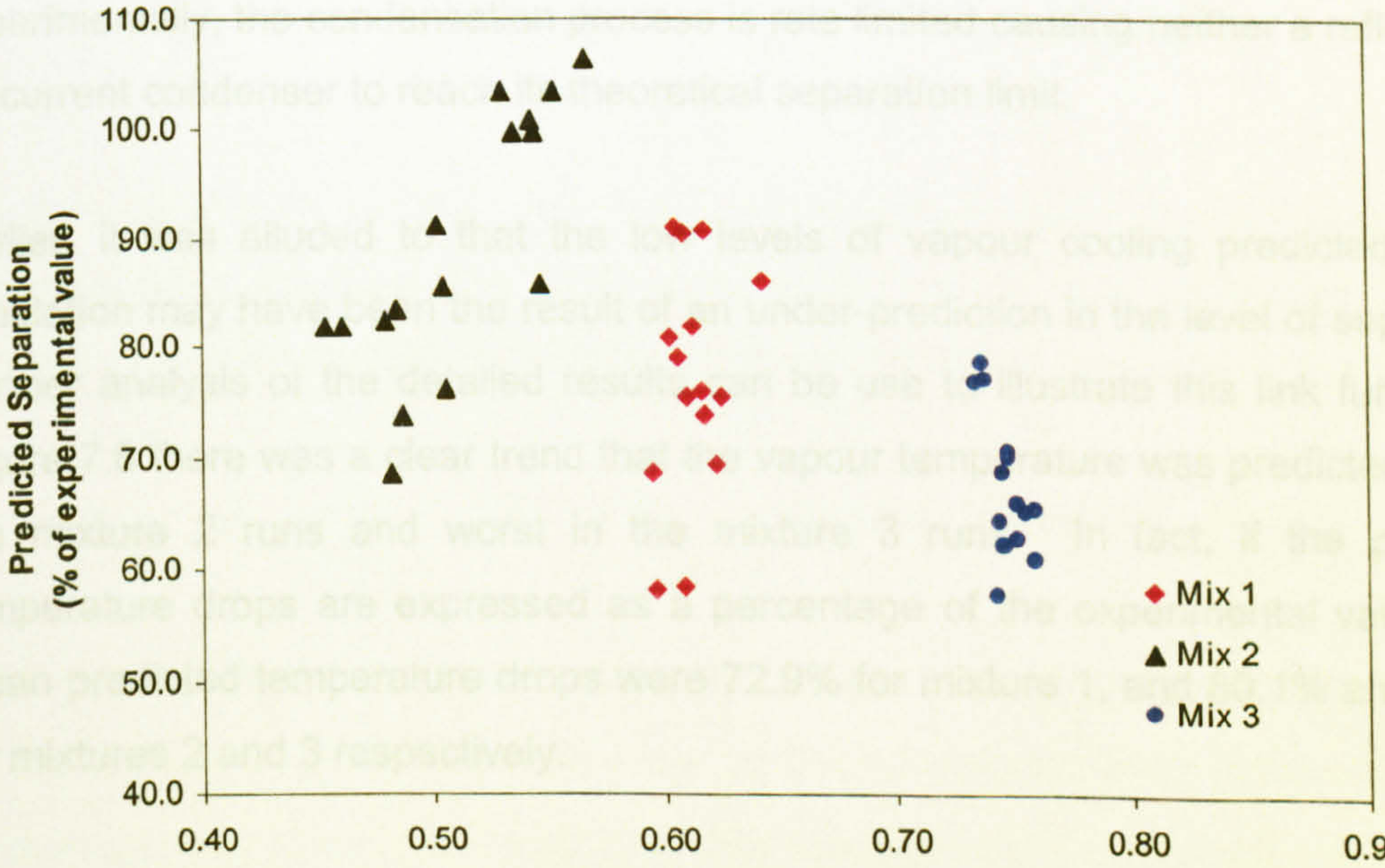

Figure 7.8: Predicted reflux condenser separations ($\tilde{y}_{P,o} - \tilde{y}_{P,i}$) as a % of the separation measured experimentally

In order to test this hypothesis, the simulation was compared to a similar film theory based simulation set up in co-current mode. To this end, the function fn_ColDrew_CoCurr was written. The code for this is included in appendix G. The co-current model represented a condenser tube with exactly the same cross section, inlet conditions and feed fraction to be condensed. The only differences were that the vapour was in downflow orientation with coolant in upflow and that heat transfer coefficients were based purely on standard correlations.

The outlet vapour compositions (referred to the pentane mole fraction) are plotted along with the reflux model results in Figure 7.7. Very low separations were predicted for the simulated co-current condenser. In all cases the model predicted less separation in co-current mode than reflux mode and much less than was measured experimentally.

It should be remembered though that in a normal situation, a co-current condenser would be operated at a much higher loading than a reflux condenser. This would improve the heat transfer characteristics of the vapour and promote better mass transfer. What these results do, is confirm that at the inlet conditions measured experimentally, the condensation process is rate limited causing neither a reflux nor a co-current condenser to reach its theoretical separation limit.

Earlier, it was alluded to that the low levels of vapour cooling predicted by the simulation may have been the result of an under-prediction in the level of separation. Further analysis of the detailed results can be use to illustrate this link further. In Figure 7.6 there was a clear trend that the vapour temperature was predicted best in the mixture 2 runs and worst in the mixture 3 runs. In fact, if the predicted temperature drops are expressed as a percentage of the experimental values, the mean predicted temperature drops were 72.9% for mixture 1, and 80.1% and 61.3% for mixtures 2 and 3 respectively.

This trend is repeated in Figure 7.7 and Figure 7.8 where the best predictions of vapour composition were in the mixture 2 runs. Analysis of the detailed results showed that the five runs in mixture 2 where the vapour temperature was predicted to within 0.4°C were the five runs where the simulated vapour composition was closest to the experimental value.

7.5.4 Discussion on separation

The analysis of Webb & Al-Shammari (2002) can be used to prove that in this case the low separations were the result of the facility geometry and operating conditions which did not promote good separation. In the film theory model of Colburn & Drew (1937), the local mass flux was defined by

$$\dot{n}_T = \beta_v \ln\left[\frac{r_i - \tilde{y}_{iS}}{r_i - \tilde{y}_{iB}}\right] \tag{2.40}$$

where r_i is the ratio of the flux of component i to total flux, S is the condensate surface and B is the bulk vapour.

Webb & Al-Shammari (2002) rearranged this equation to show that the level of separation was totally dependent on the ratio of mass flux to mass transfer coefficient. Denoted by ϕ_M this value was termed the mass transfer rate factor.

$$\frac{(r_i - \tilde{y}_{iS})}{(r_i - \tilde{y}_{iB})} = \exp\left[\frac{\dot{n}_T}{\beta_v}\right] = \exp(\phi_M) \tag{7.21}$$

They showed that as the rate factor approached zero, the surface vapour composition approached the bulk composition giving the maximum possible difference between the inlet vapour composition and that of the liquid.

$$\text{As} \quad \phi_M \to 0, \quad \tilde{y}_{iS} \to \tilde{y}_{iB} \quad \text{Maximum separation}$$

In the other limit of infinite rate factor, the surface vapour composition approached the value of r_i. Locally, as r_i is equal to the condensate composition, this gives condensate and vapour compositions that are equal at the surface, i.e. no local separation.

As $\phi_M \to \infty$, $\tilde{x}_{iS} \to \tilde{y}_{iS}$ No local separation

This can illustrated simply. An infinite condensation rate would lead to all of the vapour being condensed to a liquid of exactly the same composition.

Using this argument, Webb & Al-Shammari showed that in all cases of condensation, the level of separation depended solely on the mass transfer rate factor ϕ_M. They concluded that to maximise the separation achieved, condensers should therefore be designed to promote low rate factors, that is with low condensation rates and high mass transfer coefficients.

In fact, the opposite can be said about the experimental facility used in this work. In 5.5 it was shown that as a consequence of the experimental facility high condensation rates were expected. Also, the diameter of the tube, at 45mm, is large compared to normal industrial condensers. This means that at any given vapour flow rate, the vapour velocity would be lower than expected therefore leading to lower than usual heat and mass transfer coefficients.

The detailed results from Figure 7.1 can be used to illustrate the link between the mass transfer rate factor and separation through the tube. As the vapour flows up the tube, the change in its Reynolds number causes the mass transfer coefficient to decrease. The condensation rate increases through the tube driven by the greater temperature differences further up the tube. These two features combine to make the rate factor increase exponentially through the condenser.

This is apparent in Figure 7.9 where the rate factor and vapour composition profiles have been plotted against tube length. Near the bottom of the tube, the rate factor is low and change in composition is high leading to good separation. Small increases in the rate factor have little effect on the separation rate, but when it increases sharply in value the separation begins to drop off. In the top 20cm or so there is virtually no separation.

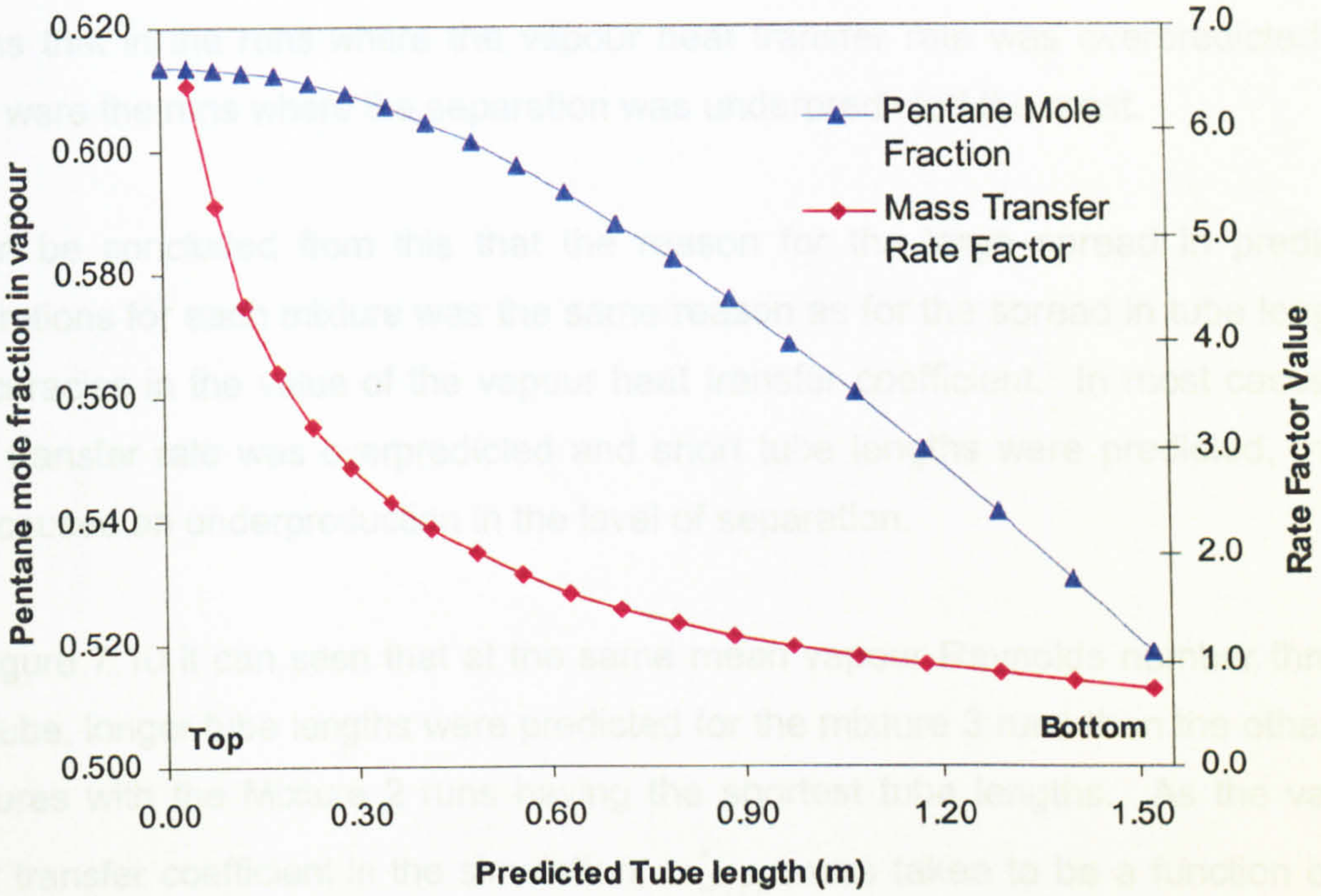

Figure 7.9: Vapour composition and mass transfer rate factor profiles for run M1.6

So far this discussion has addressed the low levels of separation measured in the experimental data and predicted by the film theory simulation. It is also necessary to consider why the simulated separations were in most cases less than the experimental separations. Referring back to Figure 7.5 and Figure 7.4 and the associated discussion, it was concluded that the large spread in the predicted tube lengths was the result of using vapour heat transfer coefficients that were different to those measured experimentally. Overprediction of the heat transfer coefficients caused an underprediction in the tube length and vice versa.

Through the heat and mass transfer analogy it is possible to show the effect that this and the rate factor had on the predicted separations. When the vapour heat transfer rate is overpredicted it follows that the mass transfer rate is also overpredicted. The mass transfer rate factor will therefore be too large causing the composition change to be reduced.

This is illustrated by Figure 7.11. In this figure, it is important to note that in all three mixtures, the level of separation was higher when larger areas were predicted. This means that in the runs where the vapour heat transfer rate was overpredicted the most were the runs where the separation was underpredicted the most.

It can be concluded from this that the reason for the large spread in predicted separations for each mixture was the same reason as for the spread in tube lengths; inaccuracies in the value of the vapour heat transfer coefficient. In most cases the heat transfer rate was overpredicted and short tube lengths were predicted, this in turn caused an underproduction in the level of separation.

In Figure 7.10 it can seen that at the same mean vapour Reynolds number through the tube, longer tube lengths were predicted for the mixture 3 runs than the other two mixtures with the Mixture 2 runs having the shortest tube lengths. As the vapour heat transfer coefficient in the simulation, $\alpha^{*}_{vP,FV}$, was taken to be a function of the vapour Reynolds number, then this figure shows the relative tube lengths at equal vapour heat transfer coefficients This means that relatively, there was a higher condensation rate in Mixture 3 than Mixture 1, and also a higher rate in Mixture 1 than Mixture 2.

Further, this explains the reason why the predicted separations differ from mixture to mixture. The mass transfer rate factor was defined as the condensation (mass transfer) rate divided by the mass transfer coefficient. Faster rates of condensation lead to larger rate factors with the associated less separation.

7.6 Film theory modelling by other workers

There are few publications available on the application of film theory models to reflux condensation and so it is difficult to conduct a full investigation into the merits of the method. Instead, a short summary of the results of previous work by Di Cave et. al (1987) and Al-Shammari (2003) on this topic is given and a short discussion presented.

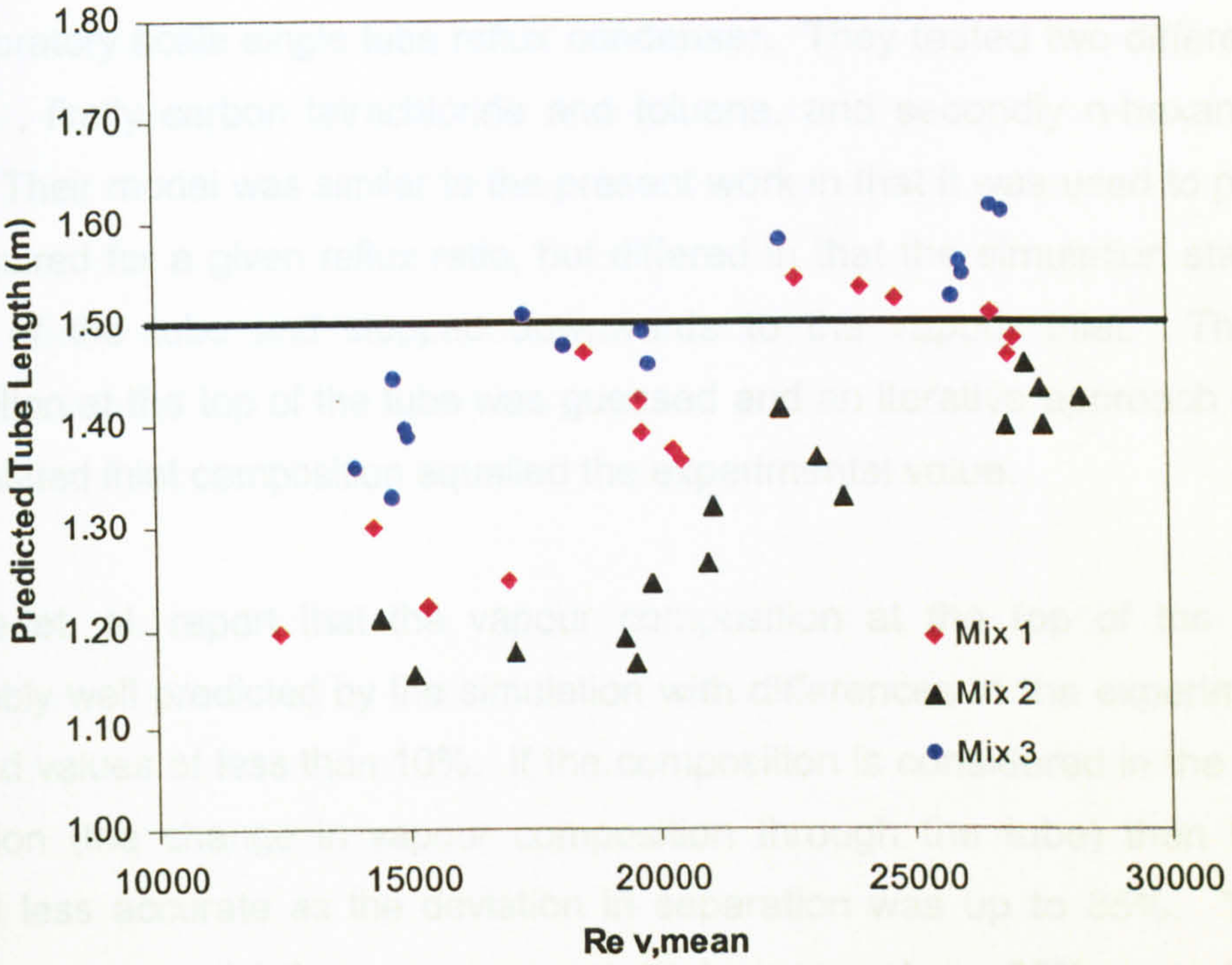

Figure 7.10: Predicted tube length against mean vapour Reynolds number

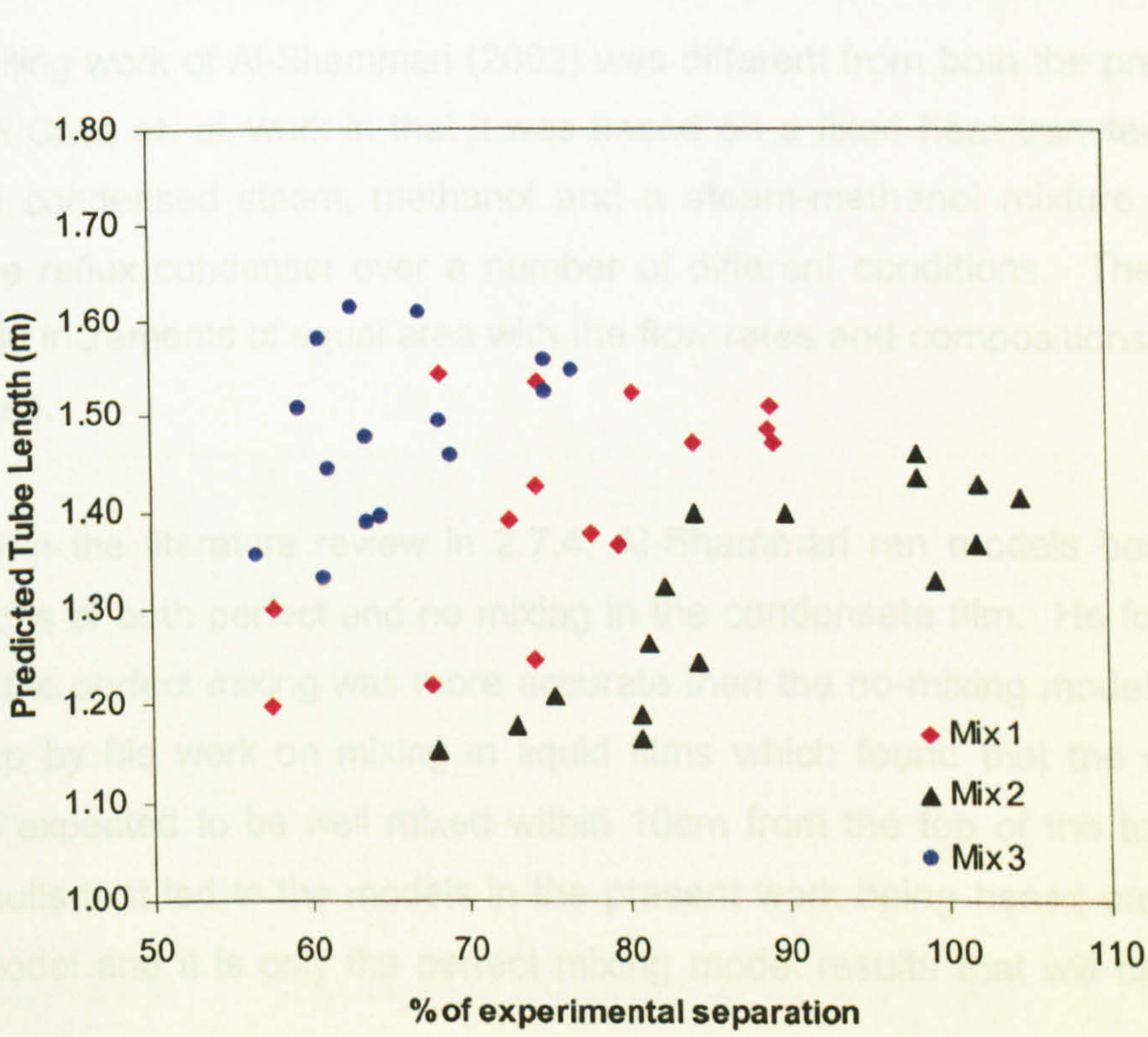

Figure 7.11: Predicted tube length against predicted separation

Di Cave et. al. (1987) compared film theory predictions to experimental data collected on a laboratory scale single tube reflux condenser. They tested two different binary mixtures , firstly carbon tetrachloride and toluene, and secondly n-hexane and n-octane. Their model was similar to the present work in that it was used to predict the area required for a given reflux ratio, but differed in that the simulation started from the top of the tube and stepped downwards to the vapour inlet. The vapour composition at the top of the tube was guessed and an iterative approach used until the simulated inlet composition equalled the experimental value.

Di Cave et. al. report that the vapour composition at the top of the tube was reasonably well predicted by the simulation with differences in the experimental and predicted values of less than 10%. If the composition is considered in the context of separation (the change in vapour composition through the tube) then the model seemed less accurate as the deviation in separation was up to 35%. The model tended to over-predict the area requirements by as much as 25% a result that they indicated was less satisfactory.

The modelling work of Al-Shammari (2002) was different from both the present work and the Di Cave et. al. work in that it was based on a fixed heat transfer area.. Al-Shammari condensed steam, methanol and a steam-methanol mixture in a large single tube reflux condenser over a number of different conditions. The tube was split into 30 increments of equal area with the flow rates and compositions calculated at each step.

As stated in the literature review in 2.7.4, Al-Shammari ran models based on the assumptions of both perfect and no mixing in the condensate film. He found that in all cases the perfect mixing was more accurate then the no-mixing model. This was backed up by his work on mixing in liquid films which found that the condensate would be expected to be well mixed within 10cm from the top of the tube. It was these results that led to the models in the present work being based on the perfect mixing model and it is only the perfect mixing model results that will be discussed here.

With a fixed area used in the models, the vapour flow rate out of the tube was reported. It was found that this was accurate to within ±5%. The reported vapour compositions were also well predicted to within ±0.05 of the actual composition. As in the other work though, it is the change in vapour composition that is more relevant. Although not discussed in the thesis, it was possible to determine the separations for some of the runs as all the necessary values were reported. In the 11 runs where the information was available, the separations predicted by the model were in the range 83.1 – 109.3% of the value measured experimentally.

An interesting result was that the vapour temperature tended to be over-predicted. All temperatures were within 3°C of the experimental value with a mean deviation of 0.8°C. This is interesting as the temperature was over-predicted in some cases where the composition change was under-predicted.

The results from these three studies are summarised in Table 7.2 below. The figures shown are deviations from the actual values measured experimentally. It is interesting to note that trends in one set of results are not necessarily reproduced in the others. For example, the required heat transfer area tended to be under-predicted in the present work whereas it was over-predicted in the Di Cave et. al. work.

Study	Prediction of area	Vapour composition	Separation ($\tilde{y}_{out} - \tilde{y}_{in}$)	Outlet Temperature
Present work	±23%	±10.1%	±43.2%	up to +4°C
Di Cave et al (1987)	up to +25%	±10%	±35%	Satisfactory agreement
Al-Shammari (2002)	Vapour flowrate to within ±5%	±11.6%	±16.9%	±3°C

Table 7.2: Summary of major results from three film theory models of reflux condensers

The compositions reported by Al-Shammari (2002) were the least accurate of the three sets of results, but when the compositions are considered in the context of separation they are by far the most accurate. This is because Al-Shammari reported separations far in excess of the other two studies. It was stated earlier that the under-prediction in vapour cooling in the present work was due to the under-prediction in separation. In the Al-Shammari work some separations were under-predicted and some over-predicted but the vapour temperature was over-predicted in almost all of the runs. This serves to highlight the fact that the vapour temperature is dependent on the vapour heat transfer coefficient as well as the composition.

Given that the importance of rate factors to the process of reflux condensation has been established, it is worth considering the rate factors in both of these works. The results published by Di Cave et al (1987) do not contain enough data for rate factors to be evaluated, but they reported separations of around one theoretical stage. This would indicate lower rate factors than in the present work, as would the fact that their tube was smaller, with an inside diameter of 18mm.

More information can be gleaned from the data published by Al-Shammari (2002). From the values given for some of the mixture runs it was possible to calculate the vapour velocities at the inlet. These ranged from 7–15m/s compared to 1.0 – 2.2 m/s in the present work indicating larger heat and mass transfer coefficients in the Al-Shammari work. Also available were the condensate mole fluxes, these were in the range $9.9*10^{-7} - 4.6*10^{-5}$ kmol/m²s, at least a factor of ten smaller than the values of $1.9*10^{-4} - 5.1*10^{-4}$ kmol/m²s in this work.

Remembering that the mass transfer rate factor was defined as the ratio of mole flux to mass transfer coefficient, it is apparent that the rate factors in the Al-Shammari work were much smaller than in this work. This explains why Al-Shammari reported separations far in excess of those reported here.

Comparing the three sets of results indicates that there is a lot of uncertainty about the application of film theory to reflux condensers. The model is very sensitive to the values used for heat and mass transfer coefficients. Al-Shammari and Di Cave et al both used standard correlations in their models, but even then there were differences. For example, for the vapour side heat transfer coefficient, Al-Shammari selected one of the Dittus Boelter (1930), Petukhov-Poop (1963) or Gnielinski (1983) correlations depending on the vapour Reynolds number whereas Di Cave et. al. used the Dittus Boelter (1930) correlation corrected for the effect of waves on the film.

The method is physically the most realistic but it may be that the reliance on correlations that were not developed for reflux condensation is the cause of the uncertainty. This was partially addressed in this work where the heat transfer coefficients were based on experimental data reported in Chapter 5.

7.7 Summary

In this chapter, the application of Colburn & Drew (1937) film theory to reflux condensation was discussed. A number of Visual Basic programs were written allowing the evaluation of local heat and mass transfer rates using the Colburn & Drew equations and the evaluation of standard downstream development equations to simulate a single tube reflux condenser. The simulation was set up to predict the required heat transfer area and resulting outlet streams for a given vapour inlet stream and reflux ratio.

The film theory model is sensitive to the values selected for heat and mass transfer coefficients. Because of this, the work reported in Chapter 5 on coolant, condensate film and vapour heat transfer coefficients was incorporated into the model. Mass transfer coefficients were calculated from heat and mass transfer analogies.

The success of the model was judged by comparison of its predictions with experimental data. The most important results were deemed to be the required heat transfer area (or predicted tube length) and vapour composition at the top of the tube. In most cases the model tended to underpredict the tube length with all differences from the actual tube length in the range –76% to +8%. The amount of separation was also under-predicted in almost all cases. Although the vapour outlet composition was reasonably well predicted, the experimental separations were small and the model predictions, mostly better than 75% were in one or two cases as low as 58% of the experimental value. Vapour outlet temperatures were for the most part slightly over-predicted but these values were not independent of the predicted compositions.

Some discussion was given to the trends in the predicted tube lengths and separations. It was found that the sensitivity of the model to the sensible vapour heat transfer coefficient resulted in the spread in the tube lengths with the tube length mostly underpredicted because the corrected correlation used tended to give larger coefficients than were measured experimentally. It was also concluded that as the mass and heat transfer rate factors were and not independent, the same cause was attributed to underpredictions and spread in simulated separations.

The results reported here were then compared to the results reported by Di Cave et al (1987) and Al-Shammari (2002) who also compared film theory models to data collected on an experimental reflux condenser. It was noticed that the trends reported in this work were not necessarily repeated in the other results. In fact, over the three sets of results there is a large spread with some values that were under-predicted in one set over-predicted in another.

It was concluded that the film theory model can be applied to reflux condensers with reasonable accuracy. This sets a good bench mark for the work in the next chapter on the equilibrium method

8 The Silver, Bell and Ghaly (Equilibrium) Method

In this chapter, experimental data are used to evaluate the strengths and weaknesses of the equilibrium method when applied to the design of a reflux condenser. Consideration is given to the choice of heat release (condensing) curve and the effect of applying the wrong type of curve. The results of the experimental analysis are then combined with a theoretical discussion and a correction to the method proposed. This correction, which is based on the heat transfer rate factor, should improve the accuracy of the method in the design of reflux and other types of condenser.

8.1 Method summary

This is a short summary of the equilibrium method, reviewing only the important equations. A full derivation of the method was given in section 2.4 in the literature review.

In the HTFS implementation of the Silver, Bell and Ghaly (equilibrium) model, the overall heat transfer coefficient was evaluated from the component resistances by

$$\frac{1}{U} = \frac{1}{\alpha_{fc}} + \frac{Z}{\alpha_v \theta_H} \tag{8.1}$$

where α_{fc} was based on the combined resistances of the condensate film, wall and coolant. Z was used to denote the ratio of sensible to total heat flux and was evaluated from

$$Z = \dot{M}_v Cp_v \frac{dT}{dh} \tag{8.2}$$

The simplicity of the model comes from the use of an idealised temperature-enthalpy relationship defined by a condensation curve. Through the use of this curve, the need for mass transfer rate equations is omitted. This leads to a trade off as this simplicity naturally leads to a loss of accuracy compared to more detailed models.

The vapour heat transfer coefficient was evaluated using a standard correlation for heat transfer to a dry stationary wall corrected for the effect of mass transfer on the gas film. The heat transfer correction factor, θ_H, was incorporated by implementing film theory and had the effect of reducing the vapour heat transfer coefficient. The inclusion of this correction makes the method become iterative, and so some of the simplicity is lost.

$$\theta_H = \frac{\phi_H}{e^{\phi_H} - 1} \tag{8.3}$$

$$\phi_H = \frac{\dot{m} Cp_v}{\alpha_v} \tag{8.4}$$

8.2 Condensation curves

There are two types of condensation curves, integral and differential. Traditionally, the integral curve is most commonly applied but there are situations when it is theoretically more appropriate to apply a differential curve.

8.2.1 Integral

It is assumed that the bulk vapour and bulk condensate leave in equilibrium such as in a closed cell with heat removal. This type of condensation would be expected in a co-current condenser when the two phases travel in the same direction and remain in contact.

8.2.2 *Differential (unmixed)*

This differential curve represents a process where the condensate is removed from contact with the vapour as it forms, hence the vapour is in equilibrium only with locally forming condensate. The curve is calculated by dividing the process into a number of stages with a fraction of the vapour condensed in each stage. A mass balance is required to determine the bulk condensate composition.

This type of curve describes behaviour in a vertical condenser (reflux and co-current) where there is no mixing in the condensate film and may be a good approximation to a horizontal condenser where the condensate forms on the outside of tubes and falls into a liquid pool. This is the type of curve recommended by ESDU for the design of a reflux condenser.

8.2.3 *Differential (mixed)*

More recently, Jibb et al (1999) proposed a second type of differential curve. The process is divided into a number of stages as in the unmixed differential curve, but in this case the vapour leaving each stage is taken to be in equilibrium with the bulk condensate. This describes a reflux condenser with a fully mixed condensate. Because of the counter-current nature of a reflux condenser, the calculation of this curve is more complicated. For example, when starting the calculation from the bottom of the tube, the composition of the condensate further up the tube is unknown. The outlet condensate composition must be guessed and an iterative approach used until the compositions converge at the top of the tube to solve the mass balance. The separation predicted by this curve is better than the other two as the rectification effect is incorporated.

8.3 Experimental analysis

8.3.1 *Implementation of the method*

It is common practice for the equilibrium method to be applied over a number of stages with the total area requirement equal to the sum of the areas of the individual

stages. The number of stages is selected such that the temperature-enthalpy relationship can be regarded as linear in each stage.

In this body of work, the experimental tube was considered purely as a single stage. There were a number of key reasons for this simplification:

- Compositions and mass balance details were only available at the tube inlet and outlet.
- Mean heat transfer coefficients over the full length of the tube were known to be more accurate than the equivalent local values as discussed in 5.4.2 and 5.6.2.
- Considering the tube as a single stage reduced the number of calculations required. This was important as the iterations made the solution very processor intensive.

It will be shown later that the temperature-enthalpy (T-h) relationship over the full tube was relatively linear thus justifying this simplification.

To allow the condensation curves and T-h relationship to be evaluated, a Visual Basic function, fn_yP_FromTheta, was written. This function returned the vapour composition expected if a known amount of vapour feed was condensed.

Consider Figure 2.15. For any given vapour inlet composition, the position of tie line DF is fixed by the value of θ, where θ represents the fraction of the feed remaining in the vapour phase after condensation. The function used an iterative approach to fix the position of the tie such that θ was equal to a value specified as an input. In practice, this value was obtained from the mass balance. The vapour composition at the outlet was then returned to the spreadsheet, allowing both the condensate composition and dew point temperatures to be found from fn_EqLiqComp and fn_Tdew respectively (see 3.2.3). Enthalpies were then calculated at the inlet and outlet points.

8.3.1.1 Integral curve

With the full tube length considered as a single design stage, the method described above was used to obtain the outlet temperature and compositions. To allow the condensate enthalpy to be evaluated, the film temperature at the bottom of the tube was assumed from equation (8.5)

$$T_{f,out} = 0.68T_{v,in} + 0.32T_{c,out} \tag{8.5}$$

This borrows from the work of Rosenhow (1956), but is modified so that the unknown wall temperature is replaced by the coolant temperature at the bottom of the tube. This value was measured in this work, and is specifiable in any design.

The heat released was then taken as the enthalpy difference between the enthalpy of the inlet vapour and the combined enthalpy of the vapour and condensate at their respective outlets.

8.3.1.2 Differential curve

The required condensate duty was split into 5 stages with the assumption of equal amounts condensed in each stage. A mass balance was therefore required over each stage to determine the value of θ, with the outlet compositions and dew point temperature found using the method described above. The T-h relationship was evaluated by plotting the total heat released at each stage. A best fit curve was then calculated to allow a mean value of dT/dh over the full length of tube.

8.3.2 T-h relationship and separation

The actual temperature-enthalpy relationship measured experimentally was evaluated in two ways. The first was using the heat gained by the coolant and vapour flow rate as described by equation (8.6). Specific enthalpies, based on measured temperatures and compositions, were also used as in equation (8.7). It was found that there was very little difference in the values obtained by the two methods.

$$\frac{dT}{dh} = \frac{T_{v,in} - T_{v,out}}{\frac{\dot{Q}_{c,R}}{\dot{M}_{v,in}}} \tag{8.6}$$

$$\frac{dT}{dh} = \frac{T_{v,in} - T_{v,out}}{h_{v,in} - \left(h_{v,out} + h_{f,out}\right)} \tag{8.7}$$

When comparing T-h relationships it is necessary to consider the level of separation predicted by the different condensation curves. Although the main purpose in applying the equilibrium method is to estimate area requirements, the outlet compositions predicted are vitally important. It has already been shown that the vapour was expected to be saturated through the test condenser (5.3.2). This means that the outlet temperature will tend to be driven to the dew point temperature and depend on the pressure and composition.

It therefore follows that the accuracy of the condensation curve in predicting the value of $\frac{dT}{dh}$ depends on the extent to which the curve predicts the actual separation.

In the literature review it was argued that, theoretically, the integral curve would underpredict the separation in a reflux condenser with the mixed version of the differential curve being best suited to this type of condenser.

This is contradicted by the extremely low separations measured experimentally which were always less than the one ideal stage predicted by integral condensation. Figure 8.1 displays the T-h relationships found for a typical run. The results are as expected in that as both types of curve overpredicted the separation, the gradient of the heat release curve was also overpredicted. The differential curve predicted more separation than the integral curve, resulting in a lower vapour outlet temperature and a steeper gradient.

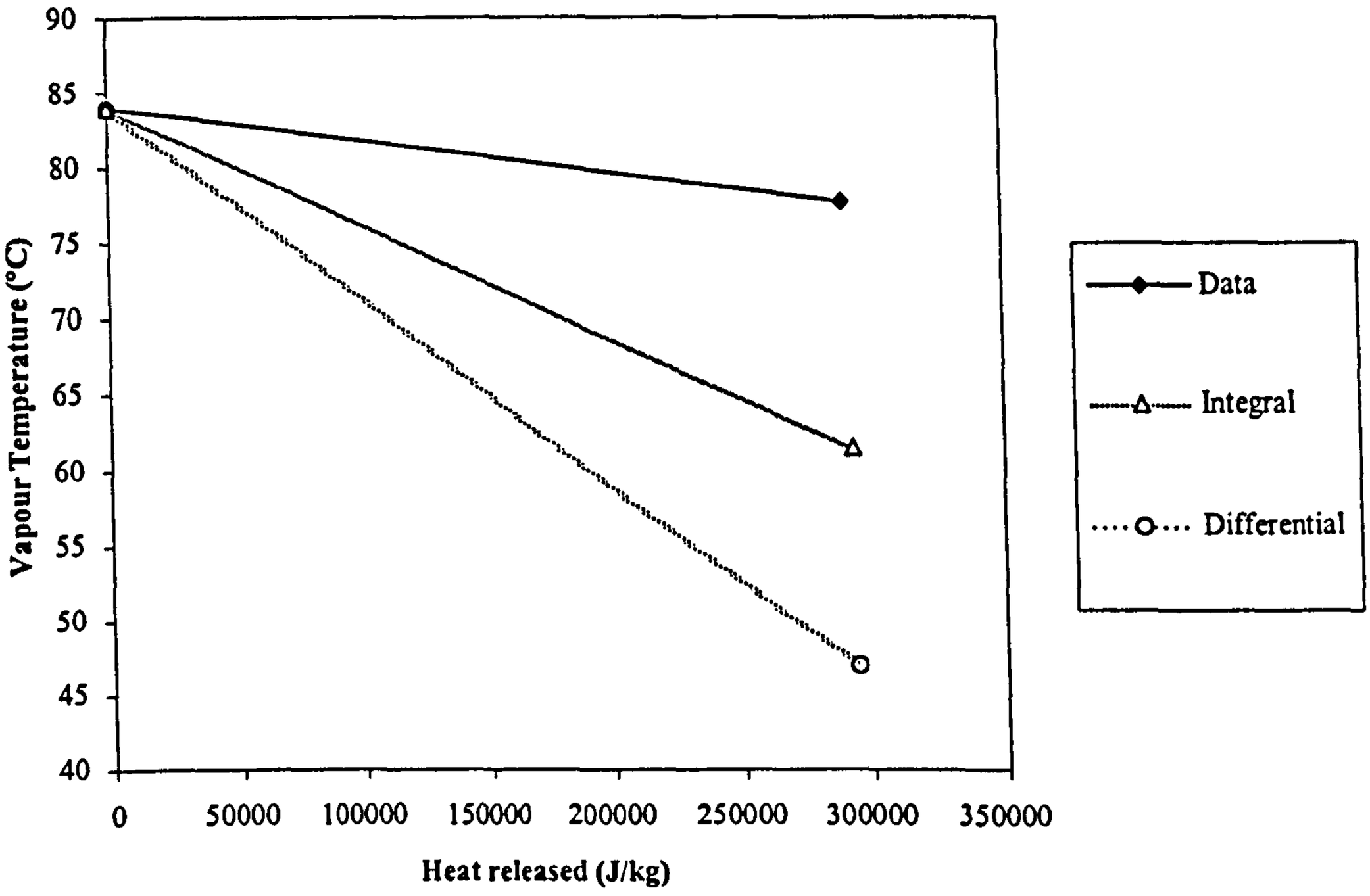

Figure 8.1: Heat release curves for run M1.1

8.3.3 Tube length predictions

To allow a full evaluation of the method, a number of tube length predictions were calculated using different values for the T-h relationship and vapour side heat transfer coefficient. These are summarised in the table below.

The most important of the predictions are those made by normal application of integral and differential condensation. The others were included purely for benchmarking purposes. For example when comparing the tube length predicted by applying one of the curves to the actual tube length, differences can arise when the vapour heat transfer coefficient used in the prediction was slightly different to the actual value measured experimentally and reported in 5.4.3.

Obviously when applying the equilibrium method for design purposes there will be no measured vapour side coefficient. In this situation where the method is being compared to actual data, it is useful not only to compare the method to the actual tube length but also to the value obtained by applying the predicted vapour heat transfer coefficient and the experimentally measured T-h relationship. This removes the vapour heat transfer coefficient as a variable and allows the effect of using condensation curves to be considered separately.

The tube length predictions for the three mixtures are displayed in Figure 8.2, with a more detailed look at the mixture 1 predictions in Figure 8.3. In the first of these figures, the tube lengths are plotted against vapour mole fraction to distinguish between the mixtures whereas the in the second, they are plotted against condensate flow. The trends in Figure 8.3 were representative of the other two mixtures.

Model	$\frac{dT}{dh}$	$\overline{\alpha}_v$	Comment
Data	Exp. data	Exp. data	Included to confirm accuracy of method when variables are well predicted
Exp. T-h	Exp. data	Predicted	Shows the extent to which the accuracy depends on $\overline{\alpha}_v$
Integral	Integral curve	Predicted	Normal application of equilibrium method as described above
Integral (no θ_H)	Integral curve	Predicted but no mass transfer correction factor	Indicates the effect of omitting the mass transfer correction factor
Differential	Differential curve	Predicted	Normal application of method as described above

Table 8.1: Summary of equilibrium method models calculated

Considering firstly the benchmarking predictions using experimental data (Figure 8.3) it can be seen that when the vapour side heat transfer and T-h relationship are well modelled then the tube length is well predicted. In all cases, the predicted tube length was within 1 cm of the actual tube length. This is only a symbolic result, as the calculation was simply a reversal of the process used to estimate the vapour heat transfer coefficient in the first place.

The importance of the vapour heat transfer coefficient can be illustrated by considering the data set labelled 'Exp. dT/dh'. These values were obtained by using the predicted vapour heat transfer coefficient with the experimentally measured T-h value. It can be seen from Figure 8.3 that the tube length is not always well predicted and seems to be a linear function of the condensate flow rate. This linearity in fact comes from the difference between the actual and predicted vapour heat transfer coefficients which was approximately linear with condensate flow rate (see Figure 5.19).

By plotting the predicted tube length against the error in the predicted heat transfer coefficient (Figure 8.4), the importance of the vapour coefficient is apparent. This is similar to Figure 7.5 in the film theory chapter. From this graph it can be seen that an overprediction of around 24% in the vapour coefficient leads to a underprediction in the area requirement of around 10%.

The vapour flow constraints imposed by flooding mean that the high vapour resistances control the process. In turn this means that the tube length obtained using this analysis is very sensitive to the value of the vapour coefficient. When it is considered that the measured vapour heat transfer coefficients were in the range 7.6 to 28.7 W/m^2, it is apparent that if the equilibrium method is to be successful, then the vapour side heat transfer must be very accurately modelled.

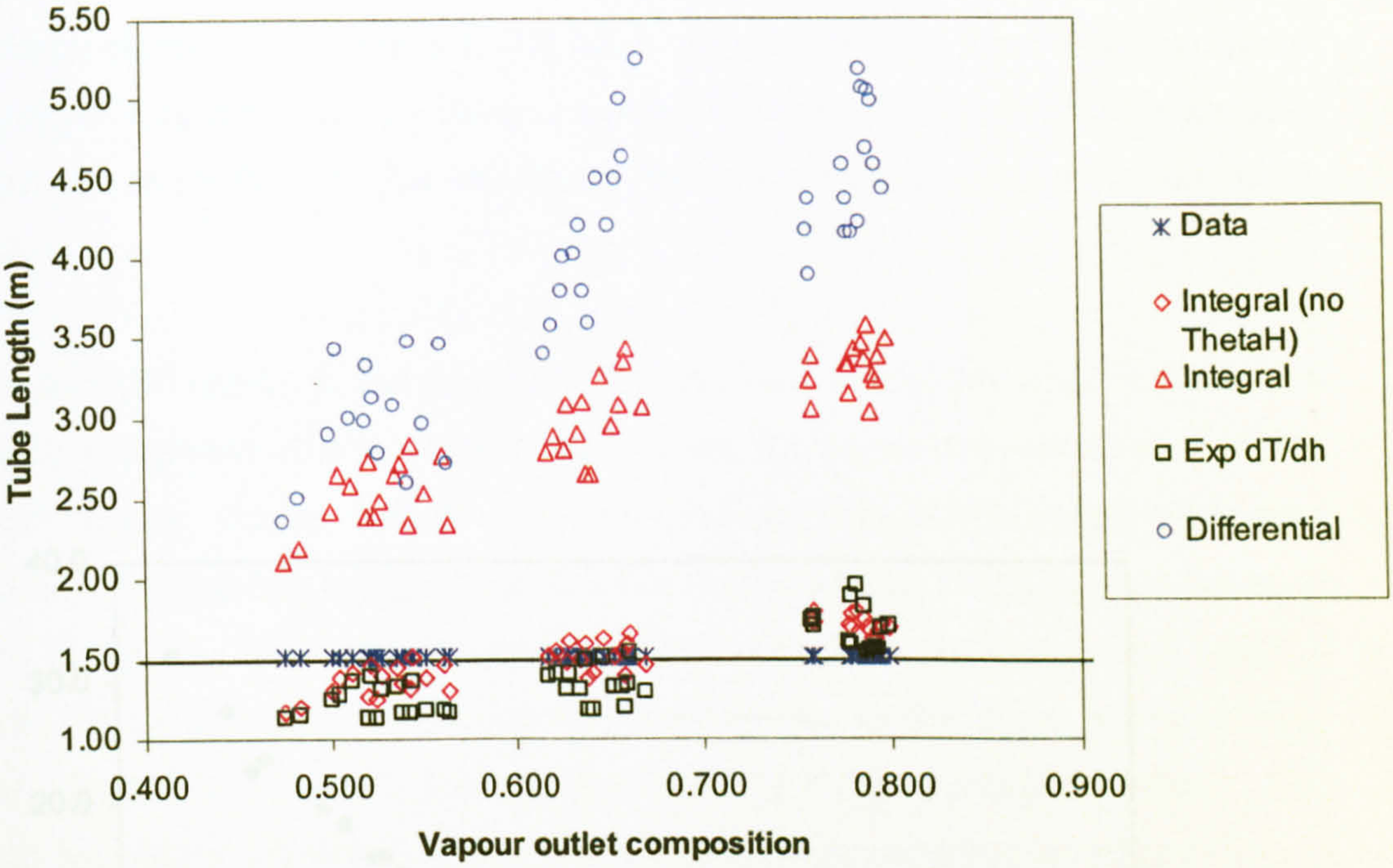

Figure 8.2: Predicted tube lengths for all mixtures

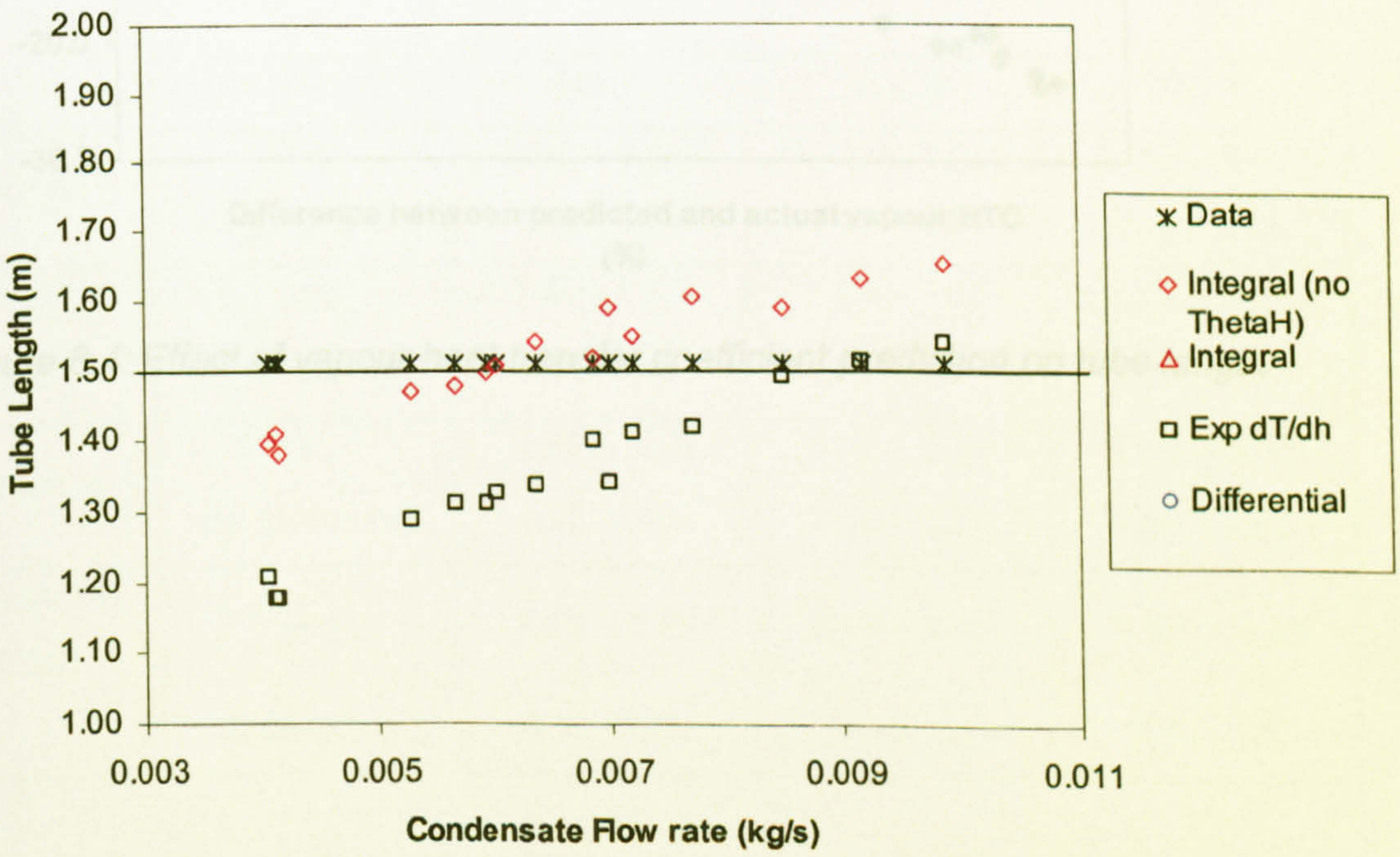

Figure 8.3: Predicted tube lengths for mixture 1 up to 2m

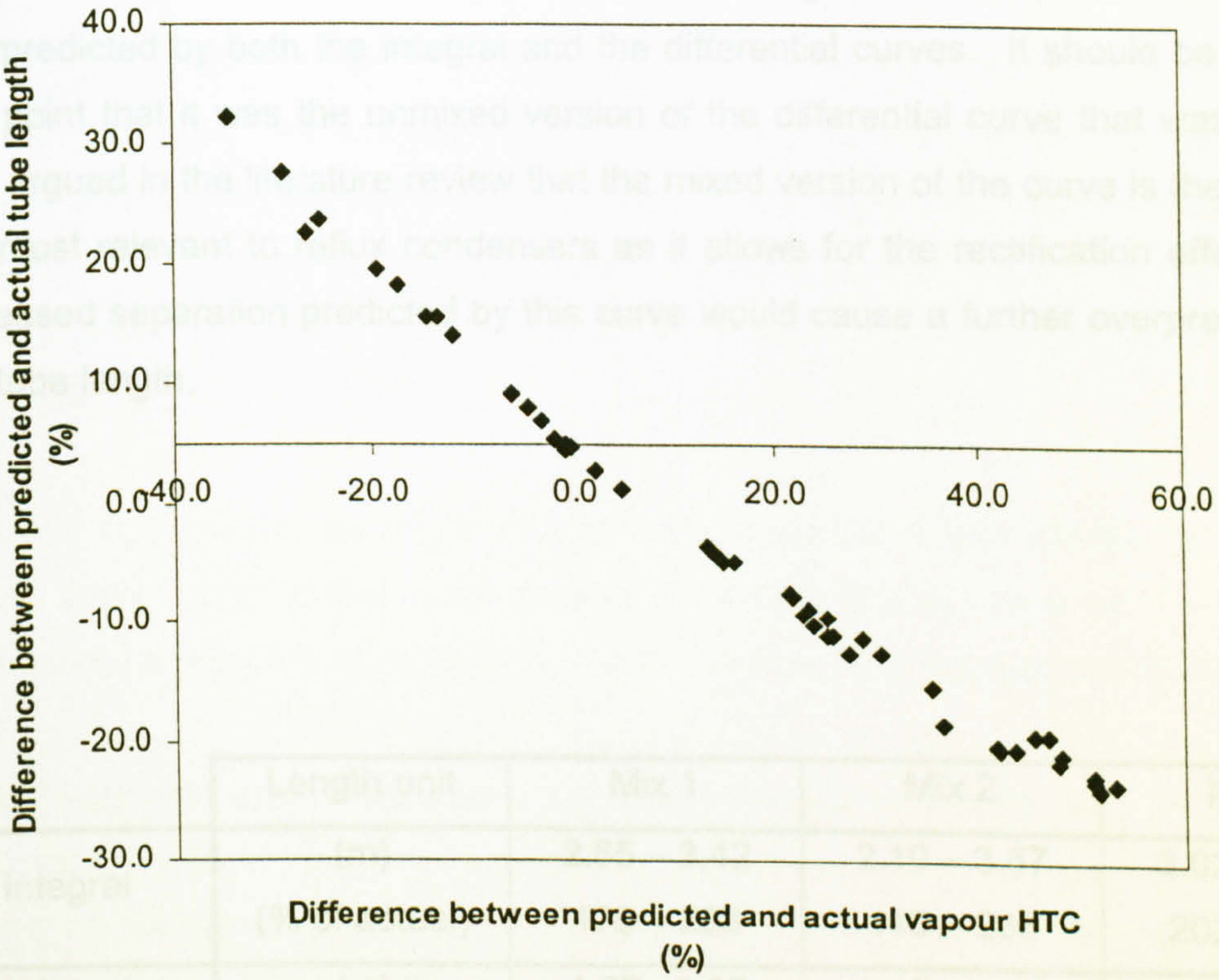

Figure 8.4: Effect of vapour heat transfer coefficient prediction on tube length

Returning to Figure 8.2 it can be seen that applying the equilibrium method with both integral and differential condensation curves resulted in tube lengths that were very much overpredicted. As expected, the tube length obtained from the differential curve is larger than that from the integral curve. There is also much more spread in the differential predictions. The results for all three mixtures are summarised in Table 7.2.

The dramatic difference in the tube lengths obtained using the experimental T-h relationship compared to the condensing curves illustrates the weakness of the equilibrium model. It was shown earlier that the gradient of this relationship was overpredicted by both the integral and the differential curves. It should be noted at this point that it was the unmixed version of the differential curve that was used. It was argued in the literature review that the mixed version of the curve is theoretically the most relevant to reflux condensers as it allows for the rectification effect. This increased separation predicted by this curve would cause a further overprediction of the tube length.

	Length unit	Mix 1	Mix 2	Mix 3
Integral	(m)	2.65 – 3.42	2.10 – 3.57	3.02 – 3.57
	(% of actual)	176 – 228	140 – 238	202 – 238
Integral (no θ_H)	(m)	1.37 –1.65	1.15 – 1.50	1.62 – 1.79
	(% of actual)	91 - 110	77 - 100	109 – 119
Differential	(m)	3.39 – 5.24	2.34 – 4.24	3.88 – 5.16
	(% of actual)	226 –349	156 – 282	259 – 344
Experimental dT/dh	(m)	1.19 – 1.84	1.14 – 1.43	1.57 – 1.98
	(% of actual)	79 – 123	76 – 95	105 – 132

Table 8.2: Summary of equilibrium method predicted tube lengths

Considering Figure 8.2 once more, it can be seen that the tube length predicted by the integral curve without the inclusion of the mass transfer correction factor is by far the most accurate of the predictions using the condensing curves. This is the version of the equilibrium method proposed by Silver (1946) and Bell & Ghaly (1972). In this version, the overprediction of the temperature-enthalpy differential coefficient (which increases the required area) is countered by the overprediction of the vapour heat transfer coefficient (which reduces the area). This is a convenient trade off that allows the condensing curves to be used.

The mass transfer correction term to the sensible vapour heat transfer coefficient, θ_H, proposed by McNaught & Emerson (1977) was defined as a function of the heat transfer rate factor. It was included to improve the modelling of the vapour side heat transfer by reducing the value obtained from a correlation for heat transfer to a dry stationary wall. It seems from the results reported above that the inclusion of the mass transfer correction factor caused the vapour resistance to be very much overpredicted.

In reflux condensers, the high vapour resistances lend themselves to high rate factors which result in low mass transfer correction factors, so it can be seen that there will be a relatively large reduction in the vapour heat transfer coefficient.

It was suggested earlier that a very high mass transfer rate factor was the reason for the poor separation measured experimentally. It was also reported by Webb & Al-Shammari (2002) that reflux condensers in industry always fail to meet their theoretical separation potential, so it seems that the problem is not confined to the experimental facility used in this work. This, and the results obtained from the equilibrium method suggest that the role of the rate factors is crucial and as such the relationship between mass and heat transfer rate factors is explored in detail later.

The main objective in applying condensation curves was to obtain the T-h relationship, but, the relationship defined by a condensation curve is an idealised situation. The weakness of the equilibrium model therefore lies in the fact that condensation curves describe idealised situations that do not seem to arise in practice. Mass transfer rate equations are ignored when in fact the separation process is rate controlled.

8.4 Link between heat and mass transfer rate factors

The mass transfer rate factor ϕ_M was defined above as the ratio of condensation rate to mass transfer coefficient (or condensation rate multiplied by mass transfer resistance). The equivalent rate factor for heat transfer is the ratio of heat transfer rate to heat transfer coefficient. This is the parameter used to evaluate θ_H the mass transfer correction term for the dry gas heat transfer coefficient.

$$\phi_H = \frac{M_v Cp_v}{\alpha_v} \tag{8.8}$$

The two parameters ϕ_M and ϕ_H are explicitly linked by virtue of heat and mass transfer analogies. As described above, conditions that promote good heat transfer also promote good mass transfer. Using a similar argument to that of Webb & Al-Shammari for the mass transfer rate factor, the relationship between the two parameters can be described.

The condensation rate is a numerator in both parameters meaning that both will increase in value with increasing mass flux. Similarly, the resistances to mass and heat transfer are also both numerators and the same can be said about increases in their values. Mass and heat transfer resistances are proportional to each other and it can be said that the behaviour of ϕ_H mirrors that of ϕ_M.

From above,

As	$\phi_M \to 0,$	$\tilde{y}_{iS} \to \tilde{y}_{iB}$	Maximum separation
Also, as	$\phi_M \to 0$	$\phi_H \to 0$	
And as	$\phi_M \to 0$	$\frac{1}{\alpha_v} \to 0$	Maximum heat transfer

In a physical situation this is illustrated by considering dew point temperatures. With good separation implied by a low value of ϕ_M, there will be a large temperature drop as the remaining vapour is driven to the dew point temperature.

The heat transfer rate factor is already incorporated into the equilibrium method to correct the dry gas heat transfer coefficient for the disruption to the laminar film caused by mass transfer. At high rate factor values, the correction term θ_H becomes significantly less than unity giving a much reduced vapour heat transfer coefficient. The area requirement then predicted by the model is much higher than without the correction. This was illustrated by the results presented in Figure 8.2 andFigure *8.3*.

The major weakness of the equilibrium method is the assumption of idealised behaviour imposed by selecting a condensation curve. Through the argument presented by Webb & Al-Shammari (2002) it has been shown that this idealised behaviour is only a limiting case and would only be expected at negligible rate factors. At high rate factor values the expected behaviour would not be well predicted by the condensation curves.

The heat transfer rate factor has been incorporated to correct the vapour resistance when departing from idealised conditions, but as yet there is no correction to the temperature-enthalpy relationship. The result is that the heat transfer rate is reduced but the temperature-enthalpy relationship is unaffected. At low rate factor values, the effect is minimal but at high values (where the heat transfer correction is significant) there will be a conflict between the rate of heat transfer and the temperature drop predicted by the condensation curve. It is therefore required to apply a correction to the value of T-h relationship to resolve this conflict.

In the film theory model, HTFS recommend applying a correction factor to the mass transfer coefficient in a similar way to the heat transfer coefficient. As the mass transfer rate equations are omitted in the equilibrium model it is not possible to apply a correction in the same way.

8.5 Proposed correction to the equilibrium method

8.5.1 Justification for a correction

This is a short summary of the discussion given above, in which the important points are revised.

Heat transfer

- Vapour heat transfer coefficients are reduced by applying a film theory based correction factor θ_H. This factor is a function of the heat transfer rate factor ϕ_H.
- Higher rate factors are expected in reflux condensers than in co-current condensers, so the correction is more significant in a reflux condenser.

Temperature-enthalpy relationship

- In the equilibrium method, the temperature–enthalpy relationship is defined by pre-selected condensation curve that describes an idealised situation.
- As condensation is a rate controlled process, the idealised situation described by a condensation curve may not occur in practice. This is the fundamental weakness of the method.
- The separation and gradient of the T-h relationship will therefore always be overpredicted by the condensation curve that seems most appropriate for the process.

In the original version of the method as proposed by Silver (1946), Bell & Ghaly (1972) and Ward (1960) the overprediction of the T-h relationship was successfully balanced by overpredicting the vapour heat transfer coefficient. The inclusion of the heat transfer correction reduced the vapour coefficient and the balance was lost.

When the equilibrium method is applied to reflux condensers, the large heat transfer correction and overprediction of $\frac{dT}{dh}$ mean that the area requirement is always overpredicted giving very conservative designs. Again it should be noted that this conflict is less of a problem in co-current condensers where lower rate factors would occur. It therefore seems that it is incorrect to apply a correction to the vapour side heat transfer without addressing the overprediction of the T-h relationship.

It is also worthwhile at this point to reiterate the reason for the vapour side heat transfer correction. Looking back to Table 7.2 it can be seen that without the correction the model was successful in predicting the tube length to within ±10 % for mixture 1, ±23 % for mixture 2 and ±19% for mixture 3. With this level of accuracy far better than the predictions with the correction included the necessity for the original heat transfer correction may be questioned.

The simplicity of the original equilibrium model came from the convenient trade off between overestimating the level of vapour heat transfer and overestimating the temperature-enthalpy gradient. The two over estimations cancelled each other out to give an area requirement that was relatively accurate.

It was stated in 2.6 that mass transfer effects present in binary mixture condensation will result in less heat transfer than an equivalent gas contacting a cooled surface. The heat transfer overestimation alluded to in the previous paragraph came from the use of a heat transfer coefficient for a cooling gas. The inclusion of the heat transfer correction factor θ_H reduces the vapour coefficient and therefore is a better model of the actual heat transfer process. Unfortunately, this has the effect of upsetting the previously convenient balance of over estimations in the equilibrium method thus leading to the requirement for a correction to reduce the gradient of the temperature-enthalpy relationship.

8.5.2 Basis for correction

Applying a rate factor based correction to the condensation curve would serve to improve the overall accuracy of the equilibrium design method when applied to reflux condensers. The correction would have two effects.

1. Correct the predicted compositions by moving away from the idealised behaviour at equilibrium and reducing the predicted separation.

2. Reduce the value of $\frac{dT}{dh}$ predicted by the condensation curve to resolve the conflict imposed when applying the vapour heat transfer correction.

With the proportional relationship between mass and heat transfer rate factors it was felt that using the heat transfer rate factor to apply a correction to more accurately model mass transfer would be justified. In this way, the effect of mass transfer on expected separation and the T-h relationship would be incorporated into the model without the need for explicit mass transfer rate equations. In this way, the major weakness of the equilibrium method can be addressed without compromising the simplicity of the model.

8.5.3 Form of the correction

The link between vapour composition and T-h relationship through the dew point temperature means that any correction to the predicted vapour composition will by definition alter the gradient of the temperature-enthalpy relationship by reducing the temperature drop.

Consider a standard T-xy diagram (Figure 8.5). If a portion of the vapour is condensed such that the fraction of flow remaining in the vapour is θ (where θ is taken as the ratio of EC to ED) then the outlet compositions given by integral condensation are $\tilde{y}^{*}_{out}$ and $\tilde{x}^{*}_{out}$.

In the limit of $\phi_M \to 0$, the tie line DE approaches AB giving $\tilde{x}_{out} = \tilde{x}_B$ and maximum separation. Conversely, with $\phi_M \to \infty$, DE approaches CF and there is no composition change.

However, in a practical situation, the mass transfer rate factor ϕ_M will not approach either limit and the position of line DE will be fixed by the value of θ. The equilibrium

values of $\tilde{y}^*_{out}$ and $\tilde{x}^*_{out}$ will only be realised if the system is allowed to reach equilibrium. As the process is rate controlled this may not happen.

It is therefore proposed to use the heat transfer rate factor to correct the outlet vapour composition giving $\tilde{y}_{corr}$. The correction will result in $\tilde{y}_{corr} < \tilde{y}^*_{out}$ hence reducing the temperature drop. A correction to the vapour composition will have a knock-on effect on the condensate composition giving $\tilde{x}_{corr}$.

The following correction is proposed

$$\tilde{y}_{corr} = \tilde{y}_{in} + F\left(\tilde{y}^*_{out} - \tilde{y}_{in}\right) \tag{8.9}$$

The condensate composition is then found by a mass balance

$$\tilde{x}_{corr} = \tilde{y}_{corr} - \left(\frac{\tilde{y}_{corr} - \tilde{y}_{in}}{1-\theta}\right) \tag{8.10}$$

where

$$F = f\left(\phi_H\right)$$

and

$$F \to 1 \text{ as } \phi_H \to 0$$

$$F \to 0 \text{ as } \phi_H \to \infty$$

8.5.4 Limits check

In the limit of $\phi_H \to \infty$, $F \to 0$ giving $\tilde{y}_{corr} = \tilde{y}_{in}$ and $\tilde{x}_{corr} = \tilde{y}_{in}$

i.e. No separation

In the limit of $\phi_H \to 0$, $F \to 1$ giving $\tilde{y}_{corr} = \tilde{y}^*_{out}$ and $\tilde{x}_{corr} = \tilde{x}^*_{out}$

i.e. Maximum separation

Further, for $\phi_H \to 0$, $\dot{n}_T \to 0$ therefore $\theta \to 1$ giving $\tilde{y}_{corr} = \tilde{y}^{\bullet}_{out} = \tilde{y}_{in}$

It is also proposed that the plot of F against ϕ_H should be exponential such that large corrections only occur when the value of the rate factor suggests a large deviation from equilibrium conditions. This would result in a more significant correction when the rate factor is higher.

It is felt by the author that this proposed correction is applicable not only to reflux condensers, but also to any condenser where the process is rate controlled. Comparing a reflux condenser to a co-current condenser again, higher rate factors would be expected in a reflux condenser hence the correction would be more significant. Also, in any vertical condenser, the correction would be more significant towards the vapour outlet where rate factor values increase as vapour Reynolds number decreases.

It should also be noted that when using the equilibrium method with the vapour heat transfer coefficient corrected by θ_H the heat transfer rate factor is already evaluated and the solution iterative. The inclusion of the correction proposed above would therefore lead to a minimal increase in the complexity of the calculations as the only additional step is the calculation of corrected compositions.

8.6 Application of correction to equilibrium method

8.6.1 Correction factor F

It has been suggested that the proposed correction to the equilibrium method would be applicable not only to reflux but to other types of condenser where the process is rate controlled. In a standard vertical co-current condenser, for example, the correction would be minimal towards the inlet where rate factors would be low, but towards the outlet, where the vapour resistance is higher, the correction would become significant. It is therefore outside the scope of this work to determine a correction factor that is widely applicable. Instead, the experimental data reported earlier will be tested with an assumed value of the factor F. The effects of applying a correction of this form can then be discussed.

The correction was applied to predictions given by both the integral and unmixed version of the differential curve. Again due to the amount of data and complexity, the mixed version of the differential curve was not considered.

As heat and mass transfer rate factors are a measure of how idealised the process is, it was decided to base F on the heat transfer rate factor ϕ_H. Further to this, the limits check above indicated that F should behave in the same manner as θ_H (the parameter used to correct the vapour side heat transfer coefficient), it was therefore assumed that this would be a suitable factor to test the proposed correction with.

The correction implemented was thus

$$\tilde{y}_{corr} = \tilde{y}_i + \theta_H \left(\tilde{y}_o^{\bullet} - \tilde{y}_i \right) \tag{8.8}$$

where θ_H was defined by equations (8.3) and (8.4).

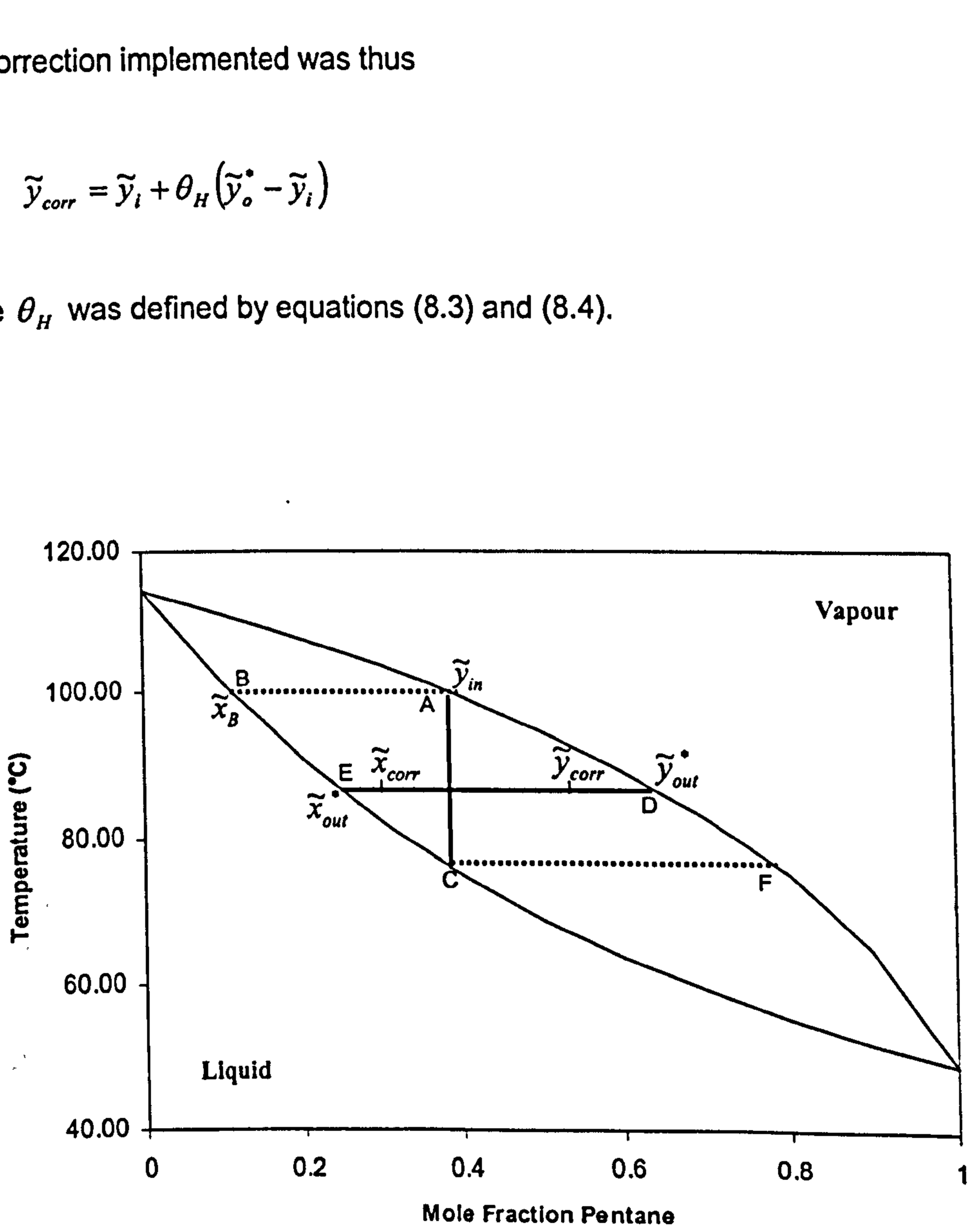

Figure 8.5: Standard T-xy diagram for partial condensation of a binary vapour mixture

8.6.2 Compositions and T-h relationship

In Figure 8.6, the heat release curves yielded for the corrected method have been added to the plot for run M1.1 that was displayed in Figure 8.1. It can be seen that correcting the vapour outlet compositions has a dramatic effect on the heat release curves. In the particular run displayed, the gradient of the T-h relationship calculated from the experimental data was very well modelled by the prediction of the corrected integral curve. This was not an uncommon result, as in all cases, the corrected integral curve predicted separations that were closest to the experimental separations. It should be noted that all predictions made in this section used a vapour heat transfer coefficient based on the Petukhov (1970) correlation modified for the relative velocity of the vapour and condensate film.

The vapour outlet compositions calculated for all three mixtures are displayed in Figure 8.7. With both types of curve, the correction dramatically improved the difference between the measured and predicted compositions. In all three mixtures, the corrected integral curve gave by far the best predictions with the accuracy almost constant over the range of compositions. This is in contrast with the corrected differential where at low outlet compositions the accuracy is fairly good but the predictions worsen as the pentane composition increases. Referring back to Figure 7.7 in the film theory chapter, it was noted that the compositions predicted by the modified integral curve were more accurate than the film theory method.

Remembering that reflux condenser separations should, in theory, be underpredicted by the integral and the unmixed version of the differential curve, Figure 8.7 indicates that the correction factor applied was not accurate for this particular condenser tube. It was stated earlier that the objective was not to define an accurate correction factor but simply to show that applying a correction of this type would improve the model. This author is of the opinion that results do indeed show that this is the case and that there is scope for an investigation into defining an accurate correction factor.

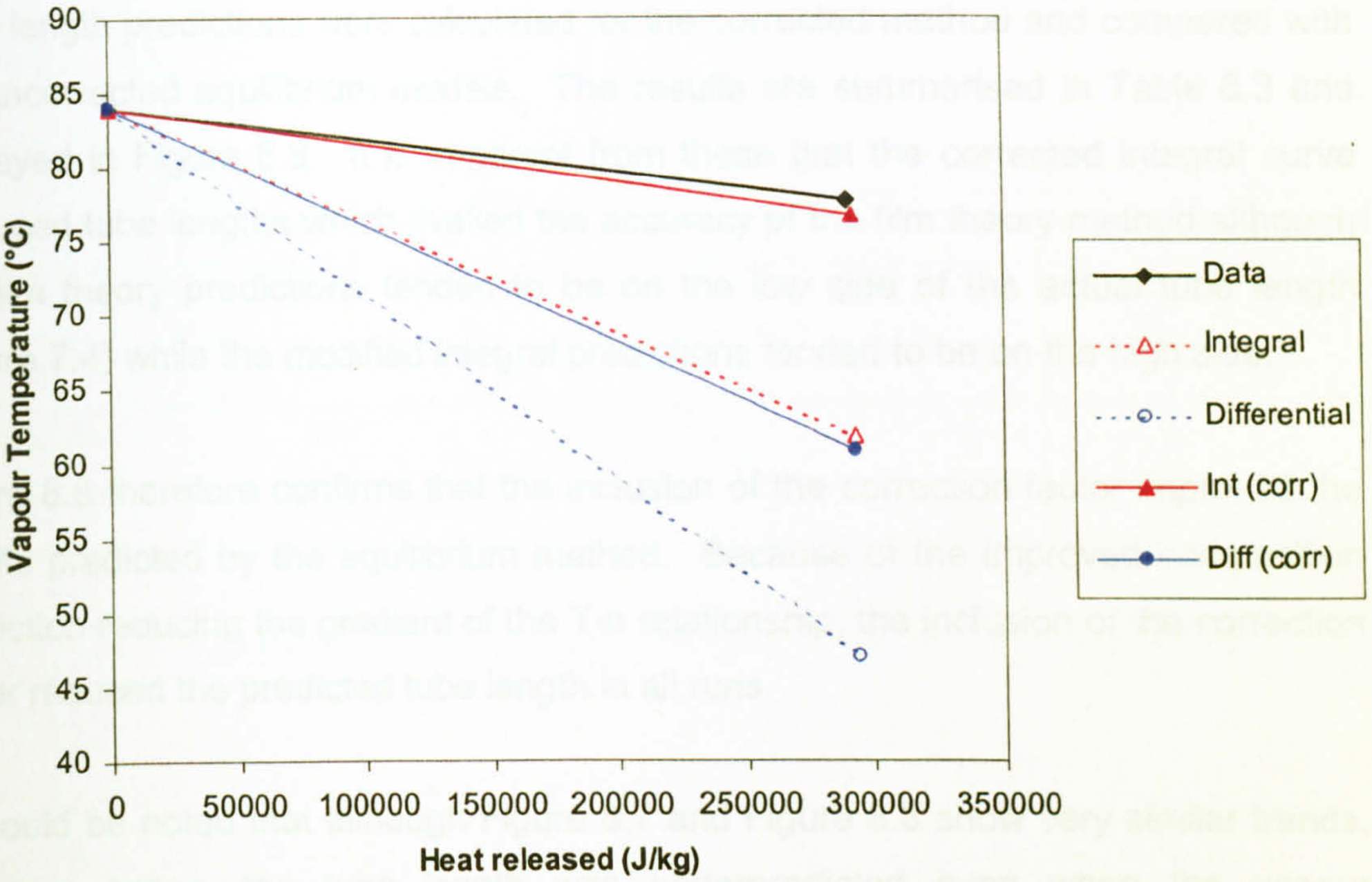

Figure 8.6: Comparison of standard and corrected heat release curves for run M1.1

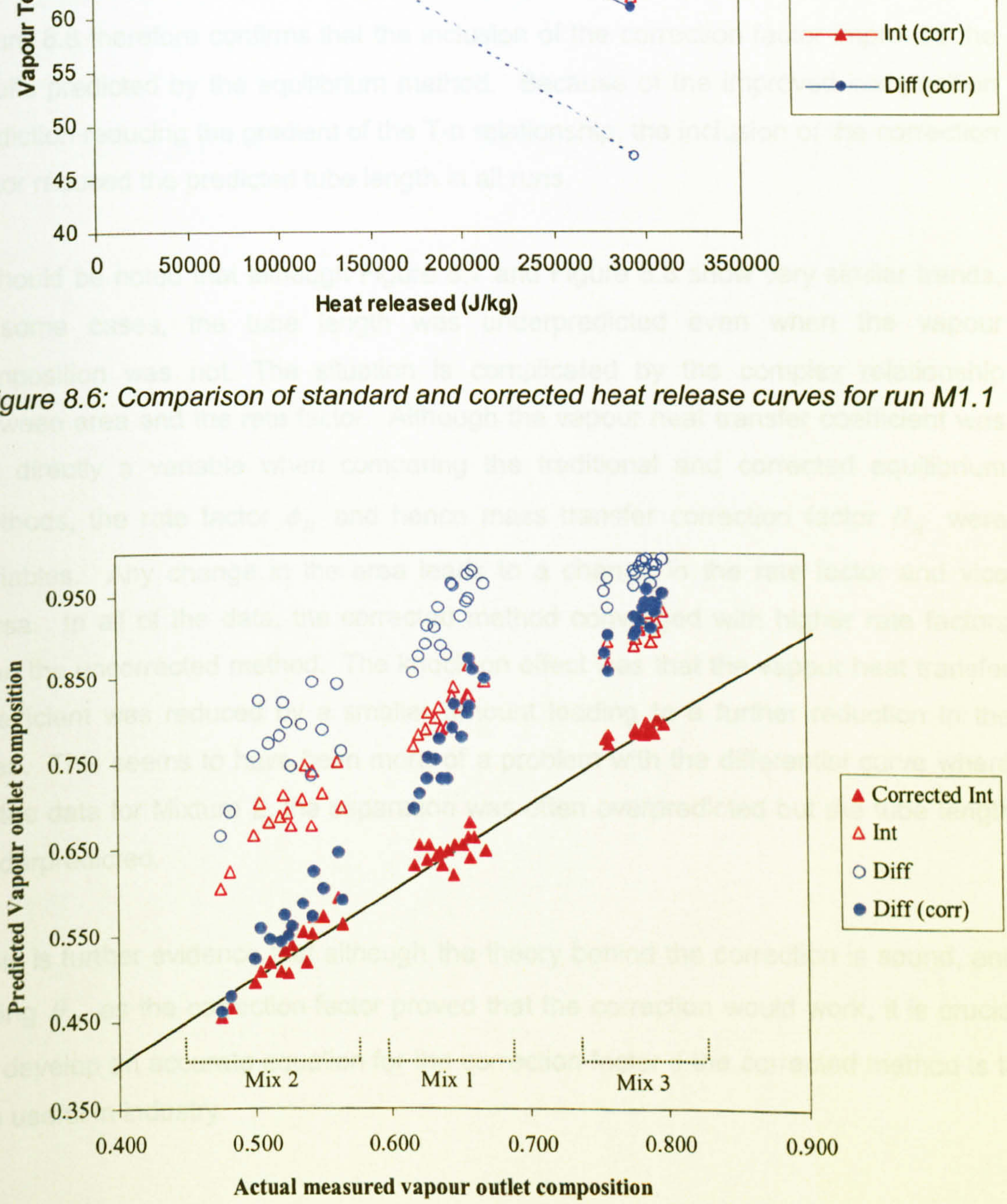

Figure 8.7: Comparison of measured and predicted vapour outlet compositions

8.6.3 Tube length predictions

Tube length predictions were calculated for the corrected method and compared with the uncorrected equilibrium models. The results are summarised in Table 8.3 and displayed in Figure 8.8. It is apparent from these that the corrected integral curve produced tube lengths which rivalled the accuracy of the film theory method although the film theory predictions tended to be on the low side of the actual tube length (Figure 7.4) while the modified integral predictions tended to be on the high side.

Figure 8.8 therefore confirms that the inclusion of the correction factor improved the results predicted by the equilibrium method. Because of the improved composition prediction reducing the gradient of the T-h relationship, the inclusion of the correction factor reduced the predicted tube length in all runs.

It should be noted that although Figure 8.7 and Figure 8.8 show very similar trends, in some cases, the tube length was underpredicted even when the vapour composition was not. The situation is complicated by the complex relationship between area and the rate factor. Although the vapour heat transfer coefficient was not directly a variable when comparing the traditional and corrected equilibrium methods, the rate factor ϕ_H and hence mass transfer correction factor θ_H were variables. Any change in the area leads to a change in the rate factor and vice versa. In all of the data, the corrected method converged with higher rate factors than the uncorrected method. The knock-on effect was that the vapour heat transfer coefficient was reduced by a smaller amount leading to a further reduction in the area. This seems to have been more of a problem with the differential curve where in the data for Mixture 2, the separation was often overpredicted but the tube length underpredicted.

This is further evidence that although the theory behind the correction is sound, and using θ_H as the correction factor proved that the correction would work, it is crucial to develop an accurate equation for the correction factor if the corrected method is to be useful in industry.

	Length unit	Mix 1	Mix 2	Mix 3
Corrected Integral	(m)	1.34 – 1.76	1.20 – 1.63	1.56 – 1.91
	(% of actual)	90 - 117	80 - 108	104 – 128
Corrected Differential	(m)	1.90 – 2.93	1.16 – 1.76	2.53 – 3.67
	(% of actual)	127 – 195	78 – 117	168 – 245

Table 8.3: Summary of corrected equilibrium method tube lengths

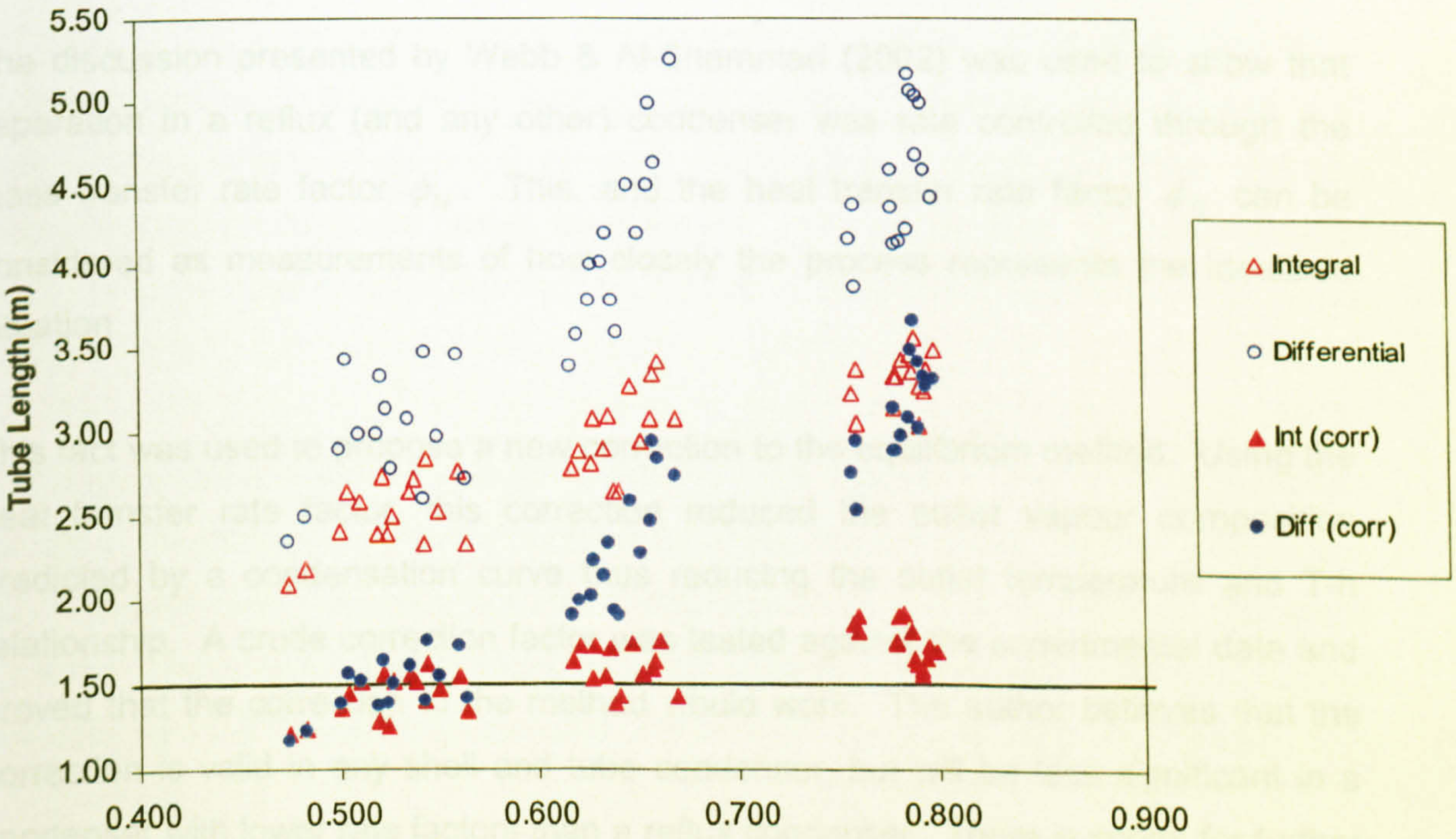

Figure 8.8: Comparison of tube lengths predicted by standard and corrected method

8.7 Summary

In this chapter, the strengths and weakness of the equilibrium method when applied to reflux condensation were addressed. It was shown that the major weakness of the method lies in the reliance on condensation curves. Although it was possible to select a condensation curve that in theory describes the process of reflux condensation, in reality the condensation curve describes an idealised situation that may not arise in reality.

Experimental data were used to show that good modelling of the vapour side heat transfer and temperature-enthalpy relationship was crucial to the success of the method. It was shown that as low vapour side heat transfer coefficients are expected in reflux condensers, small errors in predicting the coefficient led to large errors in the area requirements. The experimental facility suffered from poor separation meaning that the traditional integral and differential curves gave very poor predictions of the experimental T-h relationship resulting in tube lengths that were overpredicted by between 150% and 350%.

The discussion presented by Webb & Al-Shammari (2002) was used to show that separation in a reflux (and any other) condenser was rate controlled through the mass transfer rate factor ϕ_M. This, and the heat transfer rate factor ϕ_H can be considered as measurements of how closely the process represents the idealised situation.

This fact was used to propose a new correction to the equilibrium method. Using the heat transfer rate factor, this correction reduced the outlet vapour composition predicted by a condensation curve thus reducing the outlet temperature and T-h relationship. A crude correction factor was tested against the experimental data and proved that the correction to the method would work. The author believes that the correction is valid in any shell and tube condenser, but will be less significant in a condenser with lower rate factors than a reflux condenser. There is scope for further work to confirm this and to develop an accurate formula for the correction factor.

9 Summary, conclusions and recommendations

The main aim of this thesis was to satisfy customer demands of the sponsoring organisation, Hyprotech UK through the HTFS brand, by conducting a detailed study into the modelling of a reflux condenser. This was achieved by collecting new experimental data, comparing the results with the two major design methods for binary condensation and discussing their strengths and weaknesses.

This final chapter contains three distinct sections. Firstly, the contents of the thesis are summarised, covering all of the previous chapters. A number of conclusions are then stated, followed by recommendations for future work to take understanding of the topic further.

9.1 Summary

After a short introduction into the topic of reflux condensation and reflux condensers, the basis for the experimental and modelling work was set by conducting a literature review into the major areas of interest in reflux condenser design. This covered heat transfer in the both the vapour and condensate, flooding, and the equilibrium and film theory design methods for binary condensers. The application of these general methods to the case of reflux condensers was discussed using theoretical arguments and previously published experimental work.

The experimental facility was described in the third chapter. This chapter contained details of the major equipment, measurement systems and tools used to analyse the data. Details were given of a number of improvements that were made to the whole system. These ranged from more accurate instrumentation, new data acquisition software, to safer operating procedures and improved physical property estimation.

The objective of adding to the experimental data available on reflux condensers was met and the data presented in chapter 5. Using methods presented in the fourth chapter, the data was fully analysed and a number of important issues addressed. The quality of the data was evaluated with the improvements reported in the third chapter justified by improved heat balances and lower uncertainties. It was found that the separations measured were very small, less in fact than would be expected

in a co-current condenser with only natural separation. This is a common problem in reflux condensers, which often fail to perform to the expected level, meaning that the extra rectification (the principal reason for selecting a reflux condenser) was not achieved.

Much of the results analysis concentrated on heat transfer in the condensate film and vapour. Using single component data, the measured condensate resistance was found to be less than standard correlations for co-current flow evaluated at the same film Reynolds number. A new correlation was therefore proposed allowing more accurate estimation of the condensate resistances in the experimental facility. Analysis of the vapour side resistances in the mixture data showed that the experimental heat transfer coefficients were best predicted by correcting a standard correlation for the effect of relative vapour and condensate velocities.

Next, the issue of flooding was considered. Flooding limits the vapour flow rate resulting in the vapour resistance controlling the process, and accurate prediction of the flooding point is vitally important to avoid either flooded tubes of overly safe designs. Using a video camera and stability monitor, it was possible to define the flooding point in terms of visual observations and facility behaviour. Experimental data was then used to deduce that wave bridging was the cause of flooding in this facility and some discussion was given on three commonly used correlations for the flooding point.

The application of two standard binary condenser design tools to reflux condensers was then considered. Film theory based models were programmed into a Visual Basic simulation which allowed predictions based on the models to be compared to the experimental data. The simulation was designed to take the experimental conditions at the vapour inlet and condensate to vapour ratio at the outlet, and calculate the area requirements and vapour conditions at the top of the tube. This was achieved by guessing the condensate composition at the outlet and iterating, with heat and mass transfer rate equations evaluated over 20 increments of equal condensation. Although reasonable accuracy was achieved, the method was very sensitive to the values of vapour heat transfer coefficients.

Similar programs were written for the equilibrium method. Vapour/liquid equilibrium calculations were used to evaluate temperature-enthalpy relationships based on either integral or (unmixed) differential condensation curve thus yielding vapour

conditions at the outlet and allowing area requirements to be calculated. The method was simplified by considering the whole tube instead of a number of increments but this was justified by the linearity of the temperature-enthalpy gradients. Results showed that high rate factors caused the process to be rate controlled and as a result the method was very inaccurate for reflux condensers. Tube lengths were as much as 350% of the actual length and separations were very overpredicted. This was addressed by proposing a correction to the equilibrium method that reduced the temperature enthalpy relationship and led to lower area predictions.

9.2 Conclusions

9.2.1 Experimental work

- The databank on the reflux condensation of hydrocarbons in a single tube vertical reflux condenser has been expanded with the data collected in this project and reported in this thesis. Data were collected on two single hydrocarbons, pentane and 3,3,4-trimethyllpentane (iso-octane) and a binary mixture of pentane and iso-octane under normal refluxing conditions, and iso-octane under flooding conditions on an improved experimental facility.

- Lower resistances were measured in the condensate film than would be estimated using existing correlations for a co-current condenser. This was attributed to the effect of countercurrent flow of the vapour which although increasing the thickness of the film also increased the waviness of the film leading to higher levels of turbulence. This effect increased as the flooding point was approached.

- Vapour side resistances were found to be higher than those expected for heat transfer to a dry stationary wall. Although partially explained by the effects of mass transfer, applying the correction factor of McNaught and Emerson (1977) to reduce the heat transfer coefficient caused the data to be underpredicted. The data were best predicted by applying a further correction for the relative velocities of the condensate film and vapour. Due to countercurrent flow and the low vapour velocities imposed by flooding, the relative velocity was significantly

higher, and it was presumed that this caused the phase interface to be more disturbed thus leading to better heat transfer than in co-current flow.

9.2.2 Flooding

- The flooding databank was expanded to include not only numerical data but also video images of condensate draining from the tube. These videos are included as part of this thesis on the attached CD-ROM and provide evidence of wave bridging as the mechanism leading to flooding.

- The literature review on flooding found varying expressions of the flooding point which was one of the reasons for the large discrepancies between correlations. The other main reasons were differences in experimental set ups and the fact that some correlations were based on adiabatic air and water systems. This was addressed by separating reflux condenser flooding from adiabatic flooding by proposing a firm definition of the flooding point in a reflux condenser based on condensate drainage and pressure drop. "The vapour velocity (or set of conditions resulting in a vapour velocity) that caused condensate leaving the tube to change from film flow to a slug flow with resulting instabilities and increased pressure drop."

- When testing three commonly used correlations against this definition the method of Diehl & Koppany (1969) gave the safest predictions with the English et al (1963) modified and Alekseev (1972) correlations giving similar high accuracies. When the tube taper correction factor included in the English correlation was incorporated into the other two the Diehl & Koppany method gave very accurate results and the modified Alekseev equation overpredicted the data

9.2.3 Film theory based modelling

- Through the use of a Visual Basic simulation program written by the author, it was shown that the film theory method of Colburn & Drew (1937) could be applied to reflux condensers with reasonable accuracy. The method was found to be sensitive the values selected for vapour sensible heat transfer coefficients,

a fact that caused most of the area requirements (expressed as tube lengths) to be underpredicted.

- Most of the experimental separations were also underpredicted by the simulation. Also a result of the vapour heat transfer coefficients, this was used to highlight the importance of the mass transfer rate factor. Locally, the amount of separation depends on the value of the rate factor. Overprediction of the vapour heat transfer coefficient led to mass and heat transfer rate factors that were too high thus less separation was predicted.

- Comparison of the present work with the earlier film theory work of Di Cave et al (1987) and Al-Shammari (2002) indicated that trends in one body of work weren't always followed in others. Overall though, similar levels of accuracy were found in all three.

- Film theory modelling of a co-current condenser was also used to confirm that even though the experimental separations were very low, this was caused by high rate factors due to the tube geometry and even less separation would have been achieved in a similar co-current condenser at the same conditions.

9.2.4 Equilibrium method modelling

- The use of condensation curves and the equilibrium method of Silver (1937) and Bell & Ghaly (1972) was fully evaluated. Condensing curves describe idealised situations and although the mixed version of the differential curve is theoretically applicable to the process of reflux condensation, in practice reflux condensers fail to perform to those levels. This is because the flooding limit leads to high resistances in the vapour causing the process to be far removed from the idealised condensing curves.

- Modelling of experimental data was used to show that although more physically realistic the correction applied to reduce the dry gas vapour heat transfer coefficient for the effect of mass transfer caused large errors in the areas predicted by the method. This occurred when both the integral and differential curves were used. The error was caused by upsetting the balance between overpredicting both the vapour heat transfer coefficient and temperature-enthalpy

gradient, a balance that was key to the success of the equilibrium method. This problem is more apparent in reflux condensers as opposed to co-current condensers because the high rate factors experienced in reflux condensers cause large reductions in the vapour heat transfer coefficient.

- A new correction to the equilibrium method was proposed. Based on the heat transfer rate factor, this correction was applied to the condensation curve to reduce the amount of separation predicted and lower the gradient of the temperature-enthalpy relationship. This serves to balance the effect of reducing the vapour heat transfer coefficient leading to a reduction in the area.

- The proposed correction is applicable to all cases of binary condensation without the presence of a non condensing gas where the process is rate controlled although corrections will be more significant at higher rate factors. For example, the correction is more significant in a reflux condenser than in a standard vertical co-current condenser, and in a co0current condenser will be more significant towards the vapour outlet as vapour resistances increase.

- A simple correction factor was used to show that the proposed correction would improve the equilibrium method. Compositions and tube length predictions were both significantly better than without the correction, and with the integral curve, accuracies rivalled those of the film theory method.

9.3 Recommendations for future work

9.3.1 Flooding

It was shown earlier that the rate factors in reflux condensers are high in comparison with co-current condensers and this is the main reason reflux condensers fail to achieve their potential. It is important therefore to address this situation and design for low rate factors, but this is made difficult by the limits imposed by flooding. The issue of flooding is therefore critical to the design of reflux condensers and it is important to design a reflux condenser to operate as close to the flooding point as possible without ever actually reaching the flooding point.

The literature available on flooding weighs heavily in favour of adiabatic work, mainly air and water systems, which can behave differently to reflux condensers. Because of this, more research into flooding in reflux condensers is required. Flooding was not the main focus of this thesis, and so the experimental facility was never used to its full potential when studying flooding. There is massive scope for collecting more data on flooding, using for example different test fluids and different tube tapers. The major weakness of the flooding work in this thesis is the lack of accurate pressure drop data. If the facility is to be used for flooding, this should be addressed.

9.3.2 Film theory modelling

The results reported in this thesis suggested that the film theory model could be very accurate when the vapour side resistances were modelled accurately. Unfortunately, no local vapour heat transfer coefficients were available in the mixture work so there was an added uncertainty in the prediction of the vapour heat transfer coefficient. It would therefore be useful to collect data where local vapour coefficients were measured at a number of points in the tube. This would allow accurate local vapour coefficients to be correlated and used in the model and the true potential of the model to predict area requirements and composition change could then be evaluated.

9.3.3 Equilibrium model

The proposed correction to the HTFS version of the Silver, Bell and Ghaly equilibrium method was justified theoretically in this work and a crude correction factor was shown to improve the method. It is necessary for further research to be carried out into this correction to establish whether it will be a useful tool in the design of reflux condensers. This should concentrate on two fronts. Firstly, whether or not the correction would make significant improvements to the method in other types of condensers as suggested earlier, and secondly the evaluation of accurate correction factors. It is only through the development of accurate correction factors that the true usefulness of the method can be evaluated. This is potentially a significant amount of work especially if the correction is applicable to more than one condenser type.

9.3.4 Heat transfer enhancement

The problems caused by the high rate factors associated with reflux condensers have been well covered in this thesis. One best way of reducing the rate factors is through increasing the turbulent state of the vapour. Small increases in vapour velocity could be achieved by better understanding of the flooding point as discussed, but flooding will always limit reflux condensers to relatively low velocities. Further increases in the turbulence could potentially be achieved by heat and mass transfer enhancement through the use of tube inserts. In theory, such inserts would create eddies in the vapour thus increasing the turbulence and heat transfer coefficients and leading to lower rate factors. This would promote better separation enabling reflux condensers to operate closer to their theoretical limit.

References

Ackerman, G., *"Simultaneous heat and mass transfer with large temperature and partial pressure differences"*, Ver. Deutscher Ing. Forsch., Vol 8, (1937).

Al Shammari, SB, "*Liquid Mixing in Reflux Condensers*", Ph.D. Thesis, UMIST, Manchester, (2001)

Al-Shammari, SB, Webb, DR, Brag, R., Hedges, P.J., and Gibbard, I., "*Experimental Study of Separation in Reflux Condensers*", International Heat Transfer Conference, Grenoble, (2002).

Alekseev, V.P., Poberezkin, A.E., and Grasimov, P.V., "*Determination of Flooding Rates in Regular Packings*", Heat Transfer – Soviet Research, Vol. 4, No. 6, pp. 159-163 (1972).

Bartleman, A., "*Condensation of Pure Hydrocarbon Vapours in a Single Vertical Tube Reflux Condenser*", HTFS Research Report RS1047, (1999).

Bartleman, A., "*The Condensation of Hydrocarbons in a Vertical Reflux Condenser Tube*", Ph.D Thesis, University of Strathclyde, Glasgow, (2001).

Bell, K.J., and Ghaly, M.A., "*An Approximate Generalised Design Method for Multicomponent/Partial Condensers*", AIChE Symp. Series, Vol. 69, No. 131, pp. 72-79, (1972).

Blangetti, F., and Schlünder E.U., "*Local Heat Transfer Coefficient on Condensation in a Vertical Tube*", Proc. 6th Int. Heat Transfer Conf., Vol. 2, pp. 437-442, (1978).

Butterworth, D., (revised by McNaught, J.M.), "*Condensate Film Resistances on Vertical Surfaces (Including Tubes)*", HTFS Handbook Sheet CP2, (1975).

Butterworth, D., "*Silver Method for Multi-Component Condensation*", HTFS Handbook Sheet CM15, (1979).

Bromley, L.A., "", Ind. Eng. Chem., Vol. 44, (1952).

Carpenter, E.F., and Colburn, A.P., "*The Effect of Vapour Velocity on Condensation Inside Tubes*", Proc. of General Discussion on Heat Transfer, IMechE/ASME, pp. 20-26, (1951).

Chen, M.M., "", J. Heat Transfer, Vol 83, No. 1, (1963).

Chun, K.R., and Seban, R.A., "*Heat Transfer to Evaporating Liquid Films*", Trans. ASME, J. Heat Transfer, Vol. 93, No. 4, pp 391-396, (1971).

Chunangad, K.S., "*Sizing of Vertical Vapour-In-Tube Reflux Condensers*", MSc. Thesis, Oklahoma State University, (1992).

Clements, L.D., and Colver, C.P., "*Filmwise Condensation of Light Hydrocarbons and Their Mixtures in a Vertical Reflux Condenser*", AIChE Symp. Series, Vol. 69, No. 131, pp.18-22, (1973).

Colburn, A.P., "*Notes on the Calculation of Condensation When a Portion of the Condensate Layer is in Turbulent Motion*", Trans. AIChE, Vol. 30, pp. 187-193, (1934).

Colburn, A.P., and Drew, T.B., "*The Condensation of Mixed Vapours*", AIChE Trans. Vol. 33, pp. 197-215, (1937).

Colburn, A.P., and Hougen, O.A., "*Design of Cooler Condensers for Mixtures of Vapours With Non-condensing Gases*" Ind. Eng. Chem., Vol. 26, pp. 1178-1182, (1934).

Coulson, J.M., and Richardson, J.F., "*Coulson and Richardson's Chemical Engineering Volume 1: Fluid Flow, Heat Transfer and Mass Transfer*", 5th Ed., Pergammon, Oxford, (1997).

Cuthbertson, D., and McNaught, J.M., "*Reflux Condensation of a Single Vapour: Further Results and Flooding Studies*", HTFS Research Report RS1090

Deakin, A.W., "*A Review of Flooding Correlations for Reflux Condensers*", UKAEA Report AERA-M2923, (1977).

Deakin, A.W., Pulling, D.J., and Brogan, R., "*Flooding in Reflux Condensers*", HTFS Research Report RS249, (1978).

Diehl, J.E., and Koppany, C.R., "*Flooding Velocity Correlation for Gas-Liquid Counterflow in Tubes*", Chem. Eng. Prog. Symp. Series, Vol. 65, Part 92, pp 77-83, (1969).

Di Cave, S., Mazzarotta, B., and Sebastiani, E., "*Mathematical Model for Process Design and Simulation of Dephlegmators (Partial Condensers) for Binary Mixtures*", The Canadian J. Chem. Eng., Vol. 65, pp 559-564, (1987).

Dukler, A.E., "*Fluid Mechanics and Heat Transfer in Falling-Film Systems*", Chem. Eng. Prog. Symp. Series, Vol. 56, No. 30, pp. 1-10, (1960)

Dukler, A.E., and Smith, L., "*Two Phase Interactions in Counter-current Flow: Studies of the Flooding Mechanism*", Nureg Report No. NUREG/CR-0617, (1979).

English, K.G., Jones, W.T., and Spillers, R.C., "*Flooding in a Vertical Updraft Partial Condenser*", Chem. Eng. Progress, Vol. 61, No. 57, (1963).

ESDU, "*Reflux Condensation In Vertical Tubes*", Data Item No. 89038, (1989).

Farrant, P.E., "*An Introduction to Uncertainty Analysis for Heat Transfer Experiments*", NEL internal report, (2001).

Gross, U., *"Reflux Condensation Heat Transfer Inside a Closed Thermosyphon"*, Int. J. Heat Mass Transfer, Vol. 35, No. 2, pp 279-294, (1992).

Gross, U., Phillip, C., and Thumm, S., *"Effect of countercurrent vapour flow on film condensation heat transfer inside a vertical tube"*, International Heat Transfer Conference, Grenoble, (2002).

Hawley, D.L., and Wallis, G. B., *"Experimental study of liquid film fraction and pressure drop characteristics in vertical countercurrent annular flow"* EPRI NP-2280, Electrical Power Research Institute, Palo Alto, California, (1982).

Hewitt, G.F., *"Flooding Phenomena in Two Phase Flow"*, HTFS Handbook Sheet TP8, (1984).

Hewitt, G.F., and Wallis, G.B., *"Flooding and Associated Phenomena in Falling Film Flow in a Vertical Tube"*, UKAEA Report AERE R-4022, (1963).

Imura, H., Kusuda, H., and Funatsu, S., *"Flooding Velocity in a Counter-Current Annular Two-Phase Flow"*, Chem. Eng. Sci., Vol. 32, pp 79-87, (1977).

Incropera, F.P., and De Witt, D.P., *"Fundamentals of Heat and Mass Transfer"*, 4th Ed., John Wiley and Sons, New York, (1996).

International Standard Organisation, "*Measurement of Fluid Flow – Estimation of Uncertainty of a Flow-rate Measurement*", ISO/WD 5618.4, (1999).

Jayanti, S., Tokarz, A., and Hewitt, G.F., *"Theoretical Investigation of the Diameter Effect on Flooding in Countercurrent Flow"*, Int. J. Multiphase Flow, Vol. 22, No. 2, pp 307-324, (1996).

Jeong, J.H. and No, H.C., *"Experimental Study of the Effect of Pipe Length and Pipe-End Geometry on Flooding"*, Int. J. Multiphase Flow, Vol. 22, No. 3, pp 499-514, (1996).

Jibb, R.J., Gibbard, I., Polley, G.T., and Webb, D.R., *"The Potential for Using Heat Transfer Enhancement in Vent and Reflux Condensers"*, Eurotherm Seminar No. 62, (1998)

Kutateladze, S.S., *"Fundamentals of Heat Transfer"*, Academic Press, New York, (1963).

Koh, J.C.Y, *"An Integral Treatment of Two-Phase Boundary Layer in Film Condensation"*, J. Heat Transfer, Vol. 83, pp359-362, (1961)

Koh, J.C.Y., Sparrow, E.M., and Hartnett, J.P., *"The Two Phase Boundary Layer in Laminar Film Condensation"*, Int. J. Heat Mass Transfer, Vol. 2, pp 69-82, (1961).

Labuntsov, D.A., *"Heat Transfer in Film Condensation of Pure Steam on Vertical Surfaces"*, Teploenergetica, Vol. 4, No. 7, pp72-80, (1957).

McQuillan, K.W., and Whalley, P.B., *"A Comparison Between Flooding Correlations and Experimental Flooding Data for Gas-Liquid Flow in Vertical Circular Tubes"*, HTFS Research Report RS599, (1985).

McQuillan, K.W., Whalley, P.B., and Hewitt, G.F., *"Flooding in Vertical Two Phase Flow"*, HTFS Research Report RS598, (1985).

McNaught, J.M., *"Mass Transfer Correction Terms in Design Methods for Multicomponent/Partial Condensers"*, Condensation Heat Transfer, ASME 18th National Heat Transfer Conference, San Diego, (1979).

McNaught, J.M., *"Average Heat Transfer Coefficient for the Condensate Film on a Vertical Surface with No Vapour Shear"*, HTFS Handbook Sheet CM8, (1984).

McNaught, J.M., *"Calculation of Bulk Temperature, Composition and Flowrate in Condenser Simulation"*, HTFS Handbook Sheet CM35, (1984).

McNaught, J.M., *"Differential Condensation/Boiling Curves"*, HTFS Handbook Sheet PM38, (1984). (Referenced by McNaught (1984)

McNaught, J.M., *"Colburn-Drew Method for Condensation of Binary Mixtures of Condensing Vapours"*, HTFS Handbook Sheet CM33, (1986)

McNaught, J.M., *"Local Heat Transfer Coefficient for the Condensate Film on a Vertical Surface with No Vapour Shear"*, HTFS Handbook Sheet CM7, (1988).

McNaught, J.M., and Bartleman, A., *"Initial Results for Reflux Condensation of Hydrocarbon Vapour Mixtures"*, HTFS Research Report RS1067, (2000).

McNaught, J.M., and Emerson, W.H., *"A Development of Some Approximate Design Methods for Multi-Component Condensation"*, HTFS Research Report, RS211, (1977).

McNaught, J.M. and Walker, I.W., *"Heat Transfer During Gravity-Controlled Film-Wise Condensation in Vertical Condensers"*, HTFS Research Report RS743, (1987).

Minkowycz, W.J., and Sparrow, E.M., *"Condensation Heat Transfer in the Presence of Noncondensibles, Interfacial Resistance, Superheating, Variable Properties, and Diffusion"*, Int. J. Heat Mass Transfer, Vol. 9, pp 1125-1144, (1966).

Nusselt, W., *"Die Oberflüchenkondensation des Wasserdampfes"*, Zeitschr, VDI, Vol. 60, No. 27, pp 541-546, and Vol. 60, No. 28, pp 568-578, (1916).

Owen, R.G. and Deakin, A.W, *"A Review of Reflux Condensation"*, HTFS Research Report RS219, (1977).

Palen, J.W., Kistler, R.S., and Yang Z.F., *"What We Still Don't Know About Condensation in Tubes"*, Condensation and Condenser Design, ASME, pp 19-53, (1993).

Palen, J.W. Yang, Z.H., *"Reflux Condensation Flooding Prediction: Review of Current Status"*, Trans. IChemE, Vol. 79, Part A, (2001).

Perry, R.H. and Green, D.W., *"Perry's Chemical Engineers' Handbook"*, 7th Ed. M^{c}Graw Hill, (1997).

Poots, G., and Miles, R.G., *"Effects of Physical Properties on Laminar Film Condensation of Saturated Steam on a Vertical Flat Plate"*, Int. J. Heat Mass Transfer, Vol. 10, pp 1677-1692 (1967).

Rabas, T.J., and Arman, B., *"Effect of Exit Condition on the Performance of In-Tube Condensers"*, Heat Transfer Eng., Vol. 21, No. 1, pp 4-14, (2001).

Silver, L., *"Gas Cooling With Aqueous Condensation"*, Trans. Inst. Chem. Engs., Vol. 25, pp 30-42, (1947).

Sinnot, R.K., *"Coulson and Richardson's Chemical Engineering Volume 6: Design"*, 2nd Ed., Pergammon, Oxford, (1993).

Soliman, M., Schuster, J.R., and Berenson, P.J., *"A General Heat Transfer Correlation for Annular Flow Condensation"*, Trans. ASME J. Heat Transfer, Vol. 90, pp 267-276, (1968).

TC Ltd, "*Guide to thermocouple and resistance thermometry*", Issue 6.0, (1999).

Vijayan, M., Jayanti, S., and Balakrishnan, A.R., *"Effect of Tube Diameter on Flooding"*, Int. J. Multiphase Flow, Vol. 27, pp797-816, (2001).

Ward, D.J., *"How to Design a Multiple Component Partial Condenser"*, Petrochem. Eng., Vol. 32, No. 10, pp C42-C48, (1960).

Weast, D.C., "*Handbook of Chemistry and Physics*", 52nd Ed, The Chemical Rubber Co, (1972).

Wedd, D.R., and Al-Shammari, S.B., *"Separation in Reflux Condensers"*, International Heat Transfer Conference, Grenoble, (2002).

Whalley, P.B., *"Correlation for Flooding in Vertical Tubes"*, HTFS Handbook Sheet TM11, (1984).

Zabaras, G.J., and Dukler, A.E., *"Countercurrent Gas-Liquid Annular Flow Including the Flooding State"*, AIChe, Vol. 34, pp 389-3896, (1988).

Zapke, A., and Kröger, D.G., *"The Influence of Fluid Properties and Inlet Geometry on Flooding in Vertical and Inclined Tubes"*, Int. J. Multiphase Flow, Vol. 22, No. 3, pp 461-472, (1996).

List of figures

1.1	Schematic diagram of a vertical shell and tube reflux condenser	2
2.1	Film theory of binary mixture condensation (Colburn & Drew, 1937)	8
2.2	Filmwise condensation on a vertical surface with no vapour shear (Butterworth, 1975)	10
2.3	Typical variation of condensate heat transfer coefficient with film Reynolds number (on log-log scales) (Butterworth, 1975)	11
2.4	Colburn (1934) correlation for condensation on a vertical surface with no vapour shear	15
2.5	Comparison of Bartleman (2001) data with Nusselt (1916) and HTFS method	17
2.6	Comparison of Al-Shammari (2001) data with ESDU (1989) method	17
2.7	Wave formation as mechanism of flooding	21
2.8	Droplet entrainemt as the flooding mechanism	22
2.9	Bernoulli effect as the flooding mechanism (Rabas & Arman, 2000)	24
2.10	Pressure drop and vapour mass flux during flooding (Deakin, 1977)	25
2.11	Pressure drop v's gas mass flow rate as reported by English et al (1963)	26
2.12	Flooding studies/correlations and geometries (Imura et al, 1977)	28
2.13	Mass transfer effect on heat transfer through gas film	34
2.14	Example of a condensation (heat release) curve	35
2.15	T-xy diagram for integral condensation of pentane and iso-octane	36
2.16	T-xy diagram for partial differential condensation (4 stages) of a pentane and iso-octane mixture	38
3.1	Boiler Main Features	52
3.2	Reflux condenser test section	53
3.3	Line diagram of coolant circuit	56
3.4	Facility instrumentation diagram	58
3.5	Saturated liquid density as a function of temperature	62
3.6	Pentane vapour density as a function of temperature and pressure	63
3.7	Screenshot of the rig monitor	69
3.8	Screenshot of the stability monitor	69

4.1	Mass and energy balances over the reflux condense	72
4.2	Mass fraction against density for pentane and iso-octane	75
5.1	Heat flows in the experimental facility	104
5.2	Overall heat balance results	104
5.3	Difference between heat input and heat out against heat input	105
5.4	Difference between heat input and heat out against boiler temperature	105
5.5	CFD representation of air flow over major equipment	108
5.6	Overall heat balances with heat losses included in heat out term	109
5.7	Temperature profile for pentane run P2.2	112
5.8	Temperature profile for iso-octane run I5.2	112
5.9	Temperature profile for mixture run M1.6	115
5.10	Temperature profile for mixture run M3.1	115
5.11	Schematic diagram of condensate film on temperature probe	119
5.12	Possible causes of composition measurement error	122
5.13	Wilson plot for steam condensing over a range of coolant conditions	126
5.14	Comparison of coolant heat transfer coefficients calculated directly from data and predicted by Wilson plot correlation	126
5.15	Dimensionless local condensate film heat transfer coefficients	129
5.16	Mean condensate film heat transfer coefficients against film Reynolds number at the bottom of the tube	129
5.17	Condensate and effective vapour contributions to mean condensing side coefficient for mixture 1	133
5.18	Comparison of mean sensible vapour heat transfer coefficients and common correlations for heat transfer to a dry stationary wall	137
5.19	Comparison of mean sensible vapour heat transfer coefficients and additional corrections to Petukhov (1970) correlation	137
5.20	Measured separations through the reflux condenser	138
5.21	Heat balance expanded uncertainty against heat input for single component data	146
6.1	Digital video camera and light source for flooding observations	151
6.2	Temperature profiles for Flooding Test 3, Run 7.1 (non-flooding)	158
6.3	Temperature profile for Flooding Test 3, Run 11.1 (flooding)	158
6.4	Boiler pressure and heat load for all four flooding tests	159
6.5	Comparison of correlations for Flooding Test 1 ($T_{c,in}$ =40°C)	164

6.6	Comparison of correlations for Flooding Test 2 (Tc,in=35°C)	164
6.7	Comparison of correlations for Flooding Test 3 (Tc,in=40°C)	165
6.8	Comparison of correlations for Flooding Test 4 (Tc,in=40°C) with pressure drop also shown	165
6.9	Comparison of Flooding Test 1 (Tc, in=40°C) data with correlations modified to include English et al (1963) tube taper factor	168
6.10	Comparison of Flooding Test 3 (Tc, in=40°C) data with correlations modified to include English et al (1963) tube taper factor	168
7.1	Detailed simulation results for run M1.6	180
7.2	Detailed simulation results for run M2.10	181
7.3	Temperature profile for run M1.6	182
7.4	Tube lengths predicted by the film theory simulation	185
7.5	Predicted tube lengths against difference between calculated and meanexperimental heat transfer coefficient	185
7.6	Predicted bulk vapour temperatures at the outlet	187
7.7	Predicted vapour compositions for reflux and co-current condenser models	189
7.8	Predicted reflux condenser separations ($\tilde{y}_{P,o} - \tilde{y}_{P,i}$) as a % of the separation measured experimentally	189
7.9	Predicted tube length against mean vapour Reynolds number	195
7.10	Predicted tube length against predicted separation	195
7.11	Vapour composition and mass transfer rate factor profiles for run M1.6	193
8.1	Heat release curves for run M1.1	207
8.2	Predicted tube lengths for all mixtures	210
8.3	Predicted tube lengths for Mixture 1 up to 2m	210
8.4	Effect of vapour heat transfer coefficient prediction on tube length	211
8.5	Standard T-xy diagram for partial condensation of a binary vapour mixture	221
8.6	Comparison of standard and corrected heat release curves for run M1.1	223
8.7	Comparison of measured and predicted vapour outlet compositions	223
8.8	Comparison of tube lengths predicted by standard and corrected method	225

List of tables

3.1	Vapour Properties uncertainty analysis summary	64
3.2	VLE function summary	65
4.1	Instrument uncertainties	91
4.2	Uncertainty analysis example: Power measurement for run M2.2	94
4.3	Uncertainty analysis example: Propagated uncertainty of dump condenser heat load	98
5.1	Summary of experimental programme	101
5.2	Data rejection criteria	102
5.3	Wilson plot data summary	124
5.4	Standard uncertainties of measurements	143
5.5	Uncertainty budget for calculation of heat balance in run P2.2	145
5.6	Summary of results of overall heat balance uncertainty analysis	145
5.7	Summary of mass balance uncertainty analysis results	146
5.8	Summary of results of heat transfer coefficient uncertainty analysis	148
7.1	Tube length predictions for each mixture	184
7.2	Summary of major results from three film theory models of reflux condensers	197
8.1	Summary of equilibrium method models calculated	208
8.2	Summary of equilibrium method predicted tube lengths	212
8.3	Summary of corrected equilibrium method tube lengths	225

Appendix A: Instrument Calibrations

Pressure Transducer

The boiler pressure transducer was purchased (fully calibrated) and installed in August 2000, and was recalibrated externally by the manufacturer in July 2001. The details of these calibrations are given below and it should be noted that any uncertainty values quoted in this appendix refer solely to the calibration.

The transducer produced a current output, but the data logger recorded voltages. To combat this, a 250Ω precision resistor was used in series with the transducer and the voltage across the resistor measured.

Instrument Model:	Druck PTX510-I	
Calibrating company:	Druck Ltd (full UKAS accredited calibration)	
Range:	0 - 2.5 bar (abs)	
Uncertainty: (95% C.I.)	Generated pressure	±0.005% of reading + 0.008 mbar
	Measured current	±0.016% of reading + 1 digit

Calibration Equation: Form $P = A_1 V + A_0$

Where P = Pressure, V = voltage

Calibration date	Coefficients		Reading (V)	Calibrated value (Pa)	Drift (%)
	A_1	A_0			
Aug 00	62500	-62500	1.5	31250	-
			3.0	125000	-
			4.5	246875	-
July 01	62460	-62500	1.5	31193.2	-0.18
			3.0	124887.2	-0.09
			4.5	246689.5	-0.08

Table A.1: Pressure transducer calibration coefficients and drift

Reflux condenser flow meter

The meter used to measure the flow rate of coolant to the reflux condenser was supplied by Litre Meter in 1993 for the PhD project preceding this one. It was recalibrated in November 1999 before any data was collected for this project and again in July 2001 when some minor repairs were made. On both occasions it was calibrated by the manufacturer.

Instrument Model: Litre Meter SN220

Calibrating company: Litre Meter Limited

Range: 0.1 - 28 l/min

Uncertainty (95% C.I.): 0.4% of reading

Calibration Equation: Form $F = A_1 f + A_0$

Where F = flow rate, f = frequency

Calibration date	Coefficients		Reading (Hz)	Calibrated value (m^3/s)	Drift (%)
	A_1	A_0			
Nov 99	$6.5961*10^{-7}$	$5.6196*10^{-8}$	700	$4.618*10^{-4}$	1.55
			350	$2.309*10^{-4}$	1.56
			50	$3.305*10^{-5}$	1.71
Jul 01	$6.4880*10^{-7}$	$5.9565*10^{-8}$	700	$4.542*10^{-4}$	-1.64
			350	$2.271*10^{-4}$	-1.64
			50	$3.250*10^{-5}$	-1.63

Table A.2: Reflux condenser flowmeter calibration coefficients and drift

Dump condenser flow meter

The dump condenser coolant flow meter was also supplied by Litre Meter in 1993 for the PhD project preceding this one. It was recalibrated in November 1999 before any data was collected for this project and again in July 2001 when some worn parts were replaced.

Instrument Model: Litre Meter SN45

Calibrating company: Litre Meter Limited

Range: 0.04 – 6.3 l/min

Uncertainty (95% C.I.) 0.4% of reading

Calibration Equation: Form $F = A_1 f + A_0$

Where F = flow rate, f = frequency

Equation coefficients and drift (Figure A3)

Calibration date	Coefficients		Reading (Hz)	Calibrated value (m^3/s)	Drift (%)
	A_1	A_0			
Nov 99	$2.1793*10^{-7}$	$-1.7286*10^{-7}$	480	$1.04*10^{-4}$	0.74
			250	$5.43*10^{-5}$	0.58
			50	$1.07*10^{-5}$	-0.70
Jul 01	$2.1724*10^{-7}$	$-1.8128*10^{-7}$	480	$1.04*10^{-4}$	-0.17
			250	$5.43*10^{-5}$	-0.03
			50	$1.08*10^{-5}$	-1.12

Table A.3: Dump condenser flowmeter calibration coefficients and drift

Power transmitter

The power transmitter used to measure energy supplied to the boiler cartridge heaters was purchased and installed in December 1999 to replace a similar model that had been damaged through operating out of range. It was calibrated externally in February 2000 over some of the operating range and was recalibrated in January 2001 over the full range with more data points. Comparison of the two calibrations showed that there were minor errors in two of the data points in the original calibration giving a non-linear behaviour and a high level of drift. No experimental data quoted in this thesis was recorded before the January 2001 recalibration.

Instrument Model:	Infratek AG ITL-100 (250V/50A)		
Calibrating company:	Instrument Repairs and Calibrations, East Kilbride		
Range:	100W – 6000W		
Uncertainty: (95% C.I.)	Input	D.C.V. up to 300V	±55 ppm
		D.C.A 2.2A to 11A	±0.041%
		D.C.A. 11A to 35A	±0.5%
	Output	up to 10mA	±50 ppm
		10mA to 100mA	±100ppm

Calibration Equation: Form $F = A_1 f + A_0$

Where F = flow rate, f = frequency

Calibration date	Coefficients		Reading (V)	Calibrated value (W)	Drift (%)
	A_1	A_0			
Feb 00	2359.2	281.86	0.80	2169	-
			1.65	4175	-
			2.40	5944	-
Jan 01	2510.0	30.62	0.80	2039	-5.98
			1.65	4173	-0.02
			2.40	6057	1.90

Table A.4: Watt meter calibration coefficients and drift

Thermocouples

All of the thermocouples used on the experimental facility were Type-T (copper-copper/nickel) supplied by TC Ltd. They were all supplied to meet the standard calibration within the tolerances quoted by the manufacturer (TC Guide, 1997) over the full working range.

It was decided that although theoretically an in-house calibration could lower the uncertainty, in practice, an in-situ calibration with a temperature source and reference proved to be time consuming and unpredictable. As a result of this, in-house calibrations were neglected in favour of a periodic calibration check to determine if the thermocouples were operating within the quoted tolerances or not. Any thermocouples reading outwith the tolerance would be replaced.

Melting ice and hot water in a temperature bath were used as sources, with a precision resistance thermometer and digital display used as the reference. All thermocouples were found to be within the expected tolerances, and as such were only replaced when they became damaged.

The use of a data logger with dedicated thermocouple card meant that there was no requirement for a cold junction. The data logger card used cold junction compensation to alter the signals as if a reference junction was held at 0°C.

Instrument Model:	TC Type-T thermocouples	
Calibrating company:	TC Ltd (standard Type-T calibration)	
Range:	-185 to +300°C	
Uncertainty:	Class 1	±0.5°C
(95% CI)	Class 2	±1.0°C

Calibration Equation: Form $T = \sum_{i=1}^{n} a_i V$

Where T = temperature (°C), V = voltage (μV)

For polynomial coefficients see TC Guide (1997) page 9.

Platinum Resistance Thermometers

Five resistance thermometers (PRTs) were supplied by TC Ltd in December 2000 for boiler vapour and condenser coolant measurements. As in the thermocouples, it was felt that an in house calibration would be too inaccurate and so the manufacturer's standard calibration was used. 4-wire resistance assemblies were used to eliminate the effects of minor differences in cables or junctions.

In the cases where PRTs were used to measure temperature differences, isothermal offsets were employed. In measuring the difference between two positions A and B, an isothermal offset is the difference recorded when the two temperatures should in theory be the same. Minor variations in the thermometers may lead to slight differences between readings of the same temperature (systematic error), but by applying isothermal offsets these differences are eliminated.

With the PRTs in place, cooling water was supplied to each of the condensers with no heat input. After allowing time for the temperatures to stable, measurements were made of the inlet and outlet temperatures. Many measurements were made, over the course of 3 days, and the average difference between the inlet and the outlet was taken as the isothermal offset. The isothermal offset for the reflux condenser was found to be 0.047°C, and –0.008°C for the dump condenser. It should be noted that both of these values are lower than the quoted tolerance.

Instrument Model:	TC Pt100-1/3 (4-wire)
Calibrating company:	TC Ltd (Standard Pt100 calibration)
Range:	-200°C to +850°C
Uncertainty (95% C.I.):	±0.08°C (at 0°C), ±0.19°C (at 100°C)

Calibration Equation:

Form

up to 100°C $$R_t = R_0\left(1 + AT + BT^2 + C(T-100)T^3\right)$$

Over 100°C $$R_t = R_0\left(1 + AT + BT^2\right)$$

Where T = temperature, R_t = resistance, R_0 = resistance at 0°C (100Ω), $A = 3.9083 \times 10^{-3}\ °C^{-1}$, $B = -5.775 \times 10^{-7}\ °C^{-2}$, $C = -4.183 \times 10^{-12}\ °C^{-4}$

Densitometer

The in house calibration and accuracy of the densitometer measuring cell and digital display was discussed in detail by Bartleman (2001). The same system of calibration was used in this project except that pure pentane and iso-octane were used as the calibrating components instead of water and air. As the densitometer was only used for mixtures of pentane and iso-octane, the wide range of densities available from a water and air calibration was not used and it was felt that more accuracy could be achieved in the required range by using the two hydrocarbons.

The densitometer was expected to operate at 20°C, with a water bath providing the stable temperature. During calibration, readings were taken at 19.8, 20.0 and 20.2°C, thus allowing for small fluctuations during normal operation. Readings were taken once a day over five days, and an average value taken for the calibration constant.

Instrument Model: Paar Scientific DMA 602 Measuring Cell
Paar Scientific DMA 60 Digital Display

Calibrating company: In-house

Range: 0.627 – 0.692 kg/m³ (Pentane – Iso-octane at 20°C)

Instrument Uncertainty:	$\pm 1.5 * 10^{-6}$ g/cm³	(quoted by manufacturer)
Calibration Uncertainty	0.03 % of reading	(95% C.I.)
	(based on multiple testing of known samples)	

Calibration Equation:

Form $$k = \frac{\rho_P - \rho_I}{T_P^2 - T_I^2}$$

Where k = calibration constant

ρ_P, ρ_I = Density of Pentane, Iso-octane (kg/m³)

T_P, T_I = Oscillation period of pentane, iso-octane (s)

	Pentane		Iso-octane		Calibration constant
Temp (°C)	Density (kg/m³)	Mean period (s)	Density (kg/m³)	Mean period (s)	k (kg/m³.s²)
19.8	0.626857	3.302855	0.692933	3.364938	0.159620
20.0	0.626661	3.302594	0.692763	3.364704	0.159625
20.2	0.626464	3.302375	0.692593	3.364497	0.159669
Average	0.626661	3.302608	0.692763	3.364713	0.159638

Table A.5: Densitometer calibration coefficients

Table B1.1: Estimation of measurement uncertainties

	Measurement	Notation	Unit	$\bar{x}_i$	$s(x_i)$	$u_I(x_i)$	$u_c(\bar{x}_i)$
Boiler	Boiler Heat Input	$\dot{Q}_i$	W	3013.2	1.83	3.0	3.5
	Pressure	$P_{v,i}$	Pa	124794.7	42.33	187.2	191.9
	Vapour Temp	$T_{vR,i}$	°C	42.16	0.011	0.095	0.10
Reflux Cond Coolant	Flow Rate	$\dot{V}_{c,R}$	m³/s	5.86E-05	2.60E-07	1.17E-07	2.85E-07
	Inlet Temp	$T_{cR,i}$	°C	29.53	0.004	0.068	0.068
	TS3 Inlet Temp	$T_{cR,TS3}$	°C	31.84	0.022	0.25	0.251
	TS4 Inlet Temp	$T_{cR,TS4}$	°C	34.02	0.024	0.25	0.251
	Outlet Temp	$T_{cR,o}$	°C	36.77	0.006	0.068	0.068
Reflux Vapour	Vapour TS2 Outlet	$T_{vR,oTS2}$	°C	40.73	0.023	0.25	0.251
	Vapour TS3 Outlet	$T_{vR,oTS3}$	°C	40.77	0.020	0.25	0.251
	Vapour TS4 Outlet	$T_{vR,oTS4}$	°C	N/A	N/A	0.25	N/A
Reflux Condenser Wall Temperatures	TS2, top	$T_{w,TS2t}$	°C	30.97	0.022	0.50	0.500
	TS2, mid	$T_{w,TS2m}$	°C	32.13	0.024	0.50	0.501
	TS2, bot	$T_{w,TS2b}$	°C	34.27	0.027	0.50	0.501
	TS3, top	$T_{w,TS3t}$	°C	33.70	0.030	0.50	0.501
	TS3, mid	$T_{w,TS3m}$	°C	34.95	0.024	0.50	0.501
	TS3, bot	$T_{w,TS3b}$	°C	35.85	0.019	0.50	0.500
	TS4, top	$T_{w,TS4t}$	°C	36.35	0.030	0.50	0.501
	TS4, mid	$T_{w,TS4m}$	°C	36.96	0.019	0.50	0.500
	TS4, bot	$T_{w,TS4b}$	°C	37.78	0.029	0.50	0.501
Dump Condenser	Coolant Flow Rate	$\dot{V}_{c,D}$	m³/s	2.39E-05	1.52E-07	4.77E-08	1.59E-07
	Coolant Inlet Temp	$T_{cD,in}$	°C	15.59	0.006	0.068	0.068
	Coolant Outlet Temp	$T_{cD,out}$	°C	23.70	0.022	0.068	0.071
	Condensate Temp	$T_{f,D}$	°C	15.59	0.022	0.50	0.500
VCC Air	Inlet Temp	T_{Ai}	°C	7.49	0.132	0.25	0.283
	Outlet Temp	T_{Ao}	°C	11.46	0.019	0.25	0.251

Notes

- In cases where the instrument uncertainty, $u_I(x_i)$, is quoted as a percentage of the measurement then $u_I(x_i) = \frac{u_{I\%}}{100} * x_i$
- The steady state uncertainty, $u_s(x_i)$ is taken to be the standard deviation of the repeat scans $u_s(x_i) = s(x_i)$
- $u_c(\bar{x}_i) = \sqrt{u_i(x_i)^2 + u_s(x_i)^2}$

Table B2.1: Uncertainty budget for reflux condenser coolant heat load

Nominal Value of calculation: $\dot{Q}_R$ = 1764.1 W

Calculation inputs	Unit	Input value	Input unc	Output	Sensitivity coefficients	
		x_i	$u_c(x_i)$	$y(x_i + \Delta x_i)$	$c(x_i)$	$u_c(x_i)^2\, c(x_i)^2$
$\dot{V}_{c,R}$	m³/s	5.86*10^{-5}	2.85*10^{-7}	1772.7	3.01*10^{7}	73.79
$T_{cR,i}$	°C	29.53	0.068	1747.6	-243.9	275.07
$T_{cR,o}$	°C	36.77	0.068	1780.6	243.2	273.49
					Combined uncertainty	
					$U_c(y)$	24.8

Table B2.2: Uncertainty budget for dump condenser coolant heat load

Nominal Value of calculation: $\dot{Q}_D$ = 799.5 W

Calculation inputs	Unit	Input value	Input unc	Output	Sensitivity coefficients	
		x_i	$u_c(x_i)$	$y(x_i + \Delta x_i)$	$c(x_i)$	$u_c(x_i)^2\, c(x_i)^2$
$\dot{V}_{c,D}$	m³/s	2.39*10^{-5}	1.59*10^{-7}	813.7	8.89*10^{7}	199.80
$T_{cD,i}$	°C	15.59	0.068	801.5	29.6	4.05
$T_{cD,o}$	°C	23.61	0.071	815.4	223.2	251.13
					Combined uncertainty	
					$U_c(y)$	21.3

Table B2.3: Uncertainty budget for heat gained by air in the extraction system

Nominal Value of calculation: $\dot{Q}_A$ = 404.0 W

Calculation inputs	Unit	Input value	Input unc	Output	Sensitivity coefficients	
		x_i	$u_c(x_i)$	$y(x_i + \Delta x_i)$	$c(x_i)$	$u_c(x_i)^2\, c(x_i)^2$
$u_{A,Ex}$	m/s	4.46	0.486	448.01	90.58	1937.9
T_{Ai}	°C	7.49	0.283	375.02	-102.4	839.8
T_{Ao}	°C	11.46	0.251	429.32	101.0	642.7
					Combined uncertainty	
					$U_c(y)$	58.5

Table B2.4: Uncertainty budget for overall heat balance

Nominal Value of calculation: R_Q = 0.985 W/W

Calculation inputs	Unit	Input value	Input unc	Output	Sensitivity coefficients	
		x_i	$u_c(x_i)$	$y(x_i + \Delta x_i)$	$c(x_i)$	$u_c(x_i)^2\, c(x_i)^2$
$\dot{Q}_I$	W	3013.2	3.53	0.983	-4.10*10^{-4}	2.09*10-6
$\dot{Q}_R$	W	1764.1	24.8	0.993	3.20*10^{-4}	6.30*10-5
$\dot{Q}_D$	W	799.5	21.3	0.992	3.18*10^{-4}	4.59*10-5
$\dot{Q}_A$	W	404.0	58.5	1.004	3.27*10^{-4}	3.70*10-4
					Combined uncertainty	
					$U_c(y)$	0.022

Table B2.5: Uncertainty budget for reflux condensate mass flow rate

Nominal Value of calculation: $\dot{m}_{f,o}$ = 4.695*10^{-3} kg/s

Calculation inputs	Unit	Input value	Input unc	Output	Sensitivity coefficients	
		x_i	$u_c(x_i)$	$y(x_i + \Delta x_i)$	$c(x_i)$	$u_c(x_i)^2\, c(x_i)^2$
$\dot{Q}_R$	W	1764.1	24.8	4.761*10^{-3}	2.66*10^{-6}	4.35*10^{-9}
$T_{vR,i}$	°C	42.16	0.10	4.693*10^{-3}	-2.17*10^{-5}	4.34*10^{-12}
$\bar{T}_f$	°C	34.31	5.00	4.848*10^{-3}	3.07*10^{-5}	2.36*10^{-8}
					Combined uncertainty	
					$U_c(y)$	1.67*10^{-4}

Table B2.6: Uncertainty budget for dump condensate (vapour outlet) flow rate

Nominal Value of calculation: $\dot{m}_{v,o}$ = 1.918*10^{-3} kg/s

Calculation inputs	Unit	Input value	Input unc	Output	Sensitivity coefficients	
		x_i	$u_c(x_i)$	$y(x_i + \Delta x_i)$	$c(x_i)$	$u_c(x_i)^2\, c(x_i)^2$
$\dot{Q}_D$	W	799.5	21.3	1.97*10^{-3}	2.40*10^{-6}	2.61*10^{-9}
$T_{cD,i}$	°C	15.59	0.068	1.92*10^{-3}	-7.97*10^{-6}	2.94*10^{-13}
$T_{cD,o}$	°C	23.61	0.071	1.92*10^{-3}	1.06*10^{-6}	5.66*10^{-15}
					Combined uncertainty	
					$U_c(y)$	5.15*10^{-5}

Table B2.7: Uncertainty budget for reflux condenser vapour inlet flow rate

Nominal Value of calculation: $\dot{m}_{v,i}$ = 6.613*10^{-3} kg/s

Calculation inputs	Unit	Input value	Input unc	Output	Sens. coeffs	
		x_i	$u_c(x_i)$	$y(x_i + \Delta x_i)$	$c(x_i)$	$u_c(x_i)^2\, c(x_i)^2$
$\dot{m}_{f,o}$	kg/s	4.695*10^{-3}	1.67*10^{-4}	6.780*10^{-3}	1	2.789*10^{-8}
$\dot{m}_{v,o}$	kg/s	1.918*10^{-3}	5.15*10^{-5}	6.664*10^{-3}	1	2.652*10^{-9}
					Combined uncertainty	
					$U_c(y)$	1.75*10^{-4}

Table B2.8: Uncertainty budget for logarithmic mean temperature difference over full tube length

Nominal Value of calculation: θ_{mean} = 7.95 °C

Calculation inputs	Unit	Input value	Input unc	Output	Sensitivity coefficients	
		x_i	$u_c(x_i)$	$y(x_i + \Delta x_i)$	$c(x_i)$	$u_c(x_i)^2\, c(x_i)^2$
$T_{vR,i}$	°C	42.16	0.10	8.01	0.646	4.17*10^{-3}
$T_{vR,oTS2}$	°C	40.73	0.251	8.05	0.396	9.88*10^{-3}
$T_{cR,i}$	°C	29.53	0.068	7.92	-0.398	7.32*10^{-4}
$T_{cR,o}$	°C	36.77	0.068	7.90	-0.649	1.95*10^{-3}
					Combined uncertainty	
					$U_c(y)$	0.13

Table B2.9: Uncertainty budget for mean overall heat transfer coefficient

Nominal Value of calculation: $\overline{U}$ = 1041.8 W/m²K

Calculation inputs	Unit	Input value	Input unc	Output	Sensitivity coefficients	
		x_i	$u_c(x_i)$	$y(x_i + \Delta x_i)$	$c(x_i)$	$u_c(x_i)^2\, c(x_i)^2$
$\dot{Q}_R$	W	1764.1	24.8	1056.4	0.591	214.82
θ_{mean}	°C	7.95	0.13	1025.3	-1.29*10^2	281.23
					Combined uncertainty	
					$U_c(y)$	22.1

Table B2.10: Uncertainty budget for mean condensate film heat transfer coefficient

Nominal Value of calculation: $\overline{\alpha}_f$ = 1190.0 w/m²K

Calculation inputs	Unit	Input value	Input unc	Output	Sensitivity coefficients	
		x_i	$u_c(x_i)$	$y(x_i + \Delta x_i)$	$c(x_i)$	$u_c(x_i)^2\, c(x_i)^2$
$\overline{U}$	W/m°K	1041.8	22.09	1218.9	1.31	837.40
$\overline{\alpha}_c$	W/m°K	5857.6	100	1187.4	-2.60*10-3	0.0676
					Combined uncertainty	
					$U_c(y)$	29.0

Notes

- The uncertianty of the mean coolant htc was taken as ±100 W/m²K. This was obtained by comparing the Wilson plot data with predictions made by the correlation
- The uncertainty of the mean wall heat transfer coefficient, $\overline{\alpha}_w$, was assumed to be negligible.

Table B2.11: Uncertainty budget for local condensate htc at the bottom of TS2

Nominal Value of calculation: $\alpha_{f,TS2}$ = 2154.5 W/m²K

Calculation inputs	Unit	Input value	Input unc	Output	Sensitivity coefficient	
		x_i	$u_c(x_i)$	$y(x_i + \Delta x_i)$	$c(x_i)$	$u_c(x_i)^2\ c(x_i)^2$
$\alpha_{c,TS2}$	W/m²K	5787	100	1124.0	-10.3	$1.06*10^6$
$T_{vR,oTS3}$	°C	40.8	0.251	1086.5	$-4.26*10^3$	$1.14*10^6$
$T_{w,TS2b}$	°C	34.3	0.500	1359.4	$-1.59*10^3$	$6.32*10^5$
$T_{cR,TS3}$	°C	31.8	0.251	1001.8	$-4.59*10^3$	$1.33*10^6$
					Combined uncertainty	
					$U_c(y)$	2040.3

Table B2.12: Uncertainty budget for local condensate htc at the bottom of TS3

Nominal Value of calculation: $\alpha_{f,TS3}$ = 663.86 W/m²K

Calculation inputs	Unit	Input value	Input unc	Output	Sensitivity coefficient	
		x_i	$u_c(x_i)$	$y(x_i + \Delta x_i)$	$c(x_i)$	$u_c(x_i)^2\ c(x_i)^2$
$\alpha_{c,TS3}$	W/m²K	5927	100	674.6	0.107	114.49
$T_{vR,oTS4}$	°C	41.5	0.251	650.0	-55.12	191.41
$T_{w,TS3b}$	°C	35.9	0.501	967.3	606.53	$9.23*10^4$
$T_{cR,TS4}$	°C	34.4	0.251	532.1	-524.50	$1.73*10^4$
					Combined uncertainty	
					$U_c(y)$	331.3

Table B2.13: Uncertainty budget for local condensate htc at the bottom of TS4

Nominal Value of calculation: $\alpha_{f,TS4}$ = 1011.5 W/m²K

Calculation inputs	Unit	Input value	Input unc	Output	Sensitivity coefficient	
		x_i	$u_c(x_i)$	$y(x_i + \Delta x_i)$	$c(x_i)$	$u_c(x_i)^2\, c(x_i)^2$
$\alpha_{c,TS4}$	W/m²K	6050	100	1027.3	0.159	252.81
$T_{vR,i}$	°C	42.2	0.10	1000.3	-116.6	135.96
$T_{w,TS4b}$	°C	37.8	0.501	1469.3	914.2	$2.10*10^5$
$T_{cR,o}$	°C	36.8	0.068	961.1	-743.0	$2.55*10^3$
					Combined uncertainty	
					$U_c(y)$	461.0

Table B3.1: Calculation uncertainties reported as expanded uncertainties

All uncertainties reported in the following table are expanded using a coverage factor of 2 to give a confidence interval of approximately 95%.

Calculated value	Unit	Value	Standard uncertainty		Expanded uncertainty	
			abs	%	abs	%
$\dot{Q}_R$	W	1764.1	24.8	1.41	49.6	**2.82**
$\dot{Q}_D$	W	799.5	21.3	2.66	42.6	**5.32**
$\dot{Q}_A$	W	404.0	58.5	14.48	117.0	**28.96**
R_Q	W/W	0.985	0.022	2.23	0.044	**4.46**
$\dot{m}_{f,o}$	kg/s	$4.695*10^{-3}$	$1.67*10^{-4}$	3.56	$3.34*10^{-4}$	**7.12**
$\dot{m}_{v,o}$	kg/s	$1.918*10^{-3}$	$5.15*10^{-5}$	2.69	$1.03*10^{-4}$	**5.37**
$\dot{m}_{v,i}$	kg/s	$6.613*10^{-3}$	$1.75*10^{-4}$	2.65	$3.50*10^{-4}$	**5.29**
θ_{mean}	°C	7.95	0.13	1.64	0.26	**3.27**
$\overline{U}$	W/m²K	1041.8	22.1	2.12	44.2	**4.24**
$\overline{\alpha}_f$	W/m²K	1190.0	29.0	2.44	58.0	**4.87**
$\alpha_{f,TS2}$	W/m²K	2154.5	2040.3	94.70	4080.6	**189.40**
$\alpha_{f,TS3}$	W/m²K	663.9	331.3	49.90	662.6	**99.80**
$\alpha_{f,TS4}$	W/m²K	1011.5	461.0	45.58	922.0	**91.15**

Appendix C: Physical Properties

This appendix contains details of the work conducted by the author to predict the physical properties of n-pentane and 2,2,4-trimethylpentane (iso-octane). All data was extracted from PPDS v2.2

Liquid Properties

Table C1 below summarises the polynomial equation coefficients used to describe saturated liquid properties over the range 0 – 100 °C based on equation (C1) below. Figures C1 – C7 show the curves the equations were regressed from.

$$LProp = c_3T^3 + c_2T^2 + c_1T + c_0 \qquad \text{(C1)}$$

Component	Property	Unit	c_3	c_2	c_1	c_0
Pentane	Density	Kg/m³	-6.793E-06	-6.743E-04	-0.94573	645.88
	Heat Capacity	J/g.K	2.941E-08	8.190E-06	0.00415	2.214
	Dynamic Viscosity	Ns/m²	-5.227E-11	1.632E-08	-2.687E-06	2.724E-04
	Thermal Conductivity	W/m.K	1.013E-09	3.202E-07	-3.98E-04	0.1234
	Enthalpy	J/g	2.813E-03	1.936	2.227E+03	1.116E+01
	Latent Heat	J/g	-8.643E-06	-6.458E-04	-0.733	383.30
	Surface Tension	N/m	1.445E-10	5.781E-08	-1.13E-04	0.01828
Isooctane	Density	Kg/m³	-2.078E-06	-4.529E-04	-0.82969	709.55
	Heat Capacity	J/g.K	7.958E-09	6.192E-06	0.00405	1.964
	Dynamic Viscosity	Ns/m²	-2.455E-10	6.947E-08	-8.798E-06	6.575E-04
	Thermal Conductivity	W/m.K	2.621E-10	1.364E-07	-2.60E-04	0.1062
	Enthalpy	J/g	-3.377E-04	2.406E+00	1.991E+03	3.791E+00
	Latent Heat	J/g	-3.065E-06	2.400E-05	-0.477	314.20
	Surface Tension	N/m	5.528E-11	3.884E-08	-9.37E-05	0.02060

Table C.1: Saturated liquid physical property coefficients

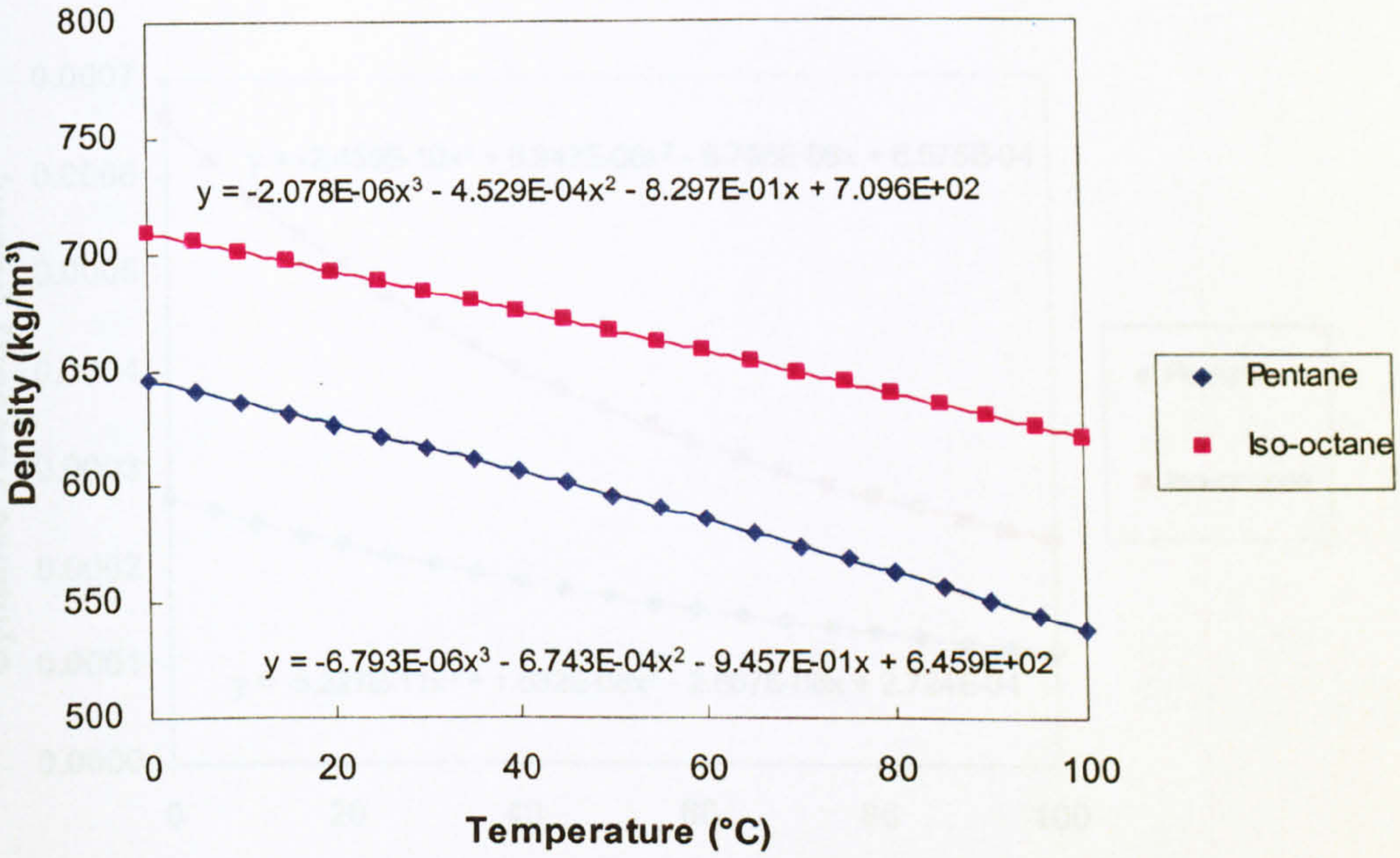

Figure C.1: Saturated liquid density

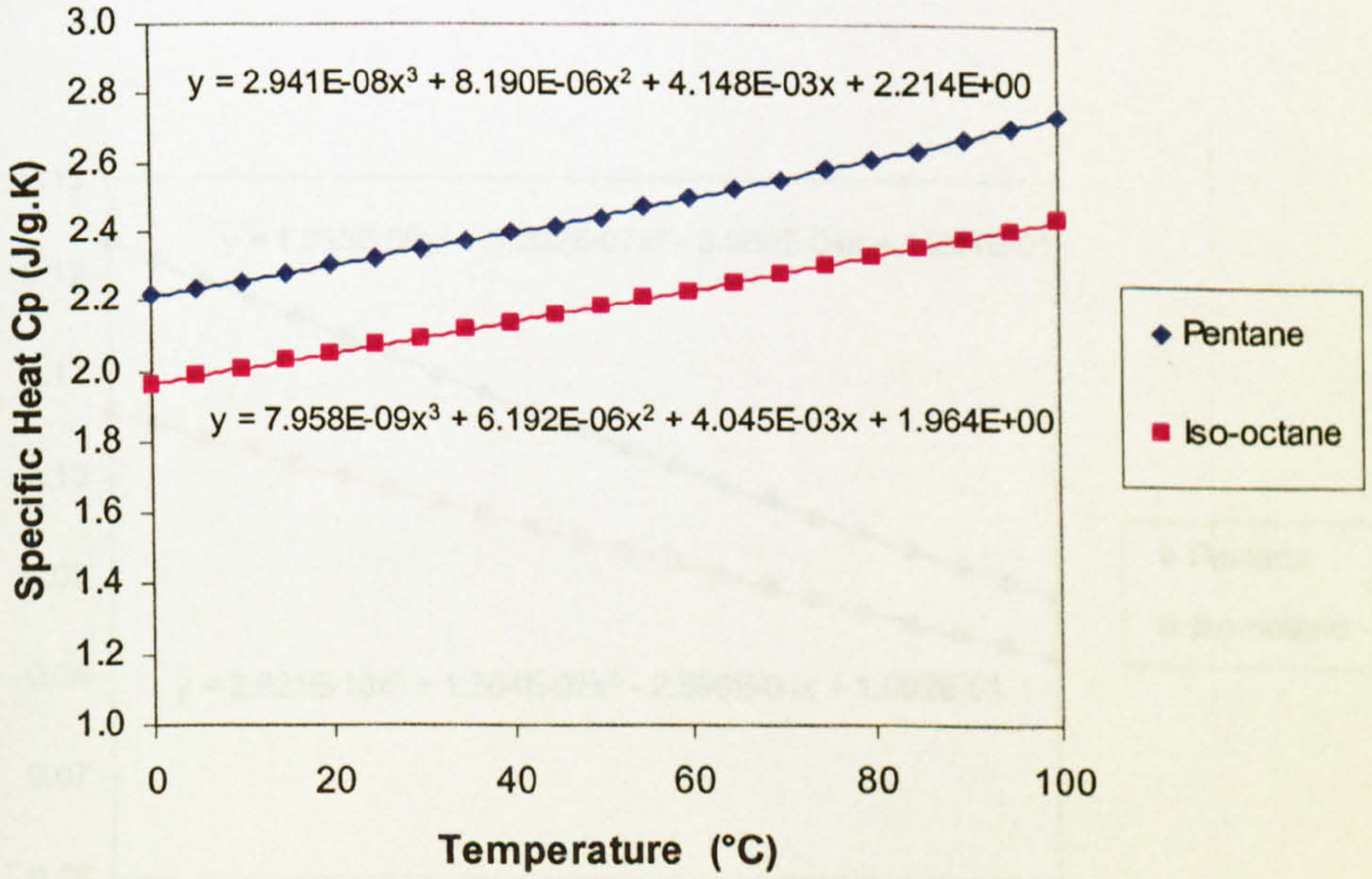

Figure C.2: Saturated liquid specific heat capacity

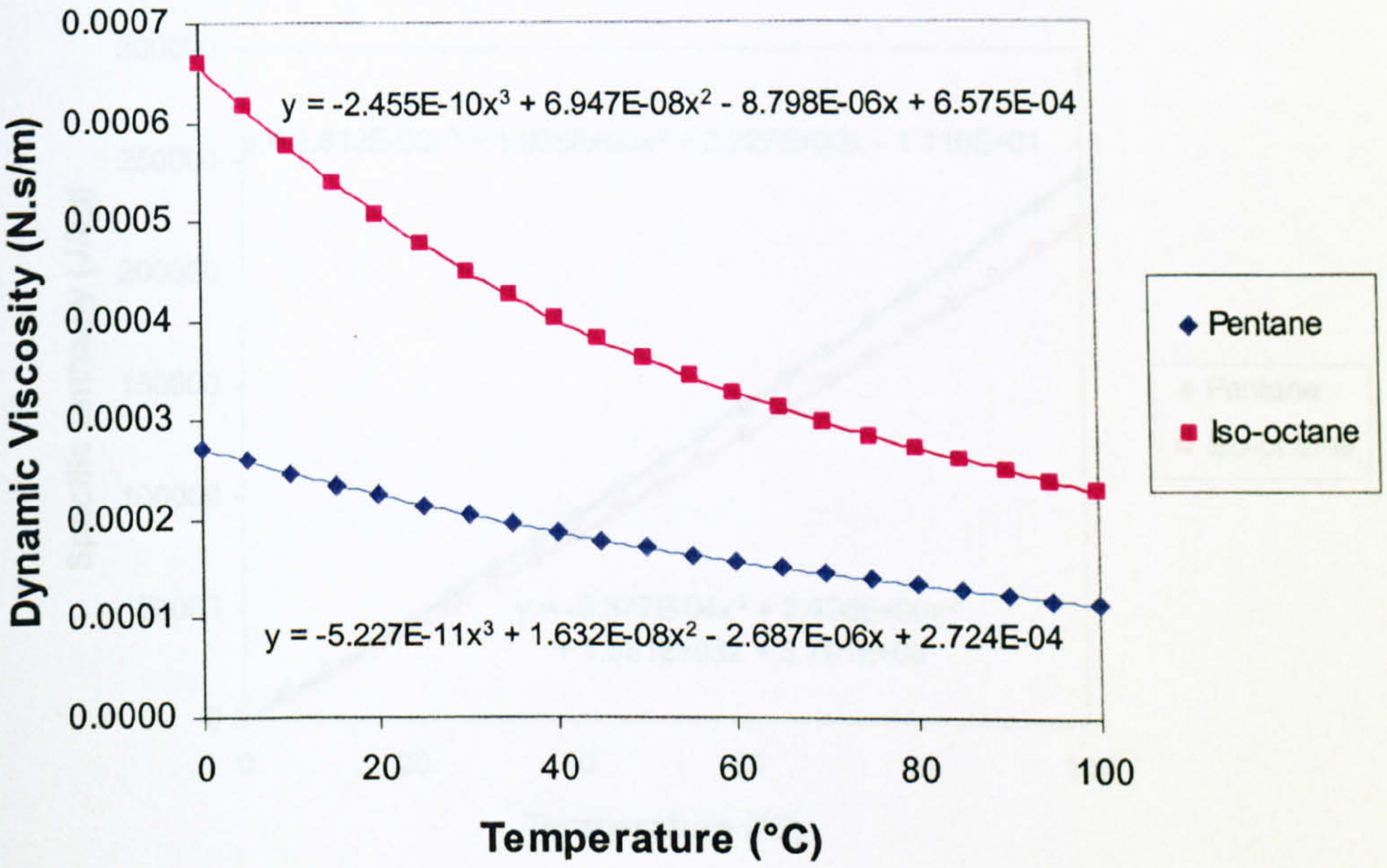

Figure C.3: Saturated liquid viscosity

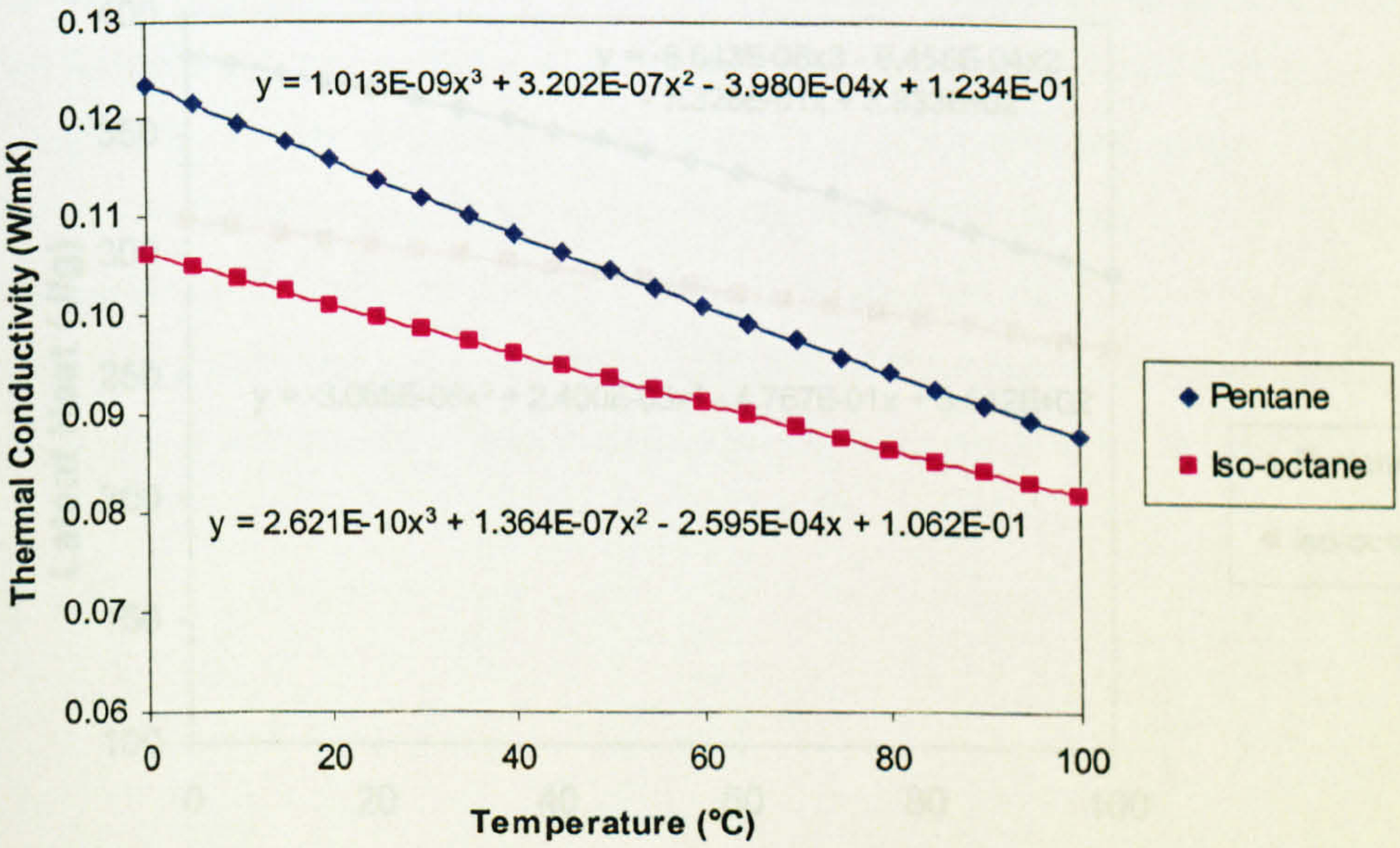

Figure C.4: Saturated liquid thermal conductivity

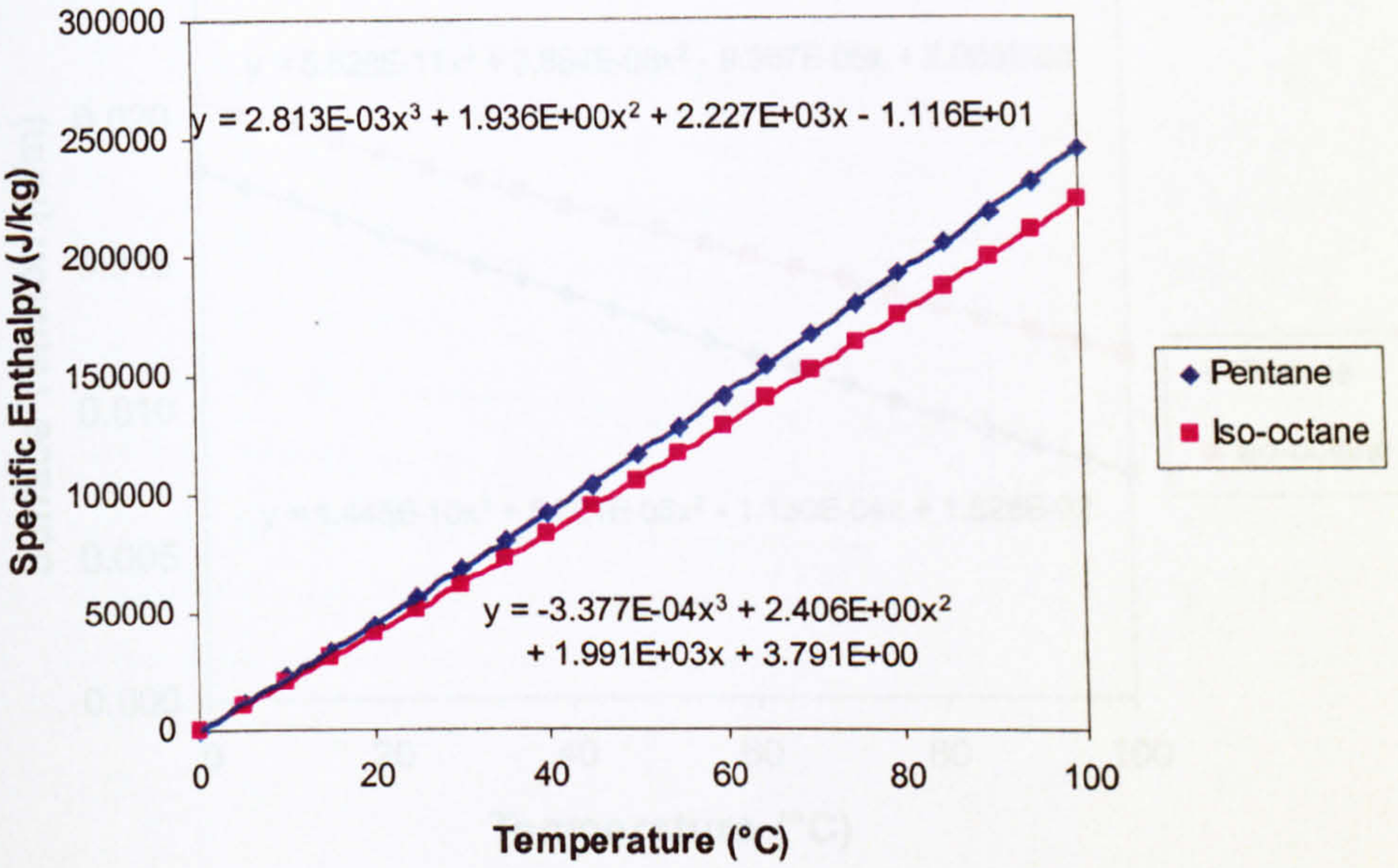

Figure C.5: Saturated liquid specific enthalpy with basis of 0°C

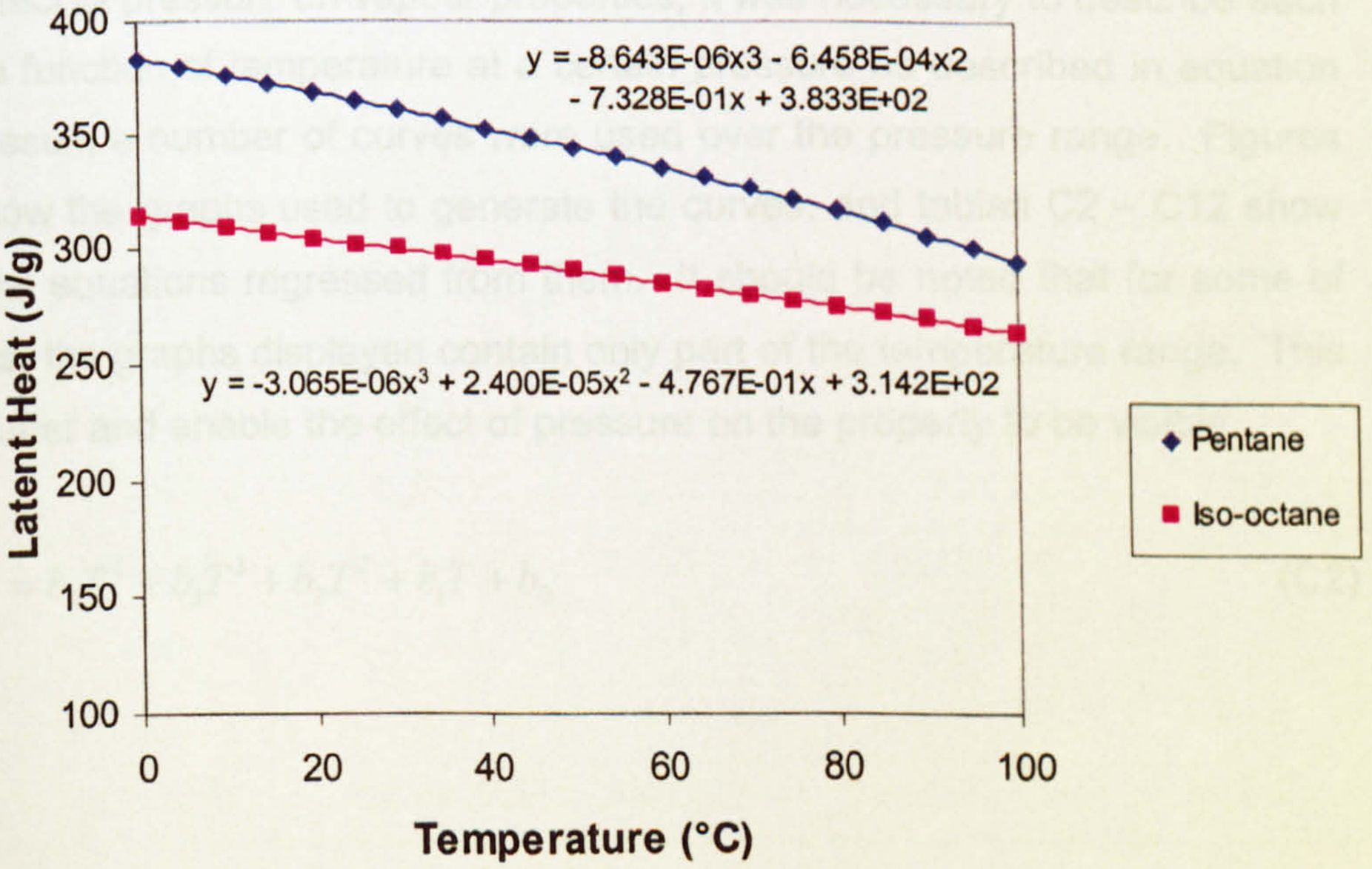

Figure C.6: Latent heat of vaporisation

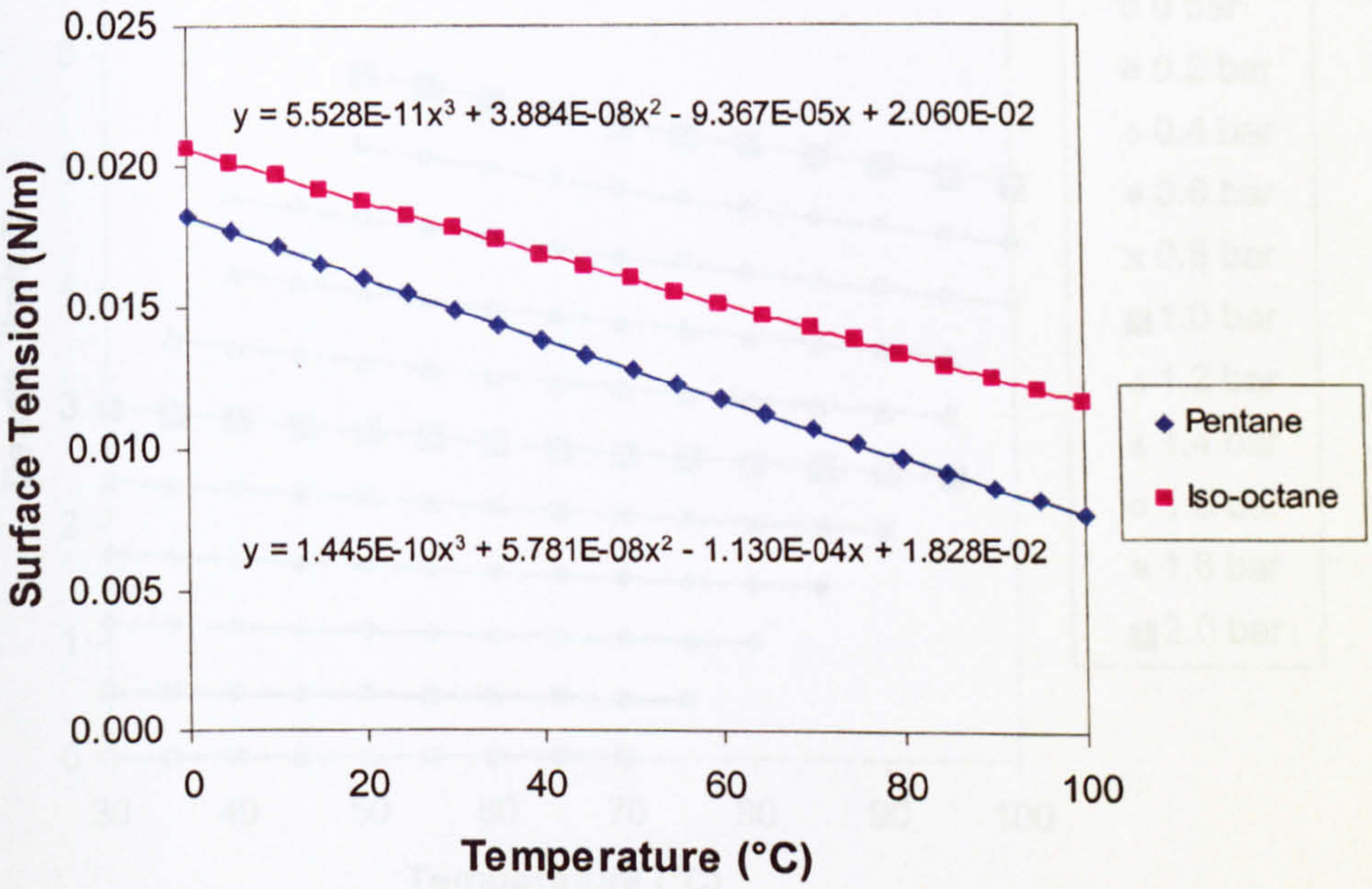

Figure C.7: Saturated liquid surface tension

Vapour properties

Due to the effect of pressure on vapour properties, it was necessary to describe each property as a function of temperature at a certain pressure as described in equation (C2). As a result, a number of curves were used over the pressure range. Figures C8 – C18 show the graphs used to generate the curves, and tables C2 – C12 show the polynomial equations regressed from them. It should be noted that for some of the properties, the graphs displayed contain only part of the temperature range. This is to avoid clutter and enable the effect of pressure on the property to be visible.

$$VProp = b_4T^4 + b_3T^3 + b_2T^2 + b_1T + b_0 \qquad \text{(C2)}$$

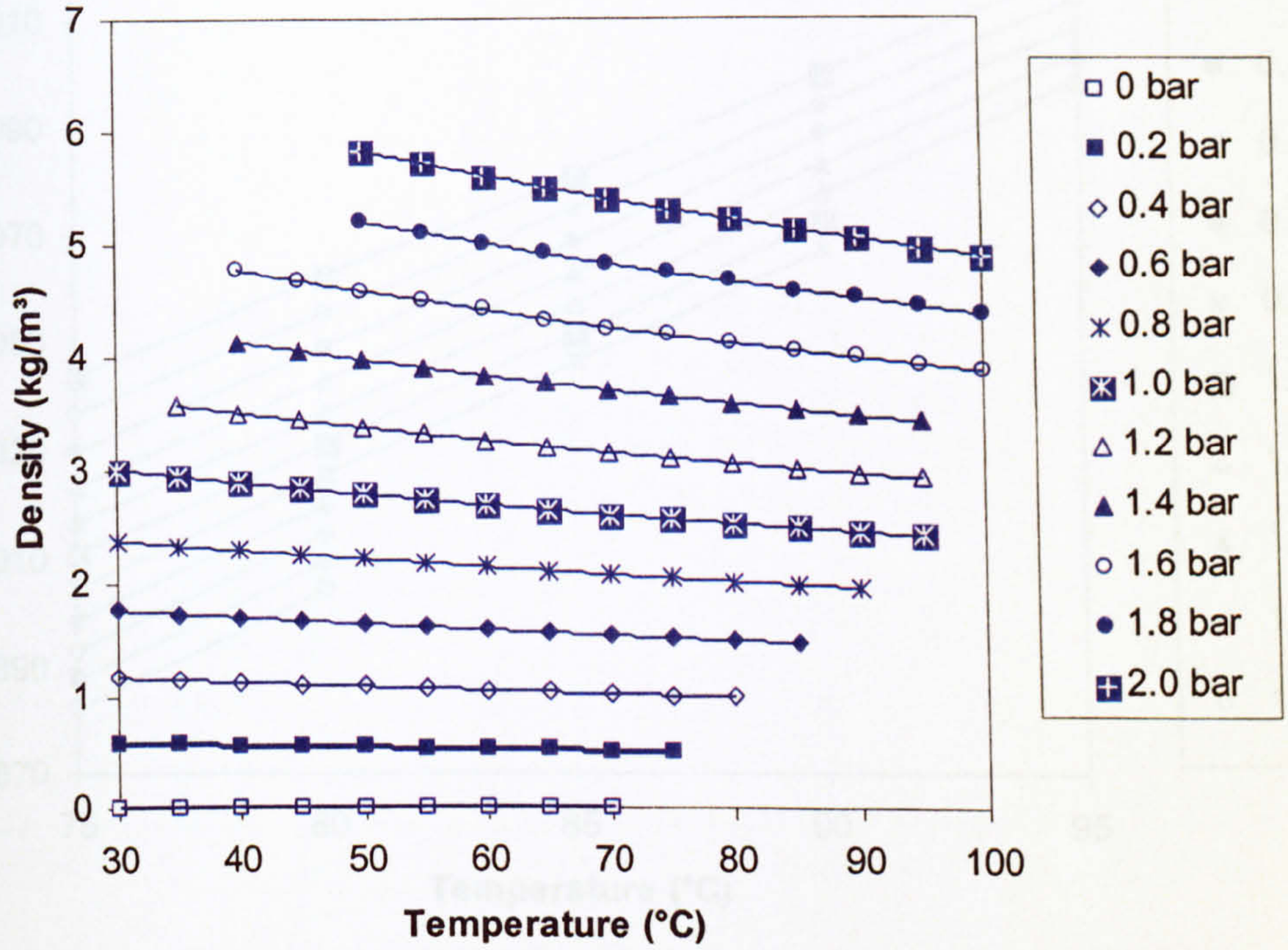

Figure C.8: Pentane vapour density

Pressure (bar)	b_4	b_3	b_2	b_1	b_0
0.0	0	0	0	0	0
0.2	7.265E-11	-3.448E-08	9.691E-06	-2.464E-03	0.644
0.4	1.982E-10	-8.773E-08	2.242E-05	-5.233E-03	1.306
0.6	3.952E-10	-1.655E-07	3.891E-05	-8.356E-03	1.987
0.8	6.890E-10	-2.753E-07	6.007E-05	-1.189E-02	2.690
1.0	1.117E-09	-4.279E-07	8.711E-05	-1.590E-02	3.416
1.2	1.719E-09	-6.355E-07	1.215E-04	-2.048E-02	4.168
1.4	2.569E-09	-9.180E-07	1.653E-04	-2.574E-02	4.949
1.6	3.763E-09	-1.302E-06	2.214E-04	-3.182E-02	5.761
1.8	5.434E-09	-1.824E-06	2.935E-04	-3.891E-02	6.610
2.0	7.790E-09	-2.540E-06	3.871E-04	-4.727E-02	7.500

Table C. 2: Pentane vapour density coefficients

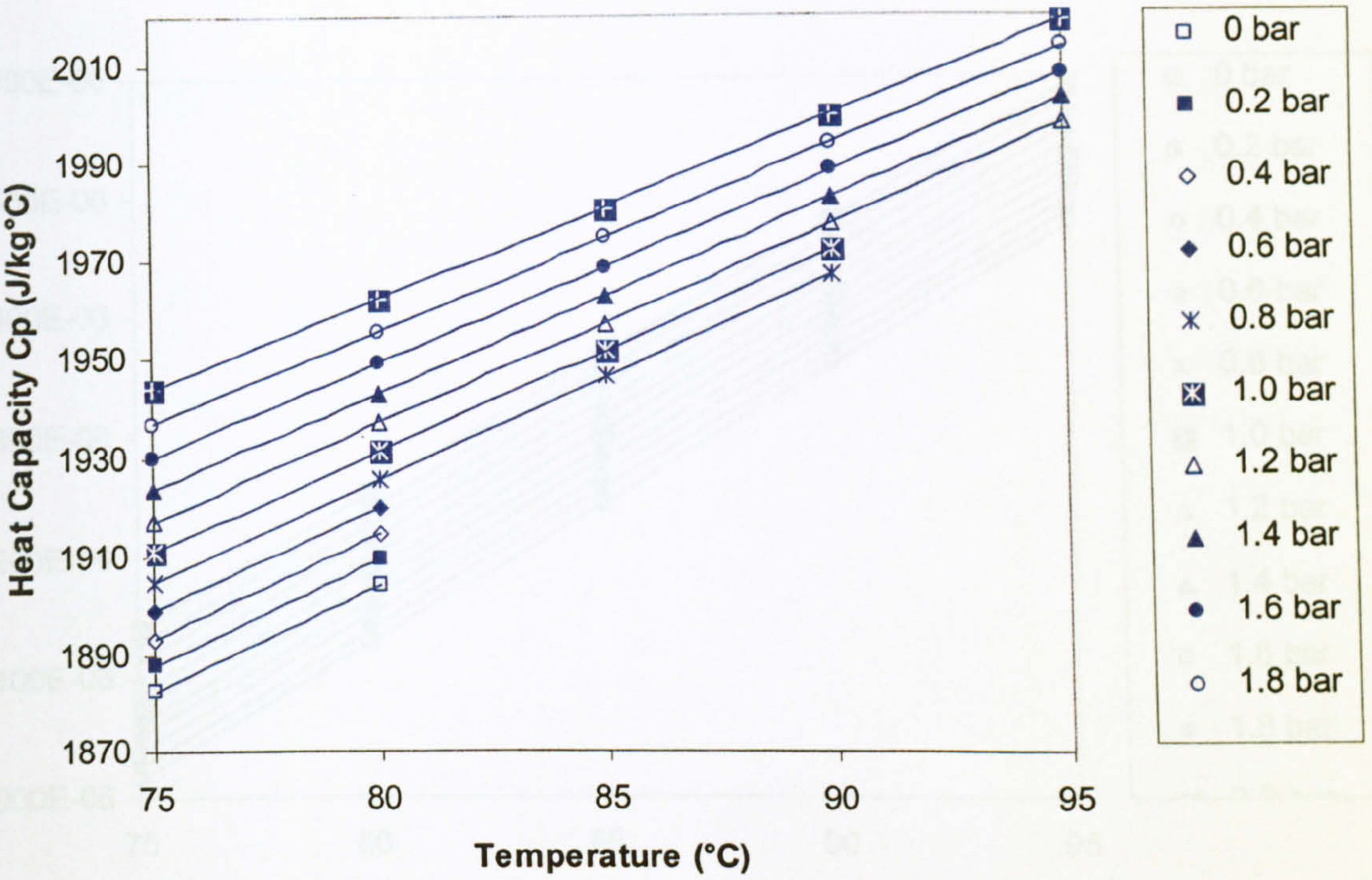

Figure C.9: Pentane vapour specific heat capacity (75 – 95°C)

Pressure (bar)	b_4	b_3	b_2	b_1	b_0
0.0	2.791E-08	-2.106E-05	4.176E-03	4.063	1.562E+03
0.2	4.957E-08	-2.946E-05	5.715E-03	3.881	1.575E+03
0.4	8.316E-08	-4.134E-05	7.668E-03	3.673	1.589E+03
0.6	1.266E-07	-5.636E-05	1.004E-02	3.434	1.605E+03
0.8	1.870E-07	-7.652E-05	1.303E-02	3.157	1.621E+03
1.0	2.697E-07	-1.032E-04	1.679E-02	2.833	1.639E+03
1.2	3.880E-07	-1.399E-04	2.164E-02	2.448	1.658E+03
1.4	5.528E-07	-1.898E-04	2.795E-02	1.984	1.680E+03
1.6	7.925E-07	-2.599E-04	3.635E-02	1.415	1.704E+03
1.8	1.135E-06	-3.581E-04	4.762E-02	0.707	1.731E+03
2.0	1.650E-06	-5.012E-04	6.325E-02	-0.199	1.762E+03

Table C.3: Pentane vapour specific heat capacity coefficients

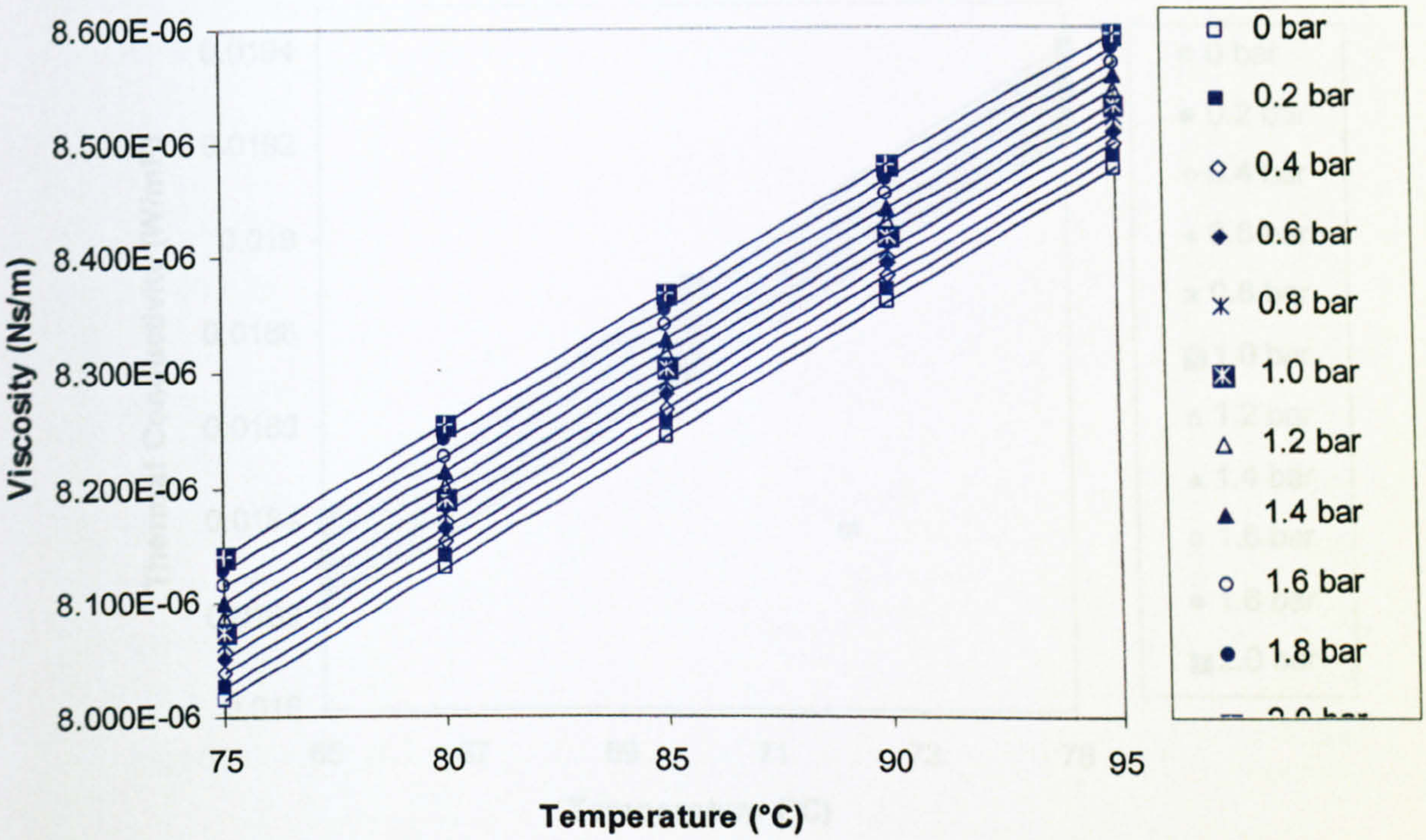

Figure C.10: Pentane vapour dynamic viscosity (75 – 95°C)

Pressure (bar)	b_4	b_3	b_2	b_1	b_0
0.0	1.976E-18	-6.702E-16	-1.007E-13	2.302E-08	6.289E-06
0.2	2.503E-18	-1.273E-15	1.176E-13	2.296E-08	6.305E-06
0.4	3.738E-18	-2.232E-15	4.061E-13	2.289E-08	6.320E-06
0.6	9.948E-18	-4.361E-15	8.157E-13	2.282E-08	6.336E-06
0.8	1.746E-17	-7.117E-15	1.336E-12	2.273E-08	6.353E-06
1.0	2.865E-17	-1.103E-14	2.012E-12	2.264E-08	6.371E-06
1.2	4.278E-17	-1.604E-14	2.858E-12	2.252E-08	6.389E-06
1.4	6.102E-17	-2.249E-14	3.913E-12	2.239E-08	6.408E-06
1.6	9.210E-17	-3.237E-14	5.335E-12	2.224E-08	6.428E-06
1.8	1.395E-16	-4.663E-14	7.231E-12	2.206E-08	6.448E-06
2.0	1.969E-16	-6.438E-14	9.592E-12	2.185E-08	6.470E-06

Table C. 4: Pentane vapour dynamic viscosity coefficients

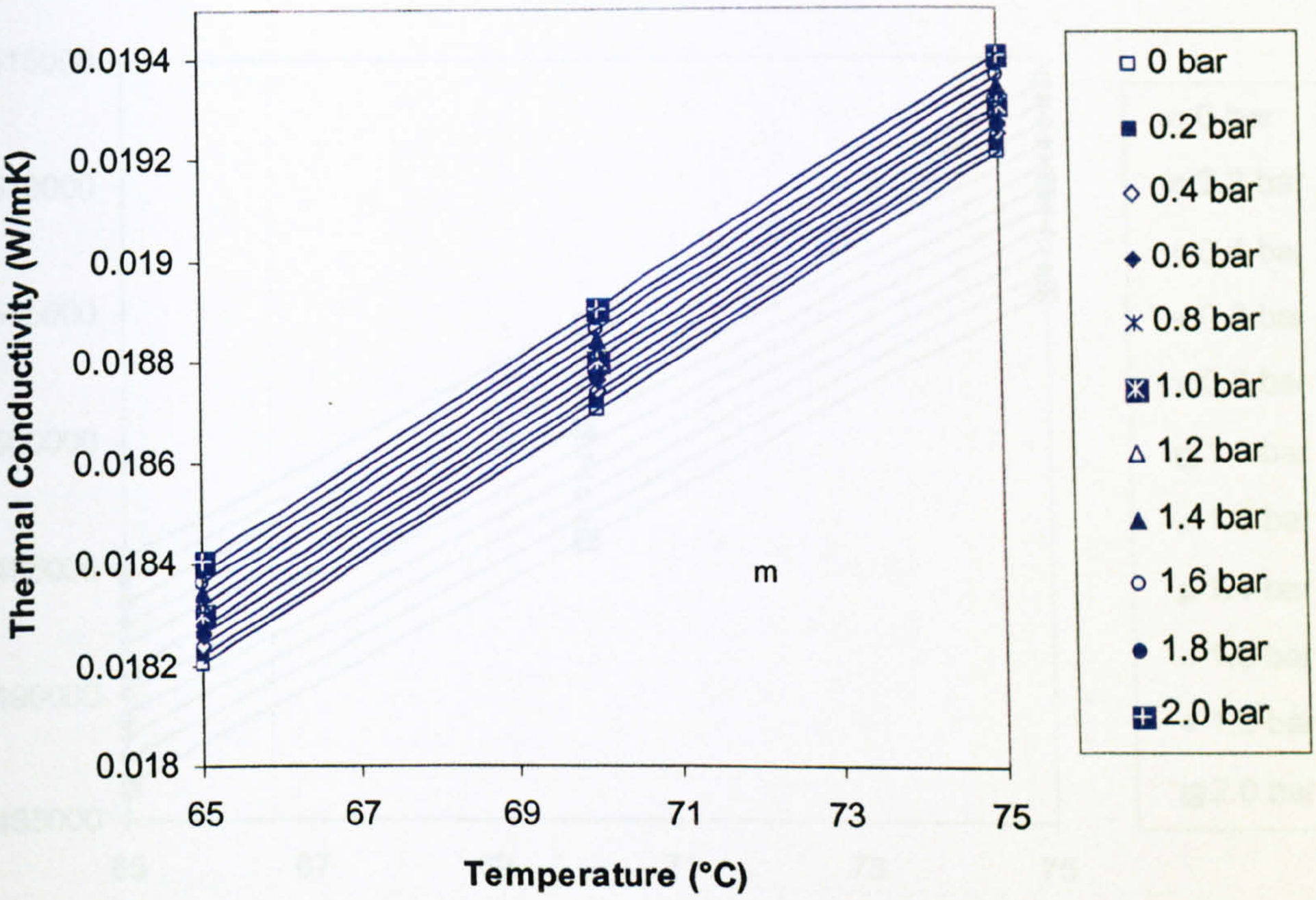

Figure C.11: Pentane vapour thermal conductivity (65 – 75°C)

Pressure (bar)	b_4	b_3	b_2	b_1	b_0
0.0	1.852E-14	-9.722E-11	1.398E-07	8.253E-05	1.227E-02
0.2	-9.675E-15	-9.175E-11	1.397E-07	8.245E-05	1.230E-02
0.4	2.330E-14	-9.991E-11	1.406E-07	8.233E-05	1.232E-02
0.6	1.455E-14	-9.930E-11	1.410E-07	8.222E-05	1.235E-02
0.8	2.465E-14	-1.034E-10	1.418E-07	8.209E-05	1.237E-02
1.0	4.986E-14	-1.107E-10	1.429E-07	8.194E-05	1.240E-02
1.2	6.425E-14	-1.174E-10	1.442E-07	8.176E-05	1.243E-02
1.4	1.056E-13	-1.300E-10	1.460E-07	8.156E-05	1.246E-02
1.6	1.466E-13	-1.432E-10	1.480E-07	8.133E-05	1.249E-02
1.8	2.293E-13	-1.677E-10	1.511E-07	8.104E-05	1.252E-02
2.0	3.150E-13	-1.941E-10	1.547E-07	8.072E-05	1.256E-02

Table C.5: Pentane vapour thermal conductivity coefficients

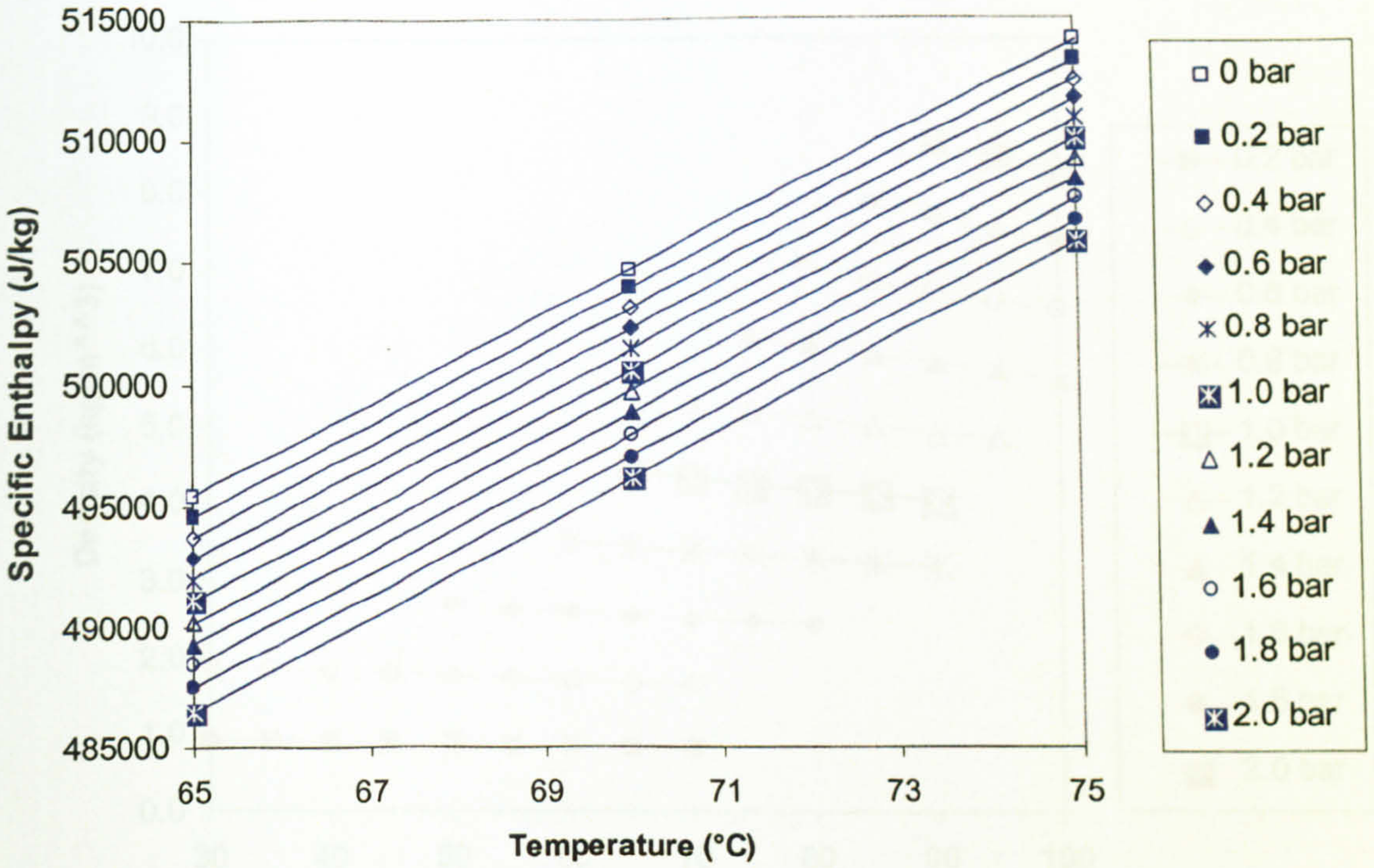

Figure C.12: Pentane vapour specific enthalpy (65 – 75°C)

(Basis: 0°C saturated liquid)

Pressure (bar)	b_4	b_3	b_2	b_1	b_0
0.0	-3.926E-06	1.279E-03	2.036	1.562E+03	3.850E+05
0.2	-4.940E-06	1.697E-03	1.948	1.575E+03	3.836E+05
0.4	-6.104E-06	2.177E-03	1.850	1.589E+03	3.821E+05
0.6	-7.641E-06	2.767E-03	1.739	1.604E+03	3.806E+05
0.8	-9.648E-06	3.494E-03	1.610	1.621E+03	3.791E+05
1.0	-1.216E-05	4.377E-03	1.462	1.638E+03	3.775E+05
1.2	-1.511E-05	5.417E-03	1.292	1.657E+03	3.758E+05
1.4	-1.919E-05	6.762E-03	1.088	1.679E+03	3.741E+05
1.6	-2.436E-05	8.432E-03	0.847	1.702E+03	3.723E+05
1.8	-3.120E-05	1.057E-02	0.555	1.728E+03	3.704E+05
2.0	-4.035E-05	1.334E-02	0.195	1.758E+03	3.684E+05

Table C.6: Pentane vapour specific enthalpy coefficients

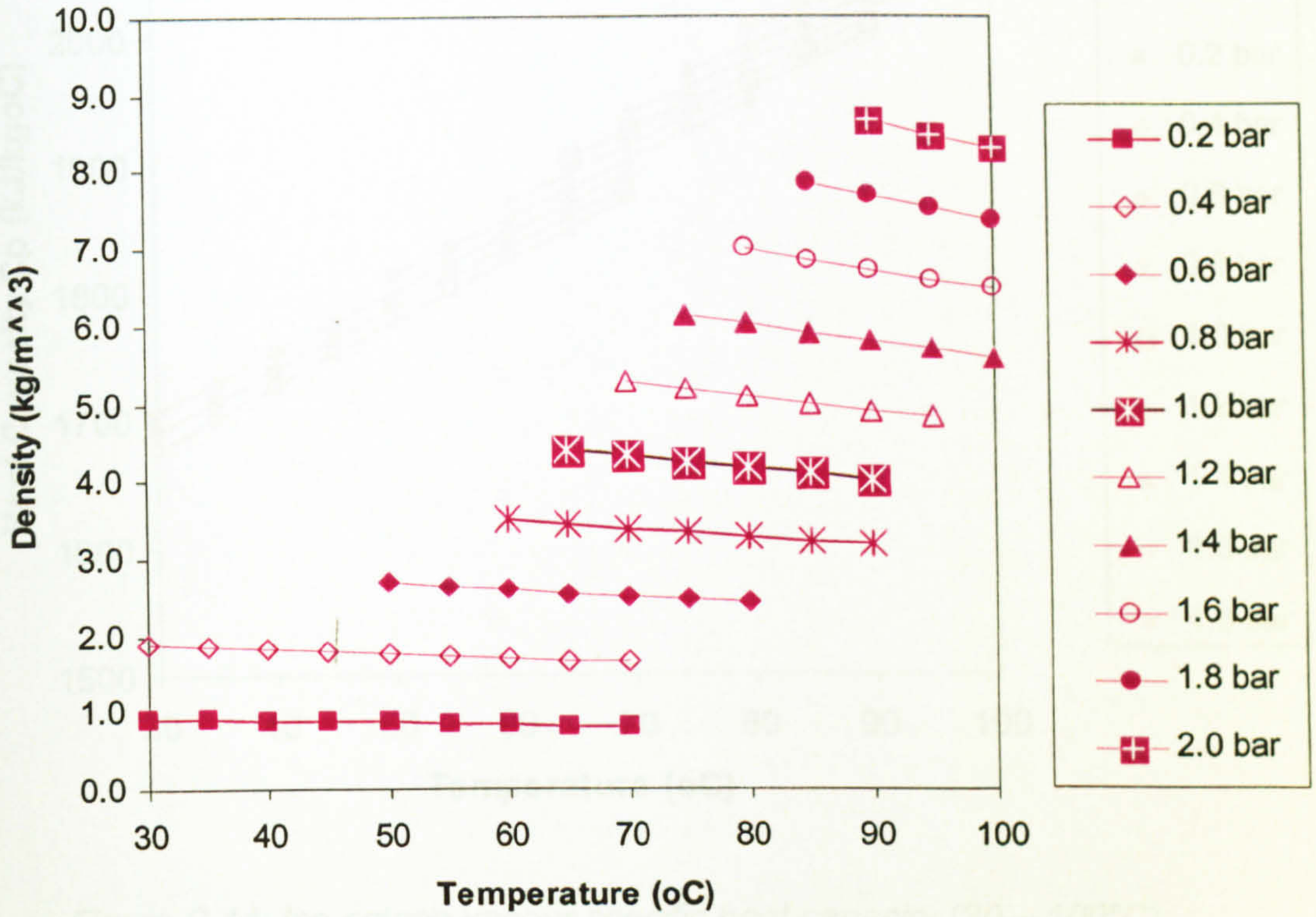

Figure C.13: Iso-octane vapour density (30 – 100°C)

Pressure (bar)	b_4	b_3	b_2	b_1	b_0
0.0	0	0	0	0	0
0.2	1.779E-10	-7.666E-08	1.884E-05	-4.239E-03	1.038
0.4	6.781E-10	-2.609E-07	5.353E-05	-9.891E-03	2.151
0.6	1.834E-09	-6.494E-07	1.151E-04	-1.760E-02	3.356
0.8	4.378E-09	-1.445E-06	2.252E-04	-2.848E-02	4.681
1.0	1.009E-08	-3.121E-06	4.307E-04	-4.471E-02	6.170
1.2	2.528E-08	-7.250E-06	8.728E-04	-7.186E-02	7.912
1.4	2.113E-09	-3.142E-06	7.610E-04	-8.902E-02	9.798
1.6	-4.630E-08	7.512E-06	7.693E-05	-8.874E-02	11.66
1.8	-7.160E-08	1.416E-05	-4.383E-04	-8.817E-02	13.56
2.0	-5.684E-08	1.280E-05	-4.771E-04	-9.542E-02	15.52

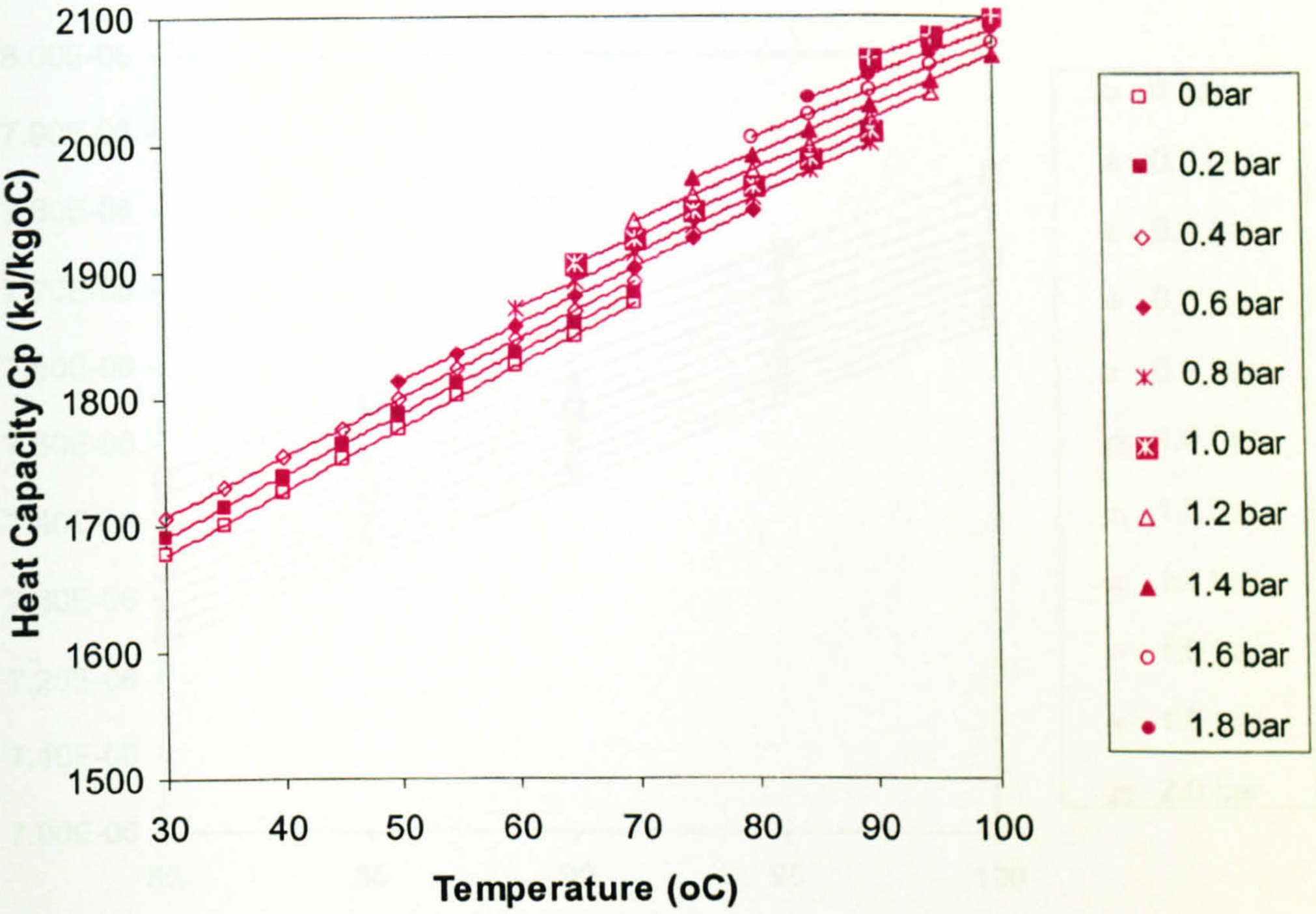

Figure C.14: Iso-octane vapour specific heat capacity (30 – 100°C)

Pressure (bar)	b_4	b_3	b_2	b_1	b_0
0.0	7.518E-09	-4.210E-06	-1.767E-03	5.123	1.524E+03
0.2	5.647E-08	-2.200E-05	1.237E-03	4.797	1.546E+03
0.4	1.580E-07	-5.553E-05	6.164E-03	4.346	1.572E+03
0.6	3.769E-07	-1.227E-04	1.486E-02	3.681	1.604E+03
0.8	8.680E-07	-2.644E-04	3.134E-02	2.623	1.646E+03
1.0	2.111E-06	-6.020E-04	6.669E-02	0.730	1.703E+03
1.2	1.477E-06	-5.674E-04	8.137E-02	-1.098	1.776E+03
1.4	-1.208E-05	2.542E-03	-1.539E-01	4.890	1.780E+03
1.6	-1.249E-05	2.987E-03	-2.248E-01	8.137	1.774E+03
1.8	-2.657E-06	1.134E-03	-1.291E-01	7.384	1.778E+03
2.0	8.477E-06	-1.211E-03	2.046E-02	4.752	1.793E+03

Table C.7: Iso-octane vapour specific heat capacity coefficients

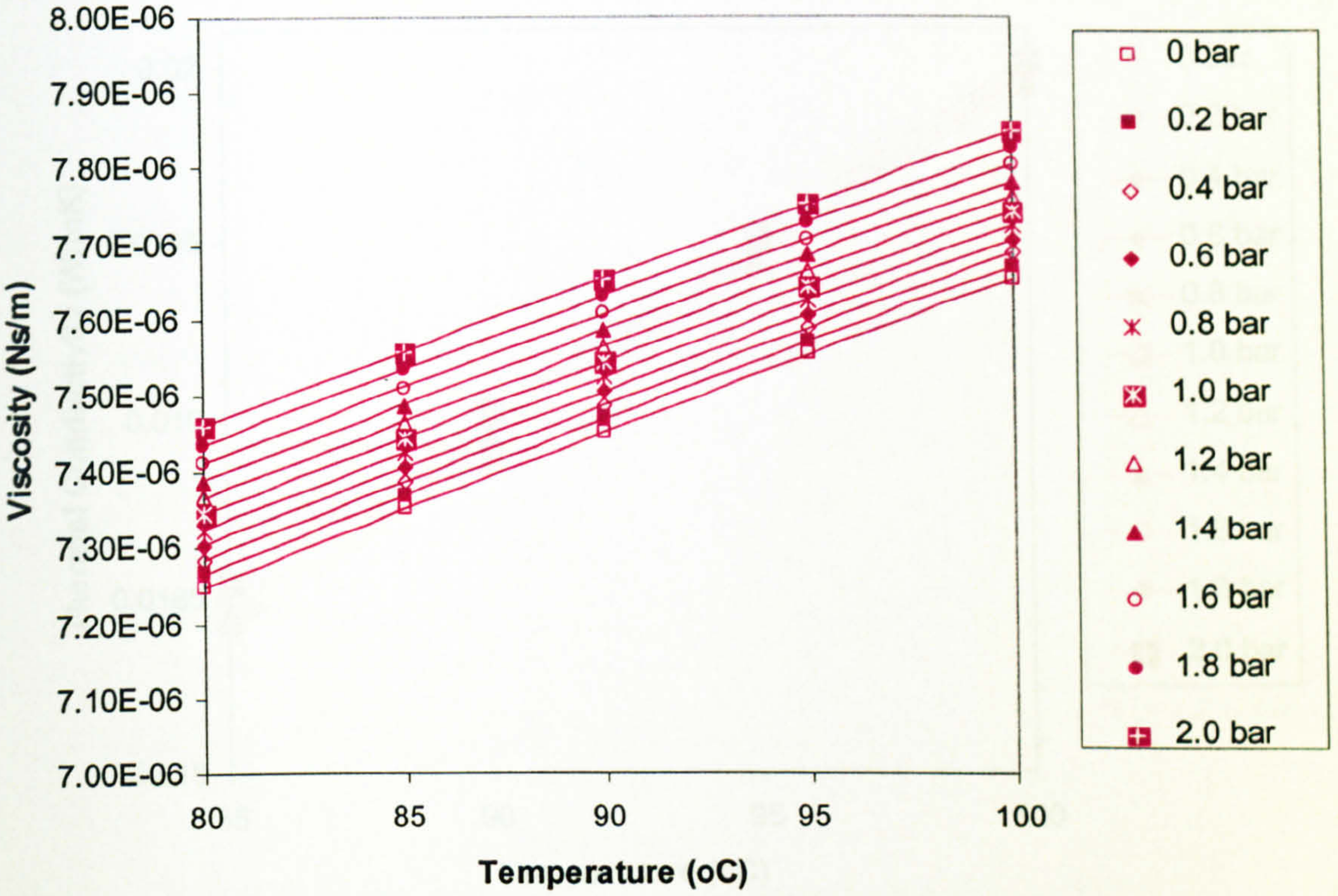

Figure C.15: Iso-octane vapour dynamic viscosity (80 – 100°C)

Pressure (bar)	b_4	b_3	b_2	b_1	b_0
0.0	4.715E-19	-4.354E-15	-1.281E-12	2.056E-08	5.616E-06
0.2	5.678E-18	-6.389E-15	-8.274E-13	2.046E-08	5.639E-06
0.4	1.701E-17	-1.063E-14	-2.303E-14	2.033E-08	5.665E-06
0.6	4.461E-17	-1.978E-14	1.423E-12	2.015E-08	5.693E-06
0.8	1.059E-16	-3.893E-14	4.063E-12	1.989E-08	5.724E-06
1.0	2.447E-16	-7.958E-14	9.037E-12	1.950E-08	5.759E-06
1.2	6.178E-16	-1.809E-13	1.986E-11	1.884E-08	5.800E-06
1.4	7.386E-17	-8.595E-14	1.760E-11	1.840E-08	5.846E-06
1.6	-1.090E-15	1.689E-13	1.502E-12	1.838E-08	5.891E-06
1.8	-1.720E-15	3.319E-13	-1.082E-11	1.836E-08	5.938E-06
2.0	-1.378E-15	3.013E-13	-1.163E-11	1.814E-08	5.987E-06

Table C.8: Iso-octane vapour dynamic viscosity coefficients

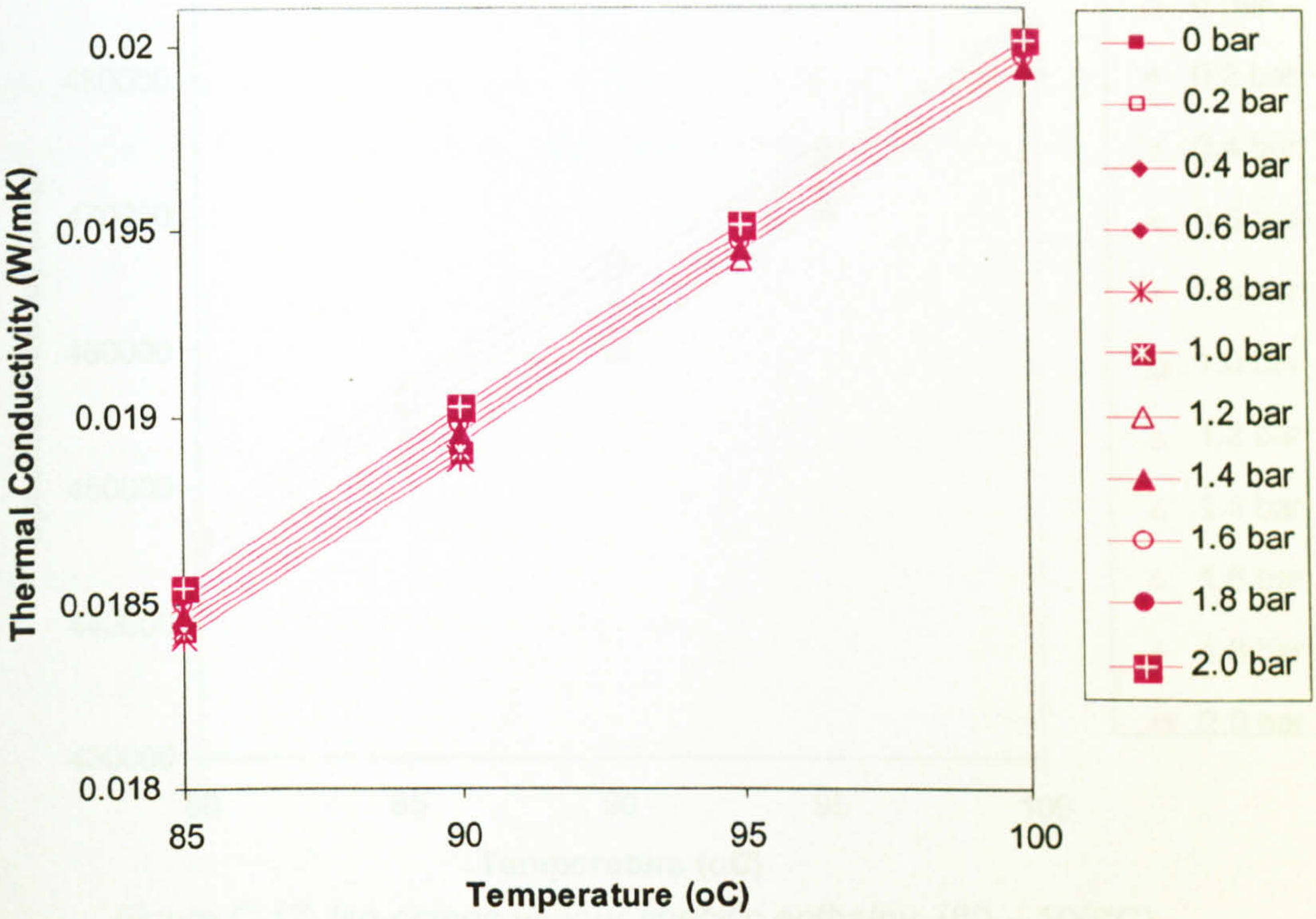

Figure C.16: Iso-octane vapour thermal conductivity (85 – 100°C)

Pressure (bar)	b_4	b_3	b_2	b_1	b_0
0.0	-1.720E-14	-1.127E-10	1.252E-07	7.787E-05	1.088E-02
0.2	3.231E-15	-1.182E-10	1.260E-07	7.776E-05	1.090E-02
0.4	1.095E-14	-1.212E-10	1.267E-07	7.762E-05	1.093E-02
0.6	4.717E-14	-1.325E-10	1.283E-07	7.743E-05	1.096E-02
0.8	8.510E-14	-1.470E-10	1.307E-07	7.716E-05	1.099E-02
1.0	2.628E-13	-1.971E-10	1.365E-07	7.673E-05	1.103E-02
1.2	6.605E-13	-3.045E-10	1.480E-07	7.603E-05	1.107E-02
1.4	5.747E-14	-1.977E-10	1.451E-07	7.559E-05	1.112E-02
1.6	-1.159E-12	6.938E-11	1.281E-07	7.556E-05	1.117E-02
1.8	-1.828E-12	2.421E-10	1.151E-07	7.555E-05	1.122E-02
2.0	-1.466E-12	2.095E-10	1.142E-07	7.533E-05	1.127E-02

Table C.9: Iso-octane vapour thermal conductivity coefficients

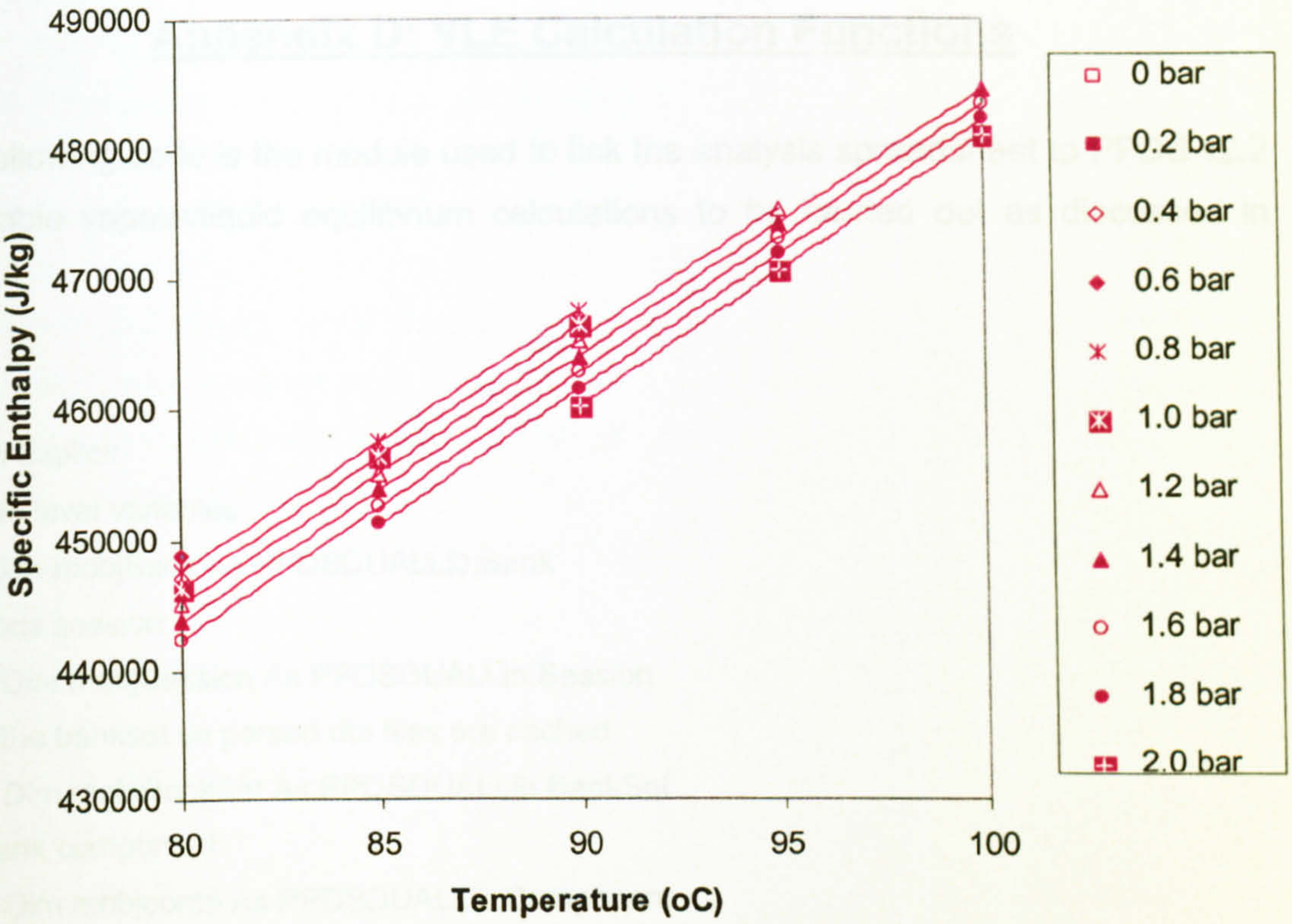

Figure C.17: Iso-octane vapour specific enthalpy (80 – 100°C)

Pressure (bar)	b_4	b_3	b_2	b_1	b_0
0.0	-6.317E-07	-6.289E-04	2.563	1.524E+03	3.144E+05
0.2	-2.497E-06	1.297E-04	2.410	1.546E+03	3.122E+05
0.4	-5.780E-06	1.321E-03	2.200	1.572E+03	3.098E+05
0.6	-1.141E-05	3.213E-03	1.906	1.603E+03	3.073E+05
0.8	-2.152E-05	6.392E-03	1.465	1.643E+03	3.045E+05
1.0	-4.127E-05	1.221E-02	0.749	1.698E+03	3.013E+05
1.2	-8.087E-05	2.333E-02	-0.499	1.777E+03	2.976E+05
1.4	1.604E-04	-2.942E-02	3.112	1.721E+03	2.947E+05
1.6	4.314E-04	-9.638E-02	8.675	1.568E+03	2.932E+05
1.8	4.341E-04	-1.088E-01	10.93	1.461E+03	2.923E+05
2.0	1.926E-04	-6.729E-02	9.421	1.432E+03	2.915E+05

Table C.10: Iso-octane vapour specific enthalpy coefficient

Appendix D: VLE Calculation Functions

The following code is the module used to link the analysis spreadsheet to PPDS v2.2 to enable vapour/liquid equilibrium calculations to be carried out as discussed in 3.2.3.

```
Option Explicit
'module level variables
    Dim mobjBank As PPDSDUALLib.Bank
'the ppds session
    Dim mobjSession As PPDSDUALLib.Session
'keep the bankset so parsed dta files are cached
    Dim mobjBankSet As PPDSDUALLib.BankSet
'the bank component
    Dim mobjcomp As PPDSDUALLib.Component
'the stream
    Dim mobjStream As PPDSDUALLib.Strm
'the results of the last search
    Dim mobjSearchResults As PPDSDUALLib.ComponentInfoSet
'the Phase object
    Dim mobjPhase As PPDSDUALLib.Phase


Function fn_EqmVapComp(fPressure, fPenFrac)
'DESC: Calculation of vapour composition in eqm with liquid input
'RELATES TO: VLE Calcs
'-------------------------------------------------------------
'MODIFICATION HISTORY
'MOD   DATE        BY                      DESCRIPTION
'1     19/11/01    D Cuthbertson, L Rowan  Initial Version
'1.1   28/01/02    D Cuthbertson           Temp removed as input as not required
'-------------------------------------------------------------
'Connect to PPDS server
    Set mobjSession = New PPDSDUALLib.Session
    mobjSession.Connect "VB Excel Sheet"
'Set up PPDS stream with components
    Set mobjStream = mobjSession.NewStream
    Set mobjcomp = mobjSession.NewComponent
```

```
        mobjcomp.Register 1, 56
        mobjStream.AddComponent mobjcomp
        Set mobjcomp = mobjSession.NewComponent
        mobjcomp.Register 1, 223
        mobjStream.AddComponent mobjcomp
'Add inputs to stream
        mobjStream.Pressure = fPressure
        mobjStream.Composition(0) = fPenFrac
        mobjStream.Composition(1) = 1 - fPenFrac
'Set up calculation method
        mobjStream.VLERouteSet.ByName "RKS/RKS"
'Perform the flash
        mobjStream.VLEFlash ppdsBubble_P, True
'Return required value
        Set mobjPhase = mobjStream.Phase(0)
        Dim ReturnVal(0 To 1)
        Dim j As Integer
        For j = 0 To mobjPhase.ComponentCount - 1
          ReturnVal(j) = mobjPhase.Composition(j)
        Next
        n_EqmVapComp = mobjPhase.Composition(0)
End Function


Function fn_EqLiqComp(fPress, Fraction)
'DESC: Calculation of liq composition in eqm with input vapour composition
'RELATES TO: VLE Calcs
'-------------------------------------------------------------
'MODIFICATION HISTORY
'MOD   DATE        BY                          DESCRIPTION
' 1    19/11/01    D Cuthbertson, L Rowan      Initial Version
'1.1   21/01/02    D Cuthbertson               Temp removed as input as not required
'-------------------------------------------------------------
'Connect to PPDS server
        Set mobjSession = New PPDSDUALLib.Session
        mobjSession.Connect "VB Excel Sheet"
'Set up PPDS stream
        Set mobjStream = mobjSession.NewStream
        Set mobjcomp = mobjSession.NewComponent
        mobjcomp.Register 1, 56
```

```
        mobjStream.AddComponent mobjcomp
        Set mobjcomp = mobjSession.NewComponent
        mobjcomp.Register 1, 223
        mobjStream.AddComponent mobjcomp
'Add inputs to stream
        mobjStream.Pressure = fPress
        mobjStream.Composition(0) = Fraction
        mobjStream.Composition(1) = 1 - Fraction
'Set up calculation method
        mobjStream.VLERouteSet.ByName "RKS/RKS"
'Perform the flash
        mobjStream.VLEFlash ppdsBubble_P, True
'Return required value
        Set mobjPhase = mobjStream.Phase(1)
        Dim ReturnVal(0 To 1)
        Dim j As Integer
        For j = 0 To mobjPhase.ComponentCount - 1
          ReturnVal(j) = mobjPhase.Composition(j)
        Next
        fn_EqLiqComp = mobjPhase.Composition(0)
End Function


Function fn_Tbub(fPress, Fraction)
'DESC: Calculation of bubble point temperature
'RELATES TO: VLE Calcs
'-----------------------------------------------------------
'MODIFICATION HISTORY
'MOD   DATE        BY                      DESCRIPTION
' 1    19/11/01    D Cuthbertson, L Rowan  Initial Version
'1.1   21/01/02    D Cuthbertson           Temp removed as input as not required
'-----------------------------------------------------------
'Connect to PPDS server
        Set mobjSession = New PPDSDUALLib.Session
        mobjSession.Connect "VB Excel Sheet"
'Set up PPDS stream
        Set mobjStream = mobjSession.NewStream
        Set mobjcomp = mobjSession.NewComponent
        mobjcomp.Register 1, 56
        mobjStream.AddComponent mobjcomp
```

```
        Set mobjcomp = mobjSession.NewComponent
        mobjcomp.Register 1, 223
    mobjStream.AddComponent mobjcomp
'Add inputs to stream
        mobjStream.Pressure = fPress
        mobjStream.Composition(0) = Fraction
        mobjStream.Composition(1) = 1 - Fraction
'Set up calculation method
        mobjStream.VLERouteSet.ByName "RKS/RKS"
'Perform the flash
        mobjStream.VLEFlash ppdsBubble_P, True
'Return required value
        Set mobjPhase = mobjStream.Phase(1)
        Dim ReturnVal(0 To 1)
        Dim j As Integer
        For j = 0 To mobjPhase.ComponentCount - 1
          ReturnVal(j) = mobjPhase.Composition(j)
        Next
        fn_Tbub = mobjStream.Temperature - 273.15
End Function

Function fn_Tdew(fPress, Fraction)
'DESC: Calculation of dew point temperature
'RELATES TO: VLE Calcs
'-------------------------------------------------------
'MODIFICATION HISTORY
'MOD   DATE        BY                      DESCRIPTION
' 1    20/11/01    D Cuthbertson, L Rowan  Initial Version
'1.1   22/01/02    D Cuthbertson           Temp removed as input as not required
'-------------------------------------------------------
'Connect to PPDS server
        Set mobjSession = New PPDSDUALLib.Session
        mobjSession.Connect "VB Excel Sheet"
'Set up PPDS stream
        Set mobjStream = mobjSession.NewStream
        Set mobjcomp = mobjSession.NewComponent
        mobjcomp.Register 1, 56
        mobjStream.AddComponent mobjcomp
        Set mobjcomp = mobjSession.NewComponent
```

```
        mobjcomp.Register 1, 223
        mobjStream.AddComponent mobjcomp
'Add inputs to stream
        mobjStream.Pressure = fPress
        mobjStream.Composition(0) = Fraction
        mobjStream.Composition(1) = 1 - Fraction
'Set up calculation method
        mobjStream.VLERouteSet.ByName "RKS/RKS"
'Perform the flash
        mobjStream.VLEFlash ppdsDew_P, True
'Return required value
        Set mobjPhase = mobjStream.Phase(1)
        Dim ReturnVal(0 To 1)
        Dim j As Integer
        For j = 0 To mobjPhase.ComponentCount - 1
        ReturnVal(j) = mobjPhase.Composition(j)
        Next
        fn_Tdew = mobjStream.Temperature - 273.15
End Function
```

```
Function fn_Pdew(fTemp, Fraction)
'DESC: Calculation of dew point pressure
'RELATES TO: VLE Calcs
'-------------------------------------------------------------
'MODIFICATION HISTORY
'MOD   DATE          BY                          DESCRIPTION
' 1    20/11/01      D Cuthbertson, L Rowan Initial Version
'1.1   24/01/02      D Cuthbertson               Temp removed as input as not required
'-------------------------------------------------------------
'Connect to PPDS server
        Set mobjSession = New PPDSDUALLib.Session
        mobjSession.Connect "VB Excel Sheet"
'Set up PPDS stream
        Set mobjStream = mobjSession.NewStream
        Set mobjcomp = mobjSession.NewComponent
        mobjcomp.Register 1, 56
        mobjStream.AddComponent mobjcomp
        Set mobjcomp = mobjSession.NewComponent
        mobjcomp.Register 1, 223
```

```
        mobjStream.AddComponent mobjcomp
'Add inputs to stream
        mobjStream.Temperature = fTemp + 273.15
        mobjStream.Composition(0) = Fraction
        mobjStream.Composition(1) = 1 - Fraction
'Set up calculation method
        mobjStream.VLERouteSet.ByName "RKS/RKS"
'Perform the flash
        mobjStream.VLEFlash ppdsDew_T, True
'Return required value
        Set mobjPhase = mobjStream.Phase(1)
        Dim ReturnVal(0 To 1)
        Dim j As Integer
        For j = 0 To mobjPhase.ComponentCount - 1
          ReturnVal(j) = mobjPhase.Composition(j)
        Next
        fn_Pdew = mobjStream.Pressure
End Function
```

Appendix E: Single Component Data And Calculation Results

Table E1.1: Experimental data for pentane tests

	Boiler			Reflux Condenser Coolant					Reflux Condenser Vapour			Extraction Air	
Run	Q_i (W)	$P_{v,i}$ (Pa)	$T_{vR,i}$ (°C)	$\dot{V}_{c,R}$ (m³/s)	$T_{cR,i}$ (°C)	$T_{cR,TS3}$ (°C)	$T_{cR,TS4}$ (°C)	$T_{cR,o}$ (°C)	$T_{vR,oTS2}$ (°C)	$T_{vR,oTS3}$ (°C)	$T_{vR,oTS4}$ (°C)	T_{Ai} (°C)	T_{Ao} (°C)
P1.1	5692.9	172812	52.57	5.88E-05	29.44	34.36	38.52	42.62	51.34	51.44	N/A	9.75	14.55
P1.2	5698.2	172776	52.56	5.89E-05	29.51	34.42	38.57	42.65	51.32	51.42	N/A	9.59	14.53
P1.3	5677.3	172778	52.56	5.88E-05	29.55	34.47	38.59	42.67	51.35	51.44	N/A	9.72	14.53
P2.1	3018.0	124602	42.12	5.85E-05	29.51	31.82	33.99	36.73	40.67	40.72	N/A	7.40	11.42
P2.2	3013.2	124795	42.16	5.86E-05	29.53	31.84	34.02	36.77	40.73	40.77	N/A	7.49	11.46
P2.3	3010.2	124894	42.19	5.86E-05	29.47	31.83	34.00	36.78	40.74	40.79	N/A	7.45	11.47
P3.1	3000.9	150955	48.14	5.77E-05	39.48	40.90	42.41	44.56	46.72	46.78	N/A	7.24	12.12
P3.2	2999.9	151153	48.18	5.79E-05	39.47	40.91	42.42	44.60	46.76	46.81	N/A	7.15	12.14
P3.3	2998.7	151311	48.22	5.79E-05	39.31	40.82	42.37	44.58	46.80	46.85	N/A	7.25	12.18
P4.1	3973.2	144841	46.84	5.94E-05	29.38	32.83	35.86	39.23	45.50	45.54	N/A	8.05	11.69
P4.2	3982.4	144812	46.83	5.95E-05	29.17	32.68	35.79	39.18	45.49	45.52	N/A	7.94	11.67
P4.3	3974.4	144726	46.82	5.93E-05	28.99	32.51	35.64	39.07	45.46	45.52	N/A	8.04	11.70
P5.1	4944.8	199872	57.47	5.98E-05	39.12	43.15	46.40	49.49	56.52	56.59	N/A	12.58	16.90
P5.2	4944.5	199784	57.45	5.97E-05	39.12	43.15	46.37	49.47	56.50	56.57	N/A	12.74	16.91
P5.3	4950.7	199808	57.46	5.99E-05	39.17	43.19	46.39	49.48	56.51	56.58	N/A	12.85	16.93
P6.1	4947.9	168633	51.77	5.97E-05	29.23	34.09	38.07	41.84	50.81	50.87	N/A	12.49	16.01
P6.2	4953.5	168672	51.78	5.98E-05	29.26	34.12	38.10	41.86	50.80	50.87	N/A	12.22	15.94
P6.3	4949.5	168681	51.78	5.97E-05	29.33	34.18	38.13	41.88	50.80	50.88	N/A	12.51	15.99
P7.1	4880.0	142426	46.33	6.01E-05	19.67	25.27	29.95	34.44	45.31	45.40	N/A	12.35	15.31
P7.2	4882.0	142403	46.33	6.02E-05	19.66	25.27	29.95	34.44	45.30	45.39	N/A	12.31	15.28
P7.3	4899.1	142375	46.32	6.00E-05	19.61	25.22	29.93	34.42	45.30	45.38	N/A	12.60	15.33
P8.1	6023.8	167465	51.53	5.96E-05	20.16	26.72	32.36	37.70	50.46	50.56	N/A	6.41	11.21
P8.2	6022.1	167677	51.57	5.96E-05	20.21	26.76	32.40	37.76	50.49	50.58	N/A	6.08	11.16
P8.3	6021.7	167831	51.60	5.97E-05	20.21	26.75	32.40	37.78	50.50	50.60	N/A	5.78	11.09
P9.1	5933.0	195608	56.73	5.93E-05	29.53	34.93	39.84	44.84	55.24	55.34	N/A	6.41	12.04
P9.2	5925.7	195721	56.75	5.95E-05	29.62	35.02	39.91	44.90	55.26	55.36	N/A	6.43	12.05
P9.3	5921.1	195722	56.75	5.94E-05	29.57	34.98	39.90	44.90	55.27	55.36	N/A	6.40	12.05

Table E1.2: Experimental data for pentane tests (ctnd)

Run	Boiler			Reflux Condenser Coolant					Reflux Condenser Vapour			Extraction Air	
	Q_i (W)	$P_{v,i}$ (Pa)	$T_{vR,i}$ (°C)	$\dot{V}_{c,R}$ (m³/s)	$T_{cR,i}$ (°C)	$T_{cR,TS3}$ (°C)	$T_{cR,TS4}$ (°C)	$T_{cR,o}$ (°C)	$T_{vR,oTS2}$ (°C)	$T_{vR,oTS3}$ (°C)	$T_{vR,oTS4}$ (°C)	T_{Ai} (°C)	T_{Ao} (°C)
P10.1	3039.4	144706	46.82	5.92E-05	29.31	32.32	35.37	39.19	45.04	45.09	N/A	6.06	9.64
P10.2	3038.3	144529	46.78	5.92E-05	29.17	32.20	35.28	39.11	45.00	45.05	N/A	5.58	9.56
P10.3	3040.8	144411	46.75	5.91E-05	29.01	32.06	35.18	39.02	44.97	45.03	N/A	5.48	9.53
P11.1	2994.8	146423	47.21	5.97E-05	29.33	33.03	36.10	39.29	46.12	46.17	N/A	8.66	13.04
P11.2	2991.2	146679	47.26	5.98E-05	29.47	33.17	36.23	39.39	46.18	46.24	N/A	8.61	13.02
P11.3	2996.0	146991	47.33	5.98E-05	29.52	33.23	36.30	39.46	46.24	46.31	N/A	8.61	12.98
P12.1	3016.1	166217	51.28	5.96E-05	39.12	41.71	43.76	46.02	50.32	50.36	N/A	9.36	13.82
P12.2	3025.8	166471	51.33	5.97E-05	39.25	41.83	43.85	46.08	50.37	50.41	N/A	9.26	13.81
P12.2	3020.6	166805	51.40	5.97E-05	39.47	42.01	44.00	46.21	50.43	50.48	N/A	9.37	13.83
P13.1	3935.6	185206	54.88	5.97E-05	39.21	42.67	45.36	48.07	53.96	54.01	N/A	8.51	13.68
P13.2	3948.7	185339	54.90	5.96E-05	39.17	42.64	45.31	48.04	53.98	54.04	N/A	8.51	13.66
P13.3	3939.3	185425	54.92	5.96E-05	39.27	42.72	45.37	48.07	54.00	54.06	N/A	8.52	13.66
P14.1	3840.9	157492	49.54	5.97E-05	29.30	33.54	37.05	40.54	48.50	48.57	N/A	8.11	13.13
P14.2	3844.2	157836	49.61	5.96E-05	29.46	33.66	37.16	40.65	48.56	48.64	N/A	8.32	13.11
P14.3	3842.9	158097	49.66	5.96E-05	29.64	33.82	37.30	40.76	48.63	48.68	N/A	8.17	13.12
P15.1	5754.2	197228	57.04	5.96E-05	20.08	27.40	34.22	40.69	55.67	55.78	N/A	8.13	11.96
P15.2	5747.7	197761	57.13	5.97E-05	20.15	27.50	34.32	40.80	55.77	55.88	N/A	8.34	12.01
P15.3	5742.0	198090	57.19	5.96E-05	20.17	27.56	34.38	40.86	55.84	55.94	N/A	8.10	12.00
P16.1	4856.8	194102	56.46	5.92E-05	39.31	42.88	45.90	49.07	55.24	55.33	N/A	8.60	14.23
P16.2	4853.2	193898	56.43	5.93E-05	39.25	42.80	45.83	49.01	55.20	55.28	N/A	8.48	14.17
P16.3	4873.7	193826	56.41	5.94E-05	39.25	42.79	45.81	48.98	55.18	55.27	N/A	8.70	14.22
P17.1	3935.0	185544	54.94	5.92E-05	39.18	42.49	45.22	48.09	53.84	53.90	N/A	9.45	14.66
P17.2	3970.7	185706	54.97	5.90E-05	39.26	42.56	45.29	48.14	53.87	53.93	N/A	9.38	14.65
P17.3	4042.6	187388	55.27	5.90E-05	39.49	42.81	45.56	48.41	54.18	54.25	N/A	9.16	14.60

Table E1.3: Experimental data for pentane tests (ctnd)

	Reflux Condenser Wall Temperatures									Dump Condenser			
Run	$T_{w,TS2t}$ (°C)	$T_{w,TS2m}$ (°C)	$T_{w,TS2b}$ (°C)	$T_{w,TS3t}$ (°C)	$T_{w,TS3m}$ (°C)	$T_{w,TS3b}$ (°C)	$T_{w,TS4t}$ (°C)	$T_{w,TS4m}$ (°C)	$T_{w,TS4b}$ (°C)	$\dot{V}_{c,D}$ (m³/s)	$T_{cD,in}$ (°C)	$T_{cD,out}$ (°C)	$T_{f,D}$ (°C)
P1.1	32.64	34.30	37.04	36.19	38.64	40.21	41.21	42.39	43.98	2.42E-05	15.01	34.04	33.31
P1.2	32.70	34.38	37.11	36.24	38.68	40.24	41.26	42.40	44.01	2.43E-05	15.05	34.03	33.36
P1.3	32.75	34.40	37.13	36.29	38.70	40.27	41.27	42.43	44.03	2.42E-05	15.07	34.07	33.46
P2.1	30.94	32.12	34.23	33.66	34.91	35.80	36.32	36.91	37.74	2.40E-05	15.56	23.64	15.53
P2.2	30.97	32.13	34.27	33.70	34.95	35.85	36.35	36.96	37.78	2.39E-05	15.59	23.70	15.59
P2.3	30.90	32.11	34.23	33.70	34.93	35.83	36.38	36.98	37.82	2.41E-05	15.56	23.70	15.61
P3.1	40.25	41.23	43.02	42.62	43.42	44.10	44.42	44.79	45.39	2.40E-05	15.29	28.27	15.95
P3.2	40.25	41.21	43.03	42.63	43.46	44.13	44.43	44.83	45.43	2.41E-05	15.31	28.34	15.98
P3.3	40.13	41.13	42.95	42.55	43.39	44.07	44.42	44.80	45.41	2.43E-05	15.27	28.35	15.99
P4.1	31.56	32.96	35.43	34.75	36.54	37.73	38.46	39.29	40.43	2.38E-05	15.08	26.43	15.37
P4.2	31.36	32.83	35.31	34.62	36.40	37.62	38.40	39.24	40.42	2.36E-05	15.31	26.47	15.37
P4.3	31.21	32.67	35.17	34.46	36.27	37.51	38.28	39.13	40.31	2.34E-05	16.00	26.77	15.60
P5.1	41.61	43.10	45.17	44.54	46.40	47.70	48.45	49.30	50.56	2.47E-05	14.72	33.20	17.81
P5.2	41.61	43.07	45.16	44.54	46.40	47.68	48.43	49.29	50.55	2.47E-05	14.72	33.18	17.79
P5.3	41.65	43.11	45.20	44.57	46.42	47.70	48.45	49.31	50.56	2.48E-05	15.03	33.24	17.85
P6.1	32.44	34.00	36.50	35.69	38.05	39.54	40.51	41.61	43.13	2.48E-05	15.18	28.68	15.63
P6.2	32.47	34.02	36.53	35.72	38.06	39.55	40.53	41.64	43.15	2.48E-05	14.99	28.63	15.66
P6.3	32.51	34.08	36.57	35.76	38.10	39.57	40.55	41.66	43.17	2.47E-05	14.49	28.47	15.50
P7.1	23.72	25.31	28.06	27.03	29.92	31.62	32.87	34.16	36.01	2.47E-05	14.85	23.13	15.05
P7.2	23.71	25.31	28.06	27.04	29.91	31.61	32.85	34.18	36.01	2.47E-05	14.85	23.10	15.12
P7.3	23.65	25.27	28.01	27.01	29.88	31.60	32.84	34.17	35.99	2.47E-05	14.88	23.10	15.13
P8.1	24.60	26.38	30.00	28.77	32.22	34.37	35.85	37.52	39.69	2.44E-05	15.08	25.80	15.39
P8.2	24.67	26.42	30.04	28.82	32.29	34.42	35.90	37.55	39.73	2.45E-05	14.87	25.73	15.24
P8.3	24.64	26.43	30.05	28.85	32.28	34.42	35.92	37.59	39.76	2.44E-05	15.06	25.80	15.16
P9.1	32.94	34.82	38.09	37.13	40.00	41.88	43.07	44.52	46.43	2.44E-05	15.03	30.71	15.77
P9.2	33.01	34.90	38.18	37.22	40.09	41.95	43.14	44.56	46.47	2.45E-05	15.25	30.81	15.83
P9.3	32.98	34.85	38.16	37.19	40.06	41.94	43.14	44.56	46.49	2.44E-05	15.56	30.96	15.98

Table E1.4: Experimental data for pentane tests (ctnd)

Run	Reflux Condenser Wall Temperatures									Dump Condenser			
	$T_{w,TS2t}$ (°C)	$T_{w,TS2m}$ (°C)	$T_{w,TS2b}$ (°C)	$T_{w,TS3t}$ (°C)	$T_{w,TS3m}$ (°C)	$T_{w,TS3b}$ (°C)	$T_{w,TS4t}$ (°C)	$T_{w,TS4m}$ (°C)	$T_{w,TS4b}$ (°C)	$\dot{V}_{c,D}$ (m³/s)	$T_{cD,i}$ (°C)	$T_{cD,o}$ (°C)	$T_{f,D}$ (°C)
P10.1	31.17	32.63	35.42	34.77	36.51	37.76	38.46	39.32	40.48	2.43E-05	15.14	17.30	14.64
P10.2	31.04	32.50	35.31	34.66	36.41	37.65	38.39	39.24	40.41	2.40E-05	15.36	17.19	14.67
P10.3	30.89	32.37	35.21	34.52	36.30	37.54	38.28	39.14	40.32	2.43E-05	15.79	17.23	14.68
P11.1	31.81	33.14	35.30	34.62	36.42	37.61	38.37	39.21	40.39	2.41E-05	15.25	16.27	14.85
P11.2	31.95	33.27	35.43	34.75	36.54	37.74	38.47	39.33	40.50	2.41E-05	15.54	16.46	14.83
P11.3	32.00	33.32	35.48	34.81	36.59	37.79	38.55	39.38	40.55	2.40E-05	15.23	16.56	14.82
P12.1	40.71	41.79	43.45	42.97	44.12	45.01	45.49	46.06	46.89	2.43E-05	14.98	23.37	15.08
P12.2	40.84	41.92	43.55	43.09	44.20	45.10	45.57	46.14	46.97	2.42E-05	15.15	23.52	15.14
P12.2	41.04	42.10	43.73	43.25	44.38	45.26	45.72	46.27	47.09	2.43E-05	14.83	23.56	15.22
P13.1	41.30	42.56	44.51	43.95	45.46	46.61	47.26	48.01	49.07	2.43E-05	14.97	27.27	14.89
P13.2	41.27	42.53	44.48	43.91	45.45	46.59	47.22	48.00	49.04	2.42E-05	15.52	27.71	15.27
P13.3	41.35	42.61	44.55	43.97	45.49	46.62	47.28	48.03	49.10	2.44E-05	14.82	27.61	15.42
P14.1	32.11	33.58	35.86	35.09	37.16	38.53	39.40	40.36	41.73	2.42E-05	15.40	20.82	14.94
P14.2	32.24	33.72	35.99	35.25	37.29	38.67	39.50	40.50	41.84	2.42E-05	15.32	20.96	15.08
P14.3	32.41	33.89	36.14	35.38	37.42	38.78	39.63	40.60	41.94	2.42E-05	14.82	20.88	15.15
P15.1	25.25	27.08	31.37	29.97	34.06	36.59	38.32	40.28	42.87	2.35E-05	15.38	15.61	13.58
P15.2	25.33	27.14	31.44	30.04	34.16	36.68	38.40	40.37	42.96	2.36E-05	15.15	15.47	13.60
P15.3	25.38	27.16	31.49	30.07	34.22	36.74	38.47	40.42	43.00	2.36E-05	15.18	15.36	13.63
P16.1	41.45	42.92	45.11	44.49	46.21	47.46	48.16	48.98	50.12	2.45E-05	15.10	34.36	20.77
P16.2	41.39	42.85	45.04	44.45	46.14	47.40	48.08	48.92	50.07	2.45E-05	14.99	34.25	20.71
P16.3	41.39	42.83	45.02	44.43	46.14	47.38	48.07	48.90	50.05	2.44E-05	15.07	34.28	20.68
P17.1	41.22	42.55	44.53	43.95	45.52	46.65	47.28	48.03	49.08	2.40E-05	14.94	27.54	15.20
P17.2	41.28	42.62	44.59	44.03	45.56	46.71	47.34	48.09	49.15	2.42E-05	15.19	27.62	15.26
P17.3	41.52	42.85	44.84	44.26	45.82	46.97	47.61	48.37	49.42	2.40E-05	14.96	27.94	15.49

Table E2.1: Heat and mass balance results for pentane tests

	Heat balance					Mass Balance				Condensate Heat Flux	Vapour Velocity	Saturation Temperature	
Run	$\dot{Q}_R$ (W)	$\dot{Q}_D$ (W)	$\dot{Q}_{A,Ex}$ (W)	$\dot{Q}_o$ (W)	$R_{\dot{Q}}$ (W/W)	$\overline{T}_f$ (°C)	$\dot{m}_{f,o}$ (kg/s)	$\dot{m}_{v,o}$ (kg/s)	$\dot{m}_{v,i}$ (kg/s)	$\dot{q}_f$ (m/s)	$u_{v,in}$ (W/m²)	$T^*_{v,in}$ (°C)	$\Delta T^*_{v,in}$ (°C)
P1.1	3222.4	1911.2	484.3	5617.9	0.987	40.25	0.00848	0.00485	0.01333	15120.2	1.70	52.73	-0.17
P1.2	3213.0	1915.0	498.5	5626.6	0.987	40.28	0.00846	0.00486	0.01332	15076.3	1.70	52.73	-0.17
P1.3	3205.3	1912.9	485.6	5603.9	0.987	40.30	0.00844	0.00486	0.01330	15040.2	1.70	52.73	-0.16
P2.1	1756.2	802.4	409.3	2967.8	0.983	34.27	0.00467	0.00192	0.00660	8240.5	1.15	42.42	-0.31
P2.2	1764.0	799.5	404.0	2967.6	0.985	34.31	0.00469	0.00192	0.00661	8277.3	1.15	42.47	-0.31
P2.3	1780.6	811.0	409.2	3000.8	0.997	34.32	0.00474	0.00195	0.00668	8354.9	1.16	42.50	-0.31
P3.1	1212.6	1292.3	496.4	3001.3	1.000	40.81	0.00327	0.00303	0.00630	5689.9	0.91	48.38	-0.24
P3.2	1232.1	1302.6	507.6	3042.4	1.014	40.84	0.00332	0.00305	0.00638	5781.5	0.92	48.42	-0.24
P3.3	1263.7	1317.4	501.6	3082.7	1.028	40.84	0.00341	0.00309	0.00650	5929.6	0.94	48.45	-0.23
P4.1	2429.5	1117.4	369.6	3916.5	0.986	36.80	0.00643	0.00263	0.00905	11399.6	1.36	47.07	-0.23
P4.2	2476.8	1088.9	380.0	3945.7	0.991	36.74	0.00655	0.00256	0.00911	11621.5	1.37	47.07	-0.24
P4.3	2483.8	1045.8	371.6	3901.2	0.982	36.67	0.00657	0.00246	0.00903	11654.4	1.36	47.05	-0.23
P5.1	2567.9	1897.4	432.0	4897.3	0.990	46.26	0.00686	0.00432	0.01118	12049.4	1.24	57.57	-0.10
P5.2	2561.9	1893.7	417.1	4872.7	0.985	46.25	0.00685	0.00431	0.01115	12020.9	1.24	57.55	-0.10
P5.3	2559.0	1878.0	407.1	4844.0	0.978	46.27	0.00684	0.00427	0.01111	12007.3	1.23	57.56	-0.10
P6.1	3130.4	1389.8	352.2	4872.5	0.985	39.89	0.00825	0.00320	0.01145	14688.8	1.49	51.93	-0.16
P6.2	3130.6	1402.5	373.1	4906.3	0.990	39.89	0.00825	0.00323	0.01148	14689.6	1.50	51.94	-0.16
P6.3	3113.1	1434.9	347.7	4895.7	0.989	39.91	0.00821	0.00330	0.01151	14607.5	1.50	51.94	-0.16
P7.1	3701.6	846.2	296.3	4844.1	0.993	33.79	0.00963	0.00199	0.01162	17368.6	1.78	46.55	-0.22
P7.2	3707.7	841.0	297.9	4846.6	0.993	33.78	0.00965	0.00197	0.01162	17397.5	1.78	46.54	-0.21
P7.3	3702.7	838.4	273.5	4814.6	0.983	33.77	0.00963	0.00197	0.01160	17374.1	1.78	46.54	-0.21
P8.1	4355.7	1084.4	489.9	5929.9	0.984	36.22	0.01123	0.00250	0.01373	20438.1	1.80	51.71	-0.18
P8.2	4355.5	1103.6	517.8	5976.9	0.993	36.26	0.01124	0.00254	0.01377	20437.2	1.81	51.75	-0.18
P8.3	4367.9	1084.4	542.1	5994.4	0.995	36.27	0.01127	0.00249	0.01376	20495.5	1.80	51.78	-0.18
P9.1	3768.0	1590.0	573.6	5931.6	1.000	42.13	0.00984	0.00360	0.01344	17680.5	1.52	56.84	-0.11
P9.2	3771.9	1581.8	572.8	5926.5	1.000	42.17	0.00985	0.00358	0.01343	17698.6	1.52	56.86	-0.11
P9.3	3783.0	1559.7	575.3	5918.0	0.999	42.16	0.00988	0.00353	0.01341	17750.8	1.52	56.86	-0.11

Table E2.2: Heat and mass balance results for pentane tests (ctnd)

Run	Heat balance					Mass Balance				Condensate Heat Flux	Vapour Velocity	Saturation Temperature	
	$\dot{Q}_R$ (W)	$\dot{Q}_D$ (W)	$\dot{Q}_{A,Ex}$ (W)	$\dot{Q}_o$ (W)	$R_{\dot{Q}}$ (W/W)	$\overline{T}_f$ (°C)	$\dot{m}_{f,o}$ (kg/s)	$\dot{m}_{v,o}$ (kg/s)	$\dot{m}_{v,i}$ (kg/s)	$\dot{q}_f$ (m/s)	$u_{v,in}$ (W/m²)	$T^*_{v,in}$ (°C)	$\Delta T^*_{v,in}$ (°C)
P10.1	2429.1	210.9	366.5	3006.5	0.989	36.55	0.00642	0.00049	0.00691	11398.2	1.04	47.04	-0.23
P10.2	2447.4	174.5	407.5	3029.4	0.997	36.49	0.00646	0.00041	0.00687	11483.6	1.04	47.01	-0.23
P10.3	2460.6	138.3	415.0	3013.9	0.991	36.42	0.00650	0.00032	0.00682	11545.7	1.03	46.98	-0.23
P11.1	2469.9	93.6	443.1	3006.6	1.004	37.05	0.00653	0.00022	0.00675	11589.4	1.01	47.42	-0.21
P11.2	2465.1	84.2	447.6	2996.9	1.002	37.13	0.00652	0.00020	0.00672	11566.9	1.00	47.47	-0.21
P11.3	2469.7	125.5	442.4	3037.7	1.014	37.17	0.00653	0.00029	0.00683	11588.6	1.01	47.54	-0.21
P12.1	1703.0	843.5	450.5	2997.0	0.994	42.50	0.00458	0.00194	0.00652	7990.9	0.86	51.47	-0.18
P12.2	1688.7	839.0	459.7	2987.4	0.987	42.57	0.00454	0.00193	0.00647	7923.9	0.85	51.52	-0.19
P12.2	1668.1	878.8	451.1	2998.0	0.993	42.67	0.00448	0.00202	0.00651	7826.9	0.86	51.58	-0.19
P13.1	2189.5	1240.6	523.8	3953.9	1.005	44.42	0.00585	0.00281	0.00866	10273.7	1.03	55.01	-0.14
P13.2	2188.7	1224.3	521.6	3934.6	0.996	44.42	0.00585	0.00278	0.00863	10270.0	1.03	55.04	-0.14
P13.3	2171.3	1292.4	519.8	3983.5	1.011	44.46	0.00581	0.00293	0.00874	10188.1	1.04	55.05	-0.14
P14.1	2788.2	538.8	508.1	3835.2	0.998	38.23	0.00735	0.00125	0.00860	13083.0	1.20	49.73	-0.19
P14.2	2769.0	562.5	484.7	3816.3	0.993	38.31	0.00730	0.00130	0.00860	12992.8	1.20	49.80	-0.19
P14.3	2753.1	605.5	501.0	3859.6	1.004	38.39	0.00726	0.00140	0.00866	12918.4	1.20	49.85	-0.19
P15.1	5114.1	13.6	389.4	5517.1	0.959	39.16	0.01309	0.00003	0.01312	23996.5	1.48	57.12	-0.08
P15.2	5129.1	22.0	372.3	5523.4	0.961	39.24	0.01313	0.00005	0.01318	24066.9	1.48	57.21	-0.08
P15.3	5126.0	9.9	396.2	5532.1	0.963	39.30	0.01313	0.00002	0.01315	24052.6	1.47	57.26	-0.08
P16.1	2390.8	1956.1	569.3	4916.2	1.012	45.40	0.00638	0.00454	0.01093	11218.1	1.25	56.58	-0.12
P16.2	2394.0	1959.0	575.7	4928.7	1.016	45.36	0.00639	0.00455	0.01094	11233.2	1.25	56.55	-0.12
P16.3	2391.8	1946.6	558.3	4896.7	1.005	45.35	0.00639	0.00452	0.01091	11222.9	1.25	56.53	-0.12
P17.1	2183.5	1254.2	525.7	3963.3	1.007	44.57	0.00584	0.00284	0.00869	10245.6	1.04	55.07	-0.13
P17.2	2167.9	1245.8	531.1	3944.8	0.993	44.61	0.00580	0.00283	0.00863	10172.3	1.03	55.10	-0.14
P17.3	2179.0	1294.1	549.1	4022.2	0.995	44.84	0.00583	0.00294	0.00877	10224.5	1.03	55.40	-0.13

Table E3.1: Local heat transfer coefficients for pentane tests

Run	Local Heat Transfer Coefficients									Intermediate Condensate Flows			
	$\alpha_{c,TS2}$ (W/m²K)	$\alpha_{f,TS2}$ (W/m²K)	$\dot{\alpha}_{f,TS2}$ (-)	$\alpha_{c,TS3}$ (W/m²K)	$\alpha_{f,TS3}$ (W/m²K)	$\dot{\alpha}_{f,TS3}$ (-)	$\alpha_{c,TS4}$ (W/m²K)	$\alpha_{f,TS4}$ (W/m²K)	$\dot{\alpha}_{f,TS4}$ (-)	$\dot{m}_{f,TS2}$ (kg/s)	$Re_{f,TS2}$ (-)	$\dot{m}_{f,TS3}$ (kg/s)	$Re_{f,TS3}$ (-)
P1.1	5943.4	1105.4	0.235	6185.9	663.9	0.141	6377.4	1011.5	0.215	0.00358	595	0.00628	961
P1.2	5951.6	1118.5	0.238	6194.2	656.2	0.140	6384.3	1016.1	0.216	0.00357	594	0.00627	961
P1.3	5948.9	1105.9	0.235	6189.7	660.2	0.141	6379.9	1017.7	0.217	0.00357	594	0.00625	958
P2.1	5781.4	2145.6	0.457	5920.0	1459.9	0.311	6042.6	1391.2	0.296	0.00186	282	0.00326	476
P2.2	5787.5	2154.5	0.459	5926.7	1489.2	0.317	6050.0	1396.6	0.297	0.00187	283	0.00328	478
P2.3	5786.7	2118.4	0.451	5925.6	1478.5	0.315	6050.8	1428.1	0.304	0.00189	287	0.00330	481
P3.1	6188.2	3495.7	0.744	6286.9	2361.4	0.503	6373.9	1938.7	0.413	0.00127	204	0.00225	352
P3.2	6210.9	3479.6	0.741	6310.0	2397.8	0.511	6398.9	1926.5	0.410	0.00130	208	0.00228	356
P3.3	6200.7	3387.2	0.721	6301.7	2326.1	0.495	6392.4	1888.3	0.402	0.00134	214	0.00234	366
P4.1	5902.6	1521.1	0.324	6088.7	1038.7	0.221	6244.6	1176.6	0.251	0.00264	418	0.00464	691
P4.2	5904.5	1524.0	0.324	6095.1	1001.0	0.213	6253.2	1203.9	0.256	0.00269	425	0.00473	705
P4.3	5879.9	1511.1	0.322	6071.3	1016.2	0.216	6230.9	1190.9	0.254	0.00268	424	0.00473	704
P5.1	6489.3	1146.0	0.244	6679.4	624.2	0.133	6815.5	1061.3	0.226	0.00311	539	0.00530	863
P5.2	6483.5	1142.8	0.243	6672.1	635.1	0.135	6808.8	1058.5	0.225	0.00310	538	0.00528	858
P5.3	6502.8	1145.1	0.244	6690.5	639.6	0.136	6826.8	1065.0	0.227	0.00311	540	0.00527	858
P6.1	6002.2	1006.6	0.214	6238.3	554.9	0.118	6415.1	954.2	0.203	0.00359	595	0.00622	947
P6.2	6008.7	1010.7	0.215	6245.3	546.1	0.116	6422.0	956.6	0.204	0.00359	594	0.00622	948
P6.3	6001.5	1002.3	0.213	6236.3	539.9	0.115	6411.9	959.7	0.204	0.00358	592	0.00619	943
P7.1	5544.2	891.5	0.190	5829.2	508.8	0.108	6052.2	922.1	0.196	0.00403	636	0.00707	1010
P7.2	5548.9	891.2	0.190	5834.1	509.4	0.108	6057.4	921.9	0.196	0.00404	638	0.00709	1012
P7.3	5531.8	888.2	0.189	5818.0	510.9	0.109	6040.5	921.6	0.196	0.00403	636	0.00708	1011
P8.1	5586.5	891.6	0.190	5920.8	562.1	0.120	6185.4	1040.3	0.222	0.00460	758	0.00823	1205
P8.2	5588.8	894.0	0.190	5923.0	567.7	0.121	6188.3	1030.9	0.219	0.00459	757	0.00822	1205
P8.3	5593.2	897.2	0.191	5927.9	568.0	0.121	6195.2	1035.9	0.221	0.00459	757	0.00823	1206
P9.1	6010.6	1100.7	0.234	6293.9	718.1	0.153	6531.3	1013.1	0.216	0.00390	670	0.00711	1107
P9.2	6031.2	1111.0	0.237	6314.2	722.7	0.154	6551.4	1003.3	0.214	0.00392	673	0.00712	1109
P9.3	6023.8	1115.3	0.237	6307.8	722.5	0.154	6546.2	1008.1	0.215	0.00392	673	0.00713	1112

Table E3.2: Local heat transfer coefficients for pentane tests (ctnd)

	Local Heat Transfer Coefficients									Intermediate Condensate Flows			
Run	$\alpha_{c,TS2}$ (W/m² K)	$\alpha_{f,TS2}$ (W/m²K)	$\alpha^{*}_{f,TS2}$ (-)	$\alpha_{c,TS3}$ (W/m²K)	$\alpha_{f,TS3}$ (W/m²K)	$\alpha^{*}_{f,TS3}$ (-)	$\alpha_{c,TS4}$ (W/m²K)	$\alpha_{f,TS4}$ (W/m²K)	$\alpha^{*}_{f,TS4}$ (-)	$\dot{m}_{f,TS2}$ (kg/s)	$Re_{f,TS2}$ (-)	$\dot{m}_{f,TS3}$ (kg/s)	$Re_{f,TS3}$ (-)
P10.1	5859.7	1874.1	0.399	6046.1	1448.5	0.308	6226.3	1263.3	0.269	0.00234	369	0.00433	644
P10.2	5858.1	1869.3	0.398	6046.6	1423.5	0.303	6227.7	1262.6	0.269	0.00235	370	0.00436	649
P10.3	5840.1	1871.8	0.399	6030.7	1401.3	0.298	6212.0	1248.8	0.266	0.00236	372	0.00440	654
P11.1	5939.5	1236.6	0.263	6127.8	736.1	0.157	6275.0	1012.6	0.216	0.00283	449	0.00485	724
P11.2	5957.3	1242.7	0.265	6145.5	740.0	0.158	6291.3	1034.2	0.220	0.00283	450	0.00486	725
P11.3	5960.2	1242.7	0.265	6149.3	725.8	0.155	6294.9	1016.1	0.216	0.00283	451	0.00487	728
P12.1	6391.8	1608.1	0.342	6520.4	924.5	0.197	6615.0	1319.4	0.281	0.00213	350	0.00350	554
P12.2	6408.9	1607.6	0.342	6536.2	939.0	0.200	6629.9	1341.4	0.286	0.00211	348	0.00347	550
P12.2	6424.2	1640.3	0.349	6549.9	965.3	0.206	6642.1	1350.8	0.288	0.00210	346	0.00344	545
P13.1	6453.2	1248.1	0.266	6614.3	699.4	0.149	6731.4	1166.6	0.248	0.00272	462	0.00453	729
P13.2	6445.9	1237.6	0.263	6606.4	715.8	0.152	6724.2	1152.1	0.245	0.00272	462	0.00452	727
P13.3	6449.8	1241.8	0.264	6609.1	698.2	0.149	6725.6	1186.3	0.253	0.00270	459	0.00449	722
P14.1	5966.7	1088.0	0.232	6179.0	617.6	0.131	6341.4	959.1	0.204	0.00318	515	0.00550	829
P14.2	5962.9	1097.7	0.234	6173.6	639.1	0.136	6336.0	970.8	0.207	0.00314	510	0.00545	823
P14.3	5976.8	1108.4	0.236	6186.9	623.3	0.133	6347.1	970.3	0.207	0.00314	509	0.00544	821
P15.1	5624.6	915.7	0.195	6021.6	589.6	0.126	6343.5	975.0	0.208	0.00506	872	0.00942	1413
P15.2	5634.8	909.7	0.194	6032.0	590.8	0.126	6354.8	967.3	0.206	0.00508	877	0.00945	1419
P15.3	5628.8	903.5	0.192	6024.7	590.5	0.126	6346.8	956.5	0.204	0.00510	880	0.00945	1419
P16.1	6418.7	1399.9	0.298	6596.1	882.6	0.188	6735.2	1112.5	0.237	0.00276	474	0.00478	775
P16.2	6426.0	1404.0	0.299	6604.0	896.9	0.191	6743.8	1131.6	0.241	0.00275	473	0.00478	775
P16.3	6430.8	1405.2	0.299	6608.9	894.8	0.191	6748.4	1131.2	0.241	0.00275	472	0.00478	774
P17.1	6398.7	1392.3	0.296	6561.3	850.1	0.181	6685.9	1127.6	0.240	0.00259	439	0.00441	710
P17.2	6385.3	1392.5	0.296	6547.5	837.9	0.178	6670.8	1157.6	0.246	0.00257	436	0.00439	707
P17.3	6404.2	1376.5	0.293	6567.1	832.7	0.177	6690.1	1152.5	0.245	0.00259	441	0.00442	714

Table E4.1: Mean heat transfer coefficients and condensate film calculations for pentane tests

	Experimental Mean Heat Transfer Coefficients							Condensate Film Analysis			
Run	θ_{mean} (°C)	$\overline{U}$ (W/m²K)	$\overline{T}_w$ (-)	$\overline{\alpha}_w$ (W/m²K)	$\overline{\alpha}_c$ (W/m²K)	$\overline{\alpha}_f$ (W/m²K)	$\overline{\alpha}_f^*$ (-)	$Re_{f,out}$ (-)	$Pr_{f,out}$ (-)	$\overline{\alpha}_{f,Nu}^*$ (-)	$\overline{\alpha}_{f,HTFS}^*$ (-)
P1.1	15.15	998.2	33.91	84754	6032.2	1129.5	0.224	1282	4.16	0.101	0.191
P1.2	15.09	999.2	33.95	84754	6040.2	1130.5	0.224	1278	4.16	0.101	0.191
P1.3	15.07	998.1	33.98	84755	6036.5	1129.2	0.224	1276	4.16	0.101	0.191
P2.1	7.93	1039.7	30.23	84672	5850.9	1187.6	0.237	670	4.24	0.126	0.221
P2.2	7.95	1041.8	30.27	84673	5857.6	1190.0	0.238	673	4.24	0.126	0.221
P2.3	7.98	1047.0	30.27	84673	5856.5	1196.9	0.239	680	4.24	0.125	0.220
P3.1	5.20	1095.2	37.03	84823	6245.4	1249.5	0.247	497	4.15	0.139	0.236
P3.2	5.22	1107.0	37.06	84823	6268.4	1264.3	0.250	505	4.15	0.138	0.235
P3.3	5.33	1112.4	37.04	84823	6258.6	1271.6	0.252	518	4.15	0.137	0.234
P4.1	11.34	1005.3	31.62	84703	5982.1	1139.7	0.227	942	4.20	0.112	0.205
P4.2	11.45	1015.4	31.54	84701	5985.6	1152.6	0.229	960	4.20	0.112	0.204
P4.3	11.56	1008.0	31.45	84699	5962.3	1143.6	0.228	961	4.21	0.111	0.204
P5.1	12.08	997.1	40.49	84900	6549.3	1117.5	0.220	1092	4.08	0.107	0.198
P5.2	12.08	995.4	40.48	84899	6543.2	1115.4	0.220	1089	4.08	0.107	0.198
P5.3	12.06	995.5	40.50	84900	6561.7	1115.1	0.220	1088	4.08	0.107	0.198
P6.1	15.01	978.6	33.77	84750	6079.9	1103.4	0.219	1243	4.16	0.102	0.193
P6.2	14.98	980.5	33.77	84750	6086.9	1105.6	0.219	1243	4.16	0.102	0.193
P6.3	14.94	977.6	33.80	84751	6078.5	1102.1	0.219	1236	4.16	0.102	0.193
P7.1	17.90	970.5	27.33	84607	5644.4	1103.0	0.220	1375	4.25	0.099	0.188
P7.2	17.89	972.4	27.32	84607	5649.0	1105.3	0.221	1377	4.25	0.099	0.188
P7.3	17.92	969.4	27.30	84607	5632.4	1101.8	0.220	1375	4.25	0.099	0.188
P8.1	21.00	973.2	28.34	84630	5709.5	1104.9	0.220	1639	4.21	0.093	0.181
P8.2	20.98	974.0	28.38	84631	5712.4	1105.9	0.220	1639	4.21	0.093	0.181
P8.3	20.99	976.5	28.37	84630	5718.1	1108.9	0.221	1644	4.21	0.093	0.181
P9.1	17.92	986.5	34.61	84769	6130.9	1112.4	0.220	1511	4.13	0.096	0.184
P9.2	17.87	990.7	34.66	84770	6151.0	1117.2	0.221	1514	4.13	0.096	0.184
P9.3	17.89	992.4	34.65	84770	6144.5	1119.6	0.222	1518	4.13	0.096	0.184

Table E4.2: Mean heat transfer coefficients and condensate film calculations for pentane tests (ctnd)

	Experimental Mean Heat Transfer Coefficients							Condensate Film Analysis			
Run	θ_{mean} (°C)	$\overline{U}$ (W/m²K)	$\overline{T}_w$ (-)	$\overline{\alpha}_w$ (W/m²K)	$\overline{\alpha}_c$ (W/m²K)	$\overline{\alpha}_f$ (W/m²K)	$\overline{\alpha}_f^*$ (-)	$Re_{f,out}$ (-)	$Pr_{f,out}$ (-)	$\overline{\alpha}_{f,Nu}^*$ (-)	$\overline{\alpha}_{f,HTFS}^*$ (-)
P10.1	11.19	1018.4	31.27	84695	5963.7	1157.0	0.230	939	4.21	0.112	0.205
P10.2	11.26	1020.0	31.19	84693	5963.0	1159.0	0.231	945	4.21	0.112	0.205
P10.3	11.35	1017.0	31.09	84691	5945.7	1155.7	0.230	949	4.21	0.112	0.204
P11.1	11.81	981.5	31.81	84707	6008.4	1108.6	0.221	960	4.20	0.112	0.204
P11.2	11.75	984.8	31.90	84709	6025.5	1112.4	0.221	959	4.20	0.112	0.204
P11.3	11.75	986.4	31.94	84710	6028.7	1114.5	0.222	961	4.20	0.111	0.204
P12.1	7.87	1016.0	37.98	84844	6436.3	1143.4	0.226	705	4.13	0.124	0.218
P12.2	7.82	1013.8	38.05	84846	6452.9	1140.4	0.225	699	4.13	0.124	0.219
P12.2	7.72	1014.1	38.18	84848	6467.4	1140.4	0.225	692	4.12	0.124	0.219
P13.1	10.27	1000.0	39.04	84868	6503.3	1121.9	0.221	917	4.10	0.113	0.206
P13.2	10.33	994.6	39.03	84867	6496.1	1115.2	0.220	916	4.10	0.113	0.206
P13.3	10.29	990.1	39.08	84868	6499.4	1109.5	0.219	910	4.10	0.114	0.206
P14.1	13.46	971.9	32.40	84720	6041.7	1095.7	0.218	1091	4.18	0.107	0.198
P14.2	13.40	970.0	32.50	84722	6038.3	1093.3	0.217	1084	4.18	0.107	0.198
P14.3	13.32	970.1	32.59	84724	6051.3	1093.2	0.217	1079	4.18	0.107	0.199
P15.1	24.73	970.1	29.95	84666	5789.5	1099.0	0.218	1960	4.17	0.088	0.174
P15.2	24.74	972.9	30.03	84667	5799.4	1102.3	0.219	1967	4.17	0.088	0.174
P15.3	24.75	971.7	30.08	84668	5791.7	1101.0	0.219	1967	4.17	0.088	0.174
P16.1	11.12	1008.8	39.71	84882	6486.6	1133.4	0.223	1008	4.09	0.110	0.202
P16.2	11.15	1007.9	39.66	84881	6494.8	1132.0	0.223	1009	4.09	0.110	0.202
P16.3	11.15	1006.8	39.66	84881	6499.7	1130.6	0.223	1008	4.09	0.110	0.202
P17.1	10.26	998.2	39.23	84872	6458.1	1120.5	0.221	916	4.10	0.113	0.206
P17.2	10.23	994.5	39.27	84873	6444.5	1116.1	0.220	910	4.10	0.114	0.206
P17.3	10.29	994.1	39.47	84877	6462.9	1115.3	0.220	916	4.10	0.113	0.206

Table E5.1: Experimental data for iso-octane tests

Run	Boiler			Reflux Condenser Coolant					Reflux Condenser Vapour			Extraction Air	
	Q_i (W)	$P_{v,i}$ (Pa)	$T_{vR,i}$ (°C)	$\dot{V}_{c,R}$ (m³/s)	$T_{cR,i}$ (°C)	$T_{cR,TS3}$ (°C)	$T_{cR,TS4}$ (°C)	$T_{cR,i}$ (°C)	$T_{vR,oTS2}$ (°C)	$T_{vR,oTS3}$ (°C)	$T_{vR,oTS3}$ (°C)	T_{Ai} (°C)	T_{Ao} (°C)
I1.1	2024.0	14624	42.38	5.84E-05	29.49	30.92	32.74	35.34	40.78	40.86	40.82	9.54	13.50
I1.2	2025.3	14684	42.48	5.85E-05	29.55	30.97	32.83	35.43	40.90	40.96	40.93	9.86	13.53
I1.3	2024.4	14754	42.58	5.84E-05	29.57	31.02	32.87	35.48	40.99	41.03	41.03	9.91	13.51
I2.1	2509.0	15992	44.57	5.85E-05	29.21	31.10	33.29	36.29	42.89	42.89	42.86	10.41	13.75
I2.2	2508.8	15988	44.56	5.82E-05	29.03	30.97	33.12	36.19	42.83	42.90	42.89	9.67	13.67
I2.3	2501.8	16003	44.59	5.82E-05	29.01	30.91	33.09	36.11	42.90	42.92	42.89	9.99	13.72
I3.1	1513.0	12605	38.82	5.84E-05	29.29	30.05	31.42	33.77	37.16	37.22	37.23	9.64	13.37
I3.2	1515.1	12642	38.90	5.83E-05	29.32	30.08	31.46	33.82	37.28	37.31	37.31	9.86	13.33
I3.3	1516.8	12707	38.98	5.82E-05	29.34	30.08	31.55	33.87	37.40	37.38	37.37	9.99	13.38
I4.1	1513.1	11846	37.39	5.81E-05	29.78	30.25	31.47	33.59	35.89	35.93	35.91	13.33	15.34
I4.2	1509.9	11803	37.30	5.82E-05	29.45	29.97	31.22	33.35	35.79	35.82	35.82	13.23	15.31
I4.3	1510.6	11775	37.24	5.82E-05	29.25	29.78	31.06	33.18	35.73	35.78	35.72	13.25	15.31
I5.1	2063.7	10821	35.30	5.81E-05	23.98	25.29	26.95	29.34	33.74	33.79	33.84	12.82	15.43
I5.2	2068.4	10824	35.29	5.82E-05	24.05	25.37	27.01	29.33	33.76	33.87	33.80	12.69	15.39
I5.3	2073.8	10834	35.32	5.81E-05	24.17	25.48	27.07	29.37	33.82	33.87	33.89	12.99	15.48
I8.1	2020.1	12601	38.79	5.83E-05	29.47	30.40	31.83	33.92	37.34	37.40	37.41	8.23	11.90
I8.2	2021.2	12641	38.84	5.81E-05	29.43	30.39	31.80	33.94	37.42	37.48	37.47	8.41	11.94
I8.3	2021.0	12646	38.87	5.80E-05	29.32	30.31	31.76	33.92	37.44	37.52	37.51	8.58	12.02
I9.1	2437.3	13911	41.17	5.80E-05	29.15	30.63	32.41	34.83	39.61	39.69	39.67	9.10	12.45
I9.2	2439.6	13904	41.14	5.80E-05	29.00	30.52	32.30	34.75	39.60	39.62	39.63	8.96	12.46
I9.3	2441.3	13908	41.15	5.81E-05	29.02	30.50	32.27	34.70	39.59	39.67	39.65	8.98	12.43
I12.1	2533.5	16594	45.54	5.82E-05	29.36	31.46	33.73	36.84	43.86	43.89	43.89	12.44	15.49
I12.2	2535.6	16651	45.62	5.84E-05	29.23	31.38	33.69	36.77	43.96	43.97	43.99	12.48	15.54
I12.3	2537.9	16699	45.69	5.84E-05	29.26	31.39	33.68	36.77	44.02	44.06	44.07	12.54	15.55
I13.1	2548.4	17034	46.19	5.85E-05	29.24	31.47	33.85	37.06	44.51	44.56	44.55	12.79	15.71
I13.2	2532.5	16993	46.13	5.83E-05	29.45	31.64	33.97	37.11	44.47	44.50	44.49	12.72	15.66
I13.3	2535.3	17012	46.16	5.82E-05	29.41	31.62	33.93	37.10	44.47	44.51	44.53	12.82	15.71

Table E5.2: Experimental data for iso-octane tests (ctnd)

Run	Reflux Condenser Wall Temperatures									Dump Condenser			
	$T_{w,TS2t}$ (°C)	$T_{w,TS2m}$ (°C)	$T_{w,TS2b}$ (°C)	$T_{w,TS3t}$ (°C)	$T_{w,TS3m}$ (°C)	$T_{w,TS3b}$ (°C)	$T_{w,TS4t}$ (°C)	$T_{w,TS4m}$ (°C)	$T_{w,TS4b}$ (°C)	$\dot{V}_{c,D}$ (m³/s)	$T_{cD,in}$ (°C)	$T_{cD,out}$ (°C)	$T_{f,D}$ (°C)
I1.1	30.42	31.39	33.31	32.85	33.90	34.58	35.21	35.54	36.25	4.26E-05	15.58	16.82	16.12
I1.2	30.51	31.44	33.38	32.91	33.99	34.68	35.28	35.62	36.33	4.26E-05	15.72	16.90	16.06
I1.3	30.52	31.48	33.42	32.96	34.03	34.72	35.32	35.69	36.39	4.26E-05	15.87	16.98	15.98
I2.1	30.40	31.55	33.63	33.10	34.36	35.17	35.79	36.36	37.35	4.26E-05	14.82	17.31	15.68
I2.2	30.24	31.35	33.47	32.99	34.23	35.01	35.63	36.26	37.28	4.26E-05	14.97	17.22	15.54
I2.3	30.24	31.34	33.47	32.91	34.17	34.96	35.60	36.20	37.19	4.26E-05	15.26	17.33	15.43
I3.1	29.81	30.54	32.27	31.88	32.79	33.29	33.56	34.02	34.61	4.25E-05	15.61	16.34	15.58
I3.2	29.85	30.62	32.31	31.92	32.83	33.36	33.61	34.05	34.66	4.26E-05	15.58	16.29	15.56
I3.3	29.86	30.65	32.38	31.95	32.81	33.44	33.66	34.11	34.65	4.25E-05	15.62	16.27	15.57
I4.1	30.06	30.75	32.39	32.10	32.81	33.29	33.49	33.89	34.36	4.26E-05	15.46	17.78	16.00
I4.2	29.81	30.47	32.10	31.81	32.53	33.00	33.27	33.65	34.10	4.27E-05	15.45	17.58	16.00
I4.3	29.61	30.30	31.96	31.62	32.34	32.84	33.08	33.49	33.97	4.26E-05	15.42	17.44	15.95
I5.1	24.92	25.67	27.32	26.96	27.95	28.53	28.93	29.51	30.19	4.20E-05	24.59	27.49	25.70
I5.2	24.96	25.76	27.43	26.99	27.99	28.57	29.00	29.48	30.21	4.19E-05	24.92	27.69	25.36
I5.3	25.09	25.85	27.49	27.08	28.07	28.63	29.04	29.56	30.23	4.20E-05	24.95	27.72	25.23
I8.1	30.11	30.87	32.41	32.03	32.87	33.43	33.68	34.15	34.68	4.23E-05	20.27	23.47	19.69
I8.2	30.04	30.82	32.42	32.03	32.87	33.40	33.66	34.16	34.73	4.22E-05	20.20	23.46	19.68
I8.3	29.97	30.75	32.36	31.97	32.81	33.36	33.63	34.14	34.70	4.23E-05	20.00	23.30	19.65
I9.1	30.10	31.01	32.74	32.32	33.35	34.00	34.36	34.96	35.76	4.23E-05	19.73	23.66	19.70
I9.2	29.96	30.91	32.63	32.17	33.24	33.91	34.25	34.84	35.68	4.23E-05	19.75	23.54	19.59
I9.3	30.00	30.91	32.60	32.18	33.20	33.87	34.24	34.81	35.58	4.23E-05	20.07	23.71	19.54
I12.1	30.70	31.85	34.06	33.52	34.86	35.65	36.18	36.94	38.00	4.28E-05	15.20	16.94	16.13
I12.2	30.59	31.77	34.00	33.43	34.79	35.61	36.12	36.88	37.94	4.28E-05	15.38	16.98	16.10
I12.3	30.62	31.80	34.03	33.44	34.81	35.62	36.13	36.89	37.98	4.28E-05	15.54	17.08	16.06
I13.1	30.65	31.85	34.14	33.58	34.96	35.80	36.35	37.16	38.29	4.29E-05	15.24	16.78	16.09
I13.2	30.83	32.00	34.29	33.72	35.09	35.91	36.42	37.23	38.32	4.29E-05	15.39	17.07	16.17
I13.3	30.81	31.99	34.27	33.69	35.05	35.91	36.43	37.20	38.30	4.29E-05	15.24	16.96	16.16

Table E6.1: Heat and mass balance results for iso-octane tests

	Heat balance					Mass Balance				Condensate Heat Flux	Vapour Velocity	Saturation Temperature	
Run	$\dot{Q}_R$ (W)	$\dot{Q}_D$ (W)	$\dot{Q}_{A,Ex}$ (W)	$\dot{Q}_o$ (W)	$R_{\dot{Q}}$ (W/W)	$\overline{T}_f$ (°C)	$\dot{m}_{f,o}$ (kg/s)	$\dot{m}_{v,o}$ (kg/s)	$\dot{m}_{v,i}$ (kg/s)	$\dot{q}_f$ (m/s)	$u_{v,in}$ (W/m²)	$T^*_{v,in}$ (°C)	$\Delta T^*_{v,in}$ (°C)
I1.1	1421.2	205.8	400.4	2027.4	1.002	36.66	0.00462	0.00059	0.00522	6668.6	5.06	43.34	-0.96
I1.2	1431.0	194.3	370.5	1995.8	0.985	36.75	0.00466	0.00056	0.00521	6714.6	5.04	43.43	-0.95
I1.3	1435.6	181.4	363.9	1980.8	0.978	36.81	0.00467	0.00052	0.00519	6736.1	4.99	43.55	-0.97
I2.1	1720.9	429.4	336.5	2486.8	0.991	37.72	0.00557	0.00122	0.00679	8074.8	6.06	45.49	-0.92
I2.2	1732.8	385.0	404.2	2522.0	1.005	37.62	0.00561	0.00109	0.00670	8130.9	5.98	45.48	-0.92
I2.3	1720.2	352.1	376.9	2449.3	0.979	37.61	0.00556	0.00100	0.00656	8071.6	5.86	45.51	-0.92
I3.1	1090.7	113.6	376.9	1581.2	1.045	34.67	0.00357	0.00033	0.00390	5117.6	4.34	39.83	-1.01
I3.2	1090.2	111.3	350.0	1551.5	1.024	34.73	0.00357	0.00032	0.00389	5115.3	4.31	39.90	-1.00
I3.3	1096.0	100.3	342.8	1539.1	1.015	34.78	0.00359	0.00029	0.00388	5142.7	4.28	40.02	-1.03
I4.1	920.8	396.8	201.3	1519.0	1.004	34.21	0.00303	0.00117	0.00420	4320.8	4.94	38.39	-1.01
I4.2	944.7	365.9	208.2	1518.8	1.006	34.00	0.00310	0.00108	0.00418	4432.6	4.94	38.31	-1.01
I4.3	952.8	343.5	205.9	1502.2	0.994	33.87	0.00313	0.00101	0.00414	4470.8	4.90	38.26	-1.01
I5.1	1297.4	492.3	262.1	2051.8	0.994	30.33	0.00420	0.00156	0.00576	6087.9	7.37	36.32	-1.02
I5.2	1279.5	468.9	271.0	2019.3	0.976	30.36	0.00414	0.00148	0.00563	6003.5	7.19	36.33	-1.05
I5.3	1258.6	468.2	248.9	1975.6	0.953	30.42	0.00408	0.00148	0.00555	5905.6	7.10	36.35	-1.04
I8.1	1078.3	551.1	372.1	2001.5	0.991	34.77	0.00353	0.00165	0.00518	5059.7	5.76	39.82	-1.03
I8.2	1091.5	557.7	359.1	2008.3	0.994	34.78	0.00358	0.00167	0.00524	5121.5	5.81	39.90	-1.05
I8.3	1110.0	566.8	349.5	2026.3	1.003	34.75	0.00363	0.00169	0.00533	5208.5	5.90	39.91	-1.03
I9.1	1371.9	679.7	339.6	2391.2	0.981	35.89	0.00447	0.00201	0.00648	6437.3	6.58	42.15	-0.98
I9.2	1387.0	653.5	354.3	2394.8	0.982	35.81	0.00452	0.00193	0.00645	6508.0	6.55	42.13	-0.99
I9.3	1371.6	625.9	349.9	2347.3	0.962	35.80	0.00447	0.00185	0.00631	6435.7	6.41	42.14	-1.00
I12.1	1808.9	296.1	305.9	2411.0	0.952	38.34	0.00585	0.00084	0.00669	8487.9	5.78	46.39	-0.85
I12.2	1829.1	270.1	306.6	2405.8	0.949	38.33	0.00591	0.00076	0.00668	8582.8	5.75	46.48	-0.85
I12.3	1824.8	260.1	301.7	2386.7	0.940	38.36	0.00590	0.00074	0.00663	8562.6	5.69	46.55	-0.85
I13.1	1901.7	260.0	291.7	2453.4	0.963	38.64	0.00614	0.00073	0.00687	8923.3	5.80	47.03	-0.84
I13.2	1855.6	285.6	294.4	2435.6	0.962	38.70	0.00600	0.00081	0.00680	8707.1	5.75	46.97	-0.84
I13.3	1862.2	293.7	289.2	2445.0	0.964	38.69	0.00602	0.00083	0.00685	8737.7	5.78	47.00	-0.84

Table E7.1: Local heat transfer coefficients for iso-octane tests

	Local Heat Transfer Coefficients									Intermediate Condensate Flows			
Run	$\alpha_{c,TS2}$ (W/m²K)	$\alpha_{f,TS2}$ (W/m²K)	$\alpha^{\bullet}_{f,TS2}$ (-)	$\alpha_{c,TS3}$ (W/m²K)	$\alpha_{f,TS3}$ (W/m²K)	$\alpha^{\bullet}_{f,TS3}$ (-)	$\alpha_{c,TS4}$ (W/m²K)	$\alpha_{f,TS4}$ (W/m²K)	$\alpha^{\bullet}_{f,TS4}$ (-)	$\dot{m}_{f,TS2}$ (kg/s)	$Re_{f,TS2}$ (-)	$\dot{m}_{f,TS3}$ (kg/s)	$Re_{f,TS3}$ (-)
I1.1	5725.9	1815.4	0.759	5846.4	1323.2	0.553	5961.9	884.5	0.370	0.00151	107	0.00291	195
I1.2	5734.1	1816.1	0.759	5856.6	1327.7	0.555	5972.2	880.1	0.368	0.00151	107	0.00294	197
I1.3	5726.1	1804.5	0.755	5848.0	1318.4	0.551	5964.2	882.3	0.369	0.00152	109	0.00294	198
I2.1	5740.8	1567.4	0.655	5880.9	1111.7	0.465	6017.7	886.5	0.371	0.00186	135	0.00354	240
I2.2	5713.0	1516.3	0.634	5851.0	1081.7	0.452	5990.6	904.0	0.378	0.00189	137	0.00353	239
I2.3	5710.0	1544.1	0.646	5849.4	1064.3	0.445	5986.8	874.9	0.366	0.00186	135	0.00353	239
I3.1	5678.7	2560.8	1.071	5775.6	2129.4	0.890	5879.0	1164.2	0.487	0.00098	67	0.00203	134
I3.2	5670.6	2518.2	1.053	5767.8	2147.3	0.898	5870.7	1157.3	0.484	0.00098	67	0.00204	134
I3.3	5660.3	2590.7	1.083	5761.7	2143.6	0.896	5862.7	1063.8	0.445	0.00097	66	0.00209	137
I4.1	5664.1	3442.7	1.439	5752.5	3051.4	1.276	5842.6	1494.2	0.625	0.00075	51	0.00169	110
I4.2	5659.1	3254.6	1.361	5749.6	2753.5	1.151	5840.5	1370.0	0.573	0.00079	53	0.00175	114
I4.3	5643.7	3226.2	1.349	5735.4	2654.5	1.110	5826.4	1389.9	0.581	0.00080	54	0.00178	116
I5.1	5394.6	1692.2	0.708	5508.3	1210.8	0.506	5614.8	932.3	0.390	0.00140	92	0.00266	166
I5.2	5403.9	1727.7	0.722	5516.8	1177.2	0.492	5619.4	976.2	0.408	0.00141	93	0.00266	166
I5.3	5404.6	1705.1	0.713	5514.8	1193.3	0.499	5616.7	945.2	0.395	0.00139	92	0.00260	163
I8.1	5687.5	2293.5	0.959	5787.4	1708.6	0.714	5875.9	1085.1	0.454	0.00111	76	0.00222	146
I8.2	5671.9	2270.5	0.949	5769.9	1669.9	0.698	5861.5	1118.5	0.468	0.00114	78	0.00221	146
I8.3	5662.2	2246.8	0.939	5762.4	1627.7	0.681	5854.6	1099.3	0.460	0.00116	80	0.00226	149
I9.1	5679.2	1725.7	0.722	5797.4	1179.6	0.493	5903.2	1009.9	0.422	0.00153	108	0.00290	193
I9.2	5673.6	1714.2	0.717	5791.4	1199.1	0.501	5898.7	1003.8	0.420	0.00157	110	0.00293	195
I9.3	5677.4	1691.6	0.707	5795.2	1166.2	0.488	5901.2	941.7	0.394	0.00153	108	0.00289	192
I12.1	5734.5	1515.3	0.634	5878.1	1061.4	0.444	6019.4	927.5	0.388	0.00202	148	0.00375	256
I12.2	5745.5	1512.0	0.632	5891.9	1048.5	0.438	6032.1	920.9	0.385	0.00205	151	0.00383	261
I12.3	5751.3	1511.9	0.632	5896.5	1057.7	0.442	6037.8	941.2	0.394	0.00204	150	0.00380	259
I13.1	5761.0	1475.7	0.617	5910.9	1031.2	0.431	6058.5	939.1	0.393	0.00212	157	0.00394	270
I13.2	5754.1	1493.7	0.625	5901.2	1046.1	0.437	6044.5	937.3	0.392	0.00208	154	0.00386	265
I13.3	5748.0	1488.2	0.622	5893.8	1069.0	0.447	6038.8	921.5	0.385	0.00209	155	0.00386	264

Table E8.1: Mean heat transfer coefficients d condensate film calculations for iso-octane tests

Run	Experimental Mean Heat Transfer Coefficients							Condensate Film Analysis			
	θ_{mean} (°C)	$\overline{U}$ (W/m²K)	$\overline{T}_w$ (-)	$\overline{\alpha}_w$ (W/m²K)	$\overline{\alpha}_c$ (W/m²K)	$\overline{\alpha}_f$ (W/m²K)	$\overline{\alpha}_f^*$ (-)	$Re_{f,out}$ (-)	$Pr_{f,out}$ (-)	$\overline{\alpha}_{f,Nu}^*$ (-)	$\overline{\alpha}_{f,HTFS}^*$ (-)
I1.1	9.00	741.1	33.72	84749	5806.2	813.8	0.283	314	9.11	0.162	0.261
I1.2	9.04	743.1	33.79	84751	5815.4	816.1	0.284	317	9.11	0.161	0.261
I1.3	9.09	741.1	33.84	84752	5806.9	813.8	0.283	318	9.10	0.161	0.261
I2.1	10.75	751.1	34.19	84760	5829.6	825.6	0.286	383	9.05	0.151	0.250
I2.2	10.86	748.4	34.05	84757	5801.0	822.7	0.285	385	9.05	0.151	0.250
I2.3	10.96	736.4	34.01	84756	5798.5	808.2	0.280	382	9.06	0.152	0.250
I3.1	6.35	805.4	32.53	84723	5758.9	892.8	0.314	237	9.23	0.178	0.279
I3.2	6.41	797.4	32.58	84724	5750.6	883.1	0.310	237	9.23	0.178	0.279
I3.3	6.48	793.7	32.61	84725	5741.9	878.6	0.308	239	9.23	0.177	0.278
I4.1	4.86	888.3	32.57	84724	5741.1	996.1	0.350	200	9.26	0.188	0.290
I4.2	5.05	877.6	32.31	84718	5736.3	982.7	0.346	205	9.28	0.187	0.288
I4.3	5.17	863.9	32.13	84714	5721.2	965.9	0.340	206	9.28	0.186	0.288
I5.1	7.71	789.8	27.78	84617	5469.3	878.2	0.314	266	9.51	0.171	0.272
I5.2	7.69	781.1	27.82	84618	5475.9	867.3	0.310	262	9.51	0.172	0.272
I5.3	7.65	772.2	27.89	84620	5475.6	856.4	0.306	258	9.51	0.173	0.273
I8.1	6.26	808.5	32.69	84726	5757.2	896.6	0.315	235	9.23	0.178	0.279
I8.2	6.32	810.8	32.68	84726	5741.2	899.6	0.316	238	9.23	0.178	0.278
I8.3	6.41	812.7	32.63	84725	5732.3	902.2	0.317	242	9.23	0.177	0.277
I9.1	8.22	782.7	33.18	84737	5752.4	865.1	0.302	301	9.16	0.164	0.264
I9.2	8.32	782.0	33.07	84735	5746.1	864.3	0.302	304	9.16	0.164	0.263
I9.3	8.34	771.6	33.04	84734	5750.4	851.6	0.298	301	9.16	0.164	0.264
I12.1	11.35	747.5	34.64	84770	5821.8	821.4	0.284	405	9.01	0.149	0.247
I12.2	11.54	743.7	34.57	84768	5832.4	816.6	0.282	410	9.01	0.148	0.246
I12.3	11.59	738.5	34.59	84769	5838.6	810.3	0.280	409	9.01	0.148	0.247
I13.1	11.94	747.6	34.75	84772	5851.2	821.0	0.284	427	9.00	0.146	0.244
I13.2	11.77	739.9	34.87	84775	5842.1	811.9	0.280	417	8.99	0.147	0.245
I13.3	11.80	740.3	34.85	84774	5835.6	812.4	0.281	418	8.99	0.147	0.245

Table E9.1: Experimental data for flooding tests

Run	Boiler			Reflux Condenser Coolant					Reflux Condenser Vapour			Extraction Air	
	Q_i (W)	$P_{v,i}$ (Pa)	$T_{vR,i}$ (°C)	$\dot{V}_{c,R}$ (m³/s)	$T_{cR,i}$ (°C)	$T_{cR,TS3}$ (°C)	$T_{cR,TS4}$ (°C)	$T_{cR,i}$ (°C)	$T_{vR,oTS2}$ (°C)	$T_{vR,oTS3}$ (°C)	$T_{vR,oTS3}$ (°C)	T_{Ai} (°C)	T_{Ao} (°C)
F1.1	1968.5	16444	45.22	5.72E-05	39.23	40.50	41.39	42.22	44.85	44.88	45.04	13.99	17.23
F1.2	1967.1	16417	45.18	5.72E-05	39.10	40.36	41.29	42.15	44.80	44.88	45.02	14.03	17.20
F1.3	1966.3	16369	45.12	5.70E-05	39.04	40.30	41.28	42.07	44.78	44.79	44.94	13.99	17.21
F1.4	2516.7	17434	46.65	5.76E-05	39.44	40.91	42.04	43.00	46.24	46.31	46.31	13.39	16.39
F1.5	2518.2	17444	46.66	5.75E-05	39.34	40.88	41.99	42.96	46.25	46.30	46.32	13.37	16.41
F1.6	2518.9	17440	46.67	5.74E-05	39.15	40.71	41.86	42.87	46.26	46.31	46.35	13.37	16.45
F1.7	4634.5	24404	55.35	5.76E-05	39.44	44.42	47.92	50.27	52.80	53.94	54.51	14.21	18.45
F1.8	4630.7	24447	55.40	5.75E-05	39.48	44.47	47.97	50.33	52.88	53.87	54.57	14.01	18.42
F1.9	4629.6	24458	55.41	5.74E-05	39.44	44.45	47.99	50.35	52.86	53.93	54.60	14.20	18.42
F1.10	3644.8	21445	51.97	5.72E-05	39.28	42.89	45.66	47.63	48.90	50.19	50.98	14.02	18.08
F1.11	3650.3	21497	52.03	5.72E-05	39.39	43.02	45.74	47.71	49.12	50.30	51.08	13.99	18.06
F1.12	3657.1	21548	52.09	5.74E-05	39.47	43.09	45.82	47.78	49.17	50.36	51.14	13.82	18.07
F2.1	2175.9	22738	53.48	5.75E-05	34.32	37.68	39.91	41.91	52.79	52.95	53.04	13.46	16.29
F2.2	2175.4	22785	53.53	5.75E-05	34.47	37.84	40.06	42.06	52.86	52.99	53.10	13.63	16.34
F2.3	2171.3	22821	53.57	5.73E-05	34.54	37.93	40.16	42.16	52.89	53.02	53.13	13.75	16.34
F2.4	2809.7	24358	55.30	5.75E-05	34.03	37.93	40.53	43.01	54.71	54.77	54.94	11.94	14.79
F2.5	2813.1	24381	55.32	5.74E-05	34.25	38.12	40.67	43.07	54.76	54.81	54.98	12.34	14.86
F2.6	2813.2	24532	55.49	5.74E-05	34.44	38.32	40.89	43.27	54.94	55.01	55.18	12.29	14.98
F2.7	3020.4	25244	56.26	5.74E-05	34.15	38.21	40.95	43.74	55.63	55.68	55.78	12.32	15.23
F2.8	3005.0	25276	56.30	5.74E-05	34.39	38.42	41.11	43.81	55.72	55.75	55.85	12.60	15.36
F2.9	3015.6	25296	56.32	5.75E-05	34.41	38.46	41.15	43.89	55.74	55.77	55.82	12.46	15.36
F2.10	3305.0	25656	56.72	5.76E-05	34.15	36.11	41.47	46.21	38.38	49.54	54.85	11.96	15.36
F2.11	3319.9	25647	56.73	5.73E-05	34.13	36.15	41.60	46.30	38.18	49.42	54.73	11.84	15.30
F2.12	3324.6	25672	56.74	5.76E-05	34.24	36.17	41.59	46.30	38.27	49.28	54.67	11.82	15.30
F2.13	3560.4	27210	58.33	5.76E-05	34.44	36.04	42.07	47.12	39.37	50.93	56.68	11.64	15.17
F2.14	3567.0	27340	58.44	5.76E-05	34.36	35.87	41.99	47.12	39.21	50.53	56.55	11.45	15.13
F2.15	3561.0	27110	58.20	5.76E-05	34.47	36.12	42.11	47.19	39.37	50.57	56.27	11.52	15.13

Table E9.2: Experimental data for flooding tests (ctnd)

Run	Reflux Condenser Wall Temperatures									Dump Condenser			
	$T_{w,TS2t}$ (°C)	$T_{w,TS2m}$ (°C)	$T_{w,TS2b}$ (°C)	$T_{w,TS3t}$ (°C)	$T_{w,TS3m}$ (°C)	$T_{w,TS3b}$ (°C)	$T_{w,TS4t}$ (°C)	$T_{w,TS4m}$ (°C)	$T_{w,TS4b}$ (°C)	$\dot{V}_{c,D}$ (m³/s)	$T_{cD,in}$ (°C)	$T_{cD,out}$ (°C)	$T_{f,D}$ (°C)
F1.1	40.22	40.66	41.04	40.77	41.31	41.72	(N/A)	42.19	42.65	2.50E-05	14.40	24.06	14.92
F1.2	40.11	40.55	40.91	40.70	41.25	41.62	(N/A)	42.13	42.56	2.50E-05	13.92	23.81	14.76
F1.3	40.04	40.50	40.88	40.64	41.17	41.57	(N/A)	42.06	42.49	2.49E-05	13.67	23.54	14.52
F1.4	40.53	41.06	41.57	41.29	41.91	42.40	(N/A)	42.95	43.42	2.52E-05	14.54	26.72	16.13
F1.5	40.46	41.02	41.51	41.22	41.86	42.35	(N/A)	42.91	43.41	2.50E-05	14.50	26.67	16.08
F1.6	40.32	40.85	41.34	41.07	41.75	42.21	(N/A)	42.82	43.33	2.52E-05	14.54	26.64	16.05
F1.7	42.13	44.03	45.90	45.09	47.25	48.35	(N/A)	49.97	51.05	2.51E-05	14.76	28.57	33.10
F1.8	42.17	44.08	45.97	45.14	47.28	48.42	(N/A)	50.04	51.10	2.51E-05	14.53	28.55	33.09
F1.9	42.12	44.06	45.94	45.15	47.29	48.43	(N/A)	50.05	51.11	2.50E-05	14.45	28.51	33.01
F1.10	41.23	42.69	44.12	43.49	45.17	46.08	(N/A)	47.45	48.38	2.49E-05	14.93	25.78	28.74
F1.11	41.38	42.76	44.18	43.57	45.25	46.18	(N/A)	47.56	48.47	2.50E-05	14.64	25.79	29.07
F1.12	41.43	42.83	44.29	43.66	45.36	46.25	(N/A)	47.63	48.55	2.50E-05	14.51	25.73	28.75
F2.1	36.79	37.62	38.75	38.22	39.54	40.36	(N/A)	41.67	42.74	2.48E-05	14.22	14.26	15.74
F2.2	36.96	37.78	38.90	38.36	39.68	40.51	(N/A)	41.82	42.89	2.47E-05	14.40	14.34	15.88
F2.3	37.03	37.87	38.98	38.43	39.76	40.61	(N/A)	41.93	42.97	2.46E-05	14.60	14.49	15.96
F2.4	36.68	37.76	39.09	38.53	40.03	41.03	(N/A)	42.58	43.97	2.52E-05	13.89	16.09	14.44
F2.5	36.88	37.95	39.25	38.69	40.18	41.17	(N/A)	42.70	44.02	2.51E-05	14.23	16.12	14.43
F2.6	37.06	38.14	39.47	38.91	40.41	41.39	(N/A)	42.89	44.22	2.51E-05	14.80	16.55	14.42
F2.7	36.93	38.05	39.35	38.78	40.36	41.40	(N/A)	43.23	44.89	2.51E-05	14.41	16.91	14.57
F2.8	37.12	38.27	39.58	39.00	40.56	41.58	(N/A)	43.34	44.94	2.50E-05	14.35	16.92	14.55
F2.9	37.15	38.29	39.59	39.01	40.60	41.64	(N/A)	43.41	45.02	2.51E-05	14.32	16.85	14.57
F2.10	34.50	35.30	37.74	36.97	40.33	42.25	(N/A)	45.48	47.61	2.49E-05	14.34	14.26	27.57
F2.11	34.53	35.32	37.77	37.01	40.39	42.34	(N/A)	45.61	47.70	2.50E-05	14.31	14.33	27.51
F2.12	34.64	35.45	37.75	37.03	40.36	42.32	(N/A)	45.60	47.72	2.49E-05	14.49	14.46	27.61
F2.13	34.80	35.24	37.76	36.96	40.73	42.90	(N/A)	46.41	48.63	2.49E-05	14.59	14.70	30.47
F2.14	34.70	35.05	37.53	36.83	40.65	42.83	(N/A)	46.36	48.64	2.50E-05	14.62	14.71	30.10
F2.15	34.82	35.22	37.76	37.07	40.75	42.91	(N/A)	46.48	48.70	2.48E-05	14.59	14.68	30.45

Table E9.3: Experimental data for flooding tests (ctnd)

Run	Boiler			Reflux Condenser Coolant					Reflux Condenser Vapour			Extraction Air	
	Q_i (W)	$P_{v,i}$ (Pa)	$T_{vR,i}$ (°C)	$\dot{V}_{c,R}$ (m³/s)	$T_{cR,i}$ (°C)	$T_{cR,TS3}$ (°C)	$T_{cR,TS4}$ (°C)	$T_{cR,i}$ (°C)	$T_{vR,oTS2}$ (°C)	$T_{vR,oTS3}$ (°C)	$T_{vR,oTS3}$ (°C)	T_{Ai} (°C)	T_{Ao} (°C)
F3.1	3052.1	24220	55.12	5.75E-05	39.15	42.18	44.26	46.23	54.58	54.64	54.72	9.30	13.53
F3.2	3047.0	24238	55.13	5.76E-05	39.21	42.19	44.29	46.25	54.60	54.67	54.77	9.52	13.55
F3.3	3047.7	24269	55.17	5.76E-05	39.35	42.33	44.39	46.31	54.64	54.70	54.83	9.43	13.57
F3.4	3066.9	24291	55.25	5.76E-05	38.39	41.45	45.64	48.79	52.28	52.43	53.98	9.43	13.62
F3.5	3070.8	24386	55.36	5.76E-05	38.13	41.44	45.63	48.81	51.96	52.38	54.00	9.37	13.60
F3.6	3073.2	24367	55.35	5.78E-05	38.07	41.71	45.76	48.90	50.71	52.23	53.96	9.48	13.61
F3.7	3236.1	26953	58.02	5.74E-05	39.15	42.71	45.16	47.54	57.47	57.53	57.66	12.56	15.71
F3.8	3236.7	26988	58.04	5.74E-05	39.20	42.76	45.21	47.55	57.55	57.57	57.70	12.39	15.66
F3.9	3237.3	27152	58.21	5.74E-05	39.37	42.96	45.36	47.70	57.70	57.78	57.86	12.22	15.65
F3.10	3468.1	30066	61.13	5.75E-05	39.28	42.43	47.80	52.04	47.20	56.90	59.65	13.44	17.62
F3.11	3456.5	29928	61.01	5.76E-05	39.27	42.64	47.94	52.09	47.21	56.93	59.43	13.42	17.60
F3.12	3455.9	29902	60.99	5.76E-05	39.20	42.36	47.72	51.97	46.90	56.53	59.59	13.56	17.60
F3.13	3807.7	33338	64.00	5.78E-05	39.38	41.15	47.93	53.04	45.20	57.60	62.61	13.90	17.92
F3.14	3801.5	33328	63.96	5.76E-05	39.43	41.70	48.29	53.23	45.95	58.61	62.71	13.94	17.93
F3.15	3805.7	33333	64.00	5.75E-05	39.45	41.46	48.24	53.33	45.47	57.93	62.68	13.83	17.96
F3.16	4210.5	25457	56.47	5.80E-05	39.36	44.39	48.31	50.91	52.97	54.65	55.59	12.93	16.78
F3.17	4202.8	25452	56.45	5.77E-05	39.33	44.40	48.31	50.92	52.99	54.69	55.53	12.91	16.80
F3.18	4207.6	25481	56.49	5.77E-05	39.25	44.35	48.26	50.90	53.11	54.75	55.52	12.79	16.87
F3.19	4534.6	26385	57.43	5.78E-05	39.08	44.69	48.85	51.62	54.25	55.77	56.61	13.34	17.25
F3.20	4548.9	26438	57.49	5.77E-05	39.13	44.67	48.85	51.63	54.22	55.76	56.66	13.20	17.23
F3.21	4536.1	26587	57.65	5.79E-05	39.42	44.93	49.04	51.82	54.41	55.98	56.81	13.14	17.27
F3.22	4839.8	27588	58.65	5.78E-05	39.46	45.42	49.78	52.64	55.62	57.02	57.80	13.05	17.43
F3.23	4840.5	27720	58.77	5.75E-05	39.31	45.37	49.78	52.71	55.75	57.23	58.05	13.34	17.58
F3.24	4829.8	27668	58.72	5.76E-05	39.11	45.23	49.65	52.63	55.53	57.15	57.94	13.41	17.61

Table E9.4: Experimental data for flooding tests (ctnd)

	Reflux Condenser Wall Temperatures									Dump Condenser			
Run	$T_{w,TS2t}$ (°C)	$T_{w,TS2m}$ (°C)	$T_{w,TS2b}$ (°C)	$T_{w,TS3t}$ (°C)	$T_{w,TS3m}$ (°C)	$T_{w,TS3b}$ (°C)	$T_{w,TS4t}$ (°C)	$T_{w,TS4m}$ (°C)	$T_{w,TS4b}$ (°C)	$\dot{V}_{c,D}$ (m³/s)	$T_{cD,in}$ (°C)	$T_{cD,out}$ (°C)	$T_{f,D}$ (°C)
F3.1	41.05	41.93	43.18	42.73	43.94	44.78	(N/A)	46.02	47.09	2.50E-05	14.80	23.18	14.76
F3.2	41.11	42.00	43.23	42.77	43.98	44.83	(N/A)	46.06	47.12	2.50E-05	14.74	23.14	14.79
F3.3	41.21	42.12	43.35	42.90	44.10	44.92	(N/A)	46.11	47.18	2.50E-05	14.55	23.09	14.79
F3.4	40.06	40.88	42.94	42.27	44.82	46.33	(N/A)	48.51	49.83	2.48E-05	14.72	15.07	14.60
F3.5	39.75	40.71	43.08	42.30	44.87	46.31	(N/A)	48.52	49.88	2.48E-05	14.66	14.95	14.90
F3.6	39.49	40.98	43.34	42.52	44.98	46.46	(N/A)	48.60	49.93	2.48E-05	14.58	14.76	15.53
F3.7	41.49	42.57	43.73	43.24	44.66	45.60	(N/A)	47.12	48.52	2.50E-05	14.53	21.83	14.70
F3.8	41.53	42.58	43.79	43.31	44.69	45.62	(N/A)	47.16	48.54	2.50E-05	14.55	21.83	14.70
F3.9	41.72	42.80	43.96	43.49	44.90	45.80	(N/A)	47.31	48.72	2.51E-05	14.47	21.74	14.70
F3.10	39.89	41.60	44.29	43.31	46.59	48.44	(N/A)	51.40	53.25	2.48E-05	14.51	14.71	29.09
F3.11	39.88	41.71	44.53	43.53	46.71	48.54	(N/A)	51.50	53.36	2.48E-05	14.52	14.62	28.74
F3.12	39.80	41.54	44.21	43.25	46.51	48.33	(N/A)	51.29	53.22	2.48E-05	14.25	14.59	28.42
F3.13	39.77	40.18	43.04	42.18	46.40	48.65	(N/A)	52.28	54.52	2.47E-05	14.33	14.46	31.57
F3.14	39.85	40.52	43.72	42.68	46.82	49.00	(N/A)	52.47	54.68	2.48E-05	14.57	14.64	30.34
F3.15	39.86	40.34	43.34	42.45	46.67	48.92	(N/A)	52.53	54.73	2.48E-05	14.86	14.84	29.93
F3.16	42.02	43.96	46.00	45.16	47.55	48.80	(N/A)	50.57	51.78	2.52E-05	14.58	22.27	32.44
F3.17	41.98	43.89	45.99	45.15	47.53	48.81	(N/A)	50.59	51.78	2.51E-05	14.55	22.29	31.61
F3.18	41.94	43.87	45.93	45.09	47.48	48.78	(N/A)	50.56	51.76	2.50E-05	14.40	22.14	32.15
F3.19	42.02	44.12	46.37	45.45	48.02	49.36	(N/A)	51.27	52.47	2.51E-05	14.38	22.89	32.72
F3.20	42.06	44.16	46.36	45.46	48.01	49.35	(N/A)	51.24	52.51	2.51E-05	14.42	22.88	32.23
F3.21	42.31	44.41	46.62	45.69	48.23	49.55	(N/A)	51.46	52.66	2.50E-05	14.73	23.05	31.64
F3.22	42.51	44.81	47.20	46.26	48.88	50.26	(N/A)	52.24	53.56	2.51E-05	14.45	24.01	32.73
F3.23	42.45	44.73	47.15	46.21	48.91	50.30	(N/A)	52.31	53.62	2.51E-05	14.25	24.16	33.82
F3.24	42.29	44.55	46.98	46.06	48.79	50.19	(N/A)	52.20	53.50	2.52E-05	13.70	23.67	32.21

Table E9.5: Experimental data for flooding tests (ctnd)

Run	Boiler			Reflux Condenser Coolant					Reflux Condenser Vapour			Extraction Air	
	Q_i (W)	$P_{v,i}$ (Pa)	$T_{vR,i}$ (°C)	$\dot{V}_{c,R}$ (m³/s)	$T_{cR,i}$ (°C)	$T_{cR,TS3}$ (°C)	$T_{cR,TS4}$ (°C)	$T_{cR,i}$ (°C)	$T_{vR,oTS2}$ (°C)	$T_{vR,oTS3}$ (°C)	$T_{vR,oTS3}$ (°C)	T_{Ai} (°C)	T_{Ao} (°C)
F4.1	1978.8	23268	54.21	6.10E-05	39.56	42.97	44.93	46.07	54.19	54.30	54.33	18.12	20.12
F4.2	1976.3	23288	54.24	6.11E-05	39.49	42.90	44.93	46.05	54.22	54.33	54.36	18.26	20.23
F4.3	1979.0	23286	54.24	6.10E-05	39.38	42.86	44.85	46.01	54.18	54.37	54.33	18.16	20.25
F4.4	2119.9	23145	54.09	6.15E-05	39.29	42.75	44.70	45.81	54.14	54.28	54.24	16.71	19.09
F4.5	2116.9	23061	54.00	6.15E-05	39.24	42.68	44.66	45.75	54.03	54.18	54.15	16.43	19.01
F4.6	2119.3	23103	54.05	6.12E-05	39.29	42.74	44.68	45.77	54.11	54.21	54.22	16.57	19.02
F4.7	2450.0	26996	58.22	6.12E-05	39.54	43.60	46.00	47.63	58.22	58.33	58.34	18.44	20.80
F4.8	2454.4	27034	58.26	6.13E-05	39.52	43.58	46.02	47.63	58.25	58.39	58.35	18.41	20.85
F4.9	2453.1	27058	58.28	6.14E-05	39.42	43.51	45.97	47.61	58.26	58.40	58.38	18.37	20.85
F4.10	2890.9	30522	61.58	6.14E-05	39.30	43.89	46.73	48.93	61.49	61.64	61.59	18.48	21.09
F4.11	2897.9	30565	61.62	6.12E-05	39.23	43.84	46.68	48.89	61.54	61.68	61.64	18.41	21.09
F4.12	2902.4	30610	61.66	6.14E-05	39.32	43.90	46.77	48.94	61.59	61.71	61.68	18.38	21.11
F4.13	3096.1	31466	62.41	6.13E-05	39.11	43.92	46.93	49.27	62.39	62.50	62.50	14.58	18.17
F4.14	3098.8	31514	62.45	6.14E-05	39.19	44.03	46.98	49.30	62.42	62.57	62.52	14.57	18.15
F4.15	3101.6	31574	62.51	6.13E-05	39.26	44.12	46.99	49.34	62.48	62.63	62.55	14.53	18.12
F4.16	3385.8	27335	58.57	6.14E-05	39.26	42.87	47.60	50.71	47.58	56.21	57.89	16.85	20.07
F4.17	3392.2	27435	58.62	6.16E-05	39.33	42.94	47.73	50.78	47.45	55.87	57.95	16.87	20.05
F4.18	3401.2	27514	58.74	6.16E-05	39.46	42.99	47.69	50.79	47.60	56.35	58.10	16.95	20.12
F4.19	3547.9	30656	61.70	6.14E-05	39.14	41.04	47.13	51.40	38.96	56.68	60.99	14.15	18.18
F4.20	3546.2	30594	61.66	6.16E-05	39.11	41.02	47.13	51.35	38.81	56.45	60.92	14.15	18.17
F4.21	3547.3	30640	61.68	6.16E-05	39.18	41.05	47.09	51.31	38.78	56.25	60.90	14.35	18.20
F4.22	3583.1	31745	62.68	6.17E-05	39.24	40.62	46.90	51.62	39.46	56.21	61.92	18.44	21.44
F4.23	3588.0	31687	62.64	6.14E-05	39.16	40.58	46.90	51.57	39.26	56.49	62.02	18.41	21.45
F4.24	3588.8	31743	62.65	6.14E-05	39.16	40.48	46.80	51.54	39.06	56.06	61.85	18.42	21.46
F4.25	4019.4	39006	68.55	6.18E-05	39.38	40.02	45.62	52.54	42.53	50.08	67.52	13.79	18.18
F4.26	4013.5	39306	68.74	6.17E-05	39.50	40.14	45.53	52.66	42.45	50.07	67.56	13.82	18.17
F4.27	4029.6	39714	69.07	6.18E-05	39.37	40.02	45.37	52.64	42.38	50.00	67.88	14.21	18.20
F4.28	4099.3	43200	71.55	6.18E-05	39.30	39.90	44.19	52.77	42.22	48.71	69.69	18.31	21.68
F4.29	4101.5	43539	71.74	6.18E-05	39.04	39.64	43.86	52.58	41.98	48.59	69.45	18.30	21.71
F4.30	4101.2	43897	72.01	6.18E-05	38.99	39.55	43.41	52.38	41.70	47.86	69.66	18.28	21.71

Table E9.6: Experimental data for flooding tests (ctnd)

	Reflux Condenser Wall Temperatures									Dump Condenser			
Run	$T_{w,TS2t}$ (°C)	$T_{w,TS2m}$ (°C)	$T_{w,TS2b}$ (°C)	$T_{w,TS3t}$ (°C)	$T_{w,TS3m}$ (°C)	$T_{w,TS3b}$ (°C)	$T_{w,TS4t}$ (°C)	$T_{w,TS4m}$ (°C)	$T_{w,TS4b}$ (°C)	$\dot{V}_{c,D}$ (m³/s)	$T_{cD,in}$ (°C)	$T_{cD,out}$ (°C)	$T_{f,D}$ (°C)
F4.1	42.06	42.49	43.41	43.00	44.07	44.90	45.35	45.91	46.57	1.81E-05	14.09	14.56	17.76
F4.2	42.04	42.47	43.41	42.95	44.05	44.86	45.36	45.87	46.54	1.83E-05	13.61	14.11	17.85
F4.3	42.01	42.34	43.32	42.86	44.03	44.83	45.27	45.82	46.46	1.82E-05	13.47	13.83	17.92
F4.4	41.83	42.17	43.25	42.82	43.92	44.76	45.21	45.79	46.40	1.85E-05	13.77	14.70	14.97
F4.5	41.79	42.10	43.20	42.76	43.88	44.71	45.13	45.73	46.30	1.82E-05	14.51	15.01	14.99
F4.6	41.82	42.17	43.27	42.80	43.91	44.73	45.20	45.74	46.35	1.84E-05	13.97	14.90	14.98
F4.7	42.44	43.04	44.24	43.72	45.09	46.08	46.64	47.39	48.27	1.82E-05	14.29	14.37	18.79
F4.8	42.43	43.03	44.24	43.72	45.09	46.07	46.66	47.37	48.25	1.82E-05	13.80	14.45	18.84
F4.9	42.36	42.95	44.17	43.66	45.04	46.03	46.62	47.34	48.22	1.84E-05	13.48	14.00	18.87
F4.10	42.50	43.26	44.64	44.07	45.68	46.85	47.57	48.49	49.66	1.83E-05	13.72	13.92	18.08
F4.11	42.47	43.21	44.60	44.02	45.64	46.80	47.56	48.44	49.63	1.81E-05	14.74	14.66	18.07
F4.12	42.53	43.29	44.69	44.09	45.73	46.88	47.61	48.51	49.68	1.82E-05	13.36	14.30	18.09
F4.13	42.44	43.24	44.75	44.11	45.81	47.06	47.85	48.83	50.20	1.83E-05	13.38	14.09	15.89
F4.14	42.49	43.29	44.80	44.20	45.88	47.12	47.91	48.91	50.27	1.82E-05	14.27	13.96	15.78
F4.15	42.60	43.33	44.83	44.28	45.90	47.19	47.96	48.98	50.32	1.82E-05	14.68	14.76	15.65
F4.16	40.40	41.62	44.16	43.30	46.17	47.99	49.01	50.35	51.70	1.84E-05	13.80	14.06	27.81
F4.17	40.46	41.56	44.22	43.37	46.26	48.11	49.12	50.43	51.77	1.84E-05	14.02	14.20	28.25
F4.18	40.59	41.71	44.29	43.39	46.25	48.11	49.13	50.47	51.81	1.85E-05	14.24	14.37	28.13
F4.19	39.70	39.92	42.25	41.54	45.35	47.71	49.12	50.77	52.58	1.79E-05	14.86	13.88	28.91
F4.20	39.66	39.80	42.14	41.51	45.35	47.73	49.05	50.80	52.56	1.81E-05	14.18	14.70	28.93
F4.21	39.73	39.92	42.12	41.52	45.34	47.67	49.07	50.72	52.56	1.81E-05	13.80	14.25	29.07
F4.22	39.81	39.79	41.46	41.04	45.03	47.57	49.08	50.89	52.84	1.81E-05	13.50	13.98	28.55
F4.23	39.70	39.77	41.50	41.04	44.99	47.54	49.07	50.90	52.80	1.82E-05	14.26	14.18	28.71
F4.24	39.73	39.70	41.30	40.91	44.92	47.49	48.99	50.86	52.78	1.83E-05	14.46	14.51	29.59
F4.25	40.01	39.75	39.93	39.81	42.75	46.75	49.00	51.63	54.35	1.81E-05	14.06	14.23	31.67
F4.26	40.11	39.86	40.06	39.92	42.45	46.67	48.98	51.67	54.46	1.81E-05	14.10	14.36	31.98
F4.27	40.00	39.74	39.93	39.83	42.31	46.55	48.85	51.59	54.47	1.81E-05	13.79	14.10	31.62
F4.28	39.92	39.71	39.79	39.71	40.82	45.45	48.22	51.51	54.89	1.82E-05	13.85	14.27	34.15
F4.29	39.67	39.44	39.53	39.46	40.54	45.22	47.94	51.32	54.73	1.82E-05	13.59	14.30	33.85
F4.30	39.64	39.37	39.42	39.33	40.07	44.65	47.58	51.10	54.56	1.81E-05	14.55	14.42	34.72

Table E10.1: Heat and mass balances for flooding tests

	Heat balance					Mass Balance				Condensate Heat Flux	Saturation Temperature	
Run	$\dot{Q}_R$ (W)	$\dot{Q}_D$ (W)	$\dot{Q}_{A,Ex}$ (W)	$\dot{Q}_o$ (W)	$R_{\dot{Q}}$ (W/W)	$\overline{T}_f$ (°C)	$\dot{m}_{f,o}$ (kg/s)	$\dot{m}_{v,o}$ (kg/s)	$\dot{m}_{v,i}$ (kg/s)	$\dot{q}_f$ (m/s)	$T^*_{v,in}$ (°C)	$\Delta T^*_{v,in}$ (°C)
F1.1	708.3	1001.6	322.1	2032.0	1.032	42.73	0.00237	0.00280	0.00517	3323.6	46.17	-0.95
F1.2	722.5	1026.4	316.0	2064.9	1.050	42.65	0.00242	0.00287	0.00528	3390.1	46.13	-0.95
F1.3	716.6	1020.1	321.1	2057.8	1.047	42.59	0.00240	0.00285	0.00524	3362.6	46.06	-0.94
F1.4	850.7	1271.8	300.1	2422.6	0.963	43.60	0.00284	0.00356	0.00640	3991.6	47.60	-0.96
F1.5	861.3	1261.9	303.1	2426.2	0.963	43.58	0.00287	0.00353	0.00640	4041.2	47.62	-0.95
F1.6	885.9	1262.6	307.6	2456.2	0.975	43.49	0.00295	0.00353	0.00648	4157.0	47.61	-0.95
F1.7	2580.1	1437.4	421.4	4439.0	0.958	49.93	0.00857	0.00431	0.01288	12106.7	56.16	-0.81
F1.8	2581.5	1459.0	438.5	4479.0	0.967	49.99	0.00857	0.00437	0.01295	12113.0	56.21	-0.81
F1.9	2591.0	1456.7	419.1	4466.8	0.965	49.99	0.00860	0.00437	0.01297	12157.4	56.22	-0.81
F1.10	1976.2	1120.0	403.7	3500.0	0.960	47.48	0.00658	0.00334	0.00991	9273.0	52.81	-0.85
F1.11	1972.9	1157.2	404.8	3534.9	0.968	47.56	0.00657	0.00345	0.01002	9257.2	52.87	-0.84
F1.12	1975.4	1164.5	422.2	3562.1	0.974	47.64	0.00658	0.00346	0.01004	9269.2	52.93	-0.84
F2.1	1811.6	-4.9	281.9	2088.6	0.960	44.43	0.00584	-0.00001	0.00583	8500.4	54.32	-0.84
F2.2	1811.6	-15.2	270.2	2066.7	0.950	44.54	0.00585	-0.00004	0.00581	8500.5	54.37	-0.84
F2.3	1811.1	-20.5	258.6	2049.2	0.944	44.62	0.00585	-0.00006	0.00579	8498.2	54.42	-0.84
F2.4	2140.6	223.0	286.4	2650.1	0.943	45.42	0.00688	0.00059	0.00748	10044.4	56.12	-0.82
F2.5	2100.5	188.9	253.3	2542.7	0.904	45.52	0.00676	0.00050	0.00726	9856.1	56.14	-0.82
F2.6	2101.3	173.8	269.5	2544.7	0.905	45.71	0.00676	0.00046	0.00722	9859.8	56.30	-0.82
F2.7	2282.7	253.3	291.9	2827.9	0.936	46.05	0.00733	0.00067	0.00800	10711.1	57.06	-0.80
F2.8	2244.4	258.8	276.2	2779.5	0.925	46.17	0.00721	0.00069	0.00790	10531.5	57.09	-0.79
F2.9	2261.1	256.6	290.3	2808.0	0.931	46.20	0.00727	0.00068	0.00795	10609.8	57.11	-0.79
F2.10	2882.5	-16.8	340.6	3206.3	0.970	46.18	0.00924	-0.00005	0.00919	13525.6	57.48	-0.76
F2.11	2891.8	-7.2	348.0	3232.6	0.974	46.23	0.00927	-0.00002	0.00925	13568.8	57.47	-0.74
F2.12	2878.3	-11.7	349.6	3216.2	0.967	46.24	0.00923	-0.00004	0.00919	13505.6	57.50	-0.76
F2.13	3025.4	1.6	354.9	3381.9	0.950	47.04	0.00967	0.00001	0.00967	14195.7	59.05	-0.72
F2.14	3049.2	-0.4	369.9	3418.7	0.958	47.01	0.00974	0.00000	0.00973	14307.8	59.18	-0.74
F2.15	3041.0	0.4	362.3	3403.7	0.956	47.02	0.00972	0.00000	0.00972	14268.9	58.95	-0.75

Table E10.2: Heat and mass balances for flooding tests (ctnd)

	Heat balance					Mass Balance				Condensate Heat Flux	Saturation Temperature	
Run	$\dot{Q}_R$ (W)	$\dot{Q}_D$ (W)	$\dot{Q}_{A,Ex}$ (W)	$\dot{Q}_o$ (W)	$R_{\dot{Q}}$ (W/W)	$\overline{T}_f$ (°C)	$\dot{m}_{f,o}$ (kg/s)	$\dot{m}_{v,o}$ (kg/s)	$\dot{m}_{v,i}$ (kg/s)	$\dot{q}_f$ (m/s)	$T^*_{v,in}$ (°C)	$\Delta T^*_{v,in}$ (°C)
F3.1	1684.8	867.1	427.5	2979.4	0.976	47.87	0.00552	0.00231	0.00783	7905.3	55.97	-0.85
F3.2	1680.5	868.8	407.3	2956.6	0.970	47.91	0.00551	0.00232	0.00782	7885.1	55.98	-0.85
F3.3	1660.2	883.8	418.8	2962.8	0.972	47.98	0.00544	0.00236	0.00780	7790.3	56.02	-0.85
F3.4	2479.7	27.1	423.4	2930.2	0.955	48.47	0.00815	0.00007	0.00822	11635.5	56.04	-0.79
F3.5	2545.7	21.3	427.1	2994.1	0.975	48.50	0.00836	0.00006	0.00842	11944.9	56.14	-0.78
F3.6	2591.4	9.0	417.4	3017.7	0.982	48.56	0.00852	0.00002	0.00854	12159.4	56.12	-0.78
F3.7	1993.0	752.3	314.9	3060.2	0.946	49.41	0.00649	0.00198	0.00847	9351.6	58.80	-0.78
F3.8	1985.5	751.2	328.3	3065.0	0.947	49.44	0.00647	0.00197	0.00844	9316.3	58.83	-0.79
F3.9	1980.0	754.4	343.4	3077.8	0.951	49.62	0.00645	0.00198	0.00843	9290.5	58.99	-0.78
F3.10	3035.3	10.9	417.2	3463.4	0.999	51.66	0.00986	0.00003	0.00990	14242.3	61.75	-0.63
F3.11	3056.5	2.1	416.6	3475.3	1.005	51.70	0.00994	0.00001	0.00995	14341.9	61.63	-0.62
F3.12	3045.6	25.9	402.9	3474.4	1.005	51.57	0.00990	0.00008	0.00998	14290.6	61.60	-0.62
F3.13	3264.4	4.7	400.2	3669.2	0.964	52.59	0.01050	0.00001	0.01051	15317.2	64.60	-0.61
F3.14	3290.6	-1.6	397.1	3686.1	0.970	52.79	0.01060	0.00000	0.01060	15440.3	64.59	-0.63
F3.15	3299.9	-11.3	410.7	3699.3	0.972	52.74	0.01062	-0.00003	0.01059	15483.8	64.60	-0.60
F3.16	2770.0	799.4	385.0	3954.4	0.939	50.51	0.00918	0.00239	0.01156	12997.4	57.28	-0.81
F3.17	2767.0	803.6	388.7	3959.3	0.942	50.50	0.00917	0.00239	0.01155	12983.7	57.27	-0.82
F3.18	2782.6	799.6	406.8	3989.0	0.948	50.49	0.00922	0.00238	0.01160	13056.8	57.30	-0.81
F3.19	3001.1	882.8	389.9	4273.8	0.942	51.13	0.00993	0.00262	0.01255	14082.1	58.23	-0.79
F3.20	2985.3	877.7	402.5	4265.5	0.938	51.16	0.00988	0.00260	0.01247	14007.6	58.28	-0.79
F3.21	2970.8	860.2	412.2	4243.2	0.935	51.35	0.00983	0.00253	0.01237	13939.8	58.43	-0.78
F3.22	3150.0	993.3	436.6	4579.9	0.946	52.11	0.01042	0.00293	0.01335	14780.8	59.42	-0.77
F3.23	3189.7	1031.9	423.3	4644.9	0.960	52.15	0.01055	0.00306	0.01361	14966.7	59.55	-0.78
F3.24	3222.2	1038.8	419.1	4680.1	0.969	52.04	0.01065	0.00305	0.01371	15119.5	59.50	-0.78

Table E10.3: Heat and mass balances for flooding tests (ctnd)

	Heat balance					Mass Balance				Cond Heat Flux	Saturation Temp	
Run	$\dot{Q}_R$ (W)	$\dot{Q}_D$ (W)	$\dot{Q}_{A,Ex}$ (W)	$\dot{Q}_o$ (W)	$R_{\dot{Q}}$ (W/W)	$\overline{T}_f$ (°C)	$\dot{m}_{f,o}$ (kg/s)	$\dot{m}_{v,o}$ (kg/s)	$\dot{m}_{v,i}$ (kg/s)	$\dot{q}_f$ (m/s)	$T^*_{v,in}$ (°C)	$\Delta T^*_{v,in}$ (°C)
F4.1	1647.7	28.7	197.5	1873.9	0.947	44.37	0.00529	0.00008	0.00537	7731.3	54.92	-0.71
F4.2	1660.5	32.0	193.9	1886.4	0.955	44.38	0.00533	0.00009	0.00542	7791.5	54.94	-0.70
F4.3	1673.9	20.4	206.3	1900.6	0.960	44.35	0.00537	0.00006	0.00543	7854.5	54.94	-0.70
F4.4	1660.0	65.6	234.4	1960.0	0.925	44.10	0.00532	0.00018	0.00550	7789.0	54.78	-0.69
F4.5	1657.4	31.9	255.7	1945.1	0.919	44.01	0.00532	0.00009	0.00540	7777.0	54.69	-0.69
F4.6	1643.1	64.8	242.3	1950.3	0.920	44.06	0.00527	0.00017	0.00544	7710.1	54.73	-0.68
F4.7	2052.7	-0.6	232.2	2284.3	0.932	46.39	0.00653	0.00000	0.00653	9631.9	58.84	-0.62
F4.8	2059.5	42.5	239.2	2341.2	0.954	46.41	0.00655	0.00011	0.00667	9663.6	58.88	-0.62
F4.9	2079.8	33.5	244.1	2357.3	0.961	46.39	0.00662	0.00009	0.00671	9758.7	58.90	-0.62
F4.10	2446.9	8.5	256.0	2711.4	0.938	47.95	0.00772	0.00002	0.00774	11481.4	62.16	-0.58
F4.11	2451.1	-12.6	262.5	2701.0	0.932	47.95	0.00773	-0.00003	0.00770	11501.2	62.20	-0.58
F4.12	2443.6	64.9	268.0	2776.5	0.957	48.01	0.00771	0.00017	0.00788	11465.9	62.24	-0.58
F4.13	2577.0	47.9	356.7	2981.6	0.963	47.91	0.00809	0.00012	0.00822	12091.9	63.00	-0.59
F4.14	2570.6	-29.8	355.5	2896.3	0.935	47.96	0.00807	-0.00008	0.00800	12061.9	63.04	-0.59
F4.15	2559.9	-0.6	356.4	2915.7	0.940	48.00	0.00804	0.00000	0.00804	12011.5	63.10	-0.59
F4.16	2907.8	13.3	317.9	3239.0	0.957	46.87	0.00927	0.00004	0.00931	13644.2	59.17	-0.60
F4.17	2917.3	7.6	313.3	3238.2	0.955	46.92	0.00930	0.00002	0.00932	13688.6	59.27	-0.65
F4.18	2886.3	3.1	311.9	3201.3	0.941	46.98	0.00920	0.00001	0.00921	13543.2	59.35	-0.61
F4.19	3114.9	-80.2	401.4	3436.1	0.968	47.40	0.00979	-0.00025	0.00953	14615.8	62.28	-0.58
F4.20	3121.4	32.4	399.8	3553.6	1.002	47.37	0.00981	0.00010	0.00991	14646.3	62.23	-0.57
F4.21	3092.0	27.8	382.7	3502.5	0.987	47.37	0.00971	0.00009	0.00980	14508.2	62.27	-0.59
F4.22	3161.0	30.0	294.6	3485.6	0.973	48.12	0.00992	0.00009	0.01002	14832.0	63.24	-0.56
F4.23	3153.7	-12.6	298.4	3439.5	0.959	48.09	0.00990	-0.00004	0.00986	14798.1	63.19	-0.56
F4.24	3147.4	-2.6	298.5	3443.3	0.959	48.07	0.00988	-0.00001	0.00987	14768.4	63.24	-0.60
F4.25	3362.4	5.9	436.9	3805.2	0.947	49.54	0.01031	0.00002	0.01033	15777.0	69.05	-0.50
F4.26	3356.6	13.6	432.0	3802.1	0.947	49.62	0.01028	0.00004	0.01033	15749.8	69.27	-0.52
F4.27	3395.1	16.8	396.2	3808.1	0.945	49.69	0.01039	0.00005	0.01044	15930.7	69.56	-0.49
F4.28	3443.0	25.9	331.0	3799.9	0.927	50.86	0.01047	0.00008	0.01055	16155.5	72.01	-0.46
F4.29	3464.6	47.3	334.8	3846.6	0.938	50.82	0.01052	0.00015	0.01067	16256.6	72.24	-0.50
F4.30	3419.8	-16.9	337.3	3740.2	0.912	50.79	0.01037	-0.00005	0.01031	16046.5	72.48	-0.47

Table E11.1: Flooding analysis results for flooding tests

	Extra Data		Pressure Drop	Tube End Conditions			Vapour Velocities				Conclusion
Run	Visual Obs	$P_{v,o}$ (Pa)	ΔP_R (Pa)	$Re_{f,o}$ (-)	$\mathrm{Pr}_{f,o}$ (-)	$Re_{v,i}$ (-)	$u_{v,exp}$ (m/s)	$u_{v,Eng}$ (m/s)	$u_{v,DK}$ (m/s)	$u_{v,MA}$ (m/s)	Tube Flooded
F1.1	1	N/A	N/A	172	8.77	17192	4.50	7.10	7.08	9.19	No
F1.2	1	N/A	N/A	175	8.77	17586	4.61	7.10	7.09	9.15	No
F1.3	1	N/A	N/A	174	8.78	17454	4.58	7.11	7.10	9.18	No
F1.4	2	N/A	N/A	208	8.72	21371	5.28	6.92	6.92	8.58	No
F1.5	2	N/A	N/A	211	8.72	21321	5.28	6.92	6.89	8.55	No
F1.6	2	N/A	N/A	217	8.73	21499	5.35	6.91	6.87	8.50	No
F1.7	5	N/A	N/A	672	8.41	27970	6.75	6.12	5.60	6.43	Yes
F1.8	5	N/A	N/A	673	8.41	28424	6.80	6.12	5.61	6.43	Yes
F1.9	5	N/A	N/A	675	8.41	28498	6.80	6.11	5.60	6.42	Yes
F1.10	10	N/A	N/A	503	8.53	35912	7.76	5.76	5.21	5.69	Yes
F1.11	10	N/A	N/A	503	8.52	36180	7.79	5.76	5.21	5.68	Yes
F1.12	10	N/A	N/A	504	8.52	36206	7.80	5.75	5.21	5.67	Yes
F2.1	2	N/A	N/A	433	8.68	12226	3.76	5.76	4.89	6.39	No
F2.2	2	N/A	N/A	433	8.67	12114	3.73	5.76	4.88	6.39	No
F2.3	2	N/A	N/A	434	8.67	12052	3.72	5.75	4.87	6.38	No
F2.4	3	N/A	N/A	515	8.63	16541	4.42	5.60	4.81	5.97	No
F2.5	3	N/A	N/A	506	8.62	17936	4.87	5.67	4.79	5.87	No
F2.6	3	N/A	N/A	508	8.61	17431	4.73	5.64	4.77	5.88	No
F2.7	5	N/A	N/A	552	8.60	18065	4.67	5.52	4.72	5.77	No
F2.8	5	N/A	N/A	544	8.59	17876	4.60	5.52	4.72	5.79	No
F2.9	5	N/A	N/A	548	8.59	17964	4.63	5.52	4.72	5.78	No
F2.10	7	N/A	N/A	697	8.59	19002	5.28	5.44	4.57	5.44	Yes
F2.11	7	N/A	N/A	700	8.59	19194	5.32	5.45	4.58	5.43	Yes
F2.12	7	N/A	N/A	697	8.59	19046	5.28	5.44	4.57	5.44	Yes
F2.13	8	N/A	N/A	736	8.55	20029	5.26	5.30	4.44	5.23	Yes
F2.14	8	N/A	N/A	741	8.55	20136	5.27	5.28	4.42	5.21	Yes
F2.15	8	N/A	N/A	740	8.55	20137	5.31	5.31	4.45	5.23	Yes

Table E11.2: Flooding analysis results for flooding tests (ctnd)

	Extra Data		Pressure Drop	Tube End Conditions			Vapour Velocities				Conclusion
Run	Visual Obs	$P_{v,o}$ (Pa)	ΔP_R (Pa)	$Re_{f,o}$ (-)	$\mathrm{Pr}_{f,o}$ (-)	$Re_{v,i}$ (-)	$u_{v,exp}$ (m/s)	$u_{v,Eng}$ (m/s)	$u_{v,DK}$ (m/s)	$u_{v,MA}$ (m/s)	Tube Flooded
F3.1	3	N/A	N/A	424	8.51	21199	4.75	5.75	5.16	6.28	No
F3.2	3	N/A	N/A	423	8.51	21190	4.74	5.74	5.16	6.28	No
F3.3	3	N/A	N/A	418	8.50	21218	4.72	5.74	5.17	6.29	No
F3.4	5	N/A	N/A	630	8.48	17339	4.98	5.61	4.73	5.76	No
F3.5	5	N/A	N/A	646	8.48	17713	5.08	5.59	4.72	5.71	No
F3.6	5	N/A	N/A	659	8.47	17899	5.16	5.60	4.72	5.69	No
F3.7	5	N/A	N/A	506	8.43	21634	4.65	5.43	4.77	5.74	No
F3.8	5	N/A	N/A	505	8.43	21568	4.63	5.43	4.76	5.74	No
F3.9	5	N/A	N/A	504	8.43	21552	4.60	5.41	4.75	5.73	No
F3.10	6	N/A	N/A	787	8.33	20371	4.91	5.07	4.20	4.96	Yes
F3.11	6	N/A	N/A	794	8.33	20431	4.95	5.08	4.21	4.96	Yes
F3.12	6	N/A	N/A	789	8.34	20636	4.97	5.08	4.22	4.97	Yes
F3.13	7	N/A	N/A	846	8.29	21408	4.74	4.83	3.97	4.64	Yes
F3.14	7	N/A	N/A	856	8.28	21539	4.77	4.83	3.97	4.63	Yes
F3.15	7	N/A	N/A	857	8.28	21465	4.77	4.83	3.97	4.63	Yes
F3.16	9	N/A	N/A	724	8.38	29035	6.70	5.58	4.87	5.48	Yes
F3.17	9	N/A	N/A	723	8.38	29015	6.69	5.58	4.88	5.48	Yes
F3.18	9	N/A	N/A	727	8.38	29089	6.71	5.57	4.87	5.47	Yes
F3.19	9	N/A	N/A	788	8.36	31489	7.03	5.48	4.78	5.29	Yes
F3.20	9	N/A	N/A	784	8.35	31276	6.97	5.48	4.78	5.29	Yes
F3.21	9	N/A	N/A	782	8.35	30907	6.88	5.46	4.76	5.28	Yes
F3.22	10	N/A	N/A	836	8.31	33656	7.17	5.38	4.68	5.12	Yes
F3.23	10	N/A	N/A	846	8.31	34455	7.28	5.37	4.68	5.09	Yes
F3.24	10	N/A	N/A	854	8.32	34642	7.34	5.37	4.68	5.09	Yes

Table E11.3: Flooding analysis results for flooding tests (ctnd)

	Extra Data		P Drop	Tube End Conditions			Vapour Velocities				Conclusion
Run	Visual Obs	$P_{v,o}$ (Pa)	ΔP_R (Pa)	$Re_{f,o}$ (-)	$\mathrm{Pr}_{f,o}$ (-)	$Re_{v,i}$ (-)	$u_{v,exp}$ (m/s)	$u_{v,Eng}$ (m/s)	$u_{v,DK}$ (m/s)	$u_{v,MA}$ (m/s)	Tube Flooded
F4.1	2	22923.8	344.1	391	8.68	11420	3.39	5.71	4.85	6.46	No
F4.2	2	22946.6	341.8	395	8.68	11541	3.41	5.70	4.85	6.44	No
F4.3	2	22949.2	336.4	398	8.68	11498	3.42	5.70	4.84	6.43	No
F4.4	1	24617.4	-1472.3	393	8.70	11901	3.48	5.73	4.89	6.47	No
F4.5	1	24557.6	-1496.8	392	8.70	11510	3.43	5.73	4.87	6.48	No
F4.6	1	24592.6	-1490.0	389	8.70	11782	3.46	5.73	4.89	6.49	No
F4.7	2	27555.9	-559.8	494	8.58	13521	3.58	5.31	4.45	5.72	No
F4.8	2	27588.3	-554.1	496	8.58	14041	3.65	5.32	4.47	5.71	No
F4.9	2	27631.1	-572.8	500	8.58	14069	3.67	5.31	4.46	5.69	No
F4.10	3	31873.0	-1350.6	593	8.50	15914	3.79	5.02	4.17	5.18	No
F4.11	3	31911.4	-1346.7	594	8.50	15707	3.76	5.01	4.16	5.17	No
F4.12	3	31974.4	-1363.9	593	8.50	16494	3.84	5.02	4.18	5.17	No
F4.13	5	33505.2	-2039.6	622	8.51	17043	3.91	4.95	4.11	5.05	No
F4.14	5	33570.9	-2056.8	620	8.50	16180	3.79	4.94	4.08	5.05	No
F4.15	5	33667.1	-2093.4	618	8.50	16418	3.81	4.94	4.09	5.05	No
F4.16	7	23233.5	4101.7	704	8.56	19330	5.04	5.29	4.43	5.26	Yes
F4.17	7	23383.7	4050.8	707	8.55	19321	5.03	5.28	4.42	5.25	Yes
F4.18	7	23352.4	4161.8	700	8.55	19050	4.96	5.27	4.41	5.25	Yes
F4.19	7	28740.2	1916.0	748	8.53	19011	4.64	4.99	4.13	4.90	Yes
F4.20	7	28586.1	2007.6	749	8.53	20507	4.84	5.01	4.17	4.91	Yes
F4.21	7	28631.6	2008.8	742	8.53	20254	4.78	5.01	4.17	4.91	Yes
F4.22	8	28901.5	2843.8	764	8.50	20649	4.72	4.93	4.09	4.80	Yes
F4.23	8	28853.5	2833.0	762	8.50	20062	4.66	4.93	4.08	4.81	Yes
F4.24	8	28832.2	2910.7	760	8.50	20143	4.65	4.92	4.08	4.81	Yes
F4.25	8	32860.8	6145.2	805	8.43	20747	4.02	4.47	3.64	4.29	Yes
F4.26	8	32978.2	6327.5	804	8.42	20783	4.00	4.45	3.63	4.28	Yes
F4.27	8	33261.1	6453.2	813	8.42	21009	4.00	4.43	3.61	4.25	Yes
F4.28	8	34983.5	8216.1	829	8.37	21133	3.73	4.26	3.45	4.06	Yes
F4.29	8	35156.8	8381.8	833	8.37	21493	3.75	4.24	3.44	4.04	Yes
F4.30	8	35288.1	8609.1	820	8.37	20355	3.59	4.22	3.40	4.03	Yes

Table E12: Key to visual observation grading

Grading	Description
1	Very smooth flowing trickle
2	Smooth condensate drainage
3	Reasonably smooth / slightly disturbed
4	Disturbances / splashing but constant flow rate
5	Small uneven pulses with drainage in between
6	Large pulses, very little drainage between
7	Intermittent drainage, pulses with no drainage between
8	Intermittent drainage; large pulses, longer gaps
9	Small uneven pulses with large gaps
10	Almost no drainage except for large flush roughly every 10s

Appendix F: Binary Mixture Data And Calculation Results

Table F1.1: Experimental data for binary mixture tests

	Boiler			Reflux Condenser Coolant					Reflux Condenser Vapour			Extraction Air	
Run	Q_i (W)	$P_{v,i}$ (Pa)	$T_{vR,i}$ (°C)	$\dot{V}_{c,R}$ (m³/s)	$T_{cR,i}$ (°C)	$T_{cR,TS3}$ (°C)	$T_{cR,TS4}$ (°C)	$T_{cR,o}$ (°C)	$T_{vR,oTS2}$ (°C)	$T_{vR,oTS3}$ (°C)	$T_{vR,oTS4}$ (°C)	T_{Ai} (°C)	T_{Ao} (°C)
M1.1	3931.1	122199	83.95	5.86E-05	34.24	38.85	41.89	44.77	77.72	76.96	79.60	16.73	20.75
M1.2	3959.0	129548	87.11	5.84E-05	39.38	43.54	46.28	48.90	80.56	80.70	82.75	16.87	21.20
M1.3	3905.8	132863	88.39	5.83E-05	41.76	45.67	48.28	50.74	81.73	82.16	84.02	17.47	21.93
M1.4	4917.6	137754	88.89	5.87E-05	29.34	35.60	40.16	44.40	82.39	79.51	84.02	20.81	24.27
M1.5	4972.2	145442	91.42	5.86E-05	34.40	40.18	44.35	48.28	84.80	82.28	86.69	20.19	24.49
M1.6	5029.6	154128	93.96	5.84E-05	39.37	44.71	48.54	52.15	87.15	85.29	89.32	19.56	24.68
M1.12	5062.2	123624	86.12	5.86E-05	34.29	39.25	42.64	45.90	80.08	80.30	82.24	16.93	21.46
M1.13	5095.6	133180	89.22	5.84E-05	39.36	43.90	47.06	50.15	82.99	83.81	85.35	17.28	22.23
M1.14	5057.2	137417	90.53	5.83E-05	41.95	46.23	49.22	52.21	84.20	85.23	86.65	16.95	22.28
M1.15	4010.4	121811	86.13	5.80E-05	39.58	43.42	45.98	48.46	79.66	80.48	81.90	16.49	21.14
M1.16	3903.8	124690	87.11	5.83E-05	41.73	45.33	47.77	50.17	80.56	81.48	82.93	16.46	21.41
M1.17	3011.6	118456	84.66	5.80E-05	39.56	43.05	45.32	47.47	77.41	78.31	79.75	18.77	22.81
M1.19	3102.5	100381	79.49	5.80E-05	39.27	41.85	43.63	45.40	73.22	74.20	75.63	15.17	19.86
M1.20	2991.5	107928	82.62	5.81E-05	41.88	44.51	46.27	47.98	76.02	76.94	(N/A)	14.43	19.45
M1.21	2562.0	102365	80.49	5.81E-05	39.38	42.01	43.74	45.40	73.21	74.54	(N/A)	15.45	20.11
M2.1	3456.1	88185	78.87	5.82E-05	39.36	41.78	43.59	45.54	73.20	74.25	(N/A)	10.76	16.40
M2.2	3940.2	75685	73.54	5.88E-05	29.20	32.63	34.98	37.30	68.55	69.47	(N/A)	10.04	15.01
M2.3	4009.7	82786	76.86	5.86E-05	34.13	37.24	39.45	41.72	71.75	72.73	(N/A)	9.49	15.33
M2.4	4030.0	89807	79.85	5.84E-05	39.25	42.00	44.07	46.26	74.79	75.86	(N/A)	9.99	16.04
M2.5	4965.1	91734	80.33	5.88E-05	29.30	33.92	37.10	40.28	74.92	75.84	(N/A)	9.32	14.54
M2.6	4954.9	98748	83.18	5.85E-05	34.35	38.54	41.47	44.57	77.75	78.76	(N/A)	8.77	14.47
M2.7	5038.8	106481	85.97	5.84E-05	39.22	43.03	45.85	48.84	80.63	81.71	(N/A)	8.20	14.25
M2.8	4918.6	90746	81.46	5.89E-05	29.39	34.11	37.36	40.60	75.80	76.71	(N/A)	9.15	15.23

Table F1.2: Experimental data for binary mixture tests (ctnd)

Run	Boiler			Reflux Condenser Coolant					Reflux Condenser Vapour			Extraction Air	
	Q_i (W)	$P_{v,i}$ (Pa)	$T_{vR,i}$ (°C)	$\dot{V}_{c,R}$ (m³/s)	$T_{cR,i}$ (°C)	$T_{cR,TS3}$ (°C)	$T_{cR,TS4}$ (°C)	$T_{cR,o}$ (°C)	$T_{vR,oTS2}$ (°C)	$T_{vR,oTS3}$ (°C)	$T_{vR,oTS4}$ (°C)	T_{Ai} (°C)	T_{Ao} (°C)
M2.9	5032.3	98779	84.52	5.87E-05	34.44	38.86	41.91	45.08	79.03	80.01	(N/A)	9.65	15.62
M2.10	2957.0	79128	77.45	5.85E-05	34.33	37.32	39.22	41.20	71.51	72.31	(N/A)	5.59	11.75
M2.11	2951.0	83745	79.69	5.84E-05	39.23	41.72	43.46	45.27	73.82	74.75	(N/A)	5.56	12.22
M2.12	4003.8	94974	83.98	5.85E-05	39.33	42.61	44.95	47.45	78.29	79.21	(N/A)	5.33	12.18
M2.13	4055.7	90148	82.09	5.86E-05	34.37	38.22	40.86	43.61	76.42	77.23	(N/A)	5.61	12.38
M2.14	3008.9	73632	75.53	5.85E-05	34.28	36.95	38.80	40.68	70.01	70.87	(N/A)	15.06	18.88
M2.15	3525.0	80871	79.62	5.85E-05	39.32	41.91	43.82	45.88	74.41	75.34	(N/A)	8.27	14.24
M2.16	3504.7	84389	81.20	5.84E-05	41.68	44.16	46.05	48.06	76.05	76.99	(N/A)	8.02	14.35
M3.1	3943.9	153292	83.33	5.92E-05	39.24	42.43	45.26	48.76	75.04	76.04	76.75	11.61	16.73
M3.2	3919.5	146492	81.53	5.92E-05	34.29	38.10	41.42	45.39	73.47	74.31	74.75	11.96	16.72
M3.3	5715.1	193414	92.64	5.93E-05	39.55	44.60	48.91	53.43	84.00	85.03	85.62	14.93	20.39
M3.4	5751.9	183532	90.59	5.98E-05	34.46	39.85	44.64	49.71	81.85	82.70	83.10	14.26	19.82
M3.7	5055.8	172499	88.21	5.97E-05	34.38	39.39	43.78	48.49	79.94	80.76	81.15	13.27	18.38
M3.8	4005.2	159617	86.07	5.94E-05	44.32	47.47	49.84	52.53	78.04	79.28	80.21	15.61	21.28
M3.9	4068.6	151108	83.97	5.98E-05	39.44	43.10	45.90	48.91	76.20	77.23	77.98	15.14	20.63
M3.11	3006.1	125152	77.27	5.96E-05	39.29	41.25	43.11	45.68	69.03	70.21	71.15	13.54	18.10
M3.12	2965.8	138578	81.32	5.94E-05	44.18	45.88	47.59	50.03	72.62	73.90	74.96	12.55	17.61
M3.13	3007.3	132072	79.59	5.98E-05	39.40	41.66	43.73	46.48	70.87	72.06	72.86	12.91	17.77
M3.14	5024.2	166127	88.62	5.86E-05	44.31	47.63	50.42	53.84	80.54	81.95	82.77	13.64	18.85
M3.15	5017.3	154846	85.90	5.94E-05	39.34	42.97	46.10	49.83	77.91	79.15	79.93	13.35	18.73
M3.16	5076.7	144718	83.26	6.01E-05	34.52	38.52	41.94	45.96	75.47	76.52	77.22	13.53	18.48
M3.17	2977.3	109302	73.15	5.97E-05	34.30	36.45	38.40	40.97	65.16	66.29	67.08	15.06	18.79
M3.18	3037.7	103103	71.07	6.00E-05	29.27	32.06	34.44	37.33	63.49	64.40	64.97	15.24	18.79

Table F1.3: Experimental data for binary mixture tests (ctnd)

Run	Reflux Condenser Wall Temperatures									Dump Condenser			
	$T_{w,TS2t}$ (°C)	$T_{w,TS2m}$ (°C)	$T_{w,TS2b}$ (°C)	$T_{w,TS3t}$ (°C)	$T_{w,TS3m}$ (°C)	$T_{w,TS3b}$ (°C)	$T_{w,TS4t}$ (°C)	$T_{w,TS4m}$ (°C)	$T_{w,TS4b}$ (°C)	$\dot{V}_{c,D}$ (m³/s)	$T_{cD,in}$ (°C)	$T_{cD,out}$ (°C)	$T_{f,D}$ (°C)
M1.1	37.59	38.67	40.05	39.46	41.23	42.39	43.20	44.25	45.85	2.52E-05	14.35	21.38	14.77
M1.2	42.40	43.35	44.58	44.07	45.66	46.73	47.45	48.41	49.88	2.54E-05	14.26	24.09	14.83
M1.3	44.63	45.57	46.65	46.18	47.67	48.68	49.32	50.22	51.67	2.54E-05	14.12	24.87	14.82
M1.4	33.79	35.34	37.32	36.43	39.12	40.81	42.07	43.58	45.85	2.52E-05	14.39	20.75	15.04
M1.5	38.45	39.92	41.73	40.96	43.38	44.97	46.12	47.54	49.63	2.53E-05	14.25	23.92	14.90
M1.6	43.07	44.44	46.12	45.42	47.64	49.10	50.11	51.43	53.42	2.52E-05	14.37	26.62	15.23
M1.12	37.95	39.16	40.48	39.84	41.80	43.13	44.04	45.20	47.06	2.53E-05	14.45	29.50	15.40
M1.13	42.67	43.81	45.06	44.48	46.27	47.52	48.37	49.47	51.23	2.53E-05	14.39	31.38	15.98
M1.14	45.07	46.10	47.41	46.85	48.55	49.74	50.53	51.58	53.31	2.53E-05	14.64	32.35	16.51
M1.15	42.44	43.34	44.46	43.97	45.44	46.46	47.11	48.00	49.45	2.52E-05	14.51	25.94	15.09
M1.16	44.40	45.26	46.31	45.86	47.24	48.21	48.82	49.68	51.08	2.53E-05	14.46	26.70	14.92
M1.17	42.19	43.04	44.02	43.54	44.86	45.74	46.28	47.03	48.29	2.52E-05	14.22	19.85	15.06
M1.19	41.44	41.92	42.58	42.25	43.27	44.03	44.43	45.08	46.16	2.42E-05	14.21	25.43	14.74
M1.20	44.04	44.57	45.22	44.94	45.93	46.66	47.05	47.66	48.73	2.47E-05	14.35	23.65	14.81
M1.21	41.56	42.08	42.77	42.44	43.43	44.14	44.53	45.11	46.10	2.46E-05	14.43	20.30	14.98
M2.1	41.30	41.67	42.56	42.20	43.22	44.06	44.54	45.24	46.42	2.41E-05	14.64	28.64	15.72
M2.2	31.94	32.49	33.67	33.16	34.55	35.53	36.18	37.01	38.38	2.40E-05	14.45	27.98	17.33
M2.3	36.60	37.12	38.18	37.73	38.99	39.93	40.54	41.35	42.71	2.41E-05	14.21	29.48	18.23
M2.4	41.41	41.90	42.84	42.42	43.60	44.53	45.09	45.88	47.21	2.40E-05	14.41	31.30	20.27
M2.5	32.81	33.68	35.28	34.60	36.47	37.77	38.65	39.78	41.62	2.39E-05	14.39	30.34	16.97
M2.6	37.47	38.27	39.80	39.18	40.86	42.11	42.93	44.03	45.81	2.39E-05	14.49	32.16	18.38
M2.7	41.94	42.70	44.30	43.74	45.30	46.53	47.32	48.37	50.08	2.39E-05	14.62	34.17	20.79
M2.8	33.01	33.93	35.46	34.77	36.69	37.99	38.87	40.06	41.96	2.38E-05	14.49	29.71	15.77

Table F1.4: Experimental data for binary mixture tests (ctnd)

	Reflux Condenser Wall Temperatures									Dump Condenser			
Run	$T_{w,TS2t}$ (°C)	$T_{w,TS2m}$ (°C)	$T_{w,TS2b}$ (°C)	$T_{w,TS3t}$ (°C)	$T_{w,TS3m}$ (°C)	$T_{w,TS3b}$ (°C)	$T_{w,TS4t}$ (°C)	$T_{w,TS4m}$ (°C)	$T_{w,TS4b}$ (°C)	$\dot{V}_{c,D}$ (m³/s)	$T_{cD,i}$ (°C)	$T_{cD,o}$ (°C)	$T_{f,D}$ (°C)
M2.9	37.77	38.63	40.09	39.47	41.24	42.52	43.36	44.52	46.38	2.38E-05	14.51	31.73	16.67
M2.10	36.70	37.09	38.28	37.80	38.91	39.77	40.27	40.98	42.14	2.37E-05	14.75	21.31	14.07
M2.11	41.22	41.54	42.54	42.17	43.13	43.96	44.42	45.06	46.19	2.38E-05	14.57	23.21	14.32
M2.12	41.79	42.37	43.68	43.18	44.49	45.52	46.17	47.04	48.53	2.38E-05	14.68	27.57	14.60
M2.13	37.29	37.99	39.44	38.87	40.38	41.49	42.22	43.18	44.77	2.37E-05	14.62	25.88	14.33
M2.14	36.55	37.02	37.74	37.42	38.49	39.26	39.70	40.38	41.55	2.39E-05	14.16	24.17	14.80
M2.15	41.43	41.86	42.63	42.22	43.33	44.19	44.71	45.46	46.73	2.32E-05	14.59	27.49	14.55
M2.16	43.68	44.06	44.89	44.51	45.57	46.45	46.96	47.69	48.96	2.33E-05	14.47	28.07	14.73
M3.1	41.47	42.58	44.90	44.35	45.91	47.11	47.82	48.68	49.97	2.01E-05	15.30	26.08	15.73
M3.2	36.98	38.22	40.79	40.14	42.02	43.38	44.26	45.25	46.73	2.00E-05	15.33	22.15	15.78
M3.3	42.94	44.42	47.10	46.35	48.82	50.51	51.59	52.93	54.86	1.93E-05	14.83	33.73	15.85
M3.4	38.17	39.71	42.70	41.84	44.60	46.49	47.73	49.21	51.33	1.91E-05	14.96	30.56	15.92
M3.7	37.89	39.34	42.13	41.33	43.86	45.59	46.71	48.05	49.95	1.91E-05	15.23	25.67	15.68
M3.8	46.61	47.65	49.04	48.56	49.87	50.84	51.40	52.16	53.35	1.92E-05	14.81	31.48	15.54
M3.9	42.10	43.22	44.82	44.25	45.83	46.94	47.64	48.52	49.82	1.91E-05	14.87	28.71	15.33
M3.11	40.80	41.53	43.28	42.87	43.90	44.69	45.13	45.70	46.61	1.89E-05	15.02	26.46	15.72
M3.12	45.53	46.22	47.84	47.47	48.42	49.15	49.51	50.04	50.89	1.91E-05	14.98	27.14	15.77
M3.13	41.13	41.97	43.78	43.32	44.47	45.32	45.83	46.44	47.44	1.90E-05	15.22	23.83	15.78
M3.14	46.67	47.72	49.78	49.25	50.80	51.99	52.69	53.60	55.00	1.92E-05	15.16	39.20	19.68
M3.15	41.90	43.05	45.35	44.75	46.52	47.83	48.62	49.62	51.09	1.93E-05	15.03	36.97	18.20
M3.16	37.39	38.62	41.03	40.37	42.31	43.72	44.63	45.72	47.34	1.91E-05	15.08	34.85	17.05
M3.17	36.03	36.78	38.47	38.02	39.13	39.91	40.38	40.97	41.90	1.91E-05	15.13	25.34	15.68
M3.18	31.44	32.32	34.25	33.72	35.09	36.03	36.62	37.35	38.39	1.89E-05	15.03	22.25	15.69

Table F2.1: Mass balance results for binary mixture tests

	Measured Compositions From Densitometer						Vapour Comp From Saturation	Mass Balance			Conden-sate Comp	Saturation Temperature	
Run	P_R (s^{-1})	$\rho_{f,R}$ (kg/m³)	$\tilde{x}_{P,R}$ (-)	P_D (s^{-1})	$\rho_{f,D}$ (kg/m³)	$\tilde{x}_{P,D}$ (-)	$\tilde{y}_{P,in}$ (-)	$\dot{m}_{f,o}$ (kg/s)	$\dot{m}_{v,o}$ (kg/s)	$\dot{m}_{v,i}$ (kg/s)	$\tilde{x}_{P,Rcalc}$ (-)	$T^*_{v,out}$ (°C)	$\Delta T^*_{v,out}$ (°C)
M1.1	3.347906	674.8	0.349	3.329220	654.8	0.659	0.559	0.00701	0.00163	0.00865	0.534	78.21	-0.49
M1.2	3.350951	678.0	0.291	3.329385	655.0	0.656	0.535	0.00638	0.00228	0.00866	0.488	80.23	0.33
M1.3	3.351439	678.5	0.282	3.329657	655.3	0.652	0.527	0.00605	0.00248	0.00853	0.470	81.30	0.42
M1.4	3.345961	672.7	0.384	3.329076	654.7	0.661	0.540	0.00988	0.00145	0.01133	0.521	81.94	0.45
M1.5	3.347915	674.8	0.349	3.330012	655.7	0.647	0.527	0.00917	0.00220	0.01137	0.496	84.60	0.20
M1.6	3.349618	676.6	0.317	3.330720	656.4	0.636	0.517	0.00849	0.00277	0.01126	0.475	87.20	-0.05
M1.12	3.351384	678.5	0.283	3.331244	657.0	0.628	0.524	0.00772	0.00351	0.01122	0.473	80.42	-0.34
M1.13	3.351846	679.0	0.274	3.331735	657.5	0.621	0.512	0.00721	0.00394	0.01115	0.447	83.28	-0.29
M1.14	3.352254	679.4	0.266	3.331980	657.8	0.617	0.507	0.00688	0.00410	0.01098	0.435	84.53	-0.33
M1.15	3.348778	675.7	0.333	3.330908	656.6	0.633	0.514	0.00594	0.00265	0.00860	0.456	79.65	0.01
M1.16	3.350309	677.3	0.304	3.331330	657.1	0.627	0.510	0.00568	0.00285	0.00853	0.446	80.78	-0.22
M1.17	3.345793	672.5	0.388	3.328489	654.1	0.669	0.525	0.00530	0.00130	0.00660	0.486	76.55	0.87
M1.19	3.354507	681.8	0.221	3.330393	656.1	0.641	0.522	0.00413	0.00256	0.00668	0.441	73.12	0.10
M1.20	3.348693	675.6	0.334	3.330621	656.3	0.638	0.505	0.00415	0.00214	0.00629	0.430	75.57	0.45
M1.21	3.347391	674.2	0.358	3.329274	654.9	0.658	0.514	0.00406	0.00135	0.00541	0.462	72.73	0.48
M2.1	3.356616	684.1	0.178	3.335427	661.4	0.563	0.447	0.00422	0.00323	0.00745	0.350	73.42	-0.23
M2.2	3.356085	683.5	0.189	3.335598	661.6	0.561	0.462	0.00549	0.00320	0.00869	0.400	68.98	-0.43
M2.3	3.356599	684.1	0.178	3.336256	662.3	0.550	0.448	0.00518	0.00360	0.00878	0.372	72.17	-0.43
M2.4	3.357113	684.6	0.168	3.336724	662.8	0.543	0.438	0.00481	0.00397	0.00878	0.344	75.02	-0.23
M2.5	3.356710	684.2	0.176	3.336638	662.7	0.544	0.442	0.00738	0.00365	0.01103	0.388	75.61	-0.69
M2.6	3.356509	684.0	0.180	3.337171	663.3	0.535	0.431	0.00690	0.00404	0.01093	0.365	78.33	-0.58
M2.7	3.356904	684.4	0.172	3.337695	663.9	0.527	0.423	0.00654	0.00448	0.01101	0.346	81.14	-0.51
M2.8	3.356847	684.3	0.173	3.338026	664.2	0.521	0.408	0.00756	0.00346	0.01103	0.352	76.38	-0.58

Table F2.2: Mass balance results for binary mixture tests (ctnd)

	Measured Compositions From Densitometer						Vapour Comp From Saturation	Mass Balance			Conden-sate Comp	Saturation Temperature	
Run	P_R (s^{-1})	$\rho_{f,R}$ (kg/m³)	$\tilde{x}_{P,R}$ (-)	P_D (s^{-1})	$\rho_{f,D}$ (kg/m³)	$\tilde{x}_{P,D}$ (-)	$\tilde{y}_{P,in}$ (-)	$\dot{M}_{f,o}$ (kg/s)	$\dot{M}_{v,o}$ (kg/s)	$\dot{M}_{v,i}$ (kg/s)	$\tilde{x}_{P,Rcalc}$ (-)	$T^*_{v,out}$ (°C)	$\Delta T^*_{v,out}$ (°C)
M2.9	3.357109	684.6	0.168	3.338649	664.9	0.511	0.399	0.00722	0.00388	0.01110	0.335	79.52	-0.50
M2.10	3.355859	683.3	0.194	3.336994	663.1	0.538	0.401	0.00472	0.00148	0.00620	0.354	71.40	0.11
M2.11	3.356260	683.7	0.185	3.337854	664.0	0.524	0.389	0.00418	0.00196	0.00614	0.320	73.78	0.04
M2.12	3.355719	683.1	0.196	3.339307	665.6	0.500	0.382	0.00558	0.00289	0.00848	0.315	78.81	-0.52
M2.13	3.355712	683.1	0.197	3.339091	665.3	0.504	0.387	0.00631	0.00253	0.00884	0.337	77.01	-0.59
M2.14	3.358289	685.9	0.143	3.338135	664.3	0.520	0.394	0.00441	0.00232	0.00673	0.321	70.14	-0.13
M2.15	3.356628	684.1	0.178	3.340351	666.7	0.483	0.363	0.00457	0.00287	0.00743	0.282	74.64	-0.24
M2.16	3.357109	684.6	0.168	3.340818	667.2	0.475	0.357	0.00445	0.00302	0.00747	0.270	76.30	-0.25
M3.1	3.333798	659.7	0.589	3.319534	644.6	0.794	0.693	0.00625	0.00199	0.00824	0.658	75.57	-0.53
M3.2	3.332095	657.9	0.615	3.31924	644.2	0.798	0.697	0.00725	0.00125	0.00850	0.679	73.78	-0.32
M3.3	3.336096	662.2	0.553	3.32067	645.8	0.779	0.672	0.00902	0.00325	0.01227	0.631	84.57	-0.57
M3.4	3.335272	661.3	0.566	3.320451	645.5	0.782	0.676	0.00996	0.00267	0.01264	0.645	82.54	-0.69
M3.7	3.333704	659.6	0.590	3.320197	645.3	0.786	0.680	0.00922	0.00180	0.01102	0.657	80.18	-0.24
M3.8	3.337033	663.1	0.538	3.320743	645.8	0.778	0.672	0.00543	0.00291	0.00834	0.610	78.25	-0.21
M3.9	3.335367	661.4	0.564	3.320782	645.9	0.778	0.676	0.00629	0.00242	0.00871	0.635	76.51	-0.31
M3.11	3.336046	662.1	0.553	3.319605	644.6	0.794	0.685	0.00426	0.00203	0.00629	0.629	69.26	-0.23
M3.12	3.338012	664.2	0.522	3.319841	644.9	0.790	0.673	0.00389	0.00216	0.00604	0.602	72.70	-0.08
M3.13	3.335588	661.6	0.561	3.319763	644.8	0.791	0.676	0.00473	0.00152	0.00625	0.636	71.11	-0.23
M3.14	3.339196	665.5	0.502	3.322141	647.3	0.759	0.654	0.00618	0.00427	0.01045	0.574	81.10	-0.55
M3.15	3.338005	664.2	0.522	3.322299	647.5	0.757	0.659	0.00687	0.00392	0.01079	0.599	78.96	-1.05
M3.16	3.336864	663.0	0.540	3.322132	647.3	0.759	0.665	0.00756	0.00351	0.01107	0.618	76.59	-1.12
M3.17	3.335674	661.7	0.559	3.320111	645.2	0.787	0.683	0.00445	0.00186	0.00631	0.637	65.70	-0.54
M3.18	3.333938	659.9	0.587	3.320006	645.1	0.788	0.688	0.00538	0.00131	0.00668	0.662	63.84	-0.36

Table F3.1: Heat balance results and heat transfer coefficients (excluding vapour) for mixture tests

	Heat Balance					Mean Heat Transfer Coefficients						Condensate Film Analysis		
Run	$\dot{Q}_R$ (W)	$\dot{Q}_D$ (W)	$\dot{Q}_{A,Ex}$ (W)	$\dot{Q}_o$ (W)	$R_{\dot{Q}}$ (W/W)	ΔT_{mean} (°C)	$\overline{U}$ (W/m²K)	$\overline{\alpha}_w$ (W/m²K)	$\overline{\alpha}_c$ (W/m²K)	$\overline{\alpha}_{CS}$ (W/m²K)	$\overline{\alpha}_f$ (W/m²K)	$\dot{q}_f$ (W/m²)	Re_f (-)	Pr_f (-)
M1.1	2559.1	733.3	396.3	3688.7	0.938	41.29	290.8	84920	6191.6	300.7	892.0	12008	752	6.33
M1.2	2300.1	1034.6	426.7	3767.9	0.952	39.68	272.0	85019	6415.7	280.4	897.9	10793	700	6.32
M1.3	2166.7	1132.7	438.4	3744.5	0.959	38.80	262.1	85063	6516.9	269.7	903.7	10167	670	6.31
M1.4	3672.1	661.6	336.5	4675.6	0.951	48.65	354.2	84875	6065.1	369.3	826.5	17230	1049	6.40
M1.5	3371.5	1011.5	418.7	4809.0	0.967	46.67	339.0	84970	6291.7	352.3	833.7	15820	1000	6.35
M1.6	3087.6	1282.0	498.8	4875.9	0.969	44.73	323.9	85064	6496.8	335.7	842.4	14488	951	6.30
M1.12	2821.0	1577.9	445.8	4850.3	0.958	42.95	308.2	84935	6226.9	319.3	858.2	13237	818	6.44
M1.13	2607.3	1787.1	486.3	4888.3	0.959	41.30	296.2	85034	6447.1	306.1	865.0	12234	787	6.38
M1.14	2474.3	1862.7	523.7	4869.0	0.963	40.25	288.4	85084	6559.6	297.7	871.0	11610	763	6.35
M1.15	2134.2	1195.7	457.9	3793.9	0.946	38.86	257.7	85014	6377.2	265.2	903.1	10014	640	6.41
M1.16	2033.0	1286.0	487.2	3812.8	0.977	37.88	251.9	85054	6497.0	259.0	909.2	9539	620	6.39
M1.17	1898.2	585.4	395.2	2883.9	0.958	37.52	237.4	85000	6348.7	243.8	933.0	8907	570	6.39
M1.19	1472.2	1126.6	464.0	3068.4	0.989	34.03	203.0	84966	6287.5	207.7	969.8	6908	432	6.48
M1.20	1469.7	952.8	497.9	2924.9	0.978	34.39	200.5	85024	6433.8	205.0	966.7	6896	441	6.47
M1.21	1446.0	595.9	460.4	2507.4	0.979	34.46	196.9	84968	6297.9	201.3	979.0	6785	425	6.50
M2.1	1489.3	1398.8	566.3	3460.2	1.001	33.58	208.1	84966	6309.4	213.0	941.6	6988	422	6.78
M2.2	1978.7	1347.0	500.2	3830.5	0.972	37.77	245.8	84773	5881.3	253.2	898.6	9285	513	6.97
M2.3	1848.0	1526.2	588.4	3968.2	0.990	36.36	238.5	84872	6113.6	245.2	905.3	8671	500	6.89
M2.4	1696.6	1686.2	609.0	3998.6	0.992	34.56	230.4	84975	6342.9	236.4	914.9	7961	481	6.80
M2.5	2682.7	1579.8	526.8	4794.3	0.966	42.78	294.3	84816	5962.5	304.8	843.7	12588	706	6.93
M2.6	2480.0	1751.2	576.3	4814.8	0.972	40.96	284.1	84915	6184.7	293.6	852.3	11637	681	6.85
M2.7	2325.3	1938.5	611.3	4884.4	0.969	39.23	278.1	85013	6411.1	286.9	859.4	10911	667	6.76
M2.8	2742.8	1506.2	613.3	4867.2	0.990	43.57	295.4	84822	5983.4	306.0	831.4	12870	714	7.05

Table F3.2: Heat balance results and heat transfer coefficients (excluding vapour) for mixture tests (ctnd)

	Heat Balance					Mean Heat Transfer Coefficients						Condensate Film Analysis		
Run	$\dot{Q}_R$ (W)	$\dot{Q}_D$ (W)	$\dot{Q}_{A,Ex}$ (W)	$\dot{Q}_o$ (W)	$R_{\dot{Q}}$ (W/W)	ΔT_{mean} (°C)	$\overline{U}$ (W/m²K)	$\overline{\alpha}_w$ (W/m²K)	$\overline{\alpha}_c$ (W/m²K)	$\overline{\alpha}_{CS}$ (W/m²K)	$\overline{\alpha}_f$ (W/m²K)	$\dot{q}_f$ (W/m²)	Re_f (-)	Pr_f (-)
M2.9	2590.3	1700.9	601.6	4898.4	0.973	41.96	289.7	84923	6219.6	299.5	838.0	12154	706	6.94
M2.10	1668.7	640.7	628.7	2942.8	0.995	36.71	213.3	84869	6098.0	218.7	919.1	7830	444	7.07
M2.11	1460.9	851.4	679.3	2995.7	1.015	34.50	198.7	84964	6321.8	203.2	936.8	6855	405	6.99
M2.12	1966.4	1275.1	698.1	3945.6	0.985	37.74	244.5	84994	6383.8	251.3	881.5	9227	551	6.94
M2.13	2247.4	1108.1	690.3	4050.8	0.999	40.24	262.1	84903	6168.4	270.1	862.2	10545	604	7.03
M2.14	1554.6	992.3	378.3	2927.9	0.973	35.29	206.7	84860	6083.9	211.8	923.9	7295	410	7.12
M2.15	1590.3	1240.9	603.9	3439.0	0.976	34.41	216.9	84969	6346.2	222.2	911.3	7462	437	7.08
M2.16	1542.3	1312.5	640.6	3499.6	0.999	33.75	214.4	85019	6456.7	219.6	914.8	7237	434	7.03
M3.1	2336.4	899.8	512.7	3751.9	0.951	35.18	311.7	84905	6483.5	322.6	955.1	10963	737	5.74
M3.2	2725.1	562.1	475.8	3766.7	0.961	37.64	339.7	84839	6262.9	353.2	933.3	12787	838	5.78
M3.3	3405.4	1511.6	540.1	5462.7	0.956	41.78	382.5	84979	6617.0	398.8	874.6	15979	1098	5.72
M3.4	3781.3	1235.5	551.5	5574.2	0.969	44.05	402.8	84911	6434.6	421.4	861.3	17743	1186	5.76
M3.7	3488.4	826.9	509.4	4828.0	0.955	42.57	384.5	84884	6385.4	401.5	879.7	16368	1085	5.78
M3.8	2013.3	1329.5	559.6	3906.7	0.975	33.63	280.9	84993	6720.3	289.5	966.2	9447	651	5.76
M3.9	2344.8	1097.4	542.3	3986.9	0.980	35.91	306.4	84921	6541.5	316.9	945.1	11002	737	5.80
M3.11	1579.8	898.0	453.5	2933.5	0.976	30.66	241.8	84868	6439.5	248.4	1023.5	7413	485	5.85
M3.12	1435.4	965.0	504.8	2907.2	0.980	29.84	225.7	84953	6655.1	231.3	1033.6	6735	455	5.81
M3.13	1752.5	675.7	484.9	2915.1	0.969	32.28	254.7	84885	6474.6	262.0	1004.1	8223	541	5.86
M3.14	2308.3	1919.6	518.9	4751.6	0.946	35.50	305.1	85002	6685.0	315.3	928.4	10831	738	5.82
M3.15	2581.0	1756.1	535.8	4877.3	0.972	37.31	324.6	84925	6531.4	336.4	915.6	12111	800	5.87
M3.16	2851.2	1569.9	492.7	4918.3	0.969	39.10	342.2	84855	6358.3	355.7	903.5	13378	859	5.91
M3.17	1654.3	806.5	369.9	2831.9	0.951	31.51	246.3	84795	6191.6	253.4	1016.3	7762	489	5.95
M3.18	2008.5	564.7	352.2	2927.0	0.964	33.98	277.4	84722	5975.4	286.7	985.7	9424	577	6.00

Table F4.1: Vapour side heat transfer coefficients

	Experimental		Correlations			Correlations with Mass Transfer Correciton Factor			Petukhov Correlation with corrections			Dimensionless Groups	
Run	$\overline{\alpha}_{v,eff}$ (W/m²K)	$\overline{\alpha}_{v}$ (W/m²K)	$\overline{\alpha}_{v,DB}$ (W/m²K)	$\overline{\alpha}_{v,P}$ (W/m²K)	$\overline{\alpha}_{v,G}$ (W/m²K)	$\overline{\alpha}^{*}_{v,DB}$ (W/m²K)	$\overline{\alpha}^{*}_{v,P}$ (W/m²K)	$\overline{\alpha}^{*}_{v,G}$ (W/m²K)	$\overline{\alpha}^{*}_{v,FV}$ (W/m²K)	$\overline{\alpha}^{*}_{v,W}$ (W/m²K)	$\overline{\alpha}^{*}_{v,FV+W}$ (W/m²K)	$\overline{Re}_{v}$ (-)	$\overline{Pr}_{v}$ (-)
M1.1	453.7	11.2	23.8	21.9	22.3	4.5	3.5	3.7	13.8	6.5	21.3	31278	5937
M1.2	407.7	12.7	25.2	23.1	23.7	6.2	4.9	5.2	15.5	8.4	23.0	31117	8218
M1.3	384.5	13.0	25.5	23.3	23.9	6.8	5.5	5.8	16.1	9.1	23.5	30559	8934
M1.4	667.7	15.2	28.7	26.1	26.9	3.8	2.7	3.0	15.0	6.2	25.4	40444	5187
M1.5	610.2	16.4	30.4	27.5	28.4	5.3	3.8	4.3	16.8	7.9	27.4	40349	7823
M1.6	558.1	17.6	31.4	28.4	29.4	6.6	5.0	5.5	18.4	9.5	29.0	39694	9798
M1.12	508.6	15.9	31.9	28.7	29.7	8.4	6.4	7.0	18.0	11.2	27.6	40513	12711
M1.13	473.8	17.2	32.8	29.5	30.6	9.8	7.6	8.3	19.5	12.7	29.2	39923	14173
M1.14	452.2	17.6	33.0	29.6	30.7	10.5	8.1	8.9	20.1	13.4	29.7	39187	14699
M1.15	375.6	12.7	25.7	23.5	24.1	7.3	5.8	6.2	16.0	9.5	23.1	31061	9633
M1.16	362.1	13.2	26.0	23.8	24.4	7.9	6.4	6.8	16.5	10.1	23.6	30745	10305
M1.17	330.0	9.9	19.3	18.1	18.2	4.2	3.5	3.5	12.5	5.8	18.1	23941	4741
M1.19	264.4	10.2	21.5	19.9	20.2	7.9	6.7	6.9	14.4	9.6	19.3	24631	9462
M1.20	260.2	9.7	20.2	18.8	19.0	6.8	5.8	5.9	13.8	8.5	18.6	22991	7855
M1.21	253.5	8.4	16.8	16.0	15.8	4.6	4.0	3.9	11.5	6.1	15.7	19903	4987
M2.1	275.3	10.9	24.1	22.0	22.5	9.7	8.1	8.5	15.6	11.5	20.9	27755	12066
M2.2	352.6	10.1	25.8	23.4	24.1	8.5	6.8	7.3	14.8	10.5	21.1	32844	12125
M2.3	336.3	11.1	26.9	24.4	25.1	9.9	8.0	8.5	16.2	11.9	22.5	32889	13522
M2.4	318.8	11.8	27.8	25.1	26.0	11.4	9.2	9.9	17.5	13.4	23.8	32643	14794
M2.5	477.2	13.8	31.2	28.0	29.0	8.8	6.6	7.3	16.8	11.3	25.4	40934	13614
M2.6	447.9	14.4	32.0	28.6	29.7	10.1	7.7	8.5	18.0	12.7	26.7	40268	14924
M2.7	430.7	15.2	33.1	29.6	30.8	11.5	9.0	9.8	19.5	14.2	28.3	40253	16415
M2.8	484.1	14.2	31.0	27.8	28.8	8.2	6.2	6.8	16.4	10.8	25.1	40928	12897

Table F4.2: Vapour side heat transfer coefficients (ctnd)

	Experimental		Correlations			Correlations with Mass Transfer Correciton Factor			Petukhov Correlation with corrections			Dimensionless Groups	
Run	$\overline{\alpha}_{v,eff}$ (W/m²K)	$\overline{\alpha}_{v}$ (W/m²K)	$\overline{\alpha}_{v,DB}$ (W/m²K)	$\overline{\alpha}_{v,P}$ (W/m²K)	$\overline{\alpha}_{v,G}$ (W/m²K)	$\overline{\alpha}^{*}_{v,DB}$ (W/m²K)	$\overline{\alpha}^{*}_{v,P}$ (W/m²K)	$\overline{\alpha}^{*}_{v,G}$ (W/m²K)	$\overline{\alpha}^{*}_{v,FV}$ (W/m²K)	$\overline{\alpha}^{*}_{v,W}$ (W/m²K)	$\overline{\alpha}^{*}_{v,FV+W}$ (W/m²K)	$\overline{Re}_{v}$ (-)	$\overline{Pr}_{v}$ (-)
M2.9	466.0	14.6	32.1	28.8	29.9	9.5	7.2	8.0	17.8	12.2	26.7	40865	14331
M2.10	286.9	7.6	18.4	17.2	17.3	4.6	3.9	3.9	11.2	6.1	15.7	23317	5586
M2.11	259.5	8.2	19.3	18.0	18.1	6.1	5.2	5.3	12.5	7.7	16.9	22951	7337
M2.12	351.5	11.4	25.7	23.4	24.0	8.0	6.4	6.8	15.4	10.0	22.0	31309	10722
M2.13	393.4	11.1	25.5	23.3	23.9	6.7	5.2	5.6	14.4	8.7	21.3	32808	9422
M2.14	274.8	8.5	20.9	19.3	19.6	6.9	5.8	6.0	12.9	8.5	17.6	25488	8821
M2.15	293.9	9.7	23.4	21.4	21.9	8.4	6.9	7.3	14.6	10.2	19.9	27873	10774
M2.16	288.9	9.9	23.9	21.8	22.3	9.0	7.4	7.8	15.1	10.8	20.5	27896	11294
M3.1	487.2	17.5	23.7	21.9	22.3	5.5	4.4	4.6	15.4	7.6	22.8	29313	7155
M3.2	568.3	16.2	22.7	21.0	21.3	3.7	2.9	3.0	13.8	5.6	21.5	30394	4515
M3.3	733.1	29.4	34.0	30.7	31.8	7.4	5.5	6.1	20.8	10.8	33.2	42503	11354
M3.4	825.2	29.5	33.5	30.1	31.2	6.0	4.3	4.8	19.3	9.1	32.0	44034	9414
M3.7	738.7	22.5	28.8	26.2	27.0	4.5	3.3	3.6	16.8	7.0	15.2	38662	6370
M3.8	413.3	18.5	25.8	23.7	24.2	8.2	6.7	7.1	17.7	10.5	15.8	29515	10396
M3.9	476.8	17.4	25.4	23.3	23.8	6.5	5.2	5.5	16.3	8.8	14.6	30998	8685
M3.11	328.0	13.9	19.7	18.4	18.6	6.3	5.4	5.5	13.7	8.0	11.9	22837	7452
M3.12	297.9	14.6	19.7	18.5	18.6	6.9	6.0	6.1	14.5	8.7	12.4	21700	7817
M3.13	354.5	13.4	18.8	17.7	17.7	4.8	4.1	4.1	13.0	6.5	10.9	22548	5540
M3.14	477.4	24.7	32.2	29.1	30.1	11.4	9.1	9.8	21.3	14.3	20.1	36770	15143
M3.15	531.9	24.2	31.9	28.8	29.8	9.9	7.7	8.4	20.0	12.8	19.0	38262	14019
M3.16	586.5	23.2	31.5	28.4	29.4	8.4	6.4	7.1	18.6	11.3	17.9	39557	12668
M3.17	337.6	12.8	19.2	17.9	18.0	5.6	4.8	4.8	12.7	7.3	11.2	23206	6894
M3.18	404.3	11.7	18.7	17.5	17.6	4.0	3.3	3.3	11.4	5.6	10.0	24737	4882

Table F5.1: Equilibrium method results

	Experimental Data			Integral Condensation Curve						Differential Condensation Curve				
		Using $\overline{\alpha}^{*}_{v,\exp}$	Using $\overline{\alpha}^{*}_{v,P}$	Condensing curve calculations				Using $\overline{\alpha}_{v,P}$	Using $\overline{\alpha}^{*}_{v,P}$	Condensing curve calculations using $\overline{\alpha}^{*}_{v,P}$				
Run	dT/dh (kg.°C/J)	L (m)	L (m)	$\widetilde{y}_{P,out}$ (-)	$\widetilde{x}_{P,out}$ (-)	$T_{v,out}$ (°C)	dT/dh (kg.°C/J)	L (m)	L (m)	$\widetilde{y}_{P,out}$ (-)	$\widetilde{x}_{P,out}$ (-)	$T_{v,out}$ (°C)	dT/dh (kg.°C/J)	L (m)
M1.1	2.15E-05	1.507	1.34	0.867	0.487	61.7	7.57E-05	3.34	1.59	0.975	0.485	46.95	1.26E-04	4.98
M1.2	2.51E-05	1.507	1.34	0.831	0.429	67.0	7.58E-05	3.07	1.54	0.943	0.403	53.92	1.25E-04	4.49
M1.3	2.67E-05	1.507	1.33	0.815	0.408	69.2	7.54E-05	2.95	1.51	0.925	0.374	57.28	1.22E-04	4.20
M1.4	2.06E-05	1.507	1.54	0.865	0.493	65.5	7.32E-05	3.42	1.65	0.981	0.503	49.50	1.24E-04	4.63
M1.5	2.30E-05	1.507	1.51	0.840	0.452	69.8	7.39E-05	3.26	1.63	0.962	0.443	54.57	1.26E-04	4.50
M1.6	2.55E-05	1.507	1.49	0.816	0.419	73.9	7.38E-05	3.09	1.59	0.936	0.394	60.36	1.23E-04	4.19
M1.12	2.46E-05	1.507	1.42	0.809	0.395	67.5	7.43E-05	3.07	1.60	0.915	0.356	56.41	1.18E-04	4.00
M1.13	2.72E-05	1.507	1.41	0.782	0.364	72.2	7.31E-05	2.88	1.55	0.877	0.318	63.15	1.11E-04	3.58
M1.14	2.86E-05	1.507	1.40	0.768	0.351	74.2	7.24E-05	2.78	1.52	0.858	0.303	66.21	1.07E-04	3.39
M1.15	2.65E-05	1.507	1.31	0.803	0.385	67.6	7.45E-05	2.89	1.50	0.911	0.346	56.49	1.19E-04	4.02
M1.16	2.79E-05	1.507	1.31	0.790	0.370	69.4	7.41E-05	2.80	1.47	0.892	0.326	59.52	1.15E-04	3.78
M1.17	2.56E-05	1.507	1.29	0.845	0.446	62.9	7.59E-05	3.07	1.47	0.965	0.438	47.79	1.29E-04	5.24
M1.19	2.88E-05	1.507	1.18	0.790	0.356	62.9	7.50E-05	2.65	1.41	0.879	0.307	54.63	1.11E-04	3.58
M1.20	2.86E-05	1.507	1.17	0.789	0.359	65.1	7.44E-05	2.65	1.38	0.890	0.314	55.49	1.15E-04	3.79
M2.1	2.88E-05	1.507	1.17	0.699	0.258	65.7	6.59E-05	2.33	1.29	0.764	0.210	61.13	8.82E-05	2.71
M2.2	2.23E-05	1.507	1.18	0.751	0.296	57.7	6.95E-05	2.76	1.46	0.844	0.246	50.17	1.02E-04	3.45
M2.3	2.47E-05	1.507	1.19	0.714	0.267	62.9	6.65E-05	2.53	1.38	0.789	0.217	57.45	9.18E-05	2.96
M2.4	2.66E-05	1.507	1.17	0.678	0.243	67.5	6.37E-05	2.33	1.31	0.736	0.197	63.75	8.30E-05	2.60
M2.5	2.28E-05	1.507	1.36	0.741	0.297	64.0	6.75E-05	2.84	1.51	0.846	0.249	55.41	1.03E-04	3.48
M2.6	2.44E-05	1.507	1.33	0.707	0.271	68.5	6.51E-05	2.65	1.44	0.795	0.223	62.01	9.34E-05	3.08
M2.7	2.58E-05	1.507	1.31	0.677	0.251	72.7	6.30E-05	2.49	1.39	0.748	0.204	67.88	8.57E-05	2.77
M2.8	2.33E-05	1.507	1.40	0.712	0.271	65.6	6.41E-05	2.73	1.46	0.822	0.224	57.26	9.77E-05	3.32

Table F5.2: Equilibrium method results (ctnd)

	Experimental Data			Integral Condensation Curve						Differential Condensation Curve				
		Using $\overline{\alpha}^{*}_{v,\exp}$	Using $\overline{\alpha}^{*}_{v,P}$	Condensing curve calculations				Using $\overline{\alpha}_{v,P}$	Using $\overline{\alpha}^{*}_{v,P}$	Condensing curve calculations using $\overline{\alpha}^{*}_{v,P}$				
Run	dT/dh (kg.°C/J)	L (m)	L (m)	$\widetilde{y}_{P,out}$ (-)	$\widetilde{x}_{P,out}$ (-)	$T_{v,out}$ (°C)	dT/dh (kg.°C/J)	L (m)	L (m)	$\widetilde{y}_{P,out}$ (-)	$\widetilde{x}_{P,out}$ (-)	$T_{v,out}$ (°C)	dT/dh (kg.°C/J)	L (m)
M2.9	2.41E-05	1.507	1.36	0.681	0.250	70.2	6.19E-05	1.41	2.58	0.773	0.203	63.77	8.92E-05	2.99
M2.10	2.24E-05	1.507	1.16	0.747	0.294	59.3	6.76E-05	1.34	2.71	(N/A)	(N/A)	(N/A)	(N/A)	(N/A)
M2.11	2.50E-05	1.507	1.13	0.692	0.250	64.6	6.33E-05	1.25	2.39	0.797	0.203	57.07	9.48E-05	3.13
M2.12	2.50E-05	1.507	1.25	0.666	0.237	70.0	6.07E-05	1.30	2.41	0.759	0.191	63.71	8.75E-05	2.89
M2.13	2.27E-05	1.507	1.29	0.703	0.263	66.0	6.35E-05	1.38	2.65	0.825	0.218	56.85	9.95E-05	3.42
M2.14	2.42E-05	1.507	1.13	0.688	0.240	61.1	6.24E-05	1.26	2.39	0.783	0.193	54.62	9.03E-05	2.99
M2.15	2.47E-05	1.507	1.14	0.624	0.202	67.6	5.64E-05	1.20	2.19	0.694	0.159	63.44	7.56E-05	2.50
M2.16	2.53E-05	1.507	1.13	0.604	0.192	69.9	5.47E-05	1.16	2.10	0.666	0.151	66.46	7.14E-05	2.34
M3.1	3.05E-05	1.507	1.69	0.918	0.624	62.8	7.41E-05	1.70	3.37	0.986	0.622	51.81	1.14E-04	4.58
M3.2	2.62E-05	1.507	1.70	0.931	0.660	59.6	7.01E-05	1.69	3.49	0.994	0.673	48.78	1.06E-04	4.42
M3.3	3.27E-05	1.507	1.88	0.900	0.594	72.6	7.42E-05	1.78	3.33	0.977	0.583	61.22	1.17E-04	4.14
M3.4	3.06E-05	1.507	1.95	0.910	0.616	69.6	7.21E-05	1.79	3.43	0.985	0.616	57.85	1.13E-04	4.15
M3.7	2.73E-05	1.507	1.82	0.919	0.635	66.4	7.09E-05	1.74	3.45	0.991	0.644	54.71	1.10E-04	4.22
M3.8	3.46E-05	1.507	1.60	0.891	0.558	67.5	7.86E-05	1.68	3.13	0.964	0.532	57.33	1.21E-04	4.37
M3.9	2.99E-05	1.507	1.61	0.906	0.591	63.9	7.60E-05	1.71	3.33	0.980	0.581	52.71	1.18E-04	4.58
M3.11	3.39E-05	1.507	1.56	0.908	0.582	57.9	7.83E-05	1.68	3.23	0.977	0.566	47.39	1.20E-04	4.98
M3.12	3.80E-05	1.507	1.55	0.894	0.554	62.7	7.97E-05	1.63	3.02	0.965	0.528	52.62	1.22E-04	4.67
M3.13	3.22E-05	1.507	1.58	0.914	0.602	58.7	7.57E-05	1.63	3.26	0.986	0.601	47.31	1.17E-04	5.03
M3.14	3.82E-05	1.507	1.71	0.867	0.511	71.5	7.94E-05	1.72	3.05	0.937	0.471	62.77	1.18E-04	3.88
M3.15	3.49E-05	1.507	1.75	0.882	0.536	67.6	7.83E-05	1.77	3.22	0.956	0.506	57.59	1.20E-04	4.17
M3.16	3.15E-05	1.507	1.77	0.895	0.562	63.9	7.68E-05	1.79	3.37	0.971	0.542	52.97	1.19E-04	4.37
M3.17	3.13E-05	1.507	1.55	0.915	0.590	53.1	7.74E-05	1.69	3.36	0.983	0.581	42.21	1.19E-04	5.16
M3.18	2.59E-05	1.507	1.56	0.930	0.632	49.3	7.32E-05	1.68	3.57	0.993	0.642	38.40	1.10E-04	5.06

Table F6.1: Corrected equilibrium method results

Run	Corrected Integral Condensation Curve							Corrected Differential Condensation Curve						
	ϕ_H (-)	θ_H (-)	$\tilde{y}_{P,corr}$ (-)	$\tilde{x}_{P,corr}$ (-)	$T_{v,out}$ (°C)	dT/dh (kg.°C/J)	L (m)	ϕ_H (-)	θ_H (-)	$\tilde{y}_{P,corr}$ (-)	$\tilde{x}_{P,corr}$ (-)	$T_{v,out}$ (°C)	dT/dh (kg.°C/J)	L (m)
M1.1	1.608	0.403	0.683	0.530	76.7	2.49E-05	1.63	0.895	0.618	0.875	0.492	60.8	7.92E-05	2.93
M1.2	1.488	0.434	0.663	0.489	79.8	2.80E-05	1.60	0.967	0.593	0.809	0.441	69.0	6.88E-05	2.46
M1.3	1.453	0.443	0.655	0.474	81.2	2.88E-05	1.57	1.002	0.581	0.780	0.425	72.2	6.41E-05	2.27
M1.4	1.701	0.380	0.664	0.522	81.8	2.25E-05	1.75	1.051	0.565	0.862	0.500	65.8	7.29E-05	2.83
M1.5	1.578	0.410	0.655	0.496	84.1	2.53E-05	1.74	1.061	0.562	0.820	0.462	71.6	6.80E-05	2.59
M1.6	1.493	0.433	0.646	0.474	86.6	2.74E-05	1.71	1.089	0.552	0.777	0.435	77.2	6.21E-05	2.34
M1.12	1.399	0.458	0.655	0.465	78.8	2.95E-05	1.73	1.090	0.552	0.757	0.420	71.8	5.76E-05	2.22
M1.13	1.399	0.458	0.655	0.465	78.8	2.95E-05	1.73	1.131	0.539	0.715	0.402	77.2	5.20E-05	2.00
M1.14	1.328	0.479	0.632	0.432	83.6	3.11E-05	1.64	1.143	0.535	0.697	0.394	79.4	4.98E-05	1.90
M1.15	1.455	0.443	0.642	0.457	79.1	2.86E-05	1.55	1.058	0.563	0.753	0.409	71.6	5.89E-05	2.13
M1.16	1.416	0.454	0.637	0.446	80.2	2.95E-05	1.53	1.077	0.556	0.732	0.400	73.9	5.58E-05	2.02
M1.17	1.678	0.385	0.649	0.495	77.8	2.40E-05	1.43	0.879	0.624	0.850	0.451	62.4	7.81E-05	2.74
M1.19	1.354	0.471	0.649	0.444	72.7	3.12E-05	1.43	1.020	0.575	0.733	0.393	67.2	5.60E-05	1.90
M1.20	1.454	0.443	0.631	0.440	76.0	2.87E-05	1.38	1.041	0.568	0.732	0.390	69.4	5.66E-05	1.93
M2.1	1.393	0.460	0.564	0.361	73.4	2.77E-05	1.35	1.324	0.480	0.592	0.340	72.0	3.46E-05	1.42
M2.2	1.433	0.449	0.593	0.388	67.3	2.75E-05	1.54	1.276	0.494	0.648	0.357	64.5	4.02E-05	1.73
M2.3	1.399	0.458	0.571	0.366	71.1	2.75E-05	1.47	0.704	0.477	0.604	0.344	69.5	3.53E-05	1.54
M2.4	1.356	0.471	0.552	0.347	74.6	2.77E-05	1.40	1.351	0.472	0.571	0.332	73.7	3.22E-05	1.40
M2.5	1.498	0.431	0.572	0.380	74.2	2.57E-05	1.63	1.384	0.463	0.625	0.355	71.4	3.72E-05	1.76
M2.6	1.460	0.442	0.554	0.361	77.4	2.59E-05	1.56	1.420	0.453	0.588	0.342	75.7	3.34E-05	1.60
M2.7	1.412	0.455	0.539	0.346	80.5	2.63E-05	1.51	1.426	0.451	0.561	0.331	79.5	3.11E-05	1.50
M2.8	1.597	0.405	0.532	0.353	75.9	2.29E-05	1.56	1.528	0.423	0.575	0.334	73.8	3.13E-05	1.63

Table F6.2: Corrected equilibrium method results (ctnd)

Run	Corrected Integral Condensation Curve							Corrected Differential Condensation Curve						
	ϕ_H (-)	θ_H (-)	$\tilde{y}_{P,corr}$ (-)	$\tilde{x}_{P,corr}$ (-)	$T_{v,out}$ (°C)	dT/dh (kg.°C/J)	L (m)	ϕ_H (-)	θ_H (-)	$\tilde{y}_{P,corr}$ (-)	$\tilde{x}_{P,corr}$ (-)	$T_{v,out}$ (°C)	dT/dh (kg.°C/J)	L (m)
M2.9	1.548	0.418	0.518	0.338	79.2	2.33E-05	1.52	1.545	0.419	0.545	0.324	77.9	2.87E-05	1.52
M2.10	1.548	0.418	0.518	0.338	79.2	2.33E-05	1.52	(N/A)	(N/A)	(N/A)	(N/A)	(N/A)	(N/A)	(N/A)
M2.11	1.700	0.380	0.505	0.337	74.7	2.12E-05	1.24	1.525	0.424	0.551	0.316	72.6	3.01E-05	1.39
M2.12	1.637	0.395	0.495	0.325	79.0	2.16E-05	1.35	1.594	0.406	0.523	0.311	77.8	2.69E-05	1.39
M2.13	1.691	0.382	0.509	0.341	76.8	2.12E-05	1.44	1.554	0.417	0.559	0.321	74.4	3.07E-05	1.57
M2.14	1.664	0.389	0.509	0.335	70.6	2.15E-05	1.28	1.556	0.416	0.544	0.317	69.1	2.82E-05	1.37
M2.15	1.645	0.393	0.467	0.301	75.3	2.02E-05	1.24	1.674	0.386	0.479	0.294	74.9	2.23E-05	1.22
M2.16	1.637	0.395	0.456	0.292	77.1	1.99E-05	1.20	1.693	0.382	0.463	0.288	76.9	2.11E-05	1.16
M3.1	1.368	0.467	0.799	0.662	75.3	2.92E-05	1.72	0.723	0.682	0.942	0.625	59.5	8.65E-05	3.26
M3.2	1.576	0.411	0.795	0.683	74.3	2.34E-05	1.69	0.805	0.651	0.955	0.666	56.1	8.21E-05	3.31
M3.3	1.296	0.488	0.785	0.635	84.3	3.13E-05	1.90	0.595	0.632	0.909	0.596	71.5	7.89E-05	2.87
M3.4	1.398	0.459	0.785	0.649	82.5	2.80E-05	1.91	0.903	0.615	0.921	0.619	68.1	7.78E-05	2.96
M3.7	1.508	0.429	0.783	0.662	80.6	2.51E-05	1.82	0.892	0.620	0.936	0.640	64.1	7.91E-05	3.08
M3.8	1.177	0.524	0.788	0.613	77.6	3.63E-05	1.73	0.708	0.688	0.903	0.557	66.1	8.49E-05	2.88
M3.9	1.310	0.484	0.789	0.636	75.8	3.14E-05	1.75	0.732	0.678	0.925	0.590	61.4	8.59E-05	3.13
M3.11	1.227	0.509	0.800	0.634	68.9	3.42E-05	1.65	0.610	0.726	0.933	0.577	54.6	9.18E-05	3.32
M3.12	1.178	0.524	0.790	0.612	72.9	3.66E-05	1.59	0.623	0.721	0.913	0.549	60.4	8.99E-05	3.01
M3.13	1.424	0.451	0.785	0.644	71.8	2.85E-05	1.56	0.650	0.710	0.944	0.602	54.6	9.12E-05	3.41
M3.14	1.091	0.552	0.772	0.576	80.2	3.95E-05	1.82	0.786	0.658	0.860	0.518	72.2	7.65E-05	2.53
M3.15	1.164	0.529	0.778	0.595	77.5	3.66E-05	1.87	0.791	0.656	0.882	0.539	67.5	7.89E-05	2.75
M3.16	1.243	0.504	0.782	0.614	74.9	3.35E-05	1.90	0.802	0.652	0.902	0.563	63.0	8.05E-05	2.94
M3.17	1.302	0.486	0.797	0.639	65.0	3.17E-05	1.65	0.615	0.724	0.942	0.587	49.3	9.21E-05	3.49
M3.18	1.534	0.422	0.791	0.665	63.8	2.48E-05	1.62	0.679	0.699	0.959	0.636	44.9	8.86E-05	3.67

Table F7.1: Film theory Simulation Results

Run	Reflux Condenser						Co-current Condenser					
	$\tilde{y}_{P,out}$ (-)	$\tilde{x}_{P,out}$ (-)	$T_{v,out}$ (°C)	$T_{c,out}$ (°C)	$\dot{Q}_T$ (W)	L (m)	$\tilde{y}_{P,out}$ (-)	$\tilde{x}_{P,out}$ (-)	$T_{v,out}$ (°C)	$T_{c,out}$ (°C)	$\dot{Q}_T$ (W)	L (m)
M1.1	0.643	0.539	79.3	34.3	2535.9	1.47	0.593	0.550	82.2	34.9	2385.8	1.23
M1.2	0.625	0.503	82.2	39.3	2321.5	1.42	0.573	0.521	85.2	40.0	2159.8	1.15
M1.3	0.618	0.489	83.5	41.6	2203.3	1.39	0.565	0.511	86.4	42.3	2042.1	1.11
M1.4	0.623	0.528	84.4	29.9	3522.8	1.54	0.573	0.535	87.2	30.8	3318.1	1.35
M1.5	0.616	0.506	86.6	34.7	3297.7	1.53	0.564	0.518	89.6	35.6	3069.6	1.30
M1.6	0.613	0.488	88.7	39.4	3076.8	1.52	0.556	0.504	92.0	40.4	2832.3	1.25
M1.12	0.617	0.482	81.2	34.2	2834.6	1.51	0.568	0.504	83.9	35.1	2622.8	1.24
M1.13	0.609	0.459	84.1	39.1	2665.6	1.48	0.557	0.487	87.0	40.0	2441.6	1.19
M1.14	0.605	0.448	85.3	41.6	2553.6	1.47	0.553	0.479	88.2	42.5	2328.4	1.17
M1.15	0.607	0.475	81.3	39.4	2164.5	1.38	0.554	0.496	84.2	40.1	2012.1	1.10
M1.16	0.603	0.463	82.3	41.5	2079.8	1.36	0.551	0.489	85.1	42.2	1924.4	1.08
M1.17	0.608	0.505	80.3	39.6	1898.7	1.30	0.556	0.517	83.2	40.0	1792.4	1.05
M1.19	0.611	0.467	75.0	39.1	1519.1	1.25	0.564	0.496	77.5	39.5	1420.4	0.97
M1.20	0.595	0.462	78.1	41.7	1506.9	1.22	0.544	0.486	80.8	42.1	1411.2	0.94
M1.21	0.597	0.487	76.3	39.3	1459.6	1.20	0.547	0.504	79.0	39.6	1382.5	0.94
M2.1	0.547	0.374	74.4	39.1	1546.9	1.24	0.498	0.411	76.7	39.6	1439.5	0.96
M2.2	0.567	0.404	68.8	29.0	2015.8	1.41	0.514	0.434	71.3	29.6	1881.5	1.09
M2.3	0.554	0.378	72.1	33.9	1904.7	1.37	0.502	0.414	74.6	34.4	1768.1	1.05
M2.4	0.543	0.354	75.1	38.9	1776.6	1.33	0.493	0.395	77.5	39.5	1640.3	1.02
M2.5	0.544	0.394	75.7	29.3	2677.0	1.46	0.492	0.420	78.2	30.1	2677.0	1.17
M2.6	0.535	0.372	78.4	34.2	2511.3	1.43	0.482	0.403	81.0	35.0	2511.3	1.13
M2.7	0.530	0.352	81.0	38.9	2395.7	1.43	0.476	0.389	83.7	39.8	2395.7	1.11
M2.8	0.505	0.365	77.2	29.5	2705.9	1.40	0.455	0.388	79.5	30.3	2705.9	1.14

Table F7.2: Film theory Simulation Results (ctnd)

Run	Reflux Condenser						Co-current Condenser					
	$\tilde{y}_{P,out}$ (-)	$\tilde{x}_{P,out}$ (-)	$T_{v,out}$ (°C)	$T_{c,out}$ (°C)	$\dot{Q}_T$ (W)	L (m)	$\tilde{y}_{P,out}$ (-)	$\tilde{x}_{P,out}$ (-)	$T_{v,out}$ (°C)	$T_{c,out}$ (°C)	$\dot{Q}_T$ (W)	L (m)
M2.9	0.501	0.347	80.1	34.4	2594.1	1.40	0.448	0.375	82.5	35.2	2594.1	1.12
M2.10	0.506	0.374	73.6	34.3	1664.2	1.21	0.437	0.391	76.0	34.7	1664.2	0.94
M2.11	0.482	0.348	75.8	39.2	1476.9	1.15	0.429	0.373	78.1	39.5	1476.9	0.89
M2.12	0.480	0.333	79.8	39.3	1981.6	1.26	0.426	0.361	82.2	39.8	1981.6	0.99
M2.13	0.485	0.350	78.0	34.4	2233.1	1.32	0.430	0.372	80.4	35.0	2233.1	1.05
M2.14	0.487	0.347	71.7	34.2	1568.3	1.18	0.437	0.373	73.8	34.6	1479.6	0.92
M2.15	0.461	0.304	75.7	39.2	1618.9	1.19	0.410	0.336	77.8	39.6	1514.9	0.92
M2.16	0.453	0.294	77.3	41.5	1575.8	1.16	0.404	0.328	79.4	42.0	1472.8	0.91
M3.1	0.760	0.674	78.4	39.4	2304.3	1.48	0.725	0.686	81.1	39.9	2161.5	1.26
M3.2	0.760	0.689	77.0	34.6	2635.2	1.51	0.726	0.695	79.5	35.2	2503.1	1.34
M3.3	0.746	0.649	87.3	39.8	3344.5	1.61	0.708	0.663	90.2	40.8	3078.8	1.39
M3.4	0.745	0.660	85.6	35.0	3641.8	1.61	0.709	0.670	88.3	36.0	3396.1	1.44
M3.7	0.746	0.669	83.4	34.9	3344.8	1.58	0.710	0.676	86.1	35.7	3145.8	1.41
M3.8	0.748	0.635	80.7	44.2	2048.6	1.46	0.709	0.655	83.5	44.8	1886.4	1.18
M3.9	0.748	0.652	78.9	39.5	2334.3	1.49	0.711	0.666	81.6	40.1	2178.1	1.26
M3.11	0.756	0.654	72.2	39.2	1595.6	1.39	0.720	0.671	74.9	39.6	1495.5	1.12
M3.12	0.747	0.636	76.2	44.1	1462.1	1.33	0.709	0.657	78.9	44.5	1359.2	1.05
M3.13	0.744	0.657	74.9	39.5	1738.3	1.35	0.707	0.669	77.5	39.8	1642.3	1.13
M3.14	0.735	0.601	83.0	44.0	2376.7	1.52	0.696	0.628	85.8	44.9	2158.3	1.23
M3.15	0.737	0.618	80.5	39.2	2601.2	1.54	0.700	0.639	83.2	40.1	2394.1	1.28
M3.16	0.738	0.635	78.2	34.6	2823.7	1.56	0.704	0.650	80.7	35.4	2630.9	1.34
M3.17	0.752	0.658	68.4	34.3	1658.7	1.39	0.718	0.672	70.8	34.6	1569.4	1.14
M3.18	0.751	0.675	66.7	29.4	1976.1	1.44	0.719	0.683	69.0	29.7	1891.0	1.24

Appendix G: Film Theory Simulation Code

The following Visual Basic code was used to create a simulation program to evaluate the film theory model of Colburn & Drew (1937). There are 5 programs and 2 functions;

fn_ColDrew_Reflux	Reflux condenser simulation
fn_ColDrew_Co-curr	Co-current condenser simulation
ColDrew_Reflux	Subroutine based program to simulate reflux condenser
ColDrew_Perfect	Heat and mass transfer calculations assuming perfect mixing
ColDrew_NoMix	Heat and mass transfer calculations assuming no-mixing at the top of the tube
OutputFile	Program to set up output file for subroutine simulation
Table Values	Used to display results in output file

```
Function fn_ColDrew_Reflux(fPsat, fTsat, fyPin, fNbulkV,_
                                        frLV, fHTCcw, fTcOut, fVolWat, iModel)
'=============================================================
'MODIFICATION HISTORY
'MOD        DATE       BY                  DESCRIPTION
'1.0        11/05/03   D Cuthbertson       Initial version  (created from Sub ColDrew_Reflux for
                                            processing of multiple runs simultaneously)
'1.1        20/05/03   D Cuthbertson       Layout tidied up
'=============================================================
        icondenser = 1
'Number of increments
        linc = 20
'Set up constants
        Const Pi = 3.141592654
        Const g = 9.80665 '[m/s**2]
        Const MWpen = 72.151
        Const MWiso = 114.232
        Const TSid = 0.045 '[m]
        Const TSl = 0.5025 '[m]
'Set up arrays
        Dim Nvap(0 To 21), Nliq(0 To 21), NliqPen(0 To 21) As Single
```

```
        Dim yP(0 To 21), xP(0 To 21), Tbulk(0 To 21) As Single
        Dim dArea(0 To 21), dLen(0 To 21), Ltot(0 To 21) As Single
        Dim Qcum(0 To 21), QFlux(0 To 21), Twater(0 To 21) As Single
'Calculate required liquid flow rate (molar)
        NCondin = 0
        NCondOut = fNbulkV * frLV
'Calculate amount of vapour to be condensed in each increment
        dNvap = NCondOut / linc
'Convert coolant vol flow to mass flow rate
        Mwat = fVolWat * fn_PropWat(fTcOut, 1)
'-----------------------------------------------------------------------------
'Starting guess for liquid composition based on vapour inlet composition
        xPoutGuess = fyPin - 0.1
'-----------------------------------------------------------------------------
'
'Initialise convergency variables for xP/NliqPen iteration
        dNliqPen = 1
        ixPloop = 1
        ilterLoop = 1
        xPloopLim = 20
        FlagLiqPen = 0
        DeltaxP = 0.01
'
Do While Abs(dNliqPen) > 0.0000000001
'
'Select value of xP depending on loop count and flagLiqPen
        If FlagLiqPen = 0 Then
                If ixPloop = 1 Then
                        xPout = xPoutGuess
                Else
                        If ixPloop < 3 Then
                                xPout = xPoutOld + DeltaxP
                                Else
'Newton-Raphson method
        xPout = xPoutOld - (dNliqPen / ((dNliqPen - dNliqPenOld) / (xPoutOld - xPoutOld2)))
                        End If
                End If
                ElseIf FlagLiqPen = 1 Then xPout = xPout + DeltaxP
                ElseIf FlagLiqPen = 2 Then xPout = xPoutGuess
                        DeltaxP = DeltaxP - 0.002
        End If
'-----------------------------------------------
'ITERATION LOOP CALCULATIONS
'-----------------------------------------------
        I = 1           'Loop Counter
```

```
'Put initial values into arrays
        Nvap(i) = fNbulkV
        Nliq(i) = NCondOut
        NliqPen(i) = NCondOut * xPout
        yP(i) = fyPin
        xP(i) = xPout
        Tbulk(i) = fTsat
        Twater(i) = fTcOut
        Ltot(i) = 0

'Start of incremental calculations
        Do While I < (Iinc + 1)
'Local molar flowrates
        NVloc = Nvap(i)
        NLloc = Nliq(i)
'Local mole fractions
        yPloc = yP(i)
        xPloc = xP(i)
'Local Temperature
        Tg = Tbulk(i)
        Tcw = Twater(i)
'Initialise values to be used in perfect/no mix models
        QwallFlux = 0
        nPen = 0
        nIso = 0
        Ucond = 0
        fdTGbydA = 0
        BetaGx = 0
        Tdew = 0
        HTCdrygas = 0
        RateFactor = 1
'Call perfect/no-mixing model for heat and mass transfer step depending on loop counter
        If I < 20 Then
            ColDrew_Perfect Icondenser, Tg, fPsat, yPloc, xPloc, NVloc, NLloc, dNvap,_
                fHTCcw, Tcw, QwallFlux, nPen, nIso, Ucond, dTGbydA, Tdew, BetaGx,_
                HTCdrygas, RateFactor
'Call no mix model at top of tube
        Else
            ColDrew_NoMix Icondenser, Tg, fPsat, yPloc, xPloc, NVloc, NLloc, dNvap,_
                fHTCcw, Tcw, QwallFlux, nPen, nIso, Ucond, dTGbydA, Tdew, BetaGx,_
                RateFactor
        End If
'-------------------------------------------------------------------------
'Calculate mass balance and area calculation over the increment
'-------------------------------------------------------------------------
```

```
        Nvap(i + 1) = Nvap(i) – dNvap                   'Vapour mole flow out of increment
        QFlux(i) = QwallFlux                            'Heat flux over increment
'
        dArea(i) = dNvap / (nPen + nIso)                'Area of increment
        dLen(i) = dArea(i) / (Pi * TSid)                'Conversion of area to length of increment
        Ltot(i + 1) = Ltot(i) + dLen(i)
'
        Qcum(i + 1) = Qcum(i) + QwallFlux * dArea(i)    'Add to total heat load
'
        NVapPen = yP(i) * Nvap(i) - nPen * dArea(i)     'Pentane vap flow out of increment
        yP(i + 1) = NVapPen / Nvap(i + 1)                       'Pentane vap mol fr out of increment
'
        Nliq(i + 1) = Nliq(i) – dNvap                   'Liquid flow into increment
        NliqPen(i + 1) = xP(i) * Nliq(i) - (nPen * dArea(i))    'Pentane liq flow into increment
'-------------------------------------------------------------------------------------------------
'Checks to make sure solution is sensible
        If i < 20 Then
          If NliqPen(i + 1) > Nliq(i + 1) Then   'Composition > 1 not possible
                  FlagLiqPen = 2
                  Exit Do
          End If
'
          If NliqPen(i + 1) < 0 Then  '-ve pentane flow not possible
                  FlagLiqPen = 1
                  Exit Do
          Else
                  FlagLiqPen = 0
          End If
        End If
'-------------------------------------------------------------------------------------------------
        xP(i + 1) = NliqPen(i + 1) / Nliq(i + 1)        'Pentane mol fr into increment
        'Tbulk(i + 1) = Tbulk(i) - dArea(i) * dTGbydA    'Vapour Temp leaving increment
        Cpwat = fn_PropWat(Twater(i), 2)                        'Water specific heat
        Twater(i + 1) = Twater(i) - (dArea(i) * QwallFlux / (Mwat * Cpwat)) 'Water temperature
'
        i = i + 1
        Loop
'
        If Abs(Nliq(i)) < 0.0000000001 Then Nliq(i) = 0

        If FlagLiqPen = 0 Then
'Store old values of xPout and dNliqPen
           xPoutOld2 = xPoutOld
           xPoutOld = xPout
```

```
        dNliqPenOld = dNliqPen
'
        dNliqPen = NliqPen(21)
'Check for non-convergence
        ixPloop = ixPloop + 1
        If ixPloop = xPloopLim Then Exit Do
        ElseIf FlagLiqPen = 1 Then
                dNliqPen = 1E+20
                i = i + 1
                ixPloop = 1
'       ElseIf FlagLiqPen = 2 Then
                dNliqPen = 2E+20
                i = i + 1
                ixPloop = 1
        End If
'
        Loop        End of iterative calculations
'
        Dim Results(0 To 10) As Single
        Results(0) = yP(linc + 1)
        Results(1) = xPout
        Results(2) = Tbulk(linc + 1)
        Results(3) = Twater(linc + 1)
        Results(4) = NliqPen(linc + 1)
        Results(5) = Qcum(linc + 1)
        Results(6) = Ltot(linc + 1)
'
        fn_ColDrew_Reflux = Results
'
End Function



Function fn_ColDrew_CoCurrent(fPsat, fTsat, fyPin, fNbulkV, frLV, fHTCcw, fTcOut, fVolWat, lModel)
'=============================================================================
'MODIFICATION HISTORY
'MOD  DATE        BY                 DESCRIPTION
'1.0  13/05/03    D Cuthbertson      Initial version    '(created from SUB ColDrew_CoCurrent)
'1.1  23/05/03    D Cuthbertson      Tidied up, changes to match reflux version
'=============================================================================
        icondenser = 2
'Number of increments
        linc = 20
'Set up constants
        Const Pi = 3.141592654
```

```
        Const g = 9.80665 '[m/s**2]
        Const MWpen = 72.151
        Const MWiso = 114.232
        Const TSid = 0.045 '[m]
        Const TSl = 0.5025 '[m]
'Set up arrays
Dim Nvap(0 To 22), Nliq(0 To 22), NliqPen(0 To 22) As Single
Dim yP(0 To 22), xP(0 To 22), Tbulk(0 To 22) As Single
Dim dArea(0 To 22), dLen(0 To 22), Ltot(0 To 22) As Single
Dim Qcum(0 To 22), QFlux(0 To 22), Twater(0 To 22) As Single
'
        NCondin = 0
        NCondOut = fNbulkV * frLV                    'Calculate required liquid mole flow rate
        dNvap = NCondOut / linc                      'Vapour  condensed in each increment
        Mwat = fVolWat * fn_PropWat(fTcOut, 1)       'Convert coolant vol flow to mass flow rate
'Loop Counter
        i = 1
'Put initial values into arrays
        Nvap(i) = fNbulkV
        Nliq(i) = NCondin
        yP(i) = fyPin
        xP(i) = 0
        Tbulk(i) = fTsat
        Twater(i) = fTcOut
'-------------------------------------------------------------
'Start of incremental calculations
'-------------------------------------------------------------
        Do While I < (linc + 1)
'
        NVloc = Nvap(i)      'Local mole flowrates
        NLloc = Nliq(i)
        yPloc = yP(i)        'Local mole fractions
        xPloc = xP(i)
        Tg = Tbulk(i)        'Local Temperature
        Tcw = Twater(i)
'Initialise values to be used in perfect/no mix models
        QwallFlux = 0
        nPen = 0
        nIso = 0
        Ucond = 0
        dTGbydA = 0
        Tdew = 0
        HTCdrygas = 0
'Call perfect/no mixing model for heat and mass transfer step depending on loop counter
        If I = 1 Then
```

```
            ColDrew_NoMix icondenser, Tg, fPsat, yPloc, xPloc, NVloc, NLloc, dNvap, fHTCcw,_
                  Tcw, QwallFlux, nPen, nIso, Ucond, dTGbydA, Tdew, BetaGx, RateFactor
            Else
            If I > 1 Then
            ColDrew_Perfect icondenser, Tg, fPsat, yPloc, xPloc, NVloc, NLloc, dNvap, fHTCcw,_
            Tcw, QwallFlux, nPen, nIso, Ucond, dTGbydA, Tdew, BetaGx, HTCdrygas, RateFactor
            End If
      End If
'-------------------------------------------------------------------------------
'Calculate mass balance and area calculation over the increment
'-------------------------------------------------------------------------------
      Nvap(i + 1) = Nvap(i) – dNvap                    'Vapour molar flow out of increment
      QFlux(i) = QwallFlux                             'Heat flux over increment
'
      dArea(i) = dNvap / (nPen + nIso)                 'Area of increment
      dLen(i) = dArea(i) / (Pi * TSid)                 'Conversion of area to length of increment
      Ltot(i + 1) = Ltot(i) + dLen(i)
      Qcum(i + 1) = Qcum(i) + QwallFlux * dArea(i)     'Add to total heat load

      NVapPen = yP(i) * Nvap(i) - nPen * dArea(i)      'Pentane vap flow out of increment
      yP(i + 1) = NVapPen / Nvap(i + 1)                'Pentane vap mole fr out of increment

      Nliq(i + 1) = Nliq(i) + dNvap                          'Liquid flow out of increment
      NliqPen(i + 1) = xP(i) * Nliq(i) + (nPen * dArea(i))   'Pentane liq flow out of increment
      xP(i + 1) = NliqPen(i + 1) / Nliq(i + 1)               'Pentane mole fr out of increment
'
'Change in bulk vapour temperature
      'Tbulk(i + 1) = Tbulk(i) - dArea(i) * dTGbydA          'Vapour temp leaving increment
      Cpwat = fn_PropWat(Twater(i), 2)                             'Water specific heat
      Twater(i + 1) = Twater(i) - dArea(i) * QwallFlux / (Mwat * Cpwat)  Water temp into increment

      i = i + 1
      Loop
'
      Dim Results(0 To 10) As Single
      Results(0) = yP(linc + 1)
      Results(1) = xP(linc + 1)
      Results(2) = Tbulk(linc + 1)
      Results(3) = Twater(linc + 1)
      Results(4) = Nliq(linc + 1)
      Results(5) = Qcum(linc + 1)
      Results(6) = Ltot(linc + 1)
'
fn_ColDrew_CoCurrent = Results
End Function
```

```
Sub ColDrew_Reflux()
'=============================================================================
'MODIFICATION HISTORY
'MOD  DATE        BY              DESCRIPTION
' 1.0   20/05/02     D Cuthbertson     Initial Version: No alterations
' 1.2   31/05/02     D Cuthbertson     +film htc now uses corr based on single component data
' 1.3   22/05/03     D Cuthbertson     +Changed to be same an fn_ColDrew_Reflux + tidy up
"=============================================================================
'-----------------
'Get unputs
'-----------------
        DataCol = InputBox("Select the column to perfrom the analysis on")
                If DataCol = "" Then Exit Sub
        iModel = InputBox("Select 1 for no-mixing or 2 for perfect mixing model")
                If iModel = "" Then Exit Sub
'
        condenser = 1                   'Reflux condenser flag
'
'Build strings so that data can be read from selected column
        strRunDate = DataCol & "7"
        strRnum = DataCol & "8"
        strTg = DataCol & "12"
        strPsat = DataCol & "11"
        stryPin = DataCol & "14"
        strNBulkV = DataCol & "15"
        strrLV = DataCol & "19"
        strHTCcw = DataCol & "27"
        strTcw = DataCol & "24"
        strMwat = DataCol & "25"
'Read variables from column using strings
        RunDate = Range(strRunDate)
        Rnum = Range(strRnum) & "_R"
        Tgin = Range(strTg)
        Psat = Range(strPsat)
        yPin = Range(stryPin)
        NBulkV = Range(strNBulkV)
        HTCcw = Range(strHTCcw)
        rLV = Range(strrLV)
        Tcwout = Range(strTcw)
        Mwat = Range(strMwat)
'Copy formats for output file
        Sheets("RefluxFormats").Select
        Cells.Select
```

```
        Selection.Copy
        Sheets("CDrew_Data").Select
'Set up constants
        Const Pi = 3.141592654
        Const g = 9.80665 '[m/s**2]
        Const MWpen = 72.151
        Const MWiso = 114.232
        Const TSid = 0.045 '[m]
        Const TSl = 0.5025 '[m]
'Set up arrays
        Dim Nvap(0 To 21), Nliq(0 To 21), NliqPen(0 To 21) As Single
        Dim yP(0 To 21), xP(0 To 21), Tbulk(0 To 21), dArea(0 To 21) As Single
        Dim dLen(0 To 21), Qcum(0 To 21), QFlux(0 To 21), Twater(0 To 21) As Single
'
        linc = 20                       'Number of increments
        NCondin = 0
        NCondOut = NBulkV * rLV         'Calculate required liquid mole flow rate
        dNvap = NCondOut / linc         Vapour condensed in each increment
'
Set up output file
OutputFile RunDate, Rnum, Tgin, Psat, NBulkV, yPin, Tcwout, HTCcw, Mwat, rLV, iModel, Icondenser
'
'-------------------------------------------------------------------------------
'Starting guess for liquid composition based on vapour inlet composition
xPoutGuess = yPin - 0.1
'-------------------------------------------------------------------------------
'Initialise convergency variables for xP/NliqPen iteration
        dNliqPen = 1
        IxPloop = 1
        IIterLoop = 1
        xPloopLim = 20
        FlagLiqPen = 0
        DeltaxP = 0.01
'
        Do While Abs(dNliqPen) > 0.0000000001
'
'Select value of xP depending on loop count and flagLiqPen
        If FlagLiqPen = 0 Then
          If ixPloop = 1 Then
                  xPout = xPoutGuess
                  Else
                  If IxPloop < 3 Then
                          xPout = xPoutOld + DeltaxP
                          Else
'Newton-Raphson convergence method
```

```
                xPout = xPoutOld - (dNliqPen / ((dNliqPen - dNliqPenOld) / (xPoutOld - xPoutOld2)))
                End If
            End If
            ElseIf FlagLiqPen = 1 Then xPout = xPout + DeltaxP
            ElseIf FlagLiqPen = 2 Then xPout = xPoutGuess
                DeltaxP = DeltaxP - 0.002
        End If
'-------------------------------------------------
'ITERATION LOOP CALCULATIONS
'-------------------------------------------------
        i = 1                   'Loop Counter
'Put initial values into arrays
        Nvap(i) = NBulkV
        Nliq(i) = NCondOut
        NliqPen(i) = NCondOut * xPout
        yP(i) = yPin
        xP(i) = xPout
        Tbulk(i) = Tgin
        Twater(i) = Tcwout
'
'Start of incremental calculations
        Do While i < (linc + 1)
'
        NVloc = Nvap(i)     'Local mole flowrates
        NLloc = Nliq(i)
        yPloc = yP(i)       'Local mole fractions
        xPloc = xP(i)
        Tg = Tbulk(i)       'Local Temperature
        Tcw = Twater(i)
'Initialise values to be used in perfect/no mix models
        QwallFlux = 0
        nPen = 0
        nIso = 0
        Ucond = 0
        fdTGbydA = 0
        BetaGx = 0
        Tdew = 0
        HTCdrygas = 0
        RateFactor = 1

'Call perfect/no-mixing model for heat and mass transfer step depending on user input and loop counter
        If iModel = 1 Then
          ColDrew_NoMix icondenser, Tg, Psat, yPloc, xPloc, NVloc, NLloc, dNvap, HTCcw, Tcw,_
                QwallFlux, nPen, nIso, Ucond, dTGbydA, Tdew, BetaGx, HTCdrygas, RateFactorM
        ElseIf iModel = 2 Then
```

```
        If I < 20 Then

'For perfect mixing model call no mix model at top of tube
        ColDrew_Perfect icondenser, Tg, Psat, yPloc, xPloc, NVloc, NLloc, dNvap, HTCcw, Tcw,_
                QwallFlux, nPen, nIso, Ucond, dTGbydA, Tdew, BetaGx, HTCdrygas, RateFactorM
        ElseIf I = 20 Then ColDrew_NoMix icondenser, Tg, Psat, yPloc, xPloc, NVloc, NLloc, dNvap,_
                        HTCcw, Tcw, QwallFlux, nPen, nIso, Ucond, dTGbydA, Tdew, BetaGx,_
                        HTCdrygas, RateFactorM
        End If
    End If
'-------------------------------------------------------------------------
'Calculate mass balance and area calculation over the increment
'-------------------------------------------------------------------------
        Nvap(i + 1) = Nvap(i) – dNvap                   'Vapour mole flow out of increment
        QFlux(i) = QwallFlux                            'Heat flux over increment
'
        dArea(i) = dNvap / (nPen + nIso)                'Area of increment
        dLen(i) = dArea(i) / (Pi * TSid)                'Conversion of area to length of increment
'
        Qcum(i + 1) = Qcum(i) + QwallFlux * dArea(i)            'Add to total heat load
'
        NVapPen = yP(i) * Nvap(i) - nPen * dArea(i)             'Pentane vap flow out of increment
        yP(i + 1) = NVapPen / Nvap(i + 1)                       'Pentane vap mol fr out of increment
'
        Nliq(i + 1) = Nliq(i) – dNvap                           'Liquid flow into increment
        NliqPen(i + 1) = xP(i) * Nliq(i) - (nPen * dArea(i))    'Pentane liq flow into increment
'-------------------------------------------------------------------------------------------
'Checks to make sure solution is sensible
        If I < 20 Then
          If NliqPen(i + 1) > Nliq(i + 1) Then          'Composition > 1 not possible
                FlagLiqPen = 2
                Exit Do
          End If
'
          If NliqPen(i + 1) < 0 Then                    '-ve pentane flow not possible
                FlagLiqPen = 1
                Exit Do
          Else
                FlagLiqPen = 0
          End If
        End If
'-------------------------------------------------------------------------------
        xP(i + 1) = NliqPen(i + 1) / Nliq(i + 1)        'Pentane mol fr into increment
        'Tbulk(i + 1) = Tbulk(i) - dArea(i) * dTGbydA   'Vapour Temp leaving increment
        Cpwat = fn_PropWat(Twater(i), 2)                        'Water specific heat
```

```
        Twater(i + 1) = Twater(i) - (dArea(i) * QwallFlux / (Mwat * Cpwat)) 'Water temperature

'Put values into table in output file
        TableValues I, Icondenser, yP, xP, Nvap, Nliq, NliqPen, Qcum, Tbulk, dLen, QwallFlux, Twater,_
          nPen, nIso, Ucond, dTGbydA, Tdew, BetaGx, HTCdrygas, RateFactorM
'
        I = I + 1
        Loop
'
        If Abs(Nliq(i)) < 0.0000000001 Then Nliq(i) = 0
'Display values out of the top increment
        TableValues I, Icondenser, yP, xP, Nvap, Nliq, NliqPen, Qcum, Tbulk, dLen, QwallFlux, Twater,_
          nPen, nIso, Ucond, dTGbydA, Tdew, BetaGx, HTCdrygas, RateFactorM
'
        If FlagLiqPen = 0 Then
'Store old values of xPout and dNliqPen
        xPoutOld2 = xPoutOld
        xPoutOld = xPout
        dNliqPenOld = dNliqPen
'
        dNliqPen = NliqPen(21)
'Check for non-convergence
        ixPloop = ixPloop + 1
      If ixPloop = xPloopLim Then Exit Do
        ElseIf FlagLiqPen = 1 Then
        dNliqPen = 1E+20
        I = I + 1
        ixPloop = 1
        TableValues I, Icondenser, yP, xP, Nvap, Nliq, NliqPen, Qcum, Tbulk, dLen, QwallFlux,_
              Twater, nPen, nIso, Ucond, dTGbydA, Tdew, BetaGx, HTCdrygas, RateFactorM

      ElseIf FlagLiqPen = 2 Then
            dNliqPen = 2E+20
            I = I + 1
            ixPloop = 1
            TableValues I, Icondenser, yP, xP, Nvap, Nliq, NliqPen, Qcum, Tbulk, dLen,_
                  QwallFlux, Twater, nPen, nIso, Ucond, dTGbydA, Tdew, BetaGx,_
                  HTCdrygas, RateFactorM
End If

'Display guess value and calculated value in output file for iteration history
        IShowIter = IIterLoop + 15 '

        strLoopNo = "V" & IShowIter
        strxPout = "W" & IShowIter
```

```
        strdNliqPen2 = "X" & iShowIter

        Range(strLoopNo) = iIterLoop
        Range(strxPout) = xPout
        Range(strdNliqPen2) = dNliqPen
'
        iIterLoop = iIterLoop + 1
        Loop
'
        Beep
        MsgBox "Model run successfully"
'
        If iModel = 1 Then
          Fname = "C:\CDrew_Models_3.0\Reflux\No Mixing\NoM_" & Rnum
        Else
          Fname = "C:\CDrew_Models_3.0\Reflux\Perfect Mixing\PM_" & Rnum
        End If
        ChDir "C:\CDrew_Models_3.0\Reflux"
        ActiveWorkbook.SaveAs FileName:=Fname, FileFormat:=xlNormal, Password:="",_
                WriteResPassword:="", ReadOnlyRecommended:=False, CreateBackup:=False
'
End Sub
```

```
Sub ColDrew_NoMix(icondenser, fTg, fPsat, fyPin, fxPout, fNvap, fNCond, fdNvap, fHTCcw, fTcw,
QwallFlux, nPen, nIso, Ucond, dTGbydA, Tdew, BetaGx, HTCdrygas, RateFactorM)
'================================================================
'MODIFICATION HISTORY
'MOD  DATE      BY              DESCRIPTION
' 1.0   05/04/02  D Cuthbertson   Initial Version
'1.1    55/05/02  D Cuthbertson   +Iterative loop changed to method of false position
'----------------------------------------------------------
'NOTES:
'       1.    Method as described in HTFS Handbook Sheet CM33
'       2.    x,y are mole fractions in liquid/vapour
'
_____________________________________
'
        Dim yPiface
        Const Pi = 3.141592654
        Const g = 9.80665 '[m/s**2]
        Const MWpen = 72.151
        Const MWiso = 114.232
        Const TSid = 0.045 '[m]
```

```
        Const TSI = 0.5025 '[m]
        TgK = fTg + 273.15
'
        Atube = (Pi * TSid ^ 2) / 4              'Cross sectional area
        Asurf = Pi * TSid * TSI * 3              'Surface area
'
'Convert mole flow rates to mass flow rates
        Mvap = fNvap * ((fyPin * MWpen) + ((1 - fyPin) * MWiso))
'
'PHYSICAL PROPERTY DATA
'=====================
'Bulk Vapour
        Den_VapIn = fn_PropHCmix(fyPin, fTg, fPsat, 6)
        Cp_VapIn = fn_PropHCmix(fyPin, fTg, fPsat, 7)
        TCond_VapIn = fn_PropHCmix(fyPin, fTg, fPsat, 9)
        DiffAB = fn_DiffAB(fTg, fPsat)
'Component specific heats at vapour temperature(calculation of Phi)
        Cp_VapPen = fn_PropHCmix(1, fTg, fPsat, 7)
        Cp_VapIso = fn_PropHCmix(0, fTg, fPsat, 7)
'================================================
'
'Mean Molecular weight of the bulk gas phase (moles)
        MWmix = (fyPin * MWpen) + ((1 - fyPin) * MWiso)
'
'Dry Gas Heat Transfer Coefficient
        HTCdrygas = fn_HTCdrygas(fPsat, fTg, fyPin, TSid, Mvap)
'
'Mass Transfer coefficient
        AA = ((DiffAB * Den_VapIn) / (MWmix * TCond_VapIn))
        BB = (TCond_VapIn) / (Cp_VapIn * Den_VapIn * DiffAB)
        '
        BetaG = HTCdrygas * AA * (BB ^ 0.4)
'
'Estimate  total molar condensing flux
        nTest = 0.0005
'-------------------------------------------------------
'1st LOOP ITERATIVE CALCULATIONS
'-------------------------------------------------------
'Initialise convergency variables
        dq = 1                   'Difference between q1 and q2
        n = 0                    'Loop counter
        nLim = 100               'Max number of loops
        Iter1 = 0
        Iter2 = 0
        dnT = -0.0001
```

```
'Repeat until solution has converged
        Do While Abs(dq) > 0.001 'Converge to 0.1%

        If n = 0 Then nT = nTest
            If n > 0 Then
                If ilter1 = 1 Then
                    If ilter2 = 0 Then
                        nT = nT + dnT
                        Else
                        'METHOD OF FALSE POSITION
                        nT = ((nTOld2 * dqOld) - (nTOld * dqOld2)) / (dqOld - dqOld2)
                    End If
                Else
                nT = nT - dnT
            End If
        End If

'Mass transfer coefficient corrected for high mass transfer rates
        RateFactorM = (nT / BetaG)
        B = (Exp(RateFactorM)) - 1
        CorrFactor = RateFactorM / B
        BetaGx = BetaG * CorrFactor
'Initialise convergency variables
        dy = 1              Difference between yPsurf and yPsurf2
        il2 = 0             'Loop COunter
        il2Lim = 100        'Max. number of loops

'-------------------------------------------------
'2nd LOOP ITERATIVE CALCULATIONS
'-------------------------------------------------
                Do While dy > 0.000001  'Converge to 0.1%

'Select value of Kpen depending on loop count
    If il2 = 0 Then
        Kpen = 0.8  'Nt = guess value in first loop
        Else
        If il2 < 3 Then   'For loops 2 and 3 use increment to guess value
                Kpen = KpenOld + 0.0005
                Else
                'Newton-Raphson
                Kpen = KpenOld - (dy / ((dy - dyOld) / (KpenOld - KpenOld2)))
        End If
    End If
```

```
            yPsurf = (fyPin * (BetaGx + nT)) / (BetaGx + (nT / Kpen))   'Vapour mole fraction at surface
            xPsurf = fn_EqLiqComp(fPsat, yPsurf)                        'Liquid mole fraction at surface

            Kpen2 = yPsurf / xPsurf                                     'Recalculate Kpen
            y2 = fyPin * ((BetaGx + nT) / (BetaGx + (nT / Kpen2)))      'Recalculate yPsurf

            dyOld = dy
            dy = (y2 - yPsurf) / yPsurf                                 'Compare yP's

                yPsurf = y2
                KpenOld2 = KpenOld
                KpenOld = Kpen
'Check for non convergence
                il2 = il2 + 1
                If il2 = il2Lim Then Exit Do
                Loop

        Tdew = fn_Tdew(fPsat, yPsurf)                                   'Condensate surface temperature
        nPen = BetaGx * (fyPin - yPsurf) + fyPin * nT                   'Condensing mole fluxes
        nIso = nT - nPen
'Calculate condensate heat transfer coefficient
        If icondenser = 1 Then
            Ncond2 = fNCond
            ElseIf icondenser = 2 Then Ncond2 = fNCond + fdNvap
        End If
        Mcond = Ncond2 * ((fxPout * MWpen) + ((1 - fxPout) * MWiso))
'Use correction to film HTC for reflux condenser
        If icondenser = 1 Then
            HTCfloc = fn_HTCfLocReflux(Mcond, TSid, fxPbulk, fyPin, Tdew, fTg, fPsat, 0)
            Else
            HTCfloc = fn_HTCfLocCM7(Mcond, TSid, fxPbulk, fyPin, Tdew, fTg, fPsat, 0)
        End If
'Calculate HTC corrected for high mass transfer rates
        Phi = ((nPen * Cp_VapPen * MWpen) + (nIso * Cp_VapIso * MWiso)) / HTCdrygas
        HTCghigh = (HTCdrygas * Phi) / ((Exp(Phi)) - 1)
Heat flux from V/L interface to coolant
        q1A = ((1 / fHTCcw) + (1 / HTCfloc))
        q1 = (Tdew - fTcw) / q1A
'Component enthalpies for local heat balance
        hgPenSurf = fn_PropHCmix(1, Tdew, fPsat, 10)
        hgPenBulk = fn_PropHCmix(1, fTg, fPsat, 10)
        DeltahvPen = fn_PropHCmix(1, Tdew, fPsat, 11)
        hgIsoSurf = fn_PropHCmix(0, Tdew, fPsat, 10)
        hgIsoBulk = fn_PropHCmix(0, fTg, fPsat, 10)
```

```
        DeltahvIso = fn_PropHCmix(0, Tdew, fPsat, 11)
'
'Heat flux from vapout to V/L interface
        q2P = nPen * (hgPenBulk - hgPenSurf + DeltahvPen) * MWpen
        q2I = nIso * (hgIsoBulk - hgIsoSurf + DeltahvIso) * MWiso
        q2 = HTCghigh * (fTg - fTcw) + q2P + q2I
'
        dq = q2 - q1
'
        If dq > 0 Then iIter1 = 1
        If n > 0 And dq < 0 Then iIter2 = 1
'
'Check for non convergence
        n = n + 1
        If n = nLim Then Exit Do
'Store old values of Dq and Nt
        nTOld2 = nTOld
        nTOld = nT
        dqOld2 = dqOld
        dqOld = dq

        Loop
        CpMol_VapIn = Cp_VapIn * Mwmix                    'Convert gas bulk Cp to molar Cp
        dTGbydA = HTCghigh * (fTg - Tdew) / (fNvap * CpMol_VapIn)
        QwallFlux = 0.5 * (q1 + q2)
        Ucond = QwallFlux / (fTg - fTcw)
'
End Sub



Sub ColDrew_Perfect(icondenser, fTg, fPsat, fyPin, fxPbulk, fNvap, fNCond, fdNvap, fHTCcw, fTcw,
QwallFlux, nPen, nIso, Ucond, dTGbydA, Tdew, BetaGx, HTCdrygas, RateFactorM)
'=================================================================
'MODIFICATION HISTORY
'MOD     DATE        BY              DESCRIPTION
'1.0     01/10/01    D Cuthbertson   Initial Version
'1.1     27/04/02    D Cuthbertson   Iterative loop improved
'1.2     03/05/02    D Cuthbertson   Tidied up, moved enthalpy calcs so that correct
                                     temperature is used
'1.3     10/05/03    D Cuthbertson   Film velocity correction to HTCvap
'-----------------------------------------------------------------------------------
'NOTES:
'       1. Method as described in HTFS Handbook Sheet CM33
```

```
'==========================================================================

'
    Dim yPiface
    Const Pi = 3.141592654
    Const g = 9.80665 '[m/s**2]
    Const MWpen = 72.151
    Const MWiso = 114.232
    Const TSid = 0.045 '[m]
    Const TSl = 0.5025 '[m]
'
    Atube = (Pi * TSid ^ 2) / 4                    'Cross sectional area
    Asurf = Pi * TSid * TSl * 3                    'Surface area
    Mvap = fNvap * ((fyPin * MWpen) + ((1 - fyPin) * MWiso)) 'Convert to mass flow rates
    MWmix = (fyPin * MWpen) + ((1 - fyPin) * MWiso)'Mean Molecular weight of the bulk gas
'
'PHYSICAL PROPERTY DATA
'==========================================
'Bulk Vapour
    Den_VapIn = fn_PropHCmix(fyPin, fTg, fPsat, 6)
    Cp_VapIn = fn_PropHCmix(fyPin, fTg, fPsat, 7)
    TCond_VapIn = fn_PropHCmix(fyPin, fTg, fPsat, 9)
    Visc_VapIn = fn_PropHCmix(fyPin, fTg, fPsat, 8)
    DiffAB = fn_DiffAB(fTg, fPsat)
'Component specific heats at vapour temperature(rate factor calculation
    Cp_VapPen = fn_PropHCmix(1, fTg, fPsat, 7)
    Cp_VapIso = fn_PropHCmix(0, fTg, fPsat, 7)
'==========================================
'
    xPsurf = fxPbulk      'Pentane mole fraction at condensate surface for PERFECT MIXING
    yPiface = fn_EqmVapComp(fPsat, xPsurf)      'Vapour Interface composition (VLE calc)
    Tdew = fn_Tdew(fPsat, yPiface)              'Condensate surface Temp (VLE calc)
'
'Condensate MASS flow rate
    If Icondenser = 1 Then
        Ncond2 = fNCond
        ElseIf Icondenser = 2 Then Ncond2 = fNCond + fdNvap
    End If
    Mcond = Ncond2 * ((fxPbulk * MWpen) + ((1 - fxPbulk) * MWiso))
'
'Vapour Heat Transfer Coefficient (with film velocity correction [v1.3 10/05/03] )
'--------------------------------------------------------------------------
    DenF = fn_PropHCmix(fxPbulk, Tdew, fPsat, 1)
    ViscF = fn_PropHCmix(fxPbulk, Tdew, fPsat, 3)
    GammaF = Mcond / (4 * TSid)
    ReF = 4 * GammaF / ViscF                    'Film Reynolds number
```

```
'
        dF1 = ((ViscF ^ 2) / (DenF ^ 2 * g)) ^ 0.333
        dF = 0.68 * dF1 * ReF ^ 0.333                   'Film Thickness
        uF = (DenF * g * dF ^ 2) / (2 * ViscF)          'Film velocity
'
        mVapuF = uF * Den_VapIn * ((Pi * TSid ^ 2) / 4)
        MvapCorr = Mvap + mVapuF
'
        'HTCdrygas = fn_HTCdrygas(fPsat, fTg, fyPin, TSid, Mvap)
        If icondenser = 1 Then
                HTCdrygas = fn_HTCpetukov(fPsat, fTg, fyPin, TSid, MvapCorr)
        Else
                HTCdrygas = fn_HTCpetukov(fPsat, fTg, fyPin, TSid, Mvap)
        End If
'
'Mass Transfer coefficient
        AA = ((DiffAB * Den_VapIn) / (MWmix * TCond_VapIn))
        BB = (TCond_VapIn) / (Cp_VapIn * Den_VapIn * DiffAB)
        BetaG = HTCdrygas * AA * (BB ^ 0.4)
'-------------------------------------------------------------------------
'ITERATIVE CALCULATIONS
'-------------------------------------------------------------------------
        nTest = 0.0005                  'Estimate total condensing flux
'Initialise convergency variables
        nLim = 100                      'Max number of loops
        iIter1 = 0
        iIter2 = 0
        dnT = -0.0001
        dq = 1                          'Difference between q1 and q2
        n = 0                           'Loop counter
'
'Set up conversion loop
Do While Abs(dq) > 0.0001 'Converge to 0.1%
'
If n = 0 Then nT = nTest
If n > 0 Then
        If iIter1 = 1 Then
                If iIter2 = 0 Then
                        If nT < 0.0002 Then
                                dnT = -0.00001
                        End If
                        nT = nT + dnT
                        Else
                        'METHOD OF FALSE POSITION
```

```
                        nT = ((nTOld2 * dqOld) - (nTOld * dqOld2)) / (dqOld - dqOld2)
                    End If
                    Else
                    nT = nT - dnT
                End If
        End If
'
'Mass transfer coefficient corrected for high mass transfer rates
        RateFactorM = (nT / BetaG)
        B = (Exp(RateFactorM)) - 1
        CorrFactor = RateFactorM / B
        BetaGx = BetaG * CorrFactor
'Condensing molar fluxes
        nPen = BetaGx * (fyPin - yPiface) + fyPin * nT
        nIso = nT - nPen
'Select correlation for HTCf based on condenser type
        If icondenser = 1 Then
                HTCfloc = fn_HTCfLocReflux(Mcond, TSid, fxPbulk, fyPin, Tdew, fTg, fPsat, 0)
                Else
                HTCfloc = fn_HTCfLocCM7(Mcond, TSid, fxPbulk, fyPin, Tdew, fTg, fPsat, 0)
        End If
'Calculate HTC corrected for high mass transfer rates
RateFactorH = ((nPen * Cp_VapPen * MWpen) + (nIso * Cp_VapIso * MWiso)) / HTCdrygas
        HTCghigh = HTCdrygas * (RateFactorH / (Exp(RateFactorH) - 1))
'
'Heat flux from V/L interface to coolant
        q1A = ((1 / fHTCcw) + (1 / HTCfloc))
        q1 = (Tdew - fTcw) / q1A

'Component enthalpies for local heat balance
        hgPenSurf = fn_PropHCmix(1, Tdew, fPsat, 10)
        hgPenBulk = fn_PropHCmix(1, fTg, fPsat, 10)
        DeltahvPen = fn_PropHCmix(1, Tdew, fPsat, 11)
        hgIsoSurf = fn_PropHCmix(0, Tdew, fPsat, 10)
        hgIsoBulk = fn_PropHCmix(0, fTg, fPsat, 10)
        DeltahvIso = fn_PropHCmix(0, Tdew, fPsat, 11)
'Heat flux from vapoutr to V/L interface
        q2P = nPen * (hgPenBulk - hgPenSurf + DeltahvPen) * MWpen
        q2I = nIso * (hgIsoBulk - hgIsoSurf + DeltahvIso) * MWiso
        q2 = HTCghigh * (fTg - fTdew) + q2P + q2I
'Compare the two heat fluxes
        dq = q2 - q1
'Set convergence flags
        If dq > 0 Then iIter1 = 1
        If n > 0 And dq < 0 Then iIter2 = 1
```

```
'Check for non convergence
        n = n + 1
        If n = nLim Then Exit Do
'Store old values of Dq and Nt
        nTOld2 = nTOld
        nTOld = nT
        dqOld2 = dqOld
        dqOld = dq
        Loop
'
CpMol_VapIn = Cp_VapIn * Mwmix                          'Convert gas bulk Cp to molar Cp
dTGbydA = HTCghigh * (fTg - Tdew) / (fNvap * CpMol_VapIn)  'Multiplier in vap cooling equation
'
QwallFlux = 0.5 * (q1 + q2)          Take heat flux as average of q1 and q2
Ucond = QwallFlux / (fTg - fTcw)     'Overall coefficient
'
End Sub


Sub OutputFile(RunDate, Rnum, Tsat, Psat, NBulkV, MolFrPVin, Tcw, HTCcw, Mwat,_
                    rLV, iModel, icondenser)
'
        Application.Workbooks.Add
        ActiveWindow.Zoom = 75
        With ActiveSheet.PageSetup
                .FitToPagesWide = 1
                .FitToPagesTall = 1
        End With
'
        If iModel = 1 Then
                Range("B1") = "Colburn_Drew Analysis: No Mixing Model"
                Else
                Range("B1") = "Colburn_Drew Analysis: Perfect Mixing Model"
                End If
'
        If icondenser = 1 Then
                Range("H1") = "Reflux Condenser"
                ElseIf icondenser = 2 Then Range("H1") = "Co-current Condenser"
        End If
'
        Range("B2") = "Date"
        Range("B3") = "Rnum"
        Range("C2") = RunDate
```

```
        Range("C3") = Rnum
'-------------------------------
'Data used for model
'===================
        Range("B5") = "DATA"
        Range("B6") = "Bulk Vapour"
        Range("B7") = "Temp"
        Range("B8") = "Press"
        Range("B9") = "Mole Flow"
        Range("B10") = "Mol Fr"
        Range("C7") = Tsat
        Range("C8") = Psat
        Range("C9") = NBulkV
        Range("C10") = MolFrPVin

        Range("D6") = "Coolant"
        Range("D7") = "Temp"
        Range("D8") = "HTC"
        Range("D9") = "Mass Flow"
        Range("E7") = Tcw
        Range("E8") = HTCcw
        Range("E9") = Mwat
        Range("F6") = "Reflux Ratio"
        Range("F7") = rLV
'-----------------------------------------------
'TABLE HEADINGS
'=============
        Range("D12") = "Flows and temperatures through the condenser"
        Range("L12") = "Results from heat and mass transfer step"
        Range("C13") = "Inc"
        Range("D13") = "yP"
        Range("E13") = "xP"
        Range("F13") = "Nvap"
        Range("G13") = "Nliq"
        Range("H13") = "NliqPen"
        Range("I13") = "Qcum"
        Range("J13") = "Tbulk"
        Range("K13") = "Twater"
        Range("L13") = "q"
        Range("M13") = "Len"
        Range("N13") = "nPen"
        Range("O13") = "nIso"
        Range("P13") = "Ucond"
        Range("Q13") = "dTGbydA"
        Range("R13") = "Tdew"
```

```
Range("S13") = "BetaGx"
Range("T13") = "RateFactor"
Range("U13") = "Vapour HTC"
Range("B14") = "Top"
Range("B34") = "Bottom"

Range("D40") = "yP bot"
Range("D41") = "yP top"
Range("D42") = "xP bot"
Range("D44") = "Tube length"
Range("D46") = "Heat load"
Range("D47") = "Tvap out"
Range("D48") = "Tcw in"
Range("D38") = "Results Summary"

Range("E40") = "=D34"
Range("E41") = "=D14"
Range("E42") = "=E34"
Range("E44") = "=M36"

If Icondenser = 1 Then
        Range("E46") = "=I14"
        Range("E47") = "=J14"
        Range("E48") = "=K14"
        Range("V14") = "Iterations"
        Range("V15") = "No."
        Range("W15") = "xPout"
        Range("X15") = "NliqPen"
        Else
        Range("E46") = "=I34"
        Range("E47") = "=J34"
        Range("E48") = "=K34"
End If

If iModel = 1 Then
        ShName = Rnum & "_NoM"
        Else
        ShName = Rnum & "_PM"
End If

Sheets("Sheet1").Name = ShName
Sheets(ShName).Select
Selection.PasteSpecial Paste:=xlFormats, Operation:=xlNone, SkipBlanks:= False,_
        Transpose: =False
Sheets(Array("Sheet2", "Sheet3")).Select
```

```
        ActiveWindow.SelectedSheets.Visible = False
        Range("A1").Select
'
End Sub


Sub TableValues(i, icondenser, yP, xP, Nvap, Nliq, NliqPen, Qcum, Tbulk, dLen, QwallFlux,_
                    Twater, nPen, nIso, Ucond, dTGbydA, Tdew, BetaGx, HTCdrygas, RateFactorM)
'
    If I = 21 Then
        If icondenser = 1 Then
            irow = 14
            ElseIf icondenser = 2 Then irow = 34
        End If
'Set up strings for output
        strinc = "C" & irow
        stryP = "D" & irow
        strxP = "E" & irow
        strNvap = "F" & irow
        strNliq = "G" & irow
        strNliqPen = "H" & irow
        strQcum = "I" & irow
        strTbulk = "J" & irow
        strTcw = "K" & irow
'Display data
        Range(strinc) = i
        Range(stryP) = yP(i)
        Range(strxP) = xP(i)
        Range(strNvap) = Nvap(i)
        Range(strNliq) = Nliq(i)
        Range(strNliqPen) = NliqPen(i)
        Range(strQcum) = Qcum(i)
        Range(strTbulk) = Tbulk(i)
        Range(strTcw) = Twater(i)
        Range("A15") = ""
        Range("M35") = "Total"
        Range("M36") = "=Sum(M14:M34)"
        Range("E14") = ""
        Range("G14") = ""
        If icondenser = 2 Then
            Range("H14") = ""
            Range("I14") = ""
        End If
```

```
        Else
            If icondenser = 1 Then
                irow = 35 - i
                ElseIf icondenser = 2 Then irow = i + 13
            End If
'Set up strings for output
            strinc = "C" & irow
            stryP = "D" & irow
            strxP = "E" & irow
            strNvap = "F" & irow
            strNliq = "G" & irow
            strNliqPen = "H" & irow
            strQcum = "I" & irow
            strTbulk = "J" & irow
            strTcw = "K" & irow
            strq = "L" & irow
            strLen = "M" & irow
            strnPen = "N" & irow
            strnIso = "O" & irow
            strUcond = "P" & irow
            strdTGbydA = "Q" & irow
            strTdew = "R" & irow
            strBetaGx = "S" & irow
            strRateFactor = "T" & irow
            strStar = "A" & irow
            strHTCdg = "U" & irow
            If icondenser = 1 Then
                strDeleteStar = "A" & irow + 1
                Else
                strDeleteStar = "A" & irow - 1
            End If
'Display data
            Range(strinc) = i
            Range(stryP) = yP(i)
            Range(strxP) = xP(i)
            Range(strNvap) = Nvap(i)
            Range(strNliq) = Nliq(i)
            Range(strNliqPen) = NliqPen(i)
            Range(strQcum) = Qcum(i)
            Range(strTbulk) = Tbulk(i)
            Range(strLen) = dLen(i)
            Range(strq) = QwallFlux
            Range(strTcw) = Twater(i)
            Range(strnPen) = nPen
            Range(strnIso) = nIso
```

```
            Range(strUcond) = Ucond
            Range(strdTGbydA) = dTGbydA
            Range(strTdew) = Tdew
            Range(strBetaGx) = BetaGx
            Range(strRateFactor) = RateFactorM
            Range(strStar) = "****"
            Range(strDeleteStar) = ""
            Range(strHTCdg) = HTCdrygas
        End If

End Sub
```

```
            Range(strUcond) = Ucond
            Range(strdTGbydA) = dTGbydA
            Range(strTdew) = Tdew
            Range(strBetaGx) = BetaGx
            Range(strRateFactor) = RateFactorM
            Range(strStar) = "****"
            Range(strDeleteStar) = ""
            Range(strHTCdg) = HTCdrygas
        End If

End Sub
```

THESIS CONTAINS CD/DVD